

## 2019000460 - 20190 00 450

JiNR-1-1,2-88\_652.



IX Международный семинар проблемам физики высоких энергий



#### ОБЪЕДИНЕННЫЙ ИНСТИТУТ ЯДЕРНЫХ ИССЛЕДОВАНИЙ

Д1,2-88-652

### Труды

# **IX** Международного семинара проблемам физики высоких энергий

(14-19 мюня 1988 г., Дубна) ТОМ И

# Proceedings of the IX International Seminar on High Energy Physics Problems

(June 14-19, 1988, Dubna) VOLUME II

#### Оргкомитет

Председатель Оргкомитета

Ученый секретарь

Члены Оргкомитета:

А.М.Балдин

В.В.Буров

И.И.Зотов

А.Л.Коваленко

Б. А. Кулаков

В.К.Лукьянов

Ю.А.Панебратцев

А.В. Радюшкин

М.И. Соловьев

В. С. Ставинский

А. П. Чеплаков

Международный семинар по проблемам физики высоких энергий "Ре-LX лятивистская ядерная физика и квантовая хромодинамика" проходил в Дубне с 14 по 19 яюня 1988 года.

Главные темы семинара:

- квантоная хромодинамика больших расстояний /общие теории, модели/;
- асимптотическое понедение адронных и ядерных реакций, кумулятивные процессы:
- мультикварковые состояния;
- структурные функции адронов и ядер;
- релятивистские ядерные столкновения.

В работе семинара приняло участие более 200 ученых, представлявших 70 научных центров из 17 стран /НРБ, ВИР, ГДР, Индия, Италия, Испания, Канада, МИР, ИИР, СРР, СССР, США, Франция, ФРГ, Швеция, Швейцария, Янония/. Было заслушано свыше 100 докладов. В сборник трудов семинара /который выходит в двух томах/ вошли доклады, подготовленные авторами для прямого репродуцирования и полученные Оргкомитетом до 1 сентября 1988 г.

Надеемся, что предлагаемый сборник с достаточной полнотой отразит научную проблематику семинара.

Оргкомитет



#### СОДЕРЖАНИЕ

V.Genchev et al.  QCD Analysis of the Nucleon Structure Function
$F_2(x,Q^2)$ Measured in Muon-Carbon Deep Inelastic Scattering 6
Л.П.Каптарь и др. Ядерные эффекты в глубоконеупругих процессах
Г.М.Ваградов Ядерные эффекты в глубоконеупругом рассеянии
Е.М.Левин Уроки ЕМС-эффекта
L.L.Frankfurt, M.I.Strikman QCD and Shadowing of Valence and Sea Quarks in Deep Inelastic
Lepton-Nucleus Scattering 44
J.P.Vary, H.J.Pirner  Quark Cluster Model - Comparisons with Recent Data
Н.П.Зотов, В.А.Салеев, В.А.Царев Жесткие процессы на ядрах
C.Ciofi degli Atti Quasi-Elastic and Deep-Inelastic Electron Scattering by Nuclei 68
B.Frois Electron Scattering and Meson-Exchange Currents
W.Meyer Physics with Polarization Degrees of Freedom at the New
Electron Stretcher Accelerator ELSA in Bonn
S.Kowalski Electromagnetic Structure of Few-Body Systems
J.M.Laget Few Body Systems at Intermediate Energies
А.В.Афанасьев, М.П.Рекало Феноменологический анализ проявлений мезонных обменных
токов в электрорасщеплении дейтрона у порога
М.П.Рекало, Г.И.Гах, А.П.Рекало Электрорасшепление векторно-поляризованных дейтронов,
2fl(e,e'p)n и дибарионные резонансы

А.И.Берлев и др. Рождение антипротонов, каонов и пионов при столкновении редигивистских ядер с энергией 3,65 ГэВ/нуклон
E.Oset et al.  Delta Excitations in Nuclei: Microscopic Description  of Pion Nuclear Reactions
V.G.Ableev et al.  Δ-Isobar Excitations of Nuclei in Charge-Exchange Reactions156
F.Chiavassa et al.  Experiments at Saturne with Ano, Spectrometer
С.А.Авраменко и др. Наблюдение релятивистских гиперядер XH при взаимодействии ЧНе (18 ГэВ/с) с легкими ядрами
M.Sano Hypernucleus Formation in High-Energy Nuclear Collisions
Р.Брандт и др. Исследование взаимодействия релятивистских ядер с мишенями из меди и 2n-геометрии
Б.И.Альясевич и др. Исследование фрагментации ядра-мишени при взаимодействии ядер 12С и 4Ме с эпергией 3,6 ГэВ/нукл с ядрами196
С.Вокал и др. Спектры $\pi^{\frac{1}{2}}$ мезонов и протонов в центральных и периферических столкновениях р, $^{12}$ С, $^{22}$ Ne с ядрами фотозмульсии при $\sim$ 4,5 A ГэВ/с
Б.У.Амеена и др. Топологические характеристики фрагментации ядер 28Si с импульсом 4,5 A РэВ/с на ядрах фотоэмульсии
Р.Р.Мехтиев, А.П.Чеплаков Анализ слектров полной поперечной энергии в $\{p,d,\alpha,C\}$ +C-взаимодействиях при 4,2 ГэВ/с228
М.И.Третьякова - EMU-O1 сотрудничество Пентральные взаимодействия ядер кислорода на тяжелых ядрах фотормульсии при энергии 200 ГэВ на нуклон
HI.Löhner et al.  Momentum Distributions of Neutral Pions in Heavy Ion Reactions at the CERN-SPS

M.C.Abreu et al.
$J/\Psi$ Production in Collisions of Oxygen and Sulphur
Ions on Heavy Targets at 200 GeV per Nucleon248
Meng Ta-chung
Stochastic Aspect of Multiparticle Production
in Relativistic Nuclear Reactions262
D.Blaschke, G.Röpke, H.Schulz
Implications From the Momentum Dependence of Heavy Quarkonium
Suppression for a Possibly Formed Quark-Gluon Plasma274
V.B.Gavrilov et al.
Possible Manifestation of Quark-Gluon Plasma
in Deep Inelastic Nuclear Reactions284
Lee G.Pondrom - CDF Collaboration
Recent Results from the CDF Detector at Fermilah288
Yu.A.Batusov et al.
Antiproton Interactions with Light Nuclei at LEAR Energies297
F.Balestra et al.
Study of Low Energy Antiproton Interaction with Nuclei
Using a Self Shunted Streamer Chamber in a Magnetic Field309
C.Chasman, O.Hansen, H.E.Wegner
The Rationale for RHIC in the Context of Recent A+A Data319
P.Kienle
Present Status of the GSI-SIS/ESR Project327

QCD ANALYSIS OF THE NUCLEON STRUCTUPE FUNCTION  $\Gamma_2(x,\mathbf{Q}^2) \text{ MEASURED IN MUON-CARBON DEEP INELASTIC SCATTERING}$ 

V.Genchev, V.G. Krivokhizhin, V.V. Kukhtin, R. Lednicky, S. Memechek, P.Reimer, 1.A. Savin, A.V. Sidorov, N.B. Skachkov, G.1. Smirnov

Presented by I. Savin

Joint Institute for Nuclear Research Dubna

#### 1. INTRODUCTION

In this paper we describe results of QCD analysis of the structure function  $F_{\chi}(x,Q^2)$  measured by the BCDMS collaboration in an experiment on muon deep inelastic scattering from carbon targets  $^{/1}$ . The method of the analysis is based on the expansion of a structure function (SF) in a Jacobi polynomial series as described in paper  $^{/2}$ . It is applied both to nonsinglet (NS) and singlet (S) structure functions the  $Q^2$ -dependence of which is predicted in the leading order (LO) and next-to-leading order (NLO) of the perturbative QCD theory. A short summary of the method and the appropriate formulae are given in Section 2.

The experimental data are obtained at incident energies of 120, 200 and 280 GeV in the region 0.25 < x < 0.80, y = 0.15-0.9 and  $Q^2 > 25 \text{ GeV}^2$ , where x and y are usual scaling variables and  $Q^2$  is the four-momentum transfer squared. In this region higher twist effects are supposed to be negligibly small and the data well suited to test the QCD predictions. Although F, is almost a singlet structure function, in

the region x > 0.3 a main contribution to it comes from a nonsinglet distribution of valence quarks because distributions of sea quarks and gluons are concentrated at smaller  $x^{/3/}$ . Taking this into consideration, we have compared the data with the QCD predictions using both the NS-(Sect.3.) and S-(Sect.4) formalisms and NLO-corrections. A consistency of these analyses proves the validity of the nonsinglet approximation in this kinematical domain.

Our main results of the NS analysis obtained with the help of the Jacobi polynomial method have been reported elsewhere  $^{/4/}$ . Here we describe the analysis in detail and estimate systematic errors in the QCD mass scale parameter  $\Lambda$  arising both from the data and from the method. To be consistent with paper  $^{/4/}$ , we have used the same cut y<0.2 removing from the data 9 points out of 166 measured in the whole y region. The dependence of the results on this and other kinematic cuts is also studied.

#### 2. BASIC FORMULAE

According to paper  $^{/2/}$ , the basic relation connecting the structure function  $F_2(x,Q^2)$  and moments  $M^{QCD}(n,Q^2)$ , calculated in the perturbative QCD, takes the form

$$\overline{F_2}(x, \dot{Q}^2) = \chi^{\alpha}(1-x)^{\beta} \sum_{k=0}^{M_{\text{MAX}}} \Theta_k^{\alpha\beta}(x) \sum_{j=0}^{k} c_j^k(\alpha_j \beta_j) \cdot M^{\dot{Q}(\lambda)}(n, \dot{Q}^2), \tag{1}$$

where  $\theta_k^{\alpha\beta}$  (x) are the Jacobi polynomials,  $x^{\alpha}(1-x)^{\beta}$  is a weight function,  $c_j(\alpha,\beta)$  are known coefficients of an expansion of the polynomial in a  $x^j$  series, n=j+2, and  $N_{MAX}$  is the number of series terms.

For calculation of the NS- and S-moments in the  $\overline{MS}$  subtraction scheme, we have used the expressions (in notations of papers  $^{/2,5/}$ ):

$$\mathsf{M}_{NS}^{\mathsf{RCD}}(\mathsf{n},\mathsf{Q}^2) = \frac{1}{6} \left\langle \Delta(\mathsf{Q}^2) \right\rangle_{\mathsf{n}} = \left[ \frac{\ell \mathsf{n}(\mathsf{Q}^2/\mathsf{A}^2)}{\ell \mathsf{n}(\mathsf{Q}^2_{\bullet}/\mathsf{A}^2)} \right]^{-\mathsf{d}_{NS}^{\mathsf{n}}} \cdot \frac{1}{6} \left\langle \Delta(\mathsf{Q}^2_{\bullet}) \right\rangle_{\mathsf{n}} \tag{2}$$

and

$$M_{S}^{(\alpha,\alpha^2)}(n,\alpha^2) = \frac{5}{18} \left\{ \langle \mathcal{E}(\alpha^2) \rangle_n (1 + \frac{\widetilde{g}^2(u^2)}{16\pi^2} \overline{B}_{z,n}^{\ \ \phi}) + \frac{\widetilde{g}(u^2)}{16\pi^2} \overline{B}_{z,n}^{\ \ G} \langle G(\alpha^2) \rangle_n \right\}, \tag{3}$$

where  $\Lambda$  is the QCh mass scale parameter,  $d_{NS}^n$  are anomalous dimensions /5/,  $\tilde{g}^2(Q^2)$ / to  $\pi^2 \in \alpha_S^2(Q^2)$  is a running constant of strong interactions, and  $\tilde{B}_{2,n}^{-\psi}$ ,  $\tilde{B}_{2,n}^G$  are known coefficients (see /5/). The running constant

$$\chi_{\mathcal{L}}^{2}(\alpha^{2}) = \left[ \frac{1}{3} \ln(\alpha^{2}/\lambda^{2}) \right]^{\frac{1}{2}} \left[ \left( 1 - \beta_{A} \ln \ln(\alpha^{2}/\lambda^{2}) \right) \frac{1}{\beta_{A}^{2}} \ln(\alpha^{2}/\lambda^{2}) \right]; \ \beta_{A} = 11 - \frac{2}{3} n_{A}, \ \beta_{A} = 102 - \frac{38}{3} n_{A}$$

is calculated for  $n_f = 4$ . Expressions for  $\Delta$ ,  $\Sigma$  and G are given in Ref. They describe  $Q^2$  evolutions of moments of nonsinglet quark, singlet quark and gluon distributions, respectively. Initial values of these moments are given or determined from the same experiment at a reference point  $Q_0^2$ . Comparing data to the QCD predictions, one can either consider initial moments as free parameters (the so-called "direct approach") or calculate them using the following relations (the "parametrication approach"):

$$\langle \Delta(Q_{e}^{2})\rangle_{n} = \int_{0}^{1} dx \, x^{n-2} \, x \, \Delta(x_{i}Q_{e}^{2}) ,$$

$$\langle \Sigma(Q_{e}^{2})\rangle_{n} = \int_{0}^{1} dx \, x^{n-2} \, x \, \Sigma(x_{i}Q_{e}^{2}) ,$$

$$\langle \Sigma(Q_{e}^{2})\rangle_{n} : \int_{0}^{1} dx \, x^{n-1} \, x \, G(x_{i}Q_{e}^{2}) ,$$

$$(4)$$

where the quark and gluon distributions have the assumed parametrizations

$$K\Delta(x,Q_{v}^{\perp}) := C_{v}^{NS} \times X_{v}^{NS} \cdot (t \cdot x)^{S_{v}^{NS}} (f \cdot y_{v}^{NS} x) . \tag{5}$$

$$\lambda \Sigma (x, Q_{\nu}^{2}) = C_{\nu}^{5} \cdot x^{\alpha_{\nu}^{5}} \cdot (1-x)^{\beta_{\nu}^{5}} + C_{\nu}^{5} (1-x)^{\beta_{\nu}^{5}}, \tag{6}$$

and

$$xG(x,Q_{\nu}^{2}): c_{q}(1-x)^{\beta_{3}}(1+y_{3}x).$$

$$(7)$$

Unknown parameters in (5-7) should be determined from the same data together with  $\Lambda$ . One of the parameters, namely  $\langle xG \rangle_2$  or  $C_g$ , is fixed by the total energy-momentum sum rule

$$\langle \Sigma(Q_e^i) \rangle_2 + \langle G(Q_e^i) \rangle_2 = 1.$$
 (8)

The final goal of the analysis is to compare the data on  $F_1$  to their QCD expectations from (1) and to find out the QCD mass scale parameter  $\Lambda$  corresponding to the best data description by the QCD formulae. We believe that a statistic error of this parameter should be defined by the statistical fluctuation of the data while uncertainties of other parameters are to be included in an estimation of the systematic error.

Particularly, to estimate the systematic error in  $\Lambda$  due to parametrization uncertainties, in the NS approximation we have performed the analysis by the two above-mentioned methods the first of which (direct) does not require a knowledge of the quark distribution while the second one assumes a certain form (5) for it.

As the input for the fitting procedure performed with the help of the MINUIT program, we have used the values of  $F_2(x,Q^2)$  calculated on the assumption that  $R = G_L/G_T = 0$  (Tables 4-6 in paper /1/). At every step of the fit we have introduced a correction assuming that  $R = R_{QCD}$ , where  $R_{QCD}$  is the QCD prediction for this parameter /6/. The initial  $(F_2^{R=0})$  and corrected  $(F_2^{RQCD})$  structure functions are connected by a relation  $F_2^{RQCD} = K(y,E,Q^2) \cdot F_2^{R=0}$ , where

$$K(y, E, Q^2) = \left[1 - y - \frac{Q^2}{4E^2} + y^2 \frac{E^2 \cdot Q^2}{2E^2}\right] / \left[1 - y - \frac{Q^2}{4E^2} + \frac{y^2 (E^2 \cdot Q^2)}{2E^2 (R_{QCD} + 1)}\right]$$
(9)

and

$$R_{QCD}(s,Q^2) = F_L^{QCD}(s,Q^2) / [(1 + 4 \uparrow f^2 \kappa / Q^2) \cdot F_L^{QCD}(s,Q^2) - F_L^{QCD}(s,Q^2)]. \tag{10}$$

The longitudinal SF,  $F_L^{\rm QCD}$ , is calculated according to Eq. (1) with the longitudinal moments given by expr./5/

$$\mathsf{M}_{L}^{\mathsf{QCD}}(n, \mathbf{Q}^2) \approx \frac{\mathsf{B}_{L,n}^{\Psi}}{\beta_{\nu} L_{n}(\alpha^{2}/\Lambda^{2})} \mathsf{M}_{2}^{\mathsf{QCD}}(n, \mathbf{Q}^2) + \frac{\mathsf{B}_{L,n}^{\mathsf{C}}}{\beta_{\nu} \ell_{n}(\alpha^{2}/\Lambda^{2})} \mathsf{S}_{\Psi}^{(2)} \cdot \mathsf{G}(\alpha^{2}/\Lambda_{n}) , \qquad (11)$$

where

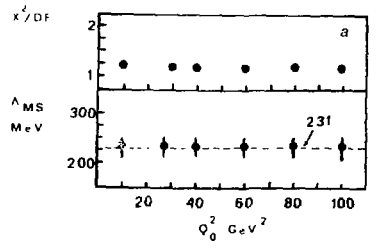
$$S_{+}^{(2)} = \frac{5}{48}$$
,  $B_{L,n}^{\Psi} = \frac{16}{3} \left[ \frac{1}{(h+3)} \right]$ ,  $B_{L,n}^{G} = \frac{32}{[(h+4)(h+2)]}$ .

#### NONSINGLET ANALYSIS

#### 3.1 Parametrization Approach

As is seen from the basic relation (1), the final value of  $\Lambda$  could, in principle, depend on variations of the weight function parameters  $\alpha$  and  $\beta$ , expansion terms  $N_{\rm MAX}$ , parameters defining the form of the NS quark distributions (5) and the reference point  $Q_{\rm c}^2$ . Using the ENC datd/7/one can show/2/ that  $\Lambda$  is practically independent of these parameters if  $N_{\rm MAX}$  is large enough. For the BCDMS data we have repeated these tests as described below.

We started with the choice of the reference point  $Q_0^2$  taking, as recommended in  $\frac{727}{N_{\rm MAX}}$ =7,  $\infty$  =-0.85 and  $\beta$ =3.0. The variation of  $Q_0^2$  within an interval of 5-100 GeV<sup>2</sup> has practically no influence on  $\Lambda$  which is stable (see Fig. 1a) around an average value of 231 MeV with point-to-point fluctuations less than 0.5 MeV. This can be taken as a systematic error in  $\Lambda$  due to arbitrariness of the reference point  $Q_0^2$ .



For further analysis we chose  $Q_0^2 = 27.5 \text{ GeV}^2$ , i.e. at the beginning of the data kinematic range.

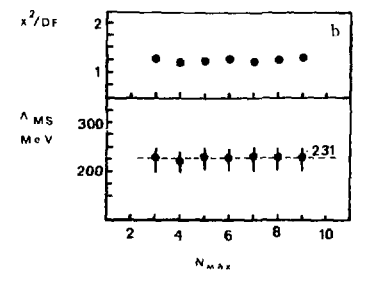


Fig. 1. Results of the nonsinglet analysis for  $\Delta$  and  $\chi^2/\mathrm{DF}$  as a function of the reference point  $Q_0^2$  (a) and the number of expansion terms  $N_{\mathrm{MAY}}$  (b).

Next we studied the stability of the results with respect to  $N_{MAX}$ . As is seen from Fig. 1b, for  $N_{MAX}$  from 3 to 9 point-to-point fluctuations in  $\Lambda$ 's are less than 5 MeV. This value gives an estimate of the systematic error in  $\Lambda$  due to  $N_{MAX}$ . Later the stability tests were extended up to  $N_{MAX}=14$  with almost the same results. The other parameters,  $C_{V}^{NS}$ ,  $\alpha_{V}^{NS}$ ,  $\beta_{V}^{NS}$ , and  $\gamma_{V}^{NS}$ , were also stable within the errors. For further tests  $N_{MAX}=7$  is used except for special cases.

The influence of the weight function form on the other parameters is seen from Fig. 2. As expected  $^{/2/}$ , all of them are stable within the errors

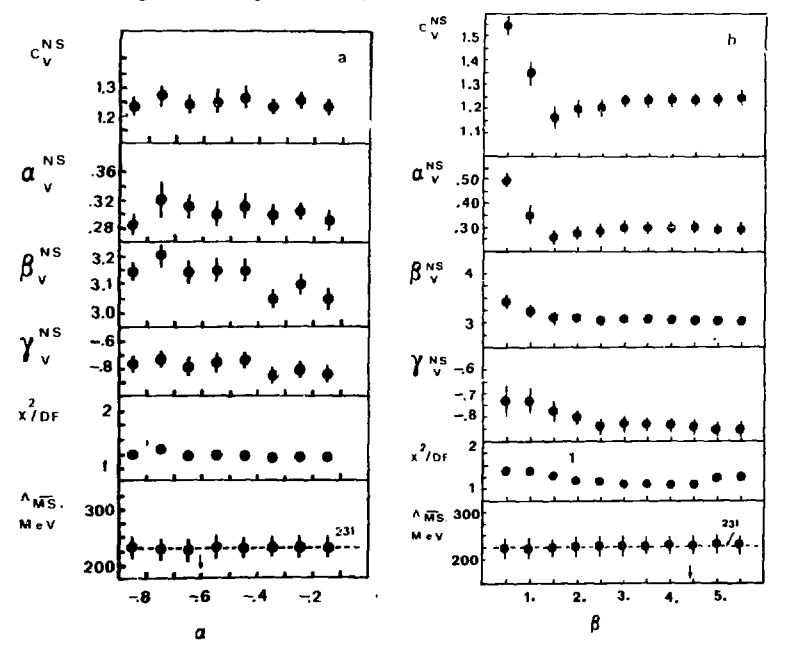


Fig. 2. Results of the nonsinglet analysis as a function of one of the weight function parameters  $\alpha$  (a) or  $\beta$  (b); the second parameter is fixed:  $\beta = 3$  and  $\alpha = -0.85$ , respectively.

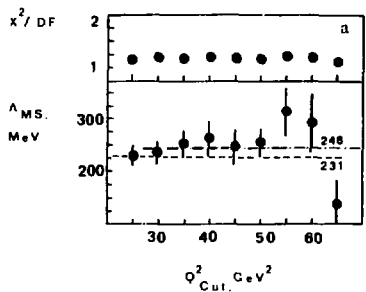
in a wide range of variations  $\{\alpha = -0.7 \pm -0.15 \text{ and } \beta = 2 \pm 5.5 \}$  in particular, the  $\Lambda$  varies by less than 3 MeV. An unpronounced  $\chi^2/\mathrm{DF}$  minimum at  $\beta = 3 \pm 4.5$  is seen in Fig. 2b. The values of  $\alpha = -0.61$  and  $\beta = 4.45$  corresponding to the fit with all free parameters indicated in Fig. 2 by arrows are used for further tests. As we have learned, the parameter fluctuations in Fig. 2 are due to a relatively low accuracy of calculations at  $N_{\mathrm{MAX}} = 7$ . These fluctuations become negligible when the calculation accuracy increases, e.g. at  $N_{\mathrm{MAX}} = 12$ .

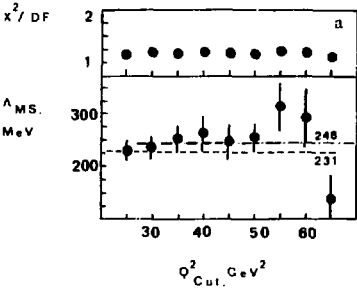
The results of stability tests with respect to various kinematic cuts are shown in Fig. 3. These tests characterize not the method of the analysis but the quality of the data.

The dependence of  $\Lambda$  on  $Q^2$  cut has been studied up to  $Q^2_{\text{cu}\overline{\textbf{t}}}65$  GeV<sup>2</sup>. Larger values are unreasonable due to losses of statistics. As is seen in Fig. 3a, the  $\Lambda'$ **s** obtained at various cuts are in statistical agreement. A small systematic increase of  $\Lambda$  with increasing  $Q^2_{\text{cut}}$  was used to estimate the corresponding systematic errors. The  $\Lambda$  averaged over the points in Fig. 3a is equal to 238 MeV. The difference between this value and a value of 231 MeV obtained without additional cuts can be considered as a measure of this type of systematic error in  $\Lambda$ . Note that the averaging over all points except the first one gives  $\Lambda$  = 216 MeV and indicates that this error could be larger.

With respect to x-cut the  $\Lambda^{'}$ s — also stable (Fig. 3b). However, a small systematic decrease of  $\Lambda$  — with increasing x<sub>cut</sub>—can be seen in Fig. 3b. We consider 5 MeV as a possible systematic error in  $\Lambda$ —due to x-cut of the data, e.g. due to the MS approximation. A small systematic decrease of  $\chi^{2}/W$  is also seen in Fig. 3b indicating that the NS approximation is more justified at x > 0.3 where the gluon and sea quark contributions become negligible.

) is stated above, we have corrected the data for  $R_{\rm QCD}$  at every step of the fitting procedure. To calculate  $R_{\rm QCD}$ , we use Expr.(11) for





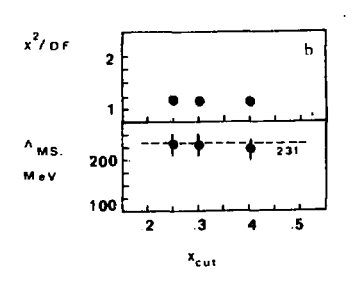


Fig. 3. Results of the nonsinglet fits for A versus 0 cut (a) or x cut (b) applied to the data.

 $M_{\rm I}$ , where the gluon distribution is taken in the form (7) with B = 8. A variation of B from 4 to 10 has a very small influence on Roch in the considered kinematic region and, consequently, on A which varies by less than 1 MeV. Since there is a 30% theoretical uncertainty in R due to higher order corrections to  $F_1^{/8}$ , we estimate the corresponding systema-

tic error in  $\Lambda$  to be 5 MeV. We have also estimated that the use of R = 0 instead of  $R_{OCD}$  increases  $\Lambda$  by 15 MeV and slightly deteriorates the X2.

Studying X of each data point, we found and excluded one point at E = 200 GeV, x = 0.275,  $Q^2 = 50 \text{ GeV}^2$  which contributed to  $X^2$  more than 10 units.

Thus, the final result of the NS analysis shown in Table 1 is based on 156 experimental points. The values of free parameters are given in the tuble. When all of them, except A , are fixed, the fit obviously gives the same values of  $\chi^2$  and  $\Lambda$  as in Table 1, but the error in A instead of 20 MeV becomes 17 MeV because now it has no contribution from uncertainties of the parameters characterizing the x distribution of F,.Comparing the errors in  $\Lambda$  obtained from the fits with free and fixed parameters and assuming that in the first case

they are summed up quadratically, one can estimate the systematic error in  $\Lambda$  due to x-distribution uncertainties of about 10 MeV.

Final Results of Monsinglet Fits

Table 1

C <sub>NS</sub>	∝ NS v	₽ <sub>v</sub> <sup>NS</sup>	۲ <sup>NS</sup>	α	В	Λ <sub>MS</sub> , MeV	<b>x</b> <sup>2</sup>
1.22	.286	3.071	830	61	4.45	232	166
±.03	±.020	±.021	±0.22	±.51	±.11	±20	

Finally, we have studied an influence of the experimental systematic errors on the results of the QCD analysis as a function of y cut applied to the data. For this study each experimental point of the undistorted set was multiplied by a factor characterizing a given type of uncertainties and a new (distorted) data set was fitted again. The factors were taken from Tables 4-6 of paper  $^{/1/}$ . The absolute differences between the values of  $\Lambda$  for the distorted and undistorted sets of data are given in Table 2 together with the total systematic error of

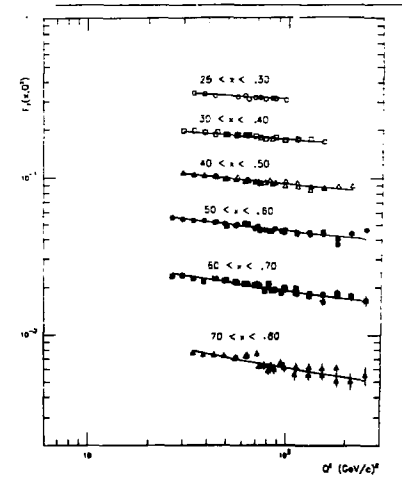
 $\Lambda$  estimated in quadratures. The number of the experimental points and the value of  $\Lambda$  for the undistorted set of  $F_2$  are also given in Table 2. We can see that the  $\Lambda's$  obtained at different  $\gamma$  cuts are statistically consistent. The cut  $\gamma$  = 0.2 reduces the systematic error in  $\Lambda$  by 20 MeV. Further reduction of the data by a stronger  $\gamma$ -cut, while increasing the statistical error, practically has no influence on the total systematic error of  $\Lambda$ .

Concluding this part we can say that the systematic errors of the polynomial expansion method are estimated and found to be small as compared with statistical and systematic errors of the data. The final value of  $\Lambda$  from the NS analysis of the data is  $\Lambda_{\overline{\text{MS}}} = 232 \pm 20 \pm 50 \text{ MeV}$ ,  $\chi^2/\text{DF} = 166/150 = 1.10$  (see also Fig.4).

Table 2

Systematic Errors in  $\Lambda_{\overline{1S}}$  Due to Experimental Uncertainties in Scattered Muon Momenta (dp/n), Incident Energy (E $_0$ ), Magnetic Field of the Spectrometer (B) and Detector Efficiencies

	У	C.15	0.20	0.25
Source	of Systematics	A di	storted - Aun	distorted <mark>,</mark> MeV
	dp/p	47	33	21
	E <sub>o</sub>	23	13	13
	В	36	19	21
Detec	tors	25	26	26
Total	syst.errors	68	47	42
No. of	data points	166	15 7	141
Undist AMS ±	orted stat.err.,MeV	208±18	231±20	248±24



<u>Fig. 4.</u> Comparison of the data on  $F_2(x,Q^2)$  and final results of the nonsinglet analysis for  $\Lambda_{\overline{MS}} = 232$  MeV (solid line).

#### 3.2 Direct Approach

Using this approach, we have performed the analysis at  $N_{\rm MAX}=5.6$  and T with  $\Lambda$  and moments  $\langle \Lambda(Q_0^2)\rangle_n$  at  $Q_0^2=27.5$  GeV<sup>2</sup> as free parameters. The weight function parameters  $\alpha$  and  $\beta$  were found and fixed at the values corresponding to the minimal  $\chi^2$ . To minimize correlations between free parameters, all moments with n>2 were normalized to the second moment. Although the results for all used  $N_{\rm MAX}$  are statistically consistent, more stable values of  $\Lambda$  were obtained at  $N_{\rm MAX}>6$ . For  $N_{\rm MAX}=7$  the results are  $\Lambda_{\rm MS}=235\pm20$  MeV,  $\chi^2/{\rm DF}=1.1$ , i.e. the same as obtained by the parametrization approach. From this coincidence one can conclude that the assumed parametrization (5) describes the experimental data well—and practically has no influence on the precision of the  $\Lambda$ —determination.

Prawing a general conclusion, one can say that both the direct and parametrization approaches to the nonsinglet analysis with next-to-leading order corrections are self-consistent and provide a good description of the data by the QCD formulae. For completeness we have performed the LO fit resulting in  $\Lambda_{1.0}^{NS} \approx 226 \pm 22$  MeV.

#### 3.3. Comparison with Other Analyses

As known, there are several practical methods (programs) of QCD analysis of structure functions, each of them having own limitations. These limitations are not always clearly indicated in papers, and applications of different programs to the same set of data could give different values of  $\Lambda$  (see examples in  $^{/4}$ ,9/).

Within the BCDMS collaboration, an alternative method of QCD-analysis based on numerical solutions of the Alta:elli-Lipatov-Parisi (ALP) evolution equations has been developed  $^{/10/}$ . We have access to other programs  $^{/11-13/}$  as well.

So, the ronsinglet analysis has been performed using all available programs for the same set of data (the set of 357 points described above).

The results (Table 3) for the first four programs are in excellent agreement.

Table 3 Results of Nonsinglet QCD Fits to  $F_{x}(x,Q^{2})$ 

Data [Program]	Λ <sub>LO</sub> (MeV)	X²/DOF	Λ <sub>MS</sub> (MeV)		
BCDMS [2]	226±22	174/152	231±20	176/152	
BCDMS [10]	215±20	174/150	235±20	178/150	
BCDMS [11]	220±20	178/151	220±20	180/151	
BCDMS [12]	224±20	190/151	233±20	198/151	
BCDMS [13]	222±25	178/152	270±25	181/151	
EMC [12]	90±20	115/80	115±10 <sup>+90</sup> -45	106/88	
EMC [2],	$Q^2 > 5 \text{ GeV}^2$		130±30		
EMC [2],	Q > 15 GeV		210±40		

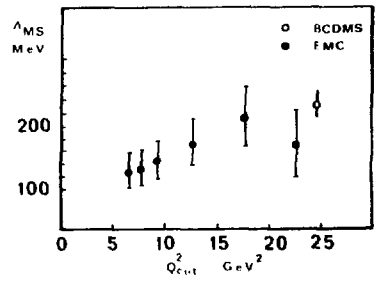
In the M.O-case the program  $^{13/}$  gave the result which is two standard deviations away from others. The reason of this deviation is not clear. Thus, for the final value of  $\Lambda$  from the nonsinglet analysis of the data, the average value obtained with programs [2,10-12] is

taken as  $\Lambda_{\overline{MS}}^{NS} = 230\pm20\pm60 \text{ MeV}$ .

where the total systematic error includes also uncertainties due to the methods.

One can compare this value with the EMC ones  $^{77}$  obtained from the analysis of F, measured in muon-iron interactions. As is seen from Table 3, the EMC and BCDMS analyses are marginally compatible within statistical and systematic errors. Why is it so? It could be due to different kinematic regions of the experiments: the EMC data as compared to the BCDMS ones extend to lower  $Q^2$  (up to 5 GeV<sup>2</sup>). Using our program, we have performed the analysis of the EMC data in the region

x = 0.35 - 0.65,  $Q^2 - 5 - 200$  and obtained the results as a function of  $Q^2$  cut applied to the data (see Fig 5). A strong systematic effect is clearly seen from this figure at  $Q^2_{cut} < 15 \text{ GeV}^2$  while in the region  $Q^2 > 15 \text{ GeV}$  the experiments are consistent within the statistical errors only. So, the EMC data at  $Q^2 < 15 \text{ GeV}^2$  probably contain a systematic



non-QCD contribution vanishing with increasing  $Q^2$ .

Fig. 5. Nonsinglet analysis of the EMC data $^{77}$ , dependence of  $\Lambda_{\overline{\rm MS}}$  on  ${
m Q}^2$  cut.

#### 4. SINGLET ANALYSIS

This type of analysis is performed by the parametrization approach assuming that the measured  $F_{\rm c}$  is a pure singlet structure function with a quark distribution parametrized by Expr.(6). Taking into account the known correlation between A and the gluon distribution parameter  $\beta_{\rm g}$  in (7), first we fixed  $\beta_{\rm g}$  = 8 and studied the stability of the fits with respect to the parameters characterizing the method. As is seen from Figs. 6 and 7, the resulting A's are independent of these parameters.

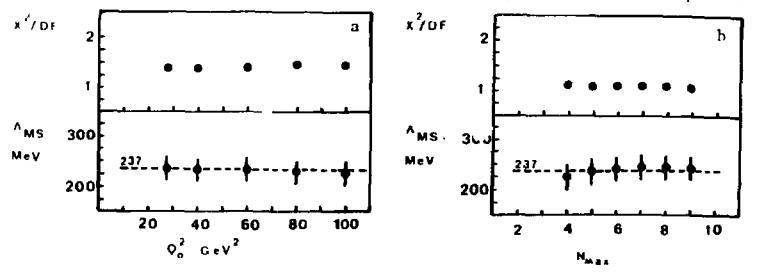


Fig. 6. Results of the singlet analysis as a function of  $Q_0$  (a) and  $N_{MAX}(h)$ . The final result of the nonsinglet fit is shown in this figure and in Fig.7 by dashed lines.

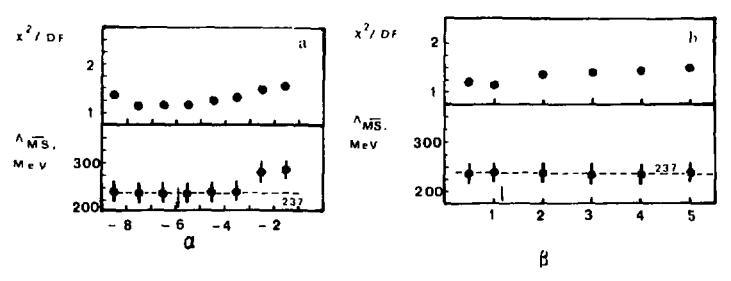
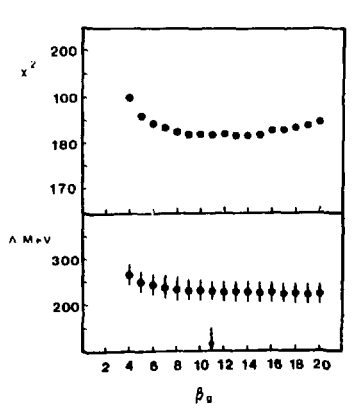


Fig. 7. Results of the singlet analysis as a function of the weight function parameters  $\alpha$  (a) and  $\beta$  (b).

ters. The tests were extended in  $Q_{0}^{2}$  up to 5 GeV<sup>2</sup> and in  $N_{MAX}$  up to 15 with practically the same results as in Fig.6. The point-to-point fluctuations in  $\Lambda$  due to the variations of  $Q_{0}^{2}$  and  $N_{MAX}$  are even less than in the case of the nonsinglet analysis. So, the systematic errors in  $\Lambda$  arising from the method are small.

For further studies aimed to determine  $\Lambda$  and  $\beta_g$ , we have taken  $Q^2 = 10 \text{ GeV}^2$ ,  $\alpha \approx -0.99$  and performed fits with  $\beta_g$  fixed in steps and other parameters being free. To guarantee a high accuracy of  $F_2$  calculations (better than 0.1%), we took  $N_{\text{MAX}} \approx 10$ . Stable



results for  $\Lambda_{\overline{\rm MS}}$  and a broad  $\chi^2$  minimum we obtained for  $\beta_{\rm g}$  between 8 and 17 (see Fig. 8) indicating a low sensitivity of the results to the shape of the distribution of the gluon contribution which is expected to be small in our kinematic region. The fit with free  $\beta_{\rm p}$  gave

<u>Fig. 8.</u> Results of the singlet fits as a function of the gluon power  $\beta_g$ .

 $A_{\overline{MS}}^{(S)} = 227 + 21$  MeV,  $\beta_g = 11_{-3}^{+6}$  and  $\mathbf{x}^2 = 182$  for 157 experimental points.

The systematic errors are the same as in the case of the non-inglet analysis.

#### 5. DISCUSSION AND CONCLUSION

The RCDMS collaboration has made the most complete comparison of the nucleon structure function  $F_{\nu}(x,Q^2)$  with perturbative QCD twist-2 predictions using the honsinglet and singlet formalisms with next-to-leading order corrections. A good agreement between the data and QCD is found in the kinematic range 0.25 < x < 0.8,  $Q^2 > 25$  GeV which is presumably free of higher twist contributions. In this region main contributions to the structure function  $F_{\nu}$  come from valence quarks. So, the nonsinglet analysis is well justified giving  $\Lambda_{\overline{MS}}^{NS} = 230 \pm 20 (\text{stat.}) \pm 60 (\text{syst.}) \text{MeV}$ , where the systematic errors are dominated by experimental uncertainties.

Veroal agreement of data with QCD and the value of  $A_{\overline{MS}}^{NS}$  = 200 ± ± 20 ± 60MeV has been also obtained by the BCDMS from the nonsinglet analysis of a proton structure function at  $Q^2>20$  GeV $^2$ /14/. Moreover, a good description of the data by QCD was obtained fitting the BCDMS nucleon and proton structure functions simultaneously. The resulting

 $\Lambda \frac{NS}{MS}$  = 215 ± 15 ± 50 is to be considered as an average value of two measurements.

The nonsinglet analysis of the EMC nucleon structure functions  $^{77/}$  performed by us in the overlapping with the BCDMS kinematic range  $x=0.3\pm0.7;~Q^2>15~GeV^2$  also gave the results consistent with QCD and  $\Lambda^{-NS}_{\overline{\rm MS}}=210\pm40~{\rm MeV}$ . The last value agrees with the BCDMS ones within the statistical errors. A satisfactory agreement of data with QCD and  $\Lambda^{+}s$  around 200 MeV has been obtained from other muon and neutrino experiments (see Rev./15) if the data are taken at  $Q^2>10~{\rm GeV}^2$  if the data are analysed in the region starting from lower  $Q^2$  ( $Q^2>3-5~{\rm GeV}^2$ ), fits have low confidence indicating that in this region the data are contaminated by non-QCD contributions or/and systematic effects.

The complete singlet treatment of the nucleon structure functions  $F_2$  including NLO corrections has been performed by the BCDMS for the first time. The result  $\Lambda_{\overline{\rm MS}}^S=227\pm21$  MeV coincides with the nonsinglet one confirming an internal consistency of the data and formalisms. Due to the limited x-range of the experiment, the singlet analysis is not sensitive to the shape of the gluon distribution. If the latter is parametrized as  ${\bf x} G({\bf x},Q_0^1)=C_g(1-{\bf x})^{\frac{3}{2}g}$ , the best solution is found for  ${\bf F}_g^{NLO}=11^{+6}_{-3}$  at  $Q_0^1=10$  GeV<sup>1</sup>. Similar results are obtained from the singlet analysis of the proton structure functions  ${14/4}$  in the range  $0.06 < {\bf x} < 0.8$ ,  $Q_0^1>8$  GeV<sup>1</sup>:

$$\Lambda_{\overline{MS}}^{S} = 205 \pm 20, \quad \beta_{g}^{NLO} = 9 \pm 2 \quad .$$

So, the gluon distribution power  $\beta_g$  is significantly higher than that previously determined in the leading order approximation  $^{/7}$ , 14/ ( $\beta_o^{LO}\simeq$ 5).

#### REFERENCES

- BCDMS, Benvenuti A.C. et al., CERN-EP/87-100 or JINR, E1-87-549, Dubna, 1987.
- Krivokhizhin V.G. et al., JINR E2-86-564. Dubna, 1986; Z.Phys., Part. and Fields, 1987, C36, p.51.
- CDHS, Abramowicz H. et al., Z.Phys., Part. and Fields 1983, C17,
   283; CHARM, Bergsma F. et al., Phys.Lett., 1983, 123B, p.269.
- 4. BCDMS, Benvenuti A.C. et al., Phys.Lett., 1987, 1958, p.97.
- 5. Buras A.J., Rev.Mod.Phys., 1980, 52, p.199.
- b. Altarelli G. and Martinelli G., Phys.Lett., 1978, 76B, p.89.
- 7. EMC, Aubert J.J. et al., Nucl. Phys., 1986, B272, p.158.
- 8. Devoto A. et al., Phys.Rev., 1984, D30, p.541.
- Savin I., in: Proc. of the XXII Intern.Conf. on High Energy Phys., Leipzig, July 19-25, 1984. Edited by A.Meyer and E.Wieczoreck, Zeuthen, 1984, vol.2, p.251.
- 10. Virchaux M. and Ouraou A., Preprint DPhPE 87-15, Saclay, France.

- 11. Gonzales-Arroyo A. et al., Nucl.Phys., 1979, B153, p.161, ibid 1979, B159, p.512;
- Gonzales-Arroyo A. and Lopez C., Nucl. Phys., 1980, B166, p.429.
- 12. Abbot L.F. et al., Phys.Rev., 1980, D22, p.582.
- 13. Furmansky W. and Petronzio R., Nucl. Phys., 1982, B195, p.237.
- 14. BCDMS, Benvenuti A.C. et al., JINR, E1-87-689, Dubna, 1987.
- 15. Voss R., in: Proc. of the 1987 Intern. Symp. on Lepton and Photon Interactions at High Energies, Hamburg.

Л.П. Каптарь, Б. Л. Резник, А.И. Титов, А.Ю. Умников Объединенный институт ядерных исследований, Лубна

Цель данного доклада - обсудить вклад ядерных эффектов в глубоконеупругом лептон-ядерном рассеянии и их влияние на информация с кварковых распределений ядер, извлекаемую из эксперимента. В области малых  $x \colon 0,1 \le x \le 0,3$  это мезонные обменные токи /МОТ/, а при  $x \ge 1$ -релятивистское ферми-движение нуклонов в ядре, учитывающее внемассовость нуклонов и многогкварковые компоненты ядерной волновом функции.

I. Представляется очевидным, что мезонные токи /MT/ должны давать вклад в глубоконеупругое рассеяние (ГНР) электронов ядрами, подобно тому, как они проявляют себя в различных электромагнитных и электрослабых ядерных процессах 1 -4/. Неудивительно поэтому, что именно мезоны явились первыми кандилатами на осъяснение ЕМС-эффекта наблюдаемого отклонения от единицы отношения структурных функции тяжелого ядра и дейтерия - R<sup>A.D</sup>. Предполагалось, что в тяжелых ядрах, из-за сильного взаимодействия нуклонов, существует некоторый избыток мезонов (пионов), приходящихся на один нуклон, по сравнению с невзаимодействующими нуклонами –  $\delta n_{\rm M}$ , которым объяснялся подъем  $P^{{\sf A}\times{\sf D}}$ при малых  $(x \le 0, 2)^{\frac{1}{3-7}}$ . Слабым местом этих работ было то, что величина  $\delta n_{\tt m}$  не вычислялась, а задавалась либо как параметр, либо как функция от неизвестных величин, которые сами являлись эффективными параметрами. Это практически означает, что вопрос о вкладе ялерных мезонов в структурную функцию ядра остается открытым. Построение самосогласованной теории МОТ в ГНР на тяжелых ядрах - дело будущего. однако проследить основные качественные моменты этой теории можно на примере точно решаемой ядерной модели - дейтрона. Поскольку адронный тензор  $W_{\mu\nu}^D$ , который содержит информацию о ГНР, определяется мнимой частыю амплитуды упругого рассеяния виртуального у-кванта дейтроном, то для нашей цели можно применить теорию МОТ, развитую для описания яДрами 1,2,4/ упругого рассеяния (УР) электронов легчайшими использованием развитой там методики выделения основных диаграми. В сечения ГНР, так же как и в УР, дают вклад разные диаграммы импульсного приближения (ИП), мезонных токов (МТ), токов отдачи, перенормировки, трехчастичных сил и т.д '4'.

Можно показать, что часть диаграмм взаимно сокращается, а часть можно учесть в диаграммах импульсного приближения , так что в итоге адронный тензор  $W^{\rm D}_{\mu\nu}$  представляется в виде суммы двух диаграмм – ИП и МТ, приведениих соответственно на рис. 1а,б, причем диаграммы МТ носят

матерференци еным харавтер, по<mark>ртому вклад от них может быть</mark> на конеременным

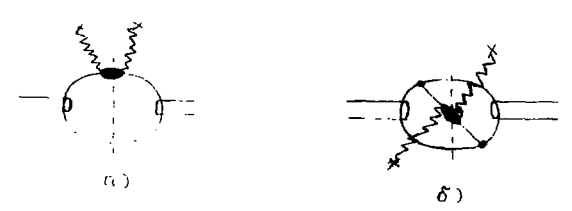


Рис 1 Лиаграммы ГНР на дейтроне.

Самосствае ванность теории подразумевает. Что при расчете диаграми МТ должны учитываться те же мезоны, которие "генерируют" NN-разимодействие в дейтроне. В наших расчетах используются два потенциала: потенциал однобозонного обмена ( $\pi$   $\sigma$   $\omega$   $\delta$   $\eta$ + $\rho$ ) боннокой группы  $^{n}$  и "парижский" потенциал $^{(n)}$ , который при r  $\geq$  0,8 fm представлен суммой  $\pi$ + $2\pi$ + $\omega$  обменных потенциалов а при r  $\leq$  0,8 fm  $\sigma$ -держит феноменологическое отталкивание.

Размет отруктурной функции дейтрона в ИП оводится к вычислению оборгки

$$F_{aD}^{IA}(x) - \int F_{aN}(x/\xi) \phi(\xi) d\xi, \qquad (1)$$

гле  $F_{a,N}(x)$  — отруктурная функция нуклона, а  $\phi(\xi)$  — распределение обязанных нуклонов в дейтроне по доле продольного импульса  $\xi=(p_0+p_3)^{-M}$ .  $p_3-M_2-M_2-M_2^{-1}$  Распределение  $\phi(\xi)$  удовлетворяет условию нормировки на барионный фарал $^{-1.0}$ 

$$\int \phi(\xi) d\xi = 1 \tag{2}$$

и связано с волновой функцией (ВФ) дейтрона (1)

$$\phi(\xi) = \int (1 + p_{x} M) |\Psi_{D}(p)|^{2} \delta(\xi - (p_{o} + p_{y}) / M) dp / (2\pi)^{3}.$$
 (3)

Нами использовалась следующая параметривация  $F_{aN}(\mathbf{x})$ :

$$F_{aN} = x(5(u_v + d_v) + 24q_s) / 18,$$
 (4)

где  $u_v^{-2}$ ,  $69x^{-7\cdot 42}(1-x)^{2\cdot 7}$ ,  $d_v^{-2}$ ,  $56x^{-6\cdot 42}(1-x)^{3\cdot 7}$ ,  $q_s^{-6}$ ,  $1x^{-1}(1-x)^7$ . Результат расчета  $F_z^{ND}$  с боннской ВФ представлен на рис. 2 в виде отношения  $R^{D\cdot N}$  (кривая 1). Качественно  $R^{D\cdot N}$  ведет себя так же, как и отношение структурных функций тяжелого ядра и нуклона  $f_z^{ND}$ , однако глубина минимума при  $f_z^{ND}$ ,  $f_$ 

$$\int_{2D}^{IA} (x) dx = (1-6) \int_{2N}^{IA} (x) dx.$$
 (5)

где расчет соответственно с ВФ дейтрона в "боннском" и "ларижском" потенциалах дает:  $\delta_{\rm p}$ =4,  $7\cdot 10^{-3}$ ;  $\delta_{\rm p}$ =5,  $0\cdot 10^{-3}$ .

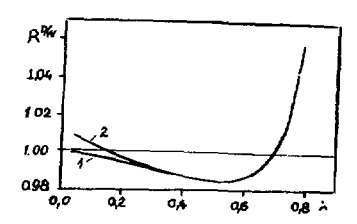


Рис. 2. Отношение структурных функций дейтрона и нуклона. Кривые: 1-импульсное приближение, 2-учет МТ (расчет с ВФ дейтрона в "боннском" потенциале).

Вклад изовекторных псевдоскалярных однопионных обменов в структурную функцию  ${\sf F_{2D}}$  имеет вид

$$\delta F_{2D}^{\pi}(x) = -\int \frac{dp_1}{(2\pi)^6} dp_2 \frac{(k_0 + k_3)}{\sqrt{2E_1 2E_2} M} F_2^{\pi}(\frac{x M}{k_0 + k_3}) \frac{g_{\pi}^2(k)}{(k^2 - m_{\pi}^2)^2} \Phi(p_1, p_2) \theta(k_0 + k_3),$$
(6)

где  $\mathbf{m}_{\pi}$  - масса пиона,  $\mathbf{k}=(\mathbf{k}_{_{\mathbf{0}}},\mathbf{k})=(\mathbf{M}_{_{\mathbf{D}}}\mathbf{-E}_{_{\mathbf{1}}}\mathbf{-E}_{_{\mathbf{2}}},\ \mathbf{p}_{_{\mathbf{1}}}\mathbf{+p}_{_{\mathbf{2}}})$  - его четырехимпульс,  $\mathbf{g}_{\pi}(\mathbf{k})$  - вершинная функция пион-нуклонного взаимодействия  $\mathbf{g}_{\pi}(\mathbf{k})$  - масса нуклона,  $\mathbf{M}_{_{\mathbf{D}}}$  - масса дейтрона,  $\mathbf{E}_{_{\mathbf{1}},_{\mathbf{2}}}=(\mathbf{M}^{2}\mathbf{+p}_{_{\mathbf{1}},_{\mathbf{2}}}^{2})^{1/2}$ . Для  $\mathbf{F}_{_{\mathbf{2}}\pi}$  нами использовались параметрирации

$$F_{a\pi}(x) = x(5q_v+20q)/9$$
,  $q_v=0,75x^{-0.9}(1-x)$ ,  $q_s=0,075(1-x)^{-5}$ . (7) Функция  $\Phi(p,p)$  связана с S- и D-компонентами дейтронной ВФ и и w соот пошением:

$$\Phi(p_1, p_2) = 4\pi [k^2 (2f(p_1)f(p_2) - 3(u(p_1)u(p_2) + w(p_1)w(p_2)P_2(\cos\theta))) + \\ + 2(P_2(\cos\theta) - 1) \cdot (p_2^2 f(p_1)w(p_2) + p_2^2 f(p_2)w(p_1))],$$
 (8)

где  $f(p) = w(p) + \sqrt{2} u(p)$ , p = |p|,  $\theta - y$ гол между p, и  $p_2$ ,  $P_2(z)$  - полином Лежандра. Результаты расчетов  $\delta F_{aD}^{\pi}$  приведены на рис. З (кривая 1). Отметим, что, в отличие от УР, в ГНР вклад МГ пропорционален интегралам перекрытия мезонных вершинных функций с ВФ дейтрона, в которой из-за отталкивания на малых расстояниях в NN-потенциале "вырезается" короткодействующая часть. Это приводит к подавлению  $2\pi$ - и  $\omega$ -мезонных вкладов, по сравнению с однопионным. Для иллюстрации на рис. 3, кривые 3,4, приведен расчет вклада  $2\pi$ -обменного тока (который, как обычно, аппроксимировался обменом скалярным  $\sigma$ -мезоном) и  $\omega$ -мезонного тока. На рис. 2, кривая 2, приведен результат расчета отношения:  $R^{D/N} = (F_1^1 A_1 F_2^2 T)/F_{\pi N}$  с использованием "боннского"

потенциала. Видно, что учет МТ приводит к подъему  $\mathbb{R}^{D \times N}$  при малых х: х  $\leq 0$ , 25. Расчет вклада ИП и МТ в энергетическое правило сумм приводит к результату

$$\langle x \rangle_{D} / \langle x \rangle_{N} = (\langle \tilde{x} \rangle_{N} + \langle x \rangle_{\pi}^{D} + \langle x \rangle_{2\pi}^{D}) / \langle x \rangle_{N} \simeq 0,998,$$
 (9)

при этом  $(\langle x \rangle_{\pi}^{D} + \langle x \rangle_{2\pi}^{D}) \times \langle x \rangle_{N} \simeq 2, 5 \cdot 10^{-3}$ ,

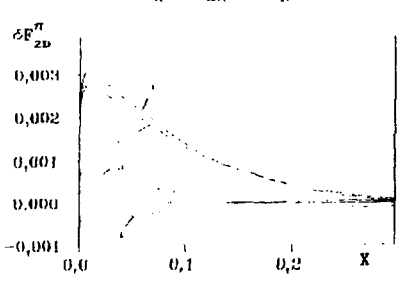


Рис.З. Вклад МТ в структурную функцию дейтрона. Кривые:2,3,4,отдельно вклад л.2л и ω-мезонов, 1-суммарный вклад всех мезонов.

что составляет  $\approx 50\%$  от  $\delta$  (см. Небольшое отличке <x>"<x>" от единицы вызвано нарушением самосогласованности расчета: область кора в "реалистических" потенциалах по сушеству задается феноменологически. Восстановить самосогласованность можно, например, путем учета многокварковой структуры дейтрона на малых расстояниях. Отметим, что развиваемый подход оперирует с пустотными мИИ-вершинами и мезонными пропагаторами и не предполагает никаких "дополнительных"

мезонов (пионов) в ядре. Добавка к структурной функции возникает естественно из-за учета обменных диаграмм. Чисто формально эту добавку можно имитировать "дополнительными" мезонами, число которых на один нуклон в дейтроне можно оценить как:  $\delta n_n^D = \langle x \rangle_n^D / (\langle x \rangle_n m_n / M) \simeq 0,4 \cdot 10^{-1}$ . Это значение  $\delta n_n^D$  меньше тех значений, которые требуются для объяснения ЕМС-эффекта на тяжелых ядрах  $(\delta n_n^A \simeq 1.2 \cdot 10^{-1})$ , однако указывает на важность последовательного учета мезонных степеней свободы в таких процессах.

II. В настоящее время становится уже общепринятым, что различие кварковых распределений в ядре и в свободном нуклоне в области средних x<sup>13</sup> объясняется эффектами фермиевского движения нуклонов с учетом связанности в ядерном потенциале 12. Учет фермиевского движения с нуклонами на массовой поверхности (с более **XCCTKHM** распределением) приводит к качественно NHOWA экспериментом поведению отношения структурных функций  $F_{x}(x)/F_{y}(x)$ . Ясно, что такая же ситуация будет наблюдаться и в граничной области  $x \sim 1$ . чисто нуклонная rze компонента исчезает. вклады мультикварковых состояний и фермиевского движения сравнимы. мультикварковых состояний (высоконыпульсной компоненты) исследовалась в кумулятивных hA-реакциях 14 при сравнительно

передачах импульса (  $Q^2 \le 10 \ \Gamma_2 B^2/c^2$ )/4/ В реакциях глубоконеупругого переданный импульс существенно (  $Q^2 \sim 100-300$  ГэВ $^2/c^2$  ), и поведение мультикваркого распределения в x ~ 1 Momen измениться из-за нарушения масштабной инвариантности. Качественный анализ  $\mathbb{Q}^2$ -зависимости структурных функций ядер при х > 1 без учета ферми-движения нуклонов был дан в работе / 1 в / . Однако, поскольку в пограничной области к ~ 1 вклад фермиевского движения существен, TO для получения количественных представляет интерес исследование суммарного вклада ферми-движения и компонент ядерной волновой функции в  $F_{2,4}(x,Q^2)$ . многокварковых задача актуальна в связи с тем, что эффект нарушения масштабной инвариантности в структурной функции свободного нуклона возрастает x --> 1.

Представим структурную функцию ялра A при данном  $Q^2$  в следующем виде:

$$F_{2A}(x) = (1 - P_e) \int dy d^4k F_{2N}(\frac{x}{y}) S(k) \delta(y^{-kq}/p_q) + P_e * F_2^{eq}(\frac{x}{2}), \tag{10}$$

где:  $-q^2 = Q^2$ , S(k)-спектральная ядерная функция с учетом связанности нуклонов,  $F^{eq}$ -шестикварковая структурная функция (в рассматриваемой области 0,8  $\leq$  x  $\leq$  1,2 основной вклад дарт шестикварковые конфигурации), P -соответствующая вероятность. Спектральная функция S(k) в оболочечной модели совпадает с одночастичным импульсным распределением. Однако, для объяснения ЕМС-эффекта, как было показано в'12/, спектральную необходимо вычислить с учетом более сложных коллективных возбуждений. Для нашей цели удобно использовать относительно простое выражение для S(k), рассчитанной спектральной Функции Антоновым--Николаевым-Петковым'17', которая описывает основные карактеристики ядра, энергетические и импульсные распределения нуклонов. импульское доспределение совпадает с теоретическими значениями. получаемыми в микроскопических расчетах других авторов 1.8. Нуклонную структурную функцию  $F_{2N}(x,Q^2)$  в (10) необходимо брать из условия хорошего описания данных рассеяния лептонов на водороде и дейтроне при данном значении Q<sup>2</sup>. К сожалению, в настоящее время в области передач импульса  $Q^2 \sim 100-300 \text{ ГэВ}^2/c^2$  данных однов лишь BCDMS-коллаборации недостаточно для надежной параметризации истинно нуклонной структурной  $F_{2N}(x,Q^2)$ , поэтому мы воспользуемся параметризацией. описывающей совокупность удовлетворительно ланных CDHS-коллабораций  $^{\prime 1}$  при  $Q^2 \sim 15-25$  Гэв $^2/c^2$ . Отметим, что параметры  $F^{eq}(x)$  определяются также из экспериментов при сравнительно небольших  $\mathbb{Q}^{\tilde{\mathbf{z}}}$ . Таким образом, мы можем рассчитать ядерную структурную функцию  $F_{a}(x,Q^{2})$ , где  $Q^{2}\sim 15$  Гэв $^{2}/c^{2}$ . Для сравнения с данными  $(\tilde{Q}^2 \sim 100-300 \; \Gamma_{\rm 3B}^2/c^2)$  необходимо решить эволюционные

Липатова-Альтарелли-Паризи<sup>гоо</sup> с начальными условиями, расчитанными по формуле (10) в точке  $Q^2 \sim 15 \, \Gamma_2 B^2/c^2$ . Однако здесь надо отметить некоторые неопределенности, связанные с выбором начальных условий. Во-первых, при сравнении ядерных данных ЕМС и ВСРМSколлаборация наблюдается небольшое систематическое различие, которое. по-видимому. существует и для нуклонных структурных функций и должно сказаться при соответствующих дифференциальных уравнений. Во-вторых. параметры мультикварковых распределений в  $F_2^{eq}(x)$ , такие, как вероятность шестикварковой конфигурации, наклон в распределении и пр., извлекаются реакций адрон-ядерного взагмодействия. Злесь неопределенности связаны с учетом вторичных ядерных эффектов, например, перерассеянием частиц, их поглощением в ядре и т.д.

Уравнения Липатова-Алтарелли-Паризи решались в лидирующем порядке с параметром квантовой хромодинамики  $\Lambda$ =(0,21-0,23) гэв/с. Нуклонные и шестикварковые структурные функции в точке  $Q_0$  брались из $^{\Lambda + 0}$ :

$$F_{2N}(x,Q_o) = 5/18\sqrt{x} (1-x)^3 (2,25+1,55(1-x))$$

$$F_2^{aq}(x,Q_o) = 5/18*\sqrt{x} (1-x)^7 + 2/3*0,23(1-x)^{11}$$
(11)

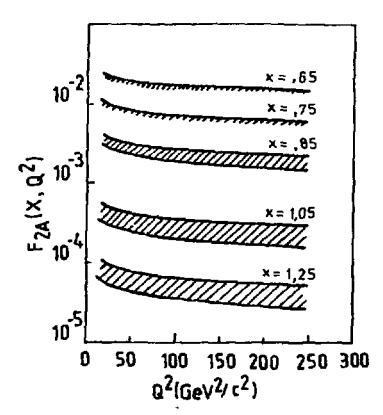


Рис. 4. Q<sup>2</sup>-авольция структурной функции углерода с учетом ферми -движения и бq-компонент. Заштрихованная область - следствие неопределенности в выборе начальных условий (см. текст).

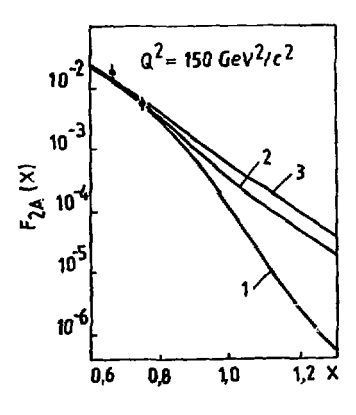


Рис. 5. Структурная функция углерода при Q<sup>2</sup> = 150 ГэВ<sup>2</sup>/с<sup>2</sup>. Кривые: 1-учет ферми-движения, 2(3)-учет 6q-компононт с 5% (10%) вероятностью.

На рис. 4 показан результат эволюции структурной функции ядра<sup>1 2</sup>С

для разных значений х с учетом поправок на связанность нуклонов и шестикварковых конфигураций Заштрихованная область отражает неопределенности в начальных условиях, о которых упоминалось выше. Вероятность шестикварковых конфигураций  $P_{\rm e}$  в углероде варьировалась в пределах от 5% до 10% .

На рис.5 приведены результаты методических расчетов ппя флнкпии углерода при  $Q^2 = 150 \text{ f} \cdot 3B^2/c^2$  в граничной кинематической области Х. Эдесь жe приводятся имеющиеся экспериментальные точки ВСРМS. Из этих двух рисунков видно. фермиевское движение нуклонов с учетом их связанности удовлетворительно описывает экспериментальные данные для к в некумулятивной области. границе нуклонной кинематики вклад шестикварковой компоненты становится сравнимым с фермиевским движением, и с ростом х мультикварковые компоненты становятся доминирующими. Видно еще, что учет внемассовости нуклонов и эффектов  $Q^2$ -эволюции приводит к смягчению высокоимпульсной компоненты в ядрах по сравнению с результатами, полученными кумулятивных hA-реакциях. Этот результат следует иметь в виду при сопоставлении различных экспериментальных данных по **СТРУКТУРНЫМ** функциям, получаемых в разных процессах- в лептон-ядерном (большие  $Q^2$ ) или адрон-ядерном рассеянии (средние  $Q^2$ ).

Отметим еще одно обстоятельство. Уравнения эволюции нами решались в лидирующем порядке. В последнее время появились расчеты с учетом поправок от высших твистов. Оказалось, что вклад от высших твистов обратно пропорционален  $Q^2$  и растет с ростом х. В нашем случае эти поправки несущественны. Действительно, в граничной области х  $\sim 0,9-1,2$  основной вклад в  $F_{2A}(x,Q^2)$  дают шестикварковые компоненты(см. рис.5), для которых масштабная переменная х в два раза меньше нуклонной, т.е.  $x_{\rm eff} \sim 0,45-0,60$ , и для таких х высшие твисты малы независимо от эначения  $Q^2$ .

Авторы выражают глубокую олагодарность А. А. Антонову, В. В. Г. грову, Е. Братковской, М. Кирхбах, В. К. Лукьянову, В. А. Николаеву, И. А. Савину, Г. А. Смирнову за многочисленные плодотворные дискуссии.

#### JUTEPATYPA

- 1. Chemtob M.- In.: Mesons in Nuclei. Amsterdam, North-Holland, 1979, p. 555.
- 2. Иванов Е.А., Труглик Э. ЭЧАЯ, 1981, 12, с. 492.
- 3. Кирхбах М., Труглик Э.- ЭЧАЯ, 1986, 17, с. 224.
- Gari M., Hyuga H.- Z. Phys., 1976, A277, p. 291; Nucl. Phys., 1976, A264, p. 409.
- 5. Ericson M., Thomas A.W. Phys. Lett., 1983, B128, p. 112.
- 6. Титов А.И. ЯФ, 1984, 40, с. 76.

- Умников А. Ю. В сб.: Ядерные реакции и кварковая структура ядер, ДВГУ, Владивосток, 1987, с. 58.
  - 7. Саперштейн Э.Е., Шматиков М.Ж.- Письма в ЖЭТФ, 1985, 41, с. 44.
- 8. Machleidt R. et al. Phys. Rep., 1987, 149, p. 1.
- 9. Lacombe M. et al. Phys. Rev., 1980, C21, p. 861.
- 10. Frankfurt L.L., Strikman M.I. Phys. Rep., 1981, 76, p. 215.
- Бирбраир Б. Л., Левин Е. М., Шуваев А. Р. В кн.: "Физика атомного ядра". Материалы XXI Зимней школы ЛИЯФ, Л., 1986, с. 3.
- 12. Akulinichev S. V., Kulagin S. A., Vagradov G. M.
- Phys. Lett., 1985, v. 1588, p. 485; Письма в ЖЭТФ, 1985, 42, с. 105.
- 13. EMC, M. Arneodo et al., CERN-EP/88-56, 1988.
- 14. Буров В. В., Лукьянов В. К., Титов А. И. ЭЧАЯ, 1984, т. 15, вып. 6, с. 1249.
- 15. BCDMS, Bollini D. et al. JINR, E1-87-549, Dubna, 1987.
- 16. Титов А. И. ЯФ, 1983, т. 38, вып. 6, с. 1582.
- 17. Antonov A. N., Nikolaev V. A., Petkov I. Zh. Z. für Phys. A, 304, 1982, p. 239., Nuovo Cim. 91A, 1986, p. 119.
- 18. Zabolitzky J. G., Ey W. Phys. Lett., 1978, B76, p. 527.
- 19. Abramowicz H. et al. Z. für Phys. C25,1984,p. 29.,
- Dydak F. Int.Symp. on Lepton and Photon Interaction at High Energies, Cornell, August 1983 (CERN-EP/83-171, 1983) 20. Altarelli G. Phys. Rep., 81,1982, p. 1.

#### ЯЛЕРНЫЕ ЭФФЕКТЫ В ГЛІУБОКОНЕУПРУГОМ РАССЕЯНИЛ

#### Г.М.Ваградов

Институт ядерных исследований АН СССР, Москва

#### Введение

Для объяснения данных по глубоконеупругому лептон-ядерному рассеянию 1 / (ВМС-эффект) привлекались различные соображения об изменении кварковой структуры нуклонов внутри ядра. С другой стороны, в рамках траниционной ядерной физики было показано $^{2}$ , что в EMC-эффекте наряду с ферми-движением определяющую роль играет и связанность нуклонов. Такой полход должен основываться на последовательном полевом описании взаимодействия высокоэнергичных частиц со связанными системами. Но эта задача пока далека от полного ее понимания,и в дан--деопрастановимся на некоторых принципиальных вопросах. Предде всего, необходимо найти такие микроскопические характеристики ядра-мишени, которне проявляются в реакциях с большими передачами митульса. Пля этого обратимся к относительно простой мезонной модели ядра, которую можно рассматривать как феноменологическую. В рамках этой модели динамические переменные ядра удается выразить через лоренц-инвариантные 4-импульсные распределения ядерных конституентов/3,4/без квантования нуклонного поля по к кому-либо одночастичному базису. Лалее. не используя операторного разложения. вим связь между структурными функциями (СФ) пдра и СФ его конституentob.

#### 2. жезонная мололь ялоа

Как иллюстрацию к задаче о релятивистском описании связанной системы рассмотрим нуклонное и скалярное поля с гамильтонианом

$$H = H_{\sigma}^{0} + H_{\sigma}^{0} + H_{\sigma}^{1}$$
,  $H_{\sigma}^{0} = \left(4\vec{y}\vec{\psi}(\vec{y})(-i\vec{y}\vec{y}+m)\psi(\vec{y}), H_{\sigma}^{0} = \frac{1}{2}\right)\left(4\vec{y}\cdot[\vec{v}^{2}+m\vec{y}\cdot\vec{v}^{2}] : -\frac{1}{2}\left(\frac{4\vec{x}}{(4\vec{x})},v_{\sigma}^{2}\vec{v}_{\sigma}\right)\right)$  (1)  $H_{\sigma}^{1} = \left(4\vec{y}\vec{\psi}(\vec{y})\vec{v}(\vec{y})\vec{v}(\vec{y}), (C_{\sigma},c_{\sigma}^{0})\right) = (2\pi)^{2}2\omega_{\sigma}\delta(\vec{v}\cdot\vec{x}), \omega_{\sigma} = \sqrt{\vec{v}^{2}+m_{\sigma}^{2}}$ . Ми будем предполагать, что все наблюдаемые физические величини в этой модели являются конечными и система. А барлонов имеет основное

COCTOSHME C HYMORIM HONHIM CHIHOM:  $\hat{P}_{\mu} \left( p > = p_{\mu} | p > \right), \qquad p_{\mu} = \frac{\langle p | H | p \rangle}{\langle p | p \rangle} - \langle o | H | o \rangle = \sqrt{M^{2} + \tilde{p}^{2}},$ 

где  $\hat{P}_{\mu}$  – оператор 4-жипульса, М – масса покол ядра в основном

состояния, 10> — вектор вакуумного состояния, 1р> нормированы гозятивистским образом: <p\p'>=(2n)^2 p\_b(\vec{p}-\vec{p})}.

Очезидно, что |p> нельзя представить в виде "фоковской строки"

$$|p\rangle_{\Phi} = \frac{1}{\sqrt{A_1}} \left( (d\vec{\kappa})_A \stackrel{\text{def}}{=} (\vec{\kappa}_1, \dots, \vec{\kappa}_A) Q_{\chi_1}^{+} \dots Q_{\kappa_A}^{+} |a\rangle \right)$$
(2)

(  $\hat{x}$  - оператор рождения свободного нуклона). Действительно, из (I) и определения вакуума (  $C_c$ 10>=0 ,  $G_c$ 10>=0 ) сразу же следует

$$\mathcal{C}_{\varphi}(\hat{p}) = \left(\frac{\langle p|H(p)\rangle}{\langle p|p\rangle}\right)_{\alpha} = \int_{(2\pi)^3}^{1} \epsilon_{\vec{k}} \, n_{\varphi}(\vec{k}, \vec{p}), \qquad \epsilon_{\vec{k}} = \sqrt{\vec{k}^2 + m^2},$$

где мф - распределение нуклонов по 3-импульсам. Таким образом, представление (2) независимо от выбора системы отсчета не отражает динамики. Динамическое описание с использованием квантования нуклонного поля по какому-либо одночастичному базису с необходимостью приводит к представлению |р> в виде бесконечной суммы "фоковских строк" с различными числами нуклонов, антинуклонов и мезонов.

Мы обратимся к другому способу описания "одночастичных" возбуждений 3.4. Для втого введем полный набор собственных векторов состояний системы из A-I барионов:

$$\hat{\hat{P}}_{\mu} \mid (\hat{p})_{r}^{A-1} = \hat{P}_{r}^{I} \mid (\hat{p})_{r}^{A-1}, \qquad \hat{p}_{r}^{I} = (\hat{p}_{o}^{I}, \vec{s}), \qquad \hat{p}_{o}^{L} = \hat{\xi}_{c}^{A-1}(\hat{p}) = \sqrt{\hat{p}^{S} + (\hat{M}_{c}^{A-1})^{2}}$$

с нормировкой  $<(p_{t}^{A-1}|\{p_{t}^{A,h}\}=\{2\pi\}^{2}\delta_{t,t}^{2}\{(3-\beta^{2})\xi_{t}^{A-1})/4^{A-1}$  (  $M_{t}^{A-1}$  – энергия покоя ядра (A-I) в состоянии L). Определим функцию в спинорном пространстве

$$\Phi_{t \in F}(y) = C_{t \in F} < (\rho - \kappa)_{t}^{A-1} |\Psi(y)| \rho > , \qquad C_{t \in F} = \left(\frac{M_{t}^{A-1}}{2\rho_{t} \mathcal{E}_{t}^{A-1}(\beta - \kappa)}\right)^{\frac{1}{2}}. \tag{3}$$

Величина  $| \Phi_{i \neq j}(y) |^{\frac{1}{4}} \overline{y}$  есть вероятность найти в состоянии  $| p_i \rangle$  барион в окрестности точки  $\overline{y}$ , а остадьнюе A-I- в состоянии  $| (p-x)^{\frac{1}{2}} \rangle$ . Воспользовавшись равенством  $\psi(y) = \overline{\psi}(y) = \overline{\psi}(y)$  можно записать (3) в виде

$$\Phi_{(\vec{k},\vec{p})}(y) = \Phi_{k}(\vec{k},\vec{p}) e^{i\vec{k}\cdot\vec{y}}, \qquad \Phi_{k}(\vec{k},\vec{p}) = \mathcal{E}_{k\vec{k}\vec{p}}(p - k) e^{i\vec{k}\cdot\vec{k}} |\psi(0)|_{p>}, \qquad (3)$$

$$\kappa^{k} = (e_{k}(\vec{k},\vec{p}), \vec{k}), \qquad e_{k}(\vec{k},\vec{p}) = \rho_{k} e^{i\vec{k}\cdot\vec{k}}.$$

Таким образом, вероятность найти в состоянии |р> барион с 4-импульсом к однородна во всем простренстве-времени. Только в модели независимих частиц Ф(н) совпадает с нормированной волновой функцией нуклона в среднем потенциале.

Функции 
$$\Phi_{L}(\vec{x},\vec{p})$$
 удовлетворяют условию:  

$$\sum_{i} \int \frac{d\vec{x}}{(2\pi)^{i}} \left[ \Phi_{L}(\vec{x},\vec{p}) \right]^{i} = \frac{1}{\langle P|P'} \int d\vec{y} \langle P|\Psi(\vec{y})\Psi(\vec{y})|P' = A + 4\Omega \int \frac{d\vec{x}}{(2\pi)^{i}}.$$
(4)

(Член, пропорциональний совему квантования  $\Omega$ , возникает из-за дирековского моря). Воспользовавшись коммутационными соотношениями для  $\psi(y)$  , получим  $\sum_{j\in \mathbb{Z}_{2}} \frac{d\vec{x}}{j(\vec{x}_{0})} \xi_{j}(\vec{x}_{0},\vec{p})|\vec{x}_{0}|^{2} \frac{1}{\langle p|p\rangle} d\vec{y} < p|\psi(\vec{y})(p,H)\psi(\vec{y})(p)=\langle p|H_{p}^{0}+H'|p\rangle/\langle p|p\rangle.$  Отсида и из (I) следует выражение для полной энергии ядра

$$\rho_{\sigma} = \sum_{r} \int \frac{d\vec{k}}{(2\pi)^{4}} \epsilon_{r} (\vec{k}, \vec{p}) \left[ \Phi_{r}(\vec{k}, \vec{p}) \right]^{2} + \int \frac{d\vec{k}}{(2\pi)^{4}} \omega_{\sigma} \eta_{\sigma}(\vec{k}, \vec{p}) - \langle \sigma| H | \sigma \rangle, \qquad \langle \sigma| H | \sigma \rangle = -4\Omega \int \frac{d\vec{k}}{(2\pi)^{4}} \epsilon_{\vec{k}, r} (5)$$

где  $n_{\sigma} = 3$ -импульсное распределение мезонов в ядре:  $n_{\sigma} < p|C_{\epsilon}^{*}C_{\epsilon}|\nu/2c_{\epsilon}p|\nu$  Полный набор векторов  $|\langle p\rangle_{\epsilon}^{k+}\rangle$  образуется из двух групп: одна относится к системе из A барионов минус один нуклон (A-N):

С учетом такого разонения (5) можно обосщить и записать 4-импульсядра

$$\beta_{p} = \left\{ \frac{d^{2}k}{(2\alpha)}, k_{p} \left\{ S_{p}(\mathbf{x}, \mathbf{p}) + S_{p}(\mathbf{x}, \mathbf{p}) + S_{q}(\mathbf{x}, \mathbf{p}) - S_{q}(\mathbf{x}) \right\} \right\}$$

$$\leq \sum_{n} = 2\pi \sum_{p} \left[ \Phi_{p}(\mathbf{x}, \mathbf{p}) \right]^{2} \delta(\mathbf{x}_{n} - \mathbf{x}_{n}(\mathbf{x}, \mathbf{p})), \qquad S_{p} = 2\pi M_{p}(\mathbf{x}, \mathbf{p}) \delta(\mathbf{x}_{n} - \mathbf{u}_{n}), \qquad S_{q} = 8\pi \Omega \delta(\mathbf{x}_{n} - \mathbf{x}_{n})$$

$$\leq \sum_{n} = 2\pi \sum_{p} \left[ \Phi_{p}(-\mathbf{x}, \mathbf{p}) \right]^{2} \delta(\mathbf{x}_{n} + \mathbf{x}_{n}(\mathbf{x}, \mathbf{p})), \qquad \widetilde{\Phi}_{p}(\mathbf{x}, \mathbf{p}) = C_{q} + C_{q}$$

Здесь, как и в (5), содержатся распределения мезонов на массовой поверхности. Это обусловлено тем, что их взаимодействия с нуклонами уже включены в  $\frac{1}{2}$ , и  $\frac{1}{2}$ , . При этом  $\frac{1}{2}$ , облагодаря связанности системы, и для числа мезонов в ядре имеем

$$\int \frac{\mathrm{d}^4 \kappa}{(2\pi)^4} \, \beta_{\rm G}(\kappa, \rho) = N_{\rm G}.$$

Легко видеть, что распределения S являются лоренц-инвариантными. Очевидно, что в более реалистической модели, когда имеется несколько мезонных полей ( или некоторых беспретных объектов), в (6)  $S_{\sigma}$  следует заменить на сумму распределений по различным мезонам (эсли взаимодействием между ними можно пренебречь).

Выражение (6), по-существу, является тождеством. Тем не менее, на основе (6) можно заключить, что связанная система представляет собой газ независимых квазичастиц со спектром масс  $m_{\lambda}$ ,  $\widetilde{m}_{\gamma}$ ,  $m_{\sigma'}$ , равномерно заполнящих все пространство с различными импульоными распределениями. При этом, поокольку  $p_{\sigma}$  — конечная величина, в  $S_{\omega}$  и  $S_{\sigma'}$   $S_{vac}$  сумыхрования по  $\widetilde{\kappa}$ ,  $\lambda$  и  $\gamma$  ограничени некоторыми интервалами, вне которых эти распределения практически обращаются в нуль. Следует иметь в виду, что однонуклонное состояние  $|\{p\}_{\alpha}\rangle$  (или  $|\{p\}_{\alpha}\rangle$ ) также содержит мезонное поле из-за собственно-энергетической часчи. Поетому из (5,6) следует исключать члени, пропорцисональные часлям нуклонов и антинуклонов.

Распределение  $S_n(\mathbf{e})$  может быть извлечено из данных по реакциям квазиупругого выбивания (e,e'p), (p, 2p) и т.п. при переданных энергиях  $\sim$  I ГэВ.

Легко установить связь изложенного формализма с известным потенциальным описанием ядер. Для этого в системе покоя ядра следует пренебречь движением центра масс и воспользоваться статическим приближением по мезонным полям, а для нуклонов — обычным нерелятивистским пределом. Из коммутационного соотношения  $[c_t,H]=\omega_t c_t+\rho_t$   $(\rho_t-g)_{dy}^{-2}\psi(y)\psi(y)^{-2}\psi(y)$  в статическом приближении  $(H-\rho_t)/\omega_t = 0$  следует

$$C_{\vec{k}}|_{p>\infty} = \frac{1}{\omega_{+}H-p} \int_{\vec{k}} |_{p>\infty} = \frac{1}{\omega_{n}} \int_{\vec{k}} |_{p>} \qquad p = (M,0). \tag{7}$$

Отсида и из нерелятивистского предела для  $\psi$  имеем

$$M^{\cong} mA + \frac{\langle p|H_{At}|e^{2}}{\langle p|p\rangle}, \qquad H_{se} = -\int \! d\vec{y} \; \vec{\psi}(\vec{y}) \frac{\vec{y}^{2}}{2m} \psi(\vec{y}) + \frac{1}{2} \int \! d\vec{y} \, d\vec{y} \; \vec{\psi}(\vec{y}) \vec{v}(\vec{y}) \vec{v}(\vec{y}) \vec{v}(\vec{y}) \psi(\vec{y}) \psi(\vec{y}),$$

где V — вкавовский потенциал:  $V(\vec{s}) = -g^2 \int d\vec{\tau} \, e^{i\vec{k}\cdot\vec{y}} (2n)^2 \omega_c^2$ . Отметим, что множитель I/2 в WW —взаимодействии возникает из—за равенства

<р $|H_{est}^o|_{p>=-\frac{1}{2}}<$ р $|H_{st}^o|_{p>=-\frac{1}{2}}<$ , которое просто получить с помощью (?). Вводя далее среднее поле V(r) для нуклона в ядре, определям соответствующую (3) одночастичную энергию

$$\epsilon_{x}(\vec{x}) = m + \frac{\vec{x}^{2}}{2m} + \int \frac{d\vec{q}}{(2\pi)^{2}} \phi_{y}^{*}(\vec{x}) V(\vec{q}) \phi_{y}(\vec{x} - \vec{q}) / |\phi_{y}(\vec{x})|^{2},$$

где  $\Phi_{\nu}(\bar{\nu})$  — фурье-образ волновой функции нуклона. (Для краткости мы опустили релятивистские поправки). Если в этом приближении и можно внчислить  $S_{\nu}$ , то значительно сложнее обстоит дело с  $S_{\nu}$ - $S_{\nu}$  и ме-зонными распределениями, для определения которых пока нет ни теоретических, ни экспериментальных идей. Хотя эффекти, связанные с антинуклонными и мезонными степенями свободы незначительны, тем не менее они могут проявляться в глубоконеупругой области.

#### 3. Структурные функции связанной системы

Чтоби вывести соотношение между СФ ядра и его конституентов, рассмотрим рассеяние виртуальных фотонов на ядре или эквивалентную задачу его взаимодействия с внешним электромагнитным полем 3.4,  $0.(9)=a.(e^{iq_3}+e^{iq_3})/2$ ,

где q, – произвольные константы, q>0 ,  $q^2<0$ .

Будем сначала считать ядро точечной частицей с внутренними степенями свободы, которые могут возбуждаться полем с (у) . Пусть гамильтониан взаимодействия ядра с этим полем имеет вид

$$H'(t) = \langle i\vec{y} \alpha_i(\vec{y},t) J'(\vec{y}) \rangle$$

где  $J''(\vec{y})$  – оператор полного тока ядра. Этот оператор имеет сложную природу, но, как мы увидим ниже, его конкретный вид для нас несуществен.

Амплитула вероятности найти япро в момент времени t в начальном состоянии (р) определяется выражением

$$T = \frac{1}{\langle p|p\rangle} i \frac{\partial}{\partial t} \langle p|U(t)|p\rangle = \frac{1}{\langle p|p\rangle} \langle p|J'(t)U(t)|p\rangle, \qquad J'(t) = e^{iHt}J'(t)e^{i$$

 $U(t) = U(t, \infty)$  — оператор временной зволиции. Из равенства  $J^{\mu}(y) = e^{i \hat{P} y} J^{\mu}(y) e^{i \hat{P} y}$  во втором порядке по a(y) и в пренебр где во втором порядке по а(у) и в пренебрежении быстро-осциллирующими членеми в (8) при t-будем иметь

$$T = \frac{\pi}{R} Q_{\mu} Q_{\nu} T^{\mu\nu}, \qquad T^{\mu\nu} = \frac{1}{2\pi} \sum_{n} \frac{\langle e_{1} I^{2} (0) (e_{1} q_{n}^{2} - \langle e_{1} q_{n}^{2} | I^{2} \langle e_{2} q_{n}^{2} - \langle e_{1} q_{n}^{2} \rangle I^{2} \rangle) e^{2}}{2 \mathcal{E}_{n} (e_{1} + q_{1}^{2} + \langle e_{2} q_{n}^{2} - \langle e_{1} q_{n}^{2} \rangle I^{2} \rangle} + (q - q). \tag{9}$$

 $\text{ 3recb } \hat{\mathbb{P}}_{k}^{1}([\rho]_{k}^{A} \succ \rho_{k}^{*}([\rho]_{k}^{A}), \quad p_{n}^{*} = \delta_{n}(\bar{p}) = \sqrt{M_{n}^{2} + \bar{p}^{*}}, \quad <(\rho')_{n}^{A}([\rho]_{k}^{A} \succ (2n)^{3} 2 E_{n}(\bar{p}) \delta_{n,n}^{A} \delta(\bar{p} - \bar{p}') \delta_{n,n}^{A} \delta(\bar{p} - \bar{p$  $M_n$  — масса покоя возбужденного ядра  $\Lambda$  в состоянии n . Определим теперь матрицу  $^{/5/}$ 

$$W_{p,y}(p,q) = i \left( T_{p,-}^* - T_{p,-}^* \right) = \left( \frac{d^{\frac{1}{2}}}{(2\pi)^2} 0} e^{iqy} \right) \qquad T_{p,p}^{\pm} = T_{p,y}\left(q,\pm iq\right). \tag{10}$$

Через W., выражается вероятность перехода в единицу времени япра из начального во все попустимые конечные состояния

$$W = \frac{\eta}{2\rho_a} a_\mu a_\nu W^{\mu\nu}. \tag{II}$$

Для ядра как точечной частици вид W., следует из тресований релятивистской инвариантности, сохранения тока и четности 15/

$$W_{\mu\nu} = 2 \left( \frac{q_1 q_2}{q_1} - q_{\mu\nu} \right) F_{\nu}(x, q^2) + \frac{2}{pq} \left( p_{\mu} - \frac{pq}{q_1} q_{\mu} \right) \left( p_{\nu} - \frac{pq}{q_2} q_{\nu} \right) F_{\nu}(x, q^2)$$
(12)

где  $f_{1,2}$  — ядерные СФ, зависящие от быёркеновских переменных  $X=Q^1/2pq$  и  $Q^2-q^2$  . Эти функции содержат информацию о внутрен ней структуре системы и обычно определяются с помощью операторного разложения.

С пругой стороны, как мы установили в разделе 2, ядро представляет собой совокупность независимых квазичастыц. Чтобы найти связь между двумя различными представлениями (точечное ядро и газ), рассмотрим сначала для упрощения связанную систему точечных заряженных бермионов ( c=! ) одного сорта и изоскалярных мезонов. Гамильтониан взаимолействия фермионов с полем Q(y)MMeet BMI:

$$H'_{-}(t) = \left(d\vec{y} \ Q_{-}(\vec{y},t)\right)^{\mu}(\vec{y}), \qquad A''(\vec{y}) = \vec{\psi}(\vec{y}) B''\psi(\vec{y}).$$

В присутствии внешнего поля Фраг (у) следует заменить на функцию

$$\Phi_{\text{egf}}^{\mathbf{r}}(t,y) = C_{\text{egf}} < (\rho - v)_{\bullet}^{\mathbf{r}-1} \bigcup_{\mathbf{r}} (t,y_{\bullet}) \psi(y) \bigcup_{\mathbf{r}} (y_{\bullet}) |\rho\rangle,$$
  $i \partial_{\mathbf{r}} U(t,t) - H_{\bullet}(t) U_{\bullet}(t,t).$ 
из уравнения движения двя оператора  $\Psi : (i\gamma \partial - w) \Psi(y) = g \Psi(y) \Psi(y),$ 

можно записать (ix 3-m- \( \int \vec{y} \) \P. = (y) = 0,

где массовый оператор  $\Sigma$  определяется соотношением

$$\sum (e_i, \vec{y}) \Psi_{LEF}(y) = C_{LEF} < (p-x)_L^{A-1} | \varphi(y) \psi(y) | p > .$$

Воспользовавшись этими уравнениями для  $\Phi_{\epsilon \epsilon \rho}(\nu)$ , запишем амплитуду рассеяния фотона вперед на квазичастице с импульсом  $\kappa^{\ell}$  :

$$t_{\epsilon} = \frac{2\rho_{e}}{\langle \rho | \rho_{e} \rangle} \int_{d\vec{y}} i \partial_{\alpha}^{\alpha} \phi_{\epsilon E \beta}^{\alpha}(y) \phi_{\epsilon E \beta}^{\alpha}(ty) \underbrace{t_{y = \infty}}_{y_{y} = \infty} \frac{2\rho_{e}}{\langle \rho | \rho_{e} \rangle} \int_{d\vec{y}} \overline{\phi}_{\epsilon E \beta}(y) (i y \partial_{-m} - \sum (\epsilon_{\epsilon}, \vec{y})) \phi_{\epsilon E \beta}^{\alpha}(t, y). \tag{13}$$

Легко показать. что

$$\frac{2\,\rho_o}{<\rho|\rho>} \sum_i \left(\frac{j_i\,\overline{k}^*}{(2\pi)^3}\right) d\vec{y} \; i\partial_e\,\varphi_{\epsilon\,\overline{k}\,\rho}^{\bullet}(y)\,\varphi_{\epsilon\,\overline{k}\,\overline{\rho}}^{\bullet}(t,y) \underset{t=y_o}{\longleftarrow} <\rho|\,\mathcal{H}_e^i(t)\,U_e(t)|\rho>/<\rho|\rho>.$$

Введем оператор рассеяния на квазичастице

$$\{iy\partial_{-m} - \sum (e_{i,\vec{y}})\} \Phi_{e\vec{e}\vec{p}}^{e}(t,y) = \int_{t-\infty}^{t} \int_{t}^{t} t(y,y') \Phi_{e\vec{e}\vec{p}}(y') .$$

По аналогии с (9) выражение (13) можно представить в виде

$$t_{t} = \frac{2\pi M_{t}}{\kappa_{t}^{0}} a_{\mu} a_{\nu} \{ \Phi_{t}(\vec{s}, \vec{p}) \}^{2} \tau^{\mu\nu}(\kappa_{t}^{1}, p, q) , \qquad m_{t}^{1} = (\kappa^{t})_{j}^{2}$$

где матрица Т\*\* определяется равенством

$$\tau^{\mu\nu} = \frac{P_{o}}{\pi < p_{i}p_{>}} \frac{\overline{\varphi}^{2}_{o}}{\overline{\varphi}_{i}(z, \beta) \overline{\varphi}_{i}(z, \beta)} \frac{\overline{\varphi}^{2}_{o}}{\delta \varphi_{o}} \int_{0}^{1} d^{3}y' \overline{\varphi}_{exp}(y) t(yy) \overline{\varphi}_{exp}(y) \Big|_{q \to 0} .$$

Заметим, что для свободного точечного фермиона  $(\phi_i(\vec{r}_i)) - \sqrt{\frac{m}{e_p}} u_{p_i}, \ \vec{u}_{p_i} u_{p_i} = \delta_{2n})$  совпадает с известным выражением для амплитуды рассеяния вперед.

Усредняя  $\tau_{rr}$  по проекции полного момента квазичастицы, в соответствии с (IO) введем матрицу  $\omega_{rr}$ 

$$4u_{\mu\nu}(\kappa_{1}^{2}\rho_{1}q) = \frac{i}{m_{1}} \left( \frac{q_{\mu}q_{\nu}}{q^{2}} - g_{\mu\nu} \right) \frac{1}{2} (x_{1}, Q^{2}) + \frac{i}{m_{1}(\kappa_{1}^{2}q)} \left( \kappa_{\mu}^{2} - \frac{(\kappa_{1}^{2}q)}{q^{2}} q_{\mu} \right) \left( \kappa_{\nu}^{2} - \frac{(\kappa_{1}^{2}q)}{q^{2}} q_{\nu} \right) \frac{1}{2} (x_{1}, Q^{2})$$
(14)

где  $\int_{\ell_1 2}$  — СФ квазичастици,  $x_2 = Q^2/2(\kappa^4 q)$ .

Вероятность перехода квазичастицы из начального во все допустимые состояния запишется в виде

$$\omega_{i} = \frac{\pi m_{i}}{\kappa_{i}^{4}} Q_{i}Q_{i}|\varphi_{i}(\xi|\hat{p})|^{2} \omega^{\dagger}(\kappa_{i}^{4}\rho_{i}q). \tag{15}$$

Сечение поглощения фотона на квазичастице определяется как

$$G_{t} = \frac{\omega_{t}}{v_{t}}$$
,  $V_{t} = \frac{1}{k_{t}^{2}q_{v}}\sqrt{(\kappa^{2}q)^{2} - (\kappa^{2})^{2}q^{2}} = \frac{(\kappa^{2}q)}{k_{t}^{2}q_{v}}\sqrt{1 - 4\frac{(\kappa^{2})^{2}\pi^{2}}{q^{2}}}$ .

 $V_t$  - поток фотонов относительно квазичастицы с импульсом  $\mathbf{k}^{\ell}$  . Поскольку для невзаимодействующих квазичастиц процесс поглощения является некогеретным, то для полного сечения будем иметь

$$G = \frac{W}{V} = \sum_{i} \int \frac{d\vec{x}}{(2\eta)} e^{i} G_{i}, \qquad V = \frac{pq}{g_{i}} q_{i} \sqrt{1 - 4 \frac{p^{2}X^{2}}{q^{2}}}, \qquad (16)$$

V — поток фотонов относительно ядра, а величина W из (II) соответствует точечному ядру.

Теперь уже легко установить связь между  $F_{\epsilon,z}$  и  $\mathfrak{f}_{\epsilon,z}$  с помощью "проекционных" матриц

$$P_{\mu\nu}^{\prime} = \frac{1}{4} \left( \frac{P_{\mu} P_{\nu}}{\rho^{2} \cdot (\underline{\rho q})^{2}} - g_{\mu\nu} \right), \qquad \qquad P_{\mu\nu}^{\prime} = \frac{Pq}{4 \left( \rho^{2} \cdot (\underline{\rho q})^{2}} \left( \frac{3 \rho_{\nu} P_{\nu}}{\rho^{2} \cdot (\underline{\rho q})^{2}} - g_{\nu\nu} \right),$$

которые приводят к равенствам

$$P_{\mu\nu}W^{\mu\nu}=F_{\mu\nu},\qquad P_{\mu\nu}'W^{\mu\nu}=F_{\mu\nu}.$$
 (17)

Воспользоваемись произвольностью коэффициентов  $\ell$ , в предельном сдучае  $Q^2 \gg m^2$  при M=A(m+p) и  $-p \ll m$  получим с учетом (II  $\sim$  I7)

$$F_{\underline{d}}(x,Q^2) = \int \frac{d^3x}{(2\pi)^3} \left( \frac{x}{X} \cdot \hat{\delta}_{\underline{d},1} + \hat{\delta}_{\underline{d},2} \right) \hat{S}(x,p) \int_{\underline{d}} (x,Q^2) , \qquad \underline{d} = 1,2.$$

 $\zeta'(\cdot,p) - 4$ -импульсное распределение фермионов. Здесь мы приняли, что при x > 1 функции  $\int_{t_1} 0$  обращаются в нуль, а X < t/A

Изложенное просто обобщается на случай составных конституентов в ядре (нуклонов, антинуклонов и мезонов с кварковой структурой):

$$F_{3}(x,Q^{3}) = \left(\frac{d^{3}x}{(2n)}, \left(\frac{x}{x}, \hat{S}_{3}, +\hat{S}_{3}, x\right) \left(\hat{S}_{x}, f_{3}^{x} + \hat{S}_{x}^{x}, f_{3}^{x} + \sum_{i} \hat{S}_{i}, f_{3}^{x} - \hat{S}_{inc}, f_{03}^{x}\right)\right)$$
(18)

где суммирование по r проводится по различным сортам мезонов. В функции  $f_{g}^{\kappa,\tilde{\kappa},r}$  включаются эффекты как внутренней структуры соответствующих квазичастиц, так и их взаимодействия со средой. Если тем не менее принять, что  $^{\mathsf{CP}}$  квазичастиц совпадают со свободными, а для  $S_{\kappa}$  воспользоваться ядерными данными, то расчеты  $^{\mathsf{CP}}$  дают удовлетворительное согласие с наблюдаемыми данными.

В пределе  $Q^2_{-\infty}$  в соответствии с теоремами КХД и с учетом (4) и (6) получим правила сумм

$$\int_{dX} F_{x}(x) = a_{x} \int_{dx} \frac{d^{3}x}{(2\pi)^{4}} \frac{nq}{pq} \left(S_{x} + \frac{S_{x}}{2} - S_{xx} + \sum_{r} S_{r}\right)$$

где константы 0, и 0, определяются как

$$\int dz \, \int_{01}^{u_{\mu}^{(j)}} (x) = a_1 + m \quad , \qquad \int dx \, \int_{01}^{u_{\mu}^{(j)}} (x) = a_2 \quad , \qquad \int dx \, \int_{0}^{u} (x) = 0 \, .$$

Заметим, что правило су м для  $F_2$  нарушается из-за наличия электромагнитного поля в я ре: это поле несет часть импульса, но не изменяет  $C\Phi$ .

## 4. Заключение

Если в зацачах о рассеянии релятивистской частици ограничиться только оценками, то ядро-мишень можно считать газом свободных нуклонов с импульсным распределением, отвечающим их ферми-движению. Но в более строгом рассмотрении необходимо учитывать их связанность и наличие в ядре полей, формирующих 🕊 -взаимодействия. При этом мы уже не в праве, как в случае слабых возбуждений. воспользоваться какимлибо частным видом ядерной волновой функции, построенной на том или ином одночастичном базисе. Чтобы выйти за рамки подобных представлений, мы обратились к методу, основанному на общих соотношениях для полевых операторов и условиях полноты векторов состояний (раздел 2). Это приводит к определению лоренц-инвариантных импульсных распределений ( спектральных функций) \$ ядерных конституентов. Однако нахождение всех этих функций наталкивается на серьезные трудности. Это вносит дополнительные усложнения в задачу о возможности выделения кварковых степеней свободы ( если за нулевое приближение к теории ядерных систем принять мезонную модель).

Очевидно, что представление ждра в виде газа независимых квазичастиц, заполняющих все пространство, не позволяет ввести понятие сечения рассеяния на ядре как целом: это можно сделать лишь для каждой из квазичастиц (аналогично случаю бесконечной среды). С другой стороны, если считать ядро точечным объектом с внутренними степенями свободы ( т.е. со спектром его возбуждений), то для него вероятность перехода в единицу времени на единичный поток палакших частиц должна совпадать с суммой соответствующих вероятностей для квазичастиц. Отсида, в частности, следует, что в соотношении (18) для СФ отсутствует потоковый множитель ( как и в конволиционной формуле ККЛ) и не требуется какой-дибо специальной нормировки спектральных функций 🖇 . В нашем полходе естественным образом осуществляется перехол от точечных конституентов к квазичастицам с внутренней структурой, для которых СФ выражается в той же форме (I8) через распределения кварков и их СФ. Заметим, что для кварков так же, как для квазичастиц теряет смысл представление об их пространственном распределении внутри ядра.

Оценки показывают  $^2$  , что в ЕМС-эффекте мезонине степени свободы играют заметную роль только при  $x = \frac{\varphi^2}{2\pi q_0} < 0.3$ , а антинуклонные, по-видимому, пренебрежимо малы. Сравнение расчетов  $^2$  с данными І свидетельствует о стабильности кварковой структури: СФ свободных и внутривдерных нуклонов совпадают в пределах точности экспериментов и внуислений. Однако мы ограничились рассмотрением модели, в которой мм - силы обязаны обмену некоторыми "белыми" объектами. Не исключено, что учет цветных взаимодействий, многокварковых образований и т.п. несколько изменит результаты расчетов 2, вероятное всего в области и > І. Но до сих пор еще не разработано сколько-нибудь надежных методов количественной оценки таких эффектов.

## Литература

- I.The EMC: Phys.Lett. (1983), <u>123B</u>, 275. The BCMDS Collab.Phys.Lett., (1985), 132B, 282.
- Акулиничев С.В., Кулагин С.А., Ваградов Г.М. Препринт ИНИ, P-0382 (1984)
   Письма в ЖЭТФ, (1985). 42.105. Phys. Lett. (1985), 158B. 475.

Physica Scripta (1986), 34, 508.

- 3. Ваградов Г.М. Краткие сообщения по физике (1987), 4, 9.
- 4. Molinari A., Vagradov G. Preprint DFTT 14/88 (1988).
- ИМИКСОН К, Зюбер К.-Б. Квантовая теория поля, т.2, Москва, "Мир" (1984).

## **УРОКИ ЕМС-ЭФФЕКТА**

## Е.М.Левин

Ленинградский институт ядерной физики АН СССР

Несмотря на шумиху вокруг ЕМС-эффекта, поднятую как экспериментаторами, так и теоретиками, мы по-прежнему далеки от построения самосогласованной теории глубоконеупругого рассеяния на ядрах. Сама же шумиха, в основном, по-моему связана с тем жизненным фактом, что мы, теоретики, оказались не готовы обсуждать жесткие процессы на ядрах, не понимали, к каким эффектам может привести более детальный учет структуры ядра. Мне кажется, что сейчас наступил подходящий момент заняться глубоконеупругым рассеянием на ядрах всерьез, развивая последовательную теорию этих процессов. В связи с этим, в данном докладе я делаю попытку систематизировать те уроки широкого обсуждения ЕМС-эффекта, которые могут быть полезны в предстоящей работе. С моей точки зрения, теоретические достижения исчерпываются следующими утверждениями:

1. Простейшая попытка редятивистского описания ядер в рамках предложенной Дираком квантовой механики на световом фронте противоречит экспериментальным данным по ЕМС-эффекту (см.обзор /1/). Таким образом, первый урок ЕМС-эффекта состоит в том, что параметр малости, который в принципе мог контролировать точность уравнения Шредкигера на световом фронте, а именно:малость вклада ненуклонных степеней свободы в ядрах, оказался неправильным, неадекватным природе. Другим недостатком динамики светового фронта является чисто теоретическое утверждение, что до сих пор не построено ни одной теоретической модели, в которой бы выполнялись предложения Стрикмана-Франкфурта. Тот факт, что мы не имеем ни одной теоретической реализации квантовой механики на световом фронте, по-моему, имеет более важное значение, чем прямое несоответствие с экспериментом.

2. Акулиничев, Ваградов и Хулагин /2/ показали, что Бодек и Ричи /3/ провели неправильное вычисление EMC-аффекта в рамках тех предположений, которые они сделали (так называемое приближение нуклонов

вне массовой поверхности). Они показали также, что корректный учет связанности нуклона в ядре может объяснить ЕМС-эффект. Это очень важный результат, который определил направление дальнейших поисков. Кроме того, вряд ли был бы вообще весь шум вокруг даб-эффекта, если бы тот результат появился раньше.

- 3. Опыт многочисленных попыток объяснить ЕМС-эффект показал, что правильная формулировка будущей теории невозможна без введения ненуклонных степеней свободы. В различных способах описания глубоконеупругого рассеяния на ядрах ненуклонные степени свободы проявляются поразному. В динамике на световом фронте мы вынуждены включать эти степени свободы явным образом для описания экспериментальных данных. В приближении нуклонов вне массовой поверхности без введения ненуклонных степеней свободы не выполняются энергетические правила сумм.
- а) Нуклоны взаимодействуют в ядре через обмен мезонов, причем эффективний лагранжиан равен:

где 🎸 - скалярное (псевдоскалярное) поле.

б) Верно предположение о свертке, то есть

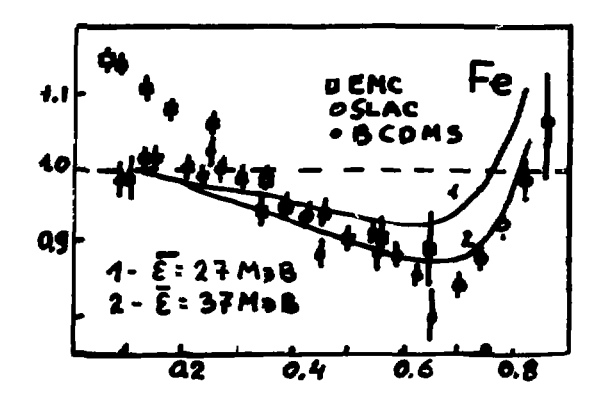
где  $F_{2A}$  ,  $F_{2N}$  и  $F_{2\phi}$  – структурные функции ядра, нуклона и скалярного (псевдоскалярного) мезона соответственно,  $\mathcal{P}_{2\phi}$  ( $\mathcal{P}_{2\phi}$ ) – вероятность найти нуклон (мезон) в ядре.

В этом подходе для отношения  $R(x) = \frac{F_{2A}(x)}{AF_{2A}(x)}$  получается формула  $\frac{1}{A}$ 

$$R(x) = 1 - \frac{1}{m} \left( \frac{\mathcal{E}}{-\langle V_c \rangle} \right) \frac{x F_{ex}(x)}{F_{ex}(x)} - \frac{1}{3m} \left( \frac{P^2}{2m} \right) \frac{x^2 F_{ex}(x)}{F_{ex}(x)} + \frac{1}{A F_{ex}(x)} \int_{y}^{0} (y) F_{ex}(y) dy$$

Идея сравнения с экспериментом этой формулы заключается в утверждении, что последнее слагсемое в ней дает вклад в области малых  $X \lesssim \frac{\rho_{F}}{\rho_{D}} \sim 0.3$  (  $P_{F}$  — импульс ферми-ядра). Поэтому в той области, где велико экспериментальное отличие R ( $\infty$ ) от I, мы можем сравнить с экспериментом формулу (3) без последнего слагаемого. В (3) E — средняя энергия отделения ядра,  $\langle V_{C} \rangle$ — средняя энергия мулона в ядре,  $\langle P^{2} \rangle$  — средний квадрат импульса в ядре. Согласие эксперимента с формулой (3) показано на рис. I. Оно вполне удовлетворительно. Само доказательство формулы (3) связано с определенным техническим достижением авторов, а именно— с доказательством теоремы вириала для взаимодействия вида (I). Именно теорема вириала обеспечивает выполнение энергетических правил сумм и позволяет выразить вклад ненуклонных степеней свободы через несколько величин (E,  $V_{C}$ ,  $\langle P^{2} \rangle$ ), относящихся к структуре ядра.

- 5. Введение в теорию больших венторных полей приводит к резкому противоречию с экспериментальными данными по ЕМС-эффекту. Лело в том. что в формуле (3) < V<sub>4</sub> > заменяется на величину среднего векторного поля в ядре, которая по различным оценкам колеблется в районе 200-300 МаВ. Непосредственно из (3) видно, что R становится порядка **R**~0,1-0,3-0,5,что находится в резком противоречии в экспериментом. Мне кажется, что это очень важный вывод из ЕМС-эффекта. Дело в том, что введение векторных полей представляет собой очень интересный, с точки зрения теории, способ построения ядра. Идея этого построения состоит в том, чтобы построить теорию взаимодействия нуклонов в ядре по аналогии с калибровочными теориями, которые добились значительного успеха в физике элементарных частиц. Предполагается, что в ядерной материи есть локальное сохранение барионного заряда. Именн докальное сохранение барионного числа приводит к появлению векторных мезонов и наличие у них масс вызывает появление хиггсовских частиц (скадярного мезона модели Валечки). Такая схема построения приводит к феноменодогии модели Валечки и других подобных им схем. К сожадению. с моей точки зрения, все эти красивые возможности закрываются экспериментальными данными по ЕМС-эффекту.
- 6. Гипотеза свертки (см. уравнение (2)) не может быть правильной, и интерференционные вклады могут и должны быть велики. В частности, они велики при эффективном взаимодействии (1). По нашим оценкам, они могут объяснить от I/3 до I/2 EMC-эффекта. Это утверждение очень важно и показывает ограниченность всех наших попыток построить теорию глубоконеупругих процессов без построения настоящей микроскопической теории ядерных сил.



7. Я хотел бы закончить перечисление уроков ЕМС-эффекта на несколько более оптимистической ноте, а именно предложить некоторое конструктивное продвижение вперед. Это связано с идеей применить для построения теории ядерной материи правила сумм квантовой хромсдинамими. Такая попытка была предпринята Е.Г.Друкаревым и мной /5/, и она оказалось успешной в описании энергии связи, равновесной плотности и сжимаемости ядерной материи. Правила сумм КХД представляют собой метод, который прямым образом применяется к жестким процессам. Еолее того, он довольно успешно описывал основные свойства их для адронного мира /5/. Поэтому мы надеемся, что правила сумм КХД окажутся адекватным методом при построении теории жестких процессов на ядрах.

## Литература

- 1. Strikman M.I., Frankfurt L.L. Phys. Rep., 1985, v.76, p.3.
- Akulinichev S.V., Kulagin S.A., Vagradov G.M. Phys.Lett., 1985, v.138B, p.485.
- 3. Bodek A., Ritchia J.K. Phys.Rev., 1981, v.23D, p.1030.
- Birbrair B.L., Levin E.M., Shuvaev A.G. Preprints LMPI-1227 (1986), -1296(1987), -1349(1987).
- 5. Drukarev E.G., Levin B.M. Preprint LNPI-1347(1987).
- Ioffe B.L. Proc. of XXII Int.Conf. on High Energy Physics, 1984, v.II, p.176.

## QCD AND SHADOWING OF VALENCE AND SEA QUARKS IN DEEP INELASTIC LEPTON-NUCLEUS SCATTERING

L.L.Frankfurt, M.I.Strikman

Leningrad Nuclear Physics Institute, Gatchina, USSR

The basic aim of this talk is to estimate the magnitude of shadowing for sea and valence quark distributions in nuclei and to consider implications of the shadowing phenomenon for the EC effect at  $x \sim 0.1$ . We also briefly consider high  $Q^2$  lepton scattering off nuclei at x > 1 and the colour transparency effect in the large angle quasielastic hadron-nucleus scattering (for details see /1/).

The recent ETC experiments/2/ have confirmed old predictions of quantum field theory, parton model, and nonperturbative QCD (with account of the scaling violation) that nuclear shadowing is the leading twist effect (see /1/ for the list of referencies). The data are at variance with the model of Brodsky et al. and believes of many interpreters of the EEC effect that shadowing is the higher twist effect.

First, let us demonstrate that large longitudinal distances are essential in nuclear shadowing. In the nucleus rest frame the average longitudinal distances in the  $Y^{H}N$  amplitude can be determined from the analysis of the  $Y^{H}N$  scattering using equations derived by B.L. Inffe neglecting scaling violation:

$$\langle P|j_{\mu}(y)j_{\lambda}(0)|P\rangle = \left[P_{\mu}P_{\lambda}\frac{2^{2}}{2y_{\mu}^{2}} - P\sigma_{\overline{\rho}y_{\mu}}^{2}\left(\frac{2}{2y_{\mu}}P_{\lambda} + \frac{2}{2y_{\mu}}P_{\mu}\right) + \delta_{\mu\lambda}\right].$$
 (1)

· (P=3/2)2] · V2 (y2, Py)/i+...

where

$$V_2(0,py) = (2\pi m_N y_3)^{-1} \int_0^1 \frac{dx}{x} F_{2N}(x) \sin(m_N y_3 x)$$
 (2)

$$F_{2N}(x) = 4 \int_{1}^{\infty} d(m_N y_3) \, V_2(o, m_N y_3) \sin(m_N y_3 x) m_N y_3 x \,. \tag{3}$$

Applying eqs.(2),(3) for  $F_2(x) \sim (1-x)^3$  and  $F_2$  valence  $\sim F_2$  win -  $F_2 \sim x$  (1-x) we find

$$1(x) = \lambda(x)/n_{m}x. \tag{4}$$

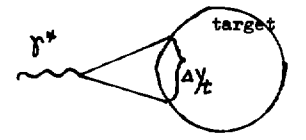
where

$$\lambda_{\text{sea}}(x) = \lambda_{\text{valence}}(x) \approx 1$$
 for  $x \le 0.5$   $\rightarrow 0$  for  $x \to 1$ . (5)

Consequently at not too large Q2 if

$$1(x)/2 > 2 R_A$$

where  $R_A$  is the nucleus radius,  $y^*$  transforms into a  $q\bar{q}$  pair (hadrons) before the nucleus.



The transverse size of  $q\bar{q}$ ,  $\Delta y_t$ , when it arrives at the target is

$$\Delta y_t \sim \frac{\kappa_t}{E_{q,(\bar{q})}} \cdot \frac{q_o}{Q^2}. \tag{6}$$

For jets aligned along \$\forall (Bjorken)

 $E_{\overline{q}} \gg E_{\overline{q}} \text{ (or } E_{\overline{q}} \gg E_{\overline{q}}) \sim (m_{\overline{q}}^2 + \kappa_{et}^2)/2m_{N} X$  and

$$\Delta y_t = \kappa_{ot} / (m_q^2 + \kappa_{ot}^2) \qquad (7)$$

lead  $^{\circ}$  to shadowing (k<sub>ot</sub>  $\sim$  0.35-0.4 GeV/c is the typical transverse momentum of a parton in the aligned jet).

For symmetric jets,

symmetric jets,
$$E_{1} \sim E_{1} \quad , \quad \Delta y_{t} \sim 1/\sqrt{Q^{2}} \tag{8}$$

and no significant shadowing is expected.

Accounting for these two components in the )\* wave function we obtain modified Gribov representation for  $\sigma_{\chi^{*}A}$  (x <<1/(4m\_NR\_A))(the main differencies from Bjorken, Zakharov and Mikolaev analyses are inclusion of unshadowed term (colour transparency of nuclei) and a more quantitative estimate of the shadowed term):

more quantitative estimate of the shadowed term):
$$\sigma_{F^*A} = \lambda A \sigma_{F^*N} + \frac{\omega}{3\pi} \int_{-\infty}^{M^2 \text{max}} \frac{R(M^2) M^2 dM^2}{(M^2 + P^2)^2}.$$
(9)
$$\cdot \left\{ \theta \left( M_0^2 - M^2 \right) + \theta \left( M^2 - M_0^2 \right) \frac{6 \kappa_0^2 t}{M^2} \right\}.$$

where  $M_{max}^2/Q^2 \sim 1/(4R_Am_N X)$ ,  $R(M^2) = \sigma(e^+e^- \rightarrow hadrons)/\sigma(e^+e^- \rightarrow M^*)$ . The factor  $6k_{ot}^2/M^2$  in eq.(9) is due to account of the small phase volume for the aligned jets  $\sim 4k_{ot}^2/M^2$  and due to alignment of  $q\bar{q}$  as a consequence of spin 1 of  $J^*$ —a factor 3/2. Finally we obtain  $A^{eff}/A = (4-\lambda) \sigma_A^*/A \sigma_{fN}^* + \lambda$ . (10)

where  $\lambda \approx 0.2$  is estimated from the application of eq.(9) to A=1. Note that  $\lambda (Q^2=0)\approx 0.2\pm 0.05$  (Really it is slightly larger since the Y-meson contribution is weakly shadowed).

Thus shadowing at  $Q^2 \sim \text{few GeV}^2$  and small x << 1/(4m<sub>N</sub>R<sub>A</sub>) should be close to one observed for the case of real photons. This is in a reasonable agreement with experimental data /2/ and really with the previous data (see /1/).

In QCD one has to take into account the gluon radiation. The aligned jet configuration with increase of  $Q^2$  transforms into configuration like

guration like

where gluon is predominantly emitted along q or  $\bar{q}$  momentum. Hence  $\Delta y_{t}(QOD \text{ aligned jet model}) \approx \Delta y_{t}(\text{aligned jet model})$ . The analysis of the QCD diagrams corresponding to the QCD aligned jet model contribution to the nuclear shadowing is given in /1/.

Thus in QCD shadowing is the leading twist effect (i)  $A_{eff}/A(w+\theta, Q^2=const)$  decreases, (ii) $A_{eff}/A(x=const, Q^2\to\infty)$ increases slowly, (iii) shadowing is present for events with high  $p_t$  jets (this effect is absent in the parton model).

The nuclear shadowing should be present for the valence distribution also, because the essential longitudinal distances in the valence and sea quark channels are similar (eq.(5)). Really the aligned jet contribution to  $V_A(x,Q^2)$  is more shadowed than for the  $\overline{q}_A$  case, since the nucleus center is black and gives negligible contribution to the difference  $\nabla_{W^+A} - \nabla_{W^-A}$  (nonvacuum reggeon exchange)

$$\frac{1}{A} \frac{V_A \text{ soft}}{V_N \text{ soft}} = \int T(b) \left(1 - \frac{1}{2} \sigma^{\text{aligned jet, N}} T(b)\right)^{A-1} d^2b \quad (11)$$

$$\approx 0.7 \quad A^{-0.33} \quad \text{for} \quad \sigma = 20 \text{ mb}$$

$$T(b) = \int P_A (\vec{b}, E) dE.$$

Thus 
$$\frac{1}{A} \frac{V_A}{V_N} = (1 - \lambda) V_A \int_{N}^{\infty} V_N + \lambda_V$$
 (12)   
  $\approx 0.6 |_{A=60} \Rightarrow 0.5 |_{A=200}$ .

Here  $\lambda_V$  characterizes contribution of nonaligned jets to  $V_N$ . From the QCD sum rule analysis of  $V_N(\mathbf{x},Q_o^2)$  made by Loffe and Kaidalov/3/we expect  $\lambda_V \leq 0.3$ .

The discussed analysis of  $A_{eff}/\Lambda$  can be extended to the region of small x:

$$\frac{A_{eff}(x,Q_{o}^{2})}{A} = \lambda + \frac{1}{A\sigma_{yyN}} \frac{A}{3\pi} \int_{0}^{\infty} \frac{R(M^{2}) M^{2} dM^{2}}{(M^{2} + Q^{2})^{2}}$$

$$\begin{cases} \theta(M_{o}^{2} - M^{2}) + \frac{6 \kappa_{o}^{2} t}{M^{2}} \theta(M^{2} - M_{o}^{2})^{2} & (A \sigma_{yy} - Re \frac{\sigma_{yy}^{2}}{2}) \\ \int d^{2}b dz_{1} dz_{2} f_{N}(b,z_{1}) f_{N}(b,z_{2}) \theta(z_{2} - z_{1}). \end{cases}$$

$$exp(-i (M^{2}/Q^{2} + 1) m_{N} \times (z_{1} - z_{2})) exp - \frac{1}{2} \sigma_{yy} \int_{0}^{\infty} f_{N}(b,z') dz'.$$
(13)

Similar expressions are valid for  $V_A/V_N$ . According to eq.(13) saturation of shadowing occurs at (see fig.1):

$$x_{\text{sat}} \sim 10^{-2} (12/A)^{\delta}$$
,  $\delta \approx 0.2$ . (14)

This  $x_{\text{sat}}$  is smaller and has weaker  $\Lambda$ -dependence than according to naive guesses. Eq.(13) is in a reasonable agreement with the R'C data /2/ (see fig.2, solid (dashed lines are calculations including shadowing for sea (sea and valence) quarks for  $\lambda_{\text{no}} = \lambda_{\text{release}} = 0.2$ ).

shadowing for sea (sea and valence) quarks for  $\lambda_{\text{sea}} = \lambda_{\text{valence}} = 0.2$ ). At  $x > (2-3) \cdot 10^{-2}$  behaviour of  $\overline{q}_A/\overline{q}_N$ ,  $V_A/V_N$  depends on the pattern of compensation of shadowing in the sum rules for the energy-momentum (Zakharov and Nikolaev)

$$\frac{1}{A}\int_{0}^{a}x_{A}\left[V_{A}(x,Q^{2})+2\bar{q}_{A}(x,Q^{2})+G_{A}(x,Q^{2})\right]dx_{A}-\int_{0}^{a}\left[A\to N\right]=0,\tag{15}$$

 $x_A = AQ^2/2 m_A q_0$ , and for the baryon number (Frankfurt and Strikman)  $\int_{0}^{A} (1/A) V_A(x_A, Q^2) dx_A - \int_{0}^{A} V_N(x, Q^2) dx = 0.$  (16)

Eq.(16) unambiguously leads to  $\xi_A(x,Q^2) \equiv \frac{1}{A} V_A(x,Q^2) / V_N(x,Q^2) > 1$  at  $0.05 \le x \le 0.15$ . In particular  $\xi_{Fe}(0.05 < x < 0.15) \sim 1.1$ . In combination with the BCDMS and new ECC data for  $F_{2A}/F_{2D}$  at  $x \sim 0.1$  this fact implies some suppression of  $\overline{q}_A$  (which is consistent with existing experimental data, see review /1/). In addition eq.(15) in this case leads to an overall enhancement of  $G_A$ . Indeed the data /2/combined with eq.(13) lead to

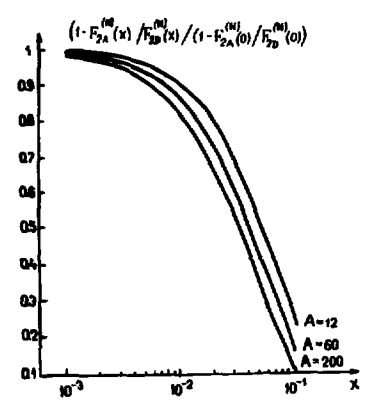
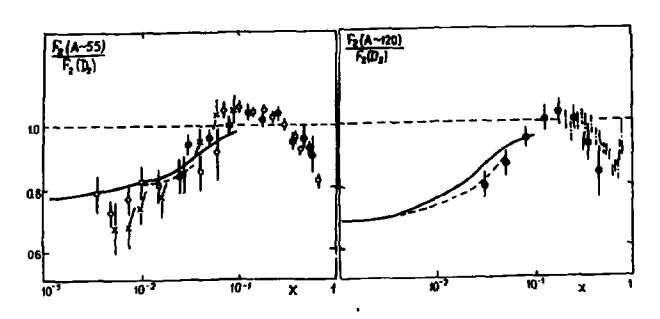


Fig. 1



F1g.2

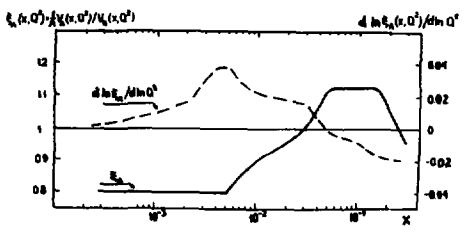


Fig.3

$$\lambda_6 = \int_{S_n}^{A} x_A \, G_{S_n}(x_A, Q^2) dx_A' \int_{Q}^{A} x \, G_N(x, Q^2) dx \approx 1.05$$

Note that in the Zakharov and Nikolaev scenario  $\lambda_{\rm G}$ =1 and 0.5F<sub>2A</sub>/F<sub>2N</sub> ~1.1 for A=118 at x~0.1 which is in variance with the data.

In the discussed Q<sup>2</sup> range scaling violation is a rather small effect (see,e.g. fig. 3) though we will consider it in the new analysis which is under way.

The simplest way to check our conclusions would be to measure the A-dependence of the charge asymmetry of the pion production in the current fragmentation region, i.e.

$$\sigma'(\uparrow^{+}A \rightarrow \not M + \pi^{+}+X) - \sigma(\not \mu + A \rightarrow \not \mu + \pi^{-}+X)\Big|_{X_{\overline{F}} > 0.2} \quad \checkmark \quad V_{A}(x,Q^{2}).$$

The FNAL experiment E-665 is well suitted for such measurements.

This iscussion has obvious implications for the EMC effect model builders: shadowing region backfires - convolution models are inapplicable for x < 0.2. Really a success of any model for x < 0.1 which does not reproduce shadowing as well is <u>really a failure</u>.

Let us discuss now the region of larger x. Skipping over the "dull" region of the E/C effect at  $x \sim 0.5$  we will consider the progress in the  $x \ge 1$  region.

Measurements of the (e,e') cross sections at  $x \geqslant 1$ ,  $q^2 \not \le 3$  GeV<sup>2</sup> were performed at SLAC. In the studied kinematics invariant mass of the produced hadron system is close to the threshold. Consequently, predominant process is production of nucleons and nuclear fragments — quark degrees of freedom are hardly excited. Thus at  $x \not = 1$  a dip is expected for the ratios like  $(A_1 > A_2)$ :

$$R(A_1, A_2, X, Q^2) = \frac{A_2}{A_4} \frac{F_{2A_1}(X, Q^2)}{F_{2A_2}(X, Q^2)} \approx \frac{\langle 1/K \rangle_{A_1}}{\langle 1/K \rangle_{A_2}}$$

A step for R is expected for  $2 \ge x \ge x_{\min}(Q^2)$ ,  $x_{\min}(Q^2 \approx 2.5 \text{ GeV}^2) \sim 1.4$ , due to dominance of pair nucleon correlations, e.g.  $R(A1,D,x>x_{\min}(Q^2)) \approx 5 \pm 1$ . Both these features are in line with the data for the Al/D and Pe/<sup>4</sup>He ratios (see /1/).

Analysic of (e,e') reactions at x >1 indicates that in heavy nuclei probability of short-range correlations is about 30%, which matches well with quenching measured for small momenta (~70% nucleons are below the Fermi surface) (see B.Frois'talk).

A new evidence in favour of large pair nucleon correlations in We was presented in the J.Guy talk who reported the results of the BEBC analysis of the reaction (-) + Ne  $\rightarrow$   $\mu$  + fast backward proton +  $\mathbf{I}$ . For events where cascade contribution was small a correlation between  $\mathbf{x}_{Bj}$  and  $\mathbf{c}$  - the light-cone fraction for a fast backward (cumulative) nucleon, was observed consistent with 1977 prediction of the pair nucleon correlation model /4/. For a comparison, similar reaction with deuteron target was studied. For large  $\mathbf{c}$  the observed decrease of  $(\mathbf{x})$  seems to be somewhat larger than the  $(\mathbf{x})$  =  $(\mathbf{x})$  decrease expected in the two nucleon approximation for the deuteron wave function. Qualitatively this pattern is consistent with prediction /1/ of the minidelocalization model of the EMC effect (suppression of point-like configurations in bound nucleons).

To measure quark distributions in nuclei at x > 1 measurements of  $F_{2A}(x,q^2 \ge 10 \text{ GeV}^2)$  are necessary (for  $A \ge 4$ ) /1/. The few nucleon correlation (FNC) model relates the slopes of  $\mathcal{A}$ -(or  $x_p$ ) distributions at  $\mathcal{A} > 1$  for production of fast backward particles "c"

$$\angle \frac{d}{dd} = \frac{d}{dd} = \left| \frac{d}{dd} - \frac{d}{dd} \right|_{d>1}$$

For  $b_p = 7$  it leads to  $b_m = 9$  which is consistent with the recent high energy data reported in the 20lin talk. For the quark distributions at x > 1 the FNC model without EMC effect leads to  $b_m = b_q$  similar to the prediction of the flucton model and the Baldin model. The pion model of the EMC effect leads to a small increase of  $b_q : b_m = b_m$ ). At the same time the suppression of the point-like configurations leads to a significant increase of the slope

 $b_q \approx 11-14$  (without change of  $b_{\chi}$ ). (Note that really the shape of the x-distribution is not purely exponential(see /1/). Thus we conclude that  $q_A(x \geqslant 1, Q^2)$  is very sensitive to the model of the EMC effect.

In the beginning of the talk we discussed that QCD predicts presence of point-like configurations in the  $Y^{\infty}$  hadron wave function. The question arises whether similar configurations are present in the quark-quon wave functions of hadrons. This property is important for interpretation of many phenomena and in particular of the EMC effect at  $x \sim 0.5$ . A perspective method to search for these configurations and for study of the microscopic nuclear structure is the investigation of the selour transparency of nuclei in large angle quasielastic reactions  $h+A \rightarrow h' + N + A'$  (see /5/).

#### References

- 1. Frankfurt L.L., Strikman M.I., Physics Rep., 1988, v. 160, p. 235.
- 2. Sloan T., Preprint CERN-EP/87-188.
- 3. Ioffe B.L., Kaidelov A.I., Phys.Lett., 1985, v.B150, p.374.
- 4. Frankfurt L.L., Strikman M.I., Phys.Lett., 1977, v. B69, p. 93.
- Farrar G.R., Liu H., Frankfurt L.L., Strikman M.I., Preprint Rutgers Univ. 88-03, 88-04, Physical Review Letters in press.

#### QUARK CLUSTER MODEL - COMPARISONS WITH RECENT DATA

James P. Vary, Avaroth Harindranath and Granddon Yen Physics Department, The Ohio State University Columbus, Ohio 43210 and

Physics Department, Iowa State University Ames, Iowa 50011, USA

H. J. Pirner

Institut für Theoretische Physik Universität Heidelberg, D-6900 Heidelberg Federal Republic of Germany

This paper reviews the quark cluster model (QCM) with emphasis on detailed comparisons with deuterium data. A critical review of the phenomenon of y scaling for these same data is presented.

#### 1. INTRODUCTION

In this review we focus on the application of the quark cluster model (QCM) to deep inelastic (DIS) lepton-deuteron scattering data. Since the same data we address within QCM has been the subject of a y scaling analysis we begin with a critical review of that particular phenomena and show that w scaling is not readily evident in the deuterium DIS data.

#### 2. CRITICAL REVIEW OF Y SCALING FOR DEUTERIUM DATA

Ever since West and Kawasoe et al. proposed1 the idea of y scaling (scaling of the inelastic lepton-nucleus scattering cross section based on quasi-clastic nucleon knock-out) there have been several experimental and theoretical attempts to understand this phenomenon. These attempts generally fall into four catagories: 1) extracting a universal scaling function F(y) and thereby trying to put stringent limits on the modification of nucleon properties in the nuclear medium?; 2) estimating the effect of final state interactions<sup>3</sup>; 3) elucidating the ambiguities in the possible choices of both the scaling variable y and the scaling function, and 4) estimating the validity of various approximations used in the derivation of y.4,5

We choose <sup>2</sup>H for a critical review of y scaling because: 1) the Deuteron (D) is the simplest of nuclei with the lowest binding energy per particle and the lowest average density. Hence our approximation of neglecting final state interactions should be more accurate. 2) D is the nucleus for which (e, e') absolute cross section datas are available over the widest kinematic range.

According to the y scaling hypothesis, in the plane wave impulse approximation the differential cross section for lepton-nucleus quasi-clastic scattering can be written as

$$\frac{d^2\sigma}{d\Omega dE'} = (Z\sigma_p + N\sigma_n)\frac{2\pi m}{|\mathbf{q}|}F(y,Q^2).$$

In this expression E' is the final lab energy of the electron, Z(N) is the proton (neutron) number of the target nucleus,  $\sigma_p$  ( $\sigma_n$ ) is the elastic electron-proton (neutron) cross section, m is the nucleon mass,  $\mathbf{q}$  is the laboratory three-vector component of the four-momentum transfer of the virtual photon and  $Q^2$  is the negative of the invariant four-momentum transfer squared. The elastic electron-nucleon cross section is given by

$$\sigma_{N} = \sigma_{Mod} [-\frac{q^{2}}{|\mathbf{q}|^{2}}G_{E}^{2} + (-\frac{1}{2}\frac{q^{2}}{|\mathbf{q}|^{2}} + tan^{2}\frac{\theta}{2})\frac{Q^{2}}{2m^{2}}G_{M}^{2}] \ .$$

It is important to note that the above expression results irrespective of whether one uses relativistic or nonrelativistic kinematics in the overall energy conserving delta function. On this point we agree with the authors of Refs. 5.7.8 and not with authors of Ref. 9.

With the conservation of relativistic energy the scaling variable y is given by y = -b + a with

$$b = \frac{|\mathbf{q}|}{2} [1 + \frac{(M_{A-1})^2 - m^2}{\Lambda^2}] ,$$

$$a = \frac{\nu + M_T}{2} [(1 - \frac{(M_{A-1} + m)^2}{12})(1 - \frac{(M_{A-1} - m)^2}{12})]^{\frac{1}{2}} .$$

where  $\Lambda^2 = (\nu + M_T)^3 - |\mathbf{q}|^2$  and  $M_{A-1} = M_T - m + \epsilon$ . Here  $M_T$  is the mass of the target and  $\epsilon$  is the binding energy.

The key issue of y scaling is whether the data indicate that  $F(y,Q^2)$  is independent of  $Q^2$ . In the impulse appoximation the scaling function F(y) is directly related to the nucleon momentum distribution function. Thus, if the experimental data exhibit y scaling we have a model-independent determination of the nucleon momentum distribution in the nucleus. Of course there is still a possible conspiracy that neglected effects cancel but more exclusive experiments could eventually test this. In fact a recent report<sup>10</sup> on (e,e'p) measurements with <sup>3</sup>He targets indicates the invalidity of the y scaling interpretation of the inclusive data. The main point of our presentation here is to exhibit the lack of y scaling in the inclusive D data.

In order to extract the function  $F(y,Q^2)$  we have to make a choice of nucleon form factors. We choose the parametrisations of Ref. 11. We have checked that alternative widely used parametrisations do not change our conclusions qualitatively.

We consider results from two experiments<sup>6</sup>. The data group into 11 sets characterized by  $Q^2 \simeq 0.8$ , 1.0, 1.5, 1.75, 2.0, 2.5, 3, 4, 6, 8, and 10 (GeV/c)<sup>2</sup>. In order to have a smooth representation of the  $y \leq 0$  data we fit to a functional form of a Gaussian centered at y=0 plus two exponentials. The form  $F(y,Q^2)=a\ e^{-bx^2}+c\ e^{dy}+f\ e^{gy}$  employs  $Q^2$  dependent coefficients. Without  $Q^2$  dependence the best fit gives  $\chi^2/d.o.f=15$ . With the restriction that the  $Q^3$  dependence of the coefficients be of polynomial form with terms  $Q^{-4}$ ,  $Q^{-2}$ ,  $Q^3$ , and  $Q^4$  and the restriction of only 10 parameters for the  $Q^3$  dependence, a best fit  $(\chi^2/d.o.f=1.26)$  was obtained which we refer to as Fit A.

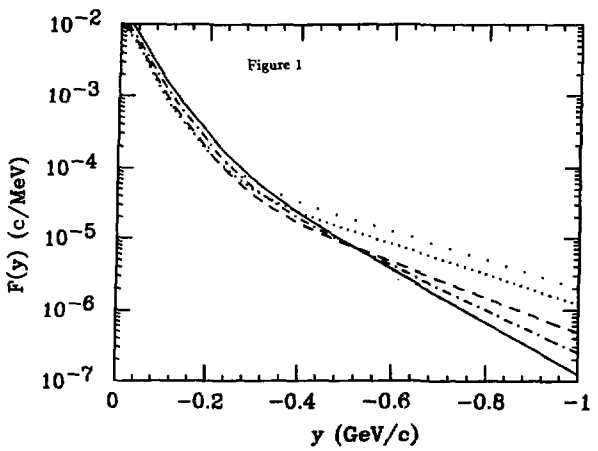


Fig.1. Fit A results for  $F(y,Q^2)$  plotted versus y for the range  $0. \le y \le -1$ .  $Q^2(GeV/c)^2 = 1.75$  (rare dots), 2.5 (dense dots), 4.0 (dashes), 6.0 (dot-dashes), and 8.0 (solid).

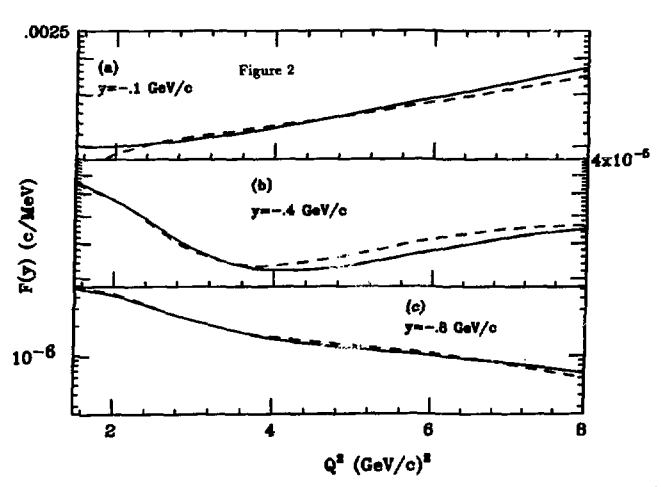


Fig.2.  $F(y,Q^2)$  versus  $Q^2$  for three different values of y . Fit A is the solid line and Fit B is the dashed line.

With the same functional dependence a separate fit (Fit B) to the 8 data sets omitting the  $Q^2$ =0.8, 1.0, and 10.0  $GeV^2/c^2$  sets yielded  $\chi^2/d.o.f = 1.17$ . The differences between Fit A and Fit B in the range  $1.5 \le Q^2 \le 8GeV^2/c^2$  can be interpreted as an indication of the uncertainty in the  $Q^2$  dependence of  $F(y,Q^2)$  dictated by the deuteron data.

Since inelastic contributions play a major role in the high energy side of the quasi elastic peak (positive y), we consider only the negative y region. The results of Fit A for  $F(y,Q^2)$  are plotted versus y in Fig. 1 for certain  $Q^2$  values in the range  $1.75 \le Q^2 \le 8GeV^2/c^2$ . We find systematic scaling violations for the entire range of y. In Fig. 2 we plot  $F(y,Q^2)$  from both fits versus  $Q^2$  for three different values of y.

For each value of y a different pattern emerges. We observe that at any value of  $Q^2$  the data do not indicate approach to scaling in the variable y. For y = -.1 GeV/c,  $F(y, Q^2)$  rises continuously with  $Q^2$ , while for y = -.4 GeV/c it exhibits a minimum at  $Q^2 \simeq 4$  (GeV/c)<sup>2</sup> and for y = -.8 GeV/c it falls uniformly over this range of  $Q^2$ . Further explanations of these features and the differences between our conclusions and the works of other authors can be found in Ref. 12.

Having now shown that the deuteron data do not exhibit y scaling we turn to the QCM explanation of this data. It should be clear that only one component of the QCM exhibits y scaling - the quasi elastic component.

## 3. MODEL ASSUMPTIONS

The quark cluster model (QCM) was proposed<sup>13-17</sup> to explain the deep inelastic electron-<sup>3</sup>He scattering (DIS) results from SLAC<sup>18</sup>. In the QCM for any application one assumes the nucleus at all times is organised into color singlet clusters. We label the clusters by their leading Fock space component in the infinite momentum frame as three-quark (3-q), six-quark (6-q) etc. clusters. Larger clusters are assumed to form by the overlap of smaller clusters. Specifically a 3-q cluster is assumed to have a critical radius,  $R_c$  such that clusters of 6, 9, etc., quarks are defined by the number of 3-q clusters joined by center of mass separations  $d \le 2 R_c$ . The overlap probabilities, and coordinate and momentum space probability distributions for these clusters are obtained in the rest frame from conventional nuclear wavefunctions.

Since we view the QCM as a model which allows us to write down the quark distributions in nuclei we expect it will be ultimately superceded by direct calculations within non- perturbative QCD. In the meantime we expect the QCM to form a basis for the uniform interpretation of a variety of high energy lepton-nucleus and hadron-nucleus interactions. In this context we are able to summarise all our efforts to date with the claim that all the data we have examined are consistent with  $R_{\rm c}=0.50\pm0.05$  fm which is the same value determined by the initial fits 13 to DIS data on  $^3$ He.

Recent improvements and applications of the QCM include application to the elastic form factor of nuclei<sup>18</sup>, precision analysis of quark cluster probabilities<sup>20</sup>, application of the QCM to the nuclear Drell- Yan process<sup>21</sup>, and to electroproduction of hadrons from nuclei<sup>22</sup>.

To apply the QCM to DIS we make two additional assumptions. First, as is customary in parton phenomenology, we assume that the participating quark (or antiquark) is quasifree. That is, we ignore initial and final state interactions. Second, since the cluster from which the participating quark originates is, by the definition of cluster configurations, spatially isolated from the remaining clusters, we assume the cluster is also quasifree. Consistent with this second assumption we assign to an i-quark cluster a mass equal to  $\frac{i}{3}$  times the nucleon mass. This last assumption is also equivalent to neglecting quark exchange processes between clusters. Encouraging support for this approximation is obtained from the demonstration by Frankfurt and Strikman<sup>23</sup> that the leading exchange graph correction to a 3-q cluster contribution to the European Muon Collaboration (EMC) effect<sup>24</sup> virtually disappears for x > 0.3.

## 4. APPLICATION OF THE QCM TO DIS DATA FROM DEUTERIUM

Since the key assumptions and development of QCM have been extensively reviewed in the literature<sup>13-17,18-33,35</sup> we will only describe here the results obtained to compare with the SLAC data.

In the QCM the total inelastic structure function can be written as the sum of the inelastic and quasielastic contributions from each of the i = 3,6,9, etc. quark clusters:

$$\nu W_2^{tot} = \Sigma_i \tilde{p}_i [\nu W_2^{inel}(i) + \nu W_2^{q-el}(i)]$$
.

where  $\hat{p}_i$  is the probability a quark chosen at random appears in the i-quark cluster. For deuterium

$$\nu W_2^{\text{tot}}(D) = \hat{p}_3[\nu W_2^{\text{inel}}(3) + \nu W_2^{\text{q-al}}(3)] + \hat{p}_0 W_2^{\text{inel}}(6)$$
.

Corrections to the model include interference effects which were discussed above and contributions of final state interactions (FSI's) which we neglect for the present.

The method of calculating  $\nu W_3^{ind}(3)$  follows the work of Ref. 27 and employs the inelastic structure function of the proton measured in the same E133 experiment. The quasielastic contribution is a conventional calculation of the (e,e'p) cross section in the plane wave impulse approximation ( with integration over the unobserved nucleon's final state.) Such a calculation of  $\nu W_3^{n-d}$  exhibits pure y-scaling.

Due to the constraints of a conference presentation we present only a small sample of our results using the Reid Soft Core<sup>26</sup> (RSC) deuteron wavefunction. In this case<sup>20</sup>  $\tilde{p}_3 = 0.953$ ,  $\tilde{p}_3 = 0.047$  when  $R_c = 0.50 Fm$ . The results at  $Q^3 = 2.5 (GeV/c)^3$  are presented in Fig. 3 and the results at  $Q^2 = 10.0 (GeV/c)^3$  are presented in Fig. 4 and are compared with E133 data from SLAC<sup>3</sup>. A very high quality description of the data is found over a large range range in  $Q^2$  and z. Since we have neglected FSI's we are not so concerned with the small but systematic deviations between the QCM and the data at the lower  $Q^3$ . With increasing  $Q^3$  the three quark inelastic component becomes comparable to the quasiclastic contribution. At high z the six quark cluster dominates the three quark cluster. Since these inelastic contributions scale with z they are the source of breakdown in y scaling at these kinematics. A more complete presentation of the QCM's description of the DIS deuterium data will be forthcoming.<sup>20</sup>.

## ACKNOWLEDGMENTS

We acknowledge useful conversations and communications with R. Arnold, P. Bosted, M. Butler,

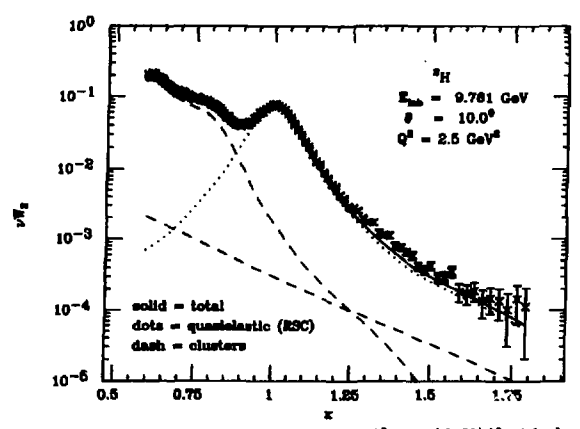


Fig.3. Comparison of SLAC E133 deuterium data near  $Q^2 = 2.5(GeV/c)^2$  with the QCM results obtained using the Reid Soft Core wavefunction. The dashed curve which dominates at  $x \le 1$  is the 3-q inelastic contribution.

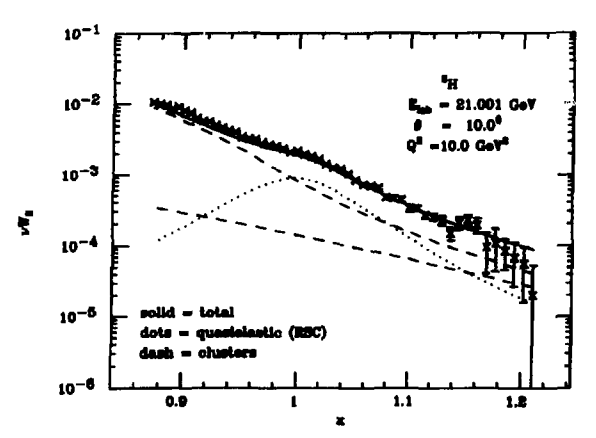


Fig.4. Same as Fig. 3 but near  $Q^2 = 10.0(GeV/c)^2$ .

S. Koonin and S. Rock. This work is supported in part by the U. S. D. O. E. under contract No. DE-FG02-87ER40371, Division of High Energy and Nuclear Physics.

#### REFERENCES

- G. B. West, Phys. Rep. 18C, 264 (1975); Y. Kawazoe, G. Takeda, and M. Matsuzaki, Prog. Theor. Phys. 54, 1394 (1975).
- 2. I. Sick, Phys. Lett. 157B, 13 (1985); R. D. Mckeown, Phys. Rev. Lett. 56, 1452 (1986).
- M. N. Butler and S. E. Koonin, Phys. Lett. B205, 123 (1988); W. Leiderman and H. Arenhovel referenced in C. Ciofi degli Atti, E. Pace, and G. Salme, Phys. Rev. C 36, 1208 (1987).
- 4. S. A. Gurvitz, S. J. Wallace, and J. Tjon, Phys. Rev. C 34, 648 (1986).
- 5. C. Ciofi degli Atti, Nucl. Phys. A463, 127c (1987).
- W. Schutz et al., Phys. Rev. Lett. 38, 259 (1977); S. Rock et al., Phys. Rev. Lett. 49, 1139 (1982); S. Rock, to be submitted to Physical Review.
- 7. J. M. Finn, R. W. Lourie, and B. H. Cottmann, Phys. Rev. C29, 2230 (1984).
- M. N. Butler (private communication); Also M. N. Butler and R. D. McKeown, Phys. Lett. B208, 171 (1988).
- P. Bosted, R. G. Arnold, S. E. Rock, and Z. Szalata, Phys. Rev. Lett. 49, 1380 (1982).
- 10. C. Marchand et al., Phys. Rev. Lett. 60, 1703 (1988).
- M. Gari and W. Krumpelman, Z. Phys. A322, 689 (1985); Phys. Lett. B173, 10 (1986).
- 12. G. Yen, A. Harindranath, J. P. Vary, and H. J. Pirner, to be published.
- 13. H. J. Pirner and J. P. Vary, Phys. Rev. Lett. 46, 1376 (1981).
- J. P. Vary, Nucl. Phys. A418,195c (1984); J. P. Vary, in Hadron Substructure in Nuclear Physics, W. -Y. Hwang and M. H. Macfarlane, eds., AIP Conf. Proc. No. 110 (New York) 1984.
- 15. H. J. Pirner, International Rev. of Nucl. Phys., Vol. II (Singapore) 1984.
- J. P. Vary and H. J. Pirner, Recent Progress in Many-Body Theories, eds.H. Kummel and M. L. Rustig (Springer-Verlag, Heidelberg, 1984) Lecture Notes in Physics 198, p. 1.
- J. P. Vary, Proceedings of the VII International Seminar on High Energy Physics Problems, Multiquark Interactions, and Quantum Chromodynamics, Dubna, 1984.
- 18. D. Dav et al., Phys. Rev. Lett. 43,1143 (1979).

- J. P. Vary, S. A. Coon, H. J. Pirner, in Few Body Problems in Physics, Vol. II, ed.
   B. Zeitnitz (North-Holland, Amsterdam, 1984), p. 683; Proc. of Int. Conf. on Nuclear Physics, ed. R. A. Ricci and P. Blasi (Tipografia Compositori, Bologna, 1983), p. 320; Hadronic Probes and Nuclear Interactions (Arizona State University) Proceedings of the Conference on Hadronic Probes and Nuclear Structure, AIP Conf. Proc. No. 133, ed. J. R. Comfort, W. R. Gibbs and B. G. Ritchie (AIP, New York, 1985).
- For a review of these overlap probabilities and the method of extrapolation to heavier nuclei, see M. Sato, S. A. Coon, H. J. Pirner and J. P. Vary, Phys. Rev. C33, 1062 (1986).
- 21. A. Harindranath and J. P. Vary, Phys. Rev. D34 3378 (1986).
- 22. A. Harindranath, K. E. Lassila, and J. P. Vary, Phys. Rev. D36, 299 (1987).
- L. L. Frankfurt and M. I. Strikman, Proceedings of the VII International Seminar on High Energy Physics Problems, Dubna, 1984 Phys. Rep. 160, 235 (1988).
- 24. J. J. Aubert et al., Phys. Lett. 123B,123 (1983).
- J. P. Vary and A. Harindranath, Proceedings of the VIII International Seminar on High Energy Physics Problems, Vol. II, Dubna D1, 2, 86-668, (1986) p.27.
- R. V. Reid, Ann. Phys. (N.Y) 50, 411 (1968).
- 27. D. Kusno and M. J. Moravscik, Phys. Rev. D20, 2734 (1979).
- 28. G. Yen, A. Harindranath, J. P. Vary, and H. J. Pirner, to be published.

## жесткие процессы на ядрах н.п. Зотов

Научно-исследовательский институт ядерной физики МГУ, Москва В.А. Салеев

# Куйбышевский государственный университет В.А. Царев

Физический институт им. П.Н. Лебедева АН СССР. Москва

## 1. Структурные функции ипер и флуктонная молель с рескейлингом

Идея о том, что структурные функции (СФ) ядер определяют физику глуфоконеуптутих и кумулятивных процессов 1,2, оказалась весьма плодотворной 3-5. Конкретная реализация этой идея на основе флуктонной моделя с рескейлингом (ФМР) 6 позволила успешно описать всю существующую совокупность экспериментальных данных по глуфоконеупругому рассению лептонов на ядрах 7 и предсказать ядерные эффекты для других дестких процессов 3.

Напомиям, что в  $^{6,7}$  со ядра выражается через со  $^{6,7}$  них флуктовов  $^{8}$ :

$$F_2^A(x,Q^2) = \sum_{k=1}^A P(k,A) F_{2,K}^A(x',Q^2),$$
 (I)

где  $x'=x/\kappa$ , а  $P(\kappa,A)$  - среднее часло  $\kappa$ -нуклонных флуктонов в ядре A, зависящее от плотности ядра и параметра  $\varepsilon$ -"раднуса когерентности." Кроме того, в модели учитывается "деформация" партонных распределений в связанных нуклонах согласно гапотеве рескейлинга $^{(9)}$ :

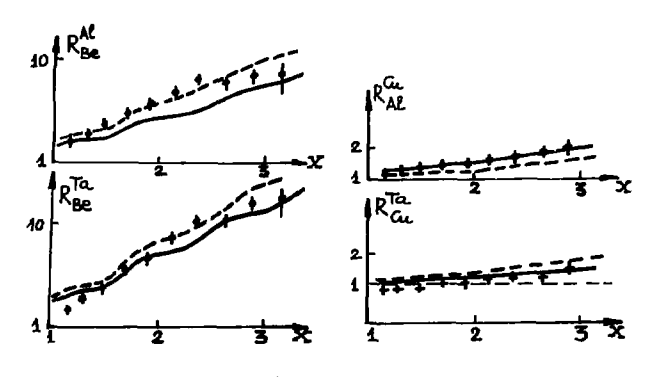
$$Q_N^A(x,Q^2) = Q_N(x, \xi_A(Q^2) \cdot Q^2). \tag{2}$$

Целью настоящего доклада является: (I) — привести новые аргументи в пользу указанного подхода, которые следуют из анализа процессов рождения  $\mathcal{F}^{+}$ —мезонов в кумулитивной области и лептонных пар на ядрах, и (2) — дать предсказания для процессов лептон-ядерных взаимодействий.

## 2. Рожиение 5 метонов в култиническ области

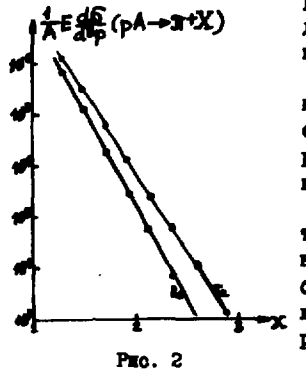
Сравним поведение СФ ядар, полученных в  $\Phi M^{6,7/}$ , с экспериментальным данным группы ИТЭФ  $^{10/}$  для выхода красилтивных  $\mathcal{F}^+$ -мезонов в широкой области  $1 \leq X \leq 3$  на развим дирах  $^{11/}$ . Параметры модали  $(C_c, S_A)$  фиксировани из сравнении с данными по глуфовоннупругому рассемии дептонов на драх  $^{7/}$ . Номым по сравнению  $c^{7/}$  изадетом динь учет больного члола флуктонов  $(\kappa=8)$  в СФ ядер.

На рис. I показано сравнение отномения СФ ядер, вичисленных в  $\Phi$ МР с данным TQ для отномений сечений рождения  $Q^{-1}$ —месонов в  $\rho A$ 



Pmc. I

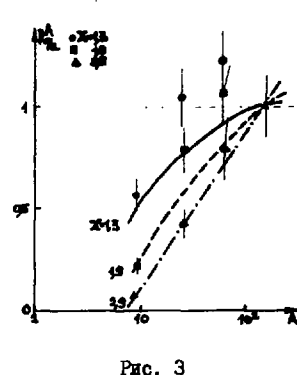
ванию действиях (A=Se, Al, Ce, To) при  $E_{\rho}$ =10, I ТэВ и  $Q_{\phi}$ =1190 в A.с. в зависимости от X /II/. Силонная и пунктирная кривые соответствуют распределению ддерной плотности по формуле Вудса-Саксона и приближению постоянной плотности, когда  $P(\kappa, A) \simeq C_{\kappa}^{A} (V_{\epsilon}/V)^{\kappa-1} \simeq A$  /8/. Теоретические кривые для отношений сФ ядер полносты передают смотрый рост отношений сечений рождения кумулятивных  $\mathcal{F}^{I}$ —мезонов, подтверждая гипотезу предельной фрагментации  $I_{\epsilon}^{I}$ , согласно которой эти сечения в области фрагментации ддра пропорциональны его квири-партонной СФ, зависимей от вментации ддра пременной X. Из рис. I также видно, что теоретические предсказания сильно зависит от предлежения о распределения плотности пунксков в ядре. Можно думить, что более



реалистические распредалении повъслят добиться лучшего согласии расчетов с экопериментом.

В рамках гипотези предельной фрагментации ФИР хорово описност такие и саму форму опектров, как это видко из рис. 2, на котором показами теоретические криме  $F = \frac{1}{2} \left( (\rho A \rightarrow \mathcal{T}^+ X) \sim \times f u_A(\kappa, q^2)^{-2} S_A(\kappa, q^2) \right)$  для ядра тептала (хримен нормирована в точие X = 1,3 на экспериментальные дляние) и для ядра беридии (без какой-мибо дополнительной нормировам). Модель такие правильно передвет A—вамисимость отношения виходов

Эт меновов на разных ядрах к ядру тантала при фиксированных  $X^{/{
m IO}/}$ . Причем теоретическое описание удучшается с ростом масштабноzпеременной 🗶 (рис. 3).



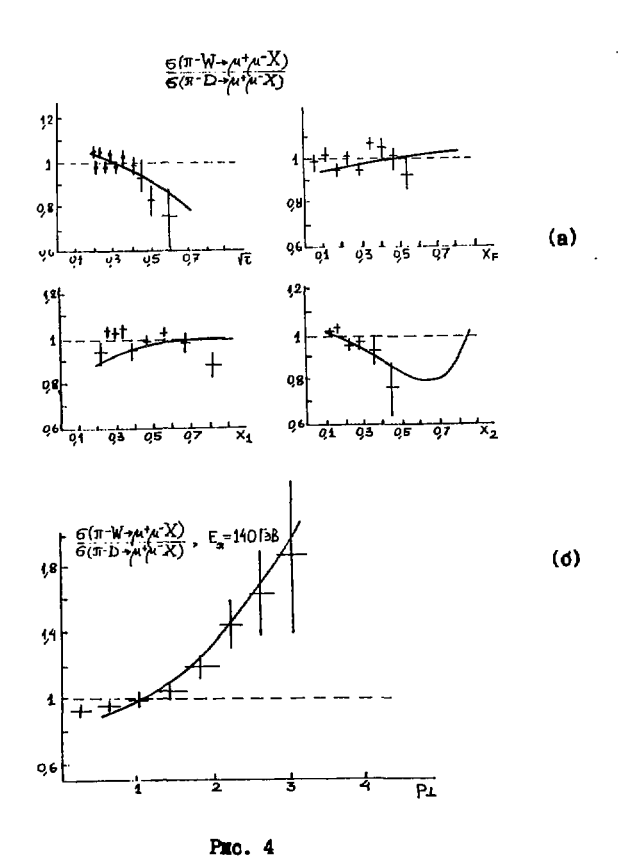
В простейшем варшанте ФМР даже при учете больного числа флуктонов (K =8) IDEECKASMBASTCE ISDEETSDEOS "ОСПЕДЛЯРУщее" ПОВедение отношения сечений, которое, по нашему мнению, не противоречит существущим данным. Не ясно, является ин этот эффект реальным. Если дальнейше экспериментальные моследования подтвердят его пресутствие, это будет сильным аргументом в пользу флуктонной модели. Однако его отсутствие не является аргументом против флуктонов, поскольку "осциллящий" могут "сглаживаться" в результате различних не учтенных эффектов (ферми-движение

флуктонов, размитие их крал и т.п.).

## 3. Якерные эффекты в пропессах рожжения дептонных пар

Как было показано в /3,6/, различие ОБ ядер и свободных нуклонов MONTHO INTERCENTS & CYMCCTRCHIRM SOTONTOM M B HOYFUX MOOTHUX INDOUGCсах на яврах. В частности, в пропоссах рожнения лептонных пар были предсказани /6/ ядерние эффекти, аналогичные ЕМС-эффекту.

Недавно коллафорацией **NA** IO было проведено экспериментальное ECCHEROBANEO RESPHEN SOCIENTOS S IIPONSCORY DORIGHER REIITONHENY IIAD HA якрах вольфрама и дейтерии 💯 -мезонами с энергией 140 и 286 ГвВ / 12/. Сравним результати нашех расчетов с этими ланными. Поскольку в экспервыенте NA 10 изучалась область х₂ €0,5, то влиянием флуктонов и ферми-движения на квариовые распределения в ядре можно было бы пренебречь. Однако представляют интерес предскавания для сечений рожителя допромения пар и их отношений в болое информационального области по Х<sub>2</sub> . Поэтому расчети проводились в ФМР/7/. Для ядра вольфрама параметр рескейлинга, входиций в (2), равен ≽ ≈2,3, а P(2, A)/A = 0, 1 (фирктоны о большим члоком нужнонов при этом не учитывались). Кинемитические условия экоперимента МА 10 соответствуют CROMPUMEM SHAVEHERM DEPENDENCE /12/:  $\sqrt{\tau_{min}^{H}} \simeq 0.27$ ,  $\sqrt{\tau_{max}^{H}} \simeq 0.65$ и Х₂≥ 0. На рис. 4а показано сращение результатов расчета для OTHOMORER S(N)/S(N) C MARKENNE /12/ MAR OTHOMORER S(N)/S(D) .



Видио, что эконориментальные данные, по существу, подтвердили величену ядерного эффекту (аналогичного БиС-эффекту) по переменной  $X_2$ , предопаванную в  $^{6}$ .

## 4. Расправаление дептониях пар по поперачному инпуньсу

Распределения по понеречному импульсу лептонных пар, рожденных в адром-ждериних веанмодействиях, заслуживают отдельного рассмотрении. Они требуют учета митили перерассенний кварков налотациюго адрона на кумионах жара /13/. Сечение процесса  $hA \to \mu^+\mu^- X$  в первом порядке теории возмущений КХД с учетом внутреннего поперечного импульса партонов из взаимодействущего адрона можно представить в следующем виде  $^{/14}$ :

$$\frac{d6}{dMdyd^2p_2} = \frac{d6^{2N}}{dMdy} \varphi_h^A(p_2) + \int d^2k_1 \frac{d6^{QCD}}{dMdyd^2p_2} \left\{ \varphi_h^A(\vec{p}_2 - \vec{k}_1) - \varphi_h^A(\vec{p}_2) \right\},\tag{3}$$

где сечения  $d6^{DV}/dM dy$  и  $d6^{DD}/dM dy d^2 p_1$  вычисляются через функции распремения партонов данного типа в ядре.

функции распределения партонов данного типа в ядре. /15/ и согласно в соответствии с аддитивной кварковой моделью /15/ и согласно процедуре учета многокварковых перерасселний /16,17/распределение кварков в адроне h по затравочному коперечному импульоу при расселнии на нуклонах ядра можно представить в виде:

$$\varphi_{A}^{A}(\vec{p}_{L}) = \sum_{n=0}^{\infty} N_{n} \varphi_{n}^{(n)}(\vec{p}_{L}), \quad \sum_{n} N_{n} = 1$$
 (4)

Здесь  $N_h$  — вероятность n перерассаний кварка из налетаннего адрона внутри ядра перед его аниппляцией. В приближении постоянной ядерной плотности  $\bar{\rho}_a = A/\frac{4}{3}\pi R_A^3$  для  $N_h$  можно получить простое выражение:

$$N_{n} = \frac{(-1)^{n}}{n!} \frac{d^{n}}{dg^{n}} N_{0}(2), N_{0}(2) = \frac{3}{2^{2}} \left[ \frac{1}{2} 2^{2} + (2-1)e^{-2} - 1 \right], \tag{5}$$

где  $\varrho = 2 \tilde{\rho}_A G_{AN}$  , а  $G_{AN} \simeq G_{NN}/3$  (  $G_{NN}$  — сечение неупритого NN — възыважения).

Распределение валентных кварков из налетаищего адрона по поперечному выпульсу после перерассенный можно записать в виде:

$$\varphi_{k}^{(n)}(\vec{p}_{1}) = \int d^{2}q_{1} \int d^{2}k_{1} \, \delta(\vec{p}_{1} - \vec{k}_{1} - \vec{q}_{1}) \, \varphi_{k}^{N}(\vec{k}_{1}) \, f_{qN}^{(n)}(\vec{q}_{1}) \, .$$

$$(6)$$

Здесь  $f_{qN}^{(n)}(\vec{q}_L)$  — опентри квари-нувлонного рассения после n взавмодействий:  $f_{qN}^{(n)}(\vec{q}_L) = f_{qN} = \frac{1}{6_{qN}} \frac{dS}{d^2q_L}(qN \to qX) =$ 

$$=(B_{q,N}^2/2\pi)e^{-B_{q,N}}q_1$$
 , где, согласно /18/,  $B_{q,N}\simeq B_{NN}=4,6$  /5 $B^{-4}$  , а  $(P_N^N(K_L)=(A^2/2\pi)e^{-AK_L}$  — распределение изарков в адроне  $k$  по "затравочному" поперечному импульсу при рассечнии на овободном нуклюне. Таким образом, перерассемиие изарков опредължется двуми параметреми:  $S_{q,N}$  и  $A$ .

Результати расчетов показывают, что отношение

$$R(p_1) = \frac{dS(\pi - W \rightarrow \mu + \mu - X)/dM dy dp_1^2}{dS(\pi - W \rightarrow \mu + \mu - X)/dM dy dp_1^2}$$
(7)

практически не зависет от у и  $M^2$  . Поэтому его можно сравнить с отновнием  $\lim_{n\to\infty} (P_L) = \lim_{n\to\infty} (P_L - \mu + \mu^- X) / 2$ 

 $\frac{dG}{d\rho_{\perp}^{2}}$  ( $\sigma$ -D- $\mu$ - $\mu$ -N), которое проинтегрировано по M и g /12/. На рис. 46 показани результати расчета отношения  $R(\rho_{\perp})$  для  $E_{g}$ =140 ГэВ при  $A \simeq 2.6$  ГэВ $^{-1}$  и  $G_{g}$ =10 мб. При этом из (6) нажии, что для ядра вольфрама  $N_{o}$ =0,54;  $N_{e}$ =0,28;  $N_{e}$ =0,12 и  $N_{e}$   $\approx$  0,06.

Следует, однако, отметить, что учет перерассеяний с указанными вдесь параметрами приводят к сильным изменениям результатов для велячин  $R(x_*)$ ,  $R(x_*)$  и т.п., рассмотренных в предыдущем разделе.

Совместное описание всех данных с учетом перерассеяния кварков по продольным и поперечным импульсам получается при других параметрах:  $6_{N} \simeq 1-2$  мб  $8_{N} \simeq 2$  ГэВ $^{-2}$  и  $N_{c} \simeq 0.4-9.2$  (при этом результати расчетов, показанные на рис. 4, практически не меняются). Такая параметри характерни не для составляющих кварков, а скорее для кварков-партонов  $^{19}$ .

## 5. Лептон-инерные взаиможействия

В этом разделе мы дадим предсказания для процессов лептон-ядерных взаимодействий, получению в рамках СМР. На рис. 5 показаны отнюшения сечений электророждения  $\mathscr{F}$ -мезонов на разных ядрах ( $eA \rightarrow e' \pi \tau X$ ), вычисленные в рамках рассматриваемой модели по бормуле  $^{20}$ :

$$\frac{N_{A}^{\mathcal{F}^{\dagger}}(x,z)}{N_{A}^{\mathcal{F}^{\dagger}}(x,z)} = \frac{4U_{v}^{A}(x)g(z) + d_{v}^{A}(x) + 5[g(z) + 7]S_{A}(x)}{4U_{v}^{A}(x)g(z) + d_{v}^{A}(x) + 5[g(z) + 7]S_{A}(x)},$$
(8)

гда  $p(z) = D^{\frac{1}{2}}(z)/D^{\frac{1}{2}}(z) \simeq 3$ , а  $S_A(x) = \overline{S}_A(x) = \overline{U}_A(x) = \overline{d}_A(x)$ . Видно, что в области x < I отновения сечений рождения  $\mathcal{T}^+$ -мезонов ведут себя подобно ЕМС-эффекту, а при x > I наблидается поведение, карактерное для  $\mathcal{T}^{(6)}$ . Отметим, что для области x < I аналогичные результати были получени в моделя кварковых кластеров  $\frac{1}{2}$ .

В докладе /22/ сыям представлени интересные экспериментальные данные для рождения K-мезонов в  $\rho A$ -веаннодействиях в кумулитивной области. Оказалось, что спектр K-мезонов в области X > I вмеет тот же наклон, что в спектри  $\mathcal{F}^{\pm}$ — в  $K^{\dagger}$ -мезонов. Поскольку в рас-

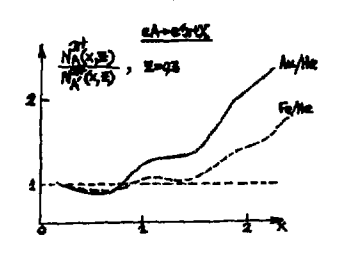


Рис. 5 мишени (см., например, /5,20/)

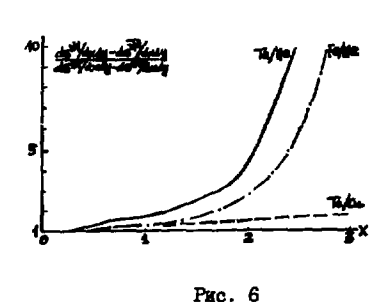
сматриваемом подходе виход  $K^-$ мевонов определяется морскими кварками из флуктона ядра, то это означает, что при x > 1 распределения морских и валентних кварков имеют один и тот же наклон:  $S_k^A(x) \sim \mathcal{U}_K^A(x)$ . В этой связи нам хотелось он сделать два замечания.

Во-первих, распределение морских кварков в ядре может бить связано с разностью сечений процессов VA-\(\alpha^{-X}\) и \(\forall A - \alpha^{-X}\). Действительно, для изоскалярной

$$\frac{d6^{VA}}{dxdy} - \frac{d6^{\overline{V}A}}{dxdy} = \left[\frac{6^2 mE}{4\pi} 2y(1-\frac{4}{2})^{x'}(F^{VA}_3 - F^{\overline{V}A}_3) = [\dots]4x'S_A(x')\right]$$
(9)

Поэтому, используя экспериментальный спектр K—мезонов, полученный в  $\rho A$ —взаимодействиях, и гипотезу предельной фрагментации  $^{/1},^{2}/$ , из (9) можно сделать предсказания для сечений  $^{/2}A$ —взаимодействий.

На рис. 6 показани результати расчетов отношений разности сечений (9) для различных ядер, выполненные в ФМР. Можно надеяться, что будущие коследования позволят проверить эти предсказания.



нуклонех, чем распределение S(X) морских кверков) будет приводить

Во-вторых, в рамках рассматриваемой модели, найденное поведение может означать, что рескейдинг для распределений валентных и морских кварков происходит по-резному. Так, еслг предположеть, что валентные кварки сосредсточени в соновном на меньших расстояняях (кор), чем морские, то рескейлинг для валентных кварков (плениях более жесткое рас-

пределение Ир (к) в свободних

к их большему смигчению по сравнению с морокими. В результате пове-

дение  $(x_{i})$  при больших x может стать близким к поведению  $S_{a}(x)$ .

Таким образом, проведенные эдесь расчеты показывают, что исследования процессов адрон- и лептон-ядерных взаимодействий в кумулятивной области представляют несомненный интерес.

## ЛИТЕРАТУРА

- I. A.M.Baldin. Proc.Conf.on Extreme States in Nuclear Systems, Dresden, 1980, 2.1; JIMR preprint E1-80-545, Dubna, 1980.
- 2. А.М. Балдин, D. А. Панебратцев, В. С. Ставинский. ДАН, 1964, 279, 1352.
- 3. Н.П.Зотов, В.А. Салеев, В.А. Царев. В сб.: "Бультикварковые взаимодействия и квантовая хромодинамика". Труды УПП Международного семинара по проблемам физики высоких энергий, Д I,2-об-665, Дубна, 1967. П.б.
- A.V.Efremov, A.B.Kaidalov, V.T.Kim, G.I. Lykasov, N.V. Slavin. JINR preprint 82-87-355. Dubna. 1987.
- 5. E.L.Berger. AND preprint AND-HEP-CP-87-45, 1987.
- Н. ІІ. Зотов, В. А. Салеев, В. А. Царев, Письма в мЭТФ, 1984, 40, 200;
   Препринт ФИАН №245, Москва, 1985.
- 7. Н.П. Зотов, В. А. Салеев, В. А. Царев. ЯФ, 1967, 45, 561.
- 8. Д.И. Блохинцев ЖЭТФ, 1957,33,1395; Б.К. Дукьянов, А.И. Титов. ЭЧАЯ, 1979,10,615; А.В. Ефремов. ЭЧАЯ, 1962,13,613.
   9. F.E.Close, R.G. Roberts, G.G. Ross. Phys. Lett., 1983,129E, 346.
- F.E.Close, R.G. Roberts, G.G. Ross. Phys. Lett., 1983, 129B, 346.
   F.E.Close, R.L. Jaffe, R.G. Roberts, G.G. Ross. Phys. Rev., 1985, D31, 1004.
- С.В.Бояринов, С.А.Герзон, М.М.Кац и др. ЯФ, 1967, 46, 1472.
- Н.П. Зотов, В.А. Салеев, В.А. Царев. Кр. сообщ. по физике ФИАН, 1967, №5.39.
- I2. P.Bordalo et al. (MA 10 Collaboration). Preprint CERN-EP/87-67, CERN-EP/87-68. Geneva. 1987.
- 13. G. I. Lykasov, Acta Phys. Polon., 1984, B15, 489.
- I4. G.Altarelli, G. Parisi, R. Petronzio. Phys. Lett. 1978, 76B, 351.
  W.J. Metcalf et al. Phys. Lett. 1980, 91B, 275.
- В. В. Анисович, М. Н. Кобринский, D. Нири, D. М. Шабельский. УФН, 1964, 144, 533.
- 16. A.B. Tapacos. 34AR, 1976, 7,771.
- I7. Г.И.Лыкасов, Б.Х.Шерконов. ЯФ, 1963, <u>38</u>, 704.
- Ів. Г.Б. Акавердян, А.В. Тарасов, В.В. Ужинский. ЯФ, 1977, 25, 666.
- 19. P.Chiappetta, H.J. Pirner. Mucl. Phys. B, 1987, 291, 765.
- 20. Ф. Клоуз. Кварки и партоны. М., "Мир", 1962.
- 21. H. Harindranath, K. E. Lassila, J. P. Vary. Phys. Rev. D, 1987, 36,299.

#### OUASI-ELASTIC AND DEEP-INELASTIC ELECTRON SCATTERING BY NUCLEI

### C. Ciofi degli Atti

INFN, Sezione Sanità, Rome, Italy V.le Regina Elena 299, I-00161 Rome, Italy and Department of Physics, University of Perugia V. Elce di Sotto, I-06100 Perugia, Italy

#### 1. Introduction

Theoretical calculations based upon microscopic models of the nucleon-nucleon interaction predict large correlation effects in the wave function of both ew-body systems and complex nuclei. The most clear manifestation of these effects is the presence in the nuclear wave function of highly excited two-nucleon configurations which lead to a strong depletion of the shell model states and to a large amount of nucleon high momentum components. Correlation effects have already been observed in (e,e'p) reactions from few body systems <sup>11</sup> and complex nuclei <sup>12,3</sup> and large effects have been predicted to occur on inclusive (e, e') cross sections <sup>14</sup> and y-scaling functions <sup>15</sup>. In this paper recent calculations of inclusive quasi-elastic and deep-inelastic processes based

In this paper recent calculations of inclusive quasi-elastic and deep-inelastic processes based upon realistic Spectral Functions and momentum distributions are reviewed and the role played by high momentum components and nucleon binding is illustrated.

## 2. Electrodisintegration, Spectral Functions and Momentum Distributions

The general expression for the cross section, describing, in Plane Wave Impulse Approximation (PWIA), the knock-out of a nucleon N from a nucleus A, is given by

$$\frac{d^{5}\sigma}{dEd\Omega_{2}d\varepsilon_{2}d\Omega_{N}d\varepsilon_{N}} \approx E_{N} k_{N} \sigma_{eN} P(k,E) \delta(\omega + M_{A} - E(k_{N}) - E(k)), \qquad (1)$$

where  $k = k_N - q$  is nucleon momentum before interaction,  $E(k_N) = (M^2 + k^2_N)^{1/2}$  is the nucleon energy in the final state,  $E(k) = ((M_{A-1} + E^{+f}_{A-1})^2 + k^2)^{1/2}$  is the recoiling energy of the final system  $(E^{+f}_{A-1})$  being the intrinsic energy of the (A-1)-nucleon system),  $E = E^f_{A-1} - E_A$  is the nucleon removal energy ( $E^f_{A-1} = E^{+f}_{A-1} + E_{A-1}$  being the eigenvalue of the (A-1)-Hamiltonian; and  $E_A(E_{A-1})$ , the ground state energy of the target (final nucleus)),  $\sigma_{eN}$  is the the electron-nucleon cross section for the scattering of an electron off an off-shell nucleon with momentum k, and, finally, P(k,E) is the nucleon Spectral Function

$$P(k,E) = (2\pi)^{-3} \sum_{f} \int dz \, e^{ik \cdot z} \, G_{f0}(z)^{2} \, \delta(E - (E^{f}_{A-1} - E_{A})) \,, \tag{2}$$

where

$$G_{f0}(z) = \int dx \dots dx \Psi^{f}_{A-1} *(x \dots x) \Psi^{0}_{A}(x \dots x.x)$$
(3)

is the overlap of the the eigenfunctions of the final (A-1) system state and the ground state of the target, respectively. The Spectral Function represents the joint probability to find in the nucleus A a nucleon with momentum k and energy E or, equivalently, the probability that the system (A-1) is left with excitation energy  $E^{f*}_{A-1}$  after a nucleon with momentum k is removed from the target.

Therefore, one can write

$$P(k,E) = P_{ex}(k,E) + P_{ex}(k,E), \qquad (4)$$

where  $P_{gr}(k,E)$  ("two-body channel" spectral function), yields the probability that the final (A-1) system is left in its ground state (corresponding to  $E^{f^w}_{A-1} = 0$  and  $E = E_{min} = |E_A \vdash |E_{A-1}|$ ), and  $P_{ex}(k,E)$  ("excited state" spectral function) yields the probability that the final (A-1) system is left in an excited state (with removal energy  $E = E^{f^w}_{A-1} + E_{min}$ ). The following relation  $V^w$  between the Spectral Function and the momentum distributions n(k) will be useful in what follows

$$n(k) = \int d\underline{z} \, d\underline{z}' e^{i\underline{k}\cdot(\underline{z}-\underline{z}')} \, \rho(\underline{z},\underline{z}') = \int_{\text{dE}}^{\text{dE}} P(k,E) = n_{gr}(k) + n_{ex}(k) \,, \tag{5}$$
Emin

where  $\rho(z,z')$  is the non diagonal one-body density matrix and

$$n_{ex}(k) = (2\pi)^{-3}! \int_{\mathbf{Z}} e^{i\underline{k}\cdot \mathbf{Z}} G_{00}(\underline{\mathbf{z}})^2$$
 (6)

where

$$n_{\mathbf{f}}(\mathbf{k}) = \iint d\mathbf{z} \, e^{i\mathbf{k} \cdot \mathbf{Z}} \, G_{\mathbf{f}\mathbf{f}}(\mathbf{z}) |^2 \tag{8}$$

is the "partial momentum distribution" of a nucleon in the A-body configuration characterized by a "spectator" (A-1) system in the virtual state f.

The knowledge of the momentum distribution allows one to calculate the spectroscopic factors defined by

$$S_{fo} = \left[ dz \right] G_{fo}(z) |^2 = \int n_f(k) k^2 dk \tag{9}$$

and normalized according to  $\sum_i S_{i,0} = 1$ . Using eqns(6) and (7), eq(4) can be rewritten as

$$P(k,E) = n_{gr}(k)\delta(E-E_{min}) + P(k,E)(1-\delta_{E,E_{min}})$$
 (10)

The Spectral Function for  ${}^{3}$ He in the T=0 state is shown in Fig. 1 and the rich removal energy structure due to the n-p continuum state can be noticed. The momentum distribution, i.e. the Spectral Function integrated over the removal energy, is shown in Fig. 2. The following important features of the three-body Spectral Function and momentum distributions should be pointed out:

i) for  $k \ge 2$  fm<sup>-1</sup> the momentum distribution is entirely determined by the three-body channel configuration in the ground state wave function, i.e. by ground-state correlations;

ii) although the components of the wave function with removal energy  $E \ge 50$  MeV have probability less than three per cent, they have large effects on the high momentum part of n(k); iii) high momentum components are strictly linked to high removal energies, so that the measurement of the former should imply the measurement of the latter.

The calculation of the full Spectral Function for complex nuclei has not yet been performed. Recently the nucleon momentum distributions in  $^4\text{He}$  /8/,  $^{12}\text{C}$ ,  $^{16}\text{O}$  and  $^{40}\text{Ca}$  /9/ have been calculated with realistic two-body interactions; the quantity  $n_{gr}$  has also been evaluated and  $n_{ex}$  was obtained as the difference between n(k) and  $n_{gr}$  (k) (see eqn (4)).

The momentum distributions  $n_{gr}(k)$  and  $n_{ex}(k)$  for <sup>3</sup>He and <sup>4</sup>He are shown in Figs. 3 and 4. It can be seen that the low-momentum part of n(k) is mostly determined by configurations in

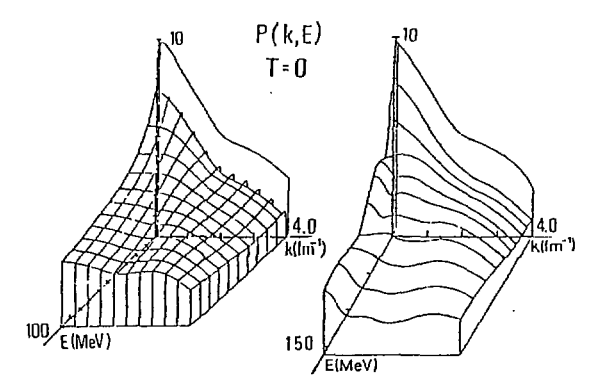


Fig. 1. Proton spectral function in  ${}^3\text{He P(K,E)}$  (eqn (2)), in the isospin T=0 state calculated using Paris  ${}^{7/l}$  (left) and RSC  ${}^{6/l}$  (right) interactions (units are fm ${}^3$  for the two-body channel and fm ${}^2$  MeV ${}^{-1}$  for the three-body channel).

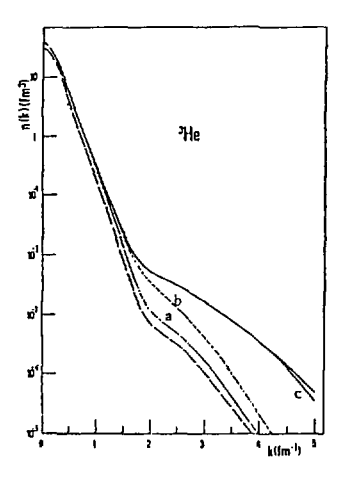


Fig. 2. The integrated spectral function in  $^3$ He. The dashed curve represents  $n_{\rm gr}$  (see eqn 6) and the curves labelled (a), (b) and (c) represent the sum of  $n_{\rm gr}$  and the three-body channel spectral function integrated from  $E_{\rm min}$  up to 12, 50 and 300 MeV, respectively. The full curve is  $n_{\rm gr}$  +  $n_{\rm ex}$  (After Ref. 6).

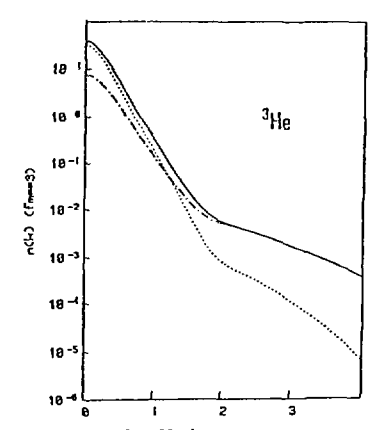


Fig. 3. Nucleon momentum distribution in <sup>3</sup>He obtained /6/ with the RSC interaction. Dotted and dash-dotted lines correspond to ngr(k) and nex(k), respectively (see eqn. 5); the full line is the total momentum distibution n(k) (After Ref.6).

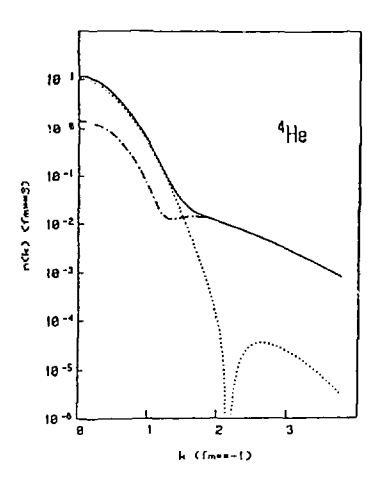
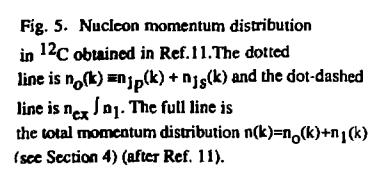


Fig. 4. The same as in Fig. 3, but for <sup>4</sup>He /8/. The momentum distributions correspond to the wave function obtained within the ATMS method using the Reid V8 interaction.



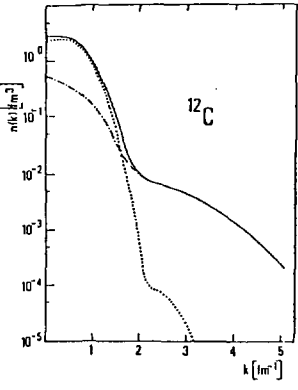


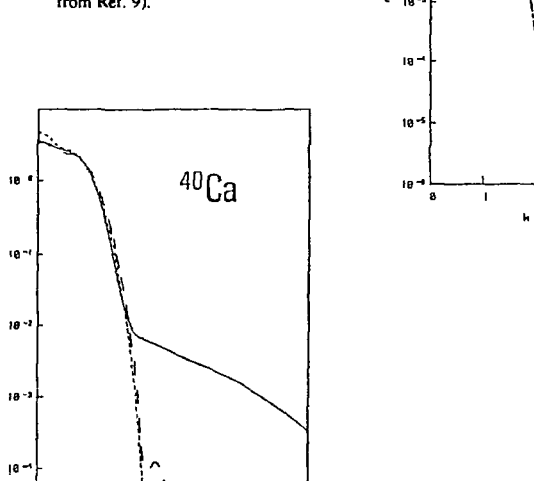
Table 1. Spectroscopic factors (eqn.10) for  $^3$ He,  $^4$ He and  $^{12}$ C calculated from the momentum distributions shown in Figs.3,4 and 5 (After Ref.11). For  $^{12}$ C

 $S_{gr} = S_o$  includes the (1s)<sup>-1</sup> state reached by knock-out of nucleons from the 1s shell.

	Sgr	Sex
3 <sub>He</sub>	0.65	0.35
<sup>4</sup> He	0.80	0.20
$^{12}C$	0.80	0.20

Fig. 6. Nucleon momentum distibutions in <sup>16</sup>O. Full curve: Ref. 9; long-dashed line: IPM with Woods-Saxon wave functions of Ref. /12/; short-dashed line: HF wave functions of Ref. /13/ (adapted from Ref. 9).

([m==(-1))



18 -1 16 0 18 -1 18 -2 18 -2 18 -2 18 -2 18 -4 18 -1

Fig. 7. The same as in Fig. 6 but for  $^{40}$ Ca. (adapted from Ref. 9).

which the spectator nucleus is in its ground state, whereas the high momentum part is entirely exhausted by the break-up channels. The results for <sup>12</sup>C, obtained with the Reid V6 interaction /10/, are presented in Fig. 5 where the separation between  $n_{gr} = n_0$  and  $n_{ex} = n_1$  is also shown (note that no include the 1s-1 state reached by knocking out nucleous from the 1s shell; see Section 5). The calculated spectroscopic factors for <sup>3</sup>He, <sup>4</sup>He and <sup>12</sup>C are shown in Table 1 and a large amount of highly excited configuration in these nuclei can be noticed.

The results for <sup>16</sup>O and <sup>40</sup>Ca are presented in Figs. 6 and 7. It can be seen that for all nuclei

considered, the inclusion of short-range and tensor correlations sharply increases n(k) in the high

momentum region (k > 1.5 - 2 fm<sup>-1</sup>) with respect to various mean field approximations.

Inclusive quasi-clastic scattering and y-scaling

The inclusive cross section can be obtained from eq.(1) by integrating over kn and E, obtaining

$$\sigma_2(\mathbf{q},\omega) = \frac{d^2\sigma}{d\omega \,d\Omega} = (Z\bar{\sigma}_{ep} + N\bar{\sigma}_{en}) \, 2\pi i \, \frac{\partial \omega}{\partial \omega} \Gamma^1 \, F(\mathbf{q},\omega) ,$$
 (11)

where the nuclear structure function F(u.ii) is

$$E_{\max}(q,\omega) = k_{\max}(q,\omega,E)$$

$$F(q,\omega) = 2\pi \int dE \qquad \int dk \ k \ P(k,E)$$

$$E_{\min} \qquad k_{\min}(q,\omega,E),$$
(12)

$$\begin{array}{lll} k_{max}(q,\omega,E_{min}) & E_{max}(q,\omega) & k_{max}(q,\omega,E) \\ =& 2\pi \int dk & k & n_{gr}(k) & + & 2\pi \int dE & \int dk & k & P_{ex}(k,E) \\ k_{min}(q,\omega,E_{min}) & E_{min} & k_{min}(q,\omega,E) \end{array} \tag{13}$$

with  $E_{max}$ ,  $k_{min}$  and  $k_{max}$  fixed by the energy conservation and  $\frac{\partial \omega}{\partial \omega} k \partial \cos \alpha$  ( $\cos \alpha = (q \cdot k)/(qk)$ ) arising from the integration over the direction of k and evaluated (together with  $\overline{\sigma}_{en(n)}$ ) at  $E=E_{min}$ and k=kmin(Emin). Let us introduce the "scaling variable" y, which is nothing but the value of kmin for  $E = E_{min}$ , i.e. by  $k_{min} = k_{min} = k_{min}$ . It is determined by the relativistic energy conservation

$$\omega + M_{A} = \sqrt{M^2 + (q \cdot k_{min})^2} + \sqrt{(M_{A-1} + E_{A-1}^{\dagger})^2 + k_{min}^2}$$
 (14)

with  $E^{+}_{A=1}=0$ . The dependence upon  $\omega$  in eq.(13) can be replaced by a dependence upon y, obtaining

$$k_{\max}(q,y,E_{\min}) = E_{\max}(q,y) \quad k_{\max}(q,y,E)$$

$$F(q,y) = 2\pi \int dk \quad k \quad n_{gr}(k) \quad + \quad 2\pi \int dE \quad \int dk \quad k \quad P_{ex}(k,E)$$

$$|y| \qquad \qquad \qquad k_{\min}(q,y,E) \quad .$$
(15)

For  $q \to \infty$ , one has:  $k_{max} = E_{max} = \infty$  and  $k_{min} = |y-(E-E_{min})|^{1/5}$  and the above equation becomes

$$F(y) = 2\pi \int_{\text{cmin}}^{6} \frac{\int_{\text{cmin}}^{6} dk \ k \ P(k, E)}{\text{by-}(E-E_{\text{min}})!}$$
 (16)

Therefore if the PWIA is a correct description of the scattering process, the following quantity, the "scaling function"

$$F_1 = \frac{\sigma_2(q,\omega)}{(Z\sigma_{en} + N\sigma_{en})} + \frac{\partial \omega}{k \partial \cos \alpha} + , \qquad (17)$$

should scale in the asymptotic limit in the variable y and should be interpreted as the structure function (16). However, because of the excitation energy of the final (A-1) system, the asymptotic scaling function does differ from the longitudinal momentum distibutions which is defined by

$$f(y) = 2\pi \int_{V} k \, n(k) \, dk \,. \tag{18}$$

Only if non relativistic kinematics is used  $^{16/}$  do egns (16) and (18) coincide. The calculation of the asymptotic scaling function requires the knowledge of the full Spectral Function, whose excitation part,  $P_{\rm ex}(k, E)$ , is exactly known only for  $^{3}$ He. For A>3 nuclei, the following approximation can be tried

$$P(k,E) = n_{gr}(k) \delta(E - E_{min}) + n_{ex}(k)\delta(E - E), \qquad (19)$$

where the quantity  $E = E^{f^*}A_{-1} + E_{min}$  can be obtained from the Koltun sum rule /34/. Thus by eq(19) the transition to the ground state of the (A-1) system is exactly taken into account, whereas the transition to all possible excited states are taken into account in an average way.

ransition to all possible excited states are taken into account in an average way.

In Figs. 8, 9 and 10 the scaling function F<sub>1</sub> ex of <sup>3</sup>He, <sup>4</sup>He and <sup>12</sup>C is shown and compared with the theoretical longitudinal momentum distilution (eq. (18)) and the asymptotic scaling function (eq. (16)). For <sup>3</sup>He eq. (16) has been calculated using the full exact spectral function <sup>16</sup>He and <sup>12</sup>C the approximation (19) has been adopted, which leads to

$$F(y) = 2\pi \int dk \, k \, n_{gr}(k) + 2\pi \int dk \, k \, n_{ex}(k)$$

$$|y| \qquad |y \cdot (E-E_{min})|$$
(20)

It can be seen that at high negative values of y, which correspond to the low energy side of the quasi clastic peak, the scaling function is almost entirely determined by the break up channels, i.e. by the excitation energy of the final (A-1) system (it should be recalled that the relation between y,  $\omega$  and  $\omega_{\text{peak}}$  is as follows: y=0 for  $\omega = \omega_{\text{peak}}$ , y>0 for  $\omega > \omega_{\text{peak}}$ , y<0 for  $\omega < \omega_{\text{peak}}$ ).

y-scaling has been used to obtain the nucleon momentum distribution n(k) in few-body systems 19-22. In the two-body system, binding effects are absent so that eqn. (16) simply becomes

$$f(y) = 2\pi \int_{|y|}^{\infty} k n(k) dk$$
(21)

from which the nucleon momentum distribution can be obtained by a simple derivative

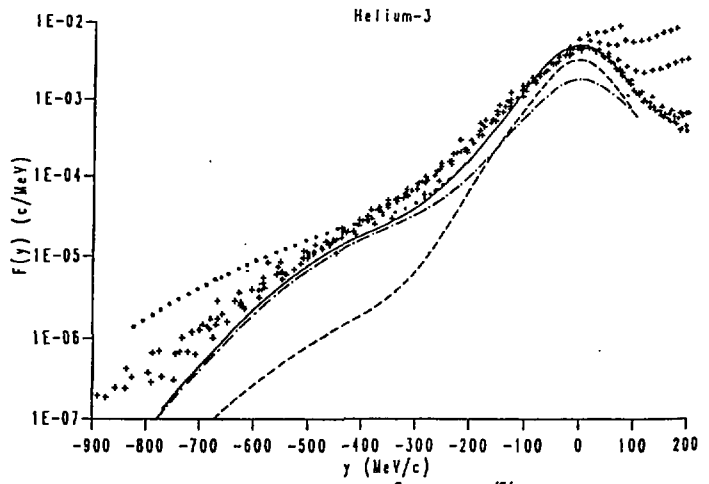


Fig. 8. The experimental scaling function of <sup>3</sup>He obtained <sup>/5/</sup> from eqn.(17) using the experimental cross section from Ref. 18. The dotted line represents the longitudinal momentum distribution (18) obtained with n(k) shown in Fig.3 whereas the full line is the asymptotic scaling function (16) obtained with the Spectral function shown in Fig.1. The dashed and dot-dashed curves represent the contribution from the two-body and three-body channels, respectively (After Ref. 5).

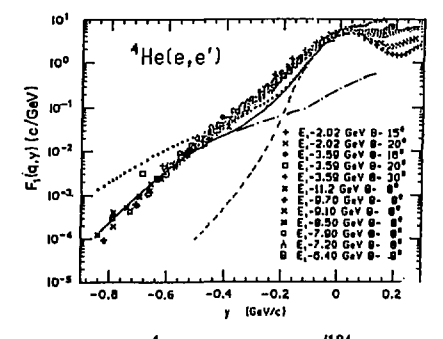


Fig. 9. The scaling function of  $^4$ He measured at SLAC  $^{/18}$ /. The dotted line represents the longitudinal momentum distribution (eqn.(18)) obtained from the momentum distribution shown in Fig. 3. The full curve has been obtained taking into account the sociation energies of the final three-body system by means of eqn(19) where  $E = E_A$ .  $^{12} + E_{min}$  with E = 100 MeV. The dashed line is the contribution from  $n_{gx}$  and the dot-dashed line the contribution from  $n_{ex}$ .

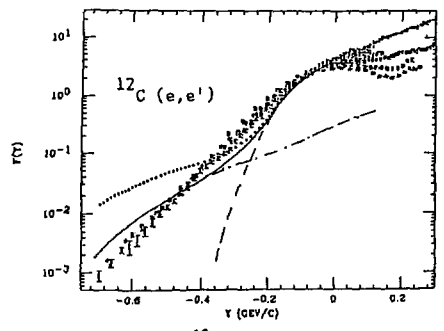


Fig. 10. The same as in Fig. 9 but for <sup>12</sup>C. The momentum distribution shown in Fig.5 has been used.

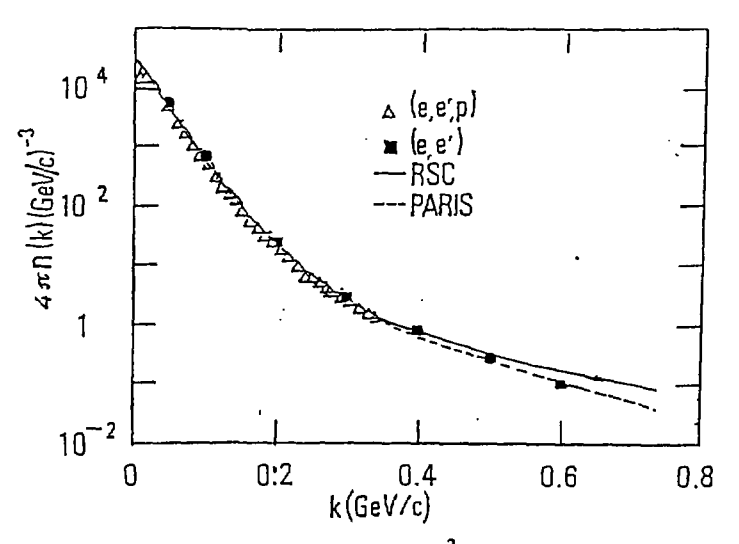


Fig.11. The nucleon momentum distribution  $n(k) = hy(k)l^2$  in deuteron. Black squares: n(k) extracted /19/ from the inclusive cross section  $^2H(e,e^*)$  /23/, using eqn.22. Triangles: n(k) extracted in Ref.24 from the exclusive  $^2H(e,e^*p)n$  cross section /25/. The full and dashed lines represent n(k) obtained from the RSC and Paris ineractions, respectively.

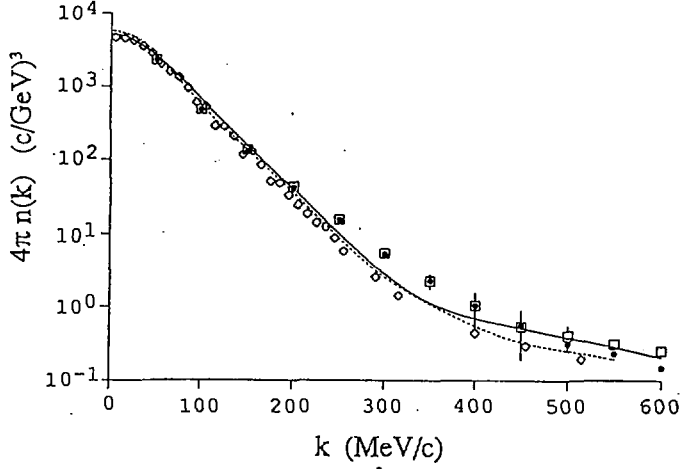


Fig. 12. The nucleon momentum distribution n(k) in <sup>3</sup>He obtained from eq. (24) by disregarding the binding correction (dots) and by calculating it using the full Spectral Function of Ref. 6 (open squares); the results corresponding to various model Spectral Functions fall between the open squares and the dots and are not shown. Diamonds: n(k) obtained <sup>11</sup>I from the exclusive cross sections <sup>3</sup>He(e,e'p)d and <sup>3</sup>He(e,e'p)d pnp including FSI and MEC corrections. Full and dashed lines: proton momentum distribution obtained from the RSC and the Paris interactions, respectively. (After Refs.20-22).

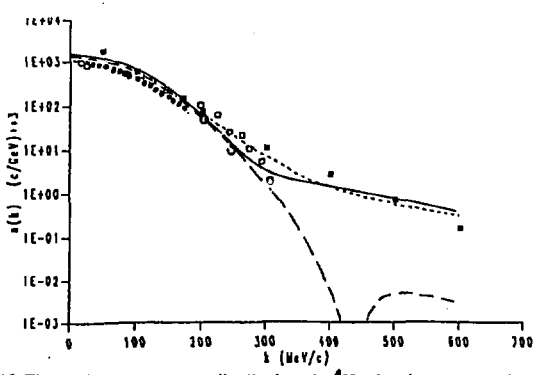


Fig. 13. The nucleon momentum distributions in <sup>4</sup>He. Black squares: n(k) extracted from the inclusive cross section of Ref. 18using eqn(23); open squares, black dots and open dots:ngr(k) obtained from the <sup>3</sup>He(e,e'p)<sup>3</sup>H reaction of Ref. 26, 27, and 28, respectively (After Refs. 21 and 22).

$$n(k) = -\frac{1}{2\pi v} \frac{df}{dv} \qquad k = tyl \cdot$$
 (22)

For A>2, the above equations do not hold and nucleon binding playes a substantial effect (cf. Figs. 8, 9 and 10). In order to take care of binding effects when extracting n(k) from the scaling function, the following procedure has been adopted 19-22. The asymptotic scaling function (16) can be rewritten as

$$F(y) = 2\pi \int_{|y|}^{\infty} \frac{dk \ k \ n_{gr}(k) + 2\pi \int_{emin}^{\infty} \frac{k_{min}(y, E)}{|y|} \int_{ex}^{k_{min}(y, E)} \frac{dk \ k \ P_{ex}(k, E)}{|y|} \equiv f(y) + B(y) , \qquad (23)$$

where the quantity B, which vanishes for deuteron, originates from nucleon binding. By taking the derivative of both sides of eq. (23), one gets

$$n(k) = -\frac{1}{2\pi y} \left\{ \frac{dF_1(y)}{dy} + \frac{dB(y)}{dy} \right\} \qquad k=|y|$$
 (24)

and the momentum distribution can be extracted from the experimental asymptotic scaling function, provided a reliable estimate of BB/dy can be made. Several of such estimates have been reported in Refs. 2D-22 and it turns out that the binding correction dB/dy is much lower than  $dF_1/dy$ , at least up to  $k = 2.5 fm^{-1}$ . The momentum distributions obtained from the scaling functions are presented in Figs. 11, for the deuteron, and in Figs. 12 and 13 for  $^3$ He and  $^4$ He. For all three nuclei, a proper procedure to minimize the effect of final state interaction has been used. In the same figures, the results obtained from exclusive (e.e.p) reactions are also presented. It can be seen that the agreement between exclusive and inclusive experiments is impressive and that the high momentum parts of the momentum distributions qualitatively agrees with theoretical calculations performed within conventional nuclear physics with realistic two-nucleon interactions.

# 4.Deep-inelastic scattering (DIS)

The relevant role played by nucleon binding in the EMC effect has been illustrated by Akulinicheve et al. <sup>199</sup> and Birbrair et al. <sup>199</sup> who have shown that if, besides the Fermi motion, also the binding of nucleons is taken into account, the EMC effect can reasonably be interpreted in terms of the Hartree-Fock (HF) picture of the nucleus. The approach of Refs.29 and 30 has however been questioned by Frankfurt and Strikman <sup>191</sup>, who argued that when relativistic effects are consistently taken into account by considering the so called flux factor in the normalization of the relativistic spectral function, the effect of nucleon binding is strongly reduced. The necessity of properly considering the flux factor has also been proved in a subsequent comprehensive paper by Birbrair et al. <sup>194</sup>, as well as by Jaffe <sup>193</sup>.

The dependence of the EMC effect upon nucleon dynamics is mainly determined (for  $x \le 1$ ) by the values of the mean removal ( $x \ge 1$ ) and kinetic ( $x \ge 1$ ) energies. As illustrated in the previous Sections, nucleon-nucleon (NN) correlations induced by realistic interactions starply increase the amount of high momentum components and consequently, the values of the mean kinetic and removal energies. Since in most calculations of the EMC effect nucleon binding has been treated within a HF picture, it has been stressed in Ref.34 that, in order to fully clarify the role played by conventional nuclear physics in DIS of electrons by nuclei, it is necessary to properly consider the effect of correlations, and an approach has been presented based upon the nucleon momentum distributions and spectral functions illustrated in previous sections. The nuclear structure function  $F_2^A(x)$  was defined according to the convolution model  $x \ge 1$ .

$$F_2^{A}(x,Q^2) = \int_{x \le z} dz \left[ f^{P}(z) F_2^{P}(x/z,Q^2) + f^{P}(z) F_2^{P}(x/z,Q^2) \right], \qquad (25)$$

where  $F_2P^{(n)}$  is the proton (neutron) structure function,  $q^2 = g^2 - V^2 = -Q^2$  the four-momentum

transfer,  $x = Q^2/2Mv$  the Bjorken scaling variable, z = (pq)/Mv, and p the four-momentum of the off-shell nucleon (in the Bjorken limit  $z \to p^+/M = (p_0 \cdot p_3)/M$ ). The function  $f^{p(n)}(z)$  is

$$f^{p(n)}(z) = \int d^4p \, S^{p(n)}(p) \, z \, \delta(z - (p \, q)/Mn)$$
, (26)

where  $S^{p(0)}$  is the invariant function describing the nuclear vertex; it is normalized according to  $f^{31/4}$  of  $f^{p}(S^{p}(p)+S^{n}(p))$  z=|dz| f  $f^{p}(z)+f^{n}(z)$  |=1 and it is related to the non relativistic spectral function P(k,E) by the following expansion:  $S^{p(0)}(p)=P^{p(0)}(k,E)$  |=1 of  $P^{p(0)}(k,E)$  |=1 of  $P^{$ 

$$f^{p(n)}(z) = 2\pi M z \int_{min}^{0} dE \int_{k}^{\infty} dk \, k \, P^{p(n)}(k, E) ,$$
 (27)

where  $E^{p(n)}_{min}$  and  $k^{p(n)}_{min}$  are determined from the kinematics of the process; in particular,  $k_{min}$  depends upon the variable z, the removal energy E and the mass of the recoiling A-1 system. In the calculations of Ref.35, the spectral function from Ref.6 has been used for the three-body system, whereas for heavier nuclei the following ansatz has been adopted

$$P(k,E) = P_0(k,E) + P_1(k,E)$$
 (28)

where

$$P_{\mathbf{O}}(\mathbf{k}, \mathbf{E}) = (2\pi)^{-3} \Sigma_{\alpha} \mid \int d\mathbf{r} e^{i\mathbf{k}\cdot\mathbf{T}} G_{\alpha o}(\mathbf{r}) \mid^{2} \delta(\mathbf{E} - \mathbf{E}_{\alpha} \mid \mathbf{E}_{\alpha})$$

$$= 1/(4\pi A) \Sigma_{\alpha} A_{\alpha} n_{\alpha}^{SRC}(\mathbf{k}) \delta(\mathbf{E} - \mathbf{E}_{\alpha} \mid \mathbf{E}_{\alpha})$$
(29)

and

$$P_{1}(k,E) = (2\pi)^{-3} \sum_{f \neq c_{1}} \left\{ \int d\mathbf{r} \, e^{i\mathbf{k} \cdot \mathbf{r}} \, G_{f0}(\mathbf{r}) \, \right\}^{2} \, \delta(E - E^{f}_{1})$$
(30)

with  $E_1^f = E_{min}^{fe}$ . In eqns (29) and (30),  $n^{SRC}$  is the many-body momentum distribution which includes the effects of NN correlations,  $A_{\alpha}$  is the number of nucleons in the orbital  $\alpha$  ( $\Sigma_{\alpha}$ ) and the sum over  $\alpha$  runs over the normally occupied HF states of the target. Within the HF approximation,  $P_1(k,E) = 0$ ,  $n_a^{SRC}(k)$  reduces to the HF momentum distribution  $n_a^{HF}(k)$ , and the spectral function of Refs.29 and 30, viz.

$$P_0 \overset{\text{HF}}{=} (k, E) = 1/(4\pi A) \sum_{\alpha} A_{\alpha} n_{\alpha} \overset{\text{HF}}{=} (k) \delta(E - | \epsilon_{\alpha}|)$$
(31)

is recovered (note that ansatz (28) differs from ansatz (19) in that in the former part of the excited final states, the hole states  $\alpha$ , are included in  $P_0$ , whereas in the latter  $P_{gr}$  contains only the ground state of the final nucleus). The nucleon momentum distribution is  $n(k) = n_0(k) + n_1(k)$ , where

$$n_{O}(k) = 4\pi \int P_{O}(k, E) dE$$
 (32)

and

$$n_1(k) = 4\pi \int P_1(k, E) dE \tag{33}$$

The momentum distributions for  $^{12}\mathrm{C}$  shown in Fig.5 are precisely  $n_0$  and  $n_1$  and the spectroscopic factors  $S_{pr}$  and  $S_{ex}$  in Table 1 are the integral of them. Eq.(27) becomes

$$f(z) = 2\pi M z \left\{ \frac{1}{4\pi A} \sum_{\alpha} A_{\alpha} \int_{k}^{\infty} \frac{SRC(k)kdk}{k_{min}^{\alpha}(z, \epsilon_{\alpha}, M_{A-1})} + \int_{E_{1min}}^{\infty} \int_{k_{min}^{\alpha}(z, E, M_{A-1})}^{\infty} \frac{P_{1}(k, E)k}{k_{min}^{\alpha}(z, E, M_{A-1})} \right\}$$
(34)

and the ratio  $R(x)=F_2^A(x)/F_2^D(x)$ , where  $F_2^D$  is the deuteron structure function per nucleon, can be calculated. A reasonable representation for  $P_1$  is  $P_1$  (k,E) =  $n_1$ (k)  $\delta(E\cdot \vec{E}_1)$ , where  $\vec{E}_1$  is the average removal energy associated with  $P_1$ . The momentum distributions  $n_\alpha^{SRC}$  and  $n_1$  have been obtained using the results of Refs. 8,9,11 and 36; the value of  $\vec{E}_1$  has been obtained using the Koltun sum rule /34/; the values of  $\varepsilon_\alpha$  have been taken from (e,e'p) reactions /37/. The values of <T> and <E> in the HF approximation and the many-body correlated approach (SRC) of Ref.35 are listed in Table 2 for  $^{12}C$  and  $^{56}Fe$ . It can be seen that correlations strongly increase the nucleon mean kinetic and removal energies.

Table 2. The values of the mean kinetic, <T>, and removal, <E>, energies calculated within the Hartree-Fock (HF) and many-body correlated (SRC) approaches.

		<t> (MeV)</t>	<e> (MeV)</e>
12 <sub>C</sub>	HF	17.0	23.0
	SRC	37.0	49.0
56 <sub>Fe</sub>	HF	15.0	25.2
	SRC	36.6	53.6

Several models for the interpretation of the EMC effect have been proposed based on the modification of nucleon properties inside the nucleus, e.g. the change of the confinement radius of a quark inside a nucleon bound in the nuclear medium  $^{/38,39/}$ ,  $^{/7}$ n Ref.34 the  $Q^2$  - rescaling of Ref. 39, has been used in the convolution formula, which amounts to replace the  $Q^2$  dependence in the nucleon structure function with  $\xi(Q^2)Q^2$ , where the rescaling parameter  $\xi$  is

$$\xi(Q^2) = \{(\lambda_A/\lambda_N)^2\} \ln(Q^2/\Lambda^2) / \ln(\mu^2/\Lambda^2) , \qquad (35)$$

 $\lambda_A$  and  $\lambda_N$  being the quark confinement radii in the bound and free nucleons, respectively. According to Ref. 39, at  $O^2 = 20$  (GeV/c)<sup>2</sup>, one has  $\Lambda = 0.25$  GeV/c and  $\mu^2 = 0.66$  (GeV/c)<sup>2</sup>.

The results of Ref. 35 for <sup>3</sup>He, <sup>12</sup>C, and <sup>56</sup>Fe are presented in Figs. 14,15 and 16, respectively. It can be seen that:

 nucleon binding within a HF picture cannot explain the EMC effect. This result, at variance with Refs. 29 and 30, is due both to the proper consideration of the flux factor in the convolution formula, as well as to the EMC effect on deuteron which reduces the denominator of R(x);

ii) NN correlations resulting from realistic interactions have large effects on the EMC effect but an appreciable discrepancy with the data in the region 0.7 ≤ x ≤ 1still remains even if rescaling is considered:

iii) if rescaling is introduced in the convolution formula within the HF model, the best agreement with data would require a 10+12 % increase in the confinement size of bound nucleons, whereas when SRC are considered an appreciably smaller increase, viz. 4 + 5 %, is obtained (the use of a larger value of  $(\lambda_A / \lambda_N)$  would result in a curve located much lower than the experimental data for all nuclei considered).

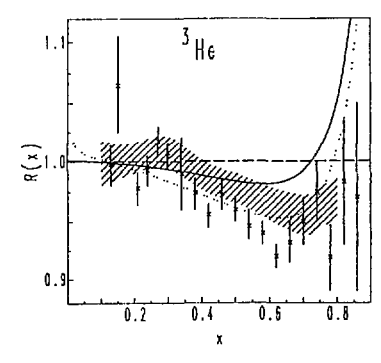
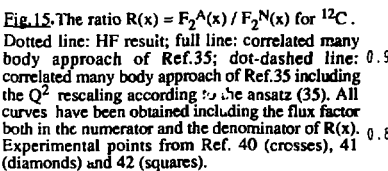
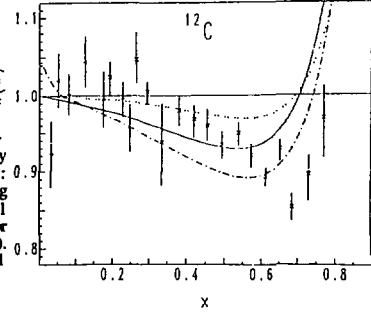


Fig.14 The ratio  $R(x) = F_2A(x) / F_2D(x)$  for <sup>3</sup>He. The full curve corresponds to the many-body structure function (eq. (25)) obtained using the spectral function from Ref.6; the dotted curve includes  $Q^2$  rescaling according to the ansatz (35). Both curves include the flux factor in the numerator and denominator of R(x). Experimental points are from Ref.40 and refer to <sup>4</sup>He. The shaded area has been obtained by rescaling the experimental data according to the A-dependence formulae given in Refs. 31 and 40. In this and in the following figure the nucleon structure function from Ref. 43 has been used.





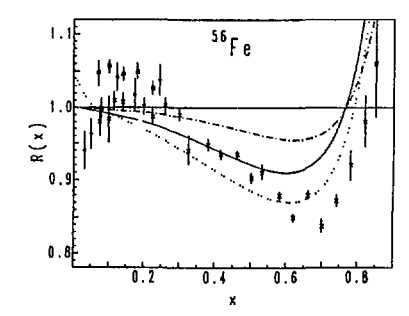


Fig.16. The same as Fig.15 for 56Fe.

In conclusion, it appears that a large part of the EMC effect in the region  $0.2 \le x \le 1$  is accounted for by realistic nucleon-nucleon correlations, but a quantitative and consistent explanation of the effect would require the explicit introduction of non-baryonic degrees of freedom, e.g. pions /44/ which, by carrying a fraction of light cone no mentum, will contribute to satisfy the momentum sum rule. Moreover, the momentum and energy dependence of possible modifications of the nucleon structure function should be considered; these modifications could consistently be incorporated in the approach of Ref.35, where the contribution from the low and the high components of nucleon momenta and binding are explicitly separated.

# REFERENCES

C. Marchand, Phys. Rev. Lett.60(1988)1703

P.K.E. de Witt Huberts, in 3rd Workshop on "Perspectives in Nuclear Physics at Intermediate Energies", May 1987, S. Boffi, C. Ciofi degli Atti and M. Giannini Eds. World Scientific, 1988, p.381

J.M. Finn, W. Bertozzi and R.W. Lourie, ibidem, p.523

C. Ciofi degli Atti, T. Katayama, G. Salme, O. Benhar and S. Liuti in "2nd Workshop on Perspectives in Nuclear Physics at Intermediate Energies", S. Boffi, C. Ciofi degli Atti and M. Giannini Eds. World Scientific 1985 p. 309, and to be published.

C. Ciofi degli Atti, E. Pace and G. Salme, Phys. Lett.177B(1983)303

C. Ciofi degli Atti, E. Pace and G. Salme, Few-Body System Supp. 1 (1986)28C. Ciofi degli Atti, Nucl. Phys. A463 (1987) 127c.

Ciofi degli Atti, E. Pace and G. Salme, Phys. Lett. (1984)14.

H. Meier-Hajduk et.al., Nucl. Phys. A395 (1983) 332, and private communication

Y. Akaishi, Nucl. Phys. A416 (1984) 409c and private communications.

O. Benhar, C. Ciofi degli Atti, S. Liuti and G. Salmè, Phys. Lett. 177 (1986) 135.

10. V.R.Pandharipande and R.B. Wiringa, Rev. Mod. Phys. 51 (1979) 821.

11. Ciofi degli Atti, O. Benhar and G. Salmè, Proceedings of the "4th Miniconference", NIKHEF, November 1985. O. Benhar, C. Ciofi degli Atti and G. Salmè, to be published.

12. L.R.B. Elton and A. Swift, Nucl. Phys. A94 (1967) 52. J.W. Negele, Phys. Rev. C1 (1970) 1260.

- J.G. Zabolitzky and W. Ey. Phys. Lett. 76B (1978) 527.
- E. Pace and G. Salmè, Phys. Lett. 110B (1982) 411.
- C. Ciofi degli Atti, Lett. Nuovo Cimento 41 (1983) 330
- S. Rock et al, Phys. Rev. C26 1592 (1982). D. Day et al, Phys. Rev. Lett. 59 (1987) 427

D. Day et al., Phys. Rev. Lett 43 (1979)1143

19. C. Ciofi degli Atti, E. Pace and G. Salmè, Phys. Rev. C36 (1987) 1208 20. C. Ciofi degii Atti, E. Pace and G. Salme, Phys. Rev. in press

21. C.Ciofi degli Atti, E. Pace and G. Salmè, Few. Body Systems, S2 (1987) 376

- C.Clofi degli Atti, E. Pace and G. Salme, in 3rd Workshop on "Perspectives in Nuclear Physics at Intermediate Energies", May 1987, S. Boffi, C. Ciofi degli Atti and M. Giannini Eds. World Scientific, 1988, p.421
- 23. P. Bosted et al, Phys. Rev. Lett. 49 (1982) 1380. H. Arenhoevel, Nucl. Phys. A384 (1982) 287.
- 25. M. Bernheim et al, Nucl. Phys. A365 (1981) 349.
- V. A. Goldshtein, Nucl. Phys. A392 (1983) 457
- 27. J.F.J. van den Brand, Private communication
- 28. A. Magnon, Private communication
- S.V. Akulinichev et al., Phys. Lett. 158B (1985), 485; Phys. Rev. Lett. 55 (1985), 2239;
- 30. B.L. Birbrair et al., Phys. Lett 166B(1986),119;31.

- 31. L.L. Frankfurt, M.I. Strikman, Phys. Lett 183B (1987)254; L.L. Frankfurt, M.I. Strikman, Phys. Rep. 160 (1988) 236;
- 32. B.L. Birbrair, E.M. Levin and Gh. Shuvaiev, Report LDK 539 (Leningrad University) 1986;

- R.L. Jaffe, Nucl. Phys. A478(1988)3c;
   D. S. Koltun, Phys. Rev. C9(1974)484;
- 37. C. Ciofi degli Atti and S. Liuti, to be published
  - C. Ciofi degli Atti and S. Liuti, Czech. J. Phys. B39(1989) (Proceedings of the Conference Mesons and Light Nuclei IV ) and to be published;
- 36. S. Fantoni and V. R. Pandharipande, Nucl. Phys. A427 (1984)473
- 37. S. Frullani and J. Mougey, Adv. Nucl. Phys. 14(1984)1;38.
- A. W. Hendry, D. B. Lichtenberg and E. Predazzi, Phys. Lett. 136B(1984)433;
   F.E. Close, R.G. Roberts, G.C. Ross, Phys. Lett. 168B (1986) 400; F.E. Close, Nucl. Phys. A478(1988)407c;
- 39. F.E. Close, R.L. Jaffe, R.G. Roberts, G.C. Ross, Phys. Rev. D31 (1985), 1004;
- 40. R.G. Arnold et al., Phys. Rev. Lett. 52 (1984) 727;
- 41. J. Ashman et al., European Muon Collaboration, Phys.Lett. 202B (1988)603;

- A.C. Benvenuti et al., BCDMS Collaboration, CERN-EP/87-13;43
   M. Glück et al., Z.Phys.C13 (1982)119;
   M. Ericson and A.Thomas, Phys. Lett. B128(1983)112 E. L. Berger and F. Coester, Phys. Rev. D32(1985)1071

# ELECTRON SCATTERING AND MESON-EXCHANGE CURRENTS

B. Frois

DPhN/HE, C.E.N. Saclay, 91191 Gif sur Yvette, France

# 1. INTRODUCTION

Nucleon-nucleon (NN) interactions are traditionally described in terms of meson-exchange processes  $^{(1-3)}$ . A complete description of the nucleus should therefore take into account all the elementary degrees of freedom in the nucleus: nucleons, their various excitations and mesons. However, the complete nuclear wave function  $\frac{1}{2}(N,A,\ldots;\pi,\rho,\ldots)$  is not known even in the deuteron, and its calculation is at present beyond our capabilities. Non-nucleonic degrees of freedom are eliminated from the complete wave function  $\frac{1}{2}$  and nuclei are described by "dressed" nucleons interacting via a two-body potential.

One usually assumes that the nuclear response to an external current is just the sum of the contributions from individual nucleons. With this assumption (the impulse approximation), the current is absorbed by a single nucleon and the process described by a one-body But the external current can be absorbed at the same time that a nucleon interacts (i.e. exchanges a meson) with another nucleon, thus the elimination of non- nucleonic degrees of freedom from the wave function requires that the one body current supplemented by a two-body current. This additional current modifies the amplitudes of transitions induced either by an axial or a vector The observation and measurement of these non-nucleonic current. contributions to the current provides a direct insight on the nature of the nucleon-nucleon interaction.

Historically, significant deviations from the impulse approximation were observed in several electromagnetic data, but the first clear signal of the presence of meson-exchange current was found in the radiative capture of thermal neutrons by protons:

$$n + p \rightarrow d + \gamma$$

where a 10% discrepancy was observed between theory and experiment. This discrepancy is relatively small but nevertherless significant,

given the precision of the experimental result and the negligible uncertainties in the theoretical description of this reaction and in the asymptotic behavior of the deuteron wave function. This discrepancy was interpreted in 1972 by Riska and Brown as the first quantitative estimate of meson-exchange currents in the deuteron.

In this process the photon has only 2.2 MeV so its wavelength is too small to probe the spatial distribution of meson-exchange currents. The inverse reaction

$$e + D \rightarrow e' + n + p$$

For an energy transfer corresponding to the deuteron break-up energy i.e. 2.2 MeV, the deuteron is broken into a neutron-proton pair with a very small relative energy E 0. If in addition, the electron is scattered at an angle  $\theta$  180°, this electrodisintegration of the deuteron leaves the two-nucleon system in a quasibound  $^{1}S_{0}$  (T = 1) state. The variation of the cross section as a function of the momentum transfer is shown in Fig. 1. Theoretical predictions which take into account only nucleon degrees of freedom have a deep minimum at  $Q^{2} = 0.5 \; (\text{GeV})^{2}$  which clearly is not observed experimentally. The filling of this minimum is entirely due to the presence of meson-exchange currents. The full calculation which includes both nucleonic and mesonic degrees of freedom is in excellent agreement with experiment: this result is now considered as the classic example of the presence of meson-exchange in nuclei.

The central problem in the unambiguous observation of meson-exchange effects was for a long time the absence of theoretical framework. The breakthrough was the derivation of a general theoretical framework for the description of meson-exchange currents by Chemtob and Rho'' in 1971. Following the prescription of chiral symmetry and current algebra, they identified a clear hierarchy of processes. Prediction for weak and electromagnetic transitions was subsequently made by Kubodera, Delorme and Rho's. They have shown

that low-energy theorems allow one to make reliable predictions of the transitions that are strongly enhanced by meson-exchange currents.

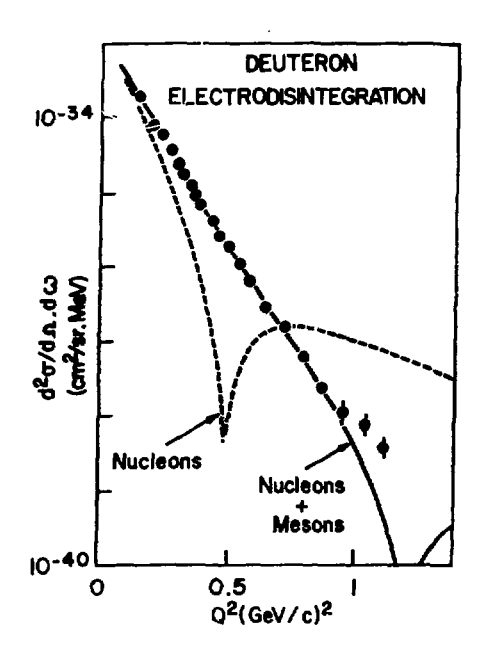


Fig. 1. Cross-section for deuteron electrodisintegration at threshold. The dashed curve represents the contribution of the one-body current. The solid curve includes the effects of two-body (meson-exchange) currents. The data are from Auditret et al. (Ref. 5). The curves depict the results of Mathiot (Ref. 5) with the Paris potential (Ref. 2).

# 2. ISOVECTOR MAGNETIC TRANSITIONS

In order to determine the range of validity of the mesonic theory, one Leeds to investigate meson-exchange currents as a function of momentum transfer. This is precisely what has been recently accomplished by electron scattering from few-nucleon systems. Electron scattering experiments disentangle charge and magnetization densities by varying the polarization of the virtual photon. The separation between isoscalar and isovector transitions can be made by studying different reactions and thus specific Leson-exchange processes can be

isolated. The interpretation of the results has essentially no ambiguity associated with the ground state wave functions of the  $\lambda=2$  and  $\lambda=3$  systems since one knows how to calculate exactly these nuclei in terms of nucleonic degrees of freedom.

The most convincing evidence for the presence of meson-exchange currents is found in magnetic isovector processes. Kubodera, Delorme and Rho'6' have shown that the contribution of two-body currents is on the same footing as nucleon currents and that a clear hierarchy of meson-exchange processes can be identified. We have already seen the classic example of the electrodisintegraton of the deuteron to the 'S The sensitivity of this reaction is due to guasibound state. destructive interference between one- and two-body a. litudes. At low momentum transfer, the wavelength of the virtual photons exchanged by electron scattering is too small to resolve meson and nucleon currents. When the momentum transfer increases, the pion-exchange is the first process which can be resolved. Its long range induces a large modification of the diffraction structure at relatively small momentum transfer. Below 0.5 (GeV/c)2, the only significant contribution is due to the pion-exchange current which is described in a natural extension of the soft-pion limit.

As the momentum transfer increases, the other meson-exchanges come into play according to the range of their interaction. Beyond  $Q^2=0.5~(\text{GeV})^2$ , one becomes sensitive to shorter range processes and in particular to the  $\rho$ -exchange and the excitation of the  $\Delta$ -isobar. The contributions of these different processes have opposite signs and tend to cancel each other. Surprisingly, the poinlike pion current contribution seems to be the only one which survives up to 1  $(\text{GeV/c})^2$ .

The <sup>3</sup>He form factors have been well known for a long time, but it is only recently that similar data for <sup>3</sup>H have been measured at MIT Bates laboratory and Saclay<sup>'10'</sup>. Thus, one can now separate  $F_S$  and  $F_V$  the isoscalar and isovector components of the A=3 form factors defined by:  $F_{S_{-V}} \propto F$  (<sup>3</sup>He)  $z \in F$  (<sup>3</sup>H).

This separation allows a direct comparison between isovector magnetic form factors of the two- and three-nucleon system. Figs. 1 and 2 show that the situation for isovector meson-exchange currents in the two- and three-nucleon system are identical. The nucleonic contribution to the cross section vanishes at a relatively small transfer due to a destructive interference between nucleonic amplitudes. When the same two-body currents which explain the isovector magnetic form factor for the electrodisintegration of the

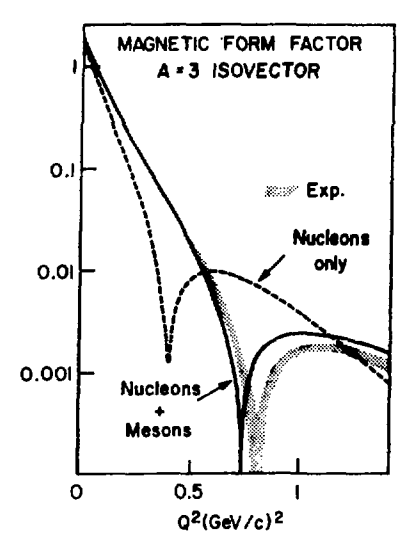


Fig. 2. Isovector magnetic form factor of the trinucleon system. The curves have the same definition as in Fig. 1. The shaded area represents the experimental result (J. Martino and S.K. Platchkov, Priv.Comm.).

deuteron are taken into account in the three-nucleon system, there is an excellent agreement between experiment and theory. Again, pion-exchange currents are the dominant contribution to the cross section up to  $Q^2 \sim 0.5 \, (\text{GeV/c})^2$ .

At higher momentum transfer, in the momentum transfer range  $0.5 \pm 0^2 \pm 1.2 (GeV/c)^2$ , isovector magnetic transitions become sensitive to medium- and short-range meson-exchange currents. Due to a cancellation between the "-exchange and the impulse approximation contributions. the differential cross-section for electrodisintegration at threshold is given almost p-exchange currents. The same is true for the three-body isovector magnetic form factor 11.12/. This form factor is of particular interest since a diffraction minimum is observed at about 0.8 (GeV/c) 2, while such a minimum has not yet been reached for the two-body system. The location of this minimum is particularly sensitive to the

cancellations between the various contributions of nuclear currents. The excellent agreement between experiment and theory for both the A=2 and A=3 systems demonstrate that mesonic theory gives an accurate description of the isovector one- and two-body currents.

# 3. ISOSCALAR MAGNETIC TRANSITIONS

Isoscalar meson-exchange currents have been observed in both the magnetic form factor of the deuteron  $B(Q^2)$  and the isoscalar part of the magnetic form factor of the trinucleon system. One of the largest contribution is due to the  $\rho n_\ell$  exchange shown in Fig. 8. In the vector dominance model, the  $\rho n_\ell$  vertex involves the following two-step process

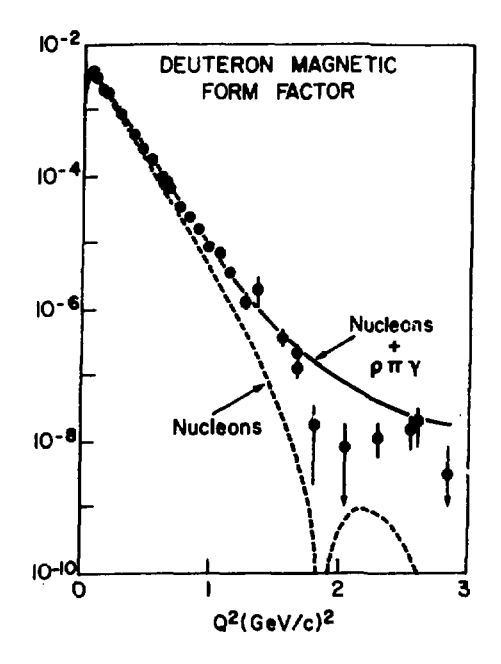


Fig. 3. Deuteron magnetic form factor  $B(Q^2)$  from Refs. 12-14. The dashed curve represents the contribution of the nucleonic (or one-body) current. The solid curve includes the effect of the dominant meson-exchange (or two-body current) due to the pay exchange current.

, (isoscalar)  $\rightarrow \omega \rightarrow \rho + \pi$ , or equivalently a 6 pion vertex. The interpretation of such vertex requires a highly non-perturbative approach.

Fig. 3 is a comparison of the experimental data with theoretical predictions for the magnetic form factor of the deuteron  $B(Q^2)$ . Besides the " $ho n_I$ " contribution, two other contributions must be included in order to have a consistent description of the electromagnetic current. The first one is a relativistic kinematical correction to the one-body current (spin-orbit and Darwin-Foldy terms). This correction contributes negatively to the magnetic moment of the deuteron (i.e. to the magnetic form factor at zero momentum transfer). Exact relativistic calculations in the impulse approximation incorporate these corrections to all orders, and show a significant decrease of the magnetic form factor for momentum larger than about 1 (GeV/C) . The second important correction originates from isobar components in the deuteron and in the three-nucleon system. contribution is positive and cancels to a large extent relativistic corrections discussed above. This explains qualitatively why a calculation which includes only the "par" exchange current 187 accounts for the experimental results 13.14 up to 1 (GeV/c)2.

The situation at higher momentum transfer indicates that the limits of this description have now been reached. Recent measurements performed at  $SLAC^{14}$  up to  $Q^2 = 3 (GeV/c)^2$  show a diffraction minimum at about 2  $(GeV/c)^2$ . This minimum cannot be explained when the " $\rho \pi /$ " contribution is the only meson-exchange current taken into account (Fig. 9). At these high momentum transfer, the intrinsic structure of the nucleon playes an important role 15, 16/. It has been shown recently by Nyman and Riska that the  $\rho\pi$ ) process can be derived in a model independent way from any effective Lagrangian constructed from Quantum Chromodynamics (this process is related to the topological structure of the nucleon and more specifically to the chiral anomaly embedded in the This first calculation based on the Skyrme Wess-Zumino term). description of the nucleon structure (Skyrmion) is in good agreement with experiment. This result is encouraging and the new description of meson-exchange currents in terms of the topological structure of the nucleon is one of the most interesting developments in this field.

# 4. BEYOND 1 (GeV/c)

Mesonic theory is a very efficient and economical description for nuclear processes involving momentum transfers up to  $1 (GeV/c)^2$ , but

for higher momentum transfers the situation is different. Besides relativistic effects, one must take into account short range processes which are essentially not known. In order to describe very short range processes, one needs to introduce more and more mesons of higher and higher mass. The one-boson approximation is no longer sufficient, and the description of the very short range component of the potential requires an infinite set of mesons strongly coupled together. It is obvious that one loses the simplicity of the mesonic description of the nuclear interaction for momentum transfers greater than 1 (GeV/c)2. In particular one should introduce not only one- and two-body operators but also three-, four- and many-body operators involving mesons and nucleons and the complete spectrum of nucleon excitations.  $Q^2 = 1 (GeV/c)^2$ , the complexity of the perturbative approach makes it untractable. One is now faced with the challenge of finding a new theoretical description for both short and long range processes in a consistent framework.

#### 5. CONCLUSIONS

Over the past few years nuclear currents have been carefully measured using high energy electrons. This study has revealed several processes dominated by meson-exchange currents. Specific meson-exchange processes have been isolated and their spatial distribution has been determined for relative distances between nucleons larger than 0.8 fm. One has clearly "seen" meson-exchange currents in nuclei.

A fully consistent description of the microscopic mechanisms in terms of mesons, nucleons and  $\Delta$  excitations has been achieved up to momentum transfers  $Q^2 \simeq 1~(\text{GeV/c})^2$ . This corresponds to relative distances between two nucleons larger than 0.8 fm. At this scale, two-body operators are constrained by general theorems and, in the long wavelength limit, meson-exchange currents are given by chiral symmetry. This explains the importance of the pion current in transitions induced by both axial and vector probes. Long range interactions are determined by a one-pion exchange while medium range interactions are described via dispersion relations in terms of  $2\pi$ -exchanges. We have shown that this fixes the limits of this theoretical framework to  $Q^2$  (  $1~(\text{GeV/c})^2$ .

In order to understand higher momentum transfer data, a description of the nucleon-nucleon interaction consistent with the nucleon substructure is needed. This requires to understand the

structure of the nucleon and to develop a theoretical framework valid for both non-perturbative long-wavelength interactions and perturbative short-wavelength interactions. This is clearly one of the most interesting challenges of nuclear physics.

#### ACKNOWLEDGEMENTS

I am very grateful to the organizers of this conference for their kind invitation and their warm hospitality. It is a great pleasure for me to meet in Dubna my colleagues from the Soviet Union.

This talk is based on a paper written in collaboration with J.F. Mathiot. I want to give him here my warmest thanks.

# REFERENCES

- 1) G.E. Brown and A.D. Jackson, The Nucleon-Nucleon Interaction, edited by North-Holland, Amsterdam 1976.
- M. Lacombe, B. Loiseau, J. M. Richard, R. Vinh Mau, J. Côté,
   P. Pirès and R. de Tourreil, Phys. Rev. C21 (1980) 861.
- 3) R. Machleidt, R. Holinde, Ch. Elster, Phys. Rep. 149, (1987' 1
- 4) D.O. Riska and G.E. Brown, Phys. Lett 38B (1972) 193.
- 5) S. Auffret et al., Phys. Rev. Lett. 55 (1985) 1362.
- W. Leidemann and H. Arenhövel, Nucl. Phys. A393 (1983) 385.
   J. F. Mathiot, Nucl. Phys. A412 (1984) 201.
- 7) M. Chemtob and M. Rho, Nucl. Phys. A163 (1971) 1.
- 8) K. Kulodera, J. Delorme and M. Rho, Phys.Rev.Lett 40 (1978) 78.
- J. Friar, B. Gibson and A. Payne,
   Ann. Rev. Nucl. Part. Sci. 36 (1986) 115.
- F.P. Juster et al., 55 (1985) 2261.
   D. Beck et al., Phys. Rev. Lett. 59 (1987) 1537.
- W. Strueve, Ch. Hajduk, P.U. Sauer and W. Theis, Nucl. Phys. A465 (1987) 651.
- 12) M. Gari and H. Hyuga, Nucl. Phys. A264 (1976) 409.
- 13) S. Auffret et al., Phys. Rev. Lett. 54 (1985) 649.
- 14) R.G. Arnold et al., Phys. Rev. Lett. 58 (1987) 1723.
- E.M. Nyman and D.O. Riska,
   Phys. Rev. Lett. 57 (1986) 3007; Nucl. Phys. A468 (1987) 473.
- 16) P.W. Sitarski, P. Blunden and E.L. Lomon, Phys. Rev. C36 (1987) 2479.

# PHYSICS WITH POLARIZATION DEGREES OF FREEDOM AT THE NEW ELECTRON STRETCHER ACCELERATOR ELSA IN BONN

W. Meyer

Physikalisches Institut der Universitaet Bonn Bonn, F.R. Germany

# 1. Introduction

Polarization experiments are an important tool to study the dynamics of elementary particle reactions. First information about a particle reaction is normally obtained by cross section measurements performed with unpolarized beams and unpolarized targets. In general these 'spin-averaged' cross sections are averages of many pure spin cross sections. Extensive experimental studies of spin effects in high or intermediate energy particle reactions have become available just since about 20 years ago. One reason for this delay is that such experiments were difficult or impossible to perform before polarized targets and polarized beams came into operation. If we are able to measure the spins of the incoming and outgoing particles as well as of the target nucleon in a certain reaction the corresponding observables give a great deal of information which is totally inaccessible to the spin-averaged cross section measurement. Hence, many of the most interesting and important features of the nucleon interaction can only be discovered by directly measuring the spin dependence with using polarized targets, polarized beams and (or) finalstate polarizations.

Polarization experiments in BONN at the 500 MeV (now closed) and 2.5 GeV electron synchrotrons have a long tradition. The recoil nucleon polarization, the target asymmetry from polarized protons and neutron targets and the beam asymmetry with polarized photons were measured for the photoproduction of mesons in the nucleon resonance region /1/. In recent years attention has been concentrated on the deuteron, especially on photodisintegration measurements with polarized deuteron targets.

In the following some remarks to the situation in the deuteron photodisintegration are made. Latest results for the target asymmetry measurement from polarized deuteron targets are presented. At the new stretcher accelerator ELSA in Bonn significant improvement of the experimental situation for  $\gamma$ -induced reactions is expected by the use of highly polarized targets in combination with a polarized tagged photon beam (PHOENICS-Experiment). The development of the radiation resistant colarized target material ammonia (NH $_3$  and ND $_3$ ) enables the use of polarized targets in electron beams /2/. Elastic efectron scattering from a tensorpolarized ND $_3$  target was performed and the measurement of the electric neutron form factor, Using a polarized electron beam and a polarized ND $_3$  target is in preparation (ELAN-Experiment).

# Deuteron photodisintegration

#### 2.1 General remarks

One of the basic problems in particle physics is the investigation of the nucleonnucleon interaction. At high energies the composite structure of the nucleon becomes apparent and the interaction is understood on the quark level. At low energies, as far as the nucleon is fundamental, the interaction is well described by the one pion exchange picture.

However, problems arise at 'higher' energies, as here the exchange of more and heavier mesons like p and w must be taken into account as well as isobar configurations. It is also not clear, how far the substructure (quarks) of the nucleons and the exchange particles must be considered.

The energy range from  $^\sim$  100 MeV to 3000 is the transition region from the classical nuclear physics to the high energy region, where the quarks are 'free' and their interaction can be described by perturbation theory. Mesonic exchange models as well as high energy quark models now try to include this intermediate energy region. The quark model opens another interesting aspect of the physics with light nuclei, as it constructs 'bags' with more than three quarks. An open question is the possible configuration of exotic states, consisting of e.g. qqq qqq ('dibaryon') as bound colourless objects /3/ /4/ /5/. The deuteron is a two nucleon system where all these aspects are relevant. The 'dibaryons' can be resonant intermediate states of such a two nucleon system. The deuteron ground state can also have a 6-quark admixture /6/. In conventional theories the 'dibaryons' are constructed e.g. as bound Na-,  $\Delta a$  - or NN-states /7/. However, both hypotheses are experimentally not proved.

In particular, the deuteron photodisintegration  $yd \rightarrow pn$  as a relatively simple reaction is a good tool for experimental and theoretical studies. The properties of the proton and neutron are well known and the binding energy of the nucleon is small. In addition, there are not problems with many particle approximation as with other heavier nuclei. However, both the theoretical and the experimental situation

in deuteron photodisintegration is unsatisfactory.

An experimental complication is given by the energy range, in which the dibaryon-resonances are predicted ( $\sqrt{s} = 2.1 - 2.4$  GeV). Here the contributions of many nucleon resonances are overlapping. It is expected that only with very precise measurements and for certain production reactions a small contribution of a collective 6-quark excitation can be detected. In addition to the direct search for resonances in the invariant mass of subsystems /8/ contributions of smaller amplitudes can be separated by measurements of polarization observables.

Due to the complicated spin structure of the deuteron photodisintegration reaction 12 complex helicity amplitudes are required to characterize completely the vd + pn process; hence 23 different observables have to be measured as a function of the

photon energy and the proton c.m.s. angle (see fig. 1).

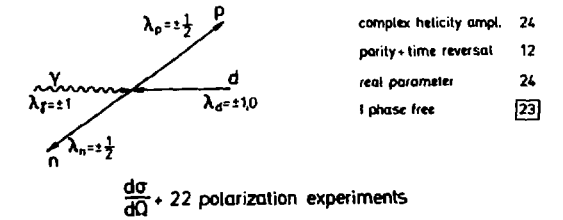


Fig.1. Proton- neutron center of mass system and helicities. For a complete description of the vd → pn reaction 23 experiments are needed.

Only few experiments have been performed to investigate single polarization quantities like target asymmetry (using a vector polarized deuteron target) /9/ beam asymmetry (using linearly polarized photons) /10/, and recoil-nucleon polarization /11/. Recently some double polarization measurements were done with linearly polarized photons, measuring the recoil proton polarization and the recoil neutron polarization. respectively /12/. Mentioned are only the most recent measurements.

# 2.2 Target asymmetry measurement from polarized deuteron targets

The latest results of the target asymmetry Ay for  $yd \rightarrow pn$  are plotted in fig. 2. The photon energy acceptance is 450 + 50 MeV, 550 + 50 MeV and 650 + 50 MeV, respectively. The errors include statisfical and systematical uncertainties. Up to now the deuteron photodisintegration is theoretically described in the nucleon-meson picture. There are a number of analyses. Some of them are based on non-relativistic calculations /13/, /14/, /15/, some on relativistic ones /16/, /17/, /18/, /19/.

References /17/ and /18/, in addition, include dibaryon resonances. Quark model calculations for the deuteron photodisintegration do not exist yet. A comparison of three analyses with the data is also shown in fig. 2. Fig. 3 shows the measured data point for the tensor asymmetry Ayy in comparison with two theoretical predictions. Although the measurement suffers from a large error, a contradition to the analyses is obvious. This first measurement demonstrates the feasibility of a tensor asymmetry experiment. On the other hand it is clear that further improved data are urgently needed. This is especially valid for the tensor observables.

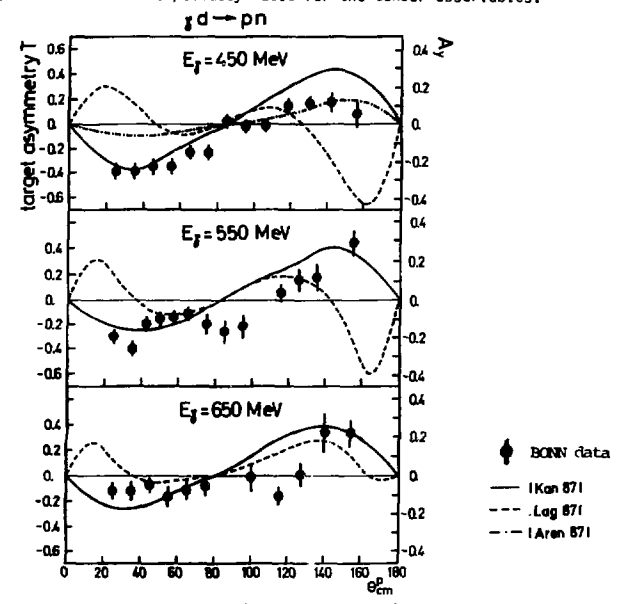


Fig.2. Target asymmetry data at  $\rm E_{\gamma}$  = 450 MeV, 550 MeV and 650 MeV together with three different theoretical calculations. At the vertical axis two different definitions for the target asymmetry are used.

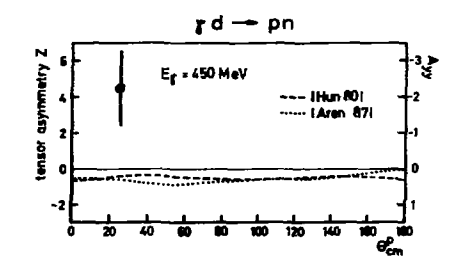


Fig.3. Tensor asymmetry data in comparison with two theoretical calculations.

# 3. Electron-deuteron scattering experiments

The elastic electron scattering off nuclei is an important tool to study short range nucleon-nucleon (N-N) interactions as well as mesonic exchange currents. At high momentum transfer  $q^2$  such experiments can also be sensitive to the above mentioned multiquark cluster inside the nuclei /20/ /21/ /22/ /23/. As an object to study this, the deuteron as the simplest nucleus is well suited.

# 3.1 Deuteron form factors

Polarization experiments are expected to play a central role in studies of the electric form factors of the nucleons. For the deuteron three form factors –  $F_C$ ,  $F_M$  and  $F_Q$ , for the charge, magnetic moment and quadrupole moment distributions – are required to specify completely its electromagnetic current. These form factors depend directly on the wave function of the deuteron. Measuring the three deuteron form factors is thus a test of our knowledge of the nucleon-nucleon interaction. The deuteron form factors are proportional to the electromagnetic form factors of the constituent nucleons and at high  $q^2$  uncertainties in (particularly the neutron form factors produce difficulties to extract information dependent only on the nucleon interaction. The cross section of the unpolarized elastic electron deuteron scattering can be written as:

$$\sigma_{\text{Unp}} = d\sigma/d\Omega_{\text{el}} = \sigma_{\text{Mott}} (A(q^2) + B(q^2) \cdot \tan^2 \frac{\sigma}{e}/2),$$

where  $^\sigma Mott = d\sigma/d\Omega Mott$  is the cross section for structureless particles,  $^\theta$  e is the laboratory scattering angle of the electron and  $q^z$  is the four momentum transfer squared. A(q^z) and B(q^z) contain the form factors of the deuteron:  $A(q^z) = F_c^{\ \ 2}(q^z) + 8/9_n^{\ \ 2} F_q^{\ \ 2}(q^z) + 2/3_n F_m^{\ \ 2}(q^z)$ 

$$A(q^2) = F_c^2(q^2) + 8/9n^2 F_q^2(q^4) + 2/3n F_m^2(q^2)$$

$$B(q^2) = 4/3n (1+n) F_m^2(q^2)$$
with  $n = q^2/4M_d^2$ .

In an unpolarized scattering experiment a separation of A(q²) and B(q²) can be achieved by accurate measurements over a range of angles  $^{6}e$ . From this,  $F_{m}$  and only a combination of  $F_{C}$  and  $F_{Q}$  can be determined. However, in the q²-range higher than D.4 (GeV/c²) it seems that  $F_{C}$  is very sensitive to various modifications of the deuteron wave function, due to mesonic exchange currents (MEC) and multiquark currents (6 quark cluster). In fig. 4 calculations for  $F_{C}$  based on the impulse approximation and modifications of the deuteron wave function due to MEC and 6-quark currents are shown.

10<sup>-1</sup>
1A+MEC+6Q
10<sup>-3</sup>
1A+MEC
100
05
100
Q<sup>2</sup> (GeV/c)<sup>2</sup>

Fig.4. Charge form factor  $F_C$  (q2) calculated by:

- impulse approximation (1A) /24/ - additional mesonic exchange currents (1A+MEC) /24/

- contribution of 2% 6-quark admixture (IA+MEC+6Q) /20/.

To separate  $F_{\rm C}$  and  $F_{\rm Q}$ , a polarization experiment is required. Especially at high q'such measurements are of great interest, since thy provide a sensitive test of the validity of perturbative QCD calculations to the electromagnetic form factors of nuclei. Carlson and Gross /25/ have shown that, with respect to the spin dependence of the elastic electron-deuteron scattering process, the results from QCD and classical nuclear physics are not the same. Therefore, a measurement of  $F_{\rm C}$  and  $F_{\rm Q}$  at high a enough q² would be a powerful tool in differentiating between these alternatives.

To achieve the separation of Fc and Fq, work has been started at the MIT-Bates Linear Accelerator Center by measuring the T20 observable by means of the determination of the recoil tensor polarization. In Novosibirsk the problem is studied by using a jet of polarized deuterium atoms as an internal target in the VEPP-2 storage ring /26/. Up to now electron scattering experiment with a polarized deuteron target did not exist. The discovery of ammonia as a polarized target material and its less sensitivity to radiation damage makes such experiments possible. In Bonn a first sensitivity to radiation damage makes such experiments that the sensitivity to radiation damage makes such experiments possible. In Bonn a first (GeV/c²) was performed. The data are in evaluation /27/.

# Planned polarization experiments at ELSA

# 4.1 Photon induced experiments

For a new generation of experiments a substantial improvement of the beam duty cycle is necessary. Several electron accelerators with high duty cycle have been proposed or are under construction. A cw-microtron for 180 MeV (Mami A) has been used in Mainz and is now being extended to 800 MeV. In the United States a superconducting continuous wave electron accelerator for 4 GeV is under construction (CEBAF). The BONN Electron Stretcher Accelerator ELSA is the first operating cw-accelerator in the GeV range. Tts relatively low intensity is ideally matched to large solid angle detectors in connection with energy marked photons (tagging systems) and polarized solid state nucleon targets. Fig. 5 shows a floor map of the Bonn accelerator facility.

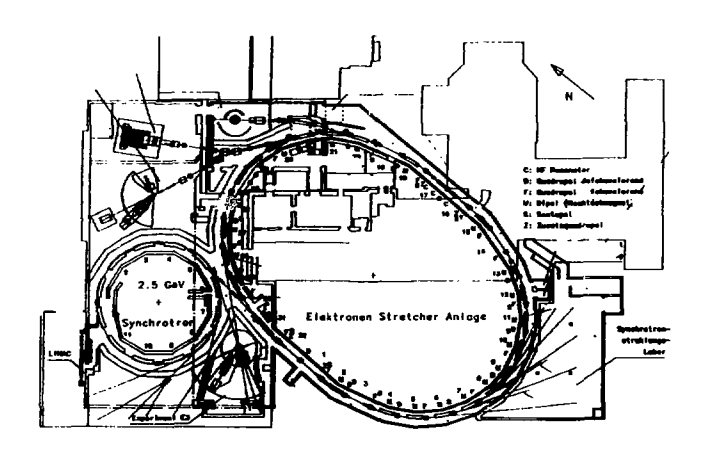


Fig.5. Floor map of the Bonn facilities: 2.5 GeV electron synchrotron and 3.5 GeV Electron Stretcher and Accelerator ELSA.

ELSA is designed to operate in two modes:

- 1) a pure stretcher mode with 95% duty factor up to 2.0 GeV
- 2) a post accelerator mode which gives energies up to 3.5 GeV to study higher mass resonances.

The estimated internal and external beam intensities are compiled in the Table.A detailed description of ELSA is given in ref. BONN IR-87-30.

Table

	Mode	Mode of operation Stretcher Post Accelerator		Pulses from
l	Stretcher			
	95% Duty Factor	60% Duty Factor	5% Duty Factor	Synchrotron
Internal Beam	12 mA	12 mA 24 mA	12 mA 24 mA 60 mA	1 2 5
External Electron Beam (average)	200 nA	5 nA 10 nA	10 nA 20 nA 50 nA	1 2 5
Bremsstrahlung from Internal Target at 1.8 GeV (photons/ min)	1011	2 x 10° 5 x 10°	5 x 10° 1 x 10°° 2 x 10°°	1 2 5

Many of the interesting photoproduction experiments at intermediate energies need detection of multiparticle final states. Therefore the rather complex magnetic detector system SAPHIR (Spectrometer Arrangement for PHoton Induced Reactions /8/ with a large acceptance is Deing built which will be operated in one of the tagged photon beams of ELSA. At the beginning there is no plan to use a polarized target within this system, as the technical problems are very serious. It seems, however, obvious that a frozen spin target is the most feasible solution. To perform (double) polarization experiments at ELSA the PHOENICS (PHOton Experiment on Nuclei In Counter Set-up) set-up for the investigation of two-body reactions is under construction. As In the case of SAPHIR these experiments will be performed with tagged photons.

#### 4.2 PHOENICS - experiment

The experimental set-up PHOENICS for the study of two body reactions at ELSA is

shown in fig. 6.

frezen apin ( crystal ) radiator (polarized) 1 m

Fig.6. Set-up PHOENICS for (double) polarization experiments, using a 'tagged' (polarized) photon beam and a frozen spin target.

The apparatus consists of a tagging spectrometer and a scintillation counter arrangement around a polarized target. A description of the bremsstrahlung tagging is given in ref. /28/. This large acceptance detection is especially useful for measurements of YN  $^+$  "N, Yd  $^+$  pn or of Y  $^3$ He  $^+$  pd etc. For a complete description of these reactions many (double) polarization experiments must be performed. As a consequence, the polarized target, which will operate in the frozen spin mode, and a polarized photon beam will play an important role in this measuring program.

An important feature of such an experimental set-up is e.g. the very high relative accuracy which can be reached. The simultaneous coverage of a large kinematical range of interest is advantageous, as changes of the beam- or target polarization, beam intensity, detector efficiency etc. will affect all data in the same way. This is a necessity for the search of small structures in energy and angular distributions caused by narrow resonances or by interference effects. In addition, the monochromatic ('tagged') photon beam offers some advantages in comparison to the conventional bremsstrahlung beam:

- the photon energy k is determined by the energy difference between the initial and the final state electron: k = Eq - E, independent from the hadron detection,
- the photon flux normalization is directly given by the counting rate of the 'tagging' counters,
- a kinematical overdetermination can be achieved by coincident detection of both outgoing particles. This is important for the suppression of (i) background at low cross section levels,
  - (ii) nuclear events in the case of a polarized proton or deuteron target,
- in the case of a polarized 'tagged' photon beam (see below) the beam polarization can be measured permanently.

By using a diamond as target linearly polarized monochromatic photons will become available. For future experiments also measurements with circularly polarized photons (produced by the bremsstrahlung of longitudinally polarized electrons) are planned. In this case, however, a new beam transport system must be built which rotates the spins (vertical in ELSA) into the desired longitudinal direction at the target over a wide energy range. With this facility seven (or more) independent experiments on YN  $^+$  mN, necessary for a complete determination of the helicity amplitudes, can be performed.

At the moment a complete measurement of the deuteron photodisintegration reaction  $\forall d$  + pn can not be realized (23 observables). The low cross section at higher energies ( $k_Y$  > 700 MeV) makes polarization experiments extremely difficult. New techniques like the use of tensor polarized deuteron targets and a polarized photon beam, however, can increase the number of possible experiments in the future.

# 4.3 Polarized electron scattering from polarized neutrons.

Elastic electron-neutron scattering is described by the electric and magnetic form factors  $F_{en}$  ( $q^2$ ) and  $F_{mn}$  ( $q^2$ ). The unpolarized cross section is given by

$$\begin{split} &\sigma unp = dc/d\Omega e | = \sigma_{MOtt} \quad [A(q^2) + B \ (q^2) * \tan^2(Oe/2)] \\ &A \ (q^2) = Fen^2 \ (q^2) + nFmn^2 \ (q^2) \\ &B(q^2) = 2n \quad (1 + n \ ) \ Fmn^2 \ (q^2) \\ &with \ n = q^2/4Mn^2 \, . \end{split}$$

In general, it is very difficult to measure the neutron form factors because there are no free neutron targets and the detection of the recoil neutrons also causes problems. The magnetic form factor  $F_{mn}$  is the best known because it is relatively large. The electric form factor  $F_{en}$  is very small and therefore generally very poorly known. Away from  $\mathbf{q}^z = \mathbf{0}$ ,  $F_{en}$  is obtained from quasi-elastic electron deuteron

scattering, however dominated by large statistical errors /29/. The most precise values of Fen, ranging from zero to about 0.10 have been obtained from elastic eD scattering /30/. There, the largest uncertainty results from the deuteron model dependence which strongly influences the extracted values of Fen. The knowledge of the neutron electric form factor is essential for accurate calculations of the electromagnetic interactions of nuclei, especially the deuteron, which is used to study the short range nuclear force, meson currents, exotic states or quark effects. For all these investigations a model independent measurement of Fen is urgently required. Therefore, it was suggested to measure the polarization of recoil neutrons produced by scattering of polarized electrons from unpolarized neutrons /31/. Due to the low efficiency (~10°) of the neutron polarimeter, such an experiment requires a high current polarized electron beam.

As shown in the elastic electron deuteron experiment with a tensor polarized target scattering off polarized electrons from polarized neutrons (ND $_3$ ) can be now considered as an alternative possibility to study  $F_{\rm en}$  at ELSA. For an orientation of the neutron spin in the electron scattering plane perpendicular to the virtual photon direction the elastic electron-neutron cross section is given by /31/:

$$d\sigma/d\Omega = (d\sigma/d\Omega)und [1 + Pe Pn An (q^2)]$$
.

where Pe is the electron polarization and Pn the effective neutron polarization inside a deuterated target material. The neutron asymmetry  $A_n = \iota \sigma (t+) - \sigma (t+) / [\sigma(t+)] + \sigma(t+)]$ 

$$A_{n} (q^{2}) = \frac{? \cdot (1+n) \cdot F_{en} \cdot F_{Mn} \cdot \tan(n_{e}/2)}{A(q^{2}) + B(q^{2}) \cdot \tan^{2}(n_{e}/2)}$$

As far as the polarized target is concerned the experiment is similar to the form factor measurement of the deuteron, as we have to use the same target material. By using the deuteron-rich and radiation-resistant target material ND, an effective neutron polarization of 0.13 can be achieved in a magnetic field of 3.5 Tesla. However, the measured neutron asymmetry is further diluted by the polarization of the incident electron beam. Acceleration of polarized electrons in the 2.5 GeV electron synchrotron in Bonn has been successfully performed some years ago /32/. In the meantime, a new source on the basis of the photoeffect on GaAs with polarized laser light is installed. In ELSA an extracted average current of 7 nA in the pure stretcher mode and an electron polarization of 0.3-0.4 is expected. The electron beam line is designed (superconducting solenoid) to supply longitudinally polarized electrons at the target. The measurement of An and hence Fen can be performed with very small systematic errors. Since the polarization of the incident electron beam can be switched on pulse-to-pulse basis the influence of changes in the detector efficiencies is very much reduced. Systematic uncertainties arising from the binding of the neutron inside the deuteron can be controlled by a simultaneous measurement of the proton asymmetry Ap  $(q^2)$  for polarized deuterons and comparing it to Ap  $(q^2)$ measured at free polarized protons, using NH, as target material:

$$V_{\text{U}}^{\text{Lie}}(d_1) = V_{\text{U}}^{\text{U}}(d_1) * \frac{V_{\text{D}}^{\text{U}}(d_2)}{V_{\text{D}}^{\text{U}}(d_2)}$$

This measurement is one of the most important electron scattering experiments which can be performed at ELSA in the near future. The nucleon form factors belong to the fundamental functions in the nuclear and particle physics. At the moment, however, the knowledge of the charge form factor of the neutron Fen is extremely unsatisfactory compared to its importance.

# References

- /1/ W. Meyer, BONN-IR-85-41
- /2/ W. Meyer, Nucl. Phys. A446 (1985) 381
- /3/ R.L. Jaffe, Phys. Rev. Lett. 38, 5 (1977) 195
- /4/ C. de Tar, Phys. Rev. D17 (1978) 323
- /5/ P.J.G. Mulders, Dissertation 1980, Nijmegen
- /6/ V.A. Matveev and P. Sorba, Lett. Nuovo Cim. 20 (1977) 435
- /7/ C.W. Wong, Phys. Rep. 136 no1 (1986) 1
- /8/ W.J. Schwille, Proc. CEBAF Workshop, Newport News 1986
- /9/ K.H. Althoff et al., Z. Phys. C26 (1984) 175
- /10/ F.V. Adamyan et al., JETP Lett. 395 (1984) 286
- /11/ A.S. Bratashevskiy et al., Preprint KhFTI 84-9, Kharkov (1984)
- /12/ V.P. Barannik et al., Nucl. Phys. A451 (1986)751
- /13/ J.M. Laget, Nucl. Phys. A312 (1978) 265
- /14/ M. Anastasio and M. Chemtob, Nucl. Phys. A364 (1981) 219
- /15/ H. Arenhövel, Nuovo Cimento 76A (1983) 256
- /16/ K. Ogawa et al., Nucl. Phys. A340 (1980) 451
- /17/ H. Huneke, BONN-IR-80-24
- /18/ H. Ikeda et al., Nucl. Phys. B172 (1980) 509
- /19/ Y. Kang, BONN-IR-86-20
- /20/ A.P. Kobushkin und V.P. Shelest, Sov. J. Part.Nucl. 14 (1978) 483
- /21/ V.A. Matveev and P. Sorba, Il Nuovo Cim. 45A (1978) 257
- /22/ V.V. Burov et al., Z. Phys. A315 (1984) 205
- /23/ M. Oka and K. Yazaki, Nucl. Phys. A402 (1983) 477
- /24/ M. Gari and H. Hyuga, Nucl. Phys. A264 (1976) 409
- /25/ C.E. Carlson and F. Gross, Phys. Rev. Lett. 53 (1984) 127
- /26/ D.K. Vesnovsky et al., Preprint INP 86-75
- /27/ H.D. Schablitzky, BONN, Disteration in preparation
- /28/ J. Arends, BONN-MS-88-03
- /29/ W. Bartel et al., Nucl. Phys. 858 (1973) 429
- /30/ S. Galster et al., Nucl. Phys. B32 (1971) 221
- /31/ R. Arnold, C.E. Carlson and F. Gross, Phys. Rev. C23 (1981) 363
- /32/ W. Brefeld et al., Nucl.Instr. and Meth. 228 (1985) 228

# ELECTROMAGNETIC STRUCTURE OF FEW-BODY SYSTEMS

#### S. Kowalski

Bates Linear Accelerator Center Laboratory for Nuclear Science and Department of Physics Massachusetts Institute of Technology Cambridge, MA 02139 USA

# I. Introduction

The study of few-body nuclear systems forms the cornerstone of our basic understanding of nuclear forces and nuclear structure. These simple systems are an ideal testing ground. The elastic form factors of the nucleon, deuteron, tritium and helium provide fundamental information on the radial distribution of charge and magnetism. Quasielastic data is important to our understanding of the momentum distribution of nucleons in nuclei.

On the theoretical side the goal has been a precise description of nuclear interactions in the nuclear medium. Current models incorporate realistic nucleon-nucleon potentials with mesonic exchange currents, isobar configurations, relativistic effects and constituent quark degrees-of-freedom.

We review in this report some of the most recent results on the electromagnetic properties of few-nucleon systems. These data are compared with the best available model descriptions. We also discuss some of the ideas for new experiments which are now being planned and which will address some of the key open questions over the next couple of years.

The present generation of high current, medium energy electron accelerators combined with improvements in detectors and experimental techniques has pushed our knowledge of the electromagnetic properties of the few-nucleon systems to higher momentum transfers and to much better accuracy. Recently we have started to exploit the measurement of spin observables as well. We note that this added capability will in the future be crucial in providing precise measurements of fundamental nuclear properties which have been precluded up to now.

# II. Neutron Electric Form Factor

The cross section for elastic scattering of unpolarized electrons from unpolarized nucleons ( $J_i \sim 1/2$ ) is given by

$$\frac{dg}{d\Omega} = \sigma_{H} f^{-1} \left[ G_{gH}^{2} (Q^{2}) + r G_{HH}^{2} (Q^{2}) \left\{ 1 + 2(1+r) \tan^{2} \frac{\theta}{2} \right\} \right].$$

where

$$\tau = -Q^2/4M_a^2.$$

The electric and magnetic form factors,  $G_{gg}(Q^2)$  and  $G_{egg}(Q^2)$ , are related to the usual  $F_{\nu}(Q^2)$  and  $F_{\nu}(Q^2)$  by

$$\sqrt{4\pi} F_{\tau} = (1+\tau)G_{FN}$$
 and  $\sqrt{4\pi} F_{\tau} = -\sqrt{2\tau(1+\tau)} G_{FN}$ 

The Rosenbluth separation of the two form factors allows for precise determination of both amplitudes only when they are comparable. In the case of the nucleons, the magnetic form factor dominates over the electric one at high momentum transfers. As a result the electric form factor is relatively poorly known.

The electric form factor, which is related to the nucleon charge distribution, is a funadmental quantity whose knowledge is important for the detailed understanding of both nucleon and nuclear structure. For the proton, reasonable knowledge of  $G_{\rm gp}$  exists only up to  $4({\rm GeV/c})^2$ . For the neutron, which is charge neutral,  $G_{\rm gp}$  is very small and as a result is very poorly known for all momentum transfers.

The Rosenbluth decomposition of electron-deuteron elastic and quasi-elastic scattering is used to provide a measure of  $G_{\rm go}$  and  $G_{\rm ph}$ . Interpretation of the results is plagued with both model dependence and large systematic errors. Fig. 1 shows some typical data for  $G_{\rm go}$  up to  $q^2\sim 1.5({\rm GeV/c})^2$ .

To improve our present knowledge of  $G_{\rm ph}$  requires the exploitation of spin observables in electron scattering. For the nucleon case  $(J_4=1/2)$  polarized electrons in combination with polarized targets or the measurement of a recoil nucleon polarization can provide accurate new information. The polarization cross section (part of the cross section which is proportional to electron helicity) for

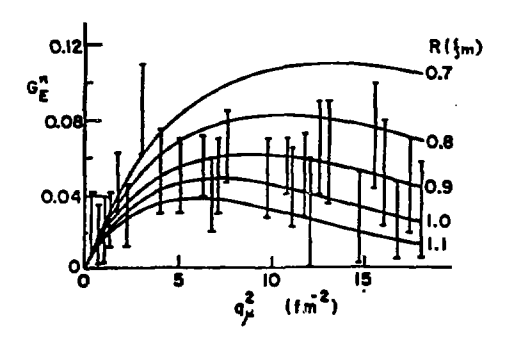


Fig. 1. Neutron electric form factor for different bag radii and existing experimental data.

scattering polarized electrons from polarized nucleons may be written as

$$\begin{split} &\Delta = - \Sigma_0 \bigg[ \overline{\mathcal{I}} \ F_{_{\!\!\!\!T}}^{\,2}(q) v_{_{\!\!\!\!T}}, \ \cos \! \theta^{\, *} + 2 \overline{\mathcal{I}} \ F_{_{\!\!\!T}}^{\,2}(q) F_{_{\!\!\!T}}^{\,2}(q) v_{_{\!\!\!TL}}^{\,2} \ \sin \! \theta^{\, *} \! \cos \! \phi^{\, *} \bigg] \ \overline{\mathcal{I}} \ F^2(q) \,, \end{split}$$
 where  $F^2(q) = v_{_{\!\!T}} F_{_{\!\!T}}^2(q) + v_{_{\!\!T}} F_{_{\!\!T}}^2(q) \,.$ 

 $\Sigma_0$  is the unpolarized cross section,  $\theta^*$  and  $\phi^*$  measure the orientation of the target polarization, and the  $\mathbf{v}_i$  are the usual kinematic factors. A measurement of the asymmetry,  $\Delta/\Sigma_0$ , or equivalently that of the recoil nucleon polarization by means of a second scattering directly involves the interference term  $\mathbf{F}_L(\mathbf{q})\mathbf{F}_T(\mathbf{q})$  which provides a measure of the small form factor and their relative sign.

Possible experiments which will be exploited to measure the neutron electric form factor  $\mathbf{G}_{\mathbf{e}_n}$  include:

$${}^{2}\vec{H}(\vec{e},e'n)p$$
 exclusive  ${}^{2}\vec{H}(\vec{e},e')x$  inclusive  ${}^{2}\vec{H}(\vec{e},e')x$  inclusive  ${}^{3}\vec{H}e(\vec{e},e')x$  inclusive

The sensitivity to  $G_{\underline{p}n}$  of the polarized-electron polarized-deuteron experiment has been evaluated by Cheung and Woloshyn<sup>2</sup>. The results for the cross section and polarization asymmetry at an electron energy of 1 GeV are shown in Fig. 2. The deuteron is polarized in the scattering plane at 45° to the incident electron direction. The neutron electric form factor has been parameterized by:

$$G_{En}(Q^2) = \frac{-\mu_n r}{(1+\eta r) \left[1 + \frac{Q^2(GeV)^2}{0.71}\right]^2}$$

with  $0<\eta<\infty$ . The asymmetry shows large sensitivity to  $G_{\rm En}$  and is measurable.

The sensitivity to  $G_{gn}$  has also been calculated for scattering from polarized  $^3$ He. In a simple picture, since the two protons in  $^3$ He have opposite spins, all of the spin-dependent effects should be primarily due to the neutron. The predicted results are shown in Fig. 3. The same parameterization was used for the neutron electric form factor and  $\beta$  is the angle in the scattering plane between the polarization axis of  $^3$ He and the incident electron direction.

An experiment to measure  $G_{\rm En}$  by scattering polarized electrons from an unpolarized deuterium target is under development at MIT-Bates<sup>4</sup>. The recoil neutron polarization will be measured using np elastic scattering. At  $Q^2 = 0.41 ({\rm GeV/c})^2$  it is projected that an uncertainty  $\Delta G_{\rm En} = \pm .016$  can be achieved. Theoretical considerations<sup>5</sup> indicate that effects due to final state interactions, mesonic exchange and isobar configurations are negligible for scattering at the quasi-free kinematics.

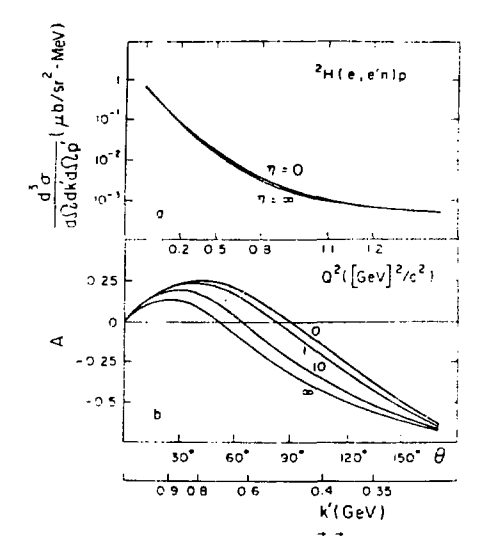


Fig. 2. Exclusive cross section for  ${}^2\vec{H}(\vec{e},e'n)p$  at quasifree kinematics for different neutron electric form factors using 1 GeV incident electrons. Asymmetry with respect to change in the electron longitudinal polarization for different neutron electric form factors. The deuteron is polarized at 45° to the incident electron direction.

A second complimentary experiment involving polarized  ${}^3\overline{\text{He}}$  is also being developed at NIT-Bates<sup>6</sup>. Closed cell targets of polarized  ${}^3\overline{\text{He}}$  with densities in excess of  $10^{19}\text{cm}^{-2}$  and polarizations of approximately 50% are available. These will allow measurements with external polarized beams at reasonable luminosities for  $Q^2 \sim (0.1-0.2)(\text{GeV/c})^2$ . A feasibility experiment to measure  $G_{\overline{\text{He}}}$  will be carried out next year, followed by a  $G_{\overline{\text{e}}}$  measurement in the future.

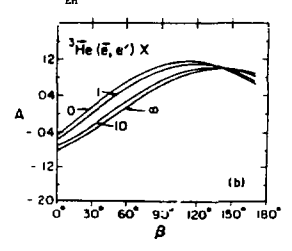


Fig. 3. Asymmetries as a function of target polarization angle  $\beta$  for inclusive polarized electron-<sup>3</sup>he scattering at the quasifree peak. Incident 1.5 GeV electrons are scattered at 60° for different choices of the neutron electric form factor.

Future experiments involving polarized targets can also make use of the internal target capabilities at the new electron stretcher-storage ring facilities which are under construction. The present technology for polarized targets would make such high luminosity internal target experiments possible. Such facilities are likely to provide our most precise measurements of  $G_{\rm gn}$  over an extended range of q. Plans are underway at HERA<sup>7</sup>, for example, to use polarized  $\vec{\bf D}$  and  $^3\vec{\bf He}$  together with polarized electrons to measure at high energies the spin-dependent structure functions of the nucleons.

# III. Deuteron Electromagnetic Structure

#### 1. Elastic Form Factors

As the simplest bound nuclear system the deuteron has been an important testing ground for our fundamental understanding of nuclear structure. Electron-deuteron scattering provides information on the short range behavior of the deuteron wave function as well as a measure of non-nucleonic degrees of freedom. Quark degrees of freedom are expected to contribute at large  $q^2$ .

A complete description of the electromagnetic properties of the deuteron (J-1) requires a measurement of three form factors: charge monopole  $(F_{\underline{u}})$ , charge quadrupole  $(F_{\underline{u}})$  and magnetic dipole  $(F_{\underline{u}})$  as a function of momentum transfer.

The cross section for elastic electron-deuteron scattering may be written as:

$$\begin{split} &\frac{d\sigma}{d\Omega} = \sigma_{\text{H}} \left[ A(q^2) + B(q^2) \tan^2 \frac{\ell}{2} \right] \\ &\text{where} \\ &A(q^2) = F_c^2(q^2) + \frac{8}{9} \eta^2 F_Q^2(q^2) + \frac{2}{3} \eta F_H^2(q^2) \\ &B(q^2) = \frac{4}{3} \eta (\eta + 1) F_H^2(q^2) \\ &\eta = q^2 / 4 M_c^2 \; . \end{split}$$

The nuclear physics is contained in the two structure functions  $A(q^2)$  which is dependent on the charge, quadrupole, and magnetic form factors, and  $B(q^2)$  which depends only on the magnetic form factor. They have been measured to high  $q^2$ .  $A(q^2)$  is known out to  $q^2 = 4(\text{GeV/c})^2$ . A recent measurement at SLAC® has determined  $B(q^2)$  out to  $q^2 = 2.77(\text{GeV/c})^2$ . It is in qualitative agreement with impulse-approximation calculations. These data provide a direct measure of  $F_{\text{N}}$  but  $F_{\text{C}}$  and  $F_{\text{Q}}$  cannot be separated in a model independent manner. The location of a possible zero in the charge monopole contribution is important to our understanding of the validity of different potential models as well as providing a measure of two-body currents.

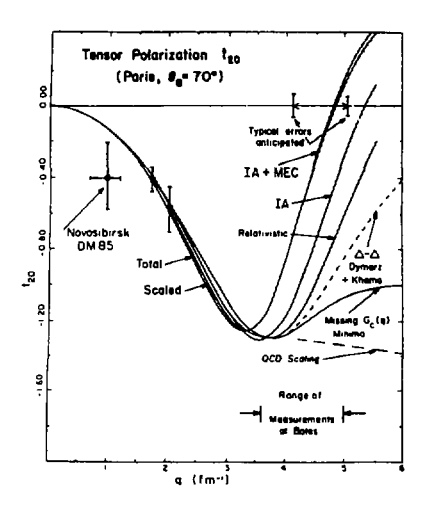


Fig. 4. Comparison between different theoretical predictions for deuteron  $\mathbf{t}_{20}$  including QCD scaling,  $\Delta$ - $\Delta$  admixtures and the effect implied by filling in of the minimum in  $G_c(\mathbf{q})$ . The Novosibirsk and Bates experimental data are shown as well as the q-range and anticipated sensitivity of a recently completed high-q  $\mathbf{t}_{20}$  experiment at Bates<sup>11</sup>.

The measurement of a spin observable allows, in principle, the complete separation of the individual multipole contributions. The  $t_{20}$  component of the tensor polarization of the recoiling deuteron is given by

$$\mathbf{t_{20}} = -\sqrt{2} \ \sigma_{_{\!M}} \left[ \frac{4}{9} \eta^2 F_{_{\!Q}}^2 + \frac{4}{3} \eta F_{_{\!C}} F_{_{\!Q}} + \frac{1}{3} \eta F_{_{\!M}}^2 \left\{ \frac{1}{2} + (1\!+\!\eta) \tan^2 \frac{\ell}{2} \right\} \right] \bigg/ \frac{d\sigma}{d\Omega} \ .$$

The most important contribution to  $t_{20}$  in the momentum transfer range  $q^2 < 1.2$  (GeV/c) $^2$  comes from the interference term  $F_cF_q$ . The observable  $t_{20}$  provides the additional handle which allows a separation of the multipole contributions.

In an earlier Bates experiment  $^{10}$  the tensor polarization was determined by measuring the polarization of the recoil deuterons in coincidence with the scattered electrons. Such an experiment involves a second analyzing scattering of known sensitivity to tensor polarized deuterons. The reaction  $\overline{\mathbf{d}}(^3\mathrm{He},\mathbf{p})$  was used as an analyzer. The extracted values of  $\mathbf{t}_{20}$  are compared with theoretical predictions for several realistic potential model calculations in Fig. 4. Also shown is an experimental point at lower q from Novosibirsk.

Extensions of these measurements to higher momentum transfer have just been completed at Bates<sup>11</sup>. These higher momentum transfers involve some

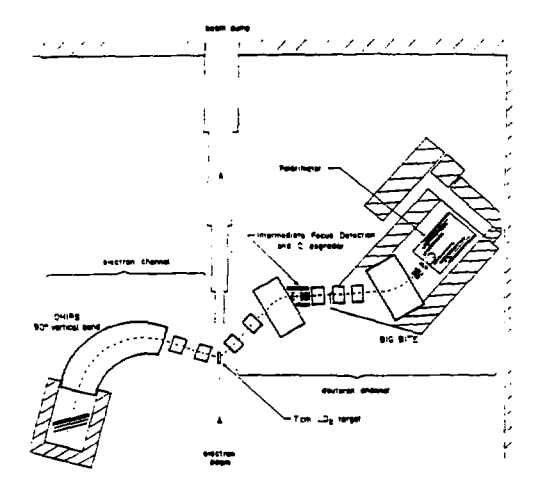


Fig. 5. Schematic layout of the Bates high-q t20 experiment.

very interesting physics. The potential model predictions are sensitive to two-body currents while perturbative QCD predictions are entirely at variance with the potential model results.

The deuteron polarimeter  $^{12}$  for these latest measurements was based on (dp) elastic scattering. The polarimeter, which was calibrated at Saturne, shows high  $T_{20}$  analyzing power for deuteron energies between 80 and 200 MeV. The energy dependence is weak and the overall polarimeter efficiency is quite high,  $-2 \times 10^{-3}$ . A schematic layout of the experiment showing the electron arm, deuteron channel and polarimeter is presented in Fig. 5.

Measurements at values of  $Q^2(fa^2)=14.2$ , 17.6 and 21.2 have been completed. The statistical uncertainty in the tensor polarization is projected to be  $\Delta t_{20}=\pm0.1$ . Detailed analysis of this data as well as an understanding of the systematic errors is presently underway. Final results are expected within the next year.

An alternative approach for determining t<sub>20</sub> involves measuring the asymmetry in elastic electron-conteron scattering from a tensor polarized target. Such measurements are presently underway at both Bonn and Novosibirsk. Holt<sup>13</sup> at ANL is developing a tensor polarized deuterium target for use as a gas jet internal to a storage ring. A target density of -10<sup>14</sup> atoms/cm<sup>2</sup> in a circulating current of 100mA results in luminosities of the order of 10<sup>32</sup>cm<sup>2</sup>s<sup>11</sup>. Such a high density of polarized deuterium nuclel is obtained by using optically-pumped polarized alkali atoms which transfer polarization to deuterium atoms by atomic spin exchange.

Densities in excess of 10<sup>15</sup> atoms/cm<sup>2</sup> appear feasible with present-day techniques.

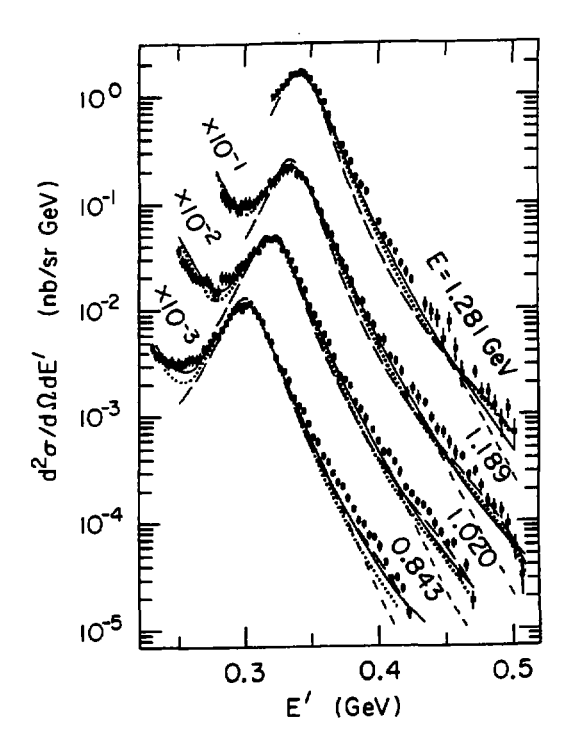


Fig. 6. Cross sections for d(e,e') as a function of scattered electron energy E' for four values of the incident energy E. The dotted curves are Lager<sup>18</sup> PWIA calculations. The short dashed arrows use the PWIA formula of McGee-Durand<sup>16</sup> with the Bonn potential. The solid curves are the full calculations of Lager<sup>18</sup> and the long dashed those due to Arcenhovel<sup>17</sup>; both using the Paris potential.

### 2. Transverse Quasielastic Scattering

Inelastic electron scattering from the deuteron provides important tests of our understanding of the nucleon-nucleon interaction. The importance of contributions such as final state interactions, mesonic exchange currents and isobar configurations beyond the simple Plane Wave Impulse Approximation can be ascertained. At the top of the quasielastic peak the impulse approximation is expected to be valid since the other effects are calculated to be small. Other interaction effects are expected to show up mainly on the high and low momentum sides of the quasielastic peak. Data at high momentum transfers can provide

information on relativistic effects and the role of constituent quarks in a proper description of the short range nucleon-nucleon interaction.

An experiment has just been completed at NPAS-SLAC on transverse (180°) inelastic electron scattering from the deuteron in the quasielastic region. Cross sections were measured 4 from breakup threshold to beyond the quasielastic peak for incident energies of 0.843, 1.020, 1.189 and 1.281 GeV, corresponding to  $0.75 \le Q^2 \le 2.57$  (GeV/c)<sup>2</sup>. These data are shown in Fig. 6. Also shown are various model predictions. The data are in reasonable agreement with nonrelativistic model calculations which include final state interactions and meson exchange currents. The largest discrepancies occur near the region of the break-up threshold and in the region of real pion production.

At the top of the quasielastic peak the models do very well in describing the process. Data in this region have often been used to extract information on the neutron elastic form factors. Values of  $G_{\rm No}$  extracted from this new data have been found to be in good agreement with both the dipole model  $G_{\rm p} = \mu_{\rm p}/(1+Q^2/0.71)^2$  and with the results from previous experiments.

### IV. 3H/3He: Three-Body Nuclear Systems

The three body nuclear systems (3H and 3He) have been fertile testing grounds for the study of nucleon interactions as we go from the simplest system, the deuteron, to more complex nuclei. Exact solutions of the non-relativistic wave equation for the ground state have been obtained using realistic two-body interactions. Experimental information on the importance of isospin dependent effects, the influence of 3-body forces, relativistic effects, non-nucleonic degrees of freedom, etc. is essential to further our basic understanding of the description of these nuclei.

For several years now we have had complete and precise data on the charge and magnetic elastic form factors for <sup>3</sup>H and <sup>4</sup>He. We have seen that the simple impulse approximation, which accounts only for nucleon currents, cannot describe the data. An explicit introduction of non-nucleonic degrees of freedom is required for a proper description. Uncertainties involving the importance of and the correct framework for incorporating relativistic effects and 3-body interactions remain.

Inclusive quasi-elastic electron scattering experiments have measured the longitudinal (scattering from charges) and transverse (scattering from currents and spins) contributions to the cross sections for several nuclei from carbon to uranium. The results are poorly described by the Plane Wave Impulse Approximation. These Saclay and Bates experiments show that the longitudinal response functions are generally predicted to be approximately 20-40% larger than the measured response. The transverse response, although having approximately the predicted magnitude at the quasielastic peak, has substantial excess strength at the large energy-transfer side of the peak. The inclusion of final state interactions is not sufficient to

resolve these differences. Other possible improvements include the use of more realistic wave functions, two-body currents, quark effects, etc. An approach which has stimulated much theoretical and experimental interest centers on the idea of "inflated" nucleons. This decreases the calculated longitudinal strength and increases the transverse/longitudinal ratio. However, conclusive experimental verification is to date lacking.

During this past year the electromagnetic response functions for the three-body mirror nuclei <sup>3</sup>H and <sup>3</sup>He have been measured in an experiment at Bates<sup>18</sup>. Combined with earlier Saclay<sup>10</sup> results on <sup>3</sup>He, these experiments have completely characterized the basic response of these simplest nuclear systems in the elastic, quasielastic,  $\Delta$  and breakup channels. Taking advantage of our ability to do "exact" calculations in the three-body systems and to isolate the isospin structure of their response functions allows for a very direct confrontation between theory and experiment. The quasielastic response for these two nuclei provide interesting and important insight into some basic open problems in nuclear structure.

The quasielastic cross section expressed in terms of the longitudinal and transverse response functions has the form:

$$\frac{d^2\sigma}{d\Omega dE_g} = \sigma_M \left[ \left[ \frac{Q^2}{q^2} \right] R_L \left( \mathbf{q}, \omega \right) \right. \\ \left. + \left. \left\{ \frac{1}{2} \, \left| \frac{Q^2}{q^2} \right| \, + \, \tan^2 \, \frac{\ell}{2} \right] \, R_T \left( \mathbf{q}, \omega \right) \right] \ , \label{eq:delta_delta_delta_delta_delta}$$

where  $\sigma_{_{\rm H}}$  is the Mott cross section, Q and q are the four- and three-momentum transfers, respectively,  $\omega$  is the energy lost by the electron in the scattering, and  $\theta$  is the electron scattering angle.

Figure 7 shows the measured longitudinal and transverse quasielastic response functions for <sup>8</sup>H and <sup>8</sup>He at a momentum transfer of 500 NeV/c. Theoretical calculations by the Hannover<sup>20</sup>, Rome<sup>21</sup>, and Illinois<sup>22</sup> groups, showing varying degrees of agreement, are included for comparison with the data. The Hannover calculation for the transverse response agrees with the observed magnitude at the peak but the width of the distribution is narrower than required. For the longitudinal response the Illinois calculation is in somewhat better agreement but both have serious deficiencies in reproducing the observed shape. The calculations appear to reflect basic difficulties in solving the continuum three-body problem which is required for a consistent treatment.

Figure 8 shows a comparison of the experimental and theoretical responses for <sup>3</sup>H and <sup>3</sup>He at 400 MeV/c, with the nucleon factor Z divided out. The ratio of the observed <sup>3</sup>H and <sup>3</sup>He peak heights are consistent with the expectation based upon one-body currents. In fact, the normalized data are more similar in peak height than any of the calculations. One also notes that the response for <sup>3</sup>H is slightly wider than that for <sup>3</sup>He. In the simplest approximation, the higher probability for high momentum components in <sup>3</sup>H than <sup>5</sup>He is expected since <sup>3</sup>He has a larger rms charge radius.

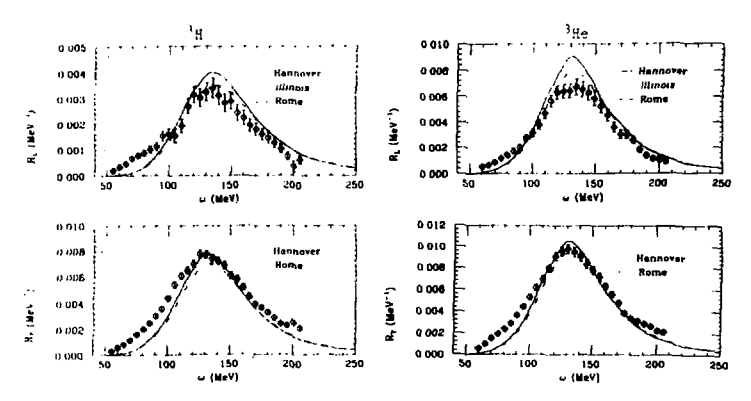


Fig. 7. <sup>3</sup>H and <sup>3</sup>He inclusive longitudinal and transverse response functions at q=500 MeV/c. The theoretical calculations are from the Illinois, Rome, and Hannover groups.

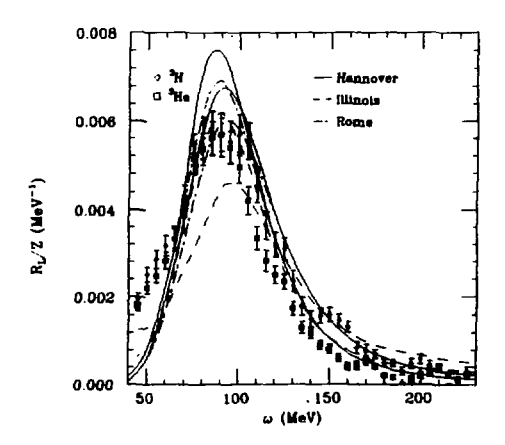


Fig. 8.  $^3$ H and  $^3$ He measured and calculated longitudinal response functions divided by 2 at q=400 MeV/c. The calculated response for  $^3$ H is always lower than  $^3$ He at the peak.

An observable which can be extracted from the measured longitudinal response functions is the so-called Goulomb Sum Rule,  $\Sigma_L(q)$ . The experimental sum rule is obtained by dividing the longitudinal response by the square of the proton charge

form factor, to obtain the 'point nucleon' response, and then an integration is performed over all  $\omega$ :

$$\Sigma_{L}\left(\mathbf{q}\right)_{\text{exp}} = \frac{\omega_{\text{exx}}}{\Sigma} \frac{R_{L}\left(\mathbf{q},\omega\right)\Delta\omega}{\left[G_{g}^{F}\left(\mathbf{Q}^{2}\right)\right]^{2}\left[\frac{1+Q^{2}/4K_{g}^{2}}{2}\right]}$$

The correction to the proton form factor, suggested by deForest<sup>23</sup>, accounts for relativistic effects due to the motion of the proton in the nucleus.

Theoretically, the sum rule depends only on the correlation structure of the ground state. It can be calculated for realistic forces on the assumption of one-body currents.

The Coulomb sum rules for <sup>3</sup>H and <sup>3</sup>He are shown in Fig. 9. Some extrapolation of the experimental data was required to account for unobserved strength at high  $\omega$ . The relatively small amount of extrapolated strength is indicated. The curves labeled 'Illinois' are exact calculations performed by the Illinois group, using only ground state wave functions<sup>24</sup>. The curves labelled 'No Correlations' were calculated using the measured elastic charge form factors<sup>28</sup>;

$$\Sigma_{L}^{nc} \; (q) \; = \; Z(1 \cdot | \, F_{ch} \; (q) \, | \, ^2/G_E^P (Q^2)^2) \; . \label{eq:def_energy}$$

This is the inelastic sum rule in the absence of correlations.

One notes that for these nuclei the experimental Coulomb Sum Rule is essentially satisfied. This is to be contrasted with the observations in heavier nuclei where the measured Coulomb Sum is suppressed by (20-40)% even out to the highest measured momentum transfers. The Illinois prediction and the data for

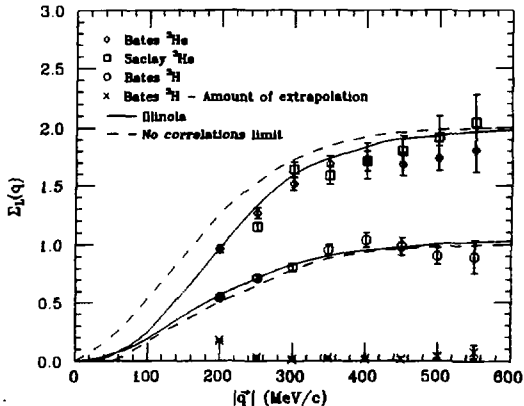


Fig. 9. Experimental and theoretical Coulomb sum rules for <sup>3</sup>H and <sup>3</sup>He.

are both quite close to the no-correlation limit. The presence of two-proton correlations is clearly evident for <sup>3</sup>He.

### V. SUBBETT

We have seen in these examples for few body systems some of the most recent contributions that the electron probe has made to our understanding of hadronic and nuclear structure. Experimental objectives have been to quantify non-nucleonic degrees of freedom and to isolate reaction mechanisms. On the theoretical front, some success has been achieved in correctly describing the very precise data which is now available. However, it still remains to be seen whether one can successfully make the transition between a description of nuclear dynamics based on meson exchange and that described by quarks and gluons.

The new generation of high current, CW accelerators now being constructed will provide new capabilities and opportunities for advancing in other directions. The exploitation of spin observables (polarized beams, polarized targets, internal target capabilities) is essential and would ensure a very strong experimental program for the next decade.

This work is supported in part by the U.S. Department of Energy under Contract No. DE-ACO2-76ER03069.

### References

- 1. T. W. Donnelly and A. S. Raskin, Annals of Physics 169, 247 (1986).
- 2. C. Y. Cheung and R. M. Woloshyn, Phys. Lett. 1278, 149 (1983).
- 3. B. Blankleider and R. M. Woloshyn, Phys. Rev. <u>G29</u>, 538 (1984).
- 4. R. Madey and S. Kowalski, Bates Proposal (1986).
- 5. W. Leidemann and H. Arenhovel, Phys. Lett. <u>8184</u>, 7 (1987).
- R. Milner, Bates Proposal (1988). T. Chupp and A. Bernstein, Bates Proposal (1988).
- 7. R. Milner, private communication.
- 8. R. Arnold et al., Phys. Rev. Lett. 35, 776 (1975).
- 9. R. Arnold et al., Phys. Rev. Lett. 58, 1723 (1987).
- 10. M. E. Schulze et al., Phys. Rev. Lett. 52, 597 (1984).
- 11. J. M. Cameron et al., Bates Proposal (1984).
- J. M. Cameron et al., Third Workshop on Perspectives in Nuclear Physics at Intermediate Energies, Trieste, May 1987.
- R. Holt, Proceedings of the Conference on Intersections Between Particle and Nuclear Physics, Steamboat Springs, edited by R. E. Mischke, AIP 123, 499 (1984).
- 14. R. Arnold et al., SLAC-PUB-4612 (1988). Submitted to Phys. Rev. Lett.
- J. Laget, Can. J. Phys. <u>62</u>, 1046(1984); J. Laget, Phys. Lett. <u>1998</u>, 493(1987).
- I. J. McGee, Phys. Rev. 161, 1640 (1967) and L. Durand, Phys. Rev. 123, 1393 (1961) as presented in W. Bartel et al., Nucl. Phys. 858, 429 (1973).
- 17. H. Arenhovel, Nucl. Phys. A393, 385 (1983).
- 18. K. Dow, Ph.D. Thesis, MIT 1987. Submitted for publication to Phys. Rev. Lett.
- 19. C. Marchard, et al., Phys. Lett. 1538, 29 (1985).
- 20. H. Meir-Hajduck et al., Nucl. Phys. <u>A395</u>, 332 (1983).
- 21. C. Ciofi degli Atti, et al., private communication (1987).
- R. Schiavilli et al., Nucl. Phys. <u>4649</u>, 219 (1986).
   T. deForest, Nucl. Phys. <u>4614</u>, 347 (1984).
- 24. R. Schiavilli, et al., Nucl. Phys. 4473, 267 (1987).
- 25. D. Beck, et al., Phys. Rev. Lett. 59, 1537 (1987).

### FEW BODY SYSTEMS AT INTERMEDIATE ENERGIES

### J.M. Laget

Service de Physique Nucléaire-Haute Energie, CEN Saclay, 91191 Gif sur Yvette, France

Few-body systems have been widely studied with hadronic as well as electromagnetic probes, the energy of which ranges from a few hundreds MeV to a few GeV. While it is fair to say that we have reached a good understanding of their static properties and their structure at large distances, we are still left with the two following open questions:

- What is the nature, and how can we study the effects, of the short range correlations in nuclei?
- What is the size and what are the effects of the three-nucleon forces?
  Those are very old problems/1,2/ which are still unsolved.

The reason is that the meson and  $\Delta$  degrees of freedom dominate all the attempts which have been made so far to study the short range behaviour of nuclei : the use of probes of increasing energy requires to take into account the deformation of the nucleon and to consider also the coupling with each mechanism which drives the nucleon-nucleon force.

While the study of these meson and  $\Delta$  degrees of freedom in nuclei has been an important achievement of the last two decades, the major task of Nuclear Physics is now to go beyond and to study nuclei in kinematical regions where their effects are strongly suppressed or with probes to which they couple weakly.

A general background can be found in my Banff's lectures<sup>3</sup>. Today, I shall update the review which I made at Fontevraud last summer<sup>4</sup>, and try to summarize the progresses which have been done in the mean time. I will deal with the following topics:

- the determination of the high momentum components of the wave functions of the few-body systems,
- the analysis of the pd capture reactions,
- the search for three-body forces.
- the study of short range correlations.

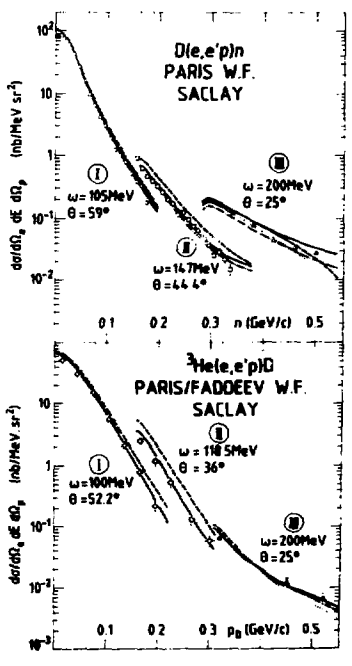
### I. THE HIGH MOMENTUM COMPONENTS OF THE NUCLEAR MAYE FUNCTION

Provided that final state interaction and meson exchange current effects are fully taken into account, the analysis'5' of the (e,e'p) reactions, recently studied at Saclay'6''7' and Amsterdam'8' for small values of the four momenta of the virtual photon, has led to strong constraints on the D and <sup>3</sup>He wave functions, up to momenta as large as 500 MeV/c.

Fig. 1 beautifully illustrates this point. It summarizes the cross sections of the  $D(e,e^+p)n$  and  $^3He(e,e^+p)d$  reactions which have been measured at Saclay/6\*77 during the past few years. The three kinematical settings have been chosen in such a way that the increase of the Mott cross section, when the electron scattering angle decreases, compensates the rapid fall-off of the nuclear wave function. These kinematics, which maximize the longitudinal component of the cross section, minimize the

effects of meson exchange currents (MEC). Although the corrections to the impulse approximation are significant and are necessary to reproduce the experiment, they do not dominate the cross section. Moreover, they are strongly constrained by gauge invariance, which links in a consistent way the wave functions of the initial and final states and the various interaction effects. The agreement with the latest solution of the Faddeev equations obtained by Hannover group<sup>79</sup> with the Paris potential<sup>710</sup>, is almost perfect.

Fig. 1. The crose sections of the D(e, e'p)n and <sup>3</sup>He(e,e'p)d reactions recently measured at Saclay'6.71 are plotted against the momentum of the undetected nuclear fragment. The electron scattering angle 6 and the energy w of the virtual photon are given for each kinematics. The dotted line curves are the impulse approximation. The dashed line curves correspond to the plane wave treatment and include the neutron exchange or the two-nucleon exchange graph. The dash-dotted line curves correspond to the distorted wave treatment. The full line curves include also the meson exchange contribution.



The corrections play a more important role in the analysis'  $^{11}$ / of the "He(e,e'p)T reaction cross section recently measured at Amsterdam'  $^{12}$ /. In fig. 2 the nucleon momentum distribution has been extracted in the frame of the Plane Wave Impulse Approximation (PMIA) for two different kinematics : the first corresponds to a backward electron scattering angle ( $\theta_{\rm e}$ = 70.4°) and minimizes the contribution of the longitudinal (Coulomb) component of the cross section, whereas the second corresponds to a forward electron scattering angle ( $\theta_{\rm p}$ = 36°) and maximizes it. Clearly the

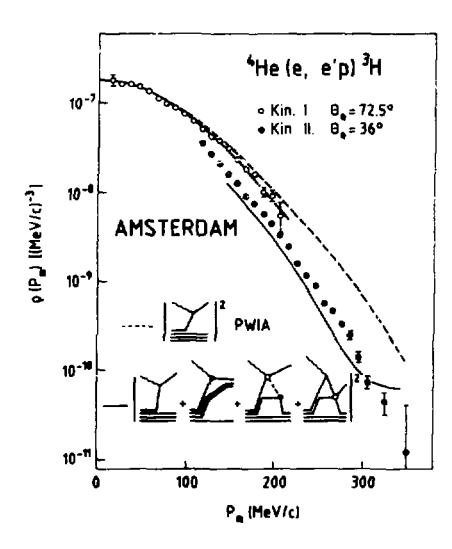


Fig. 2. The momentum distribution of the proton as extracted in the PNIA analysis of the  $^3{\rm He}({\rm e},{\rm e}'{\rm p}){\rm T}''$  reaction'  $^{12}{\rm I}'$  in two different kinematics. I: 0  $_{\rm e}$ ,= 72.5°; and II: 0  $_{\rm e}$ ,= 36°. If the PNIA were vilid, all the experimental points would have lay on the dashed curve, which is the cHeIpT> overlap integral obtained in the variational Monte-Carlo calculation reported in /13/. The full line curves include the various interaction effects depicted in the inset.

PWIA breaks down, and misses the experiments by one order of magnitude at the highest momentum; but the microscopical calculations of the various effects (see inset of fig. 2) brings the theory close to the experiment. The calculation uses the latest solution of the four-body problem obtained by the Urbana group'13' with the Y14 potential'14', in the framework of the variational Monte-Carlo method.

Since the "HelpT" overlap is a pure S-state, it exhibits a zero around p = 450 MeV/c: the interaction effects shift this minimum towards a lower momentum. This part of the momentum distribution is under study in an experiment recently performed at Saclay, the analysis of which is under way.

To summarize, the wave functions of the few-body systems have been determined by the analysis of the (e,e'p) reaction, up to 500 MeV/c for D and 3He and 300 MeV/c for "He. The extension of such an analysis to higher momenta and shorter distances, calls for electron beams of higher energies than those of the present generation of high intensity accelerators. More-

over, the separation of the transverse and longitudinal components of the cross section is the necessary step to get rid of the exchange current contribution, to minimize the corrections, and to study more directly the wave functions in the longitudinal cross section.

### II - THE pd CAPTURE REACTIONS

Therefore no freedom is left to play with the high momentum components of the three-body wave function. It can be used to analyse other channels as for instance, the pd +  $T\pi^+$  / $^{15}$ / and the pd +  $^{3}$ He $_{Y}$ / $^{16}$ / reactions. Fig. 3 represents the analysis

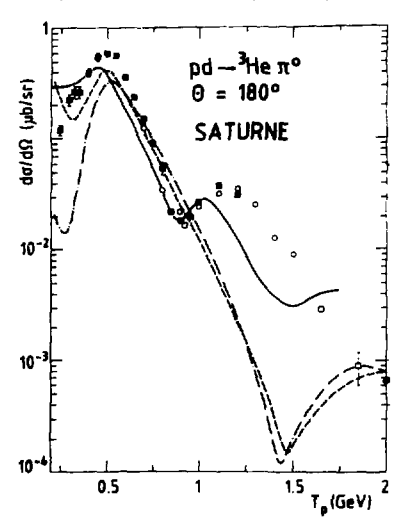


Fig. 3. The excitation function of the pd \* \$^3\text{Hm}^{10}\$ reaction cross section'\$^{17,187}\$ is plotted against the kinetic energy of the incoming proton. The full line curve represents the result of the full calculation, and includes the contribution of three-body mechanisms. They are not included in the Ashed and dot-dashed line curves. Only the Ashormation term, in the two-body pion absorption amplitude, is retained in the dot-dashed line curve.

/15/ of the excitation function at  $\theta_\pi=180^{\circ}$ , of the pd +  ${}^3{\rm He}\pi^0$  reaction /17,18/. The relevant graphs are given in fig. 4. The analysis/16/ of the 90° excitation function of the  $\gamma^3{\rm He}$  + pd reaction/19-25/ is shown on fig. 5.

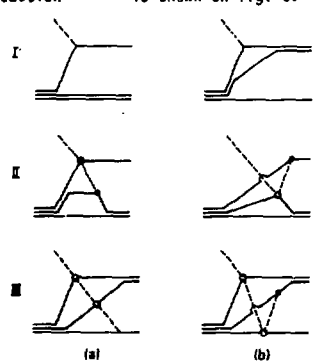


Fig. 4. The relevant graphs in the pd > Tm\* reaction. I: the one-nucleon (a) and the two-nucleon (b) exchange graphs. II: the two-body meson exchange graphs. III: the three-body meson exchange graph. Graphs III and IIIb come from the antisymmetrization of the two-body meson capture amplitude.

Due to large momentum transfers, the one-body mechanisms are strongly suppressed. Two-body mechanisms domina-

te the cross section and lead to a fair agreement with a large bulk of experimental data/3.26/. While the unpolarized differential cross sections and spin observables

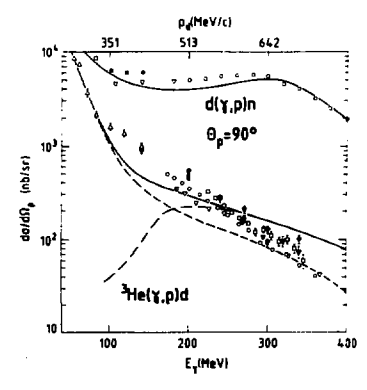


Fig. 5. The excitation functions, at  $\begin{bmatrix} \theta_p \end{bmatrix}_{c.m.} = 90^\circ$ , of the  $d(\gamma,p)n$  reaction  $^{(3)}$  21' and the  $^{(3)}$ He( $\gamma,p)d$  reaction  $^{(4)}$ -25' are plotted against the incoming photon energy. The momentum of the outgoing deuteron is also plotted as abscissa. The dotted-line curve is the contribution of the one-body mechanisms alone. The dashed-line curve includes also the two-body mechanisms. The full line curve takes also into account the meson double scattering mechanisms. Its contribution is the dash-dotted line curve.

are well reproduced at forward angles, strong deviations appear around 90° and larger angles. For instance, at 0= 90° the cross section of the pd +  $\mathrm{T}\pi^+$  and  $\gamma^3\mathrm{He}$  + pd reactions are respectively underestimated by one order of magnitude and more than a factor two. This discrepancy is really significant, since the two-body matrix elements have been calibrated against the D( $\pi$ ,p)p and D( $\gamma$ ,p)n reaction /³,  $^{26}$ /, and since we have seen that the three-body wave function has been checked in the same range of momenta.

The meson double scattering mechanism, depicted in fig. 4 for the pd +  $^3{\rm He}\pi^0$  channel and in fig. 6 for the  $\gamma^3{\rm He}$  + pd channel, accounts for a large part of the disagreement between the theory and the experiment. When the momentum transfer increases, its contribution becomes more important than the contribution of the two-body mechanisms. First, it is more likely to be shared between three rather than two nucleons. Second, one of the exchanged pion is very close to its mass shell (on its mass shell above the pion threshold), and the corresponding triangular singularity enhances this three-body amplitude.

The most spectacular evidence for this meson double-scattering mechanism is provided by the analysis'27' of the 180° excitation

function of the pd +  $^3$ He $_1$  / $^{17}$ /, which is depicted in fig. 7. Due to the larger momentum transfer and to the smallnes of the  $_1$ NN coupling constant, the one-body and two-body mechanisms are more suppressed than in the pd +  $T\pi^+$  reaction. The meson double-scattering mechanism alone is able to reproduce both the shape and the magnitude of the cross section. The minimum near  $T_p$  = 1 GeV is due to a subtle interference between the contribution of the  $S_{11}(1520)$  and  $P_{11}$  resonances ( $P_{11}(1470)$  below the threshold, and  $P_{11}(1690)$ ) which dominate the elementary  $\pi^-p$  +  $\eta n$  reaction.

Contrary to the pd +  $T\pi^+$  and the pd +  $^3He\eta$  reactions, the  $\gamma^3He$  + pd reaction has the advantages to be opened below the pion production threshold. Here both mesons are off shell and this meson double scattering is a prototype of a three-body exchange current, which is related via gauge invariance to the corresponding part of the three nucleon force. The amplitude has the same expression as above threshold, where only

on shell elementary amplitudes enter the calculation. Therefore the excitation function, shown in fig. 5, offers us the opportunity to start from a kinematical domain where the calculation is founded on solid ground, and to extrapolate below the pion threshold where the usual problems, due to the virtual nature of the exchanged mesons (form factors, heavy mesons), come into the game.

It should also be noted that, due to the strong suppression of pion absorption by T=1 nucleon pairs, only pion absorption by T=0 pairs has to be considered. Since the total isospin of the pd channel is 1/2, the formation of the A is forbidden at the first pion scattering or production vertex. On the one hand, this double scattering mechanism provides us

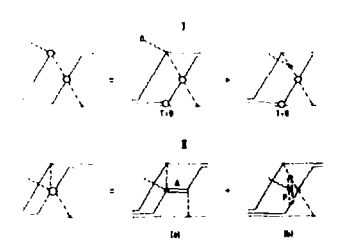
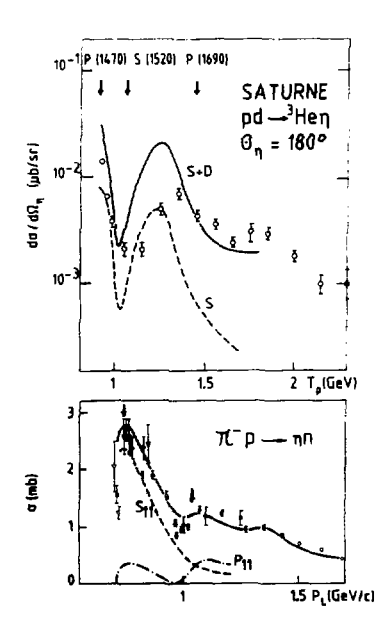


Fig. 6. The three-body exchange currents in the  $\gamma^3$ He + rd reaction.

I: The meson double scattering mechanism is decomposed into its two dominant parts. II: The two relevant graphs which do not reduce to a sequential meson scattering.



Pig. 2. The excitation function 17/ of the p.l +  $^{3}$  Hen reaction at  $\theta_{-}$ = 180° is plotted against the proton kinetic energy in the top part of the figure. The full line curve takes into account both the s and d part of the wave function of the nucleon which interacts with the n. The dashed line curve includes only the s-wave. The arrows indicate the location of the resonance which dominates the elementary n-p + nn reaction, the total cross-section of which is plotted in the bottom part of the figure igainst the incoming proton momentum. The scale is chosen in such a way that the nn invariant mass is the same as its mean value in 3He. The contribution of the Si and P11 waves are also plotted sepaparately.

with a powerful filter to create and to study the behaviour of other resonances than the  $\Delta$  in nuclei. On the other hand, only the Born terms are relevant at low energy in the pd +  $^{3}$ He $_{\Upsilon}$  reaction, and the dominant graphs are the pion photoelectric and contact terms shown in fig. 6. They are really three-nucleon exchange currents which are linked to a given part of the three-body forces.

The agreement with the pd radiative capture data is not as good as in the analycis of the pd  $\star$   $T\pi^{\dagger}$  reaction. Presumably this is a hint that other mechanisms, which do not occur in meson induced reactions, must be considered in photon induced reactions. Two examples are depicted in fig. 6 (diagram II). It is well known that  $\rho$  exchange contributes significantly to the  $\pi N$  S-wave scattering amplitudes. While the coupling of the photon to the pion is accounted for by diagram Ib, the direct coupling to the exchanged  $\rho_{\tau}$  diagram IIb, must also be considered, especially near the pion threshold and below. It is also well known/<sup>28</sup>/ that two-pion photoproduction proceeds primarily through the emission of a  $\pi\Delta$  system in a relative S-wave. When these two pions are virtual (diagram IIa) the amplitude extrapolates smoothly below the  $\pi\Delta$  threshold, and the corresponding three-body exchange current might interfer with the meson double scattering amplitude.

To summarize, meson double scattering appears to be a capital ingredient of the cross section of the  $^3\text{He}(\gamma,p)d$  reaction at high momentum transfer. However, it cannot alone reproduce all the data, and other three-body exchange currents must be considered before any definite conclusion can be reached. All these different mechanisms must be singled out and extensively studied. The flexibility of the three-body kinematics of the  $^3\text{He}(\gamma,2p)n$  or the  $^3\text{He}(e,e^!2p)n$  reactions will provide us with the way to achieve this goal and to avoid the calculation of a nine fold integral.

### III - THE THREE-BODY FORCES

The spectrum of the protons emitted at a given angle in the semi-exclusive  ${}^{3}$ He  $\{\gamma,p\}$ np reaction exhibits two peaks (fig. 8). The first is located in the high momentum part. Its top corresponds to the disintegration of a pn pair at rest in  ${}^{3}$ He, and its width is due to the Fermi motion of this pair: the corresponding model/ ${}^{29}$ / leads to a fair agreement with the Saclay experiment/ ${}^{30}$ /. The second is located at lower proton momentum and is dominated by the three-body mechanism (fig. 9). The Final State Interaction (FSI) effects are also taken into account, but do not affect significantly this picture. Such a spectrum allows to disentangle the two- and the three-body mechanisms. However the three-nucleon mechanism is dominant above the pion production threshold, and its contribution is overwhelmed by the contribution of the  ${}^{3}$ He( ${}^{\gamma}$ ,p)  ${}^{\gamma}$ NNN reaction. Therefore a second nucleon must be detected in coincidence, and the  ${}^{3}$ He( ${}^{\gamma}$ ,pp) reaction presents several advantages over the  ${}^{3}$ He( ${}^{\gamma}$ ,pn) reaction.

Contrary to the  ${}^3\text{He}(\gamma,pn)$  reaction, two-body mechanisms are strongly suppressed in the  ${}^3\text{He}(\gamma,2p)$  reaction, or the transverse part of the  ${}^3\text{He}(e,\,e^+2p)$  reaction, because (i) a pp pair has no dipole moments to couple with, (ii) the charged exchange

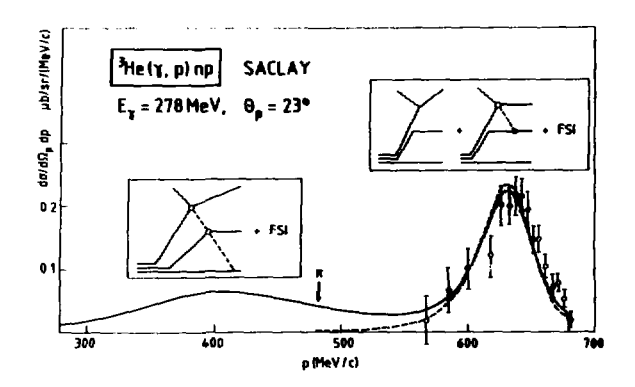


Fig. 8. The spectrum of the proton smitted at  $\theta_p=23^\circ$  in the reaction  $^3{\rm He}(\gamma,p){\rm pn}$  when the energy of the incoming photon is  ${\rm E}_{\gamma}=280$  MeV, is plotted against its momentum. The peak located at high momentum corresponds to the disintegration of a pn pair almost at rest in  $^3{\rm He}$  (dashed line curve), and is well determined by the experiment  $^{30}$ . The peak at lower momentum is due to the three-body mechanisms (full line curve). The arrow indicates the pion production threshold.

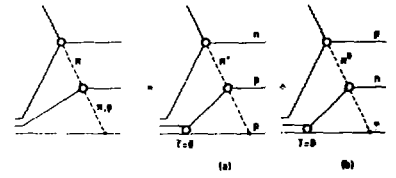


Fig. 9. The reson double scattering graph in the  $^3$ He( $\gamma$ , 2p)n reaction is expressed in terms of the two most important parts: the absorption of a positive (a) or a neutral (b) pion by a T=0 neutron proton pair.

currents are vanishing, and (iii) the formation of the  $\Delta$  as an intermediate state is forbidden (since the  $J^{\pi}=1^+$   $p\Delta^+$  S-wave cannot decay in the pp channel). When the spectator neutron is at rest, the cross section of the  ${}^3\text{He}(\gamma,2p)\text{n}$  reaction does not exceed 1 % of the cross section of the  ${}^3\text{He}(\gamma,pn)\text{p}$  reaction (fig. 10). The calculation is fully described in  $J^{3+29}/J_{\gamma}$ , and beautifully checked by the recent Saclay experiment  $J^{31}/J_{\gamma}$ . One of the detected

protons is assumed to be emitted at  $\theta P = 90^{\circ}$ , with respect to the incoming photon, in the center of mass frame of the active pair. In the pp channel, the background is due to all the graphs due to final state interactions or corresponding to pion reabsorption is a pn active pair. It does not include the pion reabsorption graph in a pp pair, which dominates the  $(\gamma, pp)$  cross section.

Fig. 11 shows the relative importance of the two- and three-body mechanisms (fig. 9) in the  $^3$ He( $\gamma$ ,pn) and  $^3$ He( $\gamma$ ,pn) reactions. The reduced cross section  $d\sigma/d\Omega$  dn is directly related to the measured cross section (being J the Jacobian):

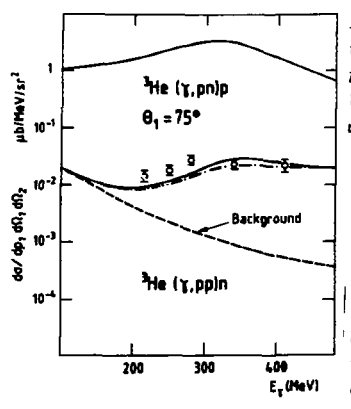


Fig. 10. The photodisintegration cross section of the pn pair (upper part), and the pp pair (lower part) at rest in <sup>3</sup>He. The full line curves include three-body mechanisms, which are not included in the dashed line curves (see text).

$$\frac{d^3\sigma}{d\rho_1 d\Omega_1 d\Omega_2} = \sqrt{1 + \frac{d^2\sigma}{d\Omega_1 d\eta}}.$$
 (1)

If the neutron is assumed to be a spectator, and if it moves in a relative S-state with respect to the active proton pair, this reduced cross section is basically the product of

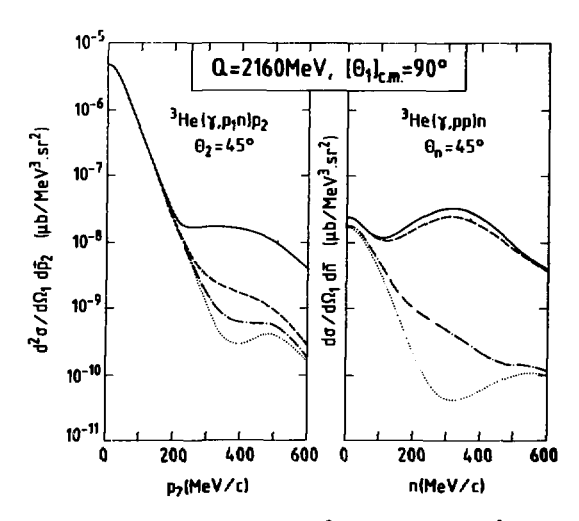


Fig. 11. The reduced cross sections of the  $^3$ He( $\gamma$ ,pn)p and the  $^3$ He( $\gamma$ ,2p)n reactions are plotted against the momentum of the undetected nucleon. The dotted and dash dotted lines represent the contributions of the two-body mechanisms, without and with final state interactions respectively. The dashed lines include the three-body graph when a  $\pi^+$  is absorbed by a np pair. The full lines include also the absorption of a  $\pi^0$  by a np pair.

its momentum distribution and the cross section of the disintegration of a pp pair (see  $/^{28}$ / for instance). The mass of the detected nucleon pair and the angle of the proton, measured in the c.m. frame of this pair with respect to the direction of the incoming photon in the Lab system, are kept constant respectively at the values W = 2160 MeV and  $[\theta_1]_{c,m} = 90^{\circ}$ . The reduced cross section is plotted against the momentum of the undetected nucleon which is emitted at 8 = 45° in the Lab frame. The plane wave cross section exhibits the variation of its momentum distribution, and the rise around 500 MeV/c comes from the antisymmetry of the outgoing three nucleons. At high momentum transfer, final state interactions become important, but the cross section is dominated by the three-body mechanisms. In the 3He(y,pn) channel, the flattening of the cross section above 200 MeV/c, at the level of 1 % of the peak corresponding to the disintegration of a pn pair at rest, is consistent with a recent study/32/ of pion capture by  ${}^{3}$ He. In the  ${}^{3}$ He( $\gamma$ , 2p) channel, two-body mechanisms are suppressed by two orders of magnitude and the cross section is entirely driven by the three-body mechanisms. As expected  $n^+$  capture followed by the emission of two protons dominates the  $(\gamma,2p)$  channel, whereas  $\pi^0$  capture leading to the emission of a pn pair dominates the (y,pn) channel.

This kinematics has been deliberately chosen in such a way to maximize the kinematical domain where the first pion propagates on shell and to enhance the effect of the triangular singularity. Indeed, the three-body mechanism dominates the cross section in a small part of the phase space. It is maximized when the neutron is emitted at 45° with a momentum around 300 MeV/c. This corresponds to the most likely kinematics of the recoil nucleon in pion photoproduction on a nucleon at rest. This characteristic behaviour of the cross section should be used to single out and study the three-body mechanisms, in a domain where the calculation is basically free of parameters. Since it depends only on the low momentum part of the three-body wave function and on shell elementary amplitudes which are calibrated independently. Such a measurement has been performed at Saclay, and its analysis is almost finished.

The next step consists of going far from the singularity in such a way that both mesons travel off shell. This graph can still be viewed as a virtual meson rescattering, but also as a genuine three-body meson exchange current, which in turn is linked to the corresponding three-body forces. An example is given in  $J^{33}$ /: here the three-body effects are sizeable when the available energy is roughly shared by the three-nucl. as. Now, the calculation heavily depends on the way the elementary amplitudes are extrapolated off-shell. While pion baryon form factor must be considered in the pion photoproduction and scattering amplitudes, the size of the corresponding cut-off mass is still an open problem in three-body forces/ $^{27}$ . While the description of S-wave pion nucleon scattering in terms of experimental phase shifts, or scattering lengths, is excellent on shell, it might not be accurate enough to extrapolate below threshold, and a more microscopic treatment, based on a low energy theorems, should be used instead. Finally, pion absorption on T = 1 pairs, as well as other three-body

mechanisms (fig. 6) which do not reduce to a meson sequential scattering, should also be considered.

All those problems are open, and the extension to the <sup>3</sup>He(e,e'2p)n reaction is expected to provide us with a way to disentangle all these mechanisms. Besides the flexibility of the three-body kinematics, this channel offers us the possibility of measuring transition form factors and to take advantage of a new degree of freedom: the variation of the four momenta of the virtual photon. It addition, the longitudinal cross section is directly linked to the short range nucleon correlations, and is the best place to study them.

### IV - THE TWO NUCLEON CORRELATIONS

The transverse cross section of the  $^3$ He(e,e'2p) reaction is strongly suppressed for the same reason as the cross section of the  $^3$ He( $\gamma$ , 2p) reaction. Charged meson exchange currents and  $\Delta$ -formation mechanisms do not contribute at all to the longitudinal cross section. This is the best place to study in detail the two-body correlations provided that final state interactions are carefully taken into account/ $^{34}$ /.

As an example fig. 12 represents the variation of the cross section, in a coplanar kinematics, against the four momenta of the virtual photon, just at the pion production threshold. The meson exchange effects are negligible, except near the photon point ( $q^2=0$ ) where the longitudinal cross section vanishes. Clearly 4 GeV is needed to measure this transition form factor up to  $|q^2|=1$  (GeV/c)<sup>2</sup> and to start studying the short range behaviour of the correlation between two nucleons.

I refer the reader to  $\frac{34}{}$  for a more detailed discussion of this topic.

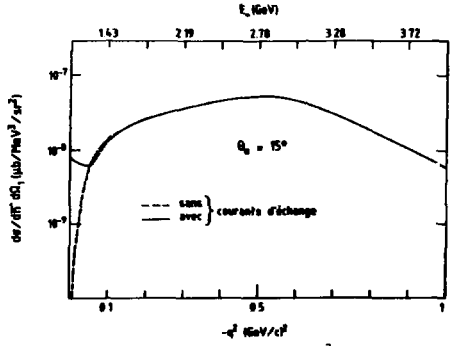


Fig. 13. The total reduced cross section of the <sup>3</sup>He(e,e'2p) reaction is plotted against the four momenta of the virtual photon. The energy of the incoming electron is also given on abscissa. The solid line curve includes the meson exchange current contribution. The dashed line curve does not.

To summarize, we have reached a good understanding of intermediate energy reactions induced in the few-body systems, in terms of complex combinations of elementary processes which can be independently singled out and checked by a suitable choice of the kinematics and the probe.

There is no need to introduce explicitly the quark degrees of freedom. The most economical, and consistent, picture relies on the description of each baryon as a small core, of radius 0.5 fm, surrounded by a meson cloud, which is polarized by the vicinity of other baryons.

In that framework, few body systems provide us with a powerfull laboratory to study the long and intermediate range part of the nucleon dynamics :

- The wave functions of the few-body systems have been determined up to 500 MeV/c, in the analysis of the (e,e'p) reactions. They agree with the latest solutions of the three- and four-body problems, when realistic potentials, as the Paris or the  $\rm V_{14}$  ones, are used.
- Two-body meson exchange mechanisms dominate the low and intermediate momentum transfer part of the cross sections, and are reasonably well under control.
- Three body mechanisms dominate the high momentum transfer part of the pd capture reaction cross sections. They allow the momentum transfer to be shared between all the nucleons, and they provide us with a powerful filter to create and to study the propagation of resonances with higher masses than the  $\Delta$  one.

What should we do now?

Obviously, we must get rid of the meson cloud, and single out those mechanisms which directly reveal the quark substructure of the baryon core.

In my opinion, three ways are open :

- The study of the (e,e'2p) reaction appears to be the most direct way to disentangle the short range two-body correlations (in the Coulomo part of the cross section) which strongly depend on the quark structure of the core and three-body mechanisms (in the transverse part) which are closely linked, via gauge invariance, to three body forces in the nuclear wave function.
- The systematic determination and the study of spin observables, in hadron induced reactions, allow us to perform a complete partial wave analysis and to pin down small amplitudes or interferences between quark and meson degrees of freedom.
- The study of the behaviour of strange baryon in a nucleus provides us with a useful tag to identify the mechanisms which drive the short range interaction between two baryons.

#### References

K. Gottfried, Ann. Phys. (NY) 21 (1963) 29;
 Y.N. Srivastava, Phys. Rev. <u>135</u> (1964) 3612.

- 2. " " & McKellar, Lecture Notes in Physics, 260 (1986) 7.
- ी। राज्या रिकार्ट, New Yistas in Electronuclear Physics, E. Tomusiak,
  - No Capitan and E. Dresster, Eds., Plenum Press, NY (1986) p. 361.
- 4. J.N. laget, Few body systems, supplementum 2 (1987) 126.
- $\delta_{*}(J_{*})$  Laget, Phys. Lett. 1998 (1987) 493.
- 3. 0. .. Leget, Filys. Lett. 1338 (1307) 433.
- M. Bernierm, et al., Nucl. Phys. <u>A365</u> (1981) 349;
   Turck-Chièze, Phys. Rev. Lett. 142B (1984) 145.
- 7. E. Jans, et al., Phys. Rev. Lett. 49 (1982) 974;
  - C. Marchand, et al., Phys. Rev. Lett. 60 (1988) 1703
- 8. P.H.M. Keizer et al., Phys. Lett. 197B (1987) 29.
- 9. Ch. Hajduk and P.U. Sauer, Nucl. Phys. A369 (1981) 321.
- 10. M. Lacombe et al., Phys. Lett. B101 (1981) 139.
- 11. J.M. Laget and R. Schiavilla, in preparation.
- 12. J.F.J. Yan den Brand et al., Phys. Rev. Lett. 60 (1988) 2006.
- 13. R. Schiavilla, V.R. Pandharipande and R.B. Wiringa, Nucl. Phys. A449 (1986) 219.
- 14. R.B. Wiringa, R.A. Smith and T. L. Ainsworth, Phys. Rev. C29 (1984) 1207.
- 15. J.M. Laget and J.F. Lecolley, Phys. Lett. 1948 (1987) 177.
- 16. J.M. Laget, preprint DPhN Saclay 2459 (1987).
- 17. P. Berthet et al., Nucl. Phys. A443 (1985) 589.
- 18. C. Kerboul et al., Phys. Lett. <u>B181</u> (1986) 28.
- 19. N.M. O'Fallon et al., Phys. Rev. C5 (1972) 1926.
- 20. P.E. Argan et al., Nucl. Phys. A237 (1975) 447.
- 21. H.J. Gassen et al., Z. Phys. 303 (1981) 303 ;
  - J. Arends et al., Nucl. Phys. A412 (1984) 509.
- 22. D.I. Sober et al., Phys. Rev. <u>C28</u> (1983) 2234.
- C.A. Heusch et al., Phys. Rev. Lett. <u>37</u> (1976) 405;
   (1976) 409;
   (1976) 960(E).
- 24. J.M. Cameron et al., Nucl. Phys. A424 (1984) 549.
- 25. W.J. Briscoe et al., Phys. Rev. C32 (1985) 1956.
- J.M. Laget, Second Workshop on Perspective in Nucl. Phys. at Intermediate Energies, S. Boffi et al., Eds. World Scientific, Singapore (1986) p. 247.
- J.M. Laget and J.F. Lecolley, preprint DPhN/Saclay n° 2510 (1988).
- 28. J.M. Laget, Phys. Rep. 69 (1981) 1.
- 29. J.M. Laget Phys. Lett. 151B (1985) 325.
- 30. N. D'Hose et al., êtme session d'Etude Biennale de Physique Nucléaire, Aussois,
  - J. Meyer ed., LYCEN 8502 (Lyon University), (1985) p.510.1; and to be published.
- 31. G. Audit et al., in preparation; private communication.
- 32. G. Backenstoss et al., Phys. Rev. Lett. 55 (1985) 2782.
- 33. J.M. Laget, preprint DPhN/Saclay 2454 (1987).
- 34. J.M. Laget, Phys. Rev. C35 (1987) 832.

# ФЕНОМЕНОЛОГИЧЕСКИЙ АНАЛИЗ ПРОЯВЛЕНИЙ МЕЗОННЫХ ОВМЕННЫХ ТОКОВ В ЭЛЕКТРОРАСШЕНИЕНИИ ЛЕЙТРОНА У ПОРОГА

## А.В. Афанасьев, M.II. Рекало

Харьковский физико-технический институт АН УССР

- 1. Пороговое электрорасщение дейтрона,  $e^- + d \rightarrow e^- + rr + \rho$  обладает рядом важных особенностей, которые делают этот процесс источником интересной информации о природе электроядерных взаимодействий при больших эначениях квадрата  $|e^2|$  переданного адронам 4-импульса, упрощая одновременно теоретическую интерпретацию процесса  $e^- + d \rightarrow e^- + rr$ -р. Перечислим некоторые из этих особенностей:
- а. Относительная простота спиновой структуры амплитуды процесса  $\delta^* + A + n + p = I$   $\delta^* виртуальный фотон <math>I$ .
- б. Квадрат переданного 4-жипульса к<sup>2</sup> однозначно связан с артументом дейтронной волновой функции (ДВФ)/в импульсном представлении/.
- в. Дифференциальное сечение процесса  $d(\mathbf{e},\mathbf{e}^*)n_{\mathcal{D}}$  у порога непосредственно связано при каждом значении  $\mathbf{x}^*$  с ДВТ, тогда как вне порога дифференциальное сечение процесса  $d(\mathbf{e},\mathbf{e}^*)n_{\mathcal{D}}$  определяется уже некоторым интегралом от квадратичных комбинаций  $S^*$  и  $D^*$ -компонент ДВТ.
- д. Более простая инклюзивная постановка опыта в  $d(\mathbf{e},\mathbf{e}^*)_{n,p}$  у порога столь же жиформативна, как и несравненно более сложная эксклюзивная постановка опыта в  $d(\mathbf{e},\mathbf{e}^*)_{n,p}$ .
- с. Связь правых отбора по изотопическому спину со спиновой структурой пороговой амплитуды.
- ж. Возможность использовать процесс  $e^+d \rightarrow e^-+n+p$  у порога для проверки свейств симметрии электромагнитного взаимодействия адронов: речь идет прекде всего о проверке  $P^-$  и  $T^-$ инвармантности [1-2], а также сохранения электромагнитного тока адронов.
- Измеренные значения диференциального сечения процесса  $d(e,e^*)_{PP}$  у порога при рассения алектронов на больше углы [3, 4] обично рассматривают как доказательство важности вклада мезонных обменных токов /МОТ/ [5]. Наиболее распространенные процедури учета МОТ являются нерелятивистскими. Между тем у порога реакции  $e^+ d \to e^+ h_2 + p$  вклад МОТ можно оценить, не апеллируя к контретной их модели. Можно воспользоваться только изотопическими свойствами тех МОТ, которые примято считать главнови в процессе  $e^+ d \to e^+ h_2 + p$ , и установить их спимовую структуру. После этого, параметризуя вклад МОТ каким либо "естественным" и правдогодобным способом, можно найти те величины, которые определяют фекоменологическую модель МОТ.

Мы выясним здесь спиновую структуру пороговой амплитуды процесса  $\delta^{\mu}d \to n+p$  в терминах электромагнитмых формфакторов. Все возможные полярмзационные эффекты в пороговом электрорасщеплении могут быть вычислены в терминах этих формфакторов. На этом пути не возникает проблемы сохранения электромагнитного тока адронов в  $e^- + d \to e^- + n+p$ , так как его параметризация с помощью формфакторов учитывает сохранение тока так же, как и для электромагнитного тока нуклона или возбуждения нуклонных резонансов. Формфакторы порогового электрорасщепления дейтрона, внчисленные в рамках релятивистского импульсного приближения /РИП/  $\{6\}$ , могут быть унитаризованы, чтобы учесть эффекти n p-выаммодействия. Для учета вкиада МОТ в формфакторе порогового перехода МГ $\to$   $3 \times 1$  вкимчена феноменологическая добавка, параметры которой найдены на основе экспериментальных данных о дифференциальном сечении процесса  $d(e,e^*)np$  у порога при рассеянии электронов на большие углы.

2. Амплитуда процесса  $\delta^* + d m_* p$  вбяжзи порога может быть записана в следующем общем виде [7] /в с.ц.м. процесса/:

Здесь  $Q_1/Q_2/$  – двухкомпонентный спинор p/n/,  $Q_1/Q_2/$  – 3-вектер поляризации дейтрона /виртуального  $Q_1^2$  – квектел,  $Q_2^2$  — единичный вектор вдоль 3-импульса  $Q_1^2$ . Формфакторы  $Q_2^2$  — характеризуют поглощение  $Q_1^2$  – квантов определенной мультипольности, а именяю, формфактор  $Q_1^2$  отвечает переходу  $M_1 \rightarrow 1 \stackrel{1}{>} 0$ ,  $Q_2 - Q_3 \rightarrow M_1 \rightarrow 3 \stackrel{1}{>} 1$ ;  $Q_2 + Q_3 \rightarrow 2 \stackrel{1}{>} 2 \rightarrow 3 \stackrel{1}{>} 1$  и  $Q_3 \rightarrow 2 \stackrel{1}{>} 3 \stackrel{1}{>} 1$ , где  $Q_3 \rightarrow 3 \stackrel{1}{>} 3 \stackrel{1}{>} 3$  отвечает продольной полиризации  $Q_1^2$ .

Расчет формфакторов  $g:(\kappa^2)$  в рамках РИП не представляет трудкостей.

Чтоби учесть эффекты  $n_P$ -взавмодействия, необходимо обеспечить выполнение условия унитарности для формфакторов  $g_i(\mathbf{x}^2, \mathbf{E}_{np})$ ,  $\mathbf{E}_{np}$ -иннетическая энергия относительного движения  $n_P$ -системы. Так, для "унитаризованного" формфактора  $g_i(\mathbf{x}^2, \mathbf{E}_{np})$  можно написать:

 $g_1(\kappa^2, E_{np}) = g_{18}(\kappa^2, E_{np}) \exp(i\delta_s)/\cos\delta_s$ , /2/где  $g_{18}$  -формфактор перехода  $M \to I S_0$  для РИИ,  $\delta_s$  -фаза синглетного n-рассеяния,  $\delta_s = \delta_s(E_{n0})$ .

Другой способ вичисления электромигнитного формфактора 91 осно-

ван на дисперсионных соотношениях [8]:

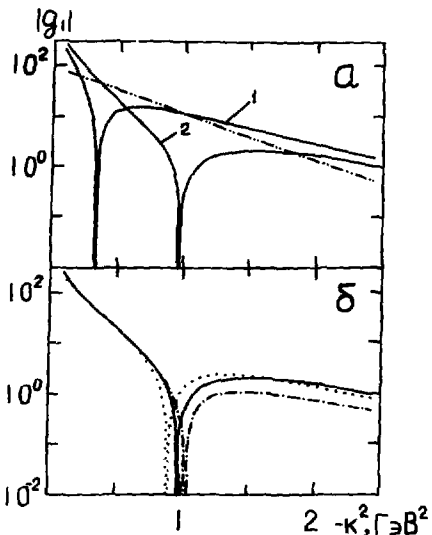


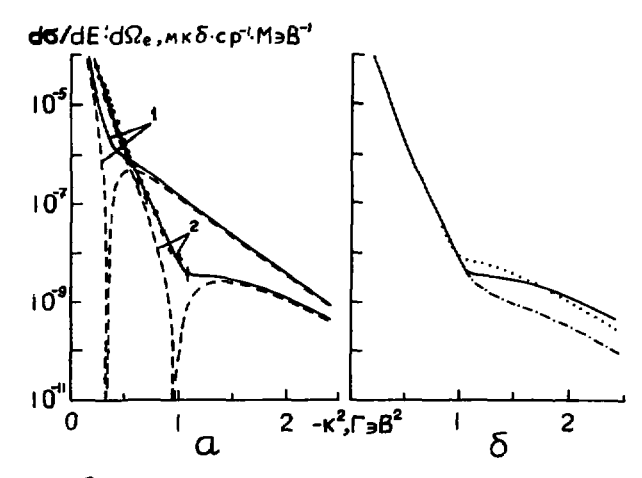
Рис. I./a/  $\kappa^2$ -зависимость формфактора  $|g_3(\kappa^2)|$ : кривая I отвечает РИП, кривая 2 - РИП-МОТ. Вилад только  $g_{MOT}^{(2)}$  изображен прерывистой линней с двойным втрихом.

/б/  $\kappa^2$ -зависимость формфактора  $|g_3(\kappa^2)|$  для развих израметризаций  $g_{MOT}$  и развих унитаризаций: точечно-пунктирная, итрих-пунктирная и сплошная кривые отвечают, соответственно  $|g_{MOT}^{(2)}|$  и / 2 /,  $|g_{MOT}^{(2)}|$  и / 2 /, а также  $|g_{MOT}^{(2)}|$  и / 3 /.

$$g_1(x) = g_{18} \exp \left\{ P(x) + i \delta_s(x) \right\}$$
 $\exp \left\{ P(x) \right\} = \left\{ \left[ x 2_{0s}^2 + (\sqrt{1-2} \frac{r_{0s}}{a_s} + 1)^2 \right] / \left[ x 2_{0s}^2 + (\sqrt{1-2} \frac{r_{0s}}{a_s} - 1) \right] \right\} \frac{1}{2}$ 

где  $x = \beta^2 = \frac{W^2}{4} - m^2$ ,  $E_{np} = W - 2m$ ,  $\sqrt{x} \cot g \delta_s(x) = -\frac{1}{a_s} + x \frac{2_{0s}^2}{2}$ ,
 $W$  — инверментная масса  $np$ -системы.

Для формфекторов  $g_2 - g_5$  можно написать:
 $g_{2-5}(x) = g_{2-5}(x) \cdot \exp \left\{ i \delta_s(x) \right\}$ ,
где  $\delta_t(x)$ -фаза триплетного  $np$ -рассеяния.



Puc. 2./a/  $n^2$ -зависимость сечения  $d^2G/dE'd\Omega_e$  при  $\theta_a=155^{\circ}$ . Пара кривых І описывает сечение для ИП, пара кривых 2 описывает сечение для РИП+МОТ, при этом втриховые линии в каждой паре изображают вилад в сечение только формфактора  $g_4(\mathbf{x}^2)$  .  $/6/\pi^2$ -зарисимость сечения  $d^26/dE'd\Omega_e$  для разных вариантов  $g_{\text{мот}}$  и разных унитаризаций. Обозначения кривых те же, что и на  $\rho$ вс. Іб.

3. Изовекторный характер  $\chi^* \bar{\mu}^* \bar{\mu}^* - \mu \chi^* \bar{\mu} \omega$ -взаимолействий приводит и тому, что отвечающие им МОТ у порога реакции  $e^- + d \rightarrow e^- + r + p$  должин характеризоваться спиновой структурой  $\stackrel{?}{\sim} U \times \hat{C}$ . Поэтому для 91 можно маписать:

 $g_{16} \rightarrow g_{16} + g_{mot}$ , а для феноменологической добавки  $g_{mot}$ , призваиной описать вилад МОТ, используем следужиме две "естественные" параметризации:

$$g_{MOT}^{(i)} = a/(1-\frac{\kappa^2}{m_x^2})^5$$
;  $g_{MOT}^{(ii)} = a \cdot \exp(\kappa^2/m_x^2)$ . 15/

Пятая степень убивания в  $g_{MeT}^{(I)}$  диктуется правилом кваркового счета. Параметры Q и  $M_{\chi}$  били майдены  $\chi^2$ -подгонкой намей модели

с учетом замени /4/ к 22 экспериментальным точкам из [3,4]. Наклучная подгонка получается для  $g_{mol}^{(2)}$  и унитаризацией /2/ с  $\alpha$  =66+I и  $M_{\rm X}$  =(0,535±0,003) ГеВ. При этом  $\chi$  2-подгонка фиксировала не только абсолотную величну  $\mathcal{G}_{\text{мот}}$ , но и ее знак /относительно амилитуди 916 , вычисляемой в РИП/.

Из рис. I видно, что добавка f мот существенно меняет величину формфактора  $g_1(\mathbf{x}^2)$  при  $-\mathbf{x}^2\lesssim 2$  Гев. При этом миникум  $|g_4(\mathbf{x}^2)|$  сдвитается в сторону больших значений  $/-\mathbf{x}^2=0,9=1,0$  Гев. По сравнению с предсказанием РИП. В дифференциальном сечении процесса  $d(\mathbf{e},\mathbf{e}^*)$  пре этот миникум заполняется виладом других мультипольных амплитуд — и прежде всего амплитуды перехода  $\mathbf{MI} \rightarrow \frac{1}{2} \mathbf{I} \quad (g_2-g_3)$  /рис.2/. При стандартном расчете МОТ изовекторной природи миникум  $|g_4(\mathbf{x}^2)|$  отодвигается в область гораздо больших значений  $(-\mathbf{x}^2)$ .

# Литература

- I. Ремало М.П. УФЖ, 3I, 491/1986/
- 2. Рекало М.П. УФЖ, 31, 805/1986/
- 3. Bernheim M., Jans B., Mougeu J. et al. Phys. Rev. Lett. ,46,402(1981)
- 4. Auffret S., Cavedon J.M., Clemens J.C. et al. ibid., 55,1362(1985)
- Sommer B. Wuel-Phys., <u>A308</u>, 263(1978); Mathiot J.F. ibid., 201 (1984); Buchmann A., Leidemann W., Arenhovel H. ibid., <u>A443</u>, 726 (1985).
- 6. Рекало М.П., Гах Г.И., Рекало А.П. УФМ, 30, II25 (1985).
- 7. Perano M.II. AD, 42, 393 (1985).
- Le Bellac M., Renard F.M., Tran Thanh Van J. Muovo Cim., 34, 450(1964)

# электрорасцепление векторно-поляризованных дейтронов, ${}^2\vec{H}$ (е , $e'\rho$ ) л и дибарионные резонансы

М.П. Рекало, Г.И.Гах, А.П. Рекало

Харьковский физико-гехнический институт АН УССР

Поиск либарионных резонансов (ДР) /I,2/ в процессах  $e^2\mathcal{H}$ —расщепления  $e^+\mathcal{H}$  +  $e^+\mathcal{J}$  (  $\mathcal{J}^*$  — ДР ),  $e^+\mathcal{H}$  +  $e^+\mathcal{L}$  +  $\rho$ ,  $e^+\mathcal{H}$  +  $e^+\mathcal{L}$  +  $\rho$ ,  $e^+\mathcal{H}$  +  $e^-\mathcal{H}$  +  $\mathcal{J}^\circ$  и г.д., имеет ряд особ яностей:

- I. Сравнительная простота инклюзивной постановки опыта для  $e^{-\frac{2}{2}H} \rightarrow e^{-\frac{2}{2}H}$ , когда не конкретизируется мода распада ДР  $d^{\frac{2}{3}}$ .
- 2. Существование целого ряда поляризационных карактеристик для процессов H(e,e/p)n и H(e,e/2,)M, чувствительных к вкладу ДР.
- 3. Заметная интерференция резонансных и нерезонансных вкладов в различных поляризационных характеристиках процессов  ${}^{2}\!\mathcal{H}(e,e')$  л.р и  ${}^{2}\!\mathcal{H}(e,e')$  д. что существенно для выявления ДР. 4. Возможность изучить  $k^{2}$ —зависимость формфакторов электровоз—
- Возможность изучить К<sup>2</sup> -зависимость формфакторов электровозсуждения ДР.
- 5. В сокое энергетическое разрешение электронных экспериментов делает их особенно пригодными для поиска узких ДР  $^{/3/}$ .

Мы рассмотрим проявления ДР в процессе  ${}^{a}H$  (e,  $e'\rho$ ) /2 . Возникающие при этом асимметрии могут оказаться чувствительными к ДР, поскольку в рамках импульсного приближения для  ${}^{a}_{+}^{a}H - n + \rho$  ( ${}^{a}_{+}^{a}$  виртуальный фотон) с вещественными амплитудами подобные асимметрии обращаются в нуль. При рассмотрении проявлений ДР в  ${}^{a}H$  (e,  $e'\rho$ ) /e0 ограничимся для простоты тремя ДР:  ${}^{a}$   ${}^{a}$   ${}^{b}$   ${}^{b}$   ${}^{a}$   ${}^{b}$   ${}^{b}$   ${}^{a}$   ${}^{b}$   ${}^$ 

$$F(0^{\dagger}) = \frac{iF(k^2)}{W^2 + iM \cdot C} \int_0^{\infty} \vec{e} \times \vec{k} \cdot \vec{U},$$

$$F(1) = \frac{iF(k^2)(\rho/\rho_1)}{W^2 - M_1^2 + iM_1\Gamma_1} \left[ f_1 \left( \vec{e} \cdot \vec{U} \cdot \hat{\vec{p}} - \vec{e} \cdot \hat{\vec{k}} \cdot \vec{k} \cdot \vec{U} \cdot \hat{\vec{p}} \right) + \right.$$

$$+ f_1 \left[ \vec{e} \cdot \vec{K} \cdot \vec{U} \cdot \vec{K} \cdot \hat{\vec{p}} \right], \qquad (2)$$

$$F(2^+) = \frac{iF(k^2)(\rho/\rho_2)}{W^2 - M_2^2 + iM_2\Gamma_2} f_2 \left( \vec{e} \cdot \vec{k} \cdot \hat{\vec{p}} \cdot \vec{U} \cdot \hat{\vec{p}} - \frac{1}{3} \vec{e} \cdot \vec{k} \cdot \vec{U} \right), \qquad (2)$$

тде  $\mathcal{G}_1(\mathcal{G}_2)$  — спиноры протона (нейтрона) в с.п.и.,  $\vec{e}$  ( $\vec{\mathcal{V}}$ ) — векторы поляризации (волновые функции)  $f^*(\mathcal{H})$ ,  $\vec{k}$  ( $\vec{\rho} = \rho \cdot \vec{\rho}$ ) — 3—импульс  $f^*($  протона) в с.ц.и.  $\rho$  — системы,  $\rho$  ( $\rho$ ).  $\rho$  — значение импульса протона при  $\mathcal{W}=\mathcal{M}_1(\mathcal{W}=\mathcal{M}_2)$ ,  $\mathcal{W}$  — инвариантная масса  $\rho$  —системы, связанная с энертией относительного движения нуклонов f — соотношением f — f — f — f — масса нуклона. Множите—ли ( $\rho$ / $\rho$ ,) и ( $\rho$ / $\rho$ ) в (2) обеспечивают пороговое поведение резонансных вкладов. Всличина f — характеризует поглощение МІ f — кванта с возбуждением ДР f — поглощение поперечного (продольного) ЕІ f —кванта с возбуждением ДР f — и, наконец, f — потлощение f — кванта с возбуждением ДР f — Параметризация (2) учитывает только образование f — системы в синглетном состоянии. Мы также предполагаем универсальную f —зависимость всех формфакторов перехода ДР—f — f — f — f — f — f — f — f — f — f — зависимость всех формфакторов перехода ДР—f — f

Фоновая часть амплитудн Г вычисляется в рамках релятивистского импульсного приближения 5. Структура дейтрона в
релятивистском формализме / описывается в терминах четырех инвариантных функций Г, С, Н и І для Н/20—вершины с одним
виртуальным нуклоном. Мы используем в расчетах параметризацию /6/
этих функций через (релятивистские) волновые дейтронные функции,
что позволяет использовать также волновые нерелятивистские функции для реалистических NN—потенциалов /7.

Величины констант  $f_0$ ,  $f_1$  и  $f_2$  были найдены с помощью  $X^2$  подгонки электронных спектров в  $f_1$  (e, e') r, в области пика квазиупругого рассеяния  $f_1$ , где с одной стороны наиболее высока точность измерений сечения, с другой — минимальна погрешность теоретических расчетов. Анализируя спектр из  $f_1$  при  $f_2$  =654 МэВ и угле рассеяния электронов  $f_2$  = 127° (9 точек в области пика квазиупругого рассеяния) и считая, что только одна константа  $f_2$  отлична от нуля, получим следующие оценки (в скобках приведено

суммарное по всем точкам значение  $\chi^2$ ):  $\pounds = 105\pm20$  (ID,6),  $\xi_f^{r} = 150\pm31$  (II,2),  $\xi_f^{r} = 1.2\pm0.4$  (I8,6),  $\xi_f = 134\pm51$  (II,3).(Заметим, что  $f_i$  имеют размерность масси, и их значения приведены в ГэВ). Анализ остальных спектров в  $^{(8)}$  дает оценки констант  $f_i$ , близкие к приведенным выше. В численных расчетах мы используем следующие значения констант  $f_0 = f_1^{\prime\prime\prime} = f_2 = 100$  и  $f_1^{\prime\prime} = 1$  . Дифференциальное сечение процесса  $f_1^{\prime\prime\prime}(e,e'\rho)$  /г. имеет вид

$$\frac{d^{3}G}{dE'dR_{e}dR_{p}} = \frac{d^{3}G}{dE'dR_{e}dR_{p}} + N\left(\frac{1}{3}xA_{x} + \frac{1}{3}yA_{y} + \frac{1}{3}zA_{z}\right),$$

$$N = \frac{\lambda^{2}}{64\pi^{3}} \frac{E'}{E} \frac{P}{MW} \left[-k^{2}(1-E)\right]^{-1}, E'' = 1 - 2\frac{\overline{K}_{AL}^{2}}{k^{2}} + \frac{1}{3}z\frac{\theta_{e}}{\omega},$$
(3)

где E (E) - энергия падающего (рассеянного) электрона в л.с.,  $d\mathcal{N}_{e}(d\mathcal{N}_{\rho})$  – телесный угол вылета рассеянного электрона в л.с. (регистрируемого протона в с.ц.и.),  $k^{2}$  – 4  $EE'sin^{2}(\partial e/2)$ ,  $k_{A.c.}$  3—импульс f'' в л.с.,  $d''SoldE'd\mathcal{N}_{e}d\mathcal{N}_{\rho}$  – сечение процесса когда все частиць не поляризованы,  $\xi$  —вектор поляризации дейтрона,  $A_i$ —анализирующие способности реакции  $\mathcal{H}$  ( e , e'  $\rho$  )/2 на векторно поляризованной мишени.

Дальнейший анализ удобно проводить в системе координат с осью 🕏 , направленной вдоль переданного 3-импульса 🖟 , плоскость ХЗ которой совпадает с плоскостью рассеяния электронов. Вектор импульса регистрируемого протона 👼 в с.ц.и. 📭-системы характеризуется полярным и азимутальным углами  $heta_
ho$  , arphi . В этой системе после выцеления кинематических переменных Е и Ф величины  $A_i$  можно представить в виде

$$A_{x} = \sin \varphi \left[ A_{x}^{(0)} + E \overline{A}_{x}^{(0)} + \sqrt{2} E(1+E) \cos \varphi A_{x}^{(1)} + E \cos 2\varphi A_{x}^{(2)} \right],$$

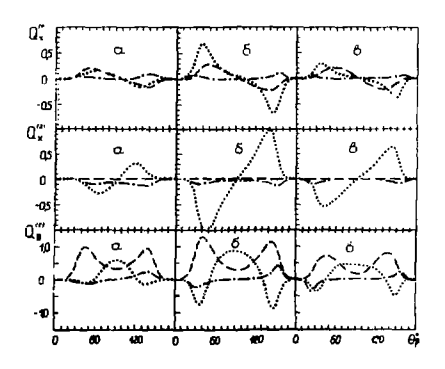
$$A_{y} = \cos \varphi \left[ A_{y}^{(1)} + E \overline{A}_{y}^{(1)} + \sqrt{2} E(1+E) \cos \varphi A_{y}^{(2)} + (4) + E \cos 2\varphi A_{y}^{(3)} \right] + \sqrt{2} E(1+E) A_{y}^{(0)},$$

$$A_{z} = \sin \varphi \left[ \sqrt{2} E(1+E) A_{z}^{(0)} + E \cos \varphi A_{z}^{(0)} \right],$$

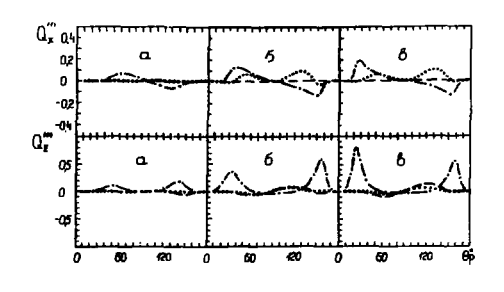
$$A_{y}^{(1)} = A_{x}^{(0)}, A_{y}^{(2)} = A_{x}^{(1)}, A_{y}^{(3)} = A_{x}^{(2)}.$$

Для компланарной кинэматики ( $\mathcal{G} = 0^\circ$ или  $180^\circ$ ) "выживает" только анализирующая функция Ау - следствие сохранения четности. В силу Т-нечетного характера асимметрий в  $\mathcal{H}(e,e'\rho)$  ле все функции  $A_{\star}^{(\kappa)}$  определяются мнимыми частями билинейных комбинаций скалярных амилитуд  $F_{B}^{(\kappa)}$  и  $F(\mathcal{F})$ процесса  $\mathcal{H}(e,e'\rho)$  ле  $(F_{B}^{(\kappa)})$  амилитуды импульсного приближения  $(F_{B}^{(\kappa)})$ . Поэтому они должны быть чувствительны и возможному вкладу ДР. Отметим, что функции  $A_{\star}^{(\kappa)}$ ,  $A_{\star}^{(\kappa)}$  и  $A_{\star}^{(\kappa)}$  определяются только поперечными компонентами ядерного гока для процесса  $(F_{\star}^{(\kappa)}\mathcal{H}) \rightarrow (F_{\star}^{(\kappa)}\mathcal{H})$ , а функции  $A_{\star}^{(\kappa)}$ ,  $A_{\star}^{(\kappa)}$  и  $A_{\star}^{(\kappa)}$  и  $A_{\star}^{(\kappa)}$  и  $A_{\star}^{(\kappa)}$  и  $A_{\star}^{(\kappa)}$  от оперечных компонент. Функции  $A_{\star}^{(\kappa)}$  и  $A_{\star}^{(\kappa)}$  и  $A_{\star}^{(\kappa)}$  от оперечных компонент. Функции  $A_{\star}^{(\kappa)}$  и  $A_{\star}^{(\kappa)}$  и  $A_{\star}^{(\kappa)}$  от оперечных компонент. Функции  $A_{\star}^{(\kappa)}$  и  $A_{\star}^{(\kappa)}$  и  $A_{\star}^{(\kappa)}$  опродольных (друг на друга), компонент.

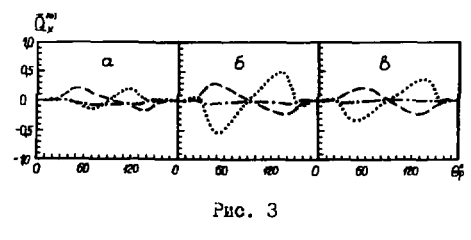
Основываясь на модели релятивистского импульсного приближения для  $f^* + f - f - p$  с учетом вклада ДР (2), мы вычислили вклады  $Q^{(*)} = A^{(*)}/(6_7 + \mathcal{E} \cdot \mathcal{E}_2)$  в эксклюзивные асимметрии  $e^2 H$  - расшепления  $(6_7 \text{ и } 6_2 - \text{поперечное и продольное сечения фоторасщепления дейтрона). Расчеты проведены для квазиупругой кинематики <math>k^2 = M^2 - W^2$  для определенности  $\mathcal{E} = 0.5$ . На рис.І представлены вклады в асимметрию  $Q^{(*)}_{\alpha}$ ,  $Q^{(*)}_{\alpha}$  и  $Q^{(*)}_{\alpha}$  как функции угла вылета протона  $\theta_p$  в с.ц.и. и р -системы для трех пар значений  $k^2$  и  $E_{np} = W - 2m$ . Видно, что асимметрии слабо меняются с изменением  $\chi^2$ , в то же время они сильно зависят от  $\theta_p$ . В пике квазиупругого рассеяния ( $\theta_p = 0^\circ$  и  $180^\circ$ ) эти асимметрии обращаются в нуль. Отметим, что различные структурные функции  $A^{(m)}_{\alpha}$  по-разному чувствительны к вкладам ДР: наибольшей чувствительностью характеризуются функции  $A^{(m)}_{\alpha}$ ,  $A^{(m)}_{\alpha}$   $A^{(m)}_{\alpha}$ 



PMC. i



Pac. 2



ог угла 🔑 отношений  $Q_{i}^{(m)} = A_{i}^{(m)} (6_{in} + \epsilon 6_{i})$ при  $\mathcal{E} = 1/2$  и кинематических условиях: а-/к%=0.5 ГаВ2 и Епо= =128 MaB; 6-/k4I PaB2 и *Ето* = 250 МаВ; с-/к¾= =I.5 ГаВ<sup>2</sup> и *Ещ* = 364 МаВ. Пунктирные линии отвечают расчету в ИП C VYETOM IP O+( £=100.  $f_1'' = f_2' = f_3 = 0$ ), TOчечные кривые - ИП + IP  $2^+(f_2=100, f_3=f_3=0)$ , штрих-пунктирные - $MII + IIP I^{-} (\cancel{f}_{*}^{r} = 100).$ f, = I . f = f = 0 ).

Рис. І-З. Зависимости

# Литература

- I. Макаров М.М. ФЭЧАЯ, 1984, 15, с. 941.
- 2. Svarc A. Bucl. Phys., 1985, A434, p.329.
- 3. Tatischeff B. Rucl. Phys., 1985, 4446, p.355.
- 4. Matveev V.A., Muradyan B.M., Tavkhelidne A.M. Lett. Huovo Cimento, 1972, 5. p.907, ibid. ,1973, 2, p.719.
- Renard F.M., Tran Thanh Van J., Le Ballac M. Buovo Cimento, 1965, 37, p.565.
- 6. Buck W.W., Gross F. Phys. Rev., 1979, <u>D20</u>, p.2361.
- Lecombe M., Loiseau B., Richard J.M. et al. Phys. Lett., 1981, <u>B101</u>, p.139.
- 8. Всаулов А.С., Рекало А.П., Рекало М.П., Тытов Ю.И. и др.ЯФ, 1987, 45, с. 410; Тытов Ю.И., Всаулов А.С., Ахмеров Р.В. и др.Письма в ЖЭТФ, 1984, 39, с.498.
- Рекало М.П., Гах Г.И., Рекало А.П. Препринт X0ТИ 83-4, 1983; препринт X0ТИ 87-1, Харьков, X0ТИ АН УССР, 1987.

# РОДДЕНИЕ АНТИПРОТОНОВ, КАОНОВ И ПИОНОВ ПРИ СТОЛКНОВЕНИИ РЕЛЯТИВИСТСКИХ ЯДЕР С ЭНЕРГИЕЙ 3.65 ГЭВ/НУКЛОН

А.И.Берлев, В.А.Краснов, А.Б.Куречин, В.С.Пантуев, М.А.Прохватилов, А.И.Решетин, С.Н.Фихиппов Институт ядерных исследований АН СССР, Москва

### Т. Ввеление

В последнее время большое внимание привлекается к исследованию рождения странных частиц и античастиц при столкновение релятивистс-KHX SIED /I/. XOTS HEROTOPHE BUILOMHERHME HEISBHO CHERKE OTHOMERES BUхода странных и нестранных частиц не дают существенного изменения этой величины при образовании кварк-глючной плазым /2,3/, можно прецположеть, что рожнение частии с необычным кварковым составом позволят исследовать механизм отолкновения ядер. Для этого необходимо сравнивать сечения рожнения странных и нестранных частии при столкновении яцер с япреми и нуклонов с япреми при опинаковых кинематических условиях. Измерение выхода заряженных к-мезонов имеет преимущества, т.к. кварковый состав К+ и К- - мезонов существенно разжичен. К- - мезон ВКЛЮЧАЕТ ТОЛЬКО МОРСКИЕ КВАРКИ. Имеет СМИСЛ НОРМИРОВАТЬ ВСЕ МЭМЕРЕния на выход положительных и отрешательных пионов, иля которых не оживается какех-либо аномальных явлений, и увеличение выхода для стояжновения илео обусловлено день увеличением эйбективного числа везимодействующих нуклонов.

Выполненные ранее эксперименты по рождению каонов стимулеровали ряд теоретических расчетов (4-7), использующих различные варманты каскадной и термодинамической модели. Однако эти эксперименты (8-10) были выполнены при энергиях до 2,1 ГэВ/нуклон, т.е. ниже порога рохдения К — мезонов в муклон-нуклонных соударениях, равного 2,5 ГэВ, что не поэволяет непосредственно сравнивать выход К и К — мезонов. Новые экспериментальные данные по измерению в одних условиях писнов и каснов на пучке ядер углерода при энергии 3,65 ГэВ/нуклон (11) были проанализарованы в рамках партонной модели

В настоящей работе приводятся более полные данные по рождению положительных и отрацательных паонов и каонов при указанной энергии на нучлон налетающего ядра /13/. Измерения выполнены на пучках ядер дейтронов и ядер углерода. В качестве мишеней были использовани углеродная и свинцовая мишени. Угох рождения 240 в лабораторной система. Импульсы мезонов в интервале 0,5 – I,I ГзВ/с.

Впервые получены данные о выходе антипротонов при столкновении релятывистских ядер углерода и меди  $^{/14/}$ . Импульс рожденных антипротонов 0,8 ГэВ/с, угол рождения  $24^{\circ}$ .

### П. Методика эксперимента

Измерения выполнены на магнитном канале установки "КАСПИЙ" Института ядерных исследований АН СССР, расположенной на выведенном цучке релятивнотских ядер синхрофазотрона Лаборатория высоких энергий ОМЯИ. Лубна. Магнитный канал, собранный по схеме QQDQQD, работал в качестве спектрометра мезонов и антипротоков, обеспечивая импульсный закват около +2%. Наличие промежуточного фокуса позволяло снязять фон в разместить счетчики времяпролетной системы. Разделение каонов и антипротоков от интенсивного физического фона пионов проводилось с использованием методики времени пролета и черенковских счетчиков, работающих в режиме полного внутреннего отражения света для быстрых частиц. При измерении каонов применялись две продетные базы, 7 м и IO м, что позволяло выделить фон квазислучайных совпаденяй. Антипротоны, имеющие существенно более визкий выход по отношению к плонам, чем каоны, дискрименировались также тремя 🛕 🗈 сцентелляционными счетчекаме. Интенсивность пучка япер дейтерея и углерода составляла около 10<sup>8</sup> ядер за импульс ускорителя. Толинн мешеней из углерода и свинца были 8-20 г/см<sup>2</sup>.

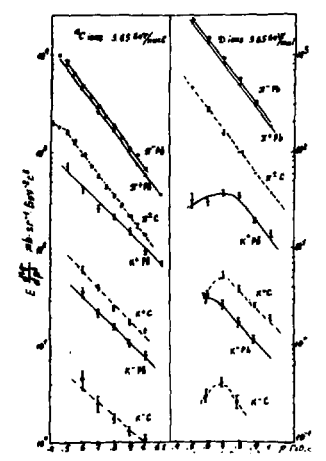
Конструкция магнетооптической системы позволела провести оценку числа протонов, проходящих через настроенную на отрацательную полярность частиц систему из-за многократного отражения от полюсов магнетов. При настройке первой части системы на положительную полярность, а второй на отращательную число протонов составило 1,3.10<sup>-5</sup> полного числа протонов при положительной полярности всего спектрометра. Обратная полярность первой и второй части спектрометра дает оценку 1,2.10<sup>-4</sup> протонов. Отсюда оценка примеся протонов к антипротонам в спектрометре не более 3.10<sup>-9</sup>, что на три порядка меньше измеряемого эффекта.

При расчете сечений рождении из данных эксперимента учитывались поправки на распад мезонов, на многократное рассеяние в воздухе и материале детекторов, поглощение первичного пучка частиц в мишени и поглощение рожденных частиц, аннигиляция антипротонов. Точность абсожотной нермировки сечений оценивается на уровне 20%.

# Ш. Результати измерения сечений

рождения пионов и каонов

Инидиванные спектры писнов и каснов, образованных при столиновении ядер углерода и дейтерия с ядрами углерода и свинца, приведены на рис. I.



Рас. I. Зависимость внваряантного сечения рождения УГ , К — мезонов ядрами углерода и дейтерия на ядрах свинца и углерода от вмпульса мезонов в лабораторной системе координат.

Спектры пнонов корошо аппроксимируются экопоненциальной SABBCEMOCTED  $G_{inv} \sim exp(-\rho/\rho_0)$ В Зависимости от импульса пионов в лабораторной системе. MADAMSTRA HARMOHOB CHERTDOB пионов одинаковы для различных налетающих ядер углерода и дейтерия и ядер мишени углерода и свинца, Д с =0.200 ± ± 0.005 ГэВ/с. Это свойство спектров плонов для столь сильно различающихся по числу нуклонов систем онло он трудно объяснить при наличии большого числа соударений образованных плонов с нуклонами. По-вишимому, сильное поглошение имведя вономп значительно уменьшает число многократных столкновений пионов до вылета из объема ядра. Если нет какой-то случайной компенсации различных эффектов, равенство наклонов спектров также указы-

вает на малую рожь перерассеяний и взаимодействий во входном канале, т.е. нуклон-нуклонных реакций, приводящих к рождению пионов. Как судет показано далее, хорошая применимость партонной модели также свидетельствует о наличии локального партон-партонного взаимодействия во входном канале.

Форма спектров каснов, образованных при столкновении дейтронов с ядрами, отклоняется от экспоненциальной зависимости. В то же время наблюдаются экспоненциальные формы спектров К<sup>+</sup> и К<sup>-</sup> – мезонов при соударении ядер углерода с ядрами углерода и свинца. Таким образования каснов на пучке дейтронов, которые можно рассматривать как два слабосвязанных нуклона, оказывается существенно различным от случая ядро-ядерных соударений.

Параметры наклонов спектров  $K^+$  и  $K^-$  -мезонов одинаковы при столиновении ядер углерода с ядрами углерода и свинца и равни  $\rho_{oK} \approx 0.27 \pm 0.01$  ГэВ/с. Однако язвестно, что  $K^+$  - мезоны в исследуемом интервале импульсов практически не поглощаются в нуклонной среде,

в то время как длина поглощения К — мезонов достигает значений около 8 Фм. Поэтому многократное рассеяние К — мезонов аналогично пионам может быть подавлено. О мелой роли взаимодействий во входном канале применими те же соображения, что и для пионов. Кроме того, оценки по партонной модели позволяют объяснить различие наклонов спектров пионов и каонов.

### ІУ. Анадыз спектров шионов и каонов

Для количественного анализа сечений рождения пионов и каснов представим данные в виде зависимости отношений инвариантных сечений к<sup>+</sup>/ $\eta$ <sup>+</sup>, к<sup>-</sup>/ $\eta$ <sup>-</sup> в зависимости от лабораторного импульса мезонов для различных комбинаций сталкивающихся ядер, см.рис.2.

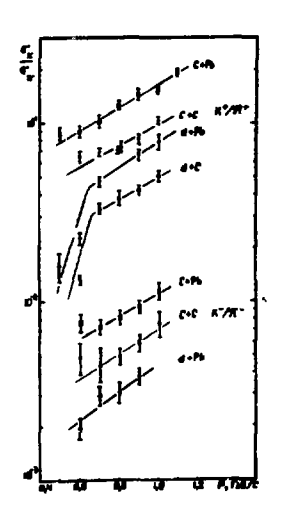


Рис. 2. Зависимость отношений сетемий К+/у+ в К-/у- — мезонов от импульсов мезонов в дабораторной системе координат дажичных комбинаций сталкивалициком ядер.

Как видно из рисунка, отношение К+/4Т+ для машени из свинца существенно превышает -ту глд ошношонто сонгитокана леродной мешени как для налетапших дейтронов, так и для налетающих ядер углерода. Аналогачное превышение наслодается пля отношения К 🖊 для налетающих ядер углерода. Извес-THO, TTO K+ - MOSORM IIDERTHчески не поглошаются в среде нуклонов в нашем плацазоне импульсов. Реакция перезарящи не дает вклада в значение выхода К<sup>+</sup> - мезонов, поскольку **ХРЕНОВЛЕООВН ХЕООО В ТОЛК** К<sup>+</sup>М≠Р К<sup>О</sup>. С другой стороны, -дкар котоворожной иносем - <sup>+</sup>но, что полино приводить к YBORNACHED OTHORRES K+AT+ для более тяжелых ядер мишени. Зависимость сочения поглошения ROTORTHO ENTITORS TO SONORS

весьма слабой. К — мезони также достаточно сильно поглощаются нуклонами вследствие процессов типа К № ≈ Т У . Однако сечение поглощения существенно зависит от энергии. Поскольку после рождения мезони распространяются в нуклонной среде, образованной составной системой сталивающихся ядер, их энергию относительно нуклонов для оценки сечения поглощения надо брать в системе координат центра масс этих ядер. Тогда одна в та же энергия мезона в лабораторной системе соответствует меньшей энергии в системе центра масс ядер для случая углеродуглеродных соударений, чем для столкновения ядер углерода с ядрами свинца. Для К - мезонов это различие приводит к разнице в вляне погдо 15 Фм. и к относительному увеличению выхода К мезонов иля более тяжелой мишени при фиксированном значении импульса К - мезона в лабораторной системе.

Для количественных оценок измеряемое сечение рождения К выражено через 🧓 - сечение при отсутствии поглощения мезонов. длину поглощения  $\lambda$  и эффективный путь в ядерном веществе L=0.7 ×  $x(R_A+R_B)$ , где  $R_A$  в  $R_B$  радвусы сталкивающихся ядер,  $R_-$ 1,15 $A^{1/3}$ фм. Такое выражение для ↓ , как показано в работе 157, эффективно учитивает поправки к используемому одномерному рассмотрению:

$$G = G_0 \exp(-L/\lambda). \tag{I}$$

где  $\lambda = (\int G_{AN}^{ads})^{-1}G_{AN}^{ads}$  — сечение поглощения мезонов нуклонами,  $\rho$  =0.17  $\phi$ m $^{-3}$  — ядерная плотность. Сечения поглощения каонов на нуклонах были взяты из обзора /16/. Производилось усреднение по протонам и нейтронам в ядре для реакций вида К № 🗢 🛪 Ү

Для оценки длини поглощения пионов нуклонами были использованы экспериментальные данные о сечениях поглодения плонов ядрами алюминая, меди и золота при энергиях 180-280 МэВ 177. Эти данные корошо описываются формулой

$$\mathcal{G}_{a}^{ab} = \pi R^{2} [-\exp(-d/\lambda)], \qquad (2)$$

гле d=4/3R - средний путь пионов, налетающих на ядро, при значении й =5 фм. Это значение принималось и для больших энергий пионов. поскольку, согласно оценкам, длина свободного пробега пионов при энергиях выше  $\Delta$  - резонанса меняется слабо /187.

После ввененя поправок на погложение отношение сечений рожиения каснов и писнов в пределах точности измерений не зависит от массового числа япер мишени для панного типа япра-снаряда. Зависимость сечений рождения от массового числа ядер мишени А можно параметривовать в форме 6~ 4 ч. Тогда параметры « для надетающих ядер углерода и дейтерия одинаковы и равны для рождения  $\pi^{\pm}$  - мезонов 0.56+0.01° дия К<sup>±</sup> мезонов 0,7I±0,0I. После учета поглощения мезонов зависимость сечения рождения бо ~ А от массового числа ядер мишени становится одинаковой для  $\pi^{\pm}$  и  $K^{\pm}$  - мезонов,  $\alpha_{\bullet} = 0.70 \pm 0.02$ .

Своеобразная зависимость сечений рождения К - мезонов от массового числа налетающего ядра-снаряда наблюдается, при сравнении отношений  $K^+AR^+$  в  $K^-AR^-$  для соударений  $C_+PR$  и  $d_+PR$  и  $K^+AR^+$  для

соударений C + C и of + C. Как видно из рис.2, относительный выход странных мезонов при одинаковом лабораторном импульсе в два раза и более выше при столкновении ядер углерода с ядрами, чем при столкновения дейтронов с ядреми. Параметризация сечений рождения мезонов в форме б ~ В в - массовое число ядра-снаряда, приводит и значениям  $\beta$  =0.69 $\pm$ 0.02 для  $\pi^{-\pm}$  — мезонов, что близко к геометричес-кому значению 2/3. Для  $\kappa^{\pm}$  — мезонов  $\beta$  =1,1 $\pm$ 0,1 при больших значениях импульсов и растет до I,5 при малых импульсах. Больший относительный выход К - мезонов по сравнению с пионами при столкновении ядер углерода с ядрами может быть обусловлен большим влиянием кластерных конфигураций в налетающем ядре или выходом на скейлинг для ядро-ядерных соударений в отличие от нуклон-ядерных соударений, как показано далее при обсуждении партонной модели. Тем не менее необходимо провести расчеты по каскадной модели, чтобы оценить величину возможного кинематического эффекта изменения отношения сечений рождения К/77 мезонов для ядер углерода в качестве налетающих частиц из-за увеличения плотности в области взаимодействия при учете в промежуточном состоянии пионов, нуклонов и д -изобар, а для рождения  $K^-$  – мезонов также дополнительный канал  $\mathcal{T}^- + Y \rightarrow K^- + N$  .

Недавно в измерениях при энергии I4,5 ГэВ/нуклон для столкновения ядер серы и золота были получены отношения полных сечений рождения к $^+/\eta^+=0$ ,19 $\pm0$ ,05 и К $^-/\eta^-=0$ ,06 $\pm0$ ,05  $^{/19}$ . Данные сравниваются со значением для  $\rho$  +  $\rho$  столкновений К $^\pm/\eta^\pm=0$ ,05+0,1. Однако наблюдаемое изменение отношения, возможно, обусловлено эффектом поглощения пионов для столкновения ядерных систем, подобно тому, как было рассмотрено ранее в настоящей работе.

Анализ по партонной модели выполнен согласно подходу, развитому в работе  $^{20}$ , где для реакции типа,

$$B + A \rightarrow \mathcal{H}^{\pm}, K^{\pm} + X \tag{3}$$

вводятся с учетом массовых поправок редятивистски-инвариантные параметры х и  $\mathbf{Z}$ , выражающие долю импульса партона от импульса нуклона в ядре мишени и в налетающем ядре. Для их нахождения используются соотношения для 4-импульсов  $\rho_g$ ,  $\rho_A$ ,  $\rho_A$  — соответственно нуклона налетающего ядра, ядра мишени и рожденного мезона:

$$(P_{R} + x P_{A} - P_{1})^{2} = (M_{R}/\beta + x M_{\alpha}/\alpha + m_{i})^{2}$$
 (4)

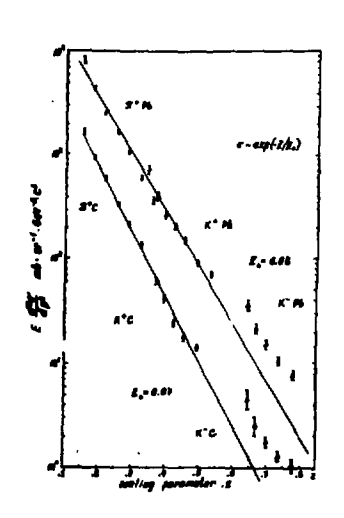
$$(Z\rho_B + \rho_A - \rho_I)^2 = (ZM_B/\beta + M\alpha/\alpha + m_i)^2,$$
 (5)

где  $M_{\beta}$  ,  $M_{cl}$  – масси налетающего ядра и ядра мижени,  $m_{i}=0$  для рождения пионов,  $m_{i}=m_{i}-m_{i}$  разница масс  $\Lambda$  – частици и нуклона,

для рождения  $K^+$  — мезонов и  $m_i = m_K$  — мезона для рождения  $K^-$  — мезона.

Поскольку в кинематических условиях настоящего эксперимента параметр и мело меняется в пределах интервала импульсов мезснов, на рис. З приведена зависимость структурных функций от в для рождения Т , к<sup>+</sup> и к<sup>-</sup> - мезоноз при ядро-ядерных соударениях. Видно, что данные по рождению плонов и к<sup>+</sup> - мезонов удовлетворительно описываются универсальной экспонентой

$$G \sim e \times P \left(-\frac{7}{2}\right)$$
 (6)



Рас. 3. Зависимость структурных функций от параметра б , для взаимодействия ядер углерода с ядрами углерода и свинца.

с показателем экспоненты  $\frac{2}{20} = 0.08$  для С + Р8 соударе – ний и 2- =0.06 для С + С соударений. Панные пля К -ROTOGREES NO MOTO BUIL BOHOESM несколько выше этой кривой. Однако желательно проведение нзмерений в более широком KEHOMETHYCKOM EHTODBEJO. YTO поэволят изучеть скейлинговое поведение для пионов в **КАОНОВ ПРИ ОЛЕНАКОВЫХ** ЗНАЧОниях параметра 💈 . Отметим, что в представлении перемен-HARMOHM CHERTDOB T H ной К+ - мезонов становятся ошнаковым. Пля налетающих лейтронов подобное скейлинговое поволение отсутствует. Обна-DYMSHEMS SAKOHOMSDHOCTH MOTYT CHAZOTOFICTBOBATE O CYMOCTвенной рожи кварк-партонного **МОХАНИЗМА РОЖЕНИЯ МОЗОНОВ В** япро-яперных соударениях.

У. Результаты взмерения выхода антипротонов в ядро-ядерных соударениях

Было зарегиотряровано 9 собитяй, которые идентибицированы как антипротоны. Импульс антипротонов в лабораторной системе  $0.8 \, \Gamma aB/c$ . Получено значение отномения сечений рождения антипротонов в пионов  $\widehat{P}/A^{-} = (4\pm I.5).10^{-6}$ , значение инвармантного сечения  $\widehat{G}_{inv}^{*} = 6,3\pm 2$  мкб.  $\Gamma aB^{-2}.op^{-1}.o^{-3}$ .

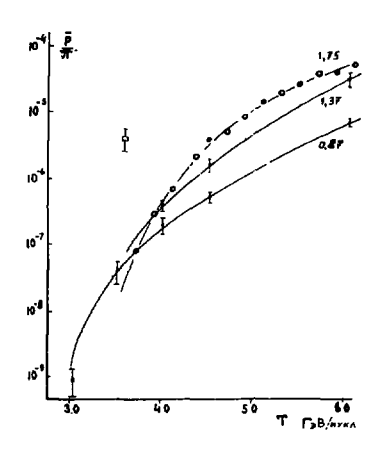


Рис. 4. Отношение выходов антипротонов и пионов в зависимости от энергии на нуклон ядер пучка. Кривые данные работ /21,23/ при импульсах вторичных частиц, указанных на кривых. Точка — результат данной работи при 0.8 ГэВ/с.

На рис.4 приведено сравнение с данными при столкновении протонов с ядрами меди. Видно, что обнаруженное увеличение выхода антипротонов по ОТНОШЕНИЮ К ПИОНАМ ПЛЯ СТОЛКНОвений яцер углерода с яцрами меци составляет около 60 по сравнению с протон-яцерными соударениями в той же кинематике 721,22/. Рождение антипротонов при энергии 3.65 ГэВ/ /нуклон является полпороговым процессом. Однако, как показали расчеты, получить обнаруженное увеличение сечения при принятом значения максимального ферми-импульса ().27 ГэВ/с пля распределения с острым краем не ущается цаже при учете рожноил иннготужемост седер имен かんチャルカ . Расчеты по моцели файерстрика дают весьма близкое значение <sup>/23/</sup>. Качественно наблюдаемый эффект соответствует партонной модели, в

которой ожидается усиление выхода антипротонов цля налетающих ядер углерода за счет наличия партонов с параметрами Z > 2. Аналогичный эффект возможен при наличии в ядрах углерода кластерных или много-кварковых конфигураций.

# ут. Заключение

Исследование рождения пионов, каонов и антипротонов при столкновении релятивистских ядер обнаруживает ряд новых эффектов, часть из которых, возможно, определяется кварк-партонной структурой ядер при высоких энергиях.

# Литература

- I. Stock R. Phys.Rep., 1976, 135, p. 261.
- 2. Muller B. Nucl. Phys., 1987, A461, p. 213.
- 3. McLerran L. Nucl. Phys., 1987, A461, p. 245.
- 4. Cugnon J., Lombard R.M. Phys. Lett., 1984, 134B, p.392.

- Zwermann W. et al. Phys.Lett., 1984, 134B, p. 397.
- 6. Olive T. et al. Phys.Lett., 1980, 95B, p. 355.
- 7. Гудима К.К., Тонеев В.Д. ОИЯИ, Р2-83-199, Дубна, 1983.
- 8. Schnetzer S. et al. Phys. Rev. Lett., 1982, 49, p. 989.
- 9. Shor A. et al. Phys.Rev.Lett., 1982, 48, p. 1597.
- IO. Barash E. et al. Phys. Lett., 1985, 161B, p. 265.
- II. Гаврилов Ю.К. и др. ОИЯИ, 1,2-84-599, Дубна, 1984, с.227.
- I2. Курепин А.Б., Пантуев В.С. ОИЯИ, I,2-86-668, Дубна, I986, с.273
- Курепин А.Б. и др. Письма в ЖЭТФ, 1988, 47, с.16.
- 14. Белдин А.А. и др. Письма в ЖЭТФ, 1988, 48, с.127.
- I5. Rundrup J. Phys.Lett., 1981, 993, p.9.
- I6. Dover C.B., Walker G.E. Phys.Rep., 1982,89,p.1.
- I7. Nakai K. et al. Phys.Rev.Lett., 1980,44,p.1446.
- Нестеров М.М., Тарасов Н.А. ЯФ, 1983, 37, с.308.
- 19. Abott T. et al. Z.Phys., 1988, 380, p. 135.
- 20. Балдин А.М. ОИЯИ, 2-82-568, Дубна, 1982.
- 2I. Dorfman D.E. et al. Phys.Rev.Lett., 1965, 14, p.995.
- Лепихин Ю.В. и др. Труди ії Симпозиума по нуклон-нуклонным и адронядерным взаимодействиям. Изд. ЛЕН АН СССР, Ленинград, 1986, с. 299.
- 23. Тонеев В.Д. и др. ЭЧАЯ, 1986, 17. с.1093.

# DELTA EXCITATIONS IN NUCLEI: MICROSCOPIC DESCRIPTION OF PION NUCLEAR REACTIONS

E. Oset, C. Garcia-Recio\*, L.L. Salcedo\* and M.J. Vicente\*

Departamento de Fisica Teórica and IFIC Centro Mixto Universidad de Valencia - CSIC Facultad de Fisica, Burjassot (Valencia) Spain

#### 1. INTRODUCTION

The diversity of pion nuclear reactions: elastic, inelastic, single charge exchange, double charge exchange and absorption has made difficult to obtain a single picture that describes simultaneously all the different channels. Partial attempts have been done using cascade calculations  $^{1,2}$ ; another attempt was done using transport equations  $^{3}$ . These studies start from free TN amplitudes or cross sections and parametrize the absorption probability in one way or another, reproducing the cross sections at a qualitative level. On the other hand more sophisticated pictures like the  $\Delta$ -h model at resonance  $^{14,5}$  and different approaches at low energy  $^{15,7}$  have been limited to the study of elastic scattering and a few other exclusive reactions and some inclusive ones like inelastic scattering  $^{18}$  or pion absorption  $^{19}$  with severe limitations like allowing for only one quasielastic collision  $^{18}$  or ignoring events with quasielastic collisions prior to pion absorption  $^{19}$ .

The work presented here combines a sophisticated calculation of the pion nucleus optical potential, using a field theoretical many body approach, with a skillful separatio, of the imaginary parts of the optical potential which can be related to the

Center for Theoretical Physics, MIT, Cambridge, Mass 02139, USA

\*\* Institute for Theoretical Physics, University of Regensburg, 8400 Regensburg,
West Germany

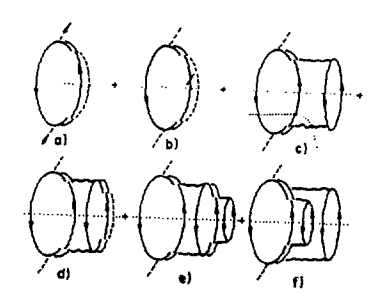
<sup>\*</sup> Supported in part by CICYT

probabilities of the Offerent reaction channels. The information obtained in this way is then used to obtain differential elastic cross sections, double differential cross sections for the inelastic, single charge exchange and double charge exchange reactions and absorption cross sections, with a remarkable success in a wide range of energies and for different nuclei.

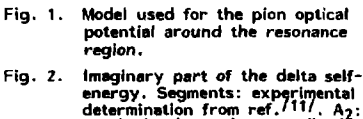
# 2. THE MODEL

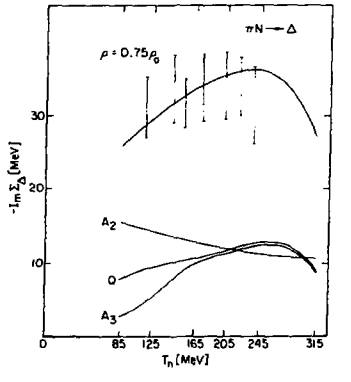
We concentrate in the region of the  $\Delta$  resonance and use the tools of the  $\Delta h$ model<sup>15</sup> to construct a microscopical pion nucleus optical potential, with the couplings of mesons to nucleons and isobars as only input. The differences with the approach of ref. 15/ are: 1) higher order terms in the number of ph excitations have been included until convergence has been found. This is accomplished at the level of 3p3h for pion absorption which has the largest phase space  $^{/10/}$ . 2) The induced interaction instead of the effective ph or Ah interaction is used. 3) The calculations are done in nuclear matter instead of in finite nuclei. Translation to nuclei is done by means of the local density approximation, but taking into account finite range effects. This allows us to perform the calculations for any nucleus while the approach of ref. 151 required a separate treatment for each nucleus, which became extremely difficult to handle for large nuclei.

The model used is depicted diagramatically in fig. 1. The pion excites a \( \Delta \) h component in the nucleus, and this A excitation can decay via Nn production (quasielastic scattering) (fig. 1a), conveniently corrected by Pauli blocking (1b), or it can decay into more complicated channels like AN + NN (two body absorption) (1c) etc. Diagrams 1e, 1f would account for three-body absorption.



potential around the resonance region.





two body obsorption contribution, Ag: three body absorption contribution. Q: higher-order quasielastic contribution.

Using standard many body techniques  $^{/12,13/}$  we can evaluate the optical potential or pion selfenergy ( $\Pi=2\omega\ V_{opt}$ ) corresponding to the diagrams in fig. 1. The wavy line stands for the ph and  $\Delta h$  induced interaction (effective interaction including ph and  $\Delta h$  excitations in an RPA sense). On the other hand let us note that if in fig. 1 we remove the external pion lines and the hole line to the left of the diagrams we are left with a set of diagrams for the  $\Delta$  selfenergy. Indeed, the diagrams of fig. 1 are calculated selfconsistently in the sense that the  $\Delta$  selfenergy is included in all the  $\Delta$  propagators, in other words, that the optical potential is of the type  $^{/14/}$ 

$$V_{\text{opt}}(q) \approx \frac{1}{\sqrt{s - M_{\Delta} + i \frac{\Gamma}{2} - \Gamma_{\Delta}}},$$
 (1)

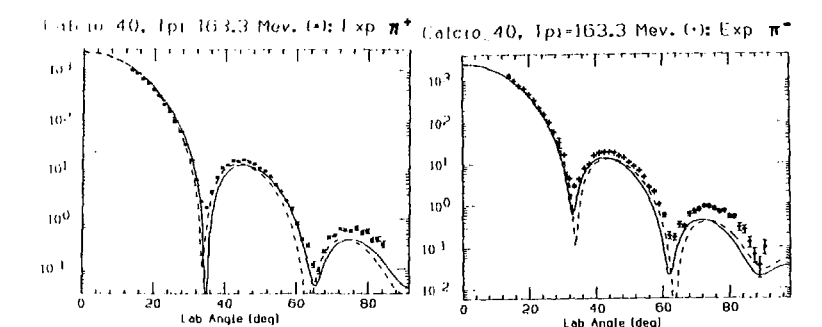
where  $\Sigma_{\Delta}$  is the  $\Delta$  selfenergy in the medium and  $\Gamma$  the free  $\Delta$  width. We thus perform first a calculation of the  $\Delta$  selfenergy in infinite matter as a function of the density, replace this function of the density in eq. (1) and then evaluate the differential cross section for pion nucleus scattering, or the total cross section via the optical theorem, in a fully quantum mechanical way, by solving the Klein-Gordon equation.

We can see the results for Im  $\Sigma_{\Delta}$  of ref./15/ in fig. 2, which compare very well with the empirical determination of ref. 11 (an effective density  $\rho=0.75\,\rho_0$  is taken for comparison). In figs. 3 and 4 we also show the results for elastic scattering for  $\pi^+$  and  $\pi^-$  differential cross sections in <sup>40</sup>Ca. The quality of the results for different nuclei is about the same as in these figures/16/. The results, as can be seen in the figures depend only a bit on shifts introduced in the real part of the  $\Delta$  selfenergy. One should notice that the level of agreement is rather good in spite of the decrease in four orders of magnitude of the cross section. The calculations include also an swave part, in addition to the p-wave part of the  $\Delta$ -h excitation which is only relevant at energies below  $T_{\pi}=100$  MeV. It is calculated in ref. <sup>16</sup>/and is in agreement with empirical determinations of low energy optical potentials for the imaginary part (we use the empirical real part).

The total reaction cross section is calculated from  $\sigma_{\rm tot}$ , obtained via the optical theorem, substracting the integrated elastic cross section. It can be seen in fig. 5 as the dashed dotted line which agrees also quite well with the experimental data /11/ except at energies below  $T_{\rm m}$  = 100 MeV where small differences can be appreciated.

Next we look at the different reaction cross sections. The difficulties in giving a full quantum mechanical treatment of this reactions have been stressed in refs. <sup>18,91</sup>. However, the many body techniques used here allow for a clear separation of all the reaction channels and one can obtain the probability that any reaction takes place at any point of the nucleus provided that the pion reaches this point. We know that a pion in infinite matter carries a phase e<sup>-i Vopt-t</sup>. Hence the probability of finding the pion in the elastic channel is proportional to

$$|\psi\rangle^2 \propto e^{2 \text{ Im } V_{\text{opt}} \cdot t} \equiv e^{-\Gamma t}$$
. (2)



Figs. 3 and 4. Differential cross sections for  $\pi^{+}$  and  $\pi^{-}$  elastic scattering on <sup>40</sup>Ca as a function of the angle.

Thus the rate at which a pion goes into any reaction channel is then given by

$$\Gamma = -\frac{1}{N}\frac{dN}{dt} = -2 \text{ Im } V_{\text{opt}} = -\frac{1}{\omega} \text{ Im } II.$$
 (3)

However, when evaluating the imaginary part of the diagrams in fig. 1, one can separate the different sources according to the different reaction channels that they represent. Indeed, the imaginary part of a Feynman diagram appears when we place on shell, in the integration over the internal variables, the lines cut by a horizontal line (dotted line in the figures). Placing on shell these particles correspond to a physical reaction channel. The channels associated to the cuts in the figure are thus clear. The ones in 1a, 1b correspond to quasielastic scattering (1b, Pauli correction); the upper cut in 1c, to two body pion absorption; the lower one in 1c, as well as the one in 1d, to higher order quasielastic scattering, while the cuts in 1e, 1f represent three-body absorption. The corresponding contributions to the  $\Delta$  selfenergy are split in fig. 2, showing the amount of two-and three-body absorption and the fact that a part of Im  $\Sigma_{\Delta}$  is not related to pion absorption but accounts for higher order quasielastic corrections.

The evaluation of the different sources of imaginary part by means of Cutkowsky rules enables us to calculate the probabilities for any reaction to take place as a function of the nuclear density. The use of the local density approximation  $(\rho \to \rho(\tau))$ , folding these functions with the range of the interaction, allows us to convert these results into local probabilities inside the nucleus for any reaction. However, there is a coupling of all these channels in the evolution of a pion through the nucleus and the evaluation of the different reaction cross sections requires especial care (a pion absorbed can no longer undergo any reaction; a pion that scatters quasielastically changes direction and energy; if there has been a charge exchange step, there has to be another one to give a contribution in the inelastic

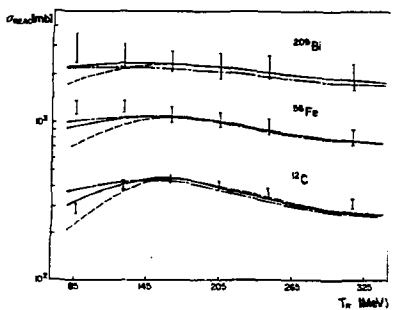
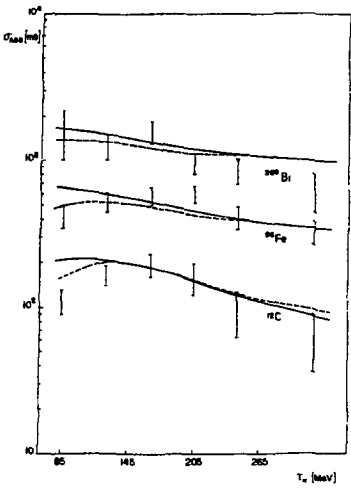


Fig. 5. Total reaction cross section. Dashed line: straight π trajectories between collisions. Continuous line: classical trajectories. Dash-dotted line: full quantum mechanical calculation.



A(π', π') x

Fig. 7. Quasielastic cross section.

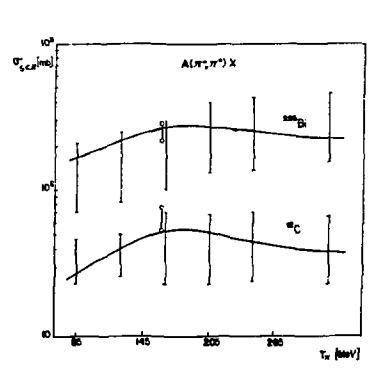


Fig. 6. Absorption cross section. Same meaning as fig. 5.

Fig. 8. Single charge exchange cross section.

channel, etc.). An easy way through all these ramifications is a computer simulation which we have used to evaluate the reaction cross sections  $^{/18/}$  and briefly discuss in the next section.

### 3. COMPUTER SIMULATION

A large number of pions are generated with random impact parameter. At regular steps, small enough to keep the reaction probabilities much smaller than one, a random number decides whether there is a quasielastic collision, absorption or nothing according to their respective probabilities. If there is absorption it counts as an absorption event. If there is a quasielastic collision then we have to determine the charge. This is particularly easy since all charge transitions are a combination of isospin factors. After that one must determine the direction in which the pion goes.

The angular distributions are provided by the same model, hence the direction (and thus the energy) of the pion is generated randomly according to these probabilities. If a pion does not undergo any of these reactions it is allowed to continue for another interval of time. At this point we have taken two prescriptions, one of them is to let the pion go in a straight line, the other one is to let it follow a classical trajectory with the real part of the optical potential Both semiclassical prescriptions give rise to about the same results, but some differences appear at low energies. However, it is quite instructive to see that both of them agree very well with the quantum calculation for the total reaction cross section mentioned before, except at small energies where some differences appear (see fig. 5). This gives us much confidence to trust the results of the simulation for the other reactions.

As a result of the calculations we obtain the absorption cross section or the double differential cross sections  $d^2\sigma/d\Omega dE$  for inelastic, single charge exchange or double charge exchange inclusive reactions. We discuss the results in the next section.

# 4. RESULTS FOR THE REACTION CHANNELS

The results of fig. 5 for the total reaction cross section have been discussed before, we simply note here the good agreement with experiment except at low energies, where the semiclassical approximations to the propagation start failing and small discrepancies start to appear. The experimental results for the reactions that we study here are from refs. [17,19,20], the last one for double charge exchange.

In fig. 6 we show the results for absorption with similar features to the reaction cross section and good agreement with experiment except at low energies.

in figs. 7 and 8 we show the results for inelestic and single charge exchange reactions respectively, using classical trajectories between collisions (which proved to agree better with the quantum calculations of fig. 5. We use this prescription in all the other figures).

in fig. 9 we show the results for the double charge exchange cross section. In apite of the smallness of the cross section the agreement is relatively good. It is actually better than it appears in the figure because the experiment of ref. 20 for

 $(\pi^+,\pi^-)$  simply detects a  $\pi^-$  in the final state and it includes the contribution from  $\pi^+$   $n \to p\pi^+\pi^-$  reactions in nuclei as well. If one adds to the calculated cross sections (which do not include the  $\pi$ ,  $2\pi$  reaction) the experimental/21/ or theoretical results/22/ for the  $\{\pi^+,\pi^+\pi^-\}$  reaction in nuclei one finds a better agreement with the data of ref. 20.

Finally we show in fig. 10 double differential cross sections for inelastic inclusive reactions. The overall agreement is good but two features deserve a comment. At small angles the theoretical quasielastic peak is somewhat narrow. This could easily be a limitation of the present prescription that takes the nucleon distribution coming from a local Fermi sea, while for small densities the momentum distribution can be different \(^{123}\). The other interesting feature is that it reproduces very well the region of low energy which comes from multiple collisions. The approach of ref. \(^{18}\) which includes only one quasielastic scattering misses that region, but takes good account of the quasielastic peak.

In fig. 11 we show double differential cross sections for the double charge exchange reaction, the smallest cross sections that comes from the simulation. The overall agreement with experiment  $^{/24/}$  is also good with the same features mentioned above. We can observe that the  $(\pi, 2\pi)$  contribution, calculated following ref.  $^{/21/}$  is large at small energies and its inclusion leads to a better agreement with experiment.

# 5. CONCLUSIONS

We have seen the results of this microscopic pion nucleus optical potential applied to all the inclusive reactions and elastic scattering in a variety of nuclei and a wide range of energies. The overall agreement with all the reactions is quite good and the small discrepancies with experiment can be traced to some of the approximations done. We studied the inclusive reactions by means of the microscopic input which provided the reaction probabilities that we used in the simulation procedure. We could show that the procedure agreed very well with the total reaction cross section calculated quantum mechanically, for pion kinetic energies bigger than 100 MeV.

We would like to stress that the many body techniques used here provide a systematic way not only to construct a microscopic optical potential but to separate the different reaction probabilities from it. The remarkable agreement for the different reactions, nuclei and energies, indicates that we have succeeded in incorporating the essential features of the reaction mechanism in the present model. Yet, in spite of its intrinsic difficulty, the relevant information used for all calculations shown here has been parametrized as a function of the density and the energy in refs. 14, 18 and is very easy to handle. The use of this information in a variety of nuclear processes involving pion propagation through nuclei at some stage, like heavy ion reactions, antiproton annihilation in nuclei etc., would be also very helpful in order to learn about peculiar features of these other reactions.



5

3

2

ı

5

Fig. 9. Double charge exchange cross section.

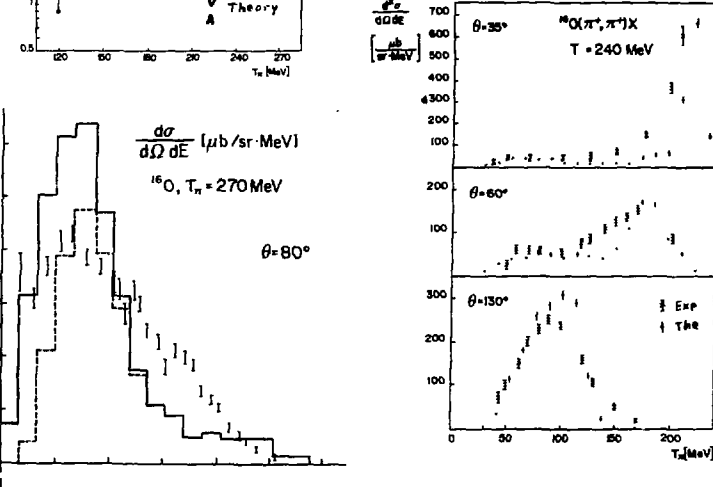


Fig. 10. Double differential cross section in inelastic scattering.

Fig. Fig.

Fig. 11. Double differential cross section for the double charge exchange reaction. The dashed histogram accounts for the (n\*, n\*) reaction alone, while the full histogram includes the (n\*, n\*n\*) events too.

0=130°

#### REFERENCES

- 1. J.N. Ginocchio and M.B. Johnson, Phys. Rev. 21 (1980) 1056
- 2. Z. Fraenkel, E. Piasetzky and G. Kalberman, Phys. Rev. C 26 (1982) 1618
- 3. J. Hüfner and M. Thies, Phys. Rev. <u>C 20</u> (1979) 273
- 4. M. Hirata, F. Lenz and K. Yazaki, Ann. of Phys. 108 (1977) 116
- 5. E. Oset and W. Weise, Nucl. Phys. A 319 (1979) 477
- 6. C. Garcia-Recio, E. Oset and L.L. Salcedo, Phys. Rev. C 37 (1988) 194
- 7. M. Kh. Khankhasayev, Czech. J. Phys. <u>B</u> 36 (1986) 257
- 8. M. Thies, Nucl. Phys. A 382 (1982) 434
- H. Ohta, M. Thies and T.H.S. Lee, Ann. of Phys. <u>163</u> (1985) 420
- 10. E. Oset, Y. Futami and H. Toki, Nucl. Phys. <u>A 448</u> (1986) 597
- 11. Y. Horikawa, M. Thies and F. Lenz, Nucl. Phys. A 345 (1980) 385
- 12. E. Oset, H. Toki and W. Weise, Phys. Reports 83 (1982) 281
- E. Oset, in "Quarks, Mesons and Isobars in Nuclei";
   R. Guardiola and A. Polls, Editors, World Scientific, 1983, page 1
- 14. E. Oset, L.L. Salcedo and D. Strottman, Phys. Lett. <u>165 B</u> (1985) 13
- 15. E. Oset and L.L. Saicedo, Nucl. Phys. A 468 (1987) 631
- 16. C. Garcia-Recio, E. Oset, L.L. Salcedo and D. Strottman, to be published
- 17. D. Ashery et al., Phys. Rev. C 23 (1981) 2173;
  - D. Ashery et al., Phys. Rev. Lett. 50 (1983) 482
- L.L. Salcedo, E. Oset, M.J. Vicente and C. Garcia-Recio, Nucl. Phys. A. in print
- 19. S.M. Levenson et al., Phys. Rev. C 28 (1983) 326
- 20. S.A. Wood et al., Phys. Rev. Lett. 54 (1985) 635
- 21. N. Grion et al., Phys. Rev. Lett. 59 (1987) 1080
- 22. E. Oset and M.J. Vicente, Nucl. Phys. A 454 (1986) 637
- M. Casas, J. Martorell, E. Moya and J. Treiner, Nucl. Phys. <u>A 473</u> (1987) 429
- S.A. Wood, Thesis, Los Alamos National Laboratory, Report No LA 9932 T. 1983

# △ - ISOBAR EXCITATIONS OF NUCLEI IN CHARGE-EXCHANGE REACTIONS

V.G.Ableev, S.M.Eliseev, V.I.Inosemtsev, B.Naumann, L.Naumann, A.A.Nomofilov, N.M.Piskunov, V.I.Sharov, I.M.Sitnik, E.A.Strokovsky, L.N.Strunov, S.A.Zaporozhets

> Joint Institute for Nuclear Research Dubna

Spin-isospin excitation of nuclear matter at high (~300 MeV) energy transferred to it are now intensively investigated both in experiment and theory. Interest in this class of reactions stems, first of all, from the fact that a nucleus can assimilate this energy not only through the excitations of the nucleonic internal degrees of freedom (i.e., the N  $\rightarrow$   $\Delta$  transitions) but also through some other kinds of excitations including collective ones, for example: intranuclear mesonic field excitations (like "spin-isospin sound"/1/); one could even exnect the isonucleus 121 formation. In general, the internal structure of the bound nucleon differs from one of the free nucleon due to medium effects. Thus, not only the A-isobar in nuclear matter but also the very N -> \Delta transition can be modified (under the influence of the nucleonic environment) as compared with the empty space case. This has to lead to differences between the observed A-excitation characteristics and the ones expected in the commonly used picture of quasi-free delta isobar production from a moving intranuclear nucleon. These differences can be more pronounced if one provides good conditions for the strong final state interaction between the A and the rest of the nucleus, i.e. when their relative momentum is small and comparable to the Fermi--momentum of nucleons in the nucleus.

Favourable conditions for interaction of a  $\Delta$ -isobar, produced in a nucleus with intranuclear nucleons were provided in our experiment  $^{/3}$ /, where a comparatively small momentum ( $\sim 300-400$  MeV/c) was transferred to  $\Delta$  since at large initial moments (from 4.40 to 18.3 GeV/c) we have detected tritons at small ( $\theta \in 0.4^\circ$ ) angles. This experiment allowed us to observe for the first time that at high energies the charge-exchange

cross section on a nucleus is mainly determined by the contribution from high (~300 MeV) spin-isospin excitation of the target-nucleus, and that the behaviour of the cross sections of  $C(^3\text{He},t)$  and  $p(^3\text{He},t)$   $\Delta^{++}$  reactions differ qualitatively from each other: i) the maximum of  $\Delta$ -peak in  $C(^3\text{He},t)$  reaction is shifted towards lower excitation energies; ii) the width of the nuclear  $\Delta$ -peak is about two times larger; iii) the ratio of the yield of  $C(^3\text{He},t)$  reaction in the  $\Delta$ -peak region to that of  $p(^3\text{He},t)$   $\Delta^{++}$  reaction

$$R_{\rm exp} = \frac{d6^{\rm C}}{d\Omega} (0^{\circ}) / \frac{d6^{\rm P}}{d\Omega} (0^{\circ})$$

is substantially greater (about two times) than the value 0.8 expected from the Glauber type calculations  $^{/4/}$ , where the known data on  $\rm NN \to N\Delta$  cross sections have been used.

Experiment<sup>6</sup> on ( $^3$ He,t) charge-exchange at smaller energies with wide variety of nuclear targets also showed the downshift and broadening of the nuclear  $\Delta$ -peak as compared to that in the charge-exchange on a free proton. The succeeding analysis<sup>5</sup> of the previously existing  $\Lambda(p,n)$  data<sup>77</sup> confirmed these features of the nuclear  $\Delta$ -excitation.

Our experimental data and the main features of the (<sup>5</sup>He,t) charge-exchange reaction are presented in Fig.1 and the Table, respectively.

Table 1. Main features of the charge-exchange reactions.

In column 4 the positions and widths of the expected non-quasi-free spectra are presented which were obtained from
the  $((^3\text{He},t))$  data by subtracting the calculated contributions from the quasi-free  $\Delta$ -production (see text on page 4)

Beam momen~ tum, GeV/c				Relative con- tribution to d6/d2 for C(3He,t) at	$R_{\rm exp} = \frac{dS}{dS^2} (0^\circ)$
	ρ( <sup>3</sup> He,t)	C( <sup>3</sup> He,t)	non-q.f.	Q > 150 MeV	. ds (0°
4.40	322 ± 2.5	274 ± 2.5	253 ± 2	62 %	1.32 ± 0.05
	138 ± 9	182 ± 16	142 ± 6		
6.81	327 ± 1.5	295 ± 1.5	275 ± 1	82 %	1.77 ± 0.03
	109 ± 5	204 ± 9	142 ± 4		
10.79	327 ± 2	305 ± 2	281 ± 2	92 %	1.95 ± 0.03
	129 ± 7	257 ± 14	153 ± 6		
18.3					2.14 ± 0.17

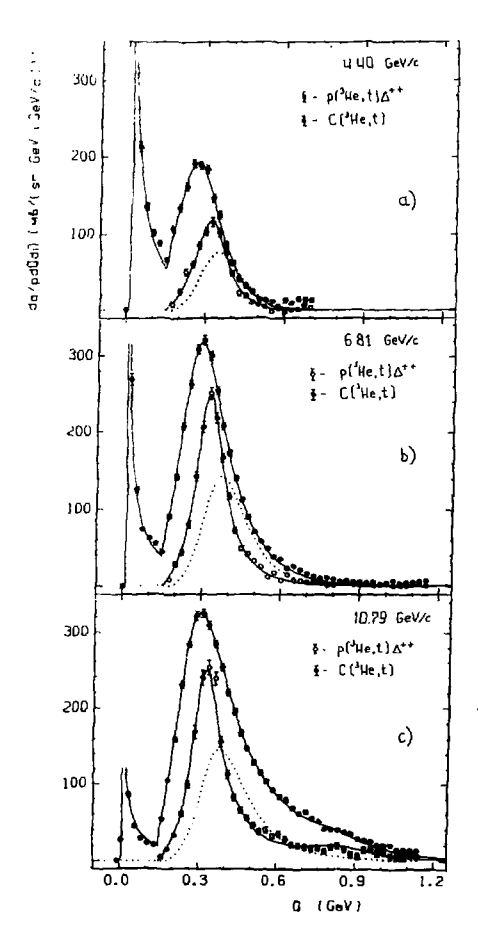


Fig. 1 a-c. Spectra of tritons from ( $^3$ He,t) charge-exchange on p and C targets as a function of Q =  $E_{_3$ He}-  $E_{_t}$  (the effects of energy resolution are taken into account/ $^4$ /). Solid lines are fitted curves. Dotted lines are the calculated (1) contributions of the quasi-free  $\Delta$ -production.

The analysis of the  $\operatorname{pt}^5\operatorname{He}$ ,t)  $\Delta^{++}$  data has shown that the spectra are well described by a  $\Delta^-$  resonance line distorted by the  $^3\operatorname{Pe}$  nucleus form factor. The Breit-Wigner parameters of the  $\Delta$ -neak, $\omega_*$  and

 $\Gamma_{\rm e}$ , are in good agreement with each other at all our energies. Their average values,  $\overline{\omega}_{\rm e}=1234$  +/- 3 MeV and  $\overline{\Gamma}_{\rm e}=116$  +/- 7 MeV, are consistent with the tahulated values/8/. Our calculations/4/ for the differential cross sections of this reaction in the Glauher-Sitenko and OPE models are in good agreement with the experimental data.

The analysis of the  $C(^3\mathrm{He},t)$  data has led us to the conclusion that it is impossible to explain the observed downshift of the  $\Delta$ -peak by quasi-free  $\Delta$ -production from a moving intranuclear nucleon (see the dotted line in Fig.1). In the case of the quasi-free production the shape of the  $\Delta$ -peak is defined by the convolution of the cross section of the "elementary"  $p(^3\mathrm{He},t)\,\Delta^{++}$  reaction on a free proton with the momentum distribution of nucleons in carbon  $p(\overline{p}_N^*)$ 

$$\frac{d\delta^{c}}{\rho d\theta d\Omega} \sim \int \! d\vec{p} \, \, g(\vec{p}_{N}) \, I(\vec{p}_{N}) \, \frac{d\delta^{p}}{\rho d\theta d\Omega} \, (t(0), \omega'(0, \vec{p}_{N})) \, . \tag{1}$$

where  $I(\overline{p}_N^2)$  is the ratio of fluxes of initial particles for the reaction  $p(^3 \text{lle}, t) \, \Delta^{**}$  on a nucleon at rest and on a nucleon moving with the momentum  $\widetilde{p}_N^2$ ; the energy of this nucleon is given by the relation

$$E_N = M_A - M_{A-1} - \frac{P_N^2}{2M_{A-1}} = m - E - \frac{P_N^2}{2(M_A - m - E)}$$
 (2)

where  $\mathbf{M}_{\tilde{\Lambda}}$  is the mass of a target-nucleus, m is the nucleon mass,  $\boldsymbol{\epsilon}$  is the binding energy

$$-\varepsilon = M - M_{A-1} - m . \tag{5}$$

where  $M_{A-1}$  is the mass of A-1 nucleon system. In the calculations we have used E=25 MeV (the average binding energy of nucleons in carbon) and the momentum distribution of nucleons in carbon following from the harmonic-oscillator model. It was assumed that the parameters  $\omega_{\rm c}$  and

 $\Gamma_o$  of the Breit-Bigner function fitting the "elementary" reaction are the same as for the reaction on a free proton (i.e., the tabulated values). As an argument  $\omega'$  we take the quantity:

$$\omega'^{2} = (Q + E_{N})^{2} - (\vec{p}_{N_{N}} - \vec{p}_{N} - \vec{p}_{N})^{2}$$
(4)

meaning the total energy squared in the c.r.s. of an intranuclear nucleon and a virtual pion exciting it. The spectra (1) have been normalized to the Glauber model estimation  $f^{Af}$  of  $-\mathrm{d}\delta^{C}/\mathrm{d}\Omega$  (0°) = 0.8  $\mathrm{d}\delta^{P}/\mathrm{d}\Omega$  (0°).

We compared our calculations (1) with experimental data  $\frac{797}{2}$  for the quasi-free  $\Delta$ -production in proton-nucleus reactions. In this experiment the quasi-free production of the  $\Delta$  isomorphy protons at 3.88 degree

on d,C,A1 and Cu nuclei has been studied through exclusive measurements of all final-state particles  $p+"n"\to p'+\Delta^o, \Delta^o\to p+\pi^-$ . Clear

 $\Delta$ -resonance peaks were observed in momentum spectra of forward (1° 48 4 5 5°) protons p' (see Fig.2) but in this case the  $\Delta$ -peaks for the C and Al targets are shifted towards larger energy transfers relative to that for the deuterium target (as opposed to cur case). The solid lines in Fig.2 show the results of our calculations (see formula (1)) taking into account the momentum resolution and the kinematical conditions of this experiment. The calculated spectra (with arbitrary normalization) agree quite well with the experimental data and confirm the conclusion of Ref. (9) about the quasi-free nature of the observed  $\Delta$ -production. One more result of the experiment is that the integrated cross sections

for d and C targets are approximately equal. It is in accordance with our Glauber model calculated value R.

Thus, from the analysis of the inclusive differential cross sections of the ( $^3$ He,t) charge-exchange on carbon nuclei and protons it follows that: i) the reaction on a nucleus at high energies proceeds mainly through the high ( $\sim 300$  MeV) spin-isospin excitation and ii) it is impossible to reduce the process of this excitation to the quasi-free production of  $\Delta$ -isobar on an individual moving intranuclear nucleon and a subsequent free motion of the isobar through the nucleus, i.e., collective effects caused by other nucleons of the nucleus are important.

As an example of possible collective effects one can exploit the picture developed by V.Dmitriev<sup>110/</sup>. He considers the formation of collective states in the following way. Delta decays mainly through pion emission. Due to a large width of the delta the pion is still at resonance and is reabsorbed by another nucleon forming again a delta-isobar but at a different space point. Thus, one has an excitation which is a superposition of the delta-hole and pionic wave in the nuclear matter; this excitation propagates through the medium oscillating between these two faces. At a very high density, where deconfinement of quarks occurs, this excitation transforms into a longitudinal spin-wave in a quark matter. This picture is close to that proposed in the pioneering paper by TF-QEricson and J.Hüfner<sup>111/</sup> for the scattering of real pions off a nucleus.

To confront the results of Ref.  $^{10}$ / with our experimental data we have subtracted from the measured  $C(^3\text{He,t})$  cross sections that part which can be reproduced by the quasi-free  $\Delta$ -production. It is reasonable to suppose that the pattern of the measured spectra is determined by both the mechanisms and they do not interfere. The parameters of the peaks after subtracting are presented in the Table (see column 4).

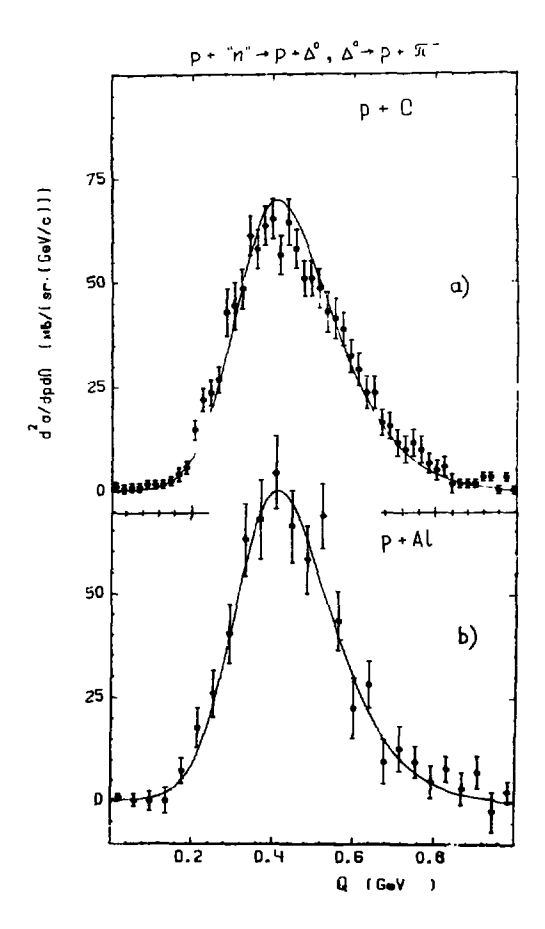


Fig. 2 a,b. Spectra of forward protons from the quasi-free  $\Delta^{\circ}$  production on C and Al targets, as a function of Q = E<sub>p</sub> - E<sub>p</sub>. Experimental data are taken from the picture of Ref. Solid lines represent results of our calculations (1) taking into account the experimental conditions of this experiment, with arbitrary normalizations.

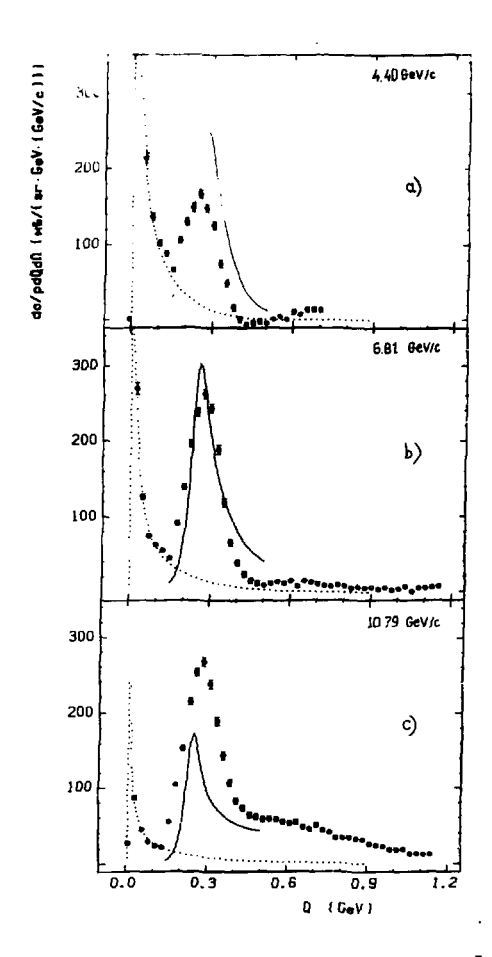


Fig. 3 a-c. The non-quasi-free parts of the  $C(\sqrt[3]{He},t)$  cross sections (were obtained from  $C(\sqrt[3]{He},t)$  data by subtracting the calculated contributions of quasi-free  $\Delta$ -production i.e., dotted lines in Fig. 1). Dotted lines in the figures are expected contributions from the 1cw-Q nuclear excitations. Solid lines show results of calculations /10/.

The non-quasi-free component of  $C(^3He,t)$  differential cross sections and the results of Ref./10/ are shown in Fig. 3. One sees the qualitative agreement of this non-quasi-free part of the experimental spectra with the calculations but a further work on this problem is, however, badly needed before one can draw more decisive conclusions about the nature of the observed collectivity.

We are grateful to the stuff members of the High Energy Laboratory, JINR, for their support to the present experiment. We are indebted to V.Dmitriev for the valuable discussions.

# References

- Dmitriev V.F., Suzuki T., Nucl-Phys. A438(1985)697;
   Chanfray G., Ericson M., Phys.Lett. B141(1984)163.
- Grishin V.G., Podgoretsky M.I., JINR, P-1508, Dubna, 1964;
   Leksin G.A., in: "Problemy Sovr.Yad.Fiziki", M., Nauka, 1972, p.511.
- Ableev V.G. et al; JINR, E1-83-486, Dubna, 1983; JETP Lett., v.40, p.763, 1984; PANIC, Books of Abstracts, Elsevier Sci. Publ. B.V., 1984, ed. by E.Guttner, B.Porh, G. zu Putlitz, v.11, p.L-24.
- V.G. Ableev et al., JINR, P1-86-435, Dubna, 1986; JINR, P1-87-374, Dubna, 1987; Yad.Fiz., v.46, p.549, 1987.
- V.G. Ableev et al., in: Proceedings of the Intern.Symp. on Mod.Devel. in Nucl.Phys., June 27- July 1, 1987, Novosibirsk, USSR, p.690, cd.by O.Sushkov, World Sci.Publ.Co., Singapore, 1988.
- 6. P. Contardo et al., Phys.Lett, B168(1986)331.
- B.E.Bonner et al., Phys.Rev.C18(1978)1418;
   V.N. Baturin et al., LNPHI, 1322, Gatchina, 1987.
- 8. Review of Particles Properties, 1982 ed., p.217, Geneva, 1982.
- 9. T.Nagae et al., Phys.Lett[B191(1987)31.
- Dmitriev V.F., INPh Preprint 86-118, Novosibirsk, 1NPh, 1986.
   Yad.Fiz., v.46, p.770, 1987.
- 11. T.E.O. Ericson, J.Hüfner, Phys.Lett.B33(1970)601.

# EXPERIMENTS AT SATURNE WITH ATT, IN SPECTROMETER

E.Chiavassa, G.Dellacasa, N. De Marco, F.Ferrero, M.Gallio, A.Musso, A.Piccotti, E.Vercellin

Dipartimento Fisica Sperimentale della Università di Torino Istituto Nazionale di Fisica Nucleare, Sezione di Torino

F. Brochard

Centre de Recherche Nucleaires et Université Louis Pasteur, Strasbourg, France

J.M. Durand

Laboratoire National Saturne, C.E.N., Saclay, France

R. Bertini

Departement de Phys. Nucleair a Moyenne Energie, Saclay, France

#### INTRODUCTION

We describe the characteristics of a spectrometer designed to study neutral mesons decaying into two gamma rays. The spectrometer has been built in Torino and is installed in a proton beam of the Saturre accelerator at Saclay National Laboratory. The spectrometer will be used in the near future to study  $\eta$  meson production in nuclei.

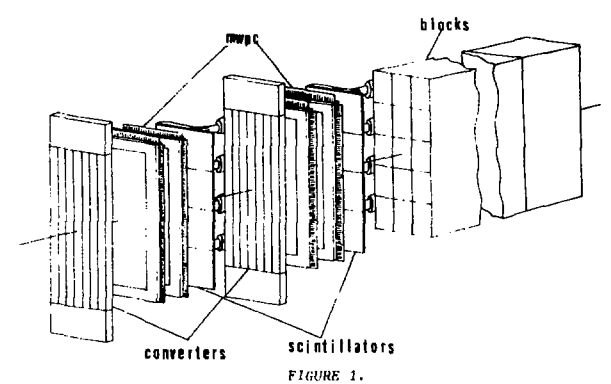
The spectrometer is similar to others already existing, principally to that operating at the Los Alamos Mesons Physics Facility (11), which has a typical energy resolution of 3 MeV for pions of 100 MeV.

Our spectrometer has been constructed with the aim to reach an energy resolution better than 2 MeV at Tm<sup>9</sup> 100 MeV and an efficiency greater than 50% for gamma of energy lower than 400 MeV. In order to obtain such characteristics we measure the energy and the direction of the two gamma rays using scintiflation glasses and MWPCs.
THE SPECTROMETER

The spectrometer consists of two identical gamma ray detectors, which mechanical support is designed to cover a wide array of experimental settings.

Each detector, as shown in fig.1, is made of two active scintillating glass converters, four MMPCs, two hodoscopes of scintillators and a total absorption counter made of 15 blocks of scintillating glass. The scintillating glass used for the converters and the calorimeter is the SCGI-C type manufactured by OHARA Optical Glass Inc.

Two sets of mechanical supports allow to position the detectors at various angles and distances from the target in two different configurations. In the first one(so-



Exploded view of a Gamma Detector of the Spectrometer.

called "one-post" configuration) the detectors are laid one upon the other horizontally on a unique support which can rotate around the target at a distance between 1 and 2 m. In the second one (so-called "two-post" configuration) the two detectors are supported by two trolleys which can pivot independently around the target. This second configuration should be used for measuring mesons produced near 0° or 180°.

The converters consist of seven bars of SCG1-C scintillating glass with front surface  $5x70~{\rm cm}^2$  and  $4.5~{\rm cm}$  thickness, corresponding to one radiation length  ${\rm X}_0$ . Each bar is viewed on both sides by two Philips XP-2012 photoraltipliers.

Behind each converter there is a couple of MWPCs which detect the charged particles emerging from the converter in order to determine the conversion point. They have an active surface of 329x576 mm<sup>2</sup> and one anode plane. The mechanical characteristics of the MWPCs are:

anode wire diameter 20 jum; anode wire spacing 2 mm;
cathode wire diameter 100 jum; cathode wire spacing 1 mm;
anode-cathode gap 7 mm; distance between anodes plane 7 cm.
On the anode plane, which has wires parallel to the smaller side of the chamber, we

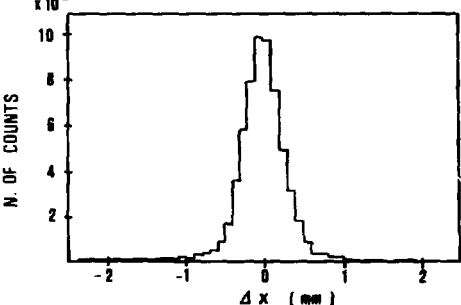
use a digital read-out system, since the 2 mm spatial resolution is sufficient for our experiments. The anode read-out uses the RMH system for a total of 2304 wires.

The orthogonal coordinate is more important for the determination of the angle between the two gamma rays; therefore we measure it by means of the centroid of the charges induced on the cathode wires. The cathode wires are connected in groups of seven and the induced signals are amplified by a linear inverting amplifier and di-

gitalized with a LeCroy 4300B ADC (FERA system). We use a total of 384 ADC channels. The spatial resolution of the analog read-out system has been measured by weans of cosmic rays and the results are shown in Fig. 2. The chambers operate with the magic gas mixture at 5200 V.  $10^2$ 

FIGURE 2.

MWPC spatial resolution
using cathode read-out.



Each couple of chambers is followed by an hodoscope made of 4 plastic scintillators with dimensions  $15x60 \text{ cm}^2$  which are used to trigger on the charged particles emerging from the converters. Each scintillator is viewed by a XP2020 Philips photomultiplier.

A third hodoscope, made of eight 10x40 cm<sup>2</sup> scintillators, 0.5 cm thick, is put in front of the first converter of each gamma detector. It detects the charged particles entering in the detector and is used as veto counter in the trigger logic.

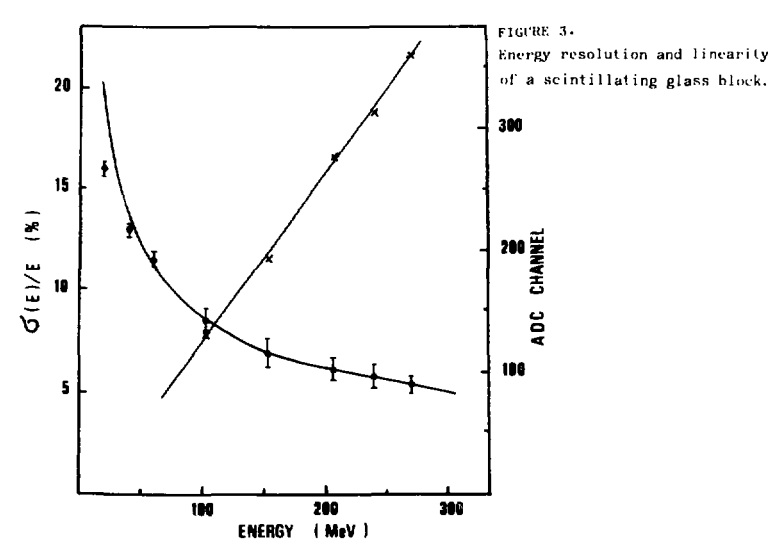
The total absorption counter is made of a 3x5 array of SCG1-C scintillating glass blocks, each with 15x15 cm $^2$  front surface and a thickness of 14 radiation length. Each block is seen by a R1512 Hamamatsu PM.

The energy resolution and linearity of a single block was tested in the energy range from 50 to 200 MeV with an electron beam at CERN SC2 and with a monochromatic gamma beam at LADON in Frascati (4). The results of these measurements are shown in fig. 3.

The signals of each one of the PMs of the converters are amplified (by a factor of 10) and sent to an ADC channel (LeCroy 4300B).

The signal from the PM of each block is sent to an ADC channel and to a linear fan-in in order to measure the light yield produced in the whole calorimeter.

To control the overall equipment and to read-out the information from chambers and ADCs we use a microVAXII computer interfaced to a Camac System Crate. Because



of the VMS heavy operative system, the microVAXII is very slow in reacting to the event trigger interrupt. To avoid a big dead time, we decided to use a front-end processor which is fully dedicated to the Camac read-out and buffers the events before sending them to the data acquisition computer. As a front-end we use a DEC J11 microprocessor directly housed in a Camac module (CES 2180 Starburst). The software for the J11 is developed on the microVAXII itself and then down-line loaded into the processor via the Camac dataway.

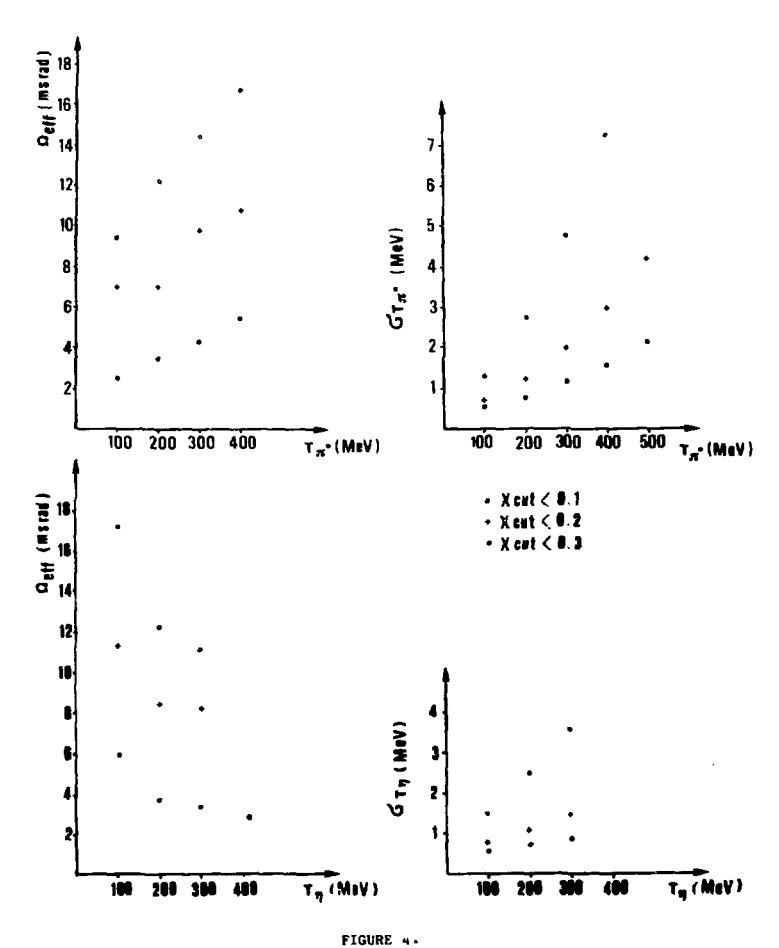
On the microVAXII side, we use the DAQ program developed at CERN for the DEC family computers.

Furthermore the front-end processor is used to select events of interest as a second level trigger. The decision algorithm is based on the calculation of the energy released by the gamma rays in each detector and it is performed in less than 100 microseconds.

With this system we can write on tape about 600 events per second (1 Kbyte long), leaving more than 70% of the microVAXII CPU free for the monitoring tasks.

Finally, to summarize the performance of the spectrometer, we calculated its energy resolution and its effective solid angle, defined as the ratio of the number of pions (or etas) which decay produces the gammas in the spectrometer to the number of pions (or etas) produced at the target. These quantities depend from the variable

Xcut, defined as the ratio between the difference and the sum of the energies of the two gammas. The results are shown in fig.4.



Effective solid angle and energy resolution of the spectrometer for  $\pi^0$  and  $\eta$  for different values of x

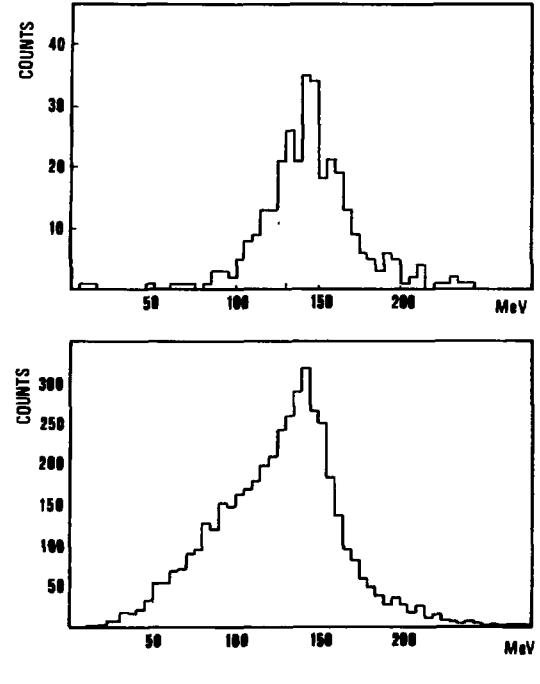


FIGURE 5.

- a) Invariant mass plot for p of 800 MeV on deuterium target. The plot is made by detecting  $^3\mathrm{He}$  particles produced in the interaction,
- b) Invariant mass plot for p of 800 MeV on deuterium target.

# TEST RUNS AT SATURNE

The spectrometer has been installed and tested at SATURNE for studying at different energies the reactions: (pp, $4\pi^{4}$ ); (pd, $^{3}$ He $\pi^{0}$ ) and (pd, $^{3}$ He $\pi^{0}$ ).

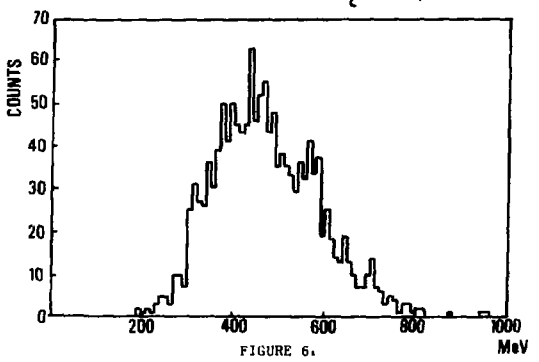
Using the first one we measured the detector response for motion of energies from 120 to 200 MeV. The detector worked properly on a proton beam of intensity 2\*10<sup>9</sup> particles per second.

The  $\pi^{\bullet}$  production on deuteron was measured with 800 MeV protons interacting on a 1 g/cm<sup>2</sup> CD2 target; we detected  $\Omega^{\bullet}$  of 270 and 300 MeV at 85° and 95° in the laboratory reference frame with the spectrometer in the "one post" configuration.

Detecting the  $^3$ He by means of a scintillator hodoscope we produced tagged  $\mathbf{f}^{\bullet}$ . The obtained invariant mass spectrum (see Fig. 5a) is peaked around 140 MeV indicating that some errors in the calibration are still existing. The width of the spectrum is about two times greater than MonteCarlo predictions, but it must be considered that the spectrometer worked in an incomplete configuration, having only one MMPC beyond each converter.

In Fig. 5b we present the same invariant mass spectrum without the  $^1$ He coincidente; the  $\pi^0$  peak clearly emerges over a continuous background.

Finally in fig. 6 we report the invariant mass spectrum for the reaction pod  $\rightarrow$  He+ $\eta$ . As target we used a 5 cm thick deuterium liquid target; the incident proton kinetic energy was 900 MeV and the spectrometer was set in the "two post" configuration For the detection of the 50 MeV $\eta$  meson produced at zero degree.



Invariant mass plot for 900 MeV proton beam on deuterium target.

Even if the data are preliminary the  $\eta$  peak appears clearly in the invariant mass spectrum.

#### EXPERIMENTS AT SATURNE

The two-gamma-rays spectrometer may be used to study the production of neutral mesons decaying through electromagnetic interaction. Among these, the  $\pi^{\circ}$  and the  $\eta$ -mesons decay in two gamma rays respectively in the 98% and 39% of the cases.

 $\pi^{\bullet}$  production has been extensively studied by means of charge exchange reaction of  $\pi^{\pm(3)}$ ; on the contrary the  $\eta$  meson production is less known.

In the last years interesting works have been done near the production threshold both with pion  $\binom{(4)}{1}$  and proton  $\binom{(5)}{1}$  beams.

As is well known, the  $\eta$  is a pseudoscalar meson belonging to the same su(3) nonet as pions and kaons. In the SU(3) diagram the  $\eta$  meson occupies the same position as the  $\Omega^0$ . The two mesons have same spin and parity but differ in isospin (I=I for  $\Omega^0$  and I=O for  $\eta$ ); the difference is due to the strange quark component of  $\eta$ .

The study of  $\eta$  -nucleon and  $\eta$ -nuclei interactions is of fundamental interst and the previously quoted experiments demonstrate their feasibility. Until now the  $\eta$ -N coupling constant is not well known and the study of nucleus interaction seems the main way to obtain useful information. We know that the  $\eta$ -N coupling constant is lower than the  $\eta$ -N coupling constant and that the  $\eta$  nucleon low energy interaction is attractive. This fact led to the prediction that  $\eta$  nucleus could exist  $^{(6)}$ . The threshold for the reaction pp -pp  $\eta$  is at proton kinetic energy  $\tau_p$ -1.26 GeV and therefore the SATURNE proton beam is well suited to study  $\eta$  production near the threshold. Furthermore choosing carefully the kinematic regions, for few reactions such as  $(pn, \eta d)$ ;  $(p^{-3}He, \eta^{-4}He, \eta^{-2})$ ;  $(pd, ^{3}He, \eta^{-4})$  and  $(dp, ^{3}He, \eta^{-4})$ , it will be possible at SATURNE to produce  $\eta$  with very low momenta.

Coherent  $\gamma$  production measurements could give precious information on  $\gamma$ -nucleon and  $\gamma$ -nuclei resonances and on the N<sup>\*</sup>behaviour in nuclei<sup>(7)</sup>. The  $\gamma$  nucleon interaction may help to understand better the specific flavour content of  $\gamma$  meson.

For all these reasons we will use our spectrometer to study  $\eta$  production in nuclei beginning with the measurements of the p+ $^6$ Li $\rightarrow \eta$ + $^7$ Be reaction with  $\eta$  at zero degree.

In the future we are considering the possibility of using a neutron beam for measuring the  $\pi + p \rightarrow d + \eta$  reaction detecting both the deuteron and the  $\eta$ .

This reaction seems of particular interest because it can be checked by well defined theoretical models.

#### REFERENCES

- 1) H.W. Baer et al., N.I.M. 180, 445 (1984)
- 2) H.W. Baer, Medium Energy Phys. World Scientific 300, 1987
- 3) G. Sanouillet et al., CEA N. 2483, 1987
- 4) J.C. Peng, Medium Energy Phys. World Scientific 336, 1987
- 5) P. Berthet et al. Nucl. Phys. A 443, 589 (1985)
- 6) L.C. Lin, LA, 11184 C, 104 (1987)
- 7) M.G. Huber, LA, 11184 C, 91 (1987)

# НАБЛЮЛЕНИЕ РЕЛЯТИВИСТСКИХ ГИПЕРЯПЕР Ж ПРИ ВЗАИМОЛЕИСТВИИ Не (18 ГэВ/с) С ЛЕТВИМИ ЯДРАМИ

Авраменко С.А., Абдуражемов А.У., Аксиненко В.Д., Анжина М.І., Баннек Б.П., Белеков D.А.( I), Бутенко В.А., Варденга Г.Д., Гаевожий К.(2), Глаголева Н.С., Голожрастов А.И., Голужена И.Г., Грачев А.Г., Дементьев Е.А., Ароздов В.А., Жильцова Л.Я., Завыялов В.Ф., Ловчев К.(3), Каминекий Н.И., Кирилов А.Д., Козубский Э.В., Кондратьев В.П.(1), Красков Л.В.(1), Кузнецов А.А., Кузнецов Е.С., Кулаков Б.А., Дукстиным D.: Аросииц В.Д., Мандрик О.D., Маньяков П.К., Матвеева Е.Н., Матимин А.Т., Матрин В.Т., Мирков ский Я.(2), Мужин С.В., Некитик Н.М., Нургожим Н.Н.(4), Оконов Э.О., Останевич Т.Г., Охраменко Л.С., Цавловский А.(2), Пакиненко Т.Д., Поль D.С.(5), Радоманов В.Б., Рожнатовская С.А., Рубина С.Г., Руколткин П.А., Ряковский В.Н., Савтов И.С., Светов А.Л., Семих С.А., Степанов И.В.(1), Таран Г.Г. (5), Хорозов С.А., Хусайнов Е.К.(4), Шевченко И.Е.(1).

- (1) Лениигранский госупарственный университет
- (2) Ипотитут рациотехники Варшавского политехнического института
- (3) MANAS EAH, Codons
- (4) MOBO AH KasCCP, Ama-Ata
- (5) Физический институт АН СССР им. П.Н.Лебедева, Москва

Объединенный институт ядерных исследований, Лубна

Зисперимент по исследованию образования и распила редитивателии гиперацер водорода провожился на спектрометре ГИБС в виведением кучке ядер Не (18 ГаВ/с) окихрофазотрона дво ОМЯН. Основная регистрирующая часть установки - стримерная камера (2xIxO,6 м<sup>3</sup>) в мегинтном поле  $\sim 0.9$  Tg. Handrichear heorem upb atmockedness labrates. March (CHo. 20 см) устанавливальсь в I2 и I8 см перед чувствительным объемом камеры. Траттерная онотемя, предназначенная для отбора реанный образо-DANER II DECEARE DOLLTURECTORIE FRESPRESD, COCTORER ES TOOK POYER OFFICEтилиминих очетчиков, работанних в амилитущим рекиме, и бногрой адектроники. Группа А. расположения исред инискър, сребативала или попавания в инионь одной и только одной альбо-частини. Гочина В фикопровеле отсутствие двухарящией частици между минокъв и чувствительним объемом намеры. Группа С срабатывана, когна за чувствительным OGSONOM RAMODH CHORA HOMBARRACH HRYZBADERHAR VACTEUR. TREFFEDERS CHOтема давала окумал на регистрацию собитил при одновременном срабативании всех групи отетчиков. Таким образом, догика триггерной спотеми OHRE OPERITEDOBREE ER OTGOD GREEVIERT DERKUER OGDREGDERE E DECKERE DELETERICTCER PRESPUED:

$${}^{4}\text{He} + \text{CH}_{2} \longrightarrow {}^{4}\text{H} + \cdots {}^{3}\text{He} + \text{I}\Gamma + n \qquad (2)$$

$${}^{4}\text{He} + \text{CH}_{2} \longrightarrow {}^{3}\text{H} + \cdots {}^{3}\text{He} + \text{I}\Gamma \qquad (3)$$

Тритони, образовавшиеся при неупругом взаимодействии альфа-частиц в мишени, могут в газе камери перезарядиться в <sup>3</sup>Не. Такая реакция тоже удовлетвориет критериям отбора собитий тритером. Для нас наиболее существенна реакция перезарядки с образованием отрицательного заряженного пиона -

$$^{3}\text{H} + \text{Ne} \rightarrow ^{3}\text{He} + \text{II}^{-} + \dots$$
 (4)

поскольку именно она может имитировать распады гиперядер (реакции (I-3) ).

В эксперименте положение счетчиков группы С выбиралось так, чтоон эффективность регистрации реакции (I) онла максимальной. Моделирование, проведенное в рамках простой модели /I/, показало, что в
этом случае геометрические эффективности регистрации реакций (I) и
(2,3) равни ~ 100% и ~ 50% соответственно. Что касается реакции (4),
то геометрическая эффективность ее регистрации омла принята такой ме,
как и для реакций (2,3), поскольку импульсно-угловие распределения
<sup>3</sup>не во всех этих реакциях приолизительно одинакови. Меньшая ( по
сравнению с (I)) геометрическая эффективность регистрации реакций
(2,3) связана с тем, что за счет большей кривизны траектории <sup>3</sup>не в
магнитном поле часть их не попадает в счетчики группы С.

На фотографиях реакции (I-3) должны вметь одинаковый вид: от вхола в камеру до вершины (точки распада) - трек однозарядной частыцы, из вершины выходит трек положительной двухзарящной частицы и трек отрешательного песна. Такой до выи могут иметь собител, соответствуюште реакции перезарящия (4). Опнако в большинстве случаев реакция перезарянке сопровоженется испусканием дополнительных частии из япрамежени ( Ne ) вин ярким стримером в вериние ( вонивалия газа камеры ядром отдачк). Таким образом, "чистая" вершина является признаком расцада геперияра. Другой особенностью, позволяющей выделять реакими (I) на фоне реакций (2-4), является величина выпульса образовавшейся в результате распада или перезаряцки квухварядной частици. В реакциях (2-4) ее выпульс вмеет, как правило, величну около 12 ГаВ/с ( ~ 4 ГаВ/с на нужнон), а в реакции (I) - около 16 ГаВ/с ( тоже ~ 4 ГаВ/с на нуклон). Точность измерения импульса инукларянной TACTELLE D CHARTDOMOTOS - HOCKOJEKO IDOMOTOD - HOSBOJEST MATARHO DASдолять эти олучан. К, наконец, смам сильным критерием является величина забентивной масон спотемы 48 + П.

Эффективность идентификации гиперадер 4н по комбинации перанх

двух критериев можно иллострировать тем, что из 15 собитий, удовлетворяниях требованиям – чистая вершина и импульс вторичного гелия больше  $14 \, \Gamma$ 9B/с, — все  $15 \,$  имеют эффективную массу с точностью до нескольких маВ ( разрешение установки по эффективной массе), разную массе гиперядра  $^{A}_{H}$  (3,9225  $\Gamma$ 9B /2/). При этом в II собитиях ( из этих I5) первичные треки имели длину, достаточную для надежной визуальной оценки разницы ионизации между первичным ( Z =I) и вторичным ( Z =2) треками. В двух случаях из—за высоковольтных пробоев в камере (пятен) вершины собитий не видны. Эти собития были идентифицированы как  $^{A}_{H}$  по комбинации признаков — импульс вторичного гелия и эффективная масса. Таким образом, результаты, которые приводятся ниже, основаны на регистрации 17 случаев распада  $^{A}_{H}$   $\rightarrow$   $^{A}_{H}$  +  $^{B}$  -  $^{A}_{H}$ 

Мы получили сечение образования  $^4_{
m H}$  в пучке  $^4_{
m He}$  ( 18 ГаВ/с) на СН $_2$  мишени, равное 0,4 $^4_0$ ,2 мкб. При расчете сечения предполагалось, что время жизни  $^4_{
m H}$  - 2х $^{10}$ - $^{10}$ с; что доля двухчастичных распадов с отридательно заряженным пионом составляет 50% ( по данным работ /3-7/) и что сечение неупругого взаимодействия  $^4_{
m He}$  с ядрами равно сечению неупругого взаимодействия  $^4_{
m He}$  с ядрами равно сечению сказывается на величине сечения образования  $^4_{
m He}$ . Так, если предположить, что сечение неупругого взаимодействия  $^4_{
m He}$  на 40% больше, чем у  $^4_{
m He}$ , то величина сечения образования изменится прислизительно на 10%. Ощиска, приведенная нами для величини сечения образования  $^4_{
m He}$ , включает в себя не только статистическую ощиску, но и неопределенности перечисленных параметров, а также возможные ощиски в определении эф-

фективностей детекторов.

В расоте /8/ по результатам первого облучения установки ( 5 случаев распада АН) ми приводили оценку сечения образования этого гиперядра 0,2 мкб. При наборе этой статистики мишень стояла практически вплотную к группе В счетчиков. Это могло би в принципе привести к тому, что часть случаев образования АН, сопровожданиямся испусканием в небольшом телесном угле нескольких однозарядних частиц, не регистрировалась ( несколько однозарядних частиц могут в группе В счетчиков имитировать сигнал от двужзарядной частицы). И хотя моделирование показало, что этот эффект незначителен, при дальнейшем наборе статистики расстояние между мишенью и группой В счетчиков было увеличено на 6 см ( размер счетчиков — 4x6 см²), а верхние пороги дискриминаторов группы В устанавливались так, чтоби свести и минимуму потери событий с двумя частицами, сопровождающими образованиееся гиперадро. Собпадение в пределах ошебок обокх результатов говорит о том, что рассмотренный эффект большой роли не играет.

Иамеренное сечение образования 4 хорошо согласуется с теорети-

ческим расчетом ( 0,29 мко на углеродной мишени в пучке <sup>4</sup>Не с импульсом 18 ГаВ/с), с котором на этом семинаре рассказывал профессор М.Сано ( см. также /9/). Труднее согласовать полученное нами сечение с сечением образования гиперидер кислорода в пучке <sup>16</sup>0 при енергии 2, I ГаВ на нуклон, которое по данинм /IO/ равно 28±14 мко. Как качественные соображения, так и непосредственные расчети /9/ показывают, что сечения обоих процессов долини бить одного порядка величинь. Не исключено, что данине /IO/ содержат значительную примесь фоновых процессов, поскольку при идентификации собитий использовались довольно слабые критерии.

На части статистики в расочей зоне длиной II5 см было подсчитано число случаев перезарядки  $^3$ H +  $^{N}e \rightarrow ^3$ He +  $^{\Pi}$  .... Соответствующее сечение  $^{I+1}_{-0.5}$  мб (  $^{25}$  случаев перезарядки). Эта величина близка к сечению перезарядки  $^3$ He + C  $\rightarrow ^3$ H + ..., равному I,2 мкб ( по данным работн /II/,), но относящемуся к заметно меньшей энергии - 3 ГэВ ( в нашем эксперименте энергия тритонов около IO ГэВ). Поскольку, однако, в этом (3–IO ГэВ) интервале энергетическая зависимость сечения перезарядки сищается незначительной ( мн благодарии профессору М.Сано за это замечание), то совпадение нашего и из работы /II/ сечений можно рассматривать как подтверщение правильного учета эффективности аппаратуры в нашем эксперименте.

Время жизни гиперядер  $^{A}$ Н, измеренное в нашем эксперименте, равно  $(2,2^{+0.5}_{-0.4})$ х  $10^{-10}$ с, что несколько больше, чем усредненное по более ранным экспериментам значение – I,6х $10^{-10}$ С (см.обзор /I2/), и заметно отличается от результата теоретического расчета (I,3х $10^{-10}$ С), приведенного в /I3/. Отметим, что во всех предшествующих экспериментах время жизни  $^{A}$ Н измерялось с низкознергичными гиперядрами, образовавшимися в результате захвата ядрами гелия или ядрами эмульски медленных К мезонов. В таких постановках экспериментов возникает ряд сложных методических проблем /2/, связанных как с очень малой долей распадов на лету, так и с идентирикацией распавшихся на лету гиперядер.

В заключение остановимся на прослеме образования и распада <sup>3</sup>Н в нашем эксперименте. Принимая во внимание отношение сечений образования <sup>4</sup>Н и <sup>3</sup>Н по расчетам /9/, доло двухчастичных распадов с отрицательно заряженным пионом ( по данным работ /3-7/) и отношение эффективностей, на 17 зарегистрированных распадов <sup>4</sup>Н ми должни были он иметь около 10 распадов <sup>3</sup>Н. Однако в эксперименте зарегистрирован только один случай. Не исключено, конечно, что это результат флуктуации и (мли) неточности модели /1/, по которой рассчитывалось отношение эффективностей. Но можно этот результат рассматривать и как указание на неолиданные свойства гиперадра <sup>3</sup>Н ( например, малое время жизни или

からいちかい なをままし

Мы благодарны Я.Жовке, М.И.Подгорецкому, М.Сано, Г.А.Соколу, В.Н.Фетисову за обсуждение рассмотренных вопросов и полезные замечания; Н.Н.Графову и В.П.Садилову за помощь в подготовке и проведении облучений установки; Л.А.Гончаровой, С.Н.Комаровой, Л.С.Любимовой, Н.С.Щербаковой и И.И.Энгель за помощь в обработке матерыала.

# ЛИТЕРАТУРА

- Вомен Т. В сб. "Каон-ядерное взаимодействие и гиперядра", Москва, Наука, 1979, с.115.
- 2. Davis D.H. and Pniewski J. Contemp. Phys., 1986, 27, p.91.
- 3. Bertrand D. ao Nucl. Phys., 1970, B16, p.77.
- Block M.M. so Proceeding of International Conference on Hyperfragment, 3t.Cergue, 1964, CERN report 64-1, CERN, 1964, p.63.
- 5. Dalitz R.H. and Liu L. Phys. Rev'. 1959, 116, p.1312.
- 6. Колесников Н.Н. и Копылов В.А. Изв. вузов. Физика. № 3.с.44.
- Филимонов В.А. в сб.: "Каон-ядерное взаимодействие и гиперядра", М., Наука, 1979, с.240.
- 8. Avramenko 5. so preprint E1-87-337, Dubna, 1987.
- 9. Bando H., Sano M., Wakai M., Žofka J. INS-REPORT-682, Tokio, 1988.
- IO. Nield K.J. ao Phys. Rev., 1976, C13, p.1263.
- II. Contardo D. so Phys. Lett., 1986, 168B, p.331.
- I2. Бом Г. и Креккер У. ЭЧАЯ, 1972, 3, c.318.
- Джибути Р.И., Крупенникова Н.Б., Саркисен Н.Н., Циклаура Ш.М., ЯФ, 1986, 44, с.349.
- 14. Bohm J. and Wysotzki F. Nucl. Phys., 1970, B15, p.628.

# M. Sano Institute for Nuclear Study, University of Tokyo, Tanashi. Tokyo 188. Japan

# 1. Introduction

Hypernuclei are usually produced by collisions of proton, electron, pion and kaon beams on a target nucleus. High-energy heavy-ion collisions may also offer not only the possibility of producing various hypernuclei, but the possibility of producing exotic nuclear species such as multi-A hypernuclei and H-particles.

Kaons and A-particles have been measured in high-energy heavy-ion collisions 1,2) and we have learned from the experiments that their production cross sections are fairly large even at 2.1 GeV/nucleon. Therefore, experiments of high-energy heavy-ion collisions may admit to the formation of hypernucleus with fairly large cross sections and also to the observation of exotic nuclear species. Kerman and Weiss<sup>3)</sup> estimated production cross sections of hypernuclei and obtained a rather large amount of production cross section. However, their prediction seems to be unrealistic, because they did not take into account the momentum distribution of A-particles produced by collisions. The formation probability of hypernucleus depends strongly on the momentum of A-particle, since the produced A-particles have to stay in a nucleus.

Asai et al. 4) have tried to apply the coalescence model<sup>5)</sup> to a description of the hypernucleus formation and to estimate the formation cross sections at 2.1 GeV/nucleon by incorporating the various experimental and theoretical information on high-energy heavy-ion collisions. The calculation has further been extended up to energy range of about 5 GeV/nucleon by Wakai et al.<sup>6)</sup> and estimated the formation cross sections of double A-hypernucleus in addition to single A-hypernucleus.

The present work is to estimate hypernucleus formation cross sections in collisions of relativistics beams of  ${}^{1}$ He,  ${}^{7}$ Li,  ${}^{12}$ C and  ${}^{19}$ F with target of  ${}^{12}$ C at energies used in the recent Dubna experiment and to evaluate the secondary ( $\mathbf{w}^+\mathbf{k}^+$ ) formation. The formation probability of H-particle is also estimated.

# 2. Hypernucleus Formation Cross Sections

The details of the calculation method of hypernucleus formation cross sections based on the coalescence model are described in previous papers  $^{i,\,6}$  and only a summary is given here.

According to the coalescence model, the formation cross section of  $\Lambda$ -hypernucleus is expressed by the product of  $\Lambda$ -particle and nuclear fragment production cross sections as follows:

$$\frac{\gamma}{\sigma_{r}} \frac{d^{3}\sigma_{o}^{(\Lambda F)}}{d\kappa_{o}^{3}} = \left[ \frac{m_{\Lambda}^{\star m_{F}}}{m_{\Lambda}^{m_{F}}} \right]^{3} S_{\Lambda F} \left[ \frac{\gamma}{\sigma_{r}} \frac{d^{3}\sigma_{o}^{(\Lambda)}}{d\kappa_{o}^{3}} \right] \left[ \frac{\gamma}{\sigma_{r}} \frac{d^{3}\sigma_{o}^{(F)}}{d\kappa_{o}^{3}} \right], \quad (1)$$

where  $k_c$  is the momentum per particle,  $m_A = M_A/M_n$ ,  $m_F = M_F/M_n$ ,  $Y = \lfloor 1 + (k_c/M_n)^2 \rfloor^{1/2}$ ,  $M_n$  is the nucleon mass,  $M_A$  is the A-particle mass,  $M_F$  is the fragment mass, and  $\sigma_P$  is the reaction cross section.  $S_{AF}$  is the coalescence factor and is given by assuming the harmonic oscillator wave function for the A-particle in the hypernucleus as

$$S_{AF} = (2\pi)^3 \sum_{n_k} (2k+1) \mathcal{N}_{AF}(n_k)$$
 (2)

The sum runs over bound state (nl) of A-particle.  $\mathscr{G}_{\mathrm{AF}}$ (nl) is give by

$$\mathcal{G}_{\Lambda F}(n\ell) = \begin{cases} (\sqrt{\pi}\alpha)^{-3} & \text{for os-state,} \\ (\sqrt{\pi}\alpha)^{-3} (\ell_{\Lambda F}/\alpha)^2 & \text{for op-state,} \end{cases}$$
 (3)

where  $\alpha=(b_{\Lambda}^2+f_{\Lambda f}^2)^{1/2}$ ,  $\beta_{\Lambda F}=(\beta_{\Lambda}^2+\beta_{F}^2)^{1/2}$ ,  $b_{\Lambda}$  is the harmonic oscillator size parameter given by  $[(f_{\Lambda}^2/M_{\Lambda})/f_{h_{\Lambda}}]^{1/2}$  and  $\beta_{f}$  is the parameter of a gaussian form for source function of particle i. In the numerical calculations, we employ a parameter value of  $b_{\Lambda}$  associated with the frequency  $f_{h_{\Lambda}}=30\,A^{-1/3}$ MeV. Here we take the parameter values for  $\beta_{\Lambda F}$  as specified in Table 1 and for Ne-Ne reaction  $\beta_{\Lambda F}=5.53$ fm is adopted, which originates from the choice  $\beta_{\Lambda}=\beta_{F}$  (= 3.91 fm). Those values correspond to the extent of the normal nucleus consisting of the projectile and target nucleons and the rms radius is given by  $b_{\Lambda}=3.57$  fg.

For the production cross sections of the A-particle and nuclear fragment F, we recent to the model calculations which reproduce the existing data quite well. Inclusive cross section  $d^3e^{(\Lambda)}/dk_0^2$  of A-particle production is evaluated by means of a statistical phase space model  $^{(\Lambda)}$  as a sum of contributions of subprocesses in which M nucleons in the projectile A interact with N nucleons in the target E:

$$E^{\frac{d^3\sigma(\Lambda)}{dp^3}} - \sum_{MN} \sigma_{AB}(M,N) \mathcal{G}_{MN}(p) . \tag{4}$$

Here  $\sigma_{AB}(M,N)$  specifies the cross section for the sub-process and  $\mathcal{F}_{MN}(p)$  denotes the distribution function of momentum p for the particle emitted in the subprocess (M,N). The cross section  $\sigma_{AB}(M,N)$  is factorized into the respective nucleon-nucleus cross section in the straight line geometry.

$$\sigma_{AB}(M,N) = \sigma_{A}(M)\sigma_{B}(N)/\sigma_{NN}, \qquad (5)$$

$$\sigma_{A}(M) = \frac{1}{M!} \int d^{2}s[\tilde{M}_{A}(s)]^{M}exp[-\tilde{M}_{A}(s)], \qquad (5)$$

$$\tilde{M}_{A}(s) = \sigma_{NN} \left\{ dz \ \rho_{A}(s,z) \right\}.$$

Here  $\rho_{A}(s,z)$  denotes the nuclear density distribution and  $\sigma_{NN}$  is the total nucleon-nucleon (N-N) cross section which is taken to be 40 mb.

where

According to the statistical phase space model, the momentum distribution  $\mathcal{J}_{MN}(p)$  is given as follows:

$$\mathcal{F}_{MN}(\mathbf{p}) = \sum_{i} n_{i} \mathcal{P}_{MN}(n_{i}) \Phi_{L}(\mathbf{p}) , \qquad (6)$$

where  $\mathcal{T}_{MN}(n_i)$  is the probability for producing  $n_i$  particles in the subprocess (M,N) involving vNN collisions and  $\phi_L(p)$  is the normalized momentum distribution of the respective products.

In the beam energy range where the possible types of particle production process are limited to

$$N + N + N + N + \alpha \pi$$
,  $(\alpha = 0, 1, 2, ...)$  (7a)  
 $N + Y + K$ ,  $(Y = A \text{ or } \Sigma)$  (7b)

, for instance, the probability  $\mathcal{P}_{\rm MN}(n_1)$  for producing  $n_{\rm w}$  pions,  $n_{\rm A}$  lambdas and  $n_{\rm r}$  sigmas is given by

$$\begin{split} \mathcal{P}_{MN}(n_{\pi},n_{\Lambda},n_{\Sigma}) &= \frac{\nu}{MN} \sum_{j_{0}=1}^{N} \sum_{j_{1}=0}^{N} \cdots \sum_{j_{\beta}=0}^{N} \frac{\nu!}{\alpha_{\pi 0}^{10} j_{\alpha}! n_{\Lambda}! n_{\Sigma}!} \\ &\times_{\alpha} \underline{1}_{0}[q_{\pi}(\alpha)]^{j_{\alpha}} q_{\Lambda}^{n_{\Lambda}} q_{\Sigma}^{n_{\Sigma}} \delta(\nu - n_{\Lambda} - n_{\Sigma} - \sum_{\alpha=0}^{\beta} j_{\alpha}) \delta(n_{\pi} - \sum_{\alpha=1}^{\beta} \alpha j_{\alpha}) \theta(M + N - n_{\Lambda} - n_{\Sigma}) \\ &+ \frac{MN - \nu}{MN} \delta_{n_{\infty}} o\delta_{n_{\pi}} o\delta_{n_{\pi}} o. \end{split}$$

Here  $\mathbf{q}_i$  are the branching ratios for the respective processes given by Eq.(7). The normalized momentum distribution becomes

$$\begin{split} \phi_{L}(p_{1}) &= \int_{j=2}^{L} \frac{d^{3}p_{j}}{E_{j}} \delta^{3} (\frac{L}{\pi}p_{j} - P_{MN}) \delta (\sum_{j=1}^{L} E_{j} - E_{MN}) \\ &= \sqrt{\int_{j=1}^{L} \frac{d^{3}p_{j}}{E_{j}}} \delta^{3} (\frac{L}{\pi}p_{j} - P_{MN}) \delta (\sum_{k=1}^{L} E_{j} - E_{MN}) \; . \end{split}$$

The subscript L denotes a set of M+N-n  $_{\Lambda}$  -n  $_{\Sigma}$  nucleons, n  $_{\Lambda}$  lambdas, n  $_{\Sigma}$ sigmas,  $n_{\pi}$  pions and  $n_{\Lambda} + n_{\tau}$  kaons.

In the energy range up to abut 5 GeV/nucleon, the following elementary reaction channels should be taken into account in addition to those in Eq.(7)

$$N + N + N + Y + K + n\pi$$
,  $(n = 1, 2, ...)$  (8a)

The set of branching ratios,  $q_{\pi}(\alpha)$ , for the process (7a) is taken from empirical formulas fitted to the experimental data of N-N scattering up to 4-5GeV, that is,  $q_{\pi}(0) = 0.350$ .  $q_{\pi}(1) = 0.228$ ,  $q_{\pi}(2) = 0.215$  and  $q_{\pi}(3) = 0.207$  at 4GeV. The isospin-averaged cross section for the combined process of N+N + N+A+K and N+N + N+E+K in Eq.(7b) is given by  $\bar{o}(N+N+Y+K) = 0.144p_{max}(K)/m_{K}(mb)$ , where  $p_{max}(K)$ is the momentum of the produced kaon of maximum energy in the c.m.s.. The isospin-averaged cross section for the process of N+N + N+Y+K+ $\pi$ is also given by  $\bar{o}(N+N+N+Y+K+\pi) = 0.898p_{max}(K)/m_{K}(mb)$ . The cross section data for the kaon pair production (8b), in the energy range of interest, are rather sparse. We use a simple linear parametrization of the cross section  $\bar{\sigma}(N+N+N+N+K+\bar{K})=0.0175~p_{max}(K)/m_K(mb)$ . The effect of the nuclear Fermi motion on the momentum distribution of the emitted particle is taken into account by using the Fermiaveraged branching ratios for the particle production processes (8a), for instance, defined as follows:

$$\bar{q}_{\Lambda}(\alpha) = \frac{1}{\sigma_{NN}} \int d^3p_{\Lambda} d^3p_{B} \Gamma(p_{\Lambda}) \Gamma(p_{B}) \bar{\sigma}(N+N+N+K+\alpha\pi) , \qquad (9)$$

where the function  $f(p_n)$  and  $f(p_n)$  describe the Yerm: momentum distributions of the nucleon in projectile A and in target B, respectively.

The main production of nuclear fragments comes from peripheral ion collisions. The nuclear fragments show typical factorization of cross sections into a target and a projectile, typical momentum distributions and isotope production ratios. In the rest frame of the projectile (or the target), the cross section is parametrized in the non-relativistic approximation as

$$\frac{d^{3}\sigma^{(F)}}{d\sigma^{3}} = \frac{\sigma_{C}}{4\pi} p \exp\left(\frac{Q_{gg}^{(F)}}{T} - \frac{p^{2}}{2\mu_{F}T}\right) / \left[2\mu_{F}T^{2}\prod_{i}\exp\left(\frac{Q_{i}^{(f)}}{T}\right)\right], \quad (10)$$

where  $Q_{gg}^{(F)}$  are the threshold Q values of various break-up channels of the projectile (or the target) into the observed fragments, T is the temperature parameter,  $\mu_F = M_n M_F (A_p - A_F)/A_p$  and  $\sigma_c = \pi r_0^2 (A_p^{1/3} + A_T^{1/3} - \delta)^2$  with  $\delta$ =1.6. The isotope yields in various ion collisions at e.g. 2.1 GeV/nucleon are well reproduced with the temperature T-8MeV.

The theoretical results are summarized in Table 1. All the hypernuclei produced with cross sections larger than 0.05µb are included. The comparison of corresponding values in Table with available experimental ones  $^{10}$  reveals a good agreement; For  $^{4}$ He beam, Ref.10 gave 0.2µb of  $^{4}$ H whereas our theoretical value is 0.29µb. For  $^{7}$ Li beam, Ref.10 suggested an upper limit only for  $^{7}$ Li production, which has been put there at 1µb. Theoretical value is 0.11µb.

Table

To al cross sections (in µb) of hypernuclei formed by projectile fragmentations

	4He+ 12C	7Li+12C	<sup>12</sup> C+ <sup>12</sup> C	19 <sub>F+</sub> 12 <sub>C</sub>	
energy(GeV/A)	3.7	3.0	3.7	3.7	
β <sub>AF</sub> (fm)	4.07	4.31	4.67	5.08	final nucleus from w A-decay
product					(if "stable")
3 <sub>H</sub>	0.44	0.53	0.46	0.59	<sup>3</sup> не
3н 4 4	0.29	0.68	0.39	0.65	<sup>4</sup> не
<sup>4</sup> не	0.27	0.10	0.39	0.30	-
, ,		0.05	0.03	0.08	-
л́' 5 ЛНе		0.25	2.58	1.94	-
6 A 6 Li		0.25	0.32	0.54	6 <sub>Li</sub>
6 ALi		0.09	0.30	0.37	-

7He       0.07       0.09       0.20       7L1         7L1       0.11       0.24       0.33       7Be         7Be       0.07       0.05       -         8L1       0.18       0.34       -         8Be       0.15       0.11       8B         ABe       0.05       0.22       9Be         9Be       2.48       1.78       -         10L1       0.01       0.09       10Be         10ABe       0.33       0.86       10B         10Be       0.28       0.48       10C         11Be       0.12       0.61       11B         11Be       0.25       0.65       11C         12Be       0       0.07       -         12Be       0       0.07       12B         12C       0.18       0.25       12N         13B       0.33       0.06       13C         13C       0.06       0.07<					
7 Be	<sup>7</sup> ΛHe	0.07	0.09	0.20	7 <sub>Li</sub>
8 Li       0.18       0.34       -         8 Be       0.15       0.11       8 B         9 Li       0.05       0.22       9 Be         9 ABe       2.48       1.78       -         10 Li       0.01       0.09       10 Be         10 Be       0.33       0.86       10 B         10 Be       0.33       0.86       10 B         10 Be       0.28       0.48       10 C         11 Be       0.12       0.61       11 B         13 Be       0.25       0.65       11 C         12 Be       0.06       0.07       -         12 Be       0.23       1.27       12 C         12 C       0.18       0.25       12 N         13 B       0.26       13 C         12 C       0.18       0.25       12 N         13 C       1.38       13 N         14 E       0.09       14 C         14 C       0.09       14 N         14 Ac       0.09       14 N         14 Ac       0.07       15 N         16 C       0.07       15 N         16 Ac       0.07       16 N	7 Λ <sup>L</sup> 1	0.11	0.24	0.33	7 <sub>Be</sub>
Be       0.15       0.11       8B         9L1       0.05       0.22       9Be         9Be       2.48       1.78       -         10L1       0.01       0.09       10Be         10Be       0.33       0.86       10B         10D       0.28       0.48       10C         11Be       0.12       0.61       11B         11Be       0.12       0.61       11B         11C       0.06       0.07       -         12Be       0.06       0.07       -         12Be       0.23       1.27       12C         12Be       0.23       1.27       12C         13C       13C       13C       13C         13Be       0.26       13C       13C         13Be       0.09       14N       0.09         14Ae       0.09       14N       0.09 <th>7 ∧Be</th> <th></th> <th>0.07</th> <th>0.05</th> <th>-</th>	7 ∧Be		0.07	0.05	-
Be       0.15       0.11       8B         9L1       0.05       0.22       9Be         9Be       2.48       1.78       -         10L1       0.01       0.09       10Be         10Be       0.33       0.86       10B         10D       0.28       0.48       10C         11Be       0.12       0.61       11B         11Be       0.12       0.61       11B         11C       0.06       0.07       -         12Be       0.06       0.07       -         12Be       0.23       1.27       12C         12Be       0.23       1.27       12C         13C       13C       13C       13C         13Be       0.26       13C       13C         13Be       0.09       14N       0.09         14Ae       0.09       14N       0.09 <th>8 ^Li</th> <th></th> <th>0.18</th> <th>0.34</th> <th>-</th>	8 ^Li		0.18	0.34	-
N	8 ABe		0.15	0.11	
N	9 Li		0.05	0.22	9 <sub>Be</sub>
10	Be		2.48	1.78	-
10 B 10 D 10 D 11 Be 10 D 11 Be 11 Be 11 B 11 B 11 B 11 B 11 B 11	10 ALi		0.01	0.09	<sup>10</sup> Be
10	10 ABe		0.33	0.86	10 <sub>B</sub>
11	10 <sub>B</sub>		0.28	0.48	
11 AB	1186		0.12	0.61	11 <sub>B</sub>
11 AC	11 <sub>B</sub>		0.25	0.65	<sup>11</sup> c
12B	1 i c		0.06	0.07	-
12B	12 Be		0	0.07	
136	12 <sub>B</sub>		0.23	1.27	<sup>12</sup> c
136	12 AC		0.18	0.25	12 <sub>N</sub>
136	13 <sub>B</sub>			0.26	<sup>13</sup> c
14 B 0.09 14 C 0.92 14 N 0.92 14 N 0.37 15 N 0.37 15 N 0.76 15 N 0.76 15 N 0.76 15 N 0.76 16 N 0.77 16 N 0.07 16 N 0.07 16 N 0.07 16 N 0.07 17 N 0.00 17 17 O 0.00 17 N 17 O 0.00 18 F 0.00 18 F 0.00 18 Ne	13c			1.38	13 <sub>N</sub>
1	14 <sub>B</sub>				<sup>1 4</sup> c
1 4 N	1 <sup>4</sup> C			0.92	1 4 N
16	1 <sup>ii</sup> N			0.37	<sup>14</sup> 0
16	15°C				15 <sub>N</sub>
16 N 1.34 16 O 1.34 16 O 1.34 17 O 1.34 17 O 1.34 18 N	15 AN			0.76	<sup>15</sup> 0
16 N 1.34 16 O 1.16 O 0.14 - 17 N 17 O 1.17 17 O 1.17 O 1.17 I 18 O 0.29 18 F 1.8 F	16 <sub>C</sub>			0.07	16 <sub>N</sub>
16 0 0.14 17 17 0 17 0 17 0 17 0 18 0 0.29 18 F 18 F 18 18 18 18 18 18 18 18 18 18 18 18 18	16 N			1.34	16 <sub>0</sub>
17 N 0.17 17 O 17 O 18	<sup>16</sup> 0			0.14	
170 0.57 17F 180 0.29 18F 18F 0.08 18Ne	17 <sub>11</sub>			0.17	17 <sub>0</sub>
18 0.08 18 Ne	17 AO				
18 r 0.08 18 Ne	180				18 <sub>F</sub>
	18 <sub>F</sub>				18 <sub>Ne</sub>
19 AF 0.13 19Ne					19 <sub>F</sub>
	19 			0.13	19 <sub>Ne</sub>

#### 3. Secondary Production Processes

The secondary hypernucleus production processes are mainly due to mesons produced at the primary stage. If those mesons can still induce the strangeness exchange reactions in nuclear fragments emerging from the primary reaction with sufficient efficiency, it represents an additional source of hypernuclei.

Limitations on the efficiency of the secondary process are the cross sections of meson productions in the relativistic ion collisions, cross sections of strangeness exchange reactions in the elementary process and especially in the process on a nuclear target and finally the kinematics (the momenta matching).

The main difference between K and  $\pi$  productions is the intensity. Remarkably enough,  $\pi$  mesons are produced almost  $10^3$  more intensively. The total cross sections for the elementary A-productions through K and  $\pi^+$  mesons do not differ by more than one order of magnitude, whereas for lower momenta the threshold of  $(\pi K)$  restion cuts off its yield. All the data suggest that the  $(\pi^+K^+)$  secondary production should be much more efficient than  $(K^-\pi^-)$  one, estimated to contribute by three orders of magnitude less than the primary process.

The total cross section  $\sigma_{\Lambda^{\begin{subarray}{c}F\end{subarray}}^{\begin{subarray}{c}F\end{subarray}}$  for producing the hypernucleus  $_{\Lambda^{\begin{subarray}{c}F\end{subarray}}^{\begin{subarray}{c}F\end{subarray}}$  via the secondary (\*K) reaction in a relativistic ion collision, based on \*\* and fragment distributions used in sect.2 is given  $^{7}$ )  $_{\epsilon}$ 

$$\sigma_{\Lambda^{F}} = \int d^{3}p_{\pi} d^{3}p_{F} \frac{d^{3}\sigma^{(\pi)}}{dp_{\pi}^{3}} \frac{1}{\sigma_{\Gamma}} \frac{d^{3}\sigma^{(F)}}{dp_{F}^{3}} \frac{1}{\sigma_{eff}} \sigma_{HY}(F(\pi^{+}K^{+})_{\Lambda}F; p_{\pi}, p_{F}). \quad (10)$$

The formation of the hypernucleus  $_{\Lambda}F$  by  $\pi$ -meson with momentum  $p_{\pi}$  in the (\*K) reaction itself, entering Eq.(10) is given by

$$\sigma_{HY}(p_{\pi}^{lab}) = \int \alpha(p_{\pi}^{lab}, e_{K}^{lab}) \frac{d\sigma}{d\Omega_{lab}}(p_{\pi}^{lab}, e_{K}^{lab}) N_{eff}(HY, p_{\pi}^{lab}, e_{K}^{lab}) d\Omega_{lab}. \tag{11}$$

in the usual laboratory frame  $(p_F^{-0},p_\pi^{-}//z)$ . In Eq.(11),  $\alpha$  is the kinematical factor for transforming from 2-body lab system to A-body lab system.  $\frac{do}{4l} (p_1^{1ab}, \theta_K^{-1ab})$  is the elementary lab differential cross section at  $\theta_K^{-1ab}$ . Effective neutron numbers  $N_{eff}$  are sharply peaked at  $\theta_K^{-1ab} = 0$  and especially for higher momenta of incoming  $\pi^{-1ab} = 0$ . Eq.(11) may be further simplified when one neglects the (very smooth) angular dependence of the factor  $\alpha$  and for  $\frac{Go}{do}$  adopts the value

corresponding to  $0_K$  = 0. Then,  $\sigma_{HY}(p_{\pi}^{lab})$  obtained under the approximation

$$\sigma_{HY}(p_{\pi}^{lab}) = \alpha(p_{\pi}, 0^{\circ}) \frac{d\sigma}{d\Omega} |_{0^{\circ}} \int_{eff} d\Omega_{lab}$$
 (12)

is peaked around  $p_{\pi}^{1ab}$ -1.1 GeV/c and fall off below 1µb only very slowly for large  $\pi$ -meson momenta ( $p_{\pi}^{1ab}$ >1.5GeV/c). A rough approximation of Eq.(10) gives the secondary ( $\pi^{*}K^{*}$ ) process contribution at 10% of the primary one obtained in sect.2. Figure 1 shows primary and secondary production cross sections

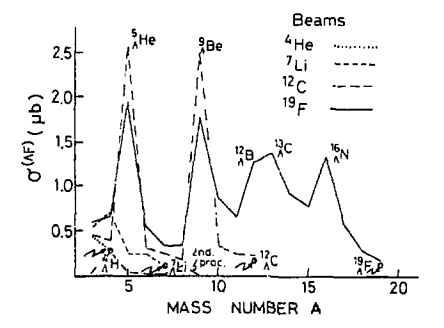


Fig. 1

for four beams indicated. Displayed are only strongest populations for each group of hyperisobares. The hyperisotopes identified in experiments are visualized by arrows.

### 4. H-particle Formation Probability

A deeply bound state of dihyperon with S=-2. Spin J=0 and flavor SU(3)[222], so called H-particle, was predicted using the MIT bag model in 1977 by Jaffe. 11) The binding energy is about 80 MeV relative to the threshold for strong decay to AA. This is a sixquark state consisting of two up quarks, two down quarks and two strange quarks with total spin and isospin zero. Since that, many calculations of the dihyperon have been performed, using relativistic quark bag models, Skyrme models, non-relativistic quark cluster model and lattice QCD. The binding energy is somewhat model dependent. The lattice QCD calculation 12) confirms the existence of a bound state below the AA threshold, but magnitude of the binding energy has not been fixed due to accuracy of numerical calculations. The nonrelativistic quark cluster model predicts a binding energy of (20±5)MeV below the AA threshold. 13,14) In despite of lack of information on the binding energy, it may be useful for experimentally exploring existence of H-particle to know the formation protability of dihyperon in high energy nuclear collisions.

The dihyperon state in  $SU(3)_f$  symmetric limit belongs to the singlet representation and can be expressed in terms of two-baryon configurations as

$$|H\rangle = \sqrt{\frac{1}{8}}|\Lambda\Lambda\rangle + \sqrt{\frac{4}{8}}|N\Xi\rangle - \sqrt{\frac{3}{8}}|\Sigma\Sigma\rangle . \tag{13}$$

In high energy nuclear collisions, many hyperons are produced. If the coalescence model is applied to the formation of dihyperon, the formation cross section of H-particle becomes

$$a^{(H)} = \frac{1}{8}\sigma^{(\Lambda\Lambda)} + \frac{4}{8}\sigma^{(N\Xi)} + \frac{3}{8}\sigma^{(\Sigma\Sigma)}$$
 (14)

Assuming a strong bound state for dihyperon and a small size (-1fm) as compared with the spatial extent of source, the coalescence factor does not depend on details of structure and is given by  $S_H(\Lambda\Lambda) = \frac{1}{2}(2\pi)^{3/2}\beta_{\Lambda}^{-3}$  etc.. In numerical calculations, a channel of N+N + N+E+K+K should be taken into account in addition to Eqs. (7) and (8). We use a simple linear parametrization of cross section of (N+N+N+E+K+K) = 4.45p\_{max}(E) \times 10^{-3} \text{mb/(GeV/c)}, which gives  $\sigma$  = 0.007mb

at plan = 10GeV/c.

Figure 2 shows the M-particle formation cross sections in Ne+Ne collisions at 5GeV/nucleon. The total cross section is -2.6µb. This gives only an upper limit of the cross section due to rough approximations taken for dihyperon wave function.

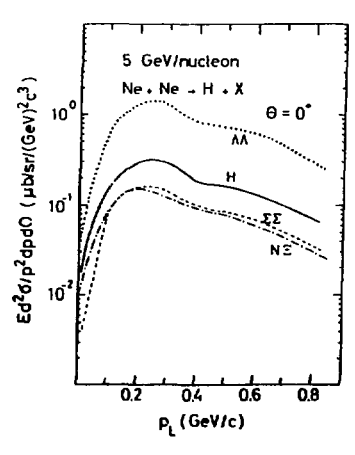


Fig. 2

#### References

- 1) S. schnetzer et al., Phys. Rev. Lett. 49 (1982) 989.
- 2) J.W. Harris et al., Phys. Rev. Lett. 47 (1981) 229.
- 3) A.K. Kerman and M.S. Weiss, Phys. Rev. C6 (1973) 408.
- 4) F. Asai. H. Bando and M. Sano, Phys. Lett. 145B (1984) 19.
- 5) H. Sato and K. Yazaki, Phys. Lett. 98B (1981) 153.

- M. Wakai, H. Bando and M. Sano, INS-Rep.-640 (1987) and to be published in Phys. Rev. C.
- 7) H. Bando, M. Sano, M. Wakai and J. Zofka, INS-Rep.-682 (1988).
- J. Knoll, Phys. Rev. C20 (1979) 773.
   F. Asai, Nucl. Phys. A356 (1981) 519.
- 9) A.S. Goldhaber, Phys. Lett. 53B (1974) 306.
- 10) S. Avramenko et al., Dubna preprint E1-87-337 (1987).
- 11) R.L. Jaffe, Phys. Rev. Lett. 38 (1977) 195.
- 12) Y. Iwasaki, T. Yoshie and Y. Tsuboi, Phys. Rev. Lett. 60 (1988) 1371.
- 13) U. Straub et al., Phys. Lett. 200 (1988) 241.
- 14) M. Oka, K. Shimizu and K. Yazaki, Nucl. Phys. A464 (1987) 700. K. Shimizu, private communication (1988),

# ИССЛЕДОВАНИЕ ВЗАИМОДЕЙСТВИЯ РЕЛЯТИВИСТСКИХ ЯЛЕР С МИШЕНЯМИ ИЗ МЕЛИ В 2П — ГЕОМЕТРИИ

Сотрудничество: Марбург-Пубна-Лейпциг

Р.Брандт, Е.Гансауге, Г.Дерш, Е.Фридлендер $^{\rm X}$ , Г.Хаасе, М.Хек, В.Шульц —

Институты ядерной жимии и ядерной физики при Университете им. Филиппса, Марбург, ФРГ

- В.С.Бутцев, М.И.Кривопустов, Б.А.Кулаков Объединенный институт ядерных исследований, Дубна,
- Э.Ю.Лангрок, Ф.Пилле -Секцая естественных наук Высшей технической школы, Лейшцаг, ГДР

### І. ВВЕДЬНИЕ

В последние годы большое внимание уделяется экспериментальному и теоретическому исследованию аномальных ядерных фрагментов, образурщихся в ядро-ядерных соударениях при релятивистских энергиях /1-26/. Анализ основных результатов по исследованию аномалонов - гипотетических объектов с аномально короткой длиной пробега в веществе, и, соответственно, повышенными сечениями взаимодействия достаточно полно изложен в обзорах /17-20/(смотри также цитированную литературу). Можно отметить, что экспериментальная и теоретическая ситуация неоднозначна и противоречива. Результати 40 работ указывают на наличие эффекта аномалонов, т.е. дают положительные результати, более 30 работ - отрищательные

Интерес к проблеме аномалонов внзван, прежде всего, различными подходами к интерпретации явления. В основу многих моделей положена гипотеза о возможных проявлениях цветовых свойств кварков и глюснов в квантовой хромодинамике. Аномалоны выступают в этих моделях как носители открытого цвета.

Поэтому, на наш взгляд, целесообразно продолжать поисковые эксперименты аномалонов с применением различных методик. Особая роль в этих исследованиях отводится ускорителям, обладающим пучками ядер с энергией выше 2 ГэВ/нуклон. Так, например, в акспериментах, выполненных с применением активационной методики /13-16/, по облучению соорки

<sup>\*</sup> постоянный адрес : Лаборатория им. Лоуренса, Калифорнийский университет, Беркли, США.

мишеней из медных дисков в пучках ядер углерода -12 (44 ГэВ) и ядер аргона-40 (72 ГэВ) наблюдено аномальное увеличение сечений образования изотопа  $^{24}$  ма по сравнению с расчетными значениями Е.М.Фридлендера. Полученные в работах  $^{713-16}$ / отношения сечений образования изотопа натрия-24 в зависимости от полной энергии налетающих ядер имеют четкую тенденцию возрастания. Для объяснения экспериментальных результатов было сделано предположение о рождении в указанных взаимодействиях частиц с необично большими поперечными импульсами, или обобраз звании экзотических объектов с временами жизни около  $10^{-10}$  с  $^{13}$ /. Па сенове этих предположений была проведена серия экспериментов по исследованию активности изотопа натрия-24 в кольцевых мишенях измеди под углами  $0^{0}$  < 9 <  $90^{0}$ , образующейся при соударениях ядер угрерода с энергией 44 ГэВ (Дубненский синхрофазотрон) и ядер гелия с энергией 4 ГъВ ( синхротрон САТУРН, Сакле) с мишенями—генераторами измеди.

### 2. ЭКСІІНРИМЕНТАЛЬНАЯ МЕТОШИКА И РЕЗУЛЬТАТЫ

В настоящих экспериментах использована активационная радиохимическая off-line методика с германиево-литиевыми детекторами на линии с ЭВМ, которая, на наш взгляд, удачно дополняет традиционные для ролятивистской ядерной физики методи. Главным критерием при выборе этой методики была более высокая статистическая обеспеченность исследований на уровне  $10^4$ , что позволяет определять отношения активностей радиоактивных нуклидов  $R_k$  с точностью не хуже (1-3)%.

Две идентичные мишени (рис.I) в виде дисков (  $\mathscr{B}$  = 80 мм, d = 10 мм) солучались в пучке ядер углерода Дубненского синхрофазотрона и в цучке ядер гелия синхротрона САТУРН (Сакле, Франция). Полный поток ядер углерода—I2 и гелия—4 за время облучения составлял  $7x10^{I2}$  и  $5x10^{I2}$  соответственно. Пучки были хорошо сфскусировани на центр мишеней ( $\pm$  I мм). Диаметр профиля пучка (  $\mathscr{B}$ =IC мм) периодически контролировался поляроклом.

Каждая мишень состояла из двух медных дисков ( k=I и 8) и шести медных колец ( k=247 ), перекрывающих диапазоны углов:  $0^0-I0^0$ ;  $10^0-I9^0$ ;  $19^0-31^0$ ;  $31^0-43^0$ ;  $43^0-52^0$  и  $52^0-90^0$  (рис.I). При столиновении ядер углерода и гелия с первым диском-мишенью возникают фрагменты ядра-снаряда и вторичные частицы , которые, в свою очередь, могут повторно взаимодействовать с кольцевным мишенями детекторами. Такая сложная конфигурация мишени была выбрана с целью определения углового распредсления вылета фрагментов и вторичных частиц в переднюю полусферу (2П-геометрия).

110 гамма-излучению изотопа <sup>24</sup>ма в каждой кольцевой мишени опре-

делялось отношение активностей  $\mathbf{R}_{\mathbf{k}}^{*} = \mathbf{A}_{\mathbf{k}}/\mathbf{A}_{\mathbf{S}}$  где  $\mathbf{A}_{\mathbf{k}}$ -активность изучаемого изотопа в  $\mathbf{k}$ -кольце,  $\mathbf{A}_{\mathbf{S}}$ -активность  $\mathbf{24}$  Na в последнем дискепетенторе (  $\mathbf{k}$  =8).

В таблице I приведены отношения активностей  $R_{K}^{*}$  изотопа <sup>24</sup> ма в кольцевых мишенях-детекторах, нормированные на активности в I и 8 дисках. Как видно из таблиць, с увеличением энергии бомбардирующего ядра выход изотопа натрия—24 значительно возрастает для всех интервалов углов от  $10^{0}$  и выше, что естественно отражает высокую множественность вторичных частиц в реакциях, вызванных потоком ядер углерода.

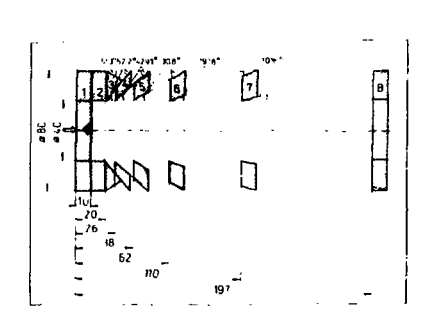


Рис. I Схематическое расположение мишеней из медных дисков (I и 8) и колец (2+7) на пучке ядер углерода-I2.

Таблица I. Экспериментальные отношения активностей  $R_{\mathbf{k}}^{\mathbf{r}}$  — изотопа  $^{24}$  Na в кольцевых мишенях—детекторах

R <sub>k</sub> ( 0 )	90 <sup>0</sup> –70 <sup>0</sup>	70°-52°	52 <sup>0</sup> -43 <sup>0</sup>	43 <sup>0</sup> –31 <sup>0</sup>	31°-19°	19 <sup>0</sup> –10 <sup>0</sup>	10°-0°
k-Homed ME-	I	2	3	4	5	6	7
не (4 ГаВ) нормировано на I-диск	0,2 <u>+</u> 0,1	0,I <u>+</u> 0,I	1,0 <u>+</u> 2,0	0,3 <u>+</u> 0,I	0 <b>,5<u>+</u>0,</b> I	0,8 <u>+</u> 0,1	90 <u>+</u> I,0
Че (4 ГаВ) нормировано на 8-лиск	0,22	0,II	0,22	0,33	0,56	0,89	= <b>I</b> 00
12С (44 ГаВ) нормировано на 1-жек 12С (44 ГаВ)	I,I <u>±</u> 0,2	0,6±0,2	1,0 <u>+</u> 0,2	3,2 <u>+</u> 0,2	5,6 <u>+</u> 0,2	7,6 <u>+</u> 0,2	115 <u>+</u> 2,0
12C (44 ГаВ) норми овано	I,0	0,5	0,9	2,8	4,9	6,8	=100

### 3. РАСЧЕТЫ ПО МОЛЕЛЯМ

В настоящее время, на наш взгляд, не существует адекватной модели для описания всех процессов, происходящих в ядро-ядерных соударениях при высоких энергиях.

В данной работе приведени результати предварительных вычислений угловых и энергетических характеристик вторичных частиц ( р , п ,  $\Pi^*$ ,  $\Pi^0$  и  $\Pi^-$ ) и легких ядер ( d , t ,  $^3$ He,  $^4$ He и  $^5$  Li ), рожденных при взаимодействии ядер углерода-I2 с энергией 44 ГэВ с первой мишенью-генератором. На этой основе проведени оценки активности изотопа натрия-24, наведенной частицами и легкими ядрами в кольцевых мишеннх (2+7) под углами  $0^0$  < 6 <  $90^\circ$ . Вычисления выполнени с использованием Дубненского варианта каскадной модели  $^{30}$ / и феноменологической модели внутриядерных взаимодействий  $^{31}$ /.

В этих вичислениях не учитывались протяженность мишени и родь третьего поколения частиц. На данном этапе вычислений ставилась задача определения роли только вторичных частиц и легких ядер в образовании изотопа натрия-24 в кольцевых мишенях.

Используя значения потоков каждого типа вторичных частиц и легких ядер N = 1 = 1, полученных в результате вычислений по моделям A = 1, определим их вклад в сечение образования изотопа натрия в кольцевых мишенях следующим выражением:

$$\mathbf{A} \stackrel{\mathbf{i}}{\mathbf{k}} (\mathbf{T}_{\mathbf{j}}) = \mathbf{\sigma} \stackrel{\mathbf{i}}{\mathbf{n}} (\mathbf{T}_{\mathbf{j}}) \stackrel{\mathbf{i}}{\mathbf{n}} \stackrel{\mathbf{i}}{\mathbf{k}} (\mathbf{T}_{\mathbf{j}}) \stackrel{\mathbf{i}}{\mathbf{n}} \stackrel{\mathbf{k}}{\mathbf{C}}_{\mathbf{u}}$$
 (I) где  $\mathbf{A} \stackrel{\mathbf{i}}{\mathbf{k}} (\mathbf{T}_{\mathbf{j}}) = \mathbf{a}_{\mathbf{k}}$  активность, образованная (  $\mathbf{i}$  ) — частицей с энергией  $\mathbf{T}_{\mathbf{j}} = \mathbf{k} (\mathbf{k})$  — кольцевой мишени,

N  $_{\rm Cu}^{\rm k}$  — число атомов меди в кольцевой мишени (k),  ${\bf G}_{\rm i,a}^{\rm i}$  ( ${\bf T}_{\rm j}$ ) — сечение образования изотопа  $^{24}$  Na при энергии  ${\bf T}_{\rm j}$  .

Для расчетов по формуле (I) требуется знание функций возбуждения изотопа 24 жа в потоке вторичных частиц и легких ядер р , и , II<sup>-</sup>, II<sup>-</sup>, II<sup>0</sup>, d , t , He, He и Li при энергиях от 300 МаВ до 5 ГаВ. Скудость экспериментальных данных о сечениях образования изотопа натрия-24 в толстых мишенях из меди при различных энергиях указанных частиц и ядер затрудняла выполнение окончательных расчетов. Поэтому для спределения полных сечений образования изотопа 24 ма в реакциях с протонами, дейтронами и ядрами углерода-I2 при энергии 3,65 ГаВ/нуклон нами было проведено дополнительное облучение мишеней из меди толщиной 0,86 г/см<sup>2</sup>.

Мониторирование первичного пучка осуществлялось методом, описанным в работе /32/, и контролировалось с помощью алюминиевых фольт по реакциям  $^{27}$  A1 (  $^{\rm p}$  ,  $^{\rm d}$  ,  $^{12}{\rm C}$ ; X)  $^{24}$  Na . Интегральный поток протонов, дейтронов и ядер углерода таким образом найден с точностью до 10%. Сечение образования изотопа  $^{24}$  Na , определенное нами в этом эксперименте, ссставляет: в реакции  $^{64}$  Cu (  $^{\rm p}$  , X)  $^{24}$  Na при энергии 8,15 ГаВ –  $^{67}$  Na = (3,4±0,5) м , в реакции  $^{64}$  Cu (  $^{\rm d}$  , X)  $^{24}$  Na при энергии 7,3 ГаВ –  $^{67}$  Na = (5,4±0,9) м о и в реакции  $^{64}$  Cu ( $^{12}{\rm C}$ , X)  $^{24}$ Na —  $^{67}$  Na = (12,3±1,8) м о.

Полученные значения сечений согласуются с результатами, содержащимися в работах /33-36/. На рис. 2 показаны значения сечений образования изотопа <sup>24</sup> на на протонах, дейтронах, П—мезонах и <sup>12</sup>с при различных энергиях; взятые из работ/33-36/ наши экспериментальные данные и расчетные значения функций возбуждения (сплошные линии), определенные путем их экстраполяции по экспериментальным значениям.

Произведя суммирование по энергии и по каждому типу частиц и яцер, определим активность изотопа натрия в каждой из кольцевых мишеней, наведенную общим потоком при энергиях от 300 МаВ до 5 ГаВ:

$$A_{k} = \sum_{i} \sum_{k} A_{k}^{i} (T_{i}). \tag{2}$$

Кроме того, необходимо учесть число ядер первичного пучка непровавимодействовавших в первой мишени, но провзаимодействовавших в восьмой мишени  $^{\mathrm{II}}$  (x), которое определим по формуле:

$$N(x) = N_{o'} e^{-G_{in'} f_{Cu'} x}, \qquad (3)$$

N  $_{\rm O}$  - поток ядер пучка (c<sup>-I</sup>),

 $\mathfrak{G}_{ ext{in}}$  — сечение неупругих взаимодействий  $^{64}$   $c_{u}$  ( $^{12}$ C,X) $^{24}$  Na при энергии 3,65 ГэВ/нуклон,

 $\rho_{\text{Cu}}$  - плотность меди (г/см<sup>2</sup>),

толщина первой мишени (x=Icm).
 Из уравнения (I) находим:

$$A_{8}^{i} = \int_{N_{8}}^{i} N(x) \cdot N_{Cu}^{8}, \qquad (4)$$

а  $\frac{1}{8}$  — доля активности, наведенной в восьмой мишени первичным пучком ядер (  $i: ^{12}{\rm C}$ ),

 $\sigma_{\rm Na}^{\rm i}$  (т<sub>j</sub>)— сечение образования натрия—24 в реакции  $^{64}$  Cu +  $^{12}{\rm C}$  при т<sub>j</sub> =3,65 ГаВ/нуклон.

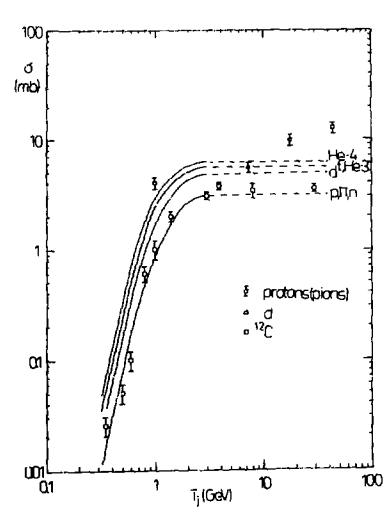


Рис. 2 функции возбуждения для изотопа  $^{24}$  на в потоке вторичных частиц и ядер типа ( і ) в реакции  $_{64}^{\rm Cu}$  ( і ,  $_{\rm X}$  )  $^{24}$  Na

Полученные значения расчетных отношений выходов активностей изотопа натрия-24 в кольцевых мишенях-детекторах приведени в таблице 2.

Таблица 2 Расчетные отношения активностей  $\kappa_{\mathbf{k}}'$  изотопа  $^{24}$  Na в кольцевых мишених-детекторах

R <sub>k</sub> *(0)	90°-70°	70°-52°	52 <sup>0</sup> –43 <sup>0</sup>	43°-31°	31º-19º	19 <sup>0</sup> ~10 <sup>0</sup>	10°-0°
мишени к-номер	I	2	3	4	5	6	7
<sup>I2</sup> C (44ГаВ) нормированс на 8-диск	0,001	eo <b>o,</b> o	0,04	0,12	ს <b>,</b> 39	I,75	=IOU

#### 4. OECYRILHIE PERVISTATOR

Прежде всего сравним экспериментальные значения отношений выходов  $\mathbf{R}_{\mathbf{k}}^{*}$  для изотопа  $^{24}$  на в шести кольцевых мишенях из меди, полученные в реакциях с ядрами углерода—12 (44 ГэВ) и ядрами гелия—4 (4 ГэВ) (таблица I).

Как видно из таблицы I, отношения выходов  $k_{\pi}^{*}$  под углами  $0^{9} < \theta < 90^{9}$  в реакции с ядрами углерода на порядок больше, чем в реакции с ядрами гелия. Этот факт свидетельствует о том, что знергия

вторичных частиц, образующихся в первой мишени в пучке ядер гелия (4 ГаВ), недостаточна для последующего образования изотопа <sup>24</sup> ма в кольцевых мишенях-детекторах. Аналогичный результат был получен нами в экспериментах по облучению сплошных мишеней из меди толщиной I ом в пучках ядер гелия /37/.

Что касается результатов, полученных в реакции с ядрами углерода-12, следует отметить два обстоятельства: во-первых, поскольку энергия первичного пучка 3,65 ГэВ/нуклон выше порога образования П-мезонов (0,8 ГаВ), то в этой реакции рождается большое число П-, П+-и П<sup>0</sup>-мезонов, и, во-вторых, доказано, что энергия вторичных частиц в большинстве случаев уже достаточна для возбуждения <sup>24</sup> Na в кольшевых мишенях ( см. рис.2).

На рис. З приведени расчетные по каскадной модели (квадратики), по феноменологической модели (треугольники) и экспериментальные (кружки) отношения активностей изотопа<sup>24</sup> № экольцевых мишенях-детекторах.

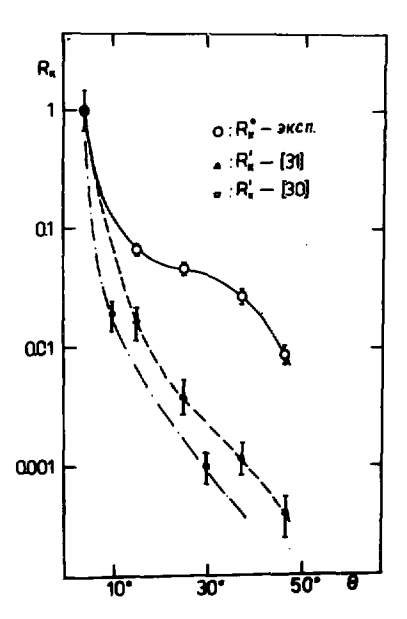


Рис. 3 Расчетние  $K_k' = R_k^* / R_8$  по каскадной — о и феноменологи— ческой —  $\Delta$  моделям и экспериментальние — C отношения активностей изотопа натрия—24.

Как видно из таблиц I и 2 и рис.3, экспери ментальные отношения активностей изотопа натрия—24 для всех диапазонов углов больше, чем расчетные. И хотя ошибка расчетов составляет (20-30)\$, расхождение экспериментальных и расчетных данных значитель ное, особенно для углов больше 20°. Возможно, это

расхождение уменьшится, если учесть родь третьего поколенчи частиц. Однако такое значительное расхождение экспериментальных значения

отношений активностей (  $R_k^*$  ) с расчетными (  $R_k^*$  ), наблюдаемое в кольцевых мишенях под углами  $20^0 < 6 < 50^\circ$ , появоляет нам сделать заключение о рождении в первых актах взаимодействия либо частиц с большими поперечными импульсами, либо неизвестных гипотетических ассоциаций, либо фрагментов с большими угловыми моментами, которые вылетают под этими углами и, при повторном взаимодействии, дают вклад в образование активности  $^{24}$ на . Поэтому вопрос о существовании аномалонов остается открытым.

### В дальнейшем предполагается:

- Продолжить экспериментальные исследования аномального уволичения сечения образования натрия-24 в ядро-ядерных соударениях с применением различных методик, в том числе и твердотельных трековых детекторов ск-39 /38/.
- Провести более тщательные расчеты угловых и энергетических характеристик вторичных и третьего поколения частиц в соударениях ядер углерода-I2 (44 ГзВ) и ядер аргона-40 (72 ГзВ) с мищенями из меди.
- Корректно учесть функции возбуждения изотопа натрия-24 при энергии до 50 ГэВ.

Авторы благодарны В.Д.Тонееву и К.Хенсгену за полезные обсуждения и помощь, оказанную во время проведения расчетов.

# Литература

- Friedlander E.L. et.al. Phys. Rev. Lett., 1980, 45, p. 1054.
   Phys. Rev., 1983, C 27, p. 1489.
- 2. Jain P.L., Dash C. Phys. Rev. Lett., 1982, 48, p. 305.
- 3. Aggerwall L.A. et.al. Pays. Lett., 1982, 111 B, p. 31.
- 4. Аганивов Г.Н. и пр., Сообщения ОИЛИ, PI-81-79, Дубиа, 1981; PI-82-795, Дубиа, 1982.
- 5. Heinrich W. et.al. Preprint Si-83-11, University of Siegen, 1983.
- Ticknell b.L., Price P.B., Report LBL-1628, 1983.
- 7. Голутени И.А. и др., Сообщения ОИЛИ, РІ-83-583, Дубиа, 1983.
- 8. Stevenson J.D. et.al. Phys.Rev.Lett., 1984, 52, p. 515.
- 9. Symons T.J.L. et.al. Phys. Rev. Lett., 1984, 52, p. 982.
- 10. Верен И. и др., Краткие сообщения ОИЛИ, 4-84, с. 10, Дубна, 1984; 9-85, с. 43, Дубна, 1985.
- 11. Price P.B. et.al. Phys. Rev. 1983, 50, p.566.
- 12. Авдейчиков В.В. и др., Ядерная физика, 1986, 44, с. 440.
- 13. Dersch G. et.al. Phys.Rev. Lett., 1985, 55, p. 1176.
- 14. Aleklett K. et.al. Proc. Intern. Symposium on Symetries and Nuclear Structure, Dubrovnik, Yugoslavia, 1986, p. 432

- 15. Aleklett K. et.al., Proc. Intern. Conference on Nuclear and Radiochemistry, ICNR-86 Bejing, China, 1986, p. 137.
- Aleklett K. et. al., Proc. Fourth Conference on Nuclear Analytical Methods, Dresden, GDR, 1987, p. 2.
- 17. Карманов В.А., УФН, 1983, 141. с. 523.
- Heinrich W. et.al., Proc. 7th High Energy Heavy Ion Study, GSI-85-10 Report, Darmstadt, 1985, p. 539.
- 19. Арбузов Б.А., Яперная физика, 1985, 42, с. 542; ЭЧАЯ, 1988, 19, с. 5.
- 20. Соловьева З.И., ЦПИИ атоминформ, вып. 1(8), 1984.
- 21. Milone A., Nuovo Cim., 1954, 12, p. 353.
- 22. Yadoga A., Nuovo Cim., 1957, 6, p. 559.
- 23. Tokunoga S., et.al., Nuovo Cim., 1957, 5, p. 517.
- Friedlander E.M., Spirchez M., Nucl. Sci. Abstr., 1961, 15, p. 2082.
- 25. Judek B., Can. J. Phys., 1986, 46, p. 343.
- 26. Cleghorn T.F., Can. J. Phys., 1986, 46, p. 572.
- Beckmann R., Dissertation, FB Physikalische Chemie, Philipps-Universitaet, Marburg, unpublished (1984).
- 28. Haustein P.E., Phys. Rev., C 20, 1979, p. 1095.
- 29. Friedlander E.M. et.al., LBL-Report 22422, 1986.
- Тудима К.К., Тожеев В.Д., Ядерная физика, 1978, 27, с. 658; Tonejev, V.D., Gudima К.К., Nucl. Phys., A 400, 1983, p. 73.
- 31. Grishin V.G., Haensgen K., Kladnitskaya E.N., Dubna Preprint, B1-85-73, Dubna, 1985; Agakishiev G.N. et.al., Computer Physics Communications, 1988, 48, p. 391.
- 32. Аверичева Т.В. и др. Сообщения ОИЯМ, I-II3I7, Дубна, 1978.
- 33. Cumming J.B. et.al., Phys. Rev., C 17, 1978, p. 1632.
- Dersch G., Dissertation, FB Physikalische Chemie, Philipps-Universitaet, Marburg, unpublished (1986).
- 35. Porile N.T., Cole G.D., Phys. Rev., 1981, 24 C, p. 2038.
- 36. Hudis J. et.al., Phys. Rev., 1962, 129, p. 434.
- 37. Brandt R. et.al., to be submitted to "Isotopenpraxis", 1988.
- Brandt R. et.al., Proc. 14th Intern. Conf. on Solid State Track Detectors, Lahore, Pakistan, 1988.

мссяндование "Рагмента ми ядра-ымпени при взальодействии ядер \*\*2°C и \*\* 4 не с онертией 3,6 гэв/нуюл с ядрами

В.П.Адьясевич, В.Г.Антоненко, М.А.Васильев, А.А.Виноградов, Ю.И.Григорьян, 1.С.Ипполитов, К.В.Караджев, А.Л.Лебедев, В.И. Ланько, Г.Л. Лебришвили, С.А.Николаев, Ю.П.Полунин, В.А.Соловьев, С.Л. Чокин, А.А.Цветков.

Институт атомной энергии им.И.В.Курчатова, Москва

### Введение

В течение нескольких лет группой из ИАЭ им.И.В.Курчатова ведутся исследования ядерно-ядерных взаимодействий на пучкам ядер син-

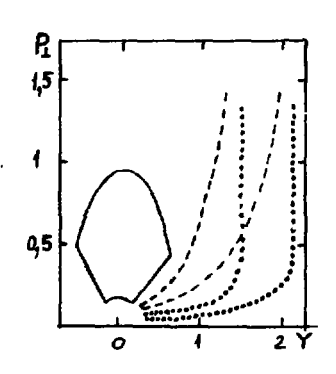


Рис. I Кинематические области на плоскости Р<sub>L</sub>, Y, покрываемые спектрометром (——) и системой измерения множественмости для протонов (—) и пионов (...). Y — быстрота, Р<sub>L</sub> поперечный импульс с фрагмента.

хрофазотрона ОИЯИ с использованием сцинтилляционных спектрометров. Кинематическая область, покрываемая такого рола спектрометром (рис. І), заселяется вторичными частицами, обусловленными, в основном, процессами фрагментации ядра-мишени. Результаты исследований инклюзивных спектров представлялись на предыдущем семинаре, а также опубликованы в рабо-Анализ [4 . 5] [1-5]. представленных в них экспериментальных данных, в сопоставлении с результатами анализа [6] данных , полученных в экспериментах, выполненных на ускорителе Бовалак в Беркли, привел к следующей картине ядро-ядерного взаимодействия при высокой энергии

В результате столкновении формируются три высоковозбужденные якерные системы (рис.2).

В области промежуточных быстрот  $Y = (Y_p + Y_k)/2$ , где:  $Y_p$  и  $Y_k$  – быстроты налетающего ядра и ядра-мишени соответственно, фрагменты, в основном, обрезуются в области центрального

файербола. Энергия возбуждения (температура) последнего увеличивается с ростом энергии, приходящейся на один нуклон налетающего ядра.

В области фрагментации ядра-мишени (налетающего ядра) фрагменты происходят из горячего мишенного источника (источника налетающего ядра), а также из холодного ка да мишени (налетающего япра). Энергия возбуждения горячего мишенного источника (источника налетающего ядра) составляет около 90 маВ/нуклон (Т 255 МаВ) и не зависит ни от энергии столкновения, ни от комбинации сталкивающихся ядер. Температура колодных источников составляет 10 маВ. что соответствует фермиевскому движению в холодном ядре.

Для уточнения этой картины и более глубокого понимания механизма ядро-ядерного взаимодействия при высокой энергии необходимо получить данные о характеристиках событий, отличающихся значениями прицельного парачетра, а также данные о

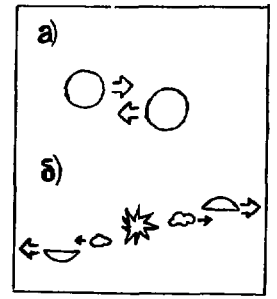


Рис. 2 Высоковозбужденные ядерные системы, образующиеся при взаимодействии релятивистских ядер в модели трех источников: а) до и б) после столкновения.

корреляциях испускаемых фрагментов. С целью обеспечения возможности получения данных такого рода экспериментальная установка ИАЭ им.И.В.Курчатова на синхрофазотроне ОИЛИ была существенно развита. Было сильно увеличено число спектрометров. В результате стали возможными измерения корреляций. Кроме этого, была запущена система измерения ассоциативной множественности. С ее помощью можно сортировать события по степени центральности (прицельному параметру). В настоящем докладе будут представлены результаты экспериментов, выполненных с использованием этих новых систем.

### 2. Летодика экспериментов

Схема экспериментальной установки изображена на рис. 3. Слектры заряженных фрагментов измеряются с помощью шести сцинтилляционных телескопов. Конструкция такого телескопа описана в работе [6]. В экспериментах, результаты которых представляются ниже, они были собраны в три пары с тем, чтобы исследовать ближние корреляции фрагментов. С целью отбора событий по прицельному параметру установлена система измерения ассоциативной множественности. Последняя представляет собий кольцо из 48 сцинтилляционных детекторов толщиной 0.9 см.

знутренний диаметр кольца - 60 см, наружный - 150 см. Система установлена пол 0° (ее ось совпадает с осью первоначального пучка) на расстоянии 2 м от мижени. Летекторы регистрируют все долетающие до них заряженные частицы. В частности, это означает, что протоны регистрируются, начиная с энергии 

45 МаВ. Кинематические области для

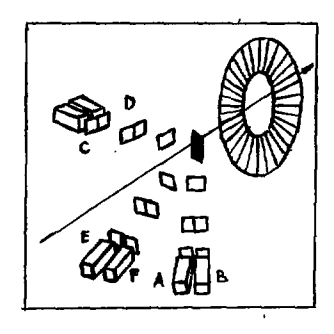


Рис. 3 Схема экспериментальной установки.

≃ 45 МаВ. Кинематические области для случаев протонов и пионов, покрываемые системой множественной регистрации, показаны на рис. Г. Видно, что они должны заселяться, в основном, за счет излучения центрального файербола. В качестве мишени использовалась свинцовая пластина толшиной Зг/см2. Измерения проводились на выведенном пучке синхрофазотрона при интенсивности тока первичных ядер 107 /импульс и при длительности импульса 300-500мс. При этом ускоритель работал в режиме с использованием устройства, устраняющего временную микроструктуру пучка. Время, на которое открывалась электронная измерительная система после срабатывания триггера (окно совпалений), устанавливалось равным 80 нс. При этих условиях доля событий с наложением взаимодействий от разных первичных илер не превышает 5%. Триггером служит запуск любого из телескопов. В режиме инклюзивных измерений для каждого из событий записывались номера детекторов системы измерения множественности, сработавних в совпадении с запуском триггера.

В режиме измерения корреляций, кроме этого, записывалась информация со всех телескопов, сработавших в совпадении с триггером, которым в этом случае служил первый сработавший телескоп.

Подробно измерительная система булет описана в отдельной ра-

# 3. Зависимость характеристик инклюзивных спектров от ассоциативной множественности

Инклюзивные спектры протонов в совпадениях со срабатываниями детекторов системы множественности были измерены для случая стол-кновения ядер <sup>12</sup>С с ядрами свинца при значениях угла вылета 45°,

 $75^{\circ}$ ,  $90^{\circ}$  и  $143^{\circ}$  и с ядрами алюминия при значениях угла вылета  $90^{\circ}$  и  $120^{\circ}$  и пля столинований япер Не с ядрами

120°, и для столкновений ядер Не с ядрами свинца при значениях угла вылета 45°, 60° 75° и 141°. Распределения событий по множественности для обоих налетающих ядер оказались не зависящими от угла вылета ассоции ированных протонов. Эти распределения показаны на рис. 4. Видно, что в случае столкновений со свинцом ядра 1° С ассоциативная множественность гораздо выше, чем в случае 10° не. В обоих случаях распределение по множественности описывается распределением Пуассона. В случае столкновений ядер 1° С с ядрами свинца среднее значение ассоциативной множественности составляет < М > = 5.2. а для не < М > = 1,5.

Отношение средних значений множественности естественно сравнивать с отношением средних чисел заряженных нуклонов-участников, входящих в состав центрального файербола, так как в систему множественности попадают ядерные фрагменты и пионы, в основ-

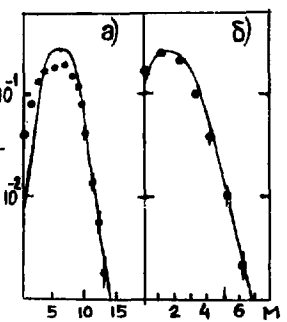


Рис. 4. Распределение по множественности для столкновений:

- а) <sup>12</sup> C+Рь, б)Не+Рь.
  - - эксперимент,
- - подгонка распределением Пуассона.

ном, от его распада, и число пионов пропорционально числу нуклоновучастников [9]. Среднее число заряженных нуклонов **-у**частников дается формулой [10]:

$$\frac{Z_{porti}}{\langle \vec{z}_{porti} \rangle} = \frac{Z_{p} \cdot R_{t}^{2} + Z_{t} \cdot R_{p}^{2}}{\left(R_{p} + R_{t}\right)^{2}}, \tag{I}$$

где  $Z_{\mathbf{p}}$  и  $Z_{\mathbf{t}}$  — зарядовые числа налетающего ядра и ядра-мишени соответственно, а  $R_{\mathbf{p}}$  и  $R_{\mathbf{t}}$  — их радиусы.

Для случаев столкновений <sup>42</sup>С +Рь и <sup>4</sup>Не+Рь формула (I) дает соответственно 9,5 и 4, I заряженных нуклонов. Их отношение 2,3 существенно меньше экспериментально наблюдаемого значения «М(<sup>42</sup>С)» «М(<sup>41</sup>С)» з,5. Возможно, что это различие связано с тем обстоятальством, что система множественности регистрирует частицы не в полном телесном угле. В случае налетающего легкого ядра Не быстрота центрального файербола должна быть меньше, чем в случае более тяжелого ядра <sup>42</sup>С, и соответственно заселяемая им кинематическая область будет сдвигаться в область задних углов, что приведет к уменьшению среднего числа заряженных частиц, попадающих в систему измерения множественности, используемую в настоящем эксперименте. Но

возможно, что это различие определяется и более глубокими причинами. В работе [II] было показано, что наблюдаемая ассоциативная множественность заряженных частиц определяется полной кинематической энергией налетающего ядра. В нашем эксперименте отношение полных кинетических энергий налетающих ядер <sup>42</sup>С и <sup>4</sup> Не есть просто отношение их массовых чисел (3,0), а наблюдаемое отношение средних множественностей (3,5) практически совпадает с нам.

Характер спектров протонов в случае налетакщего ядра <sup>42</sup>С оказался зависящим от ассоциативной множественности. На рис.5 показаны для примера импульсные спектры протонов, испускаемых под углом 45°, для столкновений с малой и большой множественностью (ядро-мишень Рь). ізидно, что в случае большой множественности инвариантное сечение спадает с импульсом гораздо медленнее, чем в случае малой множественности. Такая же картина наблюдается и для других углов вылета, хотя по мере увеличения угла различие между событиями с разной множественностью уменьшается. Если аппроксимировать зависимость инвариантного сечения от импульса экспоненциальной функцией:

то наклон спектра можно характеризовать значением параметра ро. В таблицах I и 2 приведены значения этого параметра в разных интервалах множественности для случаев столкновений <sup>42</sup> C + Рь и <sup>12</sup> C + АI для всех углов выдета нашего эксперимента.

Таблица I. Значения параметра р для столкновений <sup>42</sup>C+Рь

<b>%</b> (град.)	A43	14 < 5	M > 5	M >7	инклюзив
45	247 <u>+</u> 6	2I <b>7</b> <u>+</u> 7	324 <u>+</u> 9	342 <u>+</u> 11	296 <u>+</u> 7
75	I57 <u>+</u> 4	I63 <u>+</u> 3	193 <u>+</u> 4	195 <u>+</u> 5	I78 <u>+</u> 2
90	I30±3	I36+3	I50 <u>+</u> 2	I5I <u>+</u> 3	145 <u>+</u> 2
143	85 <u>+</u> I	<b>8</b> 7 <u>+</u> I	91 <u>+</u> 1	9I <u>+</u> I	90 <u>+</u> 1

Таблица 2. Значения параметра р<sub>о</sub> для столкновений <sup>42</sup>С+АІ

भ <u>ें (град.)</u>	W < 3	M < 4	M > 4	¥/ > 6	инклюзив
90	136 <u>+</u> 3	138 <u>+</u> 3	I56 <u>+</u> 4	I56 <u>+</u> 5	145 <u>+</u> 3
120	I07 <u>+</u> 3	I07 <u>+</u> 3	I 10 <u>+</u> 2	II2 <u>+</u> 2	109 <u>+</u> 2.

Из таблицы видно, что с увеличением множественности параметр наклона растет, и эта зависимость ослабевает по мере увеличения угла вылета. Возможно следующее объяснение этого наблюдения. С увеличением множественности (степени центральности) увеличивается вклад в сечение от излучения центрального файербола. Поскольку энергия

возбуждения последнего гораздо выше энергии возбуждения других источников, при этом в спектре будет уведичиваться доля протонов с большой энергией. Этот эффект будет ослабевать при переходе в область быстрот ядра-мишени (область задних углов). Возможно также, что и сама энергия возбуждения центрального дайербола в случае лобових столкновений выше, чем в случае периферических столкновений. Однако, чтобы установить это, необходимо било бы измерить спектры протонов при существенно больших энергиях. Иная картина наблюдается в случае легкого налетающего ядра 4не. В таблице 3 представлены значения параметра наклона ровазависимости от множественности для этого случая.

Таблица 3. Значения параметра р. для столкновений II +Ры \$\frac{1}{2} \frac{1}{2} \fra

45		232 <u>+</u> 7		230 <u>+</u> 7	234 <u>+</u> 6
60	179 <u>+</u> 5	163 <u>+</u> 3	180 <u>+</u> 4	[75 <u>+</u> 5	162 <u>+</u> 2
75	147 <u>+</u> 3	14£ <u>+</u> 2	I50 <u>+</u> 2	152 <u>±</u> 3	I49 <u>+</u> I
[4I	٤7 <u>+</u> 2	86 <u>+</u> I	€6 <u>+</u> 1	£6 <u>+</u> I	8:6 <u>+</u> I .

Из таблицы видно, что для всех типов столкновений характер спектров один и тот же. Такое различие между случаем легкого и тяжелого налетающего ядра наблюдается впервые. Оно может быть свузано с компактностью ядра Чіе. Как известно, его радиус существенно меньше того, который дается обычной формулой:  $R = \sqrt{3} \cdot \sqrt{3} \cdot \sqrt{3}$ , и близок к радиусу нуклона. Тогда возможно, что в этом случае практически нет периферических столкновений — все они происходят при полном геометрическом перекрытии налетающего ядра с ядром-мишенью. Второе возможное объяснение состоит в том, что в столкновениях ядер Не с ядрами центральный файербол вообще не образуется. Для прояснения этого вопроса необходимы дальнейшие исследования.

# 4, Дальние корреляции

Нами была измерена также зависимость вероятности запуска детектора системы измерения множественности от азимутального угла  $\mathfrak{q}$ , под которым он расположен по отношения к направления вылета частиц, зарегистрированных парой телескопов. С тем, чтоби исключить методические погрешности, связанные с возможными различиями телесных углов летекторов, динамических дапазонов регистрируемых ими частиц, эффективностей их регистрации, в действительности находилаль следующая величина (см. рис. 6):  $\mathbb{E}_{\mathbf{m}} = \left( P_{\mathbf{k}\mathbf{n}} (\mathbf{m}) - P_{\mathbf{c}\mathbf{n}} (\mathbf{m}) \right) \left[ P_{\mathbf{k}\mathbf{n}} (\mathbf{m}) + P_{\mathbf{c}\mathbf{n}} (\mathbf{m}) \right]$ 

где м — номер детектора системи измерения множественности (отсчитинаемый от вертикальной оси по направлении часовой стредки), а величини Рмв (м) и Рсс (м) — соответственно относительные вероятности запуска детектора с номером м в случае сояпадения с парой телескопов АВ или СD. Они определяются следующим образом:

гле N(m) — число запусков детектора с номером m в совпадениях с парой Ab. Аналогично определяется и величина  $P_{CD}$ . Нетрудно показать, что величина F(m) связана с обычно определяемой функцией корреляции:

 $R(m) = R(\vartheta_s, \vartheta_m, \varphi) = \frac{d_{\sigma}(\vartheta_s, \vartheta_m, \varphi)}{(d\Omega_s)^2 d\Omega_m} / \frac{d_{\sigma}(\vartheta_s, \Delta \varphi_s)}{(d\Omega_s)^2} \cdot \frac{d_{\sigma}(\vartheta_m)}{d\Omega_m},$  где  $\frac{d_{\sigma}(\vartheta_s, \vartheta_m, \varphi)}{(d\Omega_s)^2 d\Omega_m} / \frac{d_{\sigma}(\vartheta_s, \Delta \varphi_s)}{(d\Omega_s)^2} \cdot \frac{d_{\sigma}(\vartheta_m)}{d\Omega_m},$  где  $\frac{d_{\sigma}(\vartheta_s, \vartheta_m, \varphi)}{(d\Omega_s)^2} / \frac{d_{\sigma}(\vartheta_s, \Delta \varphi_s)}{(d\Omega_s)^2} \cdot \frac{d_{\sigma}(\vartheta_m)}{d\Omega_m},$  где  $\frac{d_{\sigma}(\vartheta_s, \Delta \varphi_s)}{(d\Omega_s)^2} \cdot \frac{d_{\sigma}(\vartheta_m)}{d\Omega_m} / \frac{d_{\sigma}(\vartheta_s, \Delta \varphi_s)}{(d\Omega_s)^2} \cdot \frac{d_{\sigma}(\vartheta_s, \Delta \varphi_s)}{d\Omega_m} / \frac{d_{\sigma}(\vartheta_s, \Delta \varphi_s)}{(d\Omega_s)^2} \cdot \frac{d_{\sigma}(\vartheta_s, \Delta \varphi_s)}{d\Omega_s} \cdot \frac{d_{\sigma}(\vartheta_s, \Delta \varphi_s)}{(d\Omega_s)^2} \cdot \frac{d_{\sigma}(\vartheta_s, \Delta \varphi_s)}{d\Omega_s} \cdot \frac{d_{\sigma}(\vartheta_s, \Delta \varphi_s)}{(d\Omega_s)^2} \cdot \frac{d_{\sigma}(\vartheta_s, \Delta \varphi_s)}{d\Omega_s} \cdot \frac{d_{\sigma}(\vartheta_s, \Delta \varphi_s)}{(d\Omega_s)^2} \cdot \frac{d_{\sigma}(\vartheta_s, \Delta \varphi_s)}{(d\Omega_s)^2$ 

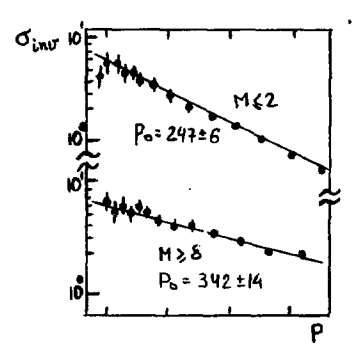


Рис. 5 Инвариантное сечение выхода протонов под углом 45<sup>0</sup> в столкновениях с малой и с большей множественностью.

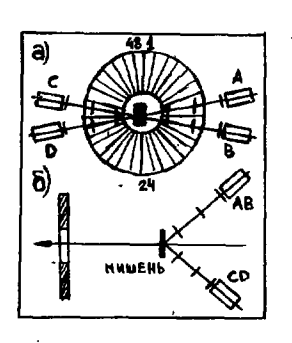


Рис.6 Схема измерения азимутальной асимметрии: а) вид по пучку, б) вид сверху

вылета пары (см.рис.6),  $d\sigma(\theta_s, \Delta q_s)/(d\Omega_s)^2$  — двойное сечение вылета пары частиц под углом  $\theta_s$  к пучку и углом  $\Delta q_s$  между ними, а  $d\sigma(\theta_m)/d\Omega_m$  — инклюзивное сечение вылета частицы под углом к пучку. Эта связь выражается соотношением:

$$F(m) = \frac{R_a(m) \cdot \sum_i f_i \cdot R_s(i) - R_s(m) \cdot \sum_i f_i \cdot R_a(i)}{R_s(m) \cdot \sum_i f_i \cdot R_s(i) - R_a(m) \cdot \sum_i f_i \cdot R_a(i)} \simeq \frac{R_a(m)}{R_s(m)},$$

гле:  $f_m$  - произведение телесного угла детектора с номером m на его эффективность, а  $R_k(m)$  и  $R_k(m)$  - соответственно антис имметричная и симметричная части функции корредиции R

Полученные нами зависимости величини № от азимутального угла для столкновении № С+Рь и Не+Рь представлени на рис.7 (a,b,c,d). Рис.7а и 7с соответствуыт случаю, когла парой телескопов регистрируются две быстрые частицы (пионы с некоторой примесыю электронов), а рис.7ь и 73 — случаю, когда регистрируются два протона. Угол вылета пары по отношению к пучку составлял 141°.

Четко наблюдается положительная корреляция в вылете быстрых частиц, попадающих в телескопы, и частиц, регистрируемых системой измерения множественности. Иними словами, имеет место преимущественный вылет быстрых частиц по одну сторону от пучка. В случае протонов знак корреляции меняется на обратный, котя эффект выражен не так четко, особенно для столкновений 4не + Рь

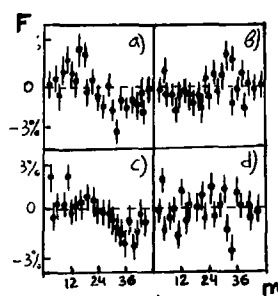


Рис. 7 Зависимость величини F(m) от номера детектора множественности для столкновений  ${}^{12}C+Pb$  (a) и b)) и  ${}^{4}$  Не  ${}^{4}$  Рb (c) и d)) при регистрации парой телескопов совпадений протонов F(b) и частиц с F(b) (a) и F(b) F(b) F(b)

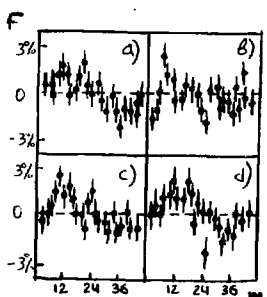


Рис. & Зависимость величины F(m) от номера детектора множественности для столкновений  $^{12}C+Pb$  (2) & b)) и  $^{12}C+l1$  (c) & d)) при регистрации событий с малой (3) & c)) и болькой (6) и d)) множественностью.

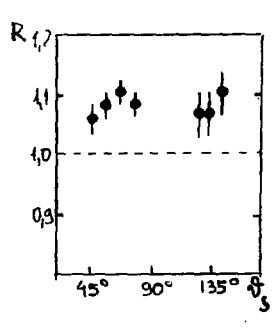


Рис. 9 Сункция корреляции R(AB,CD) в зависимости от угла  $\vartheta_c$ .

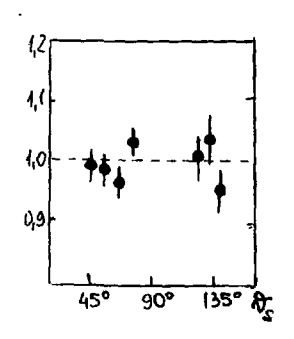


Рис.10 Контрольная величина "]" в зависимости от угла  $\Theta_{\mathsf{S}}$ .

Поназани зависит от степени центральности столкновения. На рис. 8 поназани зависимости Гим пля случаев с малой (а) и с большой ( b) множественности Педостаточная статистика не позволила слелать аналогичное разделение иля величини Грр. Вилно, что эффект положительной корреляции четко виражен в случае периферических столкновений и очень слабо заметен (если вообще наблюдается) в случае центральных столкновений. Инак картина наблюдается в случае столкновений с легким ядром (A1). Ему соответствуют рис. 8с и 8 d, на которых представлены величины Гим В обоих случаях четко видна положительная корреляция, но сколь-нибуль заметного различия событий с малой (с) и большой ( d ) множественностью не видно.

Обнаруженные корреляционные эффекты, по-видимому, свидетельствуют о явлении отскока ( bounce off ) дентрального файербола, вызванного сжатием ядерного вещества в процессе столкновения. Однако, чтобы сделать достаточно определенные выводы, необходимы более детальные исследования, которые мы планируем провести в ближайщее время.

# 5. Ближние корреляции вторичных протонов

Измерения олижних корреляций протонов были выполнены для столкновений <sup>42</sup>C+ Pb. Измерялись функции корреляции, определенные следующим образом:

$$R(AB,CD) = \sqrt{2 \cdot AB \cdot CD/(AC \cdot BD + AD \cdot BC)}$$

где AB,CD,AC и т.п. — выход пар протонов в динамическом диапазоне сцинтилляционного спектрометра, попавших соответственно в телескопы  $A \cup B, C \cup D, A \cup C \cup T \cap T$ . Очевилно, что эти функции дают отношения вероятностей вылета протонов с малым относительным углом ("рядом") и с большим относительным углом. Лля контроля олновременно измерялись еще и величины "I" =  $\sqrt{AC \cdot BD/AD/BC}$ , которые должны быть равны I, если пренебречь небольшими углами ( $5^0$ ) между телескопами в одной паре.

Было проведено два сеанса измерений. В первом использовалось только две пары телескопов (  $AB \sim CD$  ), причем углы  $\Delta q_s$  между телескопами в парах составляли соответственно  $7^0$  (пара AB ) и  $7.7^0$  (пара CD ). Измерения корреляций были выполнены при нескольких углах вылета протонов в диапазоне от  $40^0$  до  $140^0$ .

Во втором сеансе была добавлена еще одна пара телескопов ( EF ) и система измерения множественности. Углы между телескопами в парах были уменьшены до  $6.3^{\circ}$  (пара AB),  $7.1^{\circ}$  (пара CD) и  $3.2^{\circ}$  (пара CD). Измерения были выполнены для угла вылета I40.

Результаты измерений первого сеанса приведены на рис.9 и 10. Результаты второго сеанса приведены в таблицах 4 и 5. Как видно из рисунка и таблиц, наблюдается преимущественный вылет протонов с малыми относительными углами. Для всех углов вылета, при которых выполнялись измерения в первом сеансе, функция корреляции оказалась больше единицы. Зависимости ее от угла вылета не наблюдалось. Усредненное по углам значение  $R(AB,CD) = \frac{1,08 \pm 0,02}{108 \pm 0,02}$ . Из таблицы также видно, что функция корреляции не зависит от множествен—

Таблица 4. Функции корреляции для столкновений 42С + Рь

ности события.

	R(AB,CD)	R(MB,EF)	R(CD, EF)
:// <b>&gt;</b> I3	I,19 <u>+</u> 0,17	I,65+0,42	I,2I+0,23
IO < M < I2	I,22 <u>+</u> 0,I5	2, I8 <u>+</u> 0,4I	I,55 <u>+</u> 0,24
7<4<9	I,22+0,32	1,80+0,32	1,23+0,18
0 <m<6< td=""><td>I,20<u>+</u>0,I5</td><td>I,64±0,37</td><td>I,52<u>+</u>0,25</td></m<6<>	I,20 <u>+</u> 0,I5	I,64±0,37	I,52 <u>+</u> 0,25
0 < 11 < 48	I.2I±0.07	I.92±0.19	I.38±0.II

Таблица 5. Функции корреляции для столкновений Че + Рь

М	R(AB,CD)	R(AB, EF)	R(CD, EF)
0 < 14 < 48	I,43±0,52	2,26 <u>+</u> 0,40	I,44±0,72

Баиболее вероятным объяснением преимущественного вылета протонов "рядом" представляется эффект интерференции тождественных частиц
(12-14). Если это объяснение правильно, то тогда наблюдаемые результаты теоретических расчетов [14] свидетельствуют о том, что размер излучающего источника, которым в данной кинематической области
является горячий источник ядра-мишени, не превышает 3 фм. Независимость
функции корреляции от множественности говорит о том, что размер этого источника и в случае периферического, и в случае центрального
столкновения получается одним и тем же.

Для более определенного суждения о размере и форме источника необходимо получить более детальную зависимость функции корреляции от разности импульсов протонов в паре. К сожалению, импульсное и пространственное разрешение сцинтилляционных спектрометров, использоваьшихся в настоящем эксперименте, не позволяют получить такую зависимость.

### 6. Заключение

Перечислим кратко основные результаты, полученные в настоящей работе.

- І. Отношение средних значений ассоциативной множественности для случаев столкновений ядер <sup>12</sup>С и <sup>4</sup>Не с одним и тем же ядроммишенью Рь, по-видимому, определяется отношением полных кинетических энергий налетающих ядер, а не чисел заряженных нуклоновучастников, входящих в центральный файербол.
- 2. Параметры наклонов импульсных спектров протонов в случае налетающего ядра  $^{12}$ С возрастают с увеличением степени центральности столкновения (с увеличением множественности). Этот эффект усиливается с уменьшением угла вылета.

В противоположность этому, в случае налетающего ядра 4 наклон импульсного спектра протонов не зависит от множественности.

З. Наблюдается право-левая асимметрия в распределении частиц, регистрируемых системой измерения множественности, по азимутальному углу по отношения к направления вылета частиц, регистрируемых парой телескопов, в случае, когда последние прыдставляют собой пару быстрых частиц (пионы с примесью электронов), эта асимметрия соответствует преимущественному вылету продуктов реакции по одну сторону от пучка.

В случае пары протонов, наоборот, наодюдается преимущественный вылет частиц, регистрируе ых системой множественности, по другую сторону от оси пучка.

4. В случае столкновения "С+Рь измерень "ближние" норреляции протонов. Наблюдено преимущественное испускание пары протонов

с мальми относительными углами. Если эта корреляция обусловлена эффектом их интерференции, то размер излучающего источника не превосходит 3 фм.

### Литература

- I. Б.П.Адьясевич и др., Яф. т.40, вып.2(6), стр.495 (1964).
- 2. B.P.Adyasevich et al., Phys. Lett., v.142B, N4, p.245 (1984).
- 3. B. P. Adyasevich et al., Phys. Lett., v. I6IB, N1, p.55 (1985).
- 4. Б.П.Адьясевич и др., Яф. т.45, вып.2, стр.436 (1987).
- 5. Б.П.Адьясевич и др., Яф, т.46, вып.5(II), стр. I353 (1987).
- 6. V.I.Manko and S.Nagamiya, Nucl. Phys., v.A384, p.475 (1982).
- 7. S.Nagaziya et al., Phys. Rev.C, v.24, N3, p. 971 (1981).
- В.И.Манько, Трудн УШ Международного семинара по проблемам фазики высоких энергий. ОМЯИ, ДІ,2-86-668, Дубна, 1987, т.П.с.290.
- 9, J.W.Harris et al., Phys. Rev. Lett., v.58, p.463 (1987).
- IO. J.Huffner and J.Knoll, Nucl. Phys., v.A290, p.460 (1977).
- II. A.M. Poscanzer et al., Phys. Rev. C, v.21, N4, p.1321 (1980).
- I2. R. Hanbury-Brown and R.Q. Twiss, Nature, v. 178, p. 1046 (1956).
- Г.И.Копылов и М.И.Подгорецкий, Яф. 15, стр. 392 (1972).
- I4. S.E.Koonin, Phys. Lett., v.70B, p.43 (1977).

СПЕКТРЫ  $\Pi^{\pm}$  МЕЗОНОВ И ПРОТОНОВ В ЦЕНТРАЛЬНЫХ И ПЕРИФЕРИЧЕСКИХ СТОЛКНОВЕНИЯХ р.  $^{12}$ C,  $^{22}$ Ne С ЯПРАМИ ФОТОЖИЛЬСИИ ПРИ~4.5 A ГЭВ/с

С.Вокал, В.А.Лескин, К.Д.Толстов, Г.С.Шабратова

Объединенный институт ядерных исследований, Дубна

В центральных столкновениях тяжелых ионов с ядрами фотоэмульсии при энергии  $\sim 4$  ГэБ/пуклон возможно более чем двукратное увеличение илотности ядерной материи  $^{1,2}$  по сравнению с равновесной  $\rho_0 = 0.17$  фм $^{-3}$ , сопровождающееся значительным разогревом ядерного вещества  $^{3,2}$ . В таких взаимодействиях ожидаются коллективные процессы статистического характера с установлением термодинамического равновесия (термализацией) нуклонов  $^{4,4}$ . Изучение свойств ядерной материи в подобных экстремальных условиях возможно путем исследования характеристик спектров частиц, их выхода в центральных и периферических соудавинях.

В настоящей работе рассматриваются спектры релятивистских  $\Pi^{\pm}$  – мезонов и протонов, участников взаимодействия, выделенных в неупругих столкновениях р,  $^{12}\mathrm{C}$ ,  $^{22}\mathrm{Ne}$  с ядрами фотоэмульсии при  $\sim$  4,5 а ГаВ/с  $^{/5-7/}$ .

### ЭКСПЕРИМ ЭНТАЛЬНЫЙ МАТУРИАЛ

Исходный экспериментальный материал представлял собой ансамоли следов однозарядных частиц с относительной ионизацией  $g/g_o$  < I,4; скоростью  $\beta>0.75$  (s – частиц).

Виделение 11 - мезонов и протонов-участников в насорах s - частиц /6,8/ осуществлялось путем непосредственной идентификации по результатам измерений величин РВ и относительной монивании на следах с использог лием известных расчетных зависимостей 2 / 20 = † ( PB ) до области сближения рв ≃ 1.2 ГэВ/с кривых монизационных потерь. В области значений рв > 1,2 ГаВ/с выделение частиц проведено статистически с использованием спектров II+ мезонов из пр (рп)-столкновений при близких энергиях. При этом однозарядные фрагменты ядра-снаря**б**а (р. d., t. ) окли отделены от П<sup>±</sup> мезонов и протонов-участников с помощью алгоритма 787, учитывающего особенности распределения \$-частиц по углу вылета в соласти малых углов /9,10/. каждой рассматриваемой частицы и ошиску в ее измевеличину ра; рении.

# HEPPETHYECKIL PACIFICACIDADE DIOPHYHEA

Получение для столкновений р,  $^{12}$ с,  $^{22}$ Ne с ядрами фотоэмульсии экспериментальные распределения релятивистских  $^{12}$  — мезонов, протоновучастников по импульсу имели практически одинаковую форму  $^{77}$ . На подобие форм энергетических спектров (одинаковые параметры наклона при аппроксимации экспоненциальной зависимостью)  $^{1}$ ,  $^{1}$  — мезонов с импульсом  $^{1}$ Р > 0,5 ГэВ/с в лабораторной системе координат для столкновений различных ядер указивалось также в работе  $^{1}$ Г.

В таблице I представлени результаты аппроксимации распределений  $\Pi^{\pm}$  - мезонов с T > 80 WaB по кинетической эноргии в л.с. выражени- ем:

$$f(T) = C \cdot exp \quad (-T/T_0), \tag{I}$$

где  $T_{o}$ - подгоночний параметр,  $\ensuremath{\mathfrak{C}}$  - ошибка его определения.

Таблица І

Аппроксимация спектров кинетических энергий it— мезонов экспоненциальной зависимостью

Снаряд	Р <sub>о</sub> Гаж/с	T <sub>o</sub> MaB	йаБ	$\chi_5$
p_	4,5	500	20	6,7
p 12 <sub>C</sub> <sup>22</sup> Ne	4,5	500	20	C <b>,</b> 5
<sup>22</sup> Ne	4,I	<b>45</b> U	IO	1,15

Одминсковые для взаимодействий р <sup>12</sup>C, параметры Т (наклоны спектров) и близкое к ны: значение Т в <sup>22</sup>Ne + эмульсия взаимодействиях подтверждаютвивод <sup>11</sup> о слабой зависимости формы спектров и средних импульсов . — незонов от массы ядра-снаряда. Подобие форм импульсных спектров и близость средних импульсов наблюдаются также и для протонов-участников.

Известно, что g -частици ( однозарядние частици с ионизацией g /20 > 1,4, прозегом R>3 мм)  $^{12}$  в подавляющем больщинстве состоят из p, d, t — фрагыентов ядра-мишени , мягких (pg < 120 Msb/c)  $R^{\pm}$  — мезонов и замедлившихся в каскадних процессах

протонов ядра-снаряда. Определение выхода различных g -частиц сопря-

жено с рядом методических трудностей. Имеющиеся в эмульсионных работах оценки ограничены и не дают детального представления о соотношении частиц в ансамоле **Q** - фрагментов. С этой точки зрения интересно сравнить энергетический спектр частиц от фрагментации ядра

<sup>22</sup>Ne в системе его покоя со спектром **Q** - фрагментов ядер фотозмульсии. На рисунке Іа представлен полученный преобразованием 5 частиц к антилабораторной системе координат спектр кинетических энергий, где всем частицам приписана масса протона для сравнения со спектром **Q** - частиц от фрагментации ядер фотозмульски в <sup>22</sup>NeEm взаимодействиях / 13/. который показан пунктиром.

Сопоставляемые спектры, отнормированные на равное число частиц, практически одинаковы по форме. На рис. I (б.в.г.д) показаны вклады в спектр  $\varrho$  — фрагментов ядра  $^{22}$  Ne протонов—участников ( $\rho_{\text{уч}}$ ), протонов, не испытавших взаимодействие ( $\rho_{\text{фрагм}}$ ),  $\Pi^{\pm}$  — мезонов, а также сложных фрагментов—дейтронов и тритонов.

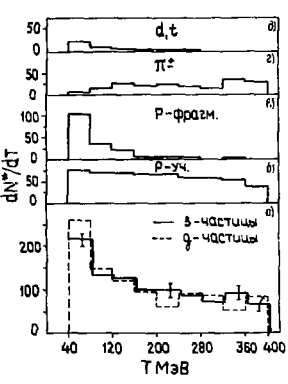


Рис. I. Распределения по кинетической энергии S — частиц из 22 Ne + эмульсия взаимо действий и Q — фрагментов ядер фотозмульсии.

В процентах эти вклады соответствуют числам: 56, 19, 20, 5. Таким образом, при фрагментации ядра  $^{22}$ Ne в системе его покоя основной вклад в g -частицы в указанном на рис. І диапазоне энергий обусловлен протонами (около 75%), 20% соответствуют вкладу  $\Pi^{\pm}$  -мезонов и 5% -вкладу d, t -фрагментов. Полученные со-

отношения дают представление об относительном выходе частиц в совокупности  $\varrho$  - фрагментов покоящегося ядра.

# СВОЙСТВА СПЕКТРОВ $\Pi^{\pm}$ —МЕЗОНОВ И ПРОТОНОВ В ЦЕНТРАЛЬНЫХ И ПЕРИФЕРИЧЕСКИХ СТОЛЮНОВЕНИИХ ЯДЕР

В табл. 2 приведены средние характеристики распределений  $\Pi^{\pm}$  -мезонов и протонов-участников по импульсу, углу вылета  $\theta$ , продольной бистроте  $\psi=1/2\ln((\pm P_{\rm H})/(\pm P_{\rm H}))$ , поперечному импульсу  $(P_{\rm LT}, P_{\rm LP})$ , относительний выход  $N_{\rm P}/N_{\rm P}$  частиц в квазицентральных и периферических  $^{22}$   $N_{\rm P}$  + эмульсия столкновениях, выделенных по суммарному заряду  $\theta$  непровзаимодействовавших фрагментов ядра-снаряда. Импульсы даны в  $^{22}$   $M_{\rm P}/N_{\rm P}$  — в градусах.

Таблица  $\gtrsim$  Средние характеристики споктров релятивистских  $IP^{\pm}$ -мезонов и протонов в зависимости от **Q** 

G.	0 + 2	7 ÷ Iù	9 + IO
~ 7 Pm> ~	6L0 ± 40	690 ± 50	720 ± 60
( Pp)	2020 ± 70	2340 ± 70	$2390 \pm 80$
< 0 <sub>€</sub> >	44 ± 3	32 ± 3	23 ± 2
< 0p>	I8 🛨 I	$12,3 \pm 0,7$	$II \pm I,2$
< y <sub>10</sub> >	0,98 <u>+</u> 0,07	I,30 <u>+</u> U,08	$1,52 \pm 0.07$
< yp>	I,27 ± 0,03	I,48 ± ∪,03	$1,53 \pm 0,04$
( btd.)	280 <u>~</u> 20	245 <u>+</u> 20	240 ± 30
〈P⊥p〉	530 ± 20	410 ± 20	400 ± 30
Nn/Np	$1,9 \pm 0,2$	$1.3 \pm 0.1$	$1,3 \pm 0,3$

В ансамоле событий с Q =0+2 в подавляющем большинстве это столкновения  $^{22}$  Ne + Aq,8r  $^{14}$ , среднее число сильновонизирующих частиц из ядра-мишени  $^{<}$  N<sub>p</sub>>  $^{<}$  26. Эта величина, отражающая в среднем степень расщепления ядер-мишеней в данной совокупности квазицентральных соударений, практически соответствует критерию отбора событий полного разрушения ядер Aq,8r  $^{/}$  15,16. Напомним, что события с N<sub>p</sub>> 7 относятся к взаимодействиям с ядрами Aq,8r , a с N<sub>p</sub> $\leq$  7 соответствуют взаимодействиям с С , N , О и перифелическим столкновениям с ядрами Aq,8r . В последней колонке табл.2 даны характеристики спектров частиц в крайне периферических столкновениях (Q =9+10). Пользуясь соотношением

$$N_{\delta a} = A_{p} - \frac{A_{p}}{Z_{p}} \cdot Q_{s}, \qquad (2)$$

определим число нуклонов ядра  $^{22}$  Ne собитий из наборов, представленных в трех последних колонках таблицы, получим соответственно:  $\sim 20$ , 7+I, 2+I.

Анализируя свойства спектров, отметим, что при переходе от центральных (квазицентральных) к крайне-периферическим <sup>22</sup> Ne + амульсия взаимодействиям ( при ~ десятикратном уменьшении числа нуклонов ядра-снаряда участников взаимодействия), наолюдается незначительное ( ~ на 20%) увеличение средних импульсов П<sup>±</sup> - мезонов и протонов, и существенное ( почти 2-кратное) уменьшение среднего угла испускания частиц, ведущее к заметному уменьшению средних поперечных импульсов (особенно протонов). Средние быстроты П<sup>±</sup> -мезонов и протонов-участников при этом возрастают и, сближаясь, становятся равными в крайне-

порифорических столкновениях. Указание на незначительную зависимость изпульсов редятивистских  $i^{\pm}$  — мезонов и протонов от числа нуклонов на их пути в ядре-ышени рассматривалось в работе  $^{77}$  как возможное проявление длины формирования.

В центральных  $^{22}$  Ne + Ag, Br — столкновениях ядер по сравнению с периферическими наслюдается значительное ( $\sim$ в I,5 раза) увеличение выхода  $\Pi^{\pm}$  — мезонов на протон-участник (см. N<sub>T</sub>/N<sub>P</sub> в тасл. 2).

Подобные свойства в поведении частиц наблюдались в  $^{12}$ С + эмульсия взаимодействиях, виделенных по  $^{22}$ С, а также в наборах событий, виделенных по степени расщепления ядра-мишени в столкновениях р,  $^{12}$ С,  $^{22}$ Ne с ядрами фотоэмульсии  $^{77}$ . Эти результати свидетельствуют о зависимости углов вылета, бистрот, относительного выхода частиц  $\Pi^{\pm}$  — мезонов и протонов-участников от числа провзаимодействовавших в событии нуклонов снаряда и мушени.

### модель файсреола и термализация протонов

В центральных соударениях ядер при значительном числе нуклонов в объеме взаимо, ействия ожидается возникловение движущегося, сильно разогретого стустка материи — фейербола 1,3, представляющего смесь нуклонов, мезонов и возоужденных барионов. Предполагается, что в ансамоле частиц файербола возможно установние термодинамического равновесия, которое достигается после того, как каждый нуклон испитывает несколько столкновений. О степени близости распадающейся системы к состоянию термодинамического равновесия можно заключить по величине отношения среднего поперечного импульса частиц к среднему продольному в событих:

 $R = \frac{2}{T} \frac{\sum_{i} P_{i} t}{\sum_{i} P_{i} t}.$  (3)

Для системы с полной термализацией R =I /4/.

В настоящей работе протоны-участники из ядра-снаряда ( $^{22}$  Ne ) были разделены на три ансамбля по степсчи расщепления ядер-мишеней в событиях, где они наблюдались. Для каждого ансамбля событий были найдены средний поперечный  $< P_{1p} > ^{x}$  и средний продольный  $< P_{1lp} > ^{x}$  импульсы протонов в системе центра масс NN — столкновений, а также величина

$$R^* = \frac{2}{\widehat{n}} \frac{\langle P_{1p} \rangle}{\langle P_{1|p} \rangle^*} \tag{4}$$

В среднем, для ограниченного класса собитий, по которым образован ансамбль протонов, величина  $R^*$  , подобно R , может характеризовать близость распавшихся на частицы систем к состоянию термодинамического равновесия.

В табл. З приводены значения  $< P_{1p} > n < P_{11p} >^*$  в МэВ/с, средних воличин R \* и  $N_{fh}/N_p$  в завысымости от степени расщепления мишени (  $N_h$  ) в выделенных ансамблях событий.

Наслидаемое в таслице увеличение фактора  $R^*$  с ростом  $N_h$  в ансамслях событий связано с уменьшением продольного и существенным увеличением поперечного движения протонов, сопровождающимся повышением на  $\sim 50\%$  выхода  $L^\pm$  — мезонов на протон-участник в квазицентральных столкновениях 20 Ne + Ag, 8r с практически полным разрушением япра-мишени.

Таблица 3 Параметр  $R^*$  в ансамблях событий  $^{22}$  Ne + эмульсия с разными  $N_h$ 

Nh	U <b>+</b> 5	6 + 25	N <sub>h</sub> ≥ 26
< PLD>	386 <u>+</u> 17	520 ± 20	564 ± 25
< P <sub>II</sub> >	500 ± 25	430 <u>+</u> 20	390 ± 25
< R <sup>*</sup> >	0,49 ± 0,04	G,77 ± U,05	U,92 ± 0,08
Nn/Np	$1,2 \pm 0,1$	$I,6 \pm 0,I$	$1.84 \pm 0.12$

Следует отметить более резкий рост величин  $\langle P_{Lp} \rangle$  и  $N_{\Omega}/N_{p}$  при переходе от событий с  $0 \le N_{h} \le 5$  к событиям с  $6 \le N_{h} \le 25$ .

чем при последующем переходе к собитини с N<sub>h</sub>≥ 26. Это указывает на заметную зависимость характеристик < P<sub>L</sub>p> и N<sub>Th</sub>/N<sub>P</sub> от чис— ла нуклонов, участников взаимодействия. Наблюдаемий скачок средних величин связан с переходом от взаимодействий с ядрами С, N , О и периферических взаимодействий с ядрами Ag, Br к непериферическия столкновениям с ядрами Ag, Br фотозмульски. Подобное изменение величин < P<sub>L</sub>p> и N<sub>Th</sub>/N<sub>P</sub> наблюдается и в ансамолях собитий, выделениях по Q<sub>2</sub> при переходе к квазицентральным столкновениям (табл.2).

Близкое к единице значение фактора  $R^*$  в центральных соударениях  $^{22}$  Ne + Ag , Br с полным разрушением ядер-мишеней, значительное увеличение относительного выхода  $H^+$  - мезонов свидетельствуют с том, что знергия направленного движения нуклонов в области перекрытия ядер преобразуется в их хаотическое движение и знергию рожденных  $H^+$  - мезонов. Это указывает на возможное проявление в подобных событиях состояний, слизких к равновесному. Отметим, что доля событий с  $N_h \ge 26$  составляет более 12% от всех 12%.

# AHIPOTOHEALIUS CHERTPOB HPOTOHOB—YYACTHIKOD II HE — MESOHOB PACHPELLILIHILM POLLS

В работе <sup>/9/</sup> спектри поперечных импульсов фрагментов ядра-снаряда с зарядом Z≥2 в л.с. из <sup>I2</sup>C + эмульсия взаимодействий (4,5 ∧ ГэВ/с) были аппроксимированы распределением

$$f(P_{\perp}) = (P_{\perp}/\sigma^2) \cdot \exp(-P_{\perp}/2\sigma^2), \qquad (5)$$

которое соответствует парциальным гауссовым распределениям по поперечным компонентам 3-импульса фрагмента в системе покоя фрагментирующего гдра. В /9/ отмечалось наличие "хвоста" больших передач в спектрах об и многозарядних фрагментов снаряда, не описываемого распределением Ралея. Подобное исследование было проведено и на материале 22 Ne + эмульски взаимодействий, где экспериментальные Рт — спектри фрагментов ядра-снаряда также неудоглетворительно описывались выражением (5). Надожная аппроксимация спектров (включая их высокоимпульсные эбласти) была проведена суммой двух распределений Ралея с заметно отличающимися параметрами, что рассматривалось как указание на существование двух независимых источников испускания фрагментов с разными "температурами" об и б2 /10/. Наличие в ансамбле спектаторных фрагментов ядра-снаряда значительной доли частиц с большими

 $ho_{
m L}$  , очевидно, должно сопровождаться адекватным свойствами спектров протонов-участников и рожденных  $\Pi^{\pm}$  - мозонов.

В табл. 4 приведены результаты ашпроксимации спектров двухралеовским распределением вида:

$$f(P_{\perp}) = \alpha (P_{\perp}/\sigma_1^2) \exp(-P_{\perp}^2/2\sigma_1^2) + (1 - \alpha)(P_{\perp}/\sigma_2^2) \exp(-P_{\perp}^2/2\sigma_2^2),$$
 (6)

где **d.** - вклад первого члена распределения. Значения импульсов даны в MaB/c.

Таблица 4
Аппроксимация спектров Р<sub>1</sub> протонов и П<sup>±</sup> — мезонов двумя распределениями Рэлея

	A <sub>p</sub>	< P₄ ⅓	1-d	< P <sub>L</sub> > <sub>2</sub>	$\widetilde{\chi}^2$	〈የኒክ	< P1 >9
	<sup>22</sup> Ne	170 <u>+</u> 17	0,5 <u>+</u> 0,I	_	•		_
Π±	12 <sub>C</sub> <b>p</b> <sup>22</sup> Ne	190 <u>±</u> 70 150±10	0,7 <u>+</u> 0,4 0,87 <u>+</u> 0,20				
P	<sup>22</sup> Ne	236 <u>±</u> 44	0,8 <u>+</u> 0,I				

Величины < Рт > п , указанные в таблице, найдени как:

 $< P_{\perp}>_{\Pi} = \alpha < P_{\perp}>_{\downarrow} + (1-\alpha) < P_{\perp}>_{2};$   $< P_{\perp}>_{\downarrow} = \sqrt{\Pi/2} \ \mathfrak{G}_{\downarrow};$   $< P_{\perp}>_{\chi} = \sqrt{\pi/2} \ \mathfrak{G}_{\chi}$ где  $< P_{\perp}>_{\downarrow}$  и  $< P_{\perp}>_{\chi}$  – математические ожидания для суммируомых распередолений.

Полученные при аппроксимации величины  $< P_L >_\Pi$  и экспериментальные  $< P_L >_B$  хорошо согласуются. Анализируя подгоночные параметры спектров  $\Pi^\pm$  — мезонов ( табл.4 ), отметим, что доля частиц с малыми  $< P_L >_I$  возрастает с увеличением  $A_p$  снаряда. Это можно объяснить возрастанием вклада периферических столкновений с увеличением массы  $A_p$ .

Большие  $P < P_L >_2$  — параметры, соответствующие более "торячему" источнику частиц, связаны с реализацией столкновений ядер при большом числе нуклонов—участников, например, во взаимодействиях  $^{22}$ Ne +A $_0$ ,B $_1$ 

сопровождающихся полным разрушением ядра-мишени и в непериферических  $^{22}$ Ne + Ag ,B  $^*$  столкновениях. Подтверждением этому является близость параметра < P<sub>1</sub> > $_2$  =560 $\pm$ 40 MaB/c и среднего импульса < P<sub>1</sub> > $_2$  =564 $\pm$ 25 MaB/c протонов в ансамоле событий  $^{1}$  N<sub>1</sub>  $\geq$  26 ( табл. 3), а также < P<sub>1</sub> > $_2$  =540 $\pm$ 25 MaB/c для событий  $^{2}$  N<sub>1</sub> > $_2$  7.

### SAKUDYEHIE

- I. Наблюдается слабая зависимость форми импульсных спектров и соответствующих средних импульсов релятивистских  $\Pi^{\pm}$  чезонов и протонов—участников от масси ядра-снаряда.
- 2. Найдены соотношения выхода частиц в ансамоле g фрагментов ядер  $^{22}$  Ne в антилаоораторной системе координат. Энергетический спектр g фрагментов ядер фотоэмульсии и спектр g фрагментов ядер  $^{22}$ Ne практически одинаковы по форме. Полученные соотношения дают представление об относительном выходе частиц в совокупности g -фрагментов покоящегося ядра.
- 3. В столкновениях <sup>22</sup>Ne + Ag, Br с полным разрушением ядер-мишений подтверждается выполнение признака термализации протонов, предсказываемой моделью файербола.

Показано, что в центральных соударениях и во взаимодействиях  $^{22}$ Ne  $^{+}$ Ag,Br с полным разрушением ядер-мишеней наблюдается превишение на  $^{45-50\%}$  выхода  $\Pi^{\pm}$  - мезонов на протон-участник над этой величиной в периферических соударениях. Подобный эффект наблюдался в непериферических взаимодействиях р,  $^{12}$ C с ядрами  $^{4}$ Ag, $^{4}$ 4 при близ-ких энергиях.

4. Показано, что спектры поперечных импульсов релятивистских П<sup>±</sup> — мезонов и протонов-участников во взаимолействиях с япрами фотоамуль-

сии состоят из двух компонент с существенно различными средними характеристиками, что может быть интерпретировано как наблюдение двух источников испускания частиц. Доля  $\mathbb{H}^{\pm}$  — мезонов с малыми поперечными импульсами возрастает с увеличением  $\mathbb{A}_{\alpha}$ .

Показано совпадение поперечного импульса, соответс::вующего висо-коимпульсной компоненте спектра протонов в <sup>22</sup>Ne + эмульсия взаимодействиях, среднего поперечного импульса протонов в собитиях полного разрушения Ag, Br ядер и среднего поперечного импульса в непериферических <sup>22</sup>Ne + Ag, Br соударениях.

Авторы благодарны С.д.Богданову и Э.Г.Бубелеву за полезные обсуждения.

## JINTEPATYPA

- I. Толстов К.Д. ОИНИ, PI-8662, дубна, 1975.
- 2. Tolstov K.D. Z.Phys.A Atoms and Nuclei, 1981, 301, 339.
- 3. Westfall G.D. et.al.-Phys. Rev. Lett., 1976, v.37, p.1202.
- 4. Тонеев В.Д. и др. ЭЧАЯ , 1986, 17,1093.
- Банник Б.П. и др. ОИЯМ, PI-13055. Дубна. 1980.
- 6. Карабова М. и др. ОИЯМ, РІ-83-14, Дубна, 1983.
- 7. Лескин В.А., Толстов К.Д. Краткие сообщения ОМЯИ, № 17-86, Дубна, 1986.
- 8. Шабратова Г.С. и др. ОММ, PI-86-303, Дубна, 1986.
- 9. Марин А. и др. ЯФ. 1980, 32, 1387.
- IU. Андреева Н.н. и др. жу, 1988, 47, с. 157.
- Курепин А.Б., Пантуев В.С. Труди УШ Международного семинара по проблемам физики высоких энергий, ОМ/И, Д1,2-86-668, т.1, с.273, Дубна, 1987.
- 12. Андреева Н.П. и др. ОГЫН, РІ-86-8, Дубна, 1986.
- Антончик В.А. и др. Яф. 1987, 46,с.1344.
- 14. Амеева Б.У. и др. ИДВЭ, 87-09. Алма-Ата, 1987.
- 15. Толстов К.д., Хошмухамедов Р.А. ОйнИ, РІ-7897, дуона, 1973.
- I6. Богданов В.Г. и др. nio, 1983, т.28, с.1493.
- Балдин А.М. ЭАМ, Т977, 8, с. 429.

# TOHOJOINYECKUE XAPARTEPUCTUKU OPAIMEHTAHUU AJEP <sup>28</sup>Si C UMITYIECOM 4,5 A PaB/c HA AUPAX OOTOOMYJECUU

Б.У.Амеева, Н.П.Андреева, З.В.Анзон, В.И.Бубнов, А.Ш.Гайтинов, Г.Ж.Елигоаева, Л.Е.Ерёменко, Г.С.Калячкина, Э.К.Канитина, И.Я.Часников, П.И.Шахова

Институт физики высоких энергий АН КазССР, Алма-Ата М.Гицок, В.Топор, М.Хайдук

М.Гицок, В.Топор, М.Хайдук
Центральный институт физики, Бухарест
С.А.Краснов, К.Д.Толстов, Г.С.Шабратова
Объединённый институт ядерных исследований, Дубна
И.Бободжанов, Т.Н.Максимкина, Г.Я.Сун-Цэин Ян
Физико-технический институт АН ТаджССР, Душаное
Ф.А.Аветян, В.М.Крищян, Н.А.Марутян, В.Р.Саркисова, Л.Г.Саркисян

Ереванский физический институт

В.Г.Богданов, К.Г.Денисенко, А.А.Плюцёв, З.И.Соловьёва

Радиевый институт им. В.Г. Хлопина АН СССР, Ленинград

Расшепление япра при его взаимодействии с япром-мишеные характеризуется испусканием вторичных частиц различного заряда и массы. Исходя из геометрических представлений о взаимодействии релятивистских япер. можно выделять зону активного взаимодействия перекрытых частей япер и их спектаторные часта. Фстоамульсконная метопика хороко иллострирует такую схему. В зоне взавмодействия происходит процесс рождения частии и практически полное разрушение подструктур ядер-участников до нуклонов. Это релятивистские и серые дучи, образованные в основном протонами и инонами. Возбуждённая спектаторная часть мишени распадается на фрагменты, образующе чёрные 6-лучи, энергия которых в лабораторной системе не превышает 26 МаВ на нужлон. Спектаторная часть снаряда фрагментирует на частилы, которые наблидеются внутри узкого конуса, срвентерованного вдоль первичного направления фраг-Mehtupynnero снаряда.

В работах 1,2 изучением топологические характеристики фрагмен-

тации релятивистских ядер  $^{12}$ С и  $^{22}$ Ng с импульсом 4,5 и 4,1 А ГаВ/с соответственно. Било показано, что наблюдаются две группи собитий: с полным расцеплением (  $^{12}$  ) спектаторной части на одно- и двухзарядные фрагменти и с сохранением фрагмента с зарядом  $\mathbf{Z}_{4} \geqslant 3$ . По мере увеличения степени перекрития ядер возрастает вклад  $^{12}$ Р и уменьшается отношение  $\mathcal{L}/\mathbf{p}$  (  $^{12}$  т.е.  $^{12}$   $^{12}$  ), поскольку подструктури всё интенсивнее разрушаются. В настоящей работе приводятся экспериментальные данные по фрагментации ядра  $^{28}$ S ( с импульсом 4,5 А ГаВ/с и проводится их сравнение с результатами указанных работ. Специальное внимание уделяется аналлзу взаимодействий с отдельными нуклонами, что представляет интерес и для космофизических задач.

### МЕТОЛИКА ЭКСПЕРИМЕНТА

При просмотре фотослоёв по следу регистрировались все неупругие взаимодействия ионов  ${}^{28}$  Si с ядрами фотозмульсии. В этих собитиях изучались характеристики всех заряженных частиц, испущенных под углом  $\Theta \le 5^{\circ}$  к направлению пучка. Заряды этих частиц оценивались с погрешностью не хуже  $\Delta Z \le I$ . Для однозарядных фрагментов на части статистики было проведено определение величины руз с относительной погрешностью около 15-20%. Это позволило провести разделение однозарядных частиц на протоны, дейтроны и ядра трития и убедиться в том, что они имеют импульси, близкие к начальному — 4,5 A ГаВ/с, т.е. являются фрагментами ядра-снаряда. Оказалось, что все многозарядные и подавляющее большинство однозарядных фрагментов сосредоточены внутри угла  $\Theta = 3^{\circ}$ . Всего проанальзировано 1980 собитий.

# топологический состав фрагментов <sup>28</sup> Si

Проведенные измерения дали возможность получить для каждого собития зарядовий состав фрагментов, а также опенить величину неперекритой ( спектаторной ) части налетающего ядра  $Q = \sum Z_f$ . Предподагая, что из зони взаимодействия испускаются в основном однозарядные фрагменти, можно определить канал распада всего ядра. В табл. І
представлени топологические жарактеристики фрагментация ядра

В левой колонке указан зарядовий состав фрагментов. Испущенные из
ядра-снаряда однозарядные фрагменти, дополняющие суммарный заряд до

14, в формуле канала реакции опущени. Данные приведены для событий с
различной степенью расшепления ядра-мишени. Количество сильномонизурицк h. -частиц в расшепления характеризует мишень ( группи ядер

Н, СNO, A<sub>2</sub>B<sub>г</sub>) и степень её разрушения. Видно, что собития ПР, в которых ядро 285; фрагментировало только на опно- и пвухзарящиме нукли-

Таблица I Топологическая дваграмма фрагментации ядра <sup>28</sup>5; на различных группах ядер фотозмульсии

Канал		NL		
реакции	_ <u>0</u> ÷ _1_	2 ÷ 7	_ ≥8	≥0
14 13 13 13 13 13 13 13 13 13 13	876954867732218511943882344212663-125315416603-2134434344212663-125315416603-2134434434212663-125315416603-22134434344212663-125315416603-124134344344212663-125315416663-124134344344212663-125315416663-12413434434424424444444444444444444444	137444042870693742357136425187 - 15871 - 156616759601 77 734	66 -5 -71-64-104-120224961638 -509 -2390 -22612 -3818278 27 9 80	470008551108895612996051705280281154321256099636238099145432125609963623809914543212560996362380991456

ды, отличаются повышенным выходом. Вклад таких событий сильнее проявляется во взаимодействиях с тяжёлой компонентой фотоэмульсии.

На рис. I приведено распределение по Q всех собитий и собитий ПР. Максимум в первом распределении соответствует первферическим

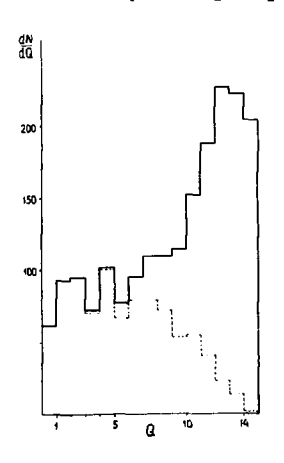
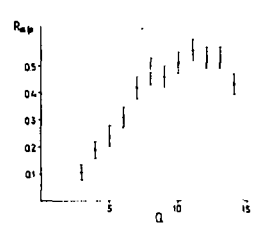


Рис.І. Распределение событий по Q . Пунктиром выделены события  $\Pi P$ .



PEC.2. SARECHMOCTS OTHORS-HER & /p or Q .

взаимодействиям с испусканием многозарядного фрагмента. При сравнении с аналогичной зависимостью для фрагментапии ядер I2<sub>C и 22 Ne /1,2/ оказывает-</sub> ся, что вклад периферических столкновений возрастает с массой фрагментирующего ядра. Вклад ПР, естественно, увеличивается при уменьшении параметра столкновения. На рис. 2 показана зависимость от Q отношения ol/p. Wa этих рисунков следует, что с уменьшением параметра соударения ( т.е. с умень-) усиливается процесс разрушения не только многозарядных, но и двухзарядных ассоциаций спектаторной части ядра.

# МНОЖЕСТВЕННОСТЬ ФРАГМЕНТОВ

В табл. 2 природени средние множественности фрагментов спектаторной части ядра  $^{28}$ Si с различными зарядами во взавмодействиях с фотозмульсией и её компонентами H, CNO, Ag Br ( $N_{\rm L}=0$ ; I,  $2\div7$ , >8 соответственно ). Для сравнения там же приведени срадние множественности фрагментов ядра  $Ne^{-/3}$ , 4/. Из таблици следует, что средняя множественность фрагментов с  $^{2}$ J $^{2}$ Si при переходе от ядра  $^{28}$ Si меняется незначительно ( $\sim 20\%$ ), а для однозарядных существенно возрастает.

При этом вклад сложных нуклядов водорода несколько увеличивается. Напомним, что при переходе от ядра  $^{12}$ С к ядру  $^{22}$  Ne доля сложных нуклядов водорода среди однозарядных фрагментов спектаторной части возродла более, чем в два раза, что связывалось с нейтронной избы-

точностью ядра <sup>22</sup> Ne <sup>/5/</sup>. Однако увеличение этого вклада, по-видимому, объясняется в первую очередь ростом массы фуагментирующего ядра.

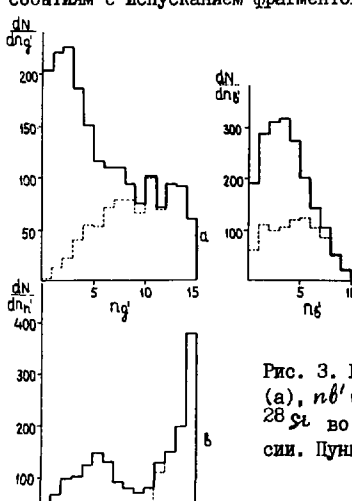
Таблица 2.

Средние множественности фрагментов-спектаторов с различными запядами

Заряд	<n<sub>f&gt; x 100</n<sub>									
	Si+H	Si+CNO	Si +AgBr	Si+Em	Ne+H	Ne+Em				
I	197+12	24I <u>+</u> II	192 <u>+</u> 7	2II <u>+</u> 5	87±3	136 <u>+</u> 2				
в т. ч	=									
P	112 <u>±</u> 8	$I40 \pm I0$	I03±55	$II9\pm4$	58±3	86 <u>±</u> 2				
d	60±5	66 <u>+</u> 6	6I±4	63 <u>±</u> 3	<b>23<u>+</u>3</b>	36 <u>+</u> 2				
t	24 <u>±</u> 3	36±4	28 <u>±</u> 2	30 <u>≭</u> 2	6±I	I4±I				
2	II7±8	I06±6	<b>76±</b> 4	96±3	95±4	<b>82</b> <u>+</u> 2				
3	4+I	4±I	5+I	4.I+0.5	4+I	5,2±0,4				
4	5 <u>+</u> I	4 <u>+</u> I	$3\pm I$	$3.8\pm0.4$	2 <u>±</u> I	4,I±0,3				
5	4 <u>+</u> I	7±I	3 <u>+</u> I	4,7±0,5	6 <b>±</b> I	5,3±0,4				
6	9±2	7 <u>+</u> I	<b>4</b> ±I	$6,I_{\pm}0,6$	$I3\pm I$	$7.6\pm0.4$				
7	8 <b>±</b> I	$7_{\pm}I$	4±I	6,0 <u>+</u> 0,6	I5±I	$7.3\pm0.4$				
B	9±2	8 <u>±</u> I	3±I	6,I±0,6	24±I	3,9±0,5				
9	7±I	7±I	3±I	5,5±0,5	I4±I	$5.5\pm0.4$				
IO	9±2	6±I	3±I	$5,4\pm0,5$	$II_{\pm}I$	$3,6\pm0,3$				
II	7±I	<b>4±</b> I	2,0±0,5	$4.0\pm0.5$						
12	11+2	5±I	0,7±0,5	$4,5\pm0,5$						
13	6±I	4±I	0,7+0,3							
<b>I4</b>	6±I	I,8±0,5	0,7±0,3							
<b>≽</b> 3	85 <u>±</u> 6	65±4	32 <u>±</u> 3	55,7 <u>±</u> 2,I	89 <u>±</u> 3	48±I				

Спектаторние фрагменти якра-снаряда в системе фрагментирующего ядра являются медленними частицьми, соответствующих 6 -фрагментам покоящегося ядра-мишени с кинетической энергией менее 26 МаВ на нужлон. Соответственно, провзаимодействованиие протони налетающего ядра, множественность которых можно оценить как I4 - Q , релятивыстские в лабораторной системе, в системе покоя налетающего ядра являются аналогами д -частиц. Таким образом, полиллется возможность получить распределение по иножественности n<sub>4</sub>, n<sub>2</sub> и n<sub>4</sub> = n<sub>5</sub> + n<sub>2</sub> для распределение по иножественности n<sub>4</sub>, n<sub>3</sub> и n<sub>4</sub> = n<sub>5</sub> + n<sub>2</sub> для распределения для всех собитий и собитий ПР приводятся раздельно, что дейт возможность конкретивировать их вклад в различные области множеотвенностей. Для прямого сравнения с распределени-

ями, полученными в лабораторной системе, многозарядные фрагменты из числа 6 -лучей исключены, поскольку они являются аналогами ядер отдачи. Такое исключение сдвигает часть гистограмми, относящуюся к событиям с испусканием фрагментов с 2+> 3, на единицу влево.



Отметим, что полученные таким образом распределения по множественности являются наиболее адекватными действительности, поскольку в экспериментах, в которых фрагментирующее ядро покоится, часть его однозарядных фрагментов может бить испущена с кинетической энергией, большей 400 мав на нужлон и, оледовательно, будет отнесена к S -частицам. Из апрокси-

Рис. 3. Распределения по множественности ng' (a), nb' (б) и nb' -частиц (в), испущенных  $^{28}$  В во взаимодействиях с ядрами фотоэмульсии. Пунктиром выделены события ПР.

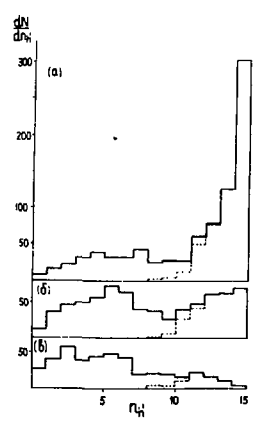
мации энергетических спектров g -частиц зависимостью  $dN/dT \sim T^{-1/6}/c$ лецует, что

в области Т= 400+IC00 МзВ может оказаться 5+IO% от общего числа быстрых одно-зарядных фрагментов, и эта доля увеличивается с массой фрагментирующего ядра, так как при этом величина у уменьшается.

15

На рис. Зв в распределении по множественности h -частиц хорошо просматривается структура, связанная с тем,

Рис. 4. Распределения по множественности і. —частиц, испущенных <sup>28</sup> Si во взаимодействиях с ядрами Ag Br (а), CNO (б) и H (в). Пунктиром виделены события ПР.



что собития ПР и с  $\mathbb{Z}_f \gg 3$  дают преимущественные вклады в различные области  $n._k$ . Аналогичный вид имеют и распределения по множественности при фрагментации ядер  $^{28}$  St на различных компонентах фотовмульски (рис. 4). Соответствующие средние значения приведены в таблице 3. Отметим, что зависимость <  $n._k$  > от массы ядра-партнёра ( H,CNO,AQ Br ) как для собитий с  $\mathbb{Z}_f \gg 3$ , так и для ПР, оказывается весьма слабой. Это характерно и для фрагментации релятивистских ядер  $^{12}$ С и  $^{22}$  Ne .

Иишень		Тип события	
	<b>Z</b> f≥ 3	ΠP	Bce
Н	4,0+4,0±0,2	II,I <u>+</u> I,4	5,2 <u>+</u> 0,3
CNO	4,9 <u>+</u> 0,3	12,2 <u>+</u> 0,8	7,5 <u>+</u> 0,3
Ag Br	6,2 <u>+</u> 0,4	I3, I <u>+</u> 0,6	II,0 <u>+</u> 0,4
Εm	4,9+0,2	I2,7 <u>+</u> 0,4	8,4 <u>+</u> 0,2

Большинство расчётов множественного образования фрагментов выполнени для средних и тяжёлих ядер  $^{7/}$ . Представляет интерес апробация этих моделей в области легких ядер на основе экспериментальных результатов по фрагментации ядер  $^{12}$ C  $^{7/}$ ,  $^{22}$ Ne  $^{12}$ Si. Наиболее критичным, на наш взгяд, может оказаться описание топологий собитий ПР и с испусканием фрагмента с  $^{2}$ J $^{>}$ 3, а также вероятность образования двух фрагментов с  $^{2}$ J $^{>}$ 3 в одном взаимодействии. Вероятность такого процесса составляет  $^{12}$ C $^{13}$ C

## **ФРАТИВЕТАЦИЯ** НА НУКЛОНАХ

В таблицах I-3 и на рис. 4а виделени характеристики фрагментации ядра  $^{28}$ Si на водородоподобной мишени (собития с  $N_h$  = 0;I), знание которых необходимо при решении ряда космофизических задач. Аналогичные данные по фрагментации релятивистских ядер  $^{22}$ Si на такой же мишени сравнивались с расчётами по различным моделям фрагментации. Каскадно-испарительная модель сильно занимает виходи двух-зарядных фрагментов  $^{/2}$ . Динамическая модель/8/ не описывает вклада полных расшельний.

Отметим, что в последнее время определённые успеха в описании распределений по масшественности в реакциях фрагментации достигнути в модели перколяции 9/, рассматривающей ядро в виде простой кубичес-

кой решётки, в которой каждый нуклен связан с соседними. Варьируя величины вероятности разрыва связи р (пареметр перколяции) и производя подсчёт и определение характериотик связанных между собой групп нуклонов (кластеров), можно попытаться достигнуть наидучшего согласия с экспериментальными данными. Результаты нашеге расчёта для кубической решётки размером экэхэ, которая ближе всего к ядру  $^{28}$  Si , представлены на рис. 5,6 совместно с экспериментальными данными для реакции  $^{28}$  Si + нуклон, полученными по массиву с  $N_{\rm h}$  =0:1. Поскольку в модели нуклоны не обладают зарядом, а в эксперименте регистрируются только заряженные фрагменты, ми преобразовали расчетное массовое распределение в зарядовое, сопоставляя фрагменты с A=3;4 с  $\mathcal{Z}_f$  =2, A=5;6 с  $\mathcal{Z}_f$  =3 и т.д. Кроме того, отдельные нейтроны, не регистрируемые ядерной фотоэмульсией, в расчёте включены в канал

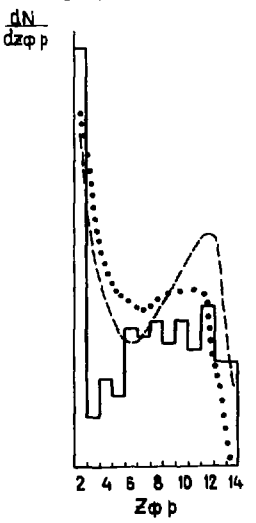


Рис. 5. Распределение по зарядам фрагментов во взаимодействиях с нуклонами. Гистограмма — эксперимент, точки — расчёт по модели перколяции с параметрами р=0,55(птриховая линия) и р=0,6 (пунктир). Нормировка по площади. Кривие, соещиниющие точки проведени от руки.

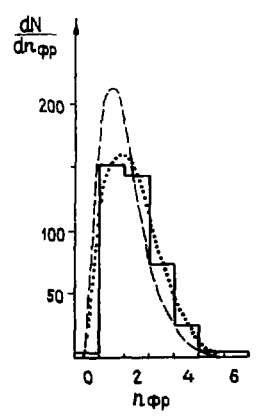


Рис. 6. Распределение по множественнос... ти фрагментов с Z<sub>J</sub>≥2 во взаимодействиях <sup>28</sup>Si с нуклонами. Обозначения те же, что на рис.5. Нормировка по площади.

А=І,что заставило нас при сравнении исключить все фрагменти с Z<sub>f</sub> =I, которым в расчёте осответствует A=I; 2. Видно, что модель перколяции неплохо описывает как зарядовое распределение, так и множественность фрагментов. Наидучшее описание достигается при p=0,6. Максимальное расхождение расчёта и эксперимента, наблюдаемое в области Z = =3+5, возможно, связано с распадом нестабильных фрагментов, не учитываемым моделыю. Кроме того, в данном варшанте расчёта не учитывается энергия связи и не минимизируется повержность образующихся фрагментов, но модель, тем не менее, передаёт общий характер распределений, иллюстрирун таким образом, какую роль играют статистические процессы в изучаемых реакциях.

## ПОЛНЫЕ РАСШЕЛЛЕНИЯ ЯЛЕР

Процесс фрагментации, в результате которого ядро распадается только на одно, и двухзарядные фрагменти (ПР), изучается уже давно. Эксперименти в основном относятся к средним (Aq Br) и тяжалым (P6) ядрам, входящим (или вводимым) в состав фотоэмульсии (6, IO-I2/. По топологическим характеристикам фрагментации релятивистских ядер I2c, 22Ne, 28Si, при их взаимодействии с различными компонентами фотоэмульсии ( H, CNO, Aq Br), можно определить и для них вероятность такого процесса. В тасл. 4 приведены обобщенные данные, полученные из анализа указанных расот, большая часть которых относится к области вероятности ПР от масси ядра-партнёра. Оказивается, что в данной энертетической области протонами с заметной вероятностым можно полностью расшепить ядра только до группы Aq Br, но уже ядра I2c вызовут полные расщепления всех элементов вплоть до урана. Вероятность ПР

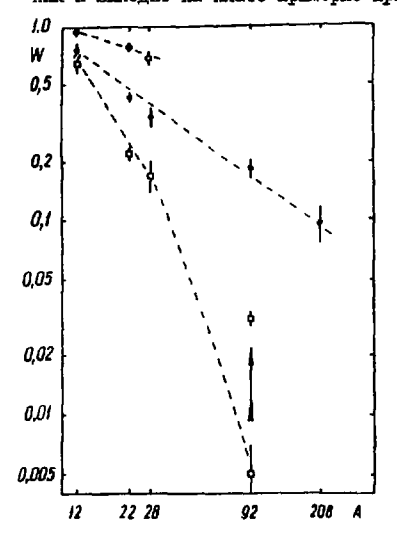
Таблица 4. Вероятность полных расшеплений в ядро-ядерных взаимодействиях при импульсе 4, I-4,5 A ГаВ/с в процентах

Снаряд Мишень	р	d.	4 <sub>He</sub>	12 <sub>C</sub>	22 <sub>Ne</sub>	28 <sub>5i</sub>	Ag Br
12 <sub>C</sub> 22 N e 28 S i	65±8 22±2 17±2 0,5±0,2 3,1±0,3 <sup>x</sup> )	2,6 <u>+</u> 0,5	6,8 <u>+</u> 0,9	75±6 43±2 37±3 18±2	20 <u>+</u> 2	26 <u>+</u> 4	94 <u>+</u> 6 77 <u>+</u> 3 66 <u>+</u> 4

х)Значение на плато.

для данного ядра завысыт от экергык ядра-партиёра. Так, вероятность

ПР ядер Ag Br под действием протонов увеличивается с энергией последних и выходит на плато примерно при IO ГаВ. Для реакций ПР более



легкого ядра <sup>12</sup>С под действием нуклонов выход этой зависимости на плато наблидается уже при энергии I Гэв /8/. Таким образом, процесс полного расщепления ядер — это общее явление для всех взаимодействующих ядер, получив—вих достаточную энергию возбум—пеняя.

Рис. 7. Зависимость вероятности полного расшепления ядер с данным А во взаимодействиях с протонами ( □ ), ядрами углерода или С N O ( ● ) и ядрами Ag Br ( O ).

# SAKJIOTEHIJE

Перечислим основние результати исследования топологических карактеристик фрагментации релятивистских ядер  $^{28}$ Si во взаимодействиях с ядрами фотозмульсии.

- Наряду с наблюдавшимися ранее / 1,2/ двумя типами расщепления неперекритой части налетамиего ядра ( ПР и с испусканием фрагмента с 2 ≥ 3) с увеличением масси снаряда заметную роль начинает играть распад с образованием двух фрагментов с 2 + ≥ 3.
- Сравнение топологических свойств фрагментации редятивистских ядер с некоторыми модельными представлениями показывает критичность таких экспериментальных данных по отношению к современным моделям фрагментации.
- Определение вероятности полных расшеплений легких ядер позволяет систематизировать вклад этого процесса в широком диапазоне масс ядер-партнёров.

Авторы выражают свою признательность техническому персоналу лабораторий за помощь в обработке данных эксперимента.

## ЛИТЕРАТУРА.

- І. Богданов В.Г., Плющёв В.А., Соловьёва З.И. Препринт РИ-177, Л., 1984.
- 2. Андреева Н.П. и др. Сообщение ОИЯИ РІ-85-692, Дубна, 1985.
- Andreeva N.P. et al. In: Proc. of XX Int. Conf. on Cosmic Rays.
   M.: Nauka, 1987, vol. 5, p. 58.
- Andreeva N.P. et al. In: Rroc. of XX Int. conf. on Cosmic Rays.
   M.: Nauka, 1987, vol. 5, p. 61.
- 5. Андреева Н.П. и др. Сообщение ОМЯИ РІ-86-828, Дубна, 1986.
- 6. Богданов В.Г. и др. ЯФ, 1983, 38, с. 1493.
- 7. Hufner J. Phys.Rep., 1985, 125, p. 129.
- 8. Б. огданов В.Г. и др. ЯФ. 1988, 47, вып. 2, с. 316.
- 9. Bauer W. et al. Nucl. Phys. A, 1986, 152, p. 699.
- IO.Tolstov K.D. Z.Phys. A, 1981, 301, p. 339.
- II.Андреева Н.П. и др. Препринт ИФВЗ 80-I5, Алма-Ата, I98I.
- I2. Вокал С. и др. Сообщение ОИЯИ PI-84-552, Дубна, I984.

# AHAMIS CHEKTFOB NOMBOM NOMEPERHOM SHEPTIM B (P,d, &,C)+C-BSAMMOMEMCTBHAX HPM 4,2 PoB/c

...ект..ев г.г., Ченлаков А.И. ·

Объединенный институт ядерных исследований. Лубна

Большой интерес визнает в последнее время данные экспериментов на ускорителе **CERN** SPS о спектрах полной ноперечной энергии вторичных частиц в лдро-ядерных соударениях. В ряде работ наблюдение собитий с большими значениями  $\mathbf{E}_{\tau}^{\text{TOT}}$  рассматривается /I/ как ситная о фазовом переходе адронной материи в состояние кварк-глюонной плазми. С другой стороны, анализ  $\mathbf{E}_{\tau}^{\text{TOT}}$ — спектров дает информацию о применимости моделей глауберовского типа, основанных на суперпозиции и независимых взаимодействий адронов /2/.

Спектри полной поперечной энергии вторичим заряженных частиц изучались нами во чзаимодействиях протонов, ядер дейтерия, гелия и углерода с ядрами углерода и в углерод-танталовых соударениях при 4,2 °A ГэВ/с. Экспериментальный материал был получен с помощью 2-м пронановой камери из дубненском синхрофазотроне. В найденных на снимках неупругих ядро-ядерных соударениях измерялись все треки заряженных частин. Полная поперечная энсргия вычислялась по формуле

Етот = ДЕт = Д ((ріт + ті - ті)), где ріт , тде ріт , т

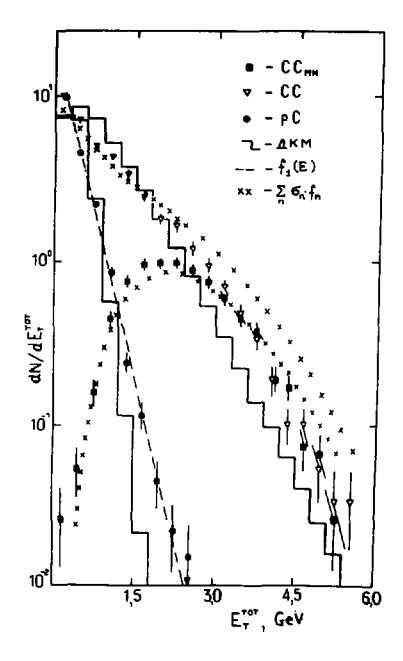
В таблице приведены использованная статистика и средние величины: множественности вторичных заряженных частиц (без спектаторов)

 $< n_{ch}>$  , члоло взаимодействующих понотонов  $< v_{ch}>$  , поперечной энергии зараженией члотоно  $< E_{T}^{i}>$  и полоной поперечной энергии в событы  $< E_{T}^{cot}>$ .

Видно, что с ростом атомного всса налетающего ядра растет как среднял множественность зарыженных частин, так и их полная поперечная эпертия. Наклопи инполизивных спектров по Е; , имперен слабо меняются для разных налетающих ядер.

	pC	<b>d</b> C	AC.	JC	JO 131
Число событий <sup>х</sup> )	3597	5 <b>1</b> 06	<b>19</b> 87	<b>421</b> 6	<b>14</b> 00
<nch></nch>	2,45±0,02	3,17±0,02	4,92±0,05	6,5 <b>2<u>+</u>0,</b> 05	I4,0 <u>+</u> 0,I
く ペゥ> < E ~>, i/ioB	1,83±0,02	I,95±0,08	3,08 <u>+</u> 0,I0	4,52 <u>+</u> 0,07	8 <b>,92<u>+</u>0,</b> 05
	<b>I</b> 50	<b>I</b> 60	170	170	<b>18</b> 0
< E <sup>TOT</sup> ≯ ld∋B	380 <u>+</u> I0	490 <u>+</u> I0	8 <b>50<u>+</u>2</b> 0	<b>I</b> 050 <u>+</u> <b>5</b> 0	<b>23</b> 80 <u>+</u> 50

х) С учётом веса для неразделенных (водогод/углегод) событий.



Puc.I.

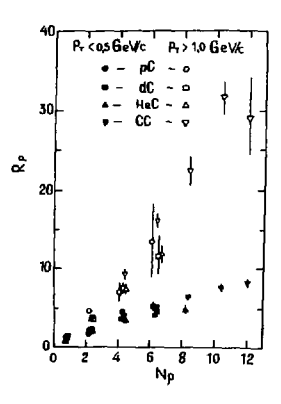
ния /6/:

$$dN^{AB}/dE_{\tau}^{TOT} = \sum_{n=1}^{A} G_{n} \cdot f_{n} (E_{\tau}^{TOT}), \qquad (I)$$

■ На рис. I приводятся экслериментальные распределения по полной поперечной энергии для неупругих pC-, CC- и CC - иногонуклонных взаимодействий. Многонуклонине взаимодействил ядер углерода отбирались при специальном просмотре /4/,они составляют ~20% неупругого 6 inel = (790+50) MO. сечения Гистограмма на рис. І - расчет по каскадной модели К. Гудимы н В. Тонесва /5/. Для наглядности, распределения нормировани на единицу в первом интервале.В использованной версии каскациой модели не учтены близкие нуклон-нуклонные корреллими. Тем не менее, согласие с моделью в целом удовлетворительное.

Распределение по Е тот можно также попытаться получить, используя расчёты по модели многократного рассея-

Едесь  $\mathbf{6}_{n}$  — вероянлести веринодействия  $\mathbf{n}$  нуклонов налетающего ядра, вичисливного в модели, а  $\mathbf{f}_{n}(\mathbf{E}_{1}^{\mathsf{TOT}})$  — вероятность наблюдать  $\mathbf{E}_{1}^{\mathsf{TOT}}$  в  $\mathbf{n}$  незавиемих  $\mathbf{p}\mathbf{C}$  — вамимоденствиях. Аналогично /7/, $\mathbf{p}\mathbf{C}$  —спектр анироксимировался с цомощью ражия — функции формулой:



Puc.2.

4 Тем но менее, определенные надежды на наблюдение "экзотики" дают данные, показанные на рис.2. Здесь представлена зависимость от числа взаимодействующих протонов. № сталкивающихся ядер роста,

 $R_{p}$ , средней множественности протонов с большим поперечным импульсом. Величина  $R_{p}$  является отношением средних множественностей при определенном  $N_{p}$  и соответструющей величине при минимальном  $N_{p} = 0$ . Значение  $N_{p}$  прямо пропоририонально величине  $E_{q}^{\text{TOT}}$  в собитии.

При изменении в неупрутих СС-взаимон, ействиях воличини  $N_P$  от 0 до 12 (  $< E_T^{vot}>$  при этом меняется от 1,2 ГэВ до 11,9 ГэВ) средняя множест-

венность протонов с  $P_{\tau} < 0.5$  ГаВ/с растет в 8 раз (от 0.7 до 5.4), а для  $P_{\tau} > 1$  ГаВ/с — растет в 30 раз (от 0.03 до 0.9). Таким образом, с ростом полной поперечной энергии все более значительный вилал в величину  $E_{\tau}^{\tau o \tau}$  дают отдельные энергичине частицы с большили  $P_{\tau}$ . Аналогичная картина повторяется также и для СТа-соударений при 4.2 A ГаВ/с, для которых енектр по  $E_{\tau}^{\tau o \tau}$  (предварительные данице) приведен на рис.3 (гистограмма — расчет ДКЫ (дубненская каскадная модаль), крестики — лодель многократного рассеянии).

В эксперименте виден также более бистрый рост средней иножественности протонов с Р<sub>7</sub>>1,6 ГэВ/с.Эти данние /4/ согласуются с известными результатами группы Кронина /8/ по наблюдению аномальной А-за-

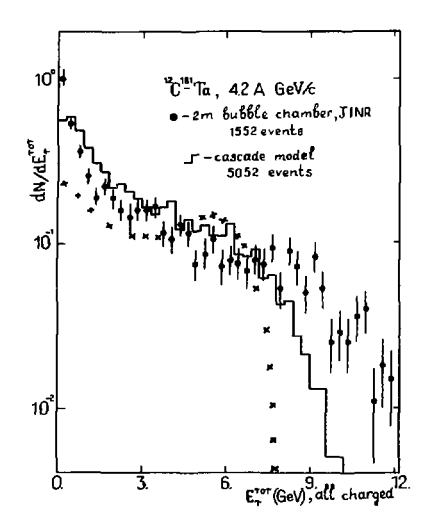


Рис.3.

висимости в образовании адронов с большими поперечивли импульсави.

Одной из важных характсристик процесса взаимодействия релятивистских ядер является наибольшая достигнутая
плотность энергии. Приведенние
аналогично /ІО/ оценки этой
величини дали для СС-многонуклонных соудараний & cc ~
~ 0.8 ГэВ/фм³, а для СТа-взаимодействий ~ I,6 ГэВ/фм³.
В обоих случаях это ниже ожидаемого порога (более 2 ГэВ)
для фазового перехода в состолим кварк-глюонной плазми.

### литература

- I.A.Bumberger et al.Phys.Lett.B184(1987)271
  - B.Berthier et al.Phys.Lett.B193(1987)417
  - R.Albrecht et al.Phys.Lett.B199(1987)297
  - L.S.Schroeder, H. Gyulassy, Nucl. Phys. A461 (1987)1
  - H.Satz et al.Z.Phys.C38(1988)3
- 2.T.Ochiai, Z.Phys.C35(1987)209; Prog.Theor.Phys.78(1987)741
  - A.Jackson, H.Bogsild, Nucl. Phys. A470(1987)669
  - A.Capella et al.Phys.Rev.D35(1987)2921
  - J.Ftacnik et al.Phys.Lett.B188(1987)279
  - J.Ranft, Phys.Lett.B188(1987)379
- 3.H.M.Agakishiev et al.JIMR, 1-82-662, Dubna, 1983
- 4-H.W.Agakishiev et al.Z.Phys.C16(1983)307
- К.К.Тудима, В.Д. Тонеев, ОЙЯМ, Р2-10431, Дубна, 1977;
   ЯФ,27 (1978), 658.
- 6. А.П.Гаспарян и др. **ЯФ,34** (1981),1328
- 7.A.L.S.Angelis et al.Phys.Lett.B141(1984)140
- 8-J.W.Cronin et al.Phys.Rev.D11(1975)3105

# дей РАЛЬные в ЗАИМОДЕЙСТВИЯ ЯДЕР КИСЛОРОДА на нажимих ядрах фотоэмульский не анаргам 200 гэв на нуклон

# шИU-01 сотрудничество

. Представляет М.И.Третьякова Эизический институт им.П.Н.Лебедева АН СССР. Москва

Представлены данные о множественности заряженных частиц и угловых характеристиках вторичных релятивистских частиц центральных взаимодействий ядер кислорода на ядрах  $A_Q$  и  $B_Z$  , которые выделялись по критериям:  $N_A > 10$  и Q = 0, где  $Q = \sum Z_{A_C} -$  суммарный заряд всех фрагментов снаряда.

Для некоторых событий плотность релятивистских частиц по псевдобыстроте достигает значений  $\rho_{\text{max}} = 140$ , что соответствует плотности энергии  $\mathcal{E} = 3$  ГэВ/+m<sup>3</sup> (с учётом нейтральных частиц).

Введение. В работе /I/ приведены данные сотрудничества ЕМЈОІ по множественности и распределениям по псевдобыстроте ливневых частиц из взаимодействий ядер кислорода, полученые в условиях перпендикулярного облучения фотоэмульсии ядрами кислорода с энергией 200 ГвВ на нуклон. Нестоящая работа посвящена изучению центральных взаимодействий ядер кислорода на тяжелых ядрах фотоэмульсии яд и во полученных в условиях горизонтального облучения слоёв фотоэмульсии.

<u>Эксперимент</u>. Стопки по 30 слоёв ядерных фотозмульсий типа EP-2 размером слоя 20х 10х0, 06 см<sup>3</sup>, облучались горизонтально пучком ядер кислорода с энергией 200 ГэВ на ускорителе CERN SPS. Интенсивность облучения  $\sim 5 \cdot 10^3$  частиц/см<sup>2</sup>. Центральные взаимодействия ядер кислорода на тяжелых ядрах фотозмульсии  $\mathcal{A}g$  и  $\mathcal{B}\tau$  отбирались по критериям:  $\mathcal{N}_{k} > 10$  и  $\mathcal{G} = 0$ , где  $\mathcal{G} = \sum \mathcal{I}_{i} -$  суммарный заряд всех фрагментов снаряда. Поиск ядерных взаимодействий проводился как просмотром вдоль следа, так и по площади. При просмотре по площади регистрировались все события без фрагментов с  $\mathcal{I} > 2$ . Для обеспечения высокой точности измерения углов вторичных частиц все измерения проводились относительно вспомогательных первичных частиц, расположенных вблизи измерлемого события.

Из событий, найденных по площади, измерялись только те, для которых  $\hat{G}=0$ , т.е. отсутствовали однозарялные фрагменты ядра снаряда, для этих событий минимальное значение пространственного угла ливневых частиц  $\hat{\theta}_{min} > 10^{-3}$  рад.

<u>Множественность заряженнях частиц</u>. На рис. І приведены распределения центральных взаимодействий по зависимости  $N_s \sim N_h$ , найденные по следу (а) и по площади (б). На рис. I(а) для сравнения приведены также характеристики событий с  $Q_s = 1$ .

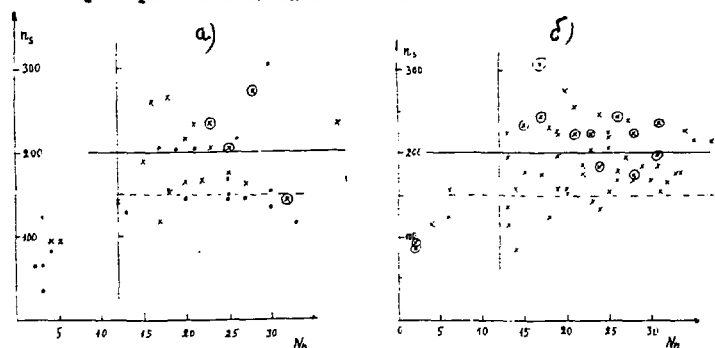


Рис. I Зависимость  $n_5 \sim Nh$ , для событий, найденных по следу (a) и по площади (б) X - Q = 0, в том числе  $\mathscr{D}$  с  $Q_{min} > 2,5 \cdot 10^{-3}$  ред;  $\mathscr{O} Q = 1$ .

В таблице I приведены средние значения  $<\mathcal{N}_5>$ ;  $<\mathcal{N}_6>$ ;  $<\mathcal{N}_6>$ ;  $<\mathcal{N}_6>$ ;  $<\mathcal{N}_6>$ . Там же для сравнения приведены средние характеристики для всех событий, найденных по следу (  $\mathcal{N}_6>$  0).

Таблица I Средние множественности заряженных частиц

Тип взаимодействий	<ns></ns>	<ne></ne>	<ng></ng>	<nn></nn>
Просмотр по след $N_h \ge 0$ ( $N = 206$ )	⊻ 62,9 <b>±</b> 4,7	4,I±0,3	4,0±0,4	8,I±0,7
Q = 0  (N = 18) (BCE $N_h > 12$ )	197±11	9,6 <b>±</b> 1,1	12,9±1,2	22,5±1,4
G = I (N = 15) (nce Na > 13)	174 <b>±1</b> 2	10,9±1,1	12,9 <b>±</b> 1,2	<b>23,8±</b> 1,5
Просмотр по площ	<u>eun</u>			
$G = \frac{0}{0}  (N = 53)$ $(N_h > 10)$	I94,5±5,5	10,7±0,7	12,8±0,7	23,5±0,9
"Особые" ( N = I5)	222±9	12,6±1,3	I2,7±1,0	25,3 <b>±</b> 1,5

Из анализа данных рис. І и табя. І следует:

- I) Для взаимодействий на ядрах Ag,  $\delta c$  в центральных взаимодействиях  $N_h \geqslant 12$ . Для центральных взаимодействий при  $n_s > 150$  данному интервалу по  $n_s$  соответствует широкое распределение по  $M_s$ .
- Средние характеристики событий с Q = 0, найденных по следу и по площади, практически совпадают.
- 3) Для событий с Q = 0 и Q = I, найденных по следу, средние характеристики близки, однако в области  $n_s > 220$  преобладают события с Q = 0, а в области  $n_s < 150$  преобладают события с Q = I.
- 4) В центральных взаимодействиях средняя множественность релятивистких и медленных заряженных частиц примерно в три раза больже по сравнению со всеми взаимодействиями ядер кислорода на ядрах фотоэмульсии (события  $N_L \geqslant 0$ ).

на рис.2 приведено распределение по  $\mathcal{N}_{\mathcal{S}}$  для центральных взаимодействий.

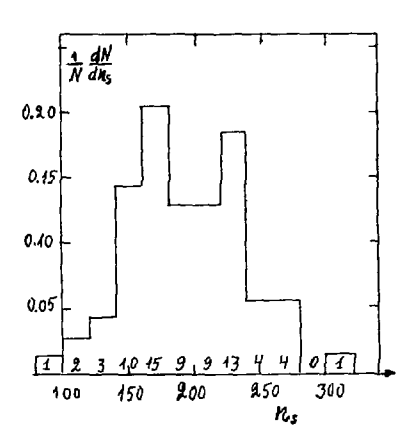


Рис. 2 Распределение по  $n_s$ событий  $^{16}0 + Mg$ , Brс G = 0.

Из рис.2 следует, что среди центральных взаимодействий доля событий с  $n_s > 200$  составляет около 45%, и с  $n_s > 250$  – около 10%. Ниже более подробно будут рассмотрены события самой высокой множественности (  $n_s > 250$ ).

Угловые характеристики центральных взаимодействий. Угловой характеристикой ливневых частиц используется псевдобыстрота  $\eta = - \ln t g \, \theta / 2$  Распределение по плотности релятивистских частиц по псевдобыстроте (числу частиц на единицу псевдобыстроты)  $\int (\eta) = (1/N) \cdot d \, N_S / d \, \gamma$ 

для различных интервалов по  $N_5$  для центральных взаимодействий приведено на рис. 3. Из анализа данных по  $P(\chi)$  следует, что плотность релятивистских частиц в центральной области растёт с ростом  $N_5$  и в области  $\gamma=2-3$  составляет:  $<P(\chi)>=48$  для всех  $N_5$ . В том числе для групп взаимодействий с  $N_5<150$  ( N=9),  $N_5=150$  – 200 ( N=31) и  $N_5>200$  ( N=31)  $<P(\chi)>=30$ ; 41; 59 соответственно.

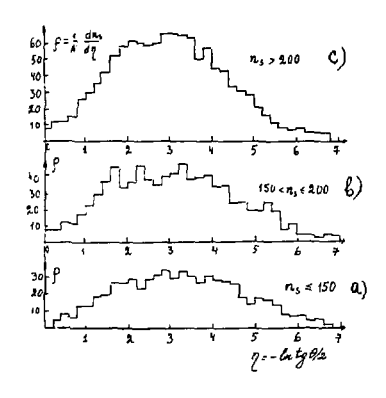


Рис. 3

Распределение ливневых частиц по псевдобыстроте из взаимодействий  $^{16}$ 0 +  $^{16}$ 9,  $^{16}$ 8 с  $^{16}$ 0 с д = 0 для различных интервалов по  $^{16}$ 9;

- a)  $N_S \leq 150$ ,
- B) I50 < Ns = 200.
- c)  $n_c > 200$ .

Из угловых характеристик индивидуальных событий определялся центр тяжести - угол вылета половины частиц 6 1/2, по которому определялся  $\chi_{c} = 1/\theta_{1/2}$  (радиан) —  $\chi_{c}$  фактор симметричной системы. По  $\chi_{c}$ Хс (рр) определялось отношение масс мишени и снаряда MT/Mc =  $= (\sqrt[3]{6})^2$  . Распределение  $M_T/M_o$  для различных интервалов взаимодействий по И6 приведено на рис. 4. Из данных рис. 4 следует, что для  $N_s \le 150$  для основной массы событий отношение  $M_T/M_c \lesssim 1$ . N<sub>S</sub> > 200 большинство событий имеют Мт/Мс ≥ І. Для интерва-150  $< n_s < 200$  М $_{\rm T}$ /М $_{\rm C} \lesssim 1$  для большинства событий, хотя  $< N_b >$ для этих классов событий практически совпадают. Вероятно, угловые характеристики индивидуальных событий при  $n_s \gg 150$  позволяют определить отношение  $M_{T}/M_{C}$ . Для событий с Q = 0 масса снаряда  $M_{C}$  близка к атомному весу снаряда, в данном случае - Мс ~ 16 и из отношения Мт / Мс определяется масса мишени.

Среди центральных взаимодействий обнаружено около 20% "особых" событий, в которых минимальный угол вылета ливневых частиц  $\theta_{min} > 2.5 \cdot 10^{-3}$  рад, в то время как  $\theta_{min} < 10^{-3}$  рад для однозарядных

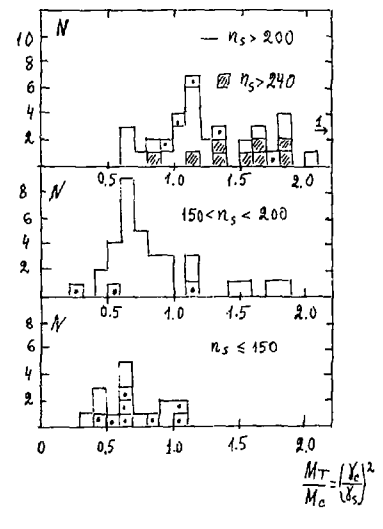
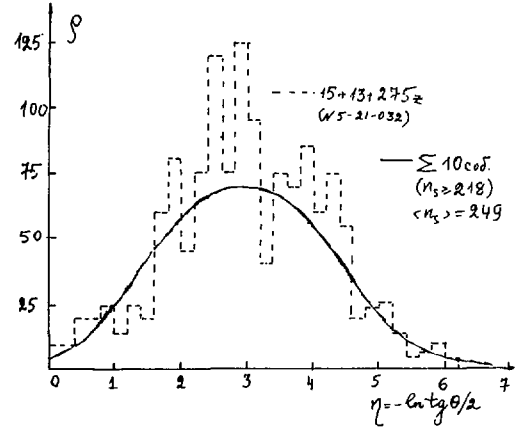


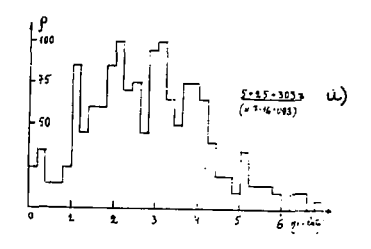
Рис. 4
Распределение событий по  $M_{T}/M_{C}$  для  $^{16}O$  +  $figB^{2}$  взаимодействий с  $G_{V}=0$  (  $\Box$  ) и  $G_{V}=1$  ( $\Box$  )

фрагментов снаряда. Средние множественности заряженных частиц для "особых" событий приведены в таблице I. Впервые "особые" события были обнаружены сотрудничеством по изучению взаммодействий ядер  $^{22}$  в фотозмульсии при  $P_0=4$ , I A ГэВ/с  $^{22}$ .

/I/ приведены результаты анализа экспериментальных данных по флуктуациям плотности ливневых частиц по псевдобыстроте, их зависимость от  $n_{\rm S}$  и интервала псевдобыстрот. Сравнение с моделью ядро-ядерных взаимодействий fritof показало их удовлетворительное согласие. Однако в этой же работе /I/ отмечено наличие плотностей fritof потмечено наличие плотностей fritof

Ниже мы более подробно рассмотрим события самой высокой множественности – с  $n_5 > 200$ . В таблице 2 приведены некоторые харыктерыстики этих событий. Из данных таблицы 2 следует, что для 5 событий из 7 масса мишени больше массы снаряда, средняя плотность  $\rho = 50$  – 75 в центральной области, для большинства этих событий полная ширина. Ар составляет примерно 3 единицы, т.е. события сравнительно узкие, в 4 из 7  $\theta_{min} > 2.10^{-3}$  рад, а в 2  $\theta_{min} > 4.10^{-3}$ , т.е. эти события являются "особыми". Характерной особенностью почти всех этих событий является наличие плотностей  $\rho > 100$  и вплоть до  $\rho = 140$  в некоторых интер-





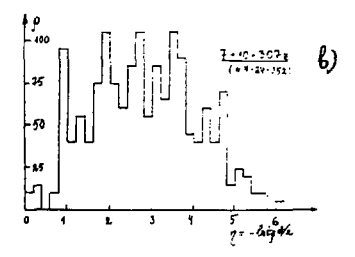


Рис. 6

Распределение ливневых частиц по псевдобыстроте для взаимо-действий  $^{16}0+\mathcal{H}_2$ ,  $\mathcal{B}_2$ :

- а) событие типа 5+25+303 д.,
- в) событие типа 7+10+307½ .

 $\frac{T \ a \ b \ n \ u \ q \ a}{2}$  Характеристики событий с  $n_s > 250$ 

n/n	» события	Тип эвезды	χς (no θ 1/2)	M <sub>T</sub> Mc	ΔZ	ρ	Omin
I	521032	15+13+275	9,8	1,12	1,6-4,6	75	0,276
2	520003	8+10+268	8,2	I,ô2	I-4,2	66	0,115
3	521013	5+11+261	10,8	0,87	1,6-4,6	66	0,127
4	716093	5+25+303 (G= I)	7,4	1,73	I-4,4	70	0,0II (0 <sub>2</sub> = 0,117)
5	522018	7 <b>+14+2</b> 55	7,4	1,84	0,5-5,2	50	$0,058$ $(\theta_2 = 0,150)$
6	724052	7+10+307	8,1	1,64	0,8-4,8 0,8-3,8	69 75	0,259
7	725038	5+I5+277	8,7	1,32	I,6 <del>-4</del> ,4	67	0,092 ( $\theta_2 = 0,172$ )

валах псевдобыстрот центральной области.

Для каждого из 7 событий с  $n_5 > 250$  было проведено сравнение распределений по псевдобыстроте со средним  $\chi^2$  на степень свободы для событий n/n I, 4, 6 оказалось больше 2-4, что даёт для вероятности случайного совпадения величину  $\sim 10^{-3}$ . На рис. 5-6 приведены распределения по псевдобыстроте для этих событий, особенностью последних является высокая плотность частиц (60-75) в центральной области, наличие подструктур и больших флуктуаций плотности частиц по псевдобыстроте. Суммарная энергия вновь рождённых частиц для этих событий составляет 0,7-0,75 от первичной.

Вероятно, вышеуказанные особенности связаны с новыми явлениями в ядро-ядерных взаимодействиях и, возможно, с образованием кварк-глюонной плазмы.

# Литература

- I. EMU-01 Collaboration, Physics Letters B, 1988, v.201, N3, 397.
- А-АНГДДЕККЛИТТУ-Б сотрудничество. Краткие сообщения ОИЯИ, № 16-86, 11; Дубна, 1986.

# MOMENTUM DISTRIBUTIONS OF NEUTRAL PIONS IN HEAVY ION REACTIONS AT THE CERN - SPS

## WA80 COLLABORATION

H. Löhner<sup>d,f</sup>, R. Albrecht<sup>a</sup>, T. C. Awes<sup>c</sup>, C. Baktash<sup>c</sup>, P. Beckmann<sup>d</sup>, F. Berger<sup>d</sup>, R. Bock<sup>a</sup>, G. Claesson<sup>a</sup>, L. Dragon<sup>d</sup>, R. L. Ferguson<sup>c</sup>, A. Franz<sup>b</sup>, S. Garpman<sup>c</sup>, R. Glasow<sup>d</sup>, H. A. Gustafisson<sup>c</sup>, H. H. Gutbrod<sup>a</sup>, K. H. Kampert<sup>d,g</sup>, B. W. Kolb<sup>a</sup>. P. Kristiansson<sup>b</sup>, I. Y. Lee<sup>c</sup>, I. Lund<sup>a,b</sup>, F. E. Obenshain<sup>c,i</sup>, A. Oskarsson<sup>c</sup>, I. Otterlund<sup>c</sup>, T. Peitzmann<sup>d</sup>, S. Persson<sup>c</sup>, F. Plasil<sup>c</sup>, A. M. Poskanzer<sup>b</sup>, M. Purschke<sup>d</sup>, H. G. Ritter<sup>b</sup>, R. Santo<sup>d</sup>, H. R. Schmidt<sup>a</sup>, T. Siemiarczuk<sup>a,j</sup>, S. P. Sorensea<sup>n,i</sup>, E. Stenlund<sup>c</sup>, and G. R. Young<sup>d</sup>

#### 1. INTRODUCTION

A systematic study of nucleus+nucleus reactions at ultrarelativistic energies has been started in 1986 with oxygen beams of 60 and 200 A-GeV in the CERN-SPS in order to investigate nuclear matter under extreme conditions of density and excitation energy. According to QCD lattice calculations<sup>(1)</sup> a first or second order transition to the deconfined phase of quarks and gluons, the quark-gluon-plasma (QGP), may occur in a finite volume of hadronic matter at energy sensities larger than the energy density inside the nucleon<sup>(2)</sup>. First "perimental results from <sup>16</sup>O + nucleus reactions<sup>(3,4)</sup> show that, in the most central events, ene. densities above 2 GeV/fm<sup>3</sup> are reached. Up to now, cosmic ray data have been the only source of information<sup>(5)</sup> and the observed rise of their transverse momenta with energy density has been interpreted as due to QGP effects<sup>(6)</sup>. Since the signature of the QGP is not well established, p + nucleus data have been taken for comparison to the nucleus+nucleus data at the same incident energy per nucleon in order to observe in the heavy ion induced reactions any deviation in the distribution of transverse momenta.

a. Gesellschaft für Schwerionenforschung (GSI), D-6100 Darmstadt , BRD

b. Lawrence Berkeley Laboratory, Berkeley, California 94720, USA

c. University of Lund, S-22362 Lund, Sweden

d. University of Münster, D-4400 Münster, BRD

e. Oak Ridge National Laboratory, Oak Ridge, Tennessee 37831, USA

f. present address: KVI, University of Groningen, NL-9747 AA Groningen BRD

g. Post Doctoral Fellowship from the German Research Community (DFG), BRD

h. Post Doctoral Fellowship from Swedish Natural Research Science Council, Sweden

i. University of Tennessee, Knoxville, Tennessee 37996, USA

j. On leave of absence from the Inst. of Nuclear Studies, PL-90681 Warsaw , Poland

#### 2. EXPERIMENT

The WA80 experiment at the CERN-SPS is designed to measure the distribution of charged particles in a large fraction of phase space, to analyse the forward and transverse energy distributions and to investigate the target fragmentation region. In addition, photons and neutral pions are identified near midrapidity in a high resolution lead glass calorimeter. This allows a detailed analysis of their transverse momenta  $(p_T)$  based on centrality selections which are determined either by measurements of the remaining projectile energy in the forward direction or the charged particle multiplicity. The experimental setup is described in detail in ref. The results presented in this paper were derived from the following detector components: the electromagnetic lead glass calorimeter (SAPHIR), the uranium scintillator sampling calorimeter at zero degree (ZDC), and the streamer tube multiplicity arrays which cover the pseudorapidity region 1.2 < n < 4.2.

SAPHIR measures the inclusive photon and  $\pi^0$  distributions at midrapidity with a pseudorapidity coverage of  $1.5 \le \eta \le 2.1$  and a solid angle of 0.13 steradian. Details of the construction and performance are given in ref./8/. The streamer tube material contributes 4% to the photon conversion probability. The target vacuum chamber contributes an additional 0.4%. Background levels during target-out operation were found negligible.

The ZDC characterizes the centrality of each collision by measuring the remaining energy of projectile spectators for lab. angles  $\leq 0.3^{\circ}$ . A strong correlation between charged particle multiplicity and energy in ZDC is observed<sup>99</sup>, so that either quantity may be used to distinguish between peripheral and central reactions.

### 3. PHOTON DISTRIBUTIONS

Inclusive spectra of photons, which dominantly originate from  $\pi^0$  decay, have been extracted from the raw data applying selection criteria based upon the electromagnetic shower development in the lead glass and the multiplicity detectors in front/8/. Systematic errors originating in misidentification are included in the error bars shown in the photon spectra.

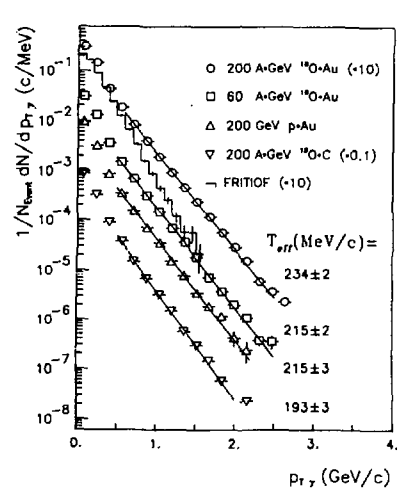
Fig. 1 shows inclusive photon  $p_T$  spectra containing about 10% of the minimum bias cross section after a selection of events with high charged particle multiplicity. The data are described by an exponential parametrization

$$dN/dp_T \sim \exp(-p_T/T_{eff})$$
 for  $p_T > 0.4 \, GeV/c$ . (1)

The slope parameters  $T_{\rm eff}$  increase slightly with increasing target- and projectile-mass and incident energy. The experimental data are compared with the Lund model FRITIOF/10/ for nucleus+nucleus interactions. The predicted inverse slopes are in general about 20% lower than the slope parameters fitted to the data.

In order to investigate the  $p_T$  distributions in more detail with respect to their centrality dependence, ratios of oxygen cross sections for a heavy ( $^{16}O + Au$ ) and a light ( $^{16}O + C$ ) target have been calculated and are presented in fig. 2 as a function of  $p_T$  for the 10% most central and the 10% most peripheral reactions as defined from the charged particle multiplicity. For central collisions an increase of this ratio by a factor of 2 is observed between  $p_T = 0.2$  GeV/c and 2 GeV/c whereas in peripheral collisions almost no dependence on  $p_T$  is visible. We conclude, that large transverse momenta are produced more efficiently in violent (central) reactions and large interacting systems, i.e. target-projectile overlap volumes. The FRITIOF model, containing the basic kinematical constraints, does not exhibit any different slope of  $p_T$  distributions for central and peripheral reactions or for different target masses and is in this respect consistent only with the most peripheral data sample.

Figure 1. Inclusive photon  $p_T$  distributions from proton and oxygen induced reactions at 200 and 60 A-GeV measured in 1.5  $\leq \eta \leq 2$ .1. Central reactions are selected with 10 % of the minimum bias cross section. For comparison with exponential parametrizations (solid lines) the histogram shows the FRITIOF model results for  $^{16}{\rm O}$  + Au at 200 A-GeV.



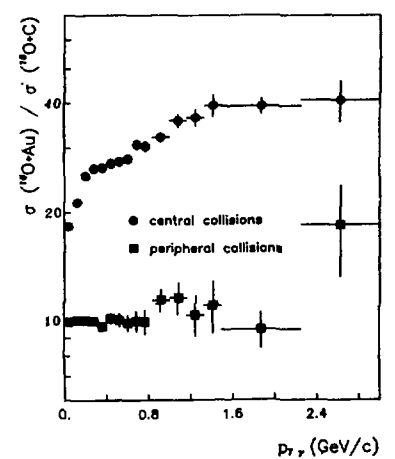


Figure 2. Ratios of inclusive photon cross sections for <sup>18</sup>O + Au and <sup>16</sup>O + C reactions at 200 A·GeV. The selections according to the charged particle multiplicity contain the 10 % most central (upper part) and the 10 % most peripheral reactions (lower part), respectively.

Since the deviation from FRITIOF is significant for  $p_T > 0.4$  GeV/c in the photon distributions, we have analyzed the  $p_T$  region above 0.4 GeV/c as a function of target mass and event centrality in a model independent way by computing algebraically the average  $p_T$  from distributions cut off at a lower  $p_T$  value C:

$$\langle p_T \rangle_{\gamma,C} = \left( \int_C^{\infty} p_T \frac{dN}{dp_T} dp_T / \int_C^{\infty} \frac{dN}{dp_T} dp_T \right) - C,$$
 (2)

using C=400 MeV/c. The resulting  $< p_T>_{\gamma C}$  is equal to the slope parameter  $T_{\rm eff}$  for a purely exponential distribution in the region  $p_T>C$ .

In order to compare the oxygen and proton induced reactions properly for different degrees of centrality and to relate the obtained  $\langle p_T \rangle_{T,C}$  values to thermodynamical models/11/, we have introduced the variable S proportional to the entropy density  $\frac{11,12}{2}$ :  $S = \frac{dN}{dn} \cdot A_{ins}^{-2/3}$ . Here (dN/dn) is the central multiplicity density which is approximated by the charged particle multiplicity in  $1.2 < \eta < 4.2$  multiplied by 1.5 in order to correct for undetected neutral particles. Ainc is the mass number of the smaller colliding nucleus in central collisions. For peripheral heavy ion collisions, however, this assumption is no longer justified. Therefore Ainc is defined to be the number of incident projectile participants, which is derived from the ZDC energy via the FRITIOF model in close resemblance to ref. 14. In this way the oxygen data are expected to correspond to the proton data for very low values of the entropy density. The resulting  $\langle p_T \rangle_{\sim 400}$  of photons is plotted as a function of the entropy density in fig. 3. The data points at highest S contain 10% of the minimum bias cross section. Their  $< p_T >_{7.400}$  increases gradually for growing size of the target-projectile overlap for 16O+C via p+Au to 16O+Au at the same incident energy and also increases with increasing beam energy. A remarkable feature of fig. 3 is the reduced increase of  $\langle p_T \rangle_{7.400}$  at intermediate and large values of the entropy density S for 16O + Au reactions at 200 A·GeV. At low entropy density the rise of  $\langle p_T \rangle_{7.400}$  may even become steeper by up to 6% due to possible systematic errors in the photon identification. Thus, the deviation from FRITIOF is obvious, since this model predicts almost no variation with centrality or target mass. Although, it has to be noted, that in the present FRITIOF version hard scattering/13/ is not yet included for nucleus+nucleus reactions. However, preliminary investigations/14,15/ seem to indicate that only a small fraction of the observed effect can be explained in this way. On the other hand, a structure like this is expected from thermodynamical and hydrodynamical studies/11,16,17/ of the QGP phase transition and is reminiscent of earlier observations of cosmic ray data<sup>16</sup>. The relative variation of  $< p_T >_{7.400}$ for p + Au at 200 GeV (fig. 3) is consistent with data obtained from p + p and  $\alpha$  +  $\alpha$ reactions at the ISR/18/. The increase to larger values of  $< p_T > \text{in } p + \bar{p}$  collider data/19/, where equivalently large entropy values are reached, is more closely resembling the <sup>16</sup>O + Au data than the p + Au data.

## π<sup>0</sup> DISTRIBUTIONS

The momentum distributions of inclusive photons analysed in the previous section allow studies of the centrality dependence for different reaction systems with good statistical accuracy. From the various sources ( $\pi^0$  and  $\eta^0$  mesons, baryon resonances) contributing photons to the observed distributions, the  $\pi^0$  are clearly dominating and expected to influence the results most strongly. However, the reaction kinematics and possible changes in the effective center of mass (CM) system make it difficult to extract absolute numbers of average transverse momenta for  $\pi^0$  from inclusive photons. Therefore, cross sections for  $\pi^0$  production and their  $p_T$  distributions have been obtained by analysing the invariant mass spectra of  $\gamma\gamma$  pairs in small intervals of  $p_T$ .

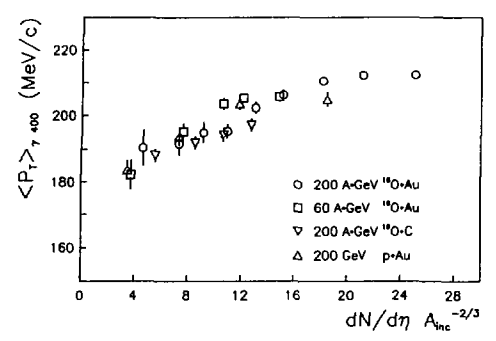


Figure 3. Experimental  $< p_T >_{7.400}$  for inclusive photons from the truncated  $p_T$  distribution (see text) as function of the entropy density estimated from the central charged particle multiplicity and the number of participating projectile nucleons which is calculated from the energy in the ZDC.

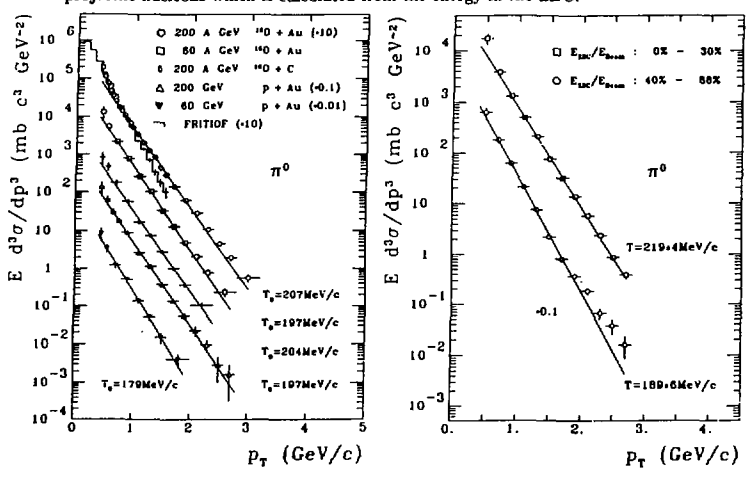


Figure 4. Invariant cross sections for  $\pi^0$  as a function of  $p_T$  from proton and oxygen induced reactions at 200 and 60 A-GeV measured in 1.5  $\leq \eta \leq$  2.1 for different target masses. For comparison with exponential parametrizations (solid lines) the histogram shows the FRITIOF model results for  $^{16}\mathrm{O}$  + Au at 200 A-GeV.

Figure 5. Invariant cross sections for  $\pi^0$  as a function of  $p_T$  from oxygen induced reactions at 200 A-GeV measured in 1.5  $\leq \eta \leq$  2.1 for the 40 % most central and the 50 % most peripheral reactions as selected by the energy measured in ZDC.

The obtained  $\pi^0$  cross sections from p + Au reactions are consistent with Fermilab data<sup>1/20/2</sup> within the error limits for  $\pi^+$  and  $\pi^-$  from p + W at 200 GeV incident energy and in approximately the same region of rapidity. Furthermore,  $\pi^0$  distributions have been studied in different regions of pseudorapidity within the acceptance of SAPHIR ranging from 1.5 to 2.1 units in  $\eta$ . From this we conclude that at most a variation of  $(6 \pm 4)\%$  in the slope of  $p_T$  distributions might originate from a change in the effective CM system when central and peripheral <sup>16</sup>O induced reactions are compared.

In fig. 4 the  $p_T$  dependence of in ariant  $\pi^0$  cross sections for minimum bias trigger conditions from proton and oxygen induced reactions is compared for different targets and energies. The slopes of these distributions can be described by an exponential parametrization

$$1/p_T dN/dp_T \sim \exp(-p_T/T_0). \tag{3}$$

Slope parameters  $T_0$  have been deduced from the same restricted transverse momentum range  $0.8~{\rm GeV/c} \le p_T \le 2~{\rm GeV/c}$  for all reaction systems. These parameters turn out to be similar for proton and oxygen induced reactions in these minimum bias data and are only weakly dependent on target mass, but are larger by at least 20 % for  $^{16}{\rm O}$  + Au at 200 A-GeV than for p + p reactions  $^{(21)}$  and for FRITIOF model predictions. This behaviour is consistent with the observations cited above which show that the linear extrapolation from p + p reactions to heavy ion reactions, as contained in this model, is doubtful. The deviation from FRITIOF by a factor of 3 at  $p_T = 1.5~{\rm GeV/c}$  may hardly be explained by multiple hard scattering since this effect produces only a 30 % increase in calculations  $^{(14)}$  of p + p reactions at 15R energies.

The spectra in fig. 4 indicate a change in slope below  $p_T \approx 0.8 \, {\rm GeV/c}$ , which is most pronounced for the heavy system. A slope parameter  $T_0 \leq 150 \, {\rm MeV/c}$  would be appropriate to describe the data for  $p_T < 0.8 \, {\rm GeV/c}$ . This effect is not seen in 250  ${\rm GeV/c}$  p + p reactions/21/, but is consistent with  $\alpha + \alpha$  reactions at the ISR/18.22.31 and weakly indicated in the p + Au data at 200  ${\rm GeV}$ . This feature is also predicted in thermodynamical models/17.24/ and in studies of the hydrodynamical expansion/16.25/ of hot hadronic systems.

Further details of the pion momentum distributions are revealed by inspecting their dependence on the impact parameter. Fig. 5 shows two distributions for the 40% most central and the 50 % most peripheral reactions as selected by the energy measured in ZDC relatively to the beam energy. The exponential curves (equ. 3) fit the data in the region  $0.8 \le p_T \le 2 \,\text{GeV/c}$ with slope parameters increasing by ≈ 15 % with increasing centrality as expected from the previous inclusive photon analysis. Deviations from a single exponential curve at low  $p_T$  for central data and at high  $p_T$  for peripheral data, which suggest a hard component, demand a systematic investigation as presented for example in fig. 6, inspired by a similar analysis performed for  $\alpha + \alpha$  and p + p reactions at ISR energies  $^{/22}$ . R<sub>ZDC</sub>( $p_T$ ) is the ratio of the ZDC-selected  $dN/dp_T$ distribution relative to the minimum plas distribution, while each distribution is normalized to unity. Here again the degree of centrality increases with decreasing energy in ZDC. We observe in complete analogy to ref. (22) that the bump at low  $p_T$  (0.8 GeV/c) for peripheral data (low multiplicity) changes to a dip for central (high multiplicity) selection. This behaviour again shows the difficulty in interpreting a single number like the average pr taken over the full pr range, because it washes out any structure in the  $p_T$  dependence, which might contain essential dynamical information.

The  $\pi^0$  analysis underlines the previous findings that the tails of the  $p_T$  distributions measured in midrapidity are enhanced beyond  $p_T=0.8$  GeV/c for high particle density or central collisions in close resemblance to hadron+hadron<sup>(21)</sup> or  $\alpha+\alpha$  reactions<sup>(22)</sup> at total CM energies between 22 and 62 GeV. There, however, the enhancement appears already for  $p_T>0.4$  GeV/c and is of the order of  $\approx 5$  % in magnitude. In the <sup>16</sup>O + Au case at 19.4 GeV total energy in the

nucleon-nucleon CM system we observe an effect of 15 %, which only in part can be explained by a variation of the effective CM system, though.

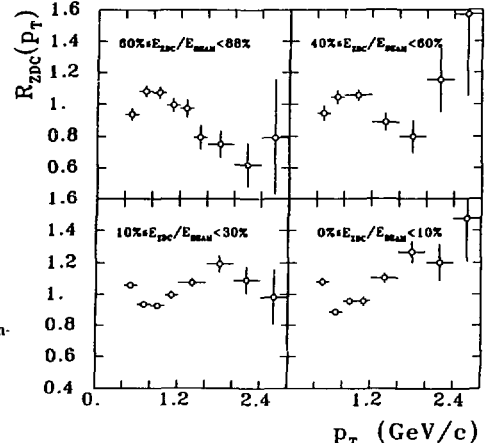


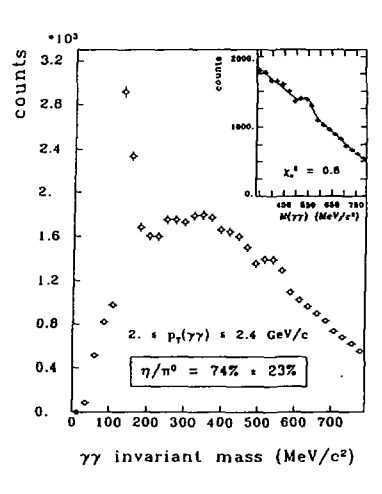
Figure 6. Ratios of ZDC-selected  $\pi^0$  distributions relative to the minimum bias distribution for  $^{16}{\rm O}$  + Au at 200 A-GeV as a function of  $p_T$ .

# 5. $\eta^0$ MESONS AND SINGLE PHOTONS

Besides the investigation of pion momentum distributions and correlation studies, the ultimate objective of photon detection in heavy ion collisions has been the detection of direct photons which promise to give a clean signal/<sup>100</sup>, <sup>270</sup>, for the expected quark gluon plasma. This analysis, however, is severely hampered by the presence of decay photons from various meson decays. Among those the  $\pi^0$  and  $\eta^0$  mesons are clearly the dominating source of single photon background. It is therefore necessary to determine the  $\eta^0/\pi^0$  production ratio in the same experiment. Due to the larger opening angle for the  $\eta^0$  decay photons, the acceptance of our detector/<sup>100</sup> is much lower than for  $\pi^0$ . Nevertheless we obtain the mass spectrum shown in fig. 7 where a clear  $\eta^0$  signal in a limited  $p_T$  region is observed with an  $\eta^0$  peak width compa-tible with the detector resolution. We derive the ratio  $\eta^0/\pi^0 = 0.74 \pm 0.23$  which is in accordance with the result of  $\eta^0/\pi^0 = 0.45 \pm 0.10$  from p + p reactions/<sup>224</sup> at 63 GeV total CM energy. Thus with the quite reasonable assumption of  $m_T$  scaling for  $\eta^0$  and  $\pi^0$  we are able to compute their contribution to the inclusive photon distribution. Heavier mesons are expected to produce only an additional small fraction of the  $\eta^0$  contribution/<sup>200</sup>.

Thus, we are now able to compute the photon/ $\pi^0$  ratio as a function of  $p_T$  and to subtract the photon/ $\pi^0$  distribution obtained from the measured meson distributions. From the observed difference spectrum we conclude that in the region  $1 \le p_T \le 2.5$  GeV/c the goal of a 5% detection level as determined by the error bars can be reached. In this region a remarkable enhancement of about 10% appears above a distribution rising slowly from 0 to about 25% at  $p_T = 3$  GeV/c. A smooth distribution of the latter type would be expected from earlier direct photon studies/<sup>29</sup>. A thorough analysis of all possible sources of systematic errors is currently under way in order to confirm the apparent photon enhancement.

Figure 7. Invariant mass spectra of  $\gamma\gamma$  pairs for  $^{16}\mathrm{O}$  + Au at 200 A-GeV. Only photons with E $_{\gamma}$  > 500 MeV and 2 GeV/c  $\leq p_{T\gamma\gamma} \leq$  2.4 GeV/c are considered. The inset shows the polynomial fit to the combinatorial background and the gaussian  $\eta^0$  mass peak with 3 % ( $\sigma$ ) mass resolution.



### 6. CONCLUSIONS

In summary, it has been shown that even in the high multiplicity environment of  $^{16}O + Au$  reactions the identification of  $\pi^0$  in the invariant mass spectrum of  $\gamma\gamma$  pairs is achieved with good accuracy in a lead glass detector. Inclusive photon spectra and  $p_T$  distributions for identified  $\pi^0$  have been presented for 60 and 200 A·GeV  $^{16}O + \text{nucleus}$  and p + nucleus reactions.

The photon spectra show in the region  $p_T > 0.4~{\rm GeV/c}$  a target mass and centrality dependence which is not predicted by the current FRITIOF model. Reactions with different initial geometry can be compared with each other when  $< p_T >$  is plotted as a function of entropy density calculated from the multiplicity and the number of projectile participants. The leveling off of a purely linear increase of  $< p_T >_{0.00}$  with entropy density for <sup>16</sup>O + Au at 200 A GeV reveals a behaviour expected in the presence of a phase transition.

The  $\pi^0$   $p_T$  distributions show at least two components, a low  $p_T$  one with an inverse slope of about 150 MeV/c and a high  $p_T$  component with a flatter slope dependent slightly on target mass. These features are not compatible with a FRITIOF type linear extrapolation from p + p data to heavy ion reactions. A description in terms of a thermodynamical evolution and hydrodynamical expansion of a hot hadronic system seems to be justified and has to be pursued in the future for quantitative comparisons. Nevertheless, hard scattering of partons needs to

be included in nucleus+nucleus interaction models, in order to study if the above observations can be explained within refined non-thermal models. Finally, investigations of  $\pi^0$  correlations and  $\eta^0/\pi^0$  ratios as well as direct photon production have been started and show reasonable results. Their analysis still needs more elaborate work but will soon provide an efficient number of observables to compare hadron+hadron, hadron+nucleus and nucleus+nucleus reactions and trace their similarities as well as their differences.

This work is partially supported by the West German BMFT and DFG, the VW-Stiftung, the United States DOE, the Swedish NFR and the Humboldt Foundation.

### References

- 1. L. McLerran and B. Svetitsky, Phys. Lett. B 98 (1981) 195;
  - T. Celik, J. Engels and H. Satz, Nucl. Phys. B 256 (1985) 670
- Jacob and H. Satz (eds.), Quark Matter Formation and Heavy Ion Collisions, Proceedings of the Bielefeld Workshop, May 1982 (World Scientific Publ. Co., 1982)
- 3. A. Bamberger et al., Phys. Lett. B 184 (1987) 271
- 4. R. Albrecht et al., WA80 collaboration, Phys. Lett. B 199 (1987) 297
- 5. T. H. Burnett et al., Phys. Rev. Lett. 57 (1986) 3249
- E.V. Shuryak and O.V. Zhirov, Phys. Lett. B 171 (1986) 99
- 7. H.H. Gutbrod et al., GSI preprint GSI-85-32, August 1985 and CERN SPSC/85 39/M406
- 8. H. Löhner et al., WA80 collaboration, Z. Phys. C 38 (1988) 97;
  - R. Albrecht et al., WA80 Collaboration, Phys. Lett. B 201 (1988) 390
- 9. I. Lund et al., WA80 collaboration, Z. Phys. C 38 (1988) 51
- 10. B. Nilsson-Almqvist and E. Stenlund, Computer Physics Com. 43 (1987) 387
- L. Van Hove, Nucl. Phys. A 447 (1985) 443c
- 12. J. D. Bjorken, Phys. Rev. D 27 (1983) 140
- 13. M. Lev and B. Petersson, Z. Physik C 21 (1983) 155
- B. Nilsson-Almqvist , proceedings of the International Europhysics Conference on High Energy Physics, Uppsala, Sweden, 1987, volume I, p. 481
- 15. E. Stenlund, private communication
- 16. M. Kataja et al., Phys. Rev. D 34 ( 1986) 2755
- 17. E. V. Shuryak, Phys. Rep. 61 (1980) 71
- A. Breakstone et al., Phys. Lett. B 183 (1987) 227
- 19. G. Arnison et al., Phys. Lett. B 118 (1982) 167;
  - T. Alexopoulos et al., Phys. Rev. Lett. 60 (1988) 1622
- 20. D. Antreasyan et al., Phys. Rev. D 19 (1979) 764
- 21. P.A. van Hal, NA22 collaboration, Thesis, University of Niimegen 1987
- 22. W. Bell et al., Z. Phys. C 27, 191 (1985)
- 23. A.L.S. Angelis et al. Phys. Lett. B 185 (1987) 213
- 24. M. Danos and J. Rafelski, Phys. Rev. D 27 (1983) 671
- 25. J. P. Blaizot and J. Y. Ollitrault, Phys. Lett. B 191 (1987) 21
- 26. R.C. Hwa and K. Kajantie, Phys. Rev. D 32 (1985) 1109
- 27. S. Raha and B. Sinha, Phys. Rev. Lett. 58 (1987) 101
- 28. T. Akesson et al., Phys. Lett. B 178 (1986) 447
- 29. M. Diakonou et al., Phys. Lett. B 91 (1980) 296

# J/¥ PRODUCTION IN COLLISIONS OF OXYGEN AND SULPHUR IONS ON HEAVY TARGETS AT 200 GEV PER NUCLEON

#### NA 38 COLLABORATION

M.C. Abreu<sup>5</sup>, M. Alimi<sup>6</sup>, C. Baglin<sup>1</sup>, A. Baldit<sup>3</sup>, M. Bedjidian<sup>6</sup>, P. Bordalo<sup>5</sup>, S. Borenstein<sup>4</sup>, J. Britz<sup>8</sup>, A. Bussière<sup>1</sup>, P. Busson<sup>4</sup>, R. Cases<sup>9</sup>, J. Castor<sup>3</sup>, C. Charlot<sup>4</sup>, B. Chaurand<sup>4</sup>, D. Contardo<sup>6</sup>, O. Drapier<sup>6</sup>, E. Descroix<sup>6</sup>, A. Devaux<sup>3</sup>, J. Fargeix<sup>3</sup>, X. Felgeyrolles<sup>3</sup>, A. Ferraz<sup>5</sup>, R. Ferreira<sup>2</sup>, P. Force<sup>3</sup>, L. Fredj<sup>3</sup>, C. Gerschel<sup>7</sup>, Ph. Gorodetzky<sup>8</sup>, J.Y. Grossiord<sup>6</sup>, A. Guichard<sup>6</sup>, J.P. Guillaud<sup>1</sup>, R. Haroutunian<sup>6</sup>, L. Kluberg<sup>4</sup>, G. Landaud<sup>3</sup>, C. Lourenco<sup>5</sup>, L. Perallas<sup>5</sup>, M. Pimenta<sup>5</sup>, J.R. Pizzi<sup>6</sup>, C. Racca<sup>8</sup>, S. Ramos<sup>5</sup>, A. Romana<sup>4</sup>, R. Salmeron<sup>4</sup>, A. Sinquin<sup>7</sup>, P. Sonderegger<sup>2</sup>, F. Staley<sup>1</sup> and J. Varela<sup>5</sup>

## Presented by L. Kluberg

The identification of the hypothetical Quark-Gluon Plasma (QGP) formation in nuclear collisions has been extensively studied in the past [1]. Several observables have been suggested for this purpose and are currently being investigated by different experiments. Most of the proposed signatures can be affected by dynamical processes so that they do not only reflect the plasma phase (if produced) but also the previous compression phase and the final expansion phase which brings matter back to our usual world of hadrons. In that sense, the lepton pair signature should be among those that

LAPP, CNRS-IN2P3, Annecy-le-Vieux, France.

<sup>2</sup> CERN, Geneva, Switzerland.

<sup>3</sup> LPC, Univ. de Ciermont-Ferrand and CNRS-IN2P3, France.

<sup>4</sup> LPNHE, Ecole Polytechnique and CNRS-IN2P3, Palaiseau, France.

<sup>5</sup> LIP, Lisbon, Portugal

<sup>6</sup> IPN, Univ. de Lyon and CNRS-IN2P3, Villeurbanne, France.

<sup>7</sup> IPN, Univ. de Paris-Sud and CNR5-IN2P3, Orsay, France.

<sup>8</sup> CRN, CNRS-IN2P3 and Univ. Louis Pasteur, Strasbourg, France.

<sup>9</sup> IFIC, Burjasot, Valencia, Spain.

keep the best track of what happened in the early stages of the collisions as the lepton interaction with the final cooling down phase is extremely weak [2]. More recently, the suppression of the  $J/\Psi$  resonance has been predicted as one of the most characteristic signatures of the QGP phase transition [3].

Experiment NA 38 [4] is a dedicated experiment for the study of muon pairs with intense incident ion beams. Its detector is based on a high resolution muon spectrometer [5] complemented with an electromagnetic calorimeter located between an uranium "active" target and a carbon hadron absorber as shown in Fig 1. The apparatus, triggerred on muon pairs, allows to measure the muon pair characteristics together with the transverse ( mainly ) electromagnetic energy produced by all the interacting participants in the reaction, on an event by event basis. Fig. 2 shows the distribution of the transverse " electromagnetic energy " for the whole sample of dimuons retained for the analysis, after subtraction of the background defined as muon pairs originating from w and K decays. The background subtraction procedure follows from an elaborated method based on the like-sign muon pair sample. The raw invariant muon pair mass distribution, shown in Fig. 3, is corrected for background and then fitted, for masses above 1.7 GeV/ $c^2$ , with two gaussians for the J/ $\Psi$  and  $\Psi'$  resonances superimposed over a continuum described by  $1/M_{\mu\mu}^{3} = M_{\mu\mu}/M_c$ . The result of the fit is expressed as the quantity S, the ratio of the fitted number of  $J/\Psi$ 's to the fitted number  $N_c$  of events in the continuum, in the dimuon mass range [ 2.7 - 3.5 GeV/c2 ]. This fitting procedure is performed for subsamples of events selected in six different transverse energy bins equally populated. Fig. 4 and 5 show, for the Oxygen data, the mass distribution and the corresponding fits for the two extreme transverse energy bins, namely [ 1 - 34 GeV ] and [ > 85 GeV ] respectively. The corresponding values for S are 13.8±1.7 and 7.2±0.9, leading to a suppression of the  $J/\Psi$  relative to the continuum of almost 50% between these two extreme energy bins. Fig. 6 shows the value of S as a function of ET.

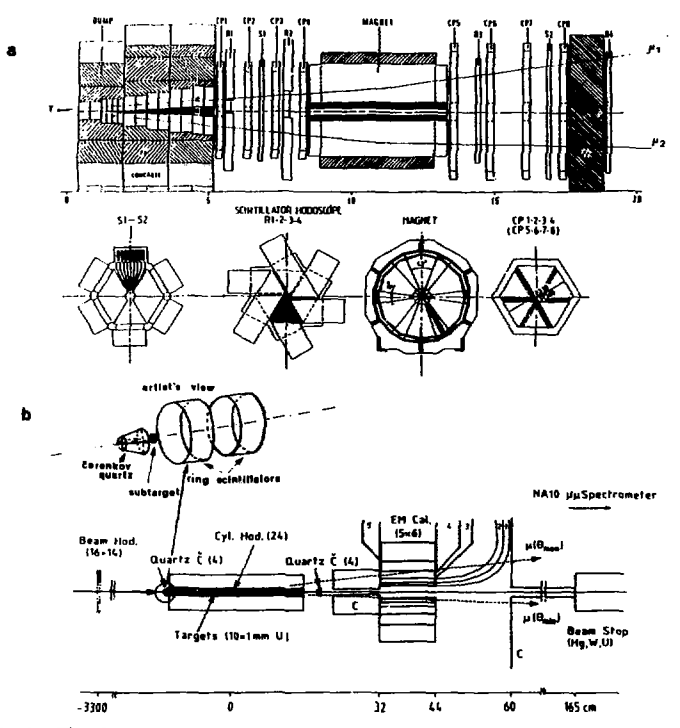


Fig. 1. The NA 38 detector. a) The muon spectrometer. b) The electromagnetic calorimeter, the multiple active target and the beam detectors.

It should be noted that the value of the fitted inverse slope parameter of the continuum, namely  $M_c$ , is stable, independent of  $E_T$  within errors, suggesting that the anomalous behaviour of the ratio S is, in fact, induced by the  $J/\Psi$ . If this would be the case, it would then be very tempting to attribute this behaviour to the formation of a quark-gluon plasma, as the plasma would screen the binding potential between the charm quark pair, hindering the formation of a  $J/\Psi$  bound state [6].

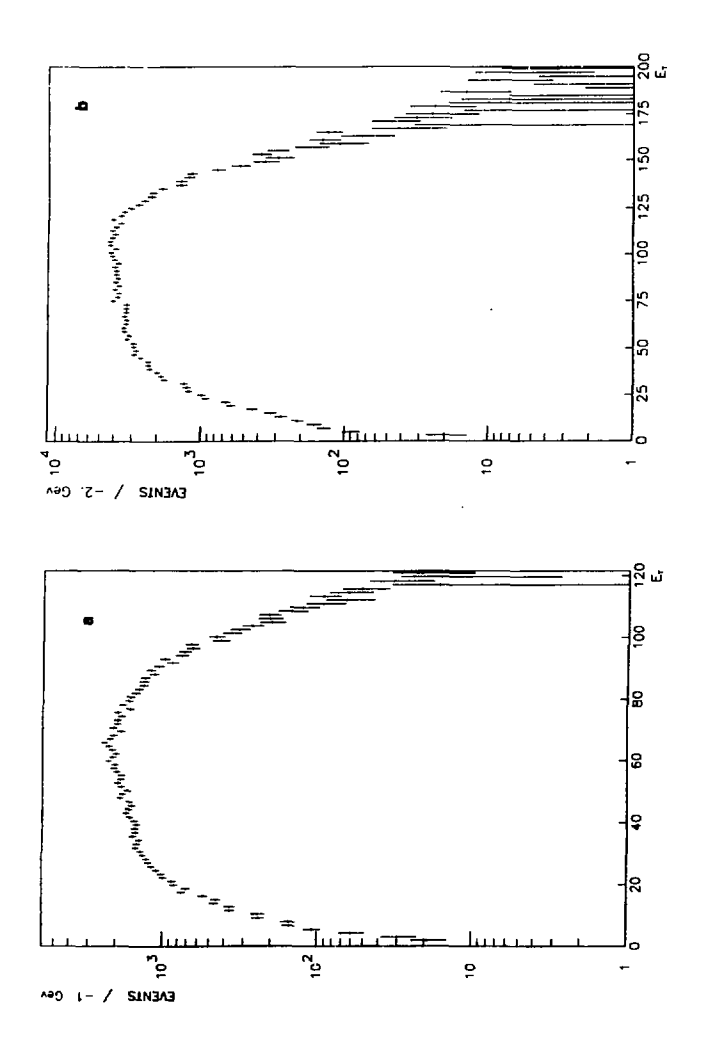


Fig. 2. The transverse 'electromagnetic energy' distribution of the selected events for a) the Oxygen-Uranium and b) the Sulphur-Uranium samples.

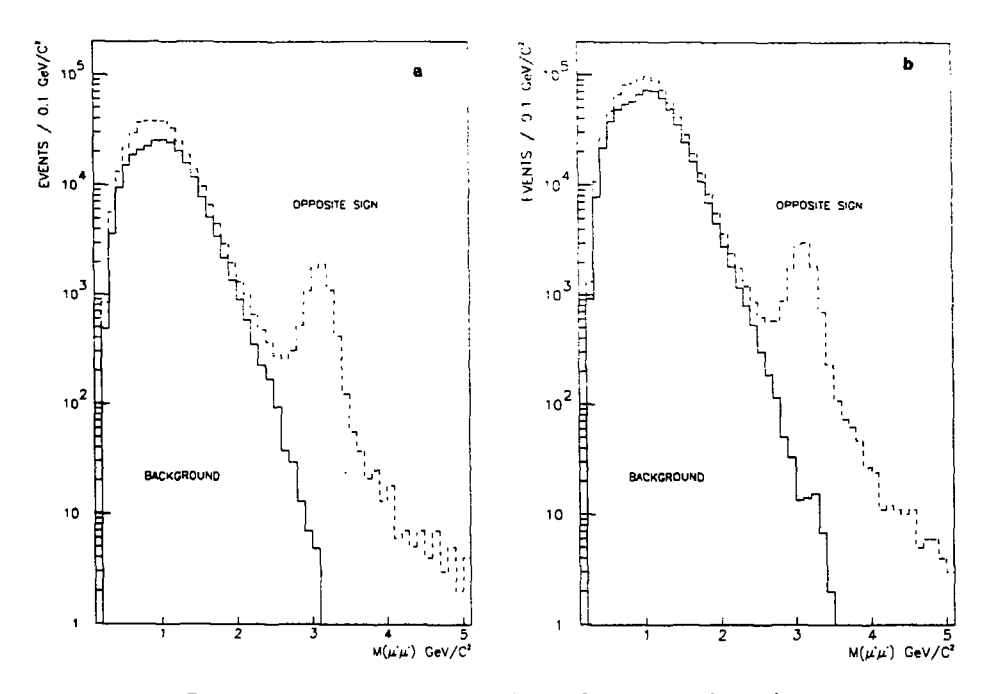


Fig. 3. The invariant muon-pair mass distribution after subtraction of events due to  $\pi$  or K decays for a) the Oxygen-Uranium and b) the Sulphur-Uranium samples.

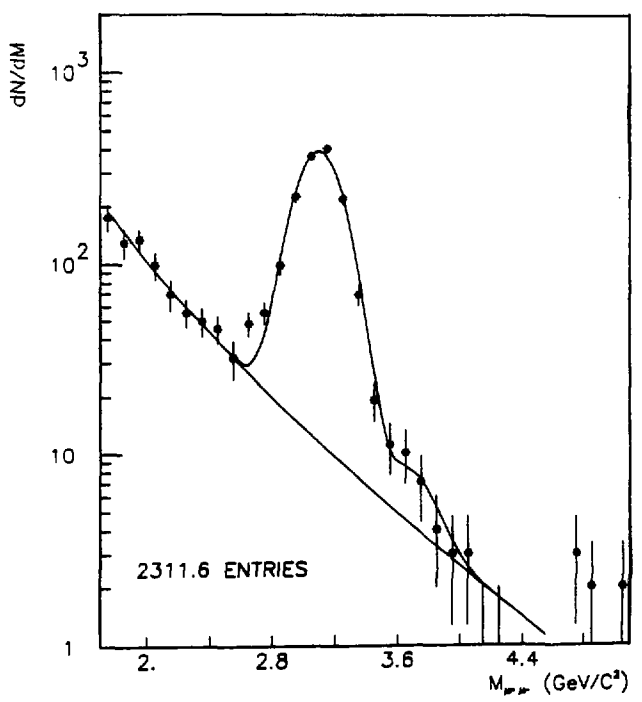


Fig. 4. The mass spectrum for muon pairs with  $1 < E_{\rm T} < 34$  GeV. The full line corresponds to the fit as described in the text.

Within the frame of this explanation, the suppression should be a function of the transverse momentum  $P_T$  of the  $J/\Psi$  [7]. This point has been investigated by studying the  $P_T$  distributions for dimuons in the mass range [  $2.7 < M_{\mu\mu} < 3.5 \, \text{GeV/c}^2$  ] i.e. for  $J/\Psi$ 's (neglecting the continuum in this mass range, which is of the order of 10%). Fig. 7 displays the distributions of  $1/PT^*dN/dP_T$  for the two extreme transverse energy bins quoted above and shows a much steeper decrease for the low transverse energy bin. This is clearly illustrated in Fig. 8 which shows the ratio of the number of events with

 $E_T > 85$  GeV, relative to the number of events with  $1 < E_T < 34$  GeV, for events in the J/ $\Psi$  mass range, as a function of  $P_T$ . This ratio is normalized to the same number of continuum events in each of the two energy bins. It is equivalent to the ratio S of J/ $\Psi$  /  $N_C$  as a function of ( $P_T$ )<sub> $\mu\mu$ </sub>, provided that the same ratio of the number of events in the two  $E_T$  bins, for events in the dimuon continuum is flat. This is the case, within the experimental errors, according to Fig. 9. Fig. 8 shows a striking  $P_T$  dependence, which is in excellent agreement with the theoretical predictions [7]. based on the screening of the binding potential between the c quarks.

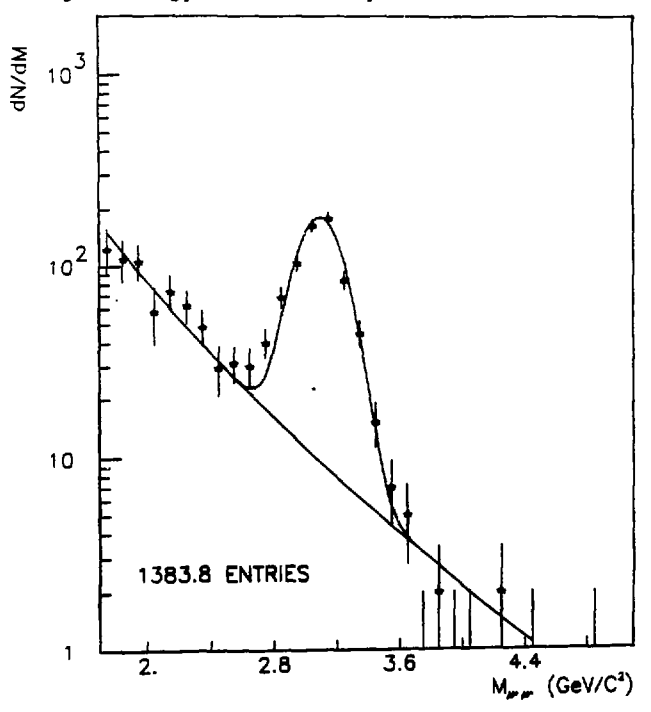


Fig. 5. Same as Fig. 4 for events with  $E_T > 85$  GeV.

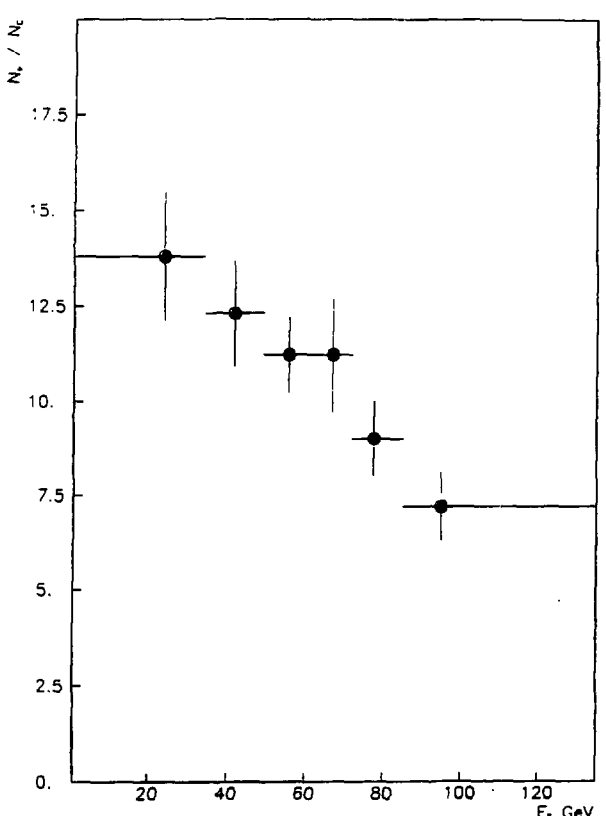


Fig. 6. The ratio  $S = N_{J/\Psi}/N_c$  as a function of transverse energy  $E_T$  for the Oxygen-Uranium sample.

A complete similar analysis has been performed on data obtained with a Copper target and also on data obtained with a 200 GeV per nucleon incident Sulphur beam on a Uranium target. Fig.10 shows the corresponding values of S as a function of  $E_T$ . The three sets of data are compared in Fig. 11 where the ratio S is displayed as a function of  $E_{T}/A_{inc}^{1/s}$  which, according to Björken's formula, is proportional, for central colli-

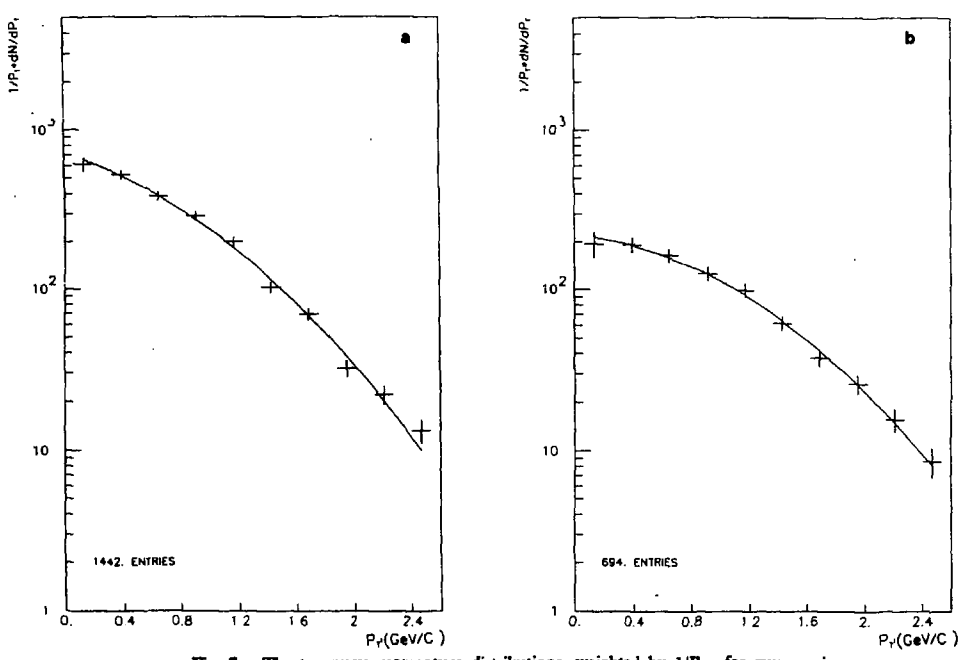


Fig. 7. The transverse momentum distributions, weighted by  $1/P_{\rm T}$ , for muon pairs with a)  $1 < E_{\rm T} < 34$  GeV and b)  $E_{\rm T} > 85$  GeV, for the Oxygen-Uranium sample.

. . .

sions, to the energy density reached in the reaction. All the data exhibit a similar behaviour and show that the production of J/Ψ relative to the muon pair continuum decreases significantly with increasing energy density.

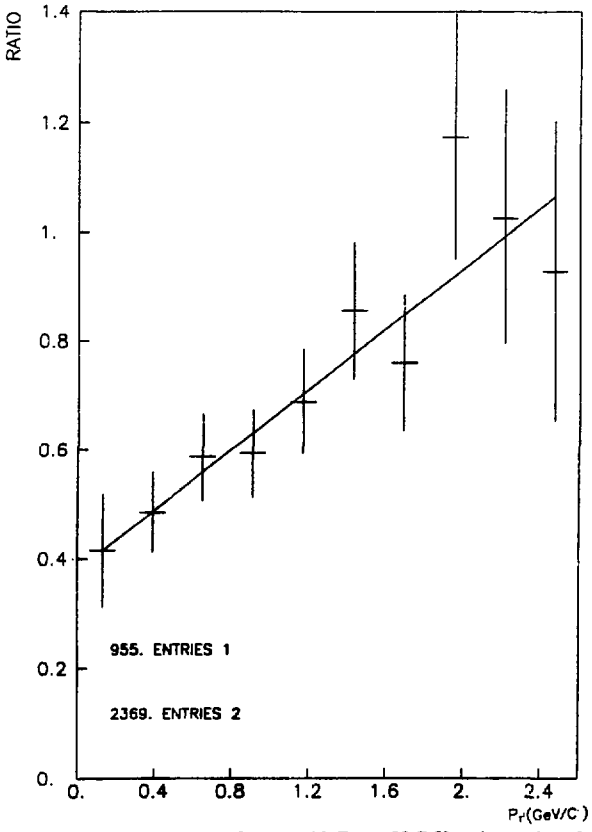


Fig. 8. The ratio of the number of events with  $E_T > 85$  GeV to the number of events with  $1 < E_T < 34$  GeV for muon pairs in the mass range [  $2.7 < M_{\mu\mu} < 3.5$  GeV/c<sup>2</sup> ] as a function of the transverse momentum  $P_T$ , for the Oxygen-Uranium sample.

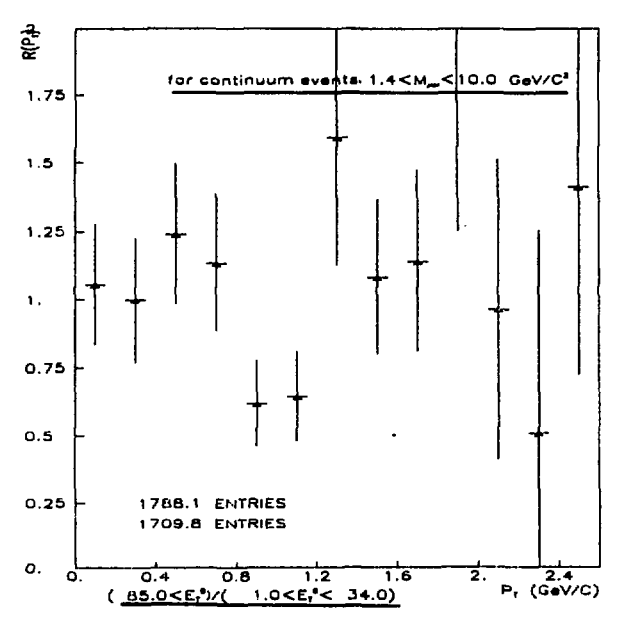


Fig. 9 . Same as Fig. 8 for events with  $M_{\mu\mu} > 1.4~{\rm GeV/c^2}$  with the mass range [  $2.7 < M_{\mu\mu} < 3.5~{\rm GeV/c^2}$  ] excluded.

As already pointed out, the results of experiment NA 38 find a natural explanation and an excellent quantitative agreement with the theoretical predictions based on the screening of the binding potential between the c quarks, let the origin of this screening be the high energy density, the partial deconfinement of quarks and gluons or some other unknown reason. Nevertheless, alternative mechanisms have been explored in order to explain these experimental results. Nuclear absorption leads to a suppression considerably weaker than observed [8]. Predictions based on inelastic scattering of J/Ψ's in a dense hadronic resonance gas [9] disagree (at least for the moment) with the observed P<sub>T</sub> effect.

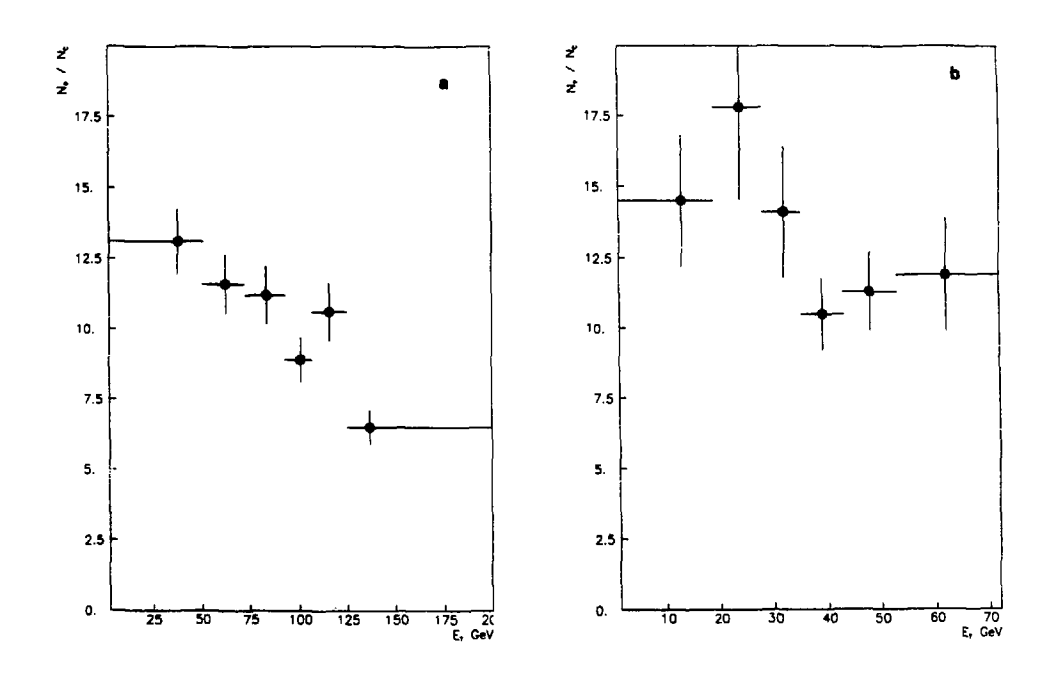


Fig. 10 . The ratio S as a function of transverse energy  $E_{\rm T}$  for  $\,$  a) the Sulphur-Uranium sample and  $\,$  b) the Oxygen-Copper sample.

In conclusion, the  $J/\Psi$  is suppressed relatively to the muon pair continuum when the energy density increases and the suppression effect is enhanced with decreasing transverse momentum. No conventional explanation is able, for the moment, to adjust quantitatively to the  $J/\Psi$  data. These data could be understood nevertheless if the observed Ion-Nucleus reactions would induce, at high energy density, a screening effect of the binding potential of the charmed quark pair, which could be a consequence of the QGP phase transition.

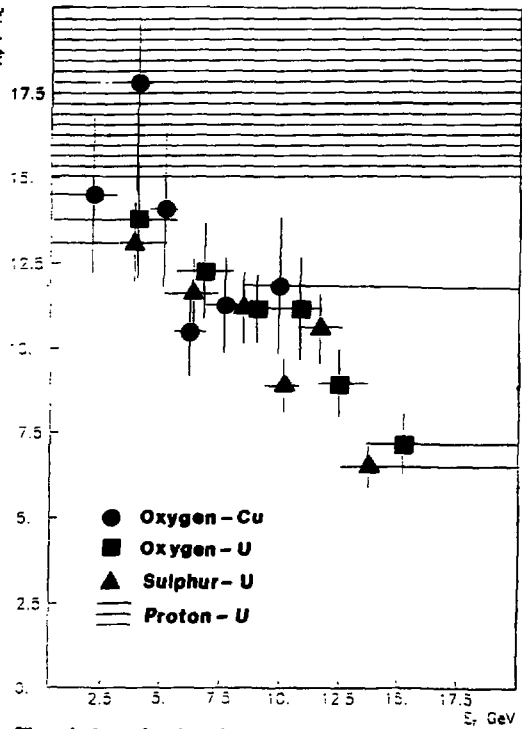


Fig. 11. The ratio S as a function of the "energy density" estimated by  $E_{\rm T}/A_{\rm inc}^{-1/2}$ . The horizontal strip corresponds to the Proton-Uranium sample studied in the same experiment, for which no  $E_{\rm T}$  dependence is observed.

#### REFERENCES

- [1] See, for example, K. Kajantie and M. Gyulassy contributions in Quark Matter Formation and Heavy Ion Collisions. Proceedings of the Bielefeld Workshop (May 1982) edited by M. Jacob and H. Satz (World Scientific Publishing Co. Singapore).
- [2] K. Kajantie et al., Phys. Rev. D34 (1986) 811.
- [3] T. Matsui and H. Satz, Phys. Lett. 178B (1986) 416.
- [4] For more details and preliminary results see A. Romana in Proceedings of the International Europhysics Conference on High Energy Physics, Uppsala (1987) 150, and A. Bussière in Proceedings of the Sixth International Conference on Ultra-Relativistic Nucleus-Nucleus Collisions – Quark Matter 1987 Nordkirchen, Z. Phys. C – Particles and Fields (1988) 117.
- [5] L. Anderson et al., Nucl. Inst. and Meth. 223 (1984) 26.
- [6] F. Karsch et al., Z. Phys. C Particles and Fields (1988) 617.
- [7] F. Karsch and R. Petronzio, Phys. Lett. B193 (1987) 105.
   F. Karsch and R. Petronzio, Z. Phys. C Particles and Fields (1988) 627.
   J.P. Blaizot and J.Y. Ollitrault, Phys. Lett. B199 (1988) 499.
   M.-C. Chu and T. Matsui, Phys. Rev. D37 (1988) 1851.
- [8] C. Gerschel and J. Hüfner, IPNO 88-04, Orsay preprint, submitted to Phys. Lett. B.
  - A. Capella, LPTHE ORSAY 88/13, Orsay preprint.
- [9] S. Gavin, M. Gyulassy and A. Jackson. LBL-24790 preprint.
   T. Ftacnik, P. Lichard and J. Pisut. COM/TH 88-1, Bratislava preprint.

#### Meng Ta-chung

## Fachbereich Physik der FU Berlin, Berlin (West)

Nuclear studies at high energies - the importance and the usefulness of which have been recognized here in Dubna already more than fifteen years ago - have attracted more and more attention recently. One of the reasons is certainly the fascinating vision that quark-gluon matter can be created and its properties can be studied in laboratories where high-energy hadrons or heavy ions are used to bombard nuclear targets.

Unfortunately, in spite of the enormous experimental and theoretical efforts, not very much is known at present about the much discussed quark-gluon plasma. In fact, at this moment, we are still in the stage of searching for an unambiguous signal for the existence of such objects. I think everybody agrees that extracting pure dynamical signals from high-energy nuclear reaction data is not trivial. In fact, due to the large number of particles which are produced in high-energy hadron-nucleus and nucleus-nucleus collisions, it is rather obvious that statistical effects have to be taken into account in all analyses.

In this talk, I shall first discuss some results on hadron-hadron collisions in order to show you that already in such simple/elementary hadronic reactions the stochastic aspect of multiparticle production processes plays a dominating role in understanding the observed phenomena. After having shown these, I shall summarize the basic ideas and the main results of the Multisource Model for hadron-nucleus and nucleus-nucleus collisions, and discuss the concept and the consequences of the NES(number of effective sources)-scaling. The papers I discuss here are written in collaboration with Cai Xu, Chao Wei-qin, Chou Kuang-chao, Huang Chao-shang, Liu Lian-sou, Peng Hong-an and Pan Ji-cai.

One class of examples which explicitly show the importance of the stochastic aspect of multiparticle production in hadron-hadron collisions is associated with the following observations. (a) There exists a simple relationship  $^{/1}$  between the charge multiplicity distributions in different rapidity intervals. (b) There is a close relationship  $^{/2}$  between minijet events and minimum bias events. (c) The transverse energy spectra in different windows of rapidity and/or azimuthal angle

<sup>\*</sup> Supported in part by Deutsche Forschungsgemeinschaft DFG Me 470/5-1 and 5-2

in different transverse energy regions are related $^{\prime 3\prime}$  to one another. (d) All these relations $^{\prime 1-3\prime}$  can be described by standard statistical methods.

In fact, it has been shown  $^{/1/}$  that the distributions  $P_w(n_w)$  of charge multiplicity  $n_w$  in finite rapidity windows w within the range of the emitting system (at a fixed total c.m.s energy  $\sqrt{s}$ ) can be calculated from:

$$P_{W}(n_{W}) = \sum_{n} P(n) {n \choose n_{W}} f_{W}^{n_{W}} (1 - f_{W})^{n - n_{W}} , \qquad (1)$$

where P(n) is the charge multiplicity distribution of the emitting system, and  $f_w = \langle n_w \rangle / \langle n \rangle$ ,  $\langle n \rangle$  is the average charge multiplicity of the emitting system and  $\langle n_w \rangle$  is that observed in the window w. Furthermore, relations similar to that given in Eq.(1) exist<sup>2,3</sup> between transverse energy distributions P(E<sub>t</sub>) and P<sub>w</sub>(E<sub>tw</sub>):

$$P_{w}(E_{tw}) = \int dE_{t}/\epsilon \ P(E_{t})B(E_{t},E_{tw};F_{w};\epsilon). \tag{2}$$

Here, P and  $P_w$  are respectively the probability densities of the transverse energies ( $E_t$  and  $E_{tw}$ ) of the system and that observed in a given rapidity and/or azimuthal angle window w;  $f_w = \langle E_{tw} \rangle / \langle E_t \rangle$  is the average chance for a unit of transverse energy to be inside w;  $\langle E_{tw} \rangle$  and  $\langle E_t \rangle$  are respectively the average value of  $E_{tw}$  and  $E_t$ .  $B(E_t, E_{tw}, f_w; \varepsilon)$  is the generalized binomial distribution for the continuous variables  $E_t/\varepsilon$  and  $E_{tw}/\varepsilon$ :

$$B(E_{t};E_{tw};f_{w};\varepsilon) = \frac{\Gamma(E_{t}/\varepsilon+1)}{\Gamma(E_{+,t}/\varepsilon+1)\Gamma(E_{t}/\varepsilon-E_{t,t}/\varepsilon+1)} f_{w}^{E_{t}w'\varepsilon} ((-f_{w})^{E_{t}/\varepsilon-E_{tw}'\varepsilon}$$
(3)

where, the energy unit & is an arbitrarily chosen s-dependent parameter.

(The relevant figures shown in the talk are omitted in the written version. The interested reader is referred to the figures in Refs. 1-3).

Another class of such examples in hadron-hadron collisions is associated with the observed regularities in midrapidity multiparticle production processes. Note that it is in the midrapidity region of hadronic reactions, where most of the exotic phenomena - especially those associated with the existence of quark-gluon plasma - are expected.

First, we recall: In 1982 when the first CERN proton-antiproton collider results were known, it was pointed out  $^{/4/}$  (See also Refs. 5 and 6) that in nondiffractive hadron-hadron collisions the multiplicity distribution P(n) = P(n|2) of charged hadrons produced in the midrapidity region is given by

$$P(n|2) = 4 \frac{n}{\langle n \rangle^2} \exp(-2\frac{n}{\langle n \rangle}),$$
 (4)

where  $\langle n \rangle$  is the average value of n (at a given  $\langle s \rangle$ ). As we can see in Figs. 1 and 2 that P(n|2) given in Eq.(4) indeed gives a very good description of the data  $^{77}$ .

Furthermore, it should be mentioned that since the transverse energy  $\rm E_t$  and the multiplicity of charged hadrons is seen/8/ to be proportional to each other, the corresponding  $\rm E_t$ -distribution is

$$P\{E_{t}|2\} = 4 \frac{E_{t}}{\langle E_{t} \rangle^{2}} \exp\{-2 \frac{E_{t}}{\langle E_{t} \rangle}\}$$

$$= \frac{v_{(II)} \cdot 4i_{1} \cdot e_{0} \cdot (2i_{1})}{v_{(II)} \cdot 4i_{2} \cdot e_{0} \cdot (2i_{1})}$$

$$= \frac{236}{6} \frac{v_{(II)} \cdot 4i_{2} \cdot e_{0} \cdot (2i_{1})}{v_{(II)} \cdot 4i_{2} \cdot e_{0} \cdot (2i_{1})}$$

$$= \frac{236}{6} \frac{v_{(II)} \cdot 4i_{2} \cdot e_{0} \cdot (2i_{1})}{v_{(II)} \cdot 4i_{2} \cdot e_{0} \cdot (2i_{1})}$$

$$= \frac{236}{6} \frac{v_{(II)} \cdot 4i_{2} \cdot e_{0} \cdot (2i_{1})}{v_{(II)} \cdot 4i_{2} \cdot e_{0} \cdot (2i_{1})}$$

$$= \frac{236}{6} \frac{v_{(II)} \cdot 4i_{2} \cdot e_{0} \cdot (2i_{1})}{v_{(II)} \cdot 4i_{2} \cdot e_{0} \cdot (2i_{1})}$$

$$= \frac{236}{6} \frac{v_{(II)} \cdot 4i_{2} \cdot e_{0} \cdot (2i_{1})}{v_{(II)} \cdot 4i_{2} \cdot e_{0} \cdot (2i_{1})}$$

$$= \frac{236}{6} \frac{v_{(II)} \cdot 4i_{2} \cdot e_{0} \cdot (2i_{1})}{v_{(II)} \cdot 4i_{2} \cdot e_{0} \cdot (2i_{1})}$$

$$= \frac{236}{6} \frac{v_{(II)} \cdot 4i_{2} \cdot e_{0} \cdot (2i_{1})}{v_{(II)} \cdot 4i_{2} \cdot e_{0} \cdot (2i_{1})}$$

Fig. 1. The scaled multiplicity distribution in the central rapidity region. The experimental data are taken from Ref. 7. The curve is obtained from Eq. (4).

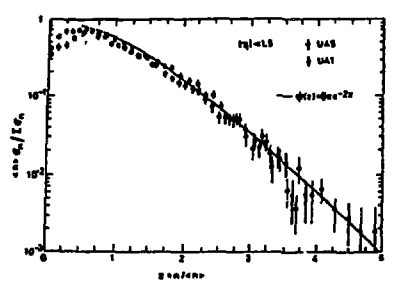


Fig. 2. The scaled multiplicity distribution in the central rapidity region, shown as a log-plot. The curve is obtained from Eq. (4). This figure is taken from the second paper of Ref. 7.

The underlying physical picture which leads to this result is that the two colliding hadrons act as two energy sources in the formation process of a system of clusters; and these clusters decay into the observed hadrons. To be more precise, it is envisaged that a central emitting system C\* is formed in every event of nondiffractive hadron-hadron collision at sufficiently high energies. In such an event, the two colliding hadrons act as two energy sources in the formation process of the C\* system [We shall from now on call it C\*(2) in order to indicate the number of sources]. Each of them may donate a random amount of its kinetic energy (in the hadron-hadron c.m.s. frame) to create the system C\*(2). The part of materi-

alization energy donated by each of the two energy sources is not associated with any specific intrinsic quantum number which could maintain the identity of that part, after the system  $\mathbb{C}^*(2)$  is formed. That is, the state of the system  $\mathbb{C}^*(2)$  after its formation is characterized by the total amount of materialization energy  $\mathbb{E}^*_{\mathbb{C}}$ , but not by the individual contributions from the two sources. In this sense, the system  $\mathbb{C}^*(2)$  "forgets its history" after it is created. Hence, in the proposed model, the relevant quantities which characterize the particle production process in the midrapidity region of nondiffractive hadron-hadron collisions are: first, the integer 2, the number of sources which contribute materialization energy  $\mathbb{E}^*_{\mathbb{C}}$  to the system  $\mathbb{C}^*(2)$ ; second, the quantity  $\langle \mathbb{E}^*_{\mathbb{C}}|2\rangle$ , the mean value of the materialization energy  $\mathbb{E}^*_{\mathbb{C}}$  in the system  $\mathbb{C}^*(2)$ . As we have shown in Refs. 5 and 6, the probability  $P_{\mathbb{C}}(\mathbb{E}^*_{\mathbb{C}}|2)$  for the system  $\mathbb{C}^*(2)$  to be in a state characterized by the materialization energy  $\mathbb{E}^*_{\mathbb{C}}$  is given by

$$\langle EE | 2 \rangle P(EE | 2) = 4 \frac{EE}{\langle EE | 2 \rangle} \exp[-2 \frac{EE}{\langle EE | 2 \rangle}],$$
 (6)

Now, since in this picture, the transverse energy  $E_{t}$  produced in the midrapidity region is due to the decay of clusters formed in the system  $C^{*}(2)$  and the corresponding materialization energy  $E_{C}^{*}$  is nothing else but the sum of the masses of such clusters which are approximately of the same size (this is in accordance with the empirical fact, see, e.g. Ref.7), we have:

$$\frac{E_{\xi}^{k}}{\langle E_{\xi}^{k} | 2 \rangle} = \frac{E_{\xi}}{\langle E_{\xi}^{-} | 2 \rangle} = \frac{n}{\langle n | 2 \rangle}.$$
 (7)

By inserting this relationship into Eq.(6) we obtain P(n|2) and  $P(E_t|2)$ , as given in Eqs.(4) and (5), where we denote hereafter the average multiplicity <n> and the average transverse energy < $E_t$ > by <n|2> and < $E_t$ |2> respectively because we are dealing with 2 sources in the hadron-hadron case.

This picture for nondiffractive hadron-hadron collisions 4-6/ taken together with the concept of effective target (ET) can be, and has already been 10,11/, extended to include hadron-nucleus collisions. Here, the elementary process is the nondiffractive interaction between a hadron and an ET. That is, a high-energy hadron-nucleus collision is a collision between the incident hadron and an effective target which is the group of nucleons along the path of the incident hadron inside the target nucleus. The ET-concept which has been proposed a long time ago 19/, is based on the following well-known facts. (a) At sufficiently high incident energies, the overwhelming majority of hadron-hadron collisions are inelastic, where in general many particles are produced. This, taken together with the fact that the average multiplicity of high-energy hadron-nucleon collisions depends only very weakly on the mass number of the nucleus, strongly suggests: The reaction time for multiparticle production in hadron-hadron reactions is very long, much longer than the time interval a high-energy hadron needs to "go through" a nucleon inside

the targets nucleus. (b) The nuclear force is of short range; and the average binding energy between the nucleons inside the target-nucleus is negligibly small compared to the kinetic energy of the incident hadron. This is why in nigh energy hadron-nucleus reaction, only the nucleons along the path of the incident hadron inside the nucleus actively take part in the collision process. This group of nucleons is called an "effective target (ET)". It should be emphasized that an ET is not a "coherent tube of hadronic matter" which has been suggested by other authors'12' at about the same time. This is because the ET usually acts gently/softly with the incident hadron and in such cases it acts as a group of individual nucleons. It can be considered as a coherent tube only when it collides violently with the incident hadron. This implies in particular that each of the collisions between the incident hadron and the  $v_{\rm ET}$  nucleons in the ET can be either diffractive or nondiffractive. We are interested only in the nondiffractive collisions between the incident hadron and the nucleons in the ET, because central emitting systems C\* (which contribute to the midrapidity region) are formed only in nondiffractive collisions. If the average chance for a hadron-nucleon collision to be nondiffractive at the given incident energy is p, the chance of having v nondiffractive collisions among the  $v_{\mathrm{E}T}$  hadron-nucleon collisions in this hadron-fit reaction is given by a binomial distribution

$$B(v_{ET}, v; p) = {v_{ET} \choose v} p^{v} (1-p)^{v_{ET}-v},$$
 (8)

In a hadron-ET collision event in which a central system C\*(1+v) is formed due to nondiffractive interaction between the incident hadron and v (of the ver) nucleons in the ET the formation process, takes place as follows. The incident hadron and the v nucleons act as 1+v energy sources. During the interaction, each of the 1+v sources contributes part of its kinetic energy to form the system  $C^*(1+v)$ ; and the amount of materialization energy each of the 1+v sources donates is random. After its formation, the system "forgets its history" in the sense that the materialization energy donates by each of the 1+v sources is not associated with any intrinsic quantum number, so that it is impossible to identify the amount of the individual contributions. That is, the state of the system C\*(1+v) is characterized by the total amount of the materialization energy  $E_{\mathbf{p}}^{\star}$  contributed from the 1+v sources. Note that E' is the sum of 1+v random variables and hence it is itself a random variable. Therefore, the relevant quantities which characterize the particle production in the midrapidity region in hadron-ET collisions, in which the incident hadron and v of the nucleons in the ET interact mondiffractively, are: first, the integer 1+v, the number of sources which contribute materialization energy E. to the system  $C^*(1+v)$ ; second, the quantity  $\langle E_C^*|1+v \rangle$  which is the mean value of  $E_C^*$ in the system C\*(1+v). As we have already pointed out in Ref.10, the probability  $P_{C}(E_{A}^{*}[1+v])$  that the system  $C^{*}(1+v)$  is in a state characterized by the materialization energy Et is

$$\langle E\xi | 1+u \rangle P(E\xi | 1+v) = \frac{(1+v)^{1+v}}{\Gamma(1+v)} \frac{\langle E\xi | 1+w \rangle}{\langle E\xi | 1+w \rangle} \cdot \exp[-(1+v) \frac{E\xi}{\langle E\xi | 1+w \rangle}]$$
 (9)

Furthermore,

$$\frac{\langle E_{\mathcal{L}}^{+}|1+\nu\rangle}{1+\nu} = \frac{\langle E_{\mathcal{L}}^{+}|2\rangle}{2}$$
 (10)

is valid/10,11,13/, provided that the kinetic energy of the 1+v sources is the same where the materialization process takes place. This condition is exactly satisfied in the hadron-nucleon c.m.s. frame, where the kinetic energy of all 1+v nucleons is the same. Furthermore, it is expected to be valid also in other Lorentz frames in which the kinetic energies of the 1+v sources are approximately the same. This is because, compared to 1ts kinetic energy, the amount of energy of each of the 1+v hadons donated to form the system C\*(1+v) is in general an extremely small quantity. By inserting Eq.(10) into Eq.(9) we obtain:

$$P(E_{\xi}^{*}[1+v) = \frac{1}{\Gamma(1+v)} \left[ \frac{2}{\langle E_{\xi}^{*}|2 \rangle} \right]^{1+v} \exp\left[ -\frac{2}{\langle E_{\xi}^{*}|2 \rangle} E_{\xi}^{*} \right]. \tag{11}$$

From this and other properties of the Multisource Model we can readily understand the observed characteristic features in hadron-nucleus collisions  $^{/14,15/}$ . Because of the limited time (for this talk) and the limited space (in the written version), let me just show you the following results as examples: (a) the ratio  $D/\langle n \rangle$  between the dispersion  $D = \langle (n-\langle n \rangle^2 \rangle^{1/2}$  and the average multiplicity  $\langle n \rangle$  as a function of the number  $N_p$  of identified protons which correspond to the grey tracks measured in emulsion experiments (See Fig. 3); (b), the multiplicity distributions and their dependence on rapidity intervals (See Figs. 4 and 5);

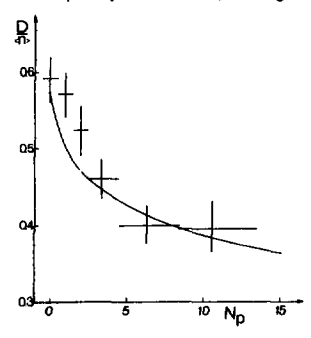


Fig. 3. The ratio of the dispersion D to the mean multiplicity  $\langle n \rangle$  as a function of Np, the number of identified protons. The data are from Ref.14 (first paper). The curve is the calculated result.

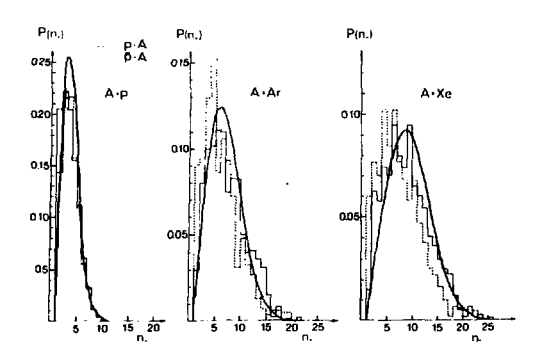


Fig. 4. Multiplicity distribution of the produced negatively charged particles for p-A and p-A collisions. The data, given by the histograms, are taken from Ref. 14 [second paper]. The solid curves are the calculated results.

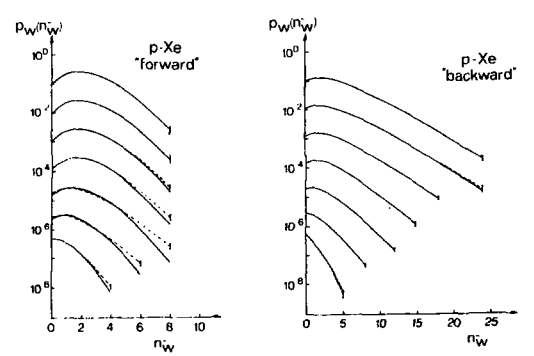


Fig.5. Multiplicity distributions for negatively charged particles in given rapidity windows w. The sizes ( $\Delta y$ ) of the rapidity windows are (counted from below) 0.5, 1.0, 1.5, 2.0, 2.5, 3.0, and 3.5, respectively. The data, taken from Ref.14 (third paper), are shown as dashed curves when they do not coincide with the corresponding solid curves. The "forward" and the "backward hemisphere" are defined in Ref.14 as the c.m.s. of the p-p system at  $p_{1ab}$ =200 GeV/c. The solid curves are the calculated results. The distributions are p+Ar collisions at  $p_{1ab}$ =200 GeV/c.

<sup>(</sup>c) the empirical formula for midrapidity transverse energy distribution in p-Au and  $\pi^{*}\text{-Au}$  collisions

$$\frac{d\sigma}{dE_{t}} = 0.173 E_{t}^{2.36} \exp(-0.727 E_{t})$$
 (12)

obtained by NA35 collaboration/15/ can be derived (See Ref.11).

The generalization of the multisource model to include nucleus-nucleus collisions is made  $^{\prime 11,13\prime}$  by taking the "effective projectiles (EP's)" into account. The concept of EP has been introduced  $^{\prime 9\prime}$  in the same way as that for ET's. (In order to see the similarity, consider the case in which a high-energy heavy ion hits a proton target!) A nucleus-nucleus collision at sufficiently high energies is, according to this picture, the simultaneous collisions of a large set of EP-ET pairs. Since we are interested only in the production processes in the midrapidity region, we consider only the nondiffractive processes between the nucleons in the EP-ET pairs. Every EP-ET collision event is associated with a number  $\mu$ , the number of nucleons that take part in nondiffractive collisions between the  $\nu_{\rm EF}$  nucleons in the EP and the  $\nu_{\rm ET}$  nucleons in the corresponding ET. The number  $\mu$  is obviously either zero (which means that there is no nondiffractive collisions) or an integer between 2 and  $\nu_{\rm EF}$   $\nu_{\rm ET}$ . For a given EP-ET pair, the probability of obtaining  $\mu$  nondiffractive nucleon-nucleon collisions is  $W(\mu|\nu_{\rm EP},\nu_{\rm ET})$   $\rho^{\mu}(1-\rho)^{\nu}$ EP+ $\nu$ ET- $^{\mu}$ , where

$$W(u|v_{EP},v_{ET}) = \sum_{\sigma=1}^{\sigma=1} {v_{EP} \choose \sigma} {v_{ET} \choose v_{E\sigma}} = {v_{EP} \choose \sigma} (13)$$

This shows in particular that the system depends only on the number  $\mu$ , but not on the specific way of composition. (That is, it does not matter how many of the  $\mu$  nucleons are from the EP and how many of them are from the ET.)

The formation process of the central system  $C^*(\mu)$  due to the nondiffractive processes among  $\mu$  nucleons in a EP-ET pair takes place as follows: The  $\mu$  nucleons act as  $\mu$  energy sources. During the interaction, every one of the  $\mu$  sources donates part of its kinetic energy for the formation of the system  $C^*(\mu)$ ; and the amount of materialization energy each of the  $\mu$  sources donates is random. After it is formed, the system  $C^*(\mu)$  "forgets its history" in the sense that the state is characterized by the total materialization energy  $E^*_{\delta}$  in  $C^*(\mu)$  but not by the  $\mu$  individual contributions of the  $\mu$  energy sources. In fact, the probability  $P(E^*_{\delta}|\mu)$  that the system  $C^*(\mu)$  is in a state characterized by  $E^*_{\delta}$  is given by Eq.(9) where the following replacements should be made: " $E^*_{\delta}$  in  $C^*(1+\nu)$ " by " $E^*_{\delta}$  in  $C^*(\mu)$ , and  $1+\nu$  by  $\mu$ . The relationship corresponding to that in Eq.(10) now reads:

$$\frac{\langle \mathcal{E}_{0}^{\dagger} | u \rangle}{u} = \frac{\langle \mathcal{E}_{0}^{\dagger} | 2 \rangle}{2} \tag{14}$$

which is exactly satisfied in the nucleon-nucleon c.m.s. frame in which all the  $\mu$  participating nucleons have the same kinetic energy; and it should be valid in all reference frames in which the kinetic energies of the above-mentioned nucleons are approximately the same. Hence, the probability  $P(E_{\nu}^{\dagger}|\mu)$  that the system  $C^{*}(\nu)$  is in a state characterized by the materialization energy  $E_{\nu}^{*}(\mu)$  is:

$$P(E\xi|\mu) = \frac{1}{\Gamma(\mu)} \left( \frac{2}{\langle E\xi|2 \rangle} \right)^{\mu} E\xi^{\mu-1} exp[-\frac{2}{\langle E\xi|2 \rangle} E\xi]. \tag{15}$$

Now, the quantity given in Eq.(14)  $\langle E_{\mathbf{k}}^{\mathbf{z}}|\mu\rangle/\mu^{-\frac{1}{2}}\langle e_{\mathbf{k}}^{\mathbf{z}}\rangle$  [which is identical to that given in Eq.(10)] is nothing else but the average materialization energy per energy-source. Hence, the quantity m definded by

$$m = E_C^*/\langle E_C^* \rangle \tag{16}$$

for a given E $\xi$  in system C\*( $\mu$ ) is of particular interest: This is because m is uniquely associated with the materialization energy E $\xi$  in C\*( $\mu$ ), and it shows how many sources there would be if each source contributes the same amount, <e $\xi$ >. From now on, we call the quantity m "the number of effective sources (NES)". In terms of m. Eq.(15) reads

$$\Omega(m \mid \mu) = \frac{1}{\Gamma(\mu)} m^{\mu-1} \exp(-m), \qquad (17)$$

where we have introduced the "NES distribution",  $\Omega(m \mid \mu)$ , by

$$\Omega(m|\mu) = \langle e_{C}^{\mu} \rangle P(E_{C}^{\mu}|\mu). \tag{18}$$

In terms of the NES-distribution, the multiplicity distribution  $P(n|\mu)$  can be written as

$$P(n|\mu) = \frac{1}{\langle n_n \rangle} \Omega \left[ \frac{n}{\langle n_n \rangle} |\mu \right], \tag{19}$$

Furthermore,  $P(E_t|\mu)$ , the distribution of the transverse energy  $(E_t^{em})$ , and  $P(E_t^{em}|\mu)$ , that of the electromagnetic part of the transverse energy  $(E_t^{em})$ , '15' can also be expressed in terms of  $\Omega(m|\mu)$  in a similar way. In fact, the distributions  $P(E_t^{em}|\mu)$  and  $P(E_t^{em}|\mu)$  can be obtained by replacing  $\langle n_u \rangle$  by  $\langle e_t \rangle$  and  $\langle e_t^{em} \rangle$  in Eq. (19) respectively. Here,  $\langle e_t \rangle$  is the average value of the transverse energy each participating nucleon contributes; and  $\langle e_t^{em} \rangle$  is the corresponding average value for the electromagnetic part of the transverse energy.

In order to compare the above-mentioned distributions with nucleus-nucleus collision data, a geometrical averaging process must be carried out. Note that EP's and ET's which interact gently/softly with each other are groups of individual nucleons; and the nucleons in each group stand more or less on a row, so that all EP's and ET's can be considered as nucleons inside cylinder-form envelopes. The axes of the cylinders are parallel to the incident axes. The cross sections of the cylin-

ders are approximately  $\pi r_0^2$  and the length is typically a few times  $r_0$ , depending of course on the size of the nucleus and the position of the cylinders in the nucleus. The positions of the interacting EP-ET pairs, and the number of nucleons in each EP or ET is determined by the geometry of the nuclei in collision. In practice we characterize the EP-ET pairs by corresponding impact parameters and perform the

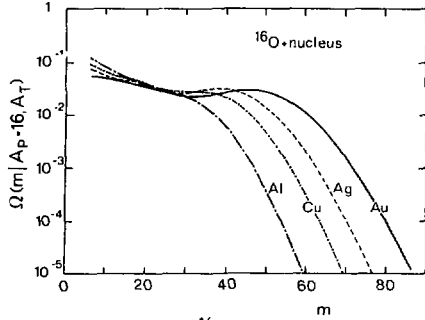


Fig.6. NES distributions for 160 ion on different nuclear targets.

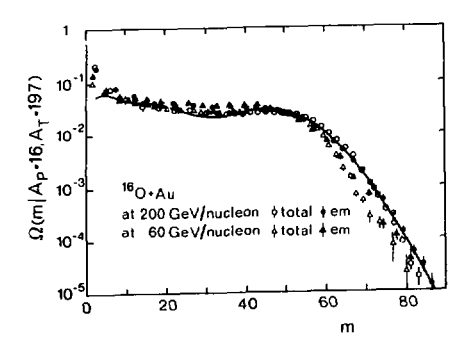


Fig.7. Test for NES-scaling is demonstrated by plotting the  $E_t$ -distribution and  $E_t^{em}$ -distribution data for 200 GeV/nucleon and 60 GeV/nucleon  $^{16}$ 0 ion on Au target in the following way:

$$\label{eq:epsilon} \langle e_t \rangle \, \frac{1}{\sigma} \, \frac{d\sigma}{dE_t} \, v_S \, \frac{E_t}{\langle e_t \rangle} \ , \qquad \langle e_t^{em} \rangle \, \frac{1}{\sigma} \, \frac{d\sigma}{dE_t^{em}} \, v_S \, \frac{E_t^{em}}{\langle e_t^{em} \rangle} \ ,$$

here do/dE  $_t$ , do/dE  $_t^{em}$  and the values for  $<e_t>$  and  $<e_t^{em}>$  are taken from Ref.15;  $\sigma$  stand for the integrated cross section which is also taken from the data.

inveraging process by a simple Monte-Carlo program to get the NES-distribution  $\mathfrak{A}(\mathfrak{m}|A_{\mathsf{P}},\mathsf{A}_{\mathsf{T}})$ , where  $\mathsf{A}_{\mathsf{P}}$  and  $\mathsf{A}_{\mathsf{T}}$  denote the mass-number of the projectile and that of the target respectively. As an example, let me show you the NES-distribution  $\mathfrak{A}(\mathfrak{m}|A_{\mathsf{P}},\mathsf{A}_{\mathsf{T}})$  for the following projectile-target combinations: "O ion on  $\mathsf{A}_{\mathsf{U}}$ ,  $\mathsf{A}_{\mathsf{G}}$ ,  $\mathsf{C}_{\mathsf{U}}$  and  $\mathsf{A}_{\mathsf{T}}$  targets. The result is shown in Fig.6. Comparison between experimental data 15 and the above-mentioned NES-scaling is shown in Fig.7.

Hence we are led to the conclusion that the midrapidity multiparticle production processes in ordinary (gentle/soft) hadron- and heavy-ion-induced reactions at sufficiently high incident energies can be summarized as follows/16/.

- (I) Midrapidity production of all scalar quantities observed in directions transverse to the collision axis are stochastic processes. There are many quantities of this kind: charge multiplicity, transverse energy, strangeness multiplicity, number of produced baryon-antibaryon pairs etc.
- (II) For a given projectile-target combination at a given incident energy, there is a scale for each of these quantities. In terms of the corresponding scaled variables, all the scaled distributions of such quantities, for a given projectile-target combination, are the same.
- (III) The existence of such scales can be understood in terms of the following simple physical picture: Every hadron that participates in such a multiparticle production process acts as an independent source a reservoir for the scalar quantities observed in the transverse directions. For every one of these quantities, the amount each source contributes in a collision event is random. Averaged over all events, the contribution from any one of the sources is the same as that from another. This average value obtained from any one of the sources is the scale for that quantity.
- (IV) This physical picture implies in particular: For any one of these quantities from any one of the sources, the probability density is a simple exponential function of the corresponding scaled variable. This means, once the above-mentioned average value of the observed quantity is known, the corresponding distribution for any given projectile-target combination can be obtained from stochastics and geometry in a straight forward way.

#### References

- 1. Chao Wei-qin, Meng Ta-chung and Pan Ji-cai, Phys. Rev. D35, 152 (1987).
- 2. Chao Wei-qin, Meng Ta-chung and Pan Ji-cai, Phys. Rev. Lett. 1399 (1987).
- 3. Meng Ta-chung and Pan Ji-cai, Phys. Rev. D37, 243 (1987).
- 4. Liu Lian-sou and Meng Ta-chung, Phys. Rev. D27, 2640 (1983).
- 5. Chou Kuang-chao, Liu Lian-sou and Meng Ta-chung, Phys. Rev. D28, 1080 (1983).

- Cai Xu, Chao Wei-quin, Huang Chao-shang and Meng Ta-shung, Phys. Rev. <u>D33</u>, 1287 (1986).
- 7. See for example, the following papers and the references given therein,
  - W. Thome et al., Nucl. Phys. B129, 365 (1977);
    - F.G. Rushbrooke, in Proceedings of the DPF Workshop on pp Options for the Supercollider, Chicago, 1984, edited by J. Pilcher and A.R. White, University of Chicago, (1984);
  - G. Ekspong, in Proceedings of the 16th International Symposium on Multiparticle Dynamics, June 9-14, 1985, Jerusalem, Israel, Ed.J. Grunhaus, Editions Frontiers, World Scientific, p. 309;
  - P. Carlson, in Proceedings of the 23rd International Conference on High-Energy Physics, 16-23 July 1986, Berkeley, Ca. USA, ed. S.C. Loken, World Scientific, p. 1346;
  - W. Kittle, in Proceedings of the 18th International Symposium on Multiparticle Dynamics 8-12, Sept. 1987, Tashkent USSR, ed. 1.M. Dremin, World Scientific (in press).
- See e.g. UA1 Collaboration, S. Geer, An. Fis. <u>A79</u>, 94 (1983); and references given therein.
- Meng Ta-chung, in Proceedings of the Topical Meeting on Multiparticle Production on Nucleus at Very High Energies, June 1976, Trieste, Italy, p. 435 (1976); Meng Ta-chung, Phys. Rev. D15, 197 (1977); Meng Ta-chung and E. Moeller, Phys. Rev. Lett. 41, 1352 (1978); Meng Ta-chung, Phys. Rev. Lett. 42, 1331 (1979).
- 10. Cai Xu, Chao Wei-qin and Meng Ta-chung, Phys. Rev. D36, 2009 (1987).
- 11. Liu Lian-sou, Meng Ta-chung and Peng Hong-an, Phys. Rev. <u>D37</u>, 3327 (1988).
- 12. G. Berlad, A. Dar, and G. Eilam, Phys. Rev. <u>D13</u>, 161 (1976);
  - S. Fredriksson, Nucl. Phys. B111, 167 (1976).
- Liu Lian-sou, Meng Ta-chung, Peng Hong-an and Pan Ji-cai, Phys. Rev. <u>D</u> (in press).
- 14. C. De Marzo et al., Phys. Rev. D26 1019 (1982);
  - C. De Marzo et al., Phys. Rev. <u>D29</u>, 2476 (1984);
  - F. Dengler et al. Z. Phys. C33 187 (1986).
- 15. NA35 Collaboration:
  - A. Bamberger at al., Phys. Lett. B184, 271 (1987);
  - T.H. Humanic, in Proceedings of the International Europhysics Conference on High-Energy Physics, June 25 - July 1, 1987 in Uppsala, Sweden, edited by O. Bother, published by University of Uppsala;
  - W. Hack, in Proceedings of Quark Matter 1987 Conference, Nordkirchen, August 23-29 (1987) in Nordkirchen, Germany (in press) and private communications.
- 16. Meng Ta-chung, Berlin preprint FUB/HEP 88-4

INTIIGATIONS PROF THE FOLENTH' DEFENDENCE OF HEAVY QUARLORIUM SUFFRESSION FOR A TOSSIBLY PORMED QUARK-GLUCK FLASKA

p. Bleschke, G. Röpke and H. Schulz<sup>+</sup> Wilhelm-Fieck-Universität, 2500 Rostock, G.D.R.

## 1. Introduction

One of the most appealing questions in the physics of high-energy nucleus-nucleus collisions is how to detect a quark-gluon plasme if it is possibly formed. Among the proposed signatures of the plasma phase the suppression of heavy querkonium production suggested by Latsui and Setz ) seems now to be confirmed experimentally by recent experiments of the MA38 Collaboration at CERN<sup>2</sup>,3). In these experiments with ultrarelativistic oxygen and sulfur beams on uranium and copper targets at 200 GeV/n, at increasing energy density of the reaction a decreasing number of J/Y counts relative to the Drell-Yanbackground was observed. A suppression ratio & has been introduced2) which is the ratio of  $J/\Psi$  abundance (normalised to the muon pair continuum) at high transverse energy ( $E_T/\Lambda^{2/3} \gtrsim 13$  GeV) to the abundance at low energy ( $E_T/\Lambda^{2/3} \lesssim 5$  GeV) where no suppression is found. Furthermore, the suppression ratio  $\mathcal{R}(p_m)$  has been given as a function of the muon pair transverse momentum  $p_T^{(3)}$ , see also Fig. 5. The analysis of the dependence of  $\mathcal{R}(p_T)$  on the longitudinal momentum  $x_p$ and the transverse energy Em of the muon pair as well as on the projectile mass number A is in progress so that in future a lot of experimental information is evailable from these dimuon measurements to set bounds to different suppression scenarios which have appeared. They try to explain the suppression pattern either in terms of more conventional physics as  $J/\Psi$  absorption in a dense hadron gas  $^{4-6)}$  or in terms of plasma physics as a Nott-effect for heavy quark bound states embedded in a quark plasma environment 7-11).

In the present contribution, we went to reexamine the scenario of Lott-dissolution by Latsui and Satz<sup>1,8)</sup> and show the shortcomings of the ingredient concepts of Debye screening and of formation time for a bound state. Finally, we give an alternate approach from the point of view of many-particle physics and chemical reaction kinetics. Ls a result, we estimate plasma parameters (radius, lifetime, temperature).

<sup>+)</sup>Central Institute for Nuclear Research, Rossendorf, 8051 Dresden, German Democratic Republic

# 2. Two-particle states and Mott transition

According to Latsui and Satz<sup>1)</sup>, the suppression of charmonium production may serve as a signal which might directly test the deconfining nature of the plasme. They proposed a scenario adopted from the concept of Debye screening in plasme physics where due to the Bott effect, the bound states dissolve at high densities. However, this often adopted static picture of the behaviour of two-particle states in a dense plasma is not correct if one is looking at the energy spectrum of the two-particle system. Consequently, the Bott- dissolution scenario has to be revisited both for the Coulomb- as well as for the quark-gluon plasma cases.

### (i) Plasma with Coulomb interaction:

The concept of a statically screened potential (Debye screening)

$$V(\mathbf{r}) = -\frac{e^2}{r} \exp(-\mathbf{r}/\mathbf{r}_0) \tag{1}$$

is well known from plasma physics. The weakening of the Coulomb potential with decreasing  $r_D=(4\pi\,ne^2/k_BT)^{-1/2}$  (n being the total charge density) implies also a shift of the bound state energies and leads finally to the destruction of the bound system at the so-called Mott density. This is illustrated in Fig. la for a hydrogen atom embedded in a plasma.

However, this picture is wrong if one is interested in the two-particle energy spectrum of the plasma. In fact, the consequent quantum statistical treatment of the two-particle properties leads to the dynamic screening of the potential and to a dynamic self-energy of the particles, which are of equal order of magnitude. Evaluating the shift of the bound state energy 12)

$$\Delta E_{\rm n} = \sum_{\rm p,\,q} \left| \Psi_{\rm n}({\rm p}) - \Psi_{\rm n}({\rm p+q}) \right|^2 \, V({\rm q}) \int \frac{{\rm d}\omega}{\pi} \, {\rm Im} \, \epsilon^{-1}({\rm q},\omega^+) \, \frac{1 + n_{\rm B}(\omega)}{E_{\rm n} - \omega - {\rm p}^2/2m} \ , \label{eq:delta-E}$$

where  $\Psi_{n}(\mathbf{p})$  is the bound state wave function,  $\mathbf{p}$  the relative momentum,  $\mathcal{E}(\mathbf{q},\omega)$  the dielectric function, and  $\mathbf{n}_{\mathrm{B}}(\omega)$  the Bose distribution function, both effects nearly compensate each other, see Fig. 1b. Since the continuum of the scattering states is shifted downwards proportional to  $-\mathrm{e}^{2}/r_{\mathrm{D}}$  (self-energy shift), the bound state energy merges at the Mott density the continuum edge. This predicted behaviour of the binding energy has been confirmed experimentally for the electron-hole plasma in strongly excited semiconductors  $^{13}$ .

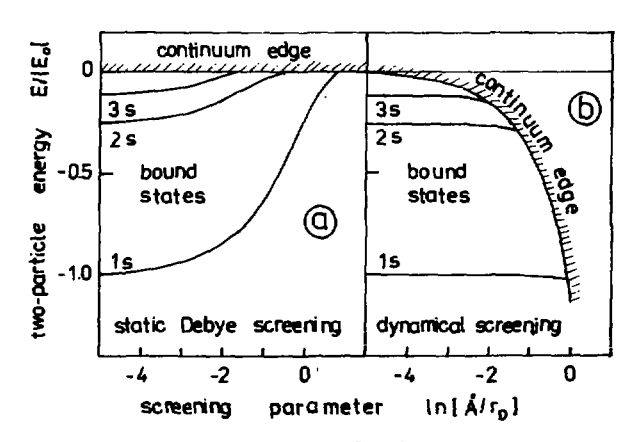


Fig. 1. Two-perticle energies in a Coulombic plasma
(a) statically screened Coulomb potential (Debye screening)
(b) dynamic screening and dynamic self-energy for the
Coulomb interaction, Ref. 12). E<sub>O</sub> - ground state energy of
the hydrogen atom; temperature k<sub>B</sub>T = 0.1 | E<sub>O</sub>|.

# (ii) Plesme with confinement interaction

According to the concept of a statically screened potential (1), an effective in-medium  $q \bar q$  potential

$$V(r,\mu) = (G/\mu)(1-\exp(-\mu r)) - (d/r)\exp(-\mu r)$$
 (2)

has been proposed<sup>8)</sup>, where  $G = 0.192 \text{ GeV}^2$  is the string tension and  $\Delta = 0.4^{-1}$  denotes the coupling constant. The screening parameter is supposed to be a function of the temperature<sup>8)</sup>. The numerical solution of the Schrödinger equation for the potential (2) leads to  $\mu$ -dependent values for the binding energies and to critical values  $\mu_c$ -where the bound states disappear<sup>8)</sup>, see Fig. 2a.

To develop a quentum statistical approach to a many-quark system, the methods worked out for ordinary Coulomb plasmas cannot immediately be applied because of the confinement nature of the quark interaction. However, it was possible to treat the many-quark system by introducing the concept of saturation of the quark-quark interaction within color-neutral clusters 14).

For given quark positions, an arbitrary decomposition into clusters (qqq or  $q\bar{q}$ ) which are color neutral, corresponds to a special string configuration. The potential energy of the many-quark system is given by the string configuration with the minimum interaction energy (most probable string configuration). This so-celled matching problem<sup>15)</sup> is similar to the resonating valence bond model of high  $T_c$  superconductivity  $t_c^{16}$ .

Evidently, for a single (color neutral) hadron the results of the quark potential model are immediately recovered. For the two-nucleon problem, spurious color- van der Waels int actions are avoided similar to the string-flip model of Lenz et al. 17). A treatment of the many-quark system using the concept of the next neighbour distribution function was given in Ref. 14, and properties of the hadronic phase as well as the transition to the quark matter phase have been described.

The energy spectra of two-particle  $c\bar{c}$  and  $b\bar{b}$  states within the model of saturated quark confinement interaction are given in Fig. 2b as a function of the temperature. Similar to the Coulomb plasma, see Fig. 1b, the bound states are not shifted as long as there is no stringflip, and the Pauli blocking is not operative because of the low density of the heavy quarks. This is in contrast to the strong medium dependence of the binding energy displayed in Fig. 2a for the

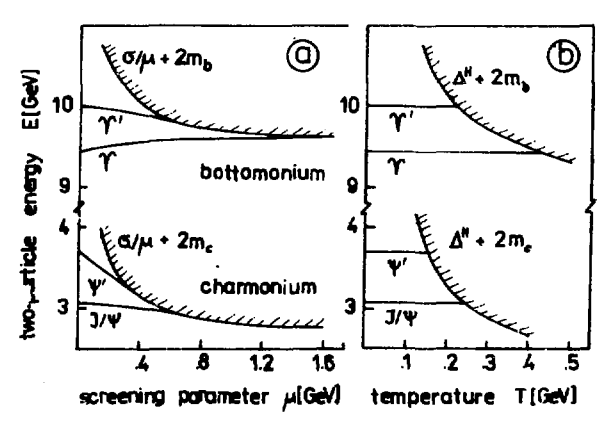


Fig. 2. Two-particle energies of heavy quarkonia in a querk plasma (a) static screening model (Ref. 8) (b) color-saturated interaction model (Refs. 11, 14).

static screening model. In contrast to the bound states, the scattering states (quasifree quarks) show a shift depending on the density of cuarks. Supposing the usual Cornell form of the  $q\bar{q}$  potential ( $\mu=C$  in Eq. (2)), one obtains for the Hertree approximation of the self-energy 11,14,16)

$$\Delta^{\rm it} = (3/4\pi)^{1/3} \left[ (4/3)6 \, n_{\rm q}^{-1/3} - (4\pi/9)^{1/3} \right] \left[ (2/3) \, \alpha \, n_{\rm q}^{1/3} \, . \quad (3)$$

At zero baryon number density, the density of quarks with flavor f is determined by the temperature according to

$$u_{\mathbf{f}}(\mathbf{T}) = \epsilon \int \frac{d^3p}{(2\pi\hbar)^3} \left\{ \exp\left[ ((p^2c^2 + m_{\mathbf{f}}^2c^4)^{1/2} + \Delta^{\mathbf{H}})/k_{\mathbf{B}}^{\mathbf{T}} \right] + 1 \right\}^{-1},$$
 (4)

where the quark masses (in GeV) are  $m_u=m_d=0.3$ ,  $m_s=0.5$ ,  $m_c=1.32$ , and  $m_b=4.75$ . Compared with the static screened potential (2), see Fig. 2a, the shift (3) of the two-particle continuum edge is directly related to the temperature of the plasma.

As can be seen from Fig. ?b, at low densities  $n_q \xrightarrow{} 0$  the formation of quasifree quarks is prohibited because of  $\stackrel{\sim}{\triangle}^H \xrightarrow{} \infty$ . According to Ref. 18, the Latt trensition to the quark gluon lasma where the light quarks move quasi freely occurs at a temperature of about  $T_c$  200 keV. At this temperature, heavy quark bound states (J/ $\psi$  and  $\gamma$ ) are stable, so that their dissolution due to the Mott effect will take place at still higher values of the temperature.

However, in the mel equilibrium the density of heavy quarkonia is low because of the thermal activation and the formation of open charm mesons, see Ref. 11. As is well known, the degree of dissociation of cc (bb) into quasi-free heavy quarks (where the string interaction is saturated by the surrounding light quarks) is given by the law of mass action

$$\frac{n_{J/\Psi}}{n_{c} \cdot n_{\bar{c}}} = \frac{\Lambda_{c}^{3}}{3 \sqrt{2}} e^{-(E_{J/\Psi} - 2m_{c} - \Delta^{H})/k_{B}T} , \quad \Lambda_{c}^{2} = 2\pi \hbar^{2}/m_{c}k_{B}T .$$

Since the density  $n_c=n_{\overline{c}}$  of charmed quarks is very low, the degree of dissociation  $n_c/(n_c+n_{J/\psi})$  is close to unity. But this chemical equilibrium state will not be attained if the plasma phase has only a short lifetime. Therefore we have to apply reaction kinetics to describe the time evolution of the chemical state of the plasma.

### 3. Reaction kinetics

After the formation of cc pairs at short distances due to hard collisions in the initial stage of the plasma cc bound states break off due to string flip processes to light querks of the surrounding. Considering the dissociated cc pair as an activation complex, the Eyring theory describes the strong tendency to the dissolution of cc pairs because of the large entropy factor, if thermodynamic equilibrium between the bound charmonium and the activated complex persists.

We apply the collision theory to estimate the reaction coefficient for the string flip process from a  $\Im Z$  bound state (Q=c,b) to another quark q (q=u,d,s) of the surrounding plasma of quasifree light quarks. This string flip to an open charm meson (quasifree heavy quark) occurs if the light quark is found at a distance which is smaller than the Q- $\bar Z$  distance of the bound quarkonium state. In this way, the string flip cross section is given by  $\sigma_Q=\pi r_Q^2$ , where we take for the quarkonia radii  $r_{J/\psi}=0.453$  fm,  $r_{\psi}=0.875$  fm and  $r_{\gamma}=0.226$  fm. The frequency factor for reactive collisions between bound heavy quarks and quasi-free light ones is given by

$$\tau_{\bar{q}}^{-1} = \sum_{\bar{q}} \int \frac{d^3p}{(2\pi\hbar)^3} \, G^*(p) \, v \, f_{\bar{q}}(p) \,,$$

where v is the relative velocity,  $f_{\overline{q}}(p)$  is the quark distribution function for  $\overline{q}$ , (cf. Eq. (4)) and the reactive cross section  $\mathfrak{S}^{\star}(p)$  accounts only for such collisions which lead to a reaction process. As usual, we assume that only such collisions give a reaction where the transferred kinetic energy exceeds a threshold value  $\Delta E_Q(T) = E_{QQ} - 2m_Q - \Delta^H(T)$  given by the dissociation energy of the bound meson into quasi-free states. As is well known from reaction kinetics, the frequency factor of reactive collisions (in quasiclassical approximation) is given by

where  $\mu_{Q\bar{q}} = m_{Q\bar{Q}} m_{\bar{q}}/(m_{Q\bar{Q}} + m_{\bar{q}})$  is the reduced mass of the quarkonium - quark collision and the light quark density  $n_{\bar{q}}(T)$  is given by Eq. (4). Since the color is fixed (color neutrality of the clusters), we have to consider only two spin directions and the different flavors. The mean time between two reactive collisions  $\tau_{Q}$  is displayed in Fig. 3 as a function of the plasma temperature T for the J/ $\Psi$ ,  $\Psi'$  and

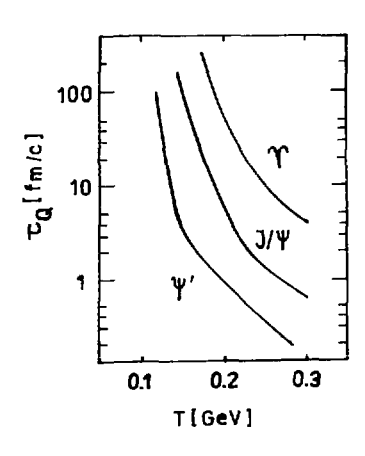


Fig. 3. Mean time interval between reactive collisions t as function of the plasma temperature T for different quarkonia states (5).

 $\gamma$  states resp., where the values for the quarkonia radii given above and the dissociation energy  $\Delta E_Q(T)$  from Fig. 2b have been used. The larger value of  $\tau_{\gamma}$  when compared with  $\tau_{J/\Psi}$  or  $\tau_{\Psi'}$  results from both the smaller value of  $r_{\gamma}$  and the larger value of the dissociation energy.

## 4. Application to high-energy nucleus-nucleus collisions

Applying this model to high-energy nucleus-nucleus collisions, we have to take into account the spacetime evolution of the plasma. For small  $x_p$ , i.e. small values of the longitudinal momentum, the extension of the plasma  $R(T_c,t)$  is characterised by the critical isotherm  $T_c$  according to  $R(T_c,t)=R_0(1-(t/t_m)^2)^{1/2}$ . Here  $R_0$  is taken as the radius of the projectile  $(R_0=1.2~\text{A}^{1/3})$  fm) and  $t_m$  is the plasma lifetime. Taking the r dependence of the initial heavy quark density in the z=0 plane  $\frac{9}{2}$  as  $\frac{2}{3}q(r)=\frac{2}{3}\frac{9}{3}(1-(r/R_0)^2)^{1/2}$ , one obtains for the suppression ratio  $\frac{19}{3}$ 

$$R_{Q}(p_{T}) = \frac{\int_{0}^{R_{0}} r dr \int_{0}^{2\pi} d\vartheta \, g_{Q}(r) \exp(-t_{Q}/\tau_{Q})}{\int_{0}^{R_{0}} 2\pi r \, g_{Q}(r) dr}, \qquad (6)$$

where  $t_Q(r, \mathcal{K}_{\mathfrak{p}_T})$  is the time of flight across the plasma for a heavy quarkonium (Q) with momentum  $p_T$ , which is emitted at distance r in the direction  $\mathcal{K}$  relatively to the axis 0-r.

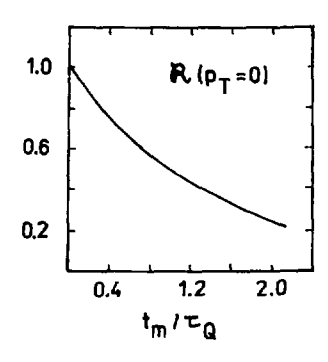


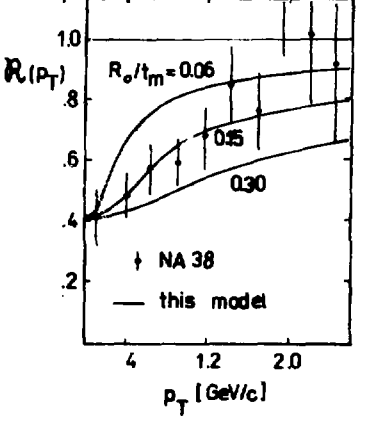
Fig. 4. Suppression ratio at venishing transverse momentum as a function of the mean number of reactive collisions  $N_Q = t_m/T_Q$ , cf. Eq. (7).

For  $p_m=0$ , the suppression is solely determined by the mean number of reactive collisions  $N_Q=t_m/\tau_Q$  during the plasma lifetime according to (cf. Fig. 4)

$$\mathcal{R}_{\mathbf{Q}}(\mathbf{p}_{\mathbf{T}}=0) = 6 \, N_{\mathbf{Q}}^{-3} \, (1 - e^{-N_{\mathbf{Q}}} (1 + N_{\mathbf{Q}} + N_{\mathbf{Q}}^2/2)) \, .$$
 (7)

For finite values of  $p_{\rm T}$ , the "speed" of the critical isotherm  $R_{\rm O}/t_{\rm m}$  occurs as the second parameter of the given approach characterising the shape of the  $\mathcal{R}(p_{\rm T})$  dependence as indicated in Fig. 5. For example, a good fit between recent experimental data of  $^{16}{\rm O+U}$  collisions and theoretical results (6) is found for  $N_{\rm Q}$ = 1.2 ( $\mathcal{R}(0)$ = 0.42) and  $R_{\rm O}/t_{\rm m}$ =0.15 c , see Fig. 5.

Fig. 5. Suppression ratio  $\mathcal{R}_{\mathbf{Q}}(\mathbf{p_{\mathbf{T}}})$  as a function of the transverse momentum. Dots with error bars: NA38 data (Ref. 3) for 0+U collisions. Full lines: model predictions for J/V suppression (6) with NJ/V =1.2 and different values of  $\mathbf{R_{O}}/\mathbf{t_{\mathbf{R}}}$  (in units of c).



For a plasme radius  $R_o=$  3 fm (corresponding to the radius of  $^{16}\text{O})$ ,  $t_{\rm m}=$  20 fm/c results for the plasma lifetime, and for the inverse collision frequency  $\tau_{x/\psi} = 16.6$  fm/c follows. According to Fig. 3, one obtains T = 175 NeV for the plasma temperature. If the radius  $\rm R_o$  of the plasme is increased so that  $\rm R_o/t_m$  is also increased, as it is expected for experiments with  $^{32}\rm S$  beams, the ratio  $\Re\left(p_{m}\right)$  as a function of  $p_{m}$  is flattened, see also Fig. 5. Furthermore, our simple model allows to predict the suppression of other heavy quarkonia. As an example, for the plasma parameters T = 175 MeV, t = 20 fm/c as derived from the J/Y suppression pettern, the suppression of  $\Upsilon$  is expected to be small ( $\Re_{\Upsilon}(p_m=0)=0.93$ ) whereas the V' state is elmost suppressed ( $\mathcal{R}_{\Psi'}(p_m=0) = 0.003$ ). Of course, our model can be improved by the account of excited quarkonia states, the xm-dependence and a refinement of the hydrodynamical model. Furthermore, reactions with the hadronic state of matter are completely neglected in the present approach but are indispensable in the vicinity of the quark-hadron phase transition. It is expected from the reactive cross sections of both phases that the possible transition from dense hadronic matter to a quark-gluon plasma phase can be seen in an abrupt change of the Em-dependence of the suppression ratio.

## 5. Conclusions

In conclusion, we presented a model calculation of the suppression of heavy quarkonia states based on a quantum statistical treatment of the many-quark system 14, which is an improved version of the more phenomenological static screening model introduced by Matsui and Satz 1,8. Instead of the quantum-mechanically not well founded concept of the formation time of a bound state, we describe the suppression of heavy quark bound states within the framework of chemical reaction kinetics which is also more coherent to other conventional approaches 4. Our simple model allows to extract the parameters of the possible plasma phase immediately from the experimental suppression patterns which are observed in different reactions 2,3,20. The estimations given here for the plasma lifetime and the plasma temperature differ from those of the static screening model 7-10, but correspond to expectations of the duration of the mixed phase during the plasma rehadronisation (see Refs. 21-23).

One of us (D.E.) is indebted to the Joint Institute for Nuclear Research for kind hospitality extended to him during the seminar.

## References

- 1) T. Matsui and H. Satz, Phys. Lett. 178B, 416 (1986).
- 2) k. C. Abreu et al. NA38 Collab., Z. Fhys. C38, 117 (1988).
- 3) 1. kluberg, lecture at this conference.
- 4) S. Gavin, M. Gyulassy and A. Jackson, LEL Report No. LEL-24790, 1988 (to be published).
- A. Gapella, J. A. Gasado, C. Fajares, A. V. Remallo and J. Tran. Than Van, Phys. Lett. B206, 354 (1908).
- 6) J. Ftečnik, P. Lichard and J. Pisut, Eratislava Report No. COLI/ TH 88-1, 1988 (to be published).
- 7) F. Kersch and R. Fetronzio, Z. Phys. C37, 627 (1988).
- 8) F. Karsch, M. T. Mehr and H. Satz, Z. Phys. C37, 617 (1988).
- 9) J. P. Blaizot and J. Y. Ollitrault, Phys. Lett. 5199, 499 (1987).
- 10) P. V. Ruuskanen and H. Satz, Z. Phys. C37, 623 (1988).
- 11) G. Röpke, D. Blaschke and H. Schulz, Phys. Lett. <u>B202</u>, 479 (1988).
- 12) W. D. Kraeft, D. Kremp, W. Ebeling and G. Röpke, Quantum Statistics of Charged Particle Systems (Plenum, New York, 1986).
- G. W. Fehrenbach, W. Schäfer, J. Treusch and R. G. Ulbrich, Phys. Rev. Lett. 49, 1281 (1982).
- 14) G. Röpke, D. Blaschke and H. Schulz, Phys. Rev. <u>D34</u>, 3499 (1986).
- 15) M. Mézard and G. Parisi, J. Physique Lett. 46, L-771 (1985).
- 16) F. W. Anderson, G. Baskeran, Z. Zou and T. Hsu, Phys. Rev. Lett. 58, 2790 (1987) and references therein.
- 17) F. Lenz, J. T. Londergan, E. J. Moniz, R. Rosenfelder, M. Stingl and K. Yazaki, Ann. Phys. (NY) 170, 65 (1986).
- 18) D. Blaschke, F. Reinholz, G. Röpke and D. Kremp, Phys. Lett. 1518, 439 (1985).
- 19) G. Röpke, D. Blaschke and H. Schulz, Phys. Rev. Lett. submitted.
- 20) S. Katsanevas et al., Phys. Rev. Lett. <u>60</u>, 2121 (1988).
- 21) J. Kapusta, Phys. Rev. <u>D36</u>, 2857 (1987).
- T. Matsui, B. Svetitsky and L. Mc Lerran, Phys. Rev. <u>D34</u>, 783, 2047 (1986).
- H. W. Barz, B. Friman, J. knoll and H. Schulz, Nucl. Phys. A (in press).

# POSSIBLE MANIFESTATION OF QUARK-GLUON PLASMA IN DEEP INFLASTIC NUCLEAR REACTIONS

V.B. Gavrilov, S.A. Gerzon, Yu.T. Kiselev, G.A. Leksin, A.V. Smirnitsky INSTITUTE OF THEORETICAL AND EXPERIMENTAL PHYSICS. MOSCOW

It is known that quantum chromodynamics predicts that hadronic matter should be in a quark-gluon plasma (QGP) state when its energy density and/or its baryon number density are sufficiently high. Theory suggests that these conditions may be achieved for high energy nuclear reactions if specific energy deposition is higher than 2GeV/fm³ and subsequent thermalization of the excited system takes place.

There are various evidences of high local energy deposition in deep inelastic hadron-nucleus reactions (DINR) at initial energy higher than several GeV. Experimental data analysis allows to say that high energy hadron passing through nuclear matter deposits energy about

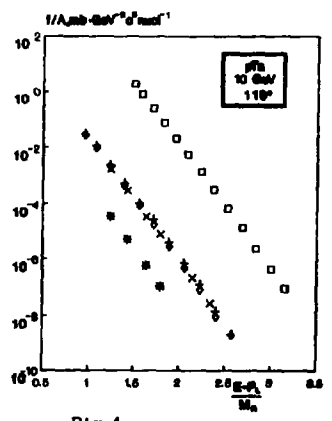
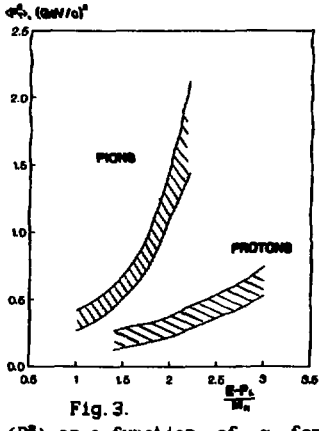


Fig. 1.  $f/A=Ed\sigma/(Ad^2p)$  as a function of  $\alpha=(E-P_L)/M_L$  for  $p(\Omega)$ ,  $\pi^+(+)$ ,  $\pi^-(+)$ ,  $k^+(\times)$  and  $k^-(\times)$ emitted at the angle of 119° in pTa interactions at 10GeV.

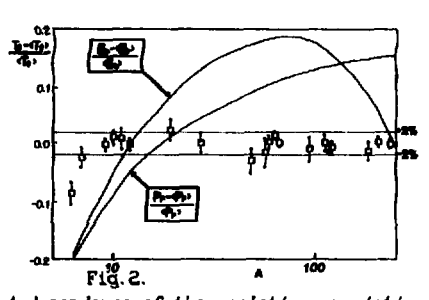
1-2GeV/fm for its excitation, and this excitation takes place near the hadron trajectory in the nucleus 11. Both direct summation of the energies of secondary particles generated at the nucleus fragmentation region and analysis of the energy dependence of cumulative particle production different nucleus lead to the mentiond above value of the energy loss for nuclear matter excitation. Under assumption about that the main part of this energy is deposited within the multiquark bags with radii r<sub>m</sub>≤ r<sub>m</sub> the energy density may reach exceed the value of 2GeV/fm3. In this case baryon number density will be \(\rho\_2\)≥ αρ, where α≈(E-P,)/N, is the light cone variable. Fig. 1 shows an example of f(a) dependence for pTa interaction at 10 GeV.

The data on inclusive particle production in DINR are in accord with scenario of isotropic of emission massless particles (quarks?) by some movina SOUTCE and subsequent hadronization of these particles in nuclear mat.ter The velocity and the temperature of this source are about B=0.5 and VeMOCL=T**Могеочег** the spectra of different  $(p,n,n^{\pm},K^{\pm},\Lambda)$ particles generated in DINR аге similar each others (Fig.1)

/3-7/ (superscaling). It is well known that the slopes of the spectra of particles produced in DINR with the momenta smaller than 1GeV/c do not depend on the atomic weight



 $\langle P_{+}^{a} \rangle$  as a function of  $\alpha$  for pions (m) and protons produced in DINR. The show the systematic errors.



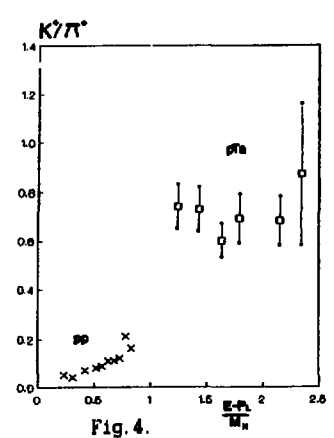
A-dependence of the relative variation of the spectra slopes (  $f \propto \exp(-T/T_s)$  ) for protons with energies 80-240Mg emitted at the angles of 119° and 160° The curves show A-dependences of the relative variations of the binding energy  $(E_{\rm p})$  and Fermi momentum  $(P_{\rm p})$ .

of target nucleus. This fact is established with an accuracy of 1-2% (Fig. 2) 8 and indicates to the locality of the process of matter excitation by high hadron.

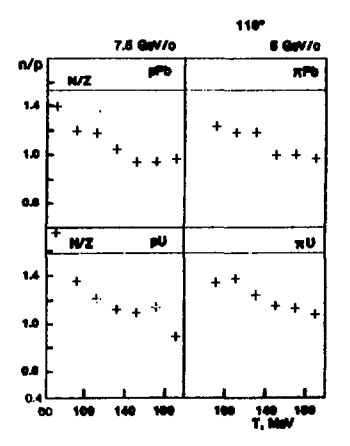
> the characteristic most. signatures of QGP there the following:

- 1. The increase of  $\langle P_{+}^2 \rangle$  with energy density exceeding threshold value.
- Enhancement of the particle production with respect to "ordinary" hadron-hadron interactions.

The experimental data show that these signatures are observed in DIMR. increase of  $\langle P_{\pi}^a \rangle$  up to the values of 1-2(GeV/c)2 with the increase of the light cone variable  $\alpha$  was observed for cumulative protons and pions 5(Fig. 3).



 $f(K^+)/f(\pi^+)$  ratio as a function of  $\alpha$  for pp  $(\bowtie)$  and pTa interactions.



of ratio the inclusive cross-sections for cumulative K+ and  $\pi^+$  production on the heavy nuclei is about 1 whereas for pp interactions the same ratio is about. 0.1 - 0.2(Fig. 4)  $^{4,6,9}$ . The enhancement of  $\Lambda$ production in DINR was also observed The isosymmetrization of yields of neutrons and protons heavy nuclei which was observed DINR (Fig. 5) 10/ may become signature of OGP.

Finally, in DINR incident particle interacts with multiquark bags in nuclei and the observed properties of these reactions are similar to those which are usually attributed to QGP. If QGP is indeed generated in DINR, it is generated as small droplets of baryon-saturated QGP differing from barion-neutral QGP which is expected to be generated at the central rapidity region for ultra-relativistic nucleus-nucleus interactions.

Fig. 5. n/p ratio as a function of nucleon energy for nucleon production at the angle of 119° in pA and  $\pi^{\pm}A$  interactions 10′.

## REFERENCES:

- V. B. Gavrilov, G. A. Leksin, ITEP-86,1986;
   PANIC'87, Abstract Book I,c-17,Kyoto,1987.
- 2) V. G. Neudatchin, Yu. M. Tchuvil'sky, Yad. Fiz., v. 46, 448, 1987.
- Yu. D. Bayukov et al., Sov. J. Nucl. Phys., v. 33, 94, 1981;
   M. V. Kossov, L. M. Voronina, ITEP-165, 1984.
- 4) A.M. Baldin et al., JINR-E1-82-472,1982; JINR-P1-83-432,1983.
- 5) S. V. Boyarinov et al., Yad. Fiz. v. 46, 1472, 1987.
- 6) S. V. Boyarinov et al., ITEP-13,1988.
- 7) L.S. Vorobyov et al., ITEP-126,1987.
- V.B. Gavrilov et al., ITEP-96,1985;
   PANIC'87. Abstract Book I.c-16.Kyoto.1987.
- 9) S. A. Gerzon, Yu. T. Kiselev, 1TEP-55, 1984.
- Yu. D. Bayukov et al., Sov. J. Nucl. Phys., v. 41, 101, 1985;
   PANIC, Book of Abstracts, v. 1, E-9, Heidelberg, 1984.

#### RECENT RESULTS FROM THE CDF DETECTOR AT FERMILAB

The CDF Collaboration\*

presented by

Lee G. Pondrom

The University of Wisconsin Madison, Wisconsin, USA

#### I. Introduction

The Tevatron Collider program at Fermilab had its first extended run from January through May of 1987. The energy of the Tevatron superconducting storage ring was 900 GeV. The Tevatron shared its tunnel with the conventional magnet main ring, which accelerated protons to 150 GeV on a 2 sec cycle to produce antiprotons. The antiprotons were captured, cooled, and accumulated at 8 GeV in a two ring facility called the antiproton source. The antiproton current stored in the source corresponded to  $\sim 3 \times 10^{11}$  antiprotons. The peak luminosity achieved during the run for proton-antiproton collisions was  $10^{29}$ cm -2 sec-1 at an center of mass energy  $\sqrt{s} \approx 1.8$  TeV.

The CDF detector was used to collect the p-p collision data described in this report. An overpass was installed for the main ring in the collision hall so that the 150 GeV beam passed 7 m above the Tevatron, over the top of the CDF apparatus. The overpass reduced the problem of backgrounds from main ring radiation - an important consideration since the antiproton source was fed continuously during a Tevatron colliding beam store. The luminosity lifetime in the Tevatron was about 10 hours. Beams were dumped and a new store inserted roughly once every 24 hours. The total integrated luminosity delivered to the collision point was 75 nb<sup>-1</sup>, while the CDF detector logged about 33 nb<sup>-1</sup> to tape.

ANL Brandeis - University of Chicago - Fermilab - INFN, Francati - Harvard - University of Illinois - KEK
 - LBL - University of Pennsylvania - INFN, University and Scuola Normale Superiore of Pisa - Purdue - Rockefeller - Rutgers - Pexas A&M - Tsukuba - University of Wisconsin

#### II. The CDF Detector

CDF is a general purpose 4  $\pi$  hadron collider detector, with a solenoidal 1.5 T magnetic field for charged particle tracking and instrumented lead (iron) plates for the measurement of total electromagnetic (hadronic) energy. The origin of the (x,y,z) master right-handed coordinate system was the mid point of the beam-beam collision region, with z directed along the proton beam, x horizontal and y vertical. The collision volume was gaussian in (x,y,z) with  $\sigma_x = \sigma_y = 60$  microns and  $\sigma_z = 40$  cm. The azimuthal angle  $\phi$  was measured in the (x,y) plane relative to the x axis. The polar angle  $\theta$  was converted into pseudorapidity  $\eta = \log(\cot(\theta/2))$ . An average "minimum bias" event had approximately equal numbers of massless particles in equal areas of  $\delta \eta \times \delta \phi$ .

The detector divided into separate regions in  $\eta$ . The central region covered  $|\eta|<1$ . The solenoid, the central tracking chamber, and the central calorimetry were all in this region. The calorimeters were constructed in towers of  $\delta\phi=15^\circ$  and  $\delta\eta=0.1$ , and were composed of plastic scintillator in between sheets of lead or iron. Drift tubes for muon identification were mounted behind the calorimeters, which presented 4.9 absorption lengths to an incident pion. Hadronic calorimetry for  $1<|\eta|<1.3$  was performed by the instrumented end wall of the magnet yoke, which had the same tower geometry and was made of scintillator and iron. Electromagnetic calorimetry between  $1<|\eta|<3.5$  and hadronic calorimetry between  $1.3<|\eta|<3.5$  was achieved with lead/gas proportional chamber or iron/gas proportional chamber systems. Gas sampling was adopted in the forward regions to avoid radiation damage to the scintillator, and to make practical the smaller physical tower sizes required by a constant  $\delta\eta$ . A pair of magnetized iron toroids on each side of the collision point analyzed muons from  $1.9<|\eta|<3.5$ . The design and performance of the detector has been described in a series of instrumentation papers (1).

#### III. The Inclusive Cross Section(2)

Figure 1 shows a detail of the parts of the detector used in the measurement of the transverse momentum spectrum of charged particles for "minimum bias" events. At least one charged particle was required to strike the proton side and the antiproton side beam-beam counter hodoscopes in coincidence with the crossing gate to furnish the minimum bias trigger. This trigger rate also defined the luminosity: at 1.8 TeV a rate of  $4300 \pm 600$  counts/sec =  $10^{29}$  cm-2 sec -1. Data were also obtained at 630 GeV for which a rate of  $3400 \pm 300$  counts/sec =  $10^{29}$  cm-2 sec -1. The uncertainties in these rates come from the error in the extrapolation to 1.8 TeV (3), the monte carlo calculations of the beam-beam counter sensitivity, and errors in the magnitudes of components of the total cross section. 55,700 triggers at 1.8 TeV and 9,400 triggers at 630 GeV comprise the present data sample. The instantaneous luminosity at 1.8 TeV ranged from 2 x  $10^{27}$  to 4 x  $10^{28}$  cm-2 sec-1, and was about 7 x  $10^{26}$  cm-2 sec-1 for the single 630 GeV run.

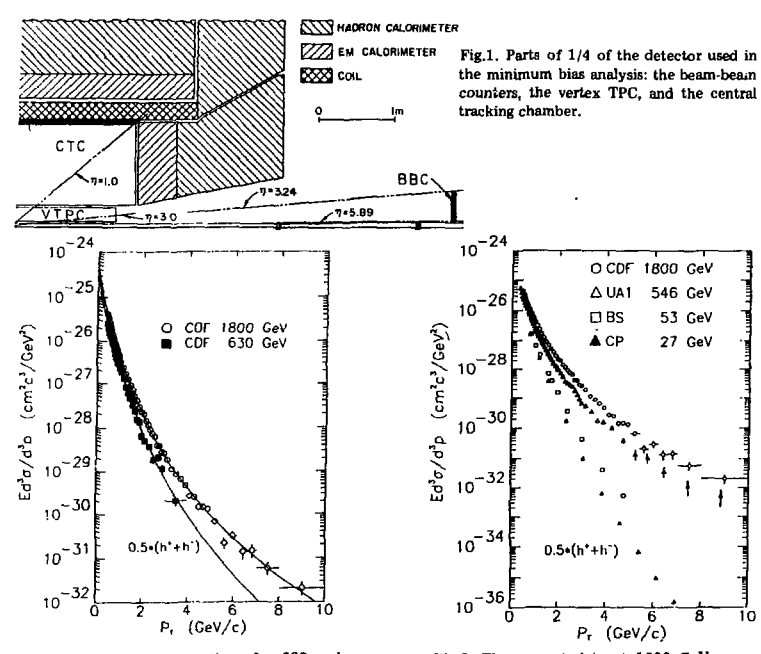


Fig.2. Inclusive cross sections for 630 and 1800 GeV. The solid curves are the fits in Table I.

Fig.3. The present data at 1800 GeV compared with UA1 at 540 GeV, the British-Scandinavian data at 53 GeV (B.Alper et al. Nucl. Phys. B87, 19 (1975)), and Chicago-Princeton data at 27 GeV (D.Antreasyan et al. Phys. Rev. D19, 764 (1979)).

The Vertex Time Projection Chamber (VTPC) was a set of eight small time projection chamber modules used to measure vertex position and the overall event topology. The acceptance of the VTPC depended on the event interaction point but typically extended to  $|\eta| = 3.5$ . The Central Tracking Chamber (CTC) was a drift chamber with 60 axial wire layers and 24 small angle  $(\pm 3^\circ)$  stereo layers in the 1.5 T axial magnetic field. The extreme inner and outer radii of the CTC sense wires were 309 mm and 1320 mm. The momentum resolution was  $\sigma p_1/p_t^2 < 0.003 (GeV/c)^{-1}$  for  $p_t > 1GeV/c$ .

Beam-gas background was eliminated from the data sample by requiring the VTPC vertex to be consistent with the beam-beam counter time of flight, and requiring at least one charged particle in both  $0 < \eta < 3$  and  $-3 < \eta < 0$  with a total of at least 4 charged particles in

the VTPC. Only tracks which traversed the entire radial width of the CTC were retained, corresponding to  $|\eta| < 1$  depending on the vertex position. The reconstruction efficiency for these tracks was 99  $\pm$  1%. The spectra of positive and negative particles were identical within errors independent of  $p_t$ . The  $p_t$  spectrum averaged for both signs of the charge was corrected for depletion from decays in flight, and for an increase due to interactions and decays of neutral strange particles.

Figure 2 shows the CDF data for 630 and 1800 GeV, and Fig 3 compares the CDF 1800 GeV data with results from lower energies. The shape of the CDF 630 GeV data agrees with the measurements of UA1 (4) and UA2 (5) at 546 GeV. The yield of charged particles for  $p_t > 2$  GeV/c increases dramatically as  $\sqrt{s}$  is increased from 27 GeV to 1800 GeV. The invariant cross sections were fit to the functional form

$$Ed^3\sigma/dp^3 = A p_o^n/(p_t + p_o)^n.$$

The results of this fit are given in Table . The parameters  $p_0$  and n are highly correlated. To compare the 630 GeV fit to UA1 (4),  $p_0$  was fixed at 1.3, which gave  $n=8.89\pm0.06$ , in reasonable agreement with the SPS result.

TABLE

$\sqrt{s}$	$A (10^{-24} cm^2/GeV^2)$	Po	n	$\chi^2$	DOF
1800	0.45±0.01	1.29±0.02	8.26±.08	102	64
630	$0.27 \pm 0.01$	1.63±0.13	10.2±.56	32	33
630	0.33±0.01	1.30 fix	8.89±.06	39	34
546(UA1)	0.46±0.01	1.30 fix	9.14±.02	29	32

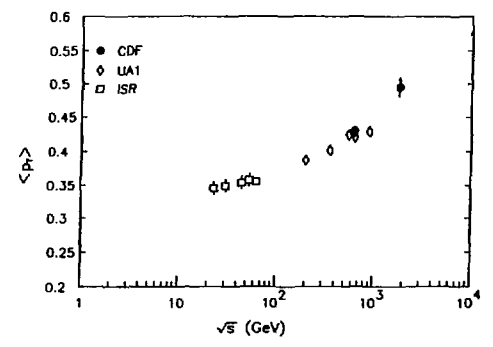


Fig.4. < pt > as a function of center of mass energy up to 1800 GeV.

In order to determine  $< p_i >$  the shape of the spectrum  $d\sigma/dp_i$  must be known as  $p_i \rightarrow 0$ . Data were eliminated for  $p_i < 0.4$  GeV/c. The unmeasured region was constrained, however, by the known multiplicity  $dN/d\eta$ . A preliminary analysis of the VTPC data yields a ratio of  $dN/d\eta$  at 1800 to  $dN/d\eta$  at 630 of 1.27  $\pm 0.04$ . Interpolation of  $dN/d\eta$  measurements at the

SPS between 200 and 900 GeV (6) gives  $dN/d\eta = 3.30 \pm 0.15$  at 630 GeV. These numbers give  $\langle p_t \rangle = 0.432 \pm 0.004$  GeV/c at 630 GeV and 0.495  $\pm$  0.014 GeV/c at 1800 GeV. These results are plotted in Fig. 4, which shows the energy dependence of  $\langle p_t \rangle$  from  $\sqrt{s} = 25$  GeV at the ISR to 1.8 TeV at the Tevatron. The increase in  $\langle p_t \rangle$  with increasing  $\sqrt{s}$  observed at the SPS continues to 1.8 TeV.

#### IV Jet Production

A narrow cone of hadrons emerging from a p-p collision at high  $E_t = E \sin \theta$  is called a jet and is attributed to the fragmentation of a color confined single parton, either a quark or a gluon. The study of these jets furnishes information on the basic parton-parton interaction which occurs within the colliding baryons (7).

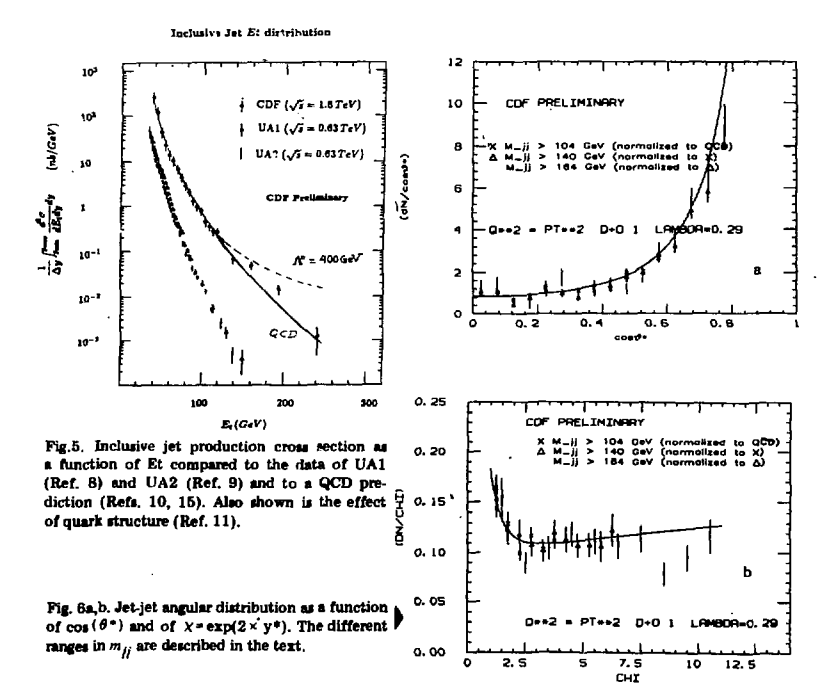
The minimum bias trigger discussed above gave very few events above  $p_t = 8 \text{ GeV/c}$ . The jet trigger was based on total transverse energy  $E_t = (EM + \text{hadronic})$  deposited in the calorimeters. The  $E_t$  threshold setting varied from 20, 30, 40, to 45 GeV depending on the luminosity. The total integrated luminosity for the jet data was 28 nb<sup>-1</sup>. No data was taken which could fill in the gap between the minimum bias results and an  $E_t$  threshold of 20 GeV.

Each of the total  $E_t$  trigger events was studied to search for clusters of towers in the calorimeter. All of the transverse energy deposited in a cone of radius R=0.6 in  $\eta-\phi$  space around a seed tower with  $E_t>2$  GeV defined a cluster. The cluster energy was then corrected for the non-linear response to low energy pions and for energy losses caused by tower boundaries and shower leakage. These corrections raised the  $E_t$  values at the lower end by  $15\pm 5$  GeV, and by  $36\pm 8$  GeV at  $E_t=200$  GeV. The errors represent systematic uncertainty. An event was used in the analysis if the total  $E_t$  in a cluster in that event exceeded the trigger threshold.

Cosmic ray bursts and background from the main ring overpass were eliminated from the high  $E_t$  end of the spectrum by rejecting events where a significant amount of energy was not in time with the beam crossing. An additional set of cuts was applied to events with  $E_t > 70$  GeV to further suppress contributions to the measured energy from spurious sources: 0.1 < (Em/TOTAL) < 0.95; 0.1 < (visible charged/TOTAL); and  $(E_t \text{ missing}/\sqrt{E_t}) < 4.8 (\text{GeV})^{1/2}$ . The first two cuts refer to the charged, neutral, and electromagnetic energy balance in the jet, and the third to the  $E_t$  balance in the event as a whole. These cuts eliminated 99% of the backgrounds while leaving the true jet cross section unaffected. The data sample was further restricted by requiring |zvertex| < 60 cm and  $|\eta$  (jet centroid)| < 0.7, 24000 events remained.

In addition to the uncertainty in luminosity described in Sec III, the inclusive jet cross section was affected by the finite energy resolution, which tended to flatten the shape, and by the uncertainty in energy scale, which could shift the curve to the right or left and thus appear as a normalization error on a steeply falling cross section. The jet energy resolution was measured by balancing the  $E_t$  of jet pairs, and the cross section curve was corrected for this effect. The combined normalization uncertainty was 50%.

Figure 5 shows the resulting inclusive jet cross section as a function of  $E_t$  compared to the data of UA1 (8) and UA2 (9) and to a curve predicted by QCD. Although the total integrated luminosity in this experiment is less than 10% of that obtained by UA1 and UA2, the increase in energy compensated, so that comparable data were obtained at high  $E_t$ . The QCD calculation used  $2 \rightarrow 2$  parton scattering and Duke-Owens I structure functions evaluated at  $Q^2 = (E_t)^2$  (10). The QCD curve was normalized to the data below  $E_t = 80$  GeV by multiplying the calculated cross section by 1.2, a factor consistent with the overall normalization uncertainty of the experimental data. The predicted cross section for composite quarks is also plotted in Fig 5, normalized the same way as the point-like QCD curve. The composite cross section is based on a four fermion interaction of the form described in Ref (11) with a mass scale of 400 GeV. This scale characterizes the strength of the binding and the size of composite states.



Final analysis of these data should give a lower limit for lambda at the 90% confidence level in the range of several hundred GeV.

The jet-jet angular distribution in the center of mass of the parton-parton collision,  $dN/d\cos(\theta^*)$ , is characterized by the angular distribution of the fundamental  $2 \to 2$  parton cross section. Although there are nine elementary reactions involving quarks, antiquarks, and gluons (12), the angular distributions are remarkably similar both to one another and to the cross section for Rutherford scattering, particularly in the region of the Coulomb pole as  $\theta \to 0$  (13). Further restrictions were placed on the inclusive jet data sample for the angular distribution analysis. One jet of  $E_t > 45$  GeV was required with  $|\eta| < 0.7$ , i.e. well contained within the central calorimetry. The azimuthal angle of the centroid of the recoil jet was required to be at  $180 \pm 20^\circ$ . A total of 4890 events remained.

If  $y_1$  and  $y_2$  are the rapidities of the two jets in the laboratory, then  $y^* = (y_1 - y_2)/2$  is the rapidity of jet #1 in the jet-jet center of mass, and  $\cos(\theta^*) = \tanh(y^*)$ . It was desirable to choose a range in  $\cos(\theta^*)$  over which the detector acceptance was uniform. This was done by calculating the minimum di-jet invariant mass  $m_{jj}$  for a given maximum value of  $\cos(\theta^*)$ :  $m_{jj} = 2 \times E_{lmin} / \sin(\theta^*)$ , where  $E_{lmin} = 45$  GeV. Thus for the range  $0 < \cos(\theta^*) < 0.6$ ,  $m_{jj} > 144$  GeV; for  $0 < \cos(\theta^*) < 0.76$ ,  $m_{jj} > 140$  GeV; and for  $0 < \cos(\theta^*) < 0.83$ ,  $m_{jj} > 164$  GeV. Lower mass data would be accepted only near  $\cos(\theta^*) = 0$  and hence would distort the curve. The highest mass bin  $m_{jj} > 164$  GeV covered the entire range in  $\cos(\theta^*)$ , but had limited statistics. Figure 6a shows the  $\cos(\theta^*)$  distributions for the three different choices of  $m_{jj}$ . The QCD curve, normalized to the 114 GeV data, was calculated using the set I structure functions of Ref (10). Figure 6b shows the same data plotted in terms of the variable  $\chi = e^{2y}$ , which expands the region near  $\cos(\theta^*) = 1$ .

#### V. W\* PRODUCTION

The production of  $W^{\pm}$  weak intermediate bosons in  $\bar{p}-p$  collisions proceeds according to the standard model via quark-antiquark annihilation (14). This process is simpler than the jet-jet reaction discussed in Sec IV because the basic partons are limited to  $q\bar{q}$ - gluons are restricted to the role of radiative corrections - and because there are no final state interactions in the  $W \to e \nu$  mode.

The characteristic topology for  $p + p \to W \to e\nu$  is a high transverse momentum electron and a balancing amount of missing transverse energy which one ascribes to the neutrino. Most of the events are very clean, with little other hadronic activity and an isolated high  $E_t$  electron. No other visible energy balances the electron  $E_t$ .

The same data sample as was used in the jet analysis described above was searched for  $W^{\pm}$  candidates. The strategy for this search was based on missing  $E_t$  in the calorimetry. For each event a total missing  $E_t$  was defined:  $E_t = \Sigma_t \vec{E}_{it}$ .

Since a dominant source of  $\mathcal{B}_t$  was mismeasured jet events, the variable  $S = \mathcal{B}_t / \sqrt{E_t}$  was useful. Starting with 400,000 jet triggers, corresponding to an integrated luminosity of 25 nb<sup>-1</sup>, the following cuts were applied:  $\mathcal{B}_t > 25$  GeV  $\rightarrow$  4178 events; at least one jet (presumably the electron) with  $E_t > 15$  GeV  $\rightarrow$  1604 events;  $\mathcal{B}_t / \sqrt{E_t} > 2.8$ , no jet opposite the first one at 180 °  $\pm$  30°, and a timing cut to eliminate cosmic rays  $\rightarrow$  115 events. Finally two electron requirements were placed on the jet: (EM energy)  $> 0.85 \times E_t$ , and a single track of measured momentum p pointing to the center of the EM shower with E/p < 2, after which 22 events remained. Figure 7 shows a plot of E/p for these 22 events. The tail at high E/p is consistent with bremmstrahlung of the electron before the momentum measurement where the radiated photon is included in the shower E. Figure 8 shows the transverse mass distribution for these events, compared with an expected curve for  $M_W = 83$  GeV (14).

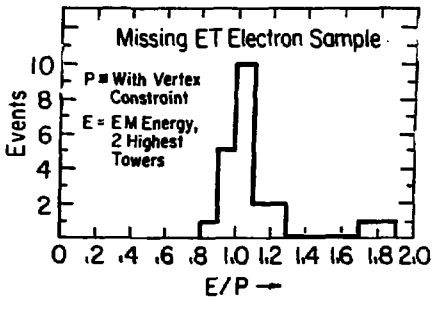


Fig.7. E/p for the 22 electron candidates obtained by scanning the data for missing  $E_t$ .

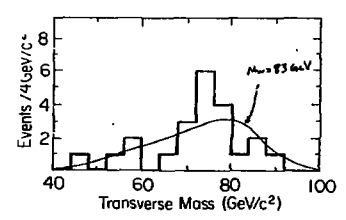
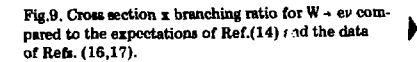
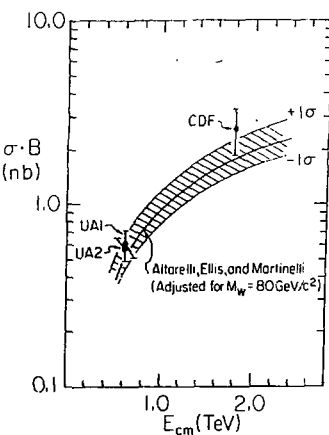


Fig.8. The 22 electron candidates plotted as a function of the variable  $M_1 = \sqrt{2(E_L \nu \times E_r e - p_I^2 \nu \cdot P_r^2 e)}$ . The data favor a slightly lower value for Mw = 80 GeV than was used in the theoretical curve.





The cross section for  $W^{\pm}$  production  $\times$  the branching ratio for decay into  $e \nu$  can be calculated from these 22 events and the 25 nb<sup>-1</sup> integrated luminosity. The events were required to have  $|\eta| < 1$ , which should contain (50 ± 5)% of all  $W \rightarrow e \nu$  events according to calculation (15). Monte carlo studies indicated that the other cuts imposed on the data sample should reduce this efficiency to (33 ± 3)%. Hence 22 ± 4.7 events  $\rightarrow$  66 ± 14 events total, and  $\sigma \times B(W \rightarrow e \nu) = 2.60 \pm 0.56 \pm 0.4$  nb, where the  $\pm$  0.4 comes from a 15% uncertainty in the 1.8 TeV normalization quoted in Sec III above. This result is plotted in Fig. 9 together w. the UA1 (16) and UA2 (17) 630 GeV numbers and the standard model expectation calculated by Ref (14). The agreement between experiment and calculation is satisfactory.

#### REFERENCES

- For calorimetry see CDF Collaboration, Nucl. Instr. Meth. A267, pp249-351 (1988); for tracking and muons see Ibid. A268, pp24-92 (1988); and for electronics and trigger see Ibid. A269, pp33-93 (1988).
- For a more complete report, see F. Abe et al. (CDF Collaboration) Phys Rev Lett 61 (to be published).
- G. Arnison et al. (UA1 Collaboration) Phys Lett 128B, 336 (1983); and R. Ansorge et al. (UA5 Collaboration), Z. Phys. C 33, 175 (1986).
- 4. G. Arnison et al. (UA1 Collaboration) Phys Lett 118B, 167 (1982).
- 5. M. Banner et al. (UA2 Collaboration) Z. Phys C 27, 329 (1985).
- 6. G. Ekspong, Nucl Phys A461, 145 (1987).
- F. Halzen, in Proceedings of the Oregon Annual Meeting of the Division of Particles and Fields of the American Physical Society, edited by R. Hwa, (World Scientific, Singapore, 1986) p 529.
- 8. G. Arnison et al. (UA1 Collaboration) Phys Lett 172B, 461 (1986).
- 9. J. Appel et al. (UA2 Collaboration) Phys Lett 160B, 349 (1985).
- 10. D. W. Duke and J. F. Owens, Phys Rev D 30, 49 (1984).
- 11. E. Eichten, K. Lane, and M. reskin, Phys Rev Lett 50, 811 (1983).
- B. L. Combridge, J. Kripfganz, and J. Ranft, Phys Lett 70B, 234 (1977).
- 13. J. R. Cudell, F. Halzen, and C. S. Kim Int Journ Mod Phys A3, 1051 (1988).
- G. Altarelli et al. Nucl Phys B246, 12 (1984); and G. Altarelli, K. Ellis, and G. Martinelli, Z Phys C27, 617 (1985).
- F. Paige and S. D. Protopopescu, ISAJET Monte Carlo, Brookhaven National Laboratory Report BNL 3804 (1986, unpublished)
- G. Arnison et al. (UA1 Collaboration) Phys Lett 166B, 484 (1986). See also K. Eggert in Physics in Collision 7, Tsukuba Japan 1987, edited by T. Kondo and K. Takahashi (World Scientific, Singapore, 1988) p 209.
- P. Bagnaia et al. (UA2 Collaboration) Z. Phys C 24, 1 (1984). See also J. Repellin in Physics in Collision 7, Tsukuba Japan 1987, edited by T. Kondo and K Takahashi (World Scientific, Singapore, 1988) p 235.

#### ANTIPROTON INTERACTIONS WITH LIGHT NUCLEI AT LEAR ENERGIES

Yu.A.Batusov, S.A.Bunyatov, I.V.Falomkin, F.Nichitiu, G.B.Pontecorvo, A.M.Rozhdestvensky, M.G.Sapozhnikov, V.I.Tretyak
Joint Institute for Nuclear Research, Dubna

F.Balestra, S.Bossolasco, M.P.Bussa, L.Busso, E.Fioramonti, L.Ferrero, A.Grasso, D.Panzieri, G.Piragino, F.Tosello Istituto di Fisica Generale A.Avogadro", University of Turin, INFN-Sezione di Torino, Italy

R.Barbieri, G.Bendiscioli, A.Rotondi, P.Salvini, A.Zenoni Dipartimento di Fisica Nupleare e Teorica, University of Pavia and INFN, Sezione di Pavia, Italy

C.Guaraldo, A.Maggiora Laboratori Nazionali di Frascati dell'INFN, Frascati, Italy

E. Lodi Rizzini Dipartimento di Automazione Industriale, University of Brecia and INFN, Sezione di Pavia, Italy

A.Haatuft, A.Halsteinslid, K.Myklebost, J.M.Olsen Physics Department, University of Bergen, Norway

F.O.Breivik, T.Jakobsen, S.O.Sorensen Physics Department, University of Oslo, Norway

(presented by M.G.Sapozhnikov)

#### 1.INTRODUCTION

One of the most intriguing problems of hadron interactions with the nucleus is the study of the renormalisation of the elementary hadron-nucleon amplitudes in nuclear matter. In contrast to ordinary hadron probes, such as pions or nucleons, antiprotons provide an extra important advantage to tag the nucleon on which the interaction takes place. Indeed, the even number of charged mesons is the signature of the annihilation on a proton in the nucleus whereas the odd number of charged mesons is the label of the antiproton annihilation on a neutron. The final state interactions (FSI) of the mesons complicate the nucleon tagging, but not too much (in the case of the lightest nuclei).

The possibility of distinguishing between annihilation on a proton and a neutron in the nucleus provides useful information on the isospin structure of the elementary NN amplitudes. This is important for testing of different quark models of annihilation. The absence of high intensity antineutron beams prevents systematic studies of np (pn)-interactions. In this situation the investigation of pn annihilation on the lightest nuclei has its merits in spite of the complications due to FSI.

The TOFRADUPP collaboration in the PS 179 experiment at CERN at LEAR facility has performed measurements of antiproton interactions with He and He nuclei in the  $\mathbf{p_L} = 0$  - 600 MeV/c region. The data on the elastic, quasielastic and annihilation reactions are presented.

A detailed description of the experimental apparatus may be found in  $^{/1/}$ , so here we shall recall only its main features. Our apparatus consists of a self-shunted streamer chamber  $^{/2/}$  placed in a magnetic

field. The chamber was filled with  $^4$ He and  $^3$ He at atmospheric pressure and served simultaneously as a target and a detector. The chamber volume was  $70 \times 90 \times 18$  cm $^3$ . The target thickness was  $15 \text{ mg/cm}^2$ . The trigger for the high voltage pulse generator of the chamber was provided by a hodoscope of thin scintillation counters placed along the beam in front of the chamber.

The important advantages of the LEAR antiproton beam are high intensity  $(10^4-10^5~{\rm p/s})$  and momentum resolution  $(\Delta p_{\rm L}/p_{\rm L}=10^{-3})$ , absence of any pion contamination and the possibility of having a beam of antiprotons with the energies down to 5 MeV  $(p_{\rm T}=105~{\rm MeV/c})$ .

It must be stressed that a streamer chamber filled with a gas at normal pressure is an ideal tool for studying charged particles with low energies. For instance, the range of a 250 keV  $\alpha$ -particle or a 160 keV proton is 1 cm long in the chamber and certainly visible. In contrast, in bubble chambers the tracks of spectator protons from pd annihilation were not detected in 73% of all events  $^{/3}/$ .

The procedure of the scanning, measurements of events and the identification of the different reaction channels is described  ${\rm in}^{/4}$ .

#### 3. DISCUSSION OF THE RESULTS

3.1 General features of antiproton interaction with lightest nuclei

The first LEAR experimental data dealt with the elastic antiproton scattering on  $^{12}\text{C}$  /5/at 300 MeV/c. They reveal the differential cross section with a typical diffraction pattern. The same situation was found for elastic scattering at 600 MeV/c as well as for other, heavier, nuclei/6/,(see, for example, Fig.1) .0wing to the huge annihilation cross section, the nucleus is practically "black" for the antiprotons providing typical "shadow" elastic scattering

We have measured the differential cross section of elastic scattering of antiprotons on  $^4{\rm He}$  at 607 MeV/c ( $T_{\rm kin}=179$  MeV). Fig.2 shows the angular distribution for a sample of 2346 elastic events. The data/8/ for pion elastic scattering on  $^4{\rm He}$  at 174 MeV is also shown for comparison. At this energy the  $\Delta_{33}$ -resonance is dominated in the  $\pi N$  scattering providing the strong inelasticities in the  $\pi A$  scattering. The total and elastic cross sections are practically the same for antiproton and pion scattering on  $^4{\rm He}$  at this energy. However, at first sight, the differential cross sections of pions and antiprotons are quite different. Nevertheless, if one estimates the black sphere effective radius  $R_{\rm eff}$ 

$$d\sigma/d\Omega|_{b.s.} = (k R_{eff}/q)^2 J_1^2 (q H_{eff})$$
 (1)

Fig.1. The differential cross sections of elastic antiproton Fit at 600 MeV/c scattering on different nucun = 135.2 ± 2.0 (mb) lei/5.6/. Full lines correspond  $\beta_0^2 = 21.8 \pm 0.6 \, |\text{GeV/c}|^2$ to the result of the Glauber model fit where parameters of an =0.035 ± 0.017 the pn-interaction were treated X 70F - 1.53 as free ones/7/. 10 4 10 3 10 4 Fig. 2. The differential cross sections of elastic antiproton scattering on 4He at 607 MeV/c (crosses). The full line cor-10 3 responds to the Glauber model calculations/10/. The dashed line is the black sphere model predictions. The data /8/ for 10 2 π- elastic scattering on 4He at 174 MeV is also shown by rhombs. 10 10<sup>-1</sup> 10 1 10 ² 10 d(sigma)/d(omega) (mb/sr) Ö 20 30 40 50 60 10 U<sub>EM</sub> (deg) 10 40.00 120.00 0.00 80.00 Scattering angle (degrees)

from the position of the minimum in the  $do/d\Omega$  of  $\pi^4$ He scattering one can find  $R_{\rm eff}$ =2.34 fm.If the effective radius of  $\hat{p}^4$ He scattering is the same, then it corresponds to the minimum in the  $do/d\Omega$  of  $\hat{p}^4$ He at  $\theta_{\rm min}$ = 40°. As is seen from Fig.2, it is really the case. One can conclude that pions at the resonance energy and antiprotons "see" the same diffraction object. However, it is known'9' that the position of the minimum in the  $\pi^4$ He elastic scattering does not change with the energy of the initial pion. So a simple diffraction pattern is not valid for  $\pi^4$ He elastic scattering at all energies. It is interesting to check what happens in the case of  $\hat{p}^4$ He elastic scattering.

The full line in Fig.2 corresponds to the results of Glauber model calculations 10. The dashed line represents the black sphere model predictions. One can see that even in the case of light nuclei the black sphere model results are in good agreement with the Glauber model calculations (at least, for scattering at small angles). Therefore, the elastic pa-scattering must be sensitive only to the gross features of the pa interaction such as a dimension of the nuclei and an average strength of the NN amplitude. More elaborate details of the antiproton-nucleus potential can hardly be definitely determined from the elastic data alone. Indeed, concrete calculations show that different theoretical models based on the Glauber approach 11. optical potential models (e.g. RMT type) 12. or the relativistic Dirac potential 13. give equally good descriptions of the elastic pa data. The uncertainties in the knowledge of the NN elementary amplitude lead to greater changes in the description of the pa scattering than transition from one theoretical model to another 13.

An interesting feature of the antiproton-nuclear dynamics discovered in the LEAR experiments was the strong suppression of the inelastic  $A(\bar{p}, \bar{p}')X$  reactions  $^{14,5}$ . For instance, in the PS 179 experiment it was measured that the cross section of the annihilationless break-up of helium, (reaction  $^{4}\text{He}(\bar{p}, \bar{p}')X$ ) is  $\sigma_{\text{bu}}=15.5\pm2.9$  mb at  $T_{\text{p}}=180$  MeV which is only 6% of the total reaction cross section  $\sigma_{\text{R}}$ . It is much smaller than in the case of  $\sigma_{\text{R}}^{4}$  He scattering where the cross section of the  $(\pi,\pi')$  reactions is around 70-80% of  $\sigma_{\text{p}}^{15/}$  in the  $\Delta$ -resonance region.

The reason for the suppression of the antiproton break-up reaction in the case of light nuclei lies in the specifics of the  $\overline{\rm NN-amplitude}/^{16,17}/.$  It is well known that in the low energy region the pp-scattering occurs mainly in a very narrow forward cone. The slope parameter in the pp differential cross section is b= 20 (GeV/c) $^{-2}$  at  $\rm T_{kin}$ = 180 MeV  $^{/18}/.$  much greater than in pp-scattering where b= 6 (GeV/c) $^{-2}$  at  $\rm T_{kin}$ = 1 Gev. So the elementary NN scattering is characterised by a small averaged momentum transfer  $\rm < q^2>$ , which in the case of antiproton-nucleus scattering is not sufficient to effectively destroy the nuclei. For instance, even at  $\rm T_{kin}$ =180 MeV

the average energy (E) transferred in NN scattering is

$$\langle E \rangle \approx (2 \text{ b m}_{\text{M}})^{-1} \approx 27 \text{ MeV}.$$
 (2)

That is comparable with the  $^4{\rm He}$  binding energy. Therefore, even a hundred MeV antiproton has not, in average, a possibility of breaking up the light nucleus.

In the case of antiproton interaction with heavy nuclei the annihilationless break-up reactions is also  $\rm small^{15}$ . As shown in /14,17/ the reason is in the large annihilation probability which prevents the annihilationless break-up reactions in all regions except a small nuclear surface ring. Therefore, one may expect that the break-up reaction is very sensitive to details of the nuclear surface. Indeed, it was calculated/ $^{14}$ / that for  $\bar{p}^{40}{\rm Ga}$  interaction a 10% change of the nuclear diffuseness parameter leads to a 10% change of the other cross sections did not practically

change. A great number of mesons created in the annihilation with average energies around the  $\Delta_{33}$  -resonance one, where the  $\pi N$  interaction reaches its maximum, and the fact that these mesons in the pA annihilation are produced just at the surface of nuclei - all these circumstances provide strong effects of the final state interaction (FSI). These FSI effects distort the momentum distribution of the spectator nucleons 19, change drastically the A to  $\overline{\rm A}$  ratio in the  $\overline{\rm pd}$  annihilation  $^{20}/$  and result in the additional destruction of the nucleus after annihilation. The FSI effects in  $\overline{\rm p}^4{\rm He}$  annihilation lead to the decreasing probability for a three-nucleon system to survive after the annihilation in a bound state. It occurs  $^{21}/$  that at 180 MeV the probability for  $^3{\rm He}$  to survive after annihilation is

$$\sigma(\bar{p}^{4}\text{He} \rightarrow ^{3}\text{He} + X)$$
 $W_{\bar{p}}(^{3}\text{He}) = ----- = (15.5 \pm 0.7) \% (3)$ 

This is three times lesser than the correspondent ratio for the pion- $^4$ He scattering at the same energy  $^{15}$ :

pion-<sup>4</sup>He scattering at the same energy<sup>15/</sup>:
$$\sigma(\pi + {}^{4}\text{He} \Rightarrow {}^{3}\text{He} + X)$$

$$W_{\pi}({}^{3}\text{He}) = ----- \approx 46 \% . (4)$$

It is a clear indication of the strength of FSI effects in the  $\bar{p} \hat{A}$  scattering.

#### 3.2 Antiproton annihilation on bound nucleons

In spite of substantial FSI effects the task of determining the cross sections for antiproton interaction with bound protons and neutrons is not insoluble. In the streamer chamber filled with helium gas the annihilation on bound proton is recognizable as an event with even number of meson tracks and a track from a heavy particle which may be a proton, a deutron or a triton. The annihilation on bound neutrons provides an odd number of meson tracks and two tracks from heavy particles. Due to FSI the number of meson and heavy particle tracks may change mainly owing to reactions of the charge-exchange type:

$$\pi^{-} + p \Rightarrow \pi^{0} + n$$
 (5)  
 $\pi^{0} + n \Rightarrow \pi^{-} + p$  (6)

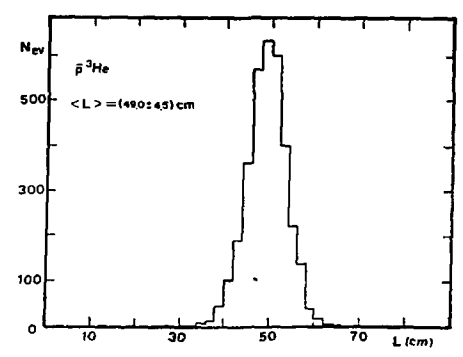


Fig. 3. Distribution of the antiproton stopping points along the beam direction in the chamber for annihilation of stopped  $\tilde{p}$  in  $^3$ He.

The detailed analysis of the FSI corrections was done in  $^{10}$ . Fortunately the distorted reactions (5)-(6) counteract each other which simplifies the analysis.

Annihilation of antiprotons stopped in  $^4\text{He}$  and  $^3\text{He}$  has been studied in PS 179 experiment. In contrast to the previous experiments with stopped antiprotons we used the beam with a well defined ( $\Delta p/p \approx 10^{-3}$ ) initial momentum 105 MeV/c. So the distribution of the antiproton stopping points along the beam direction inside the chamber volume exhibits a clear peak in a right position (see Fig. 3). Table 1 collects the data for the branching ratios for the

Table 1 collects the data for the branching ratios for the annihilation at rest on bound in <sup>4</sup>He and free protons. The third column contains the predictions of a simple statistical annihilation model <sup>22</sup>/<sub>2</sub>.

TABLE I. Branching ratios of different charge prongs states in pp annihilation at rest.

N(n <sup>-</sup> )*)	pp (free) [23]	pp (bound in <sup>4</sup> He)	theory [22]
)	4.1+0.2	4.97 ± 0.5	2.37
	43.1 ± 0.9	46.71 ± 1.64	45.5
2	47.3 ± 1.2	43.90 ± 2.53	44.9
3	4.25± 0.31	4.2 ± 1.42	4.89

<sup>\*)</sup> kaons are also included in 4He distributions

Branching ratios for the annihilation on bound neutrons is collected in the Table 2.

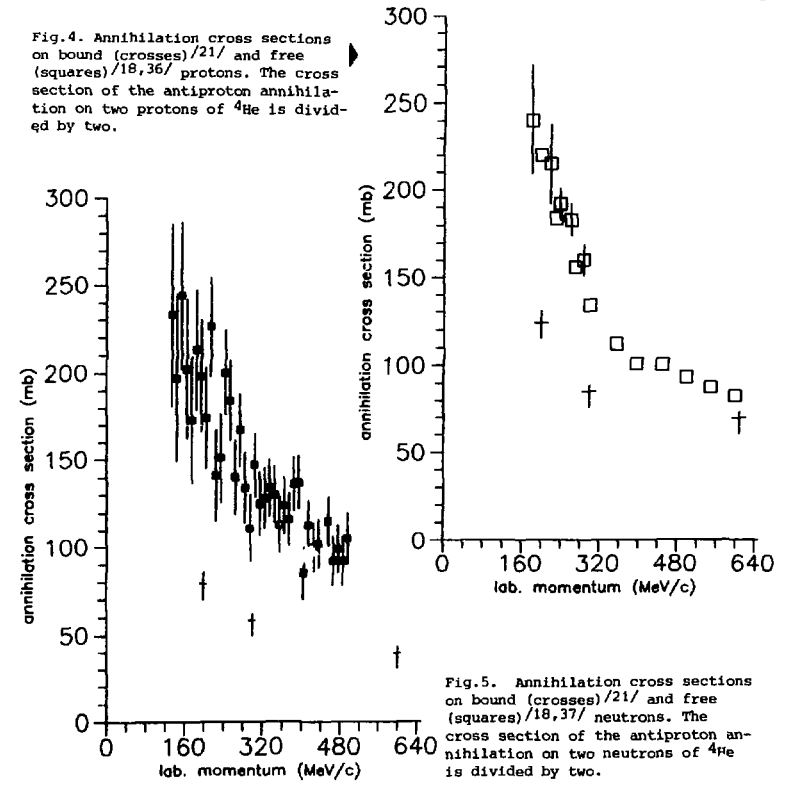
TABLE 2. Branching ratios of different charge prongs states in pn annihilation at rest.

N(π <sup>-</sup> )*)	pn (bound in d) [24]	pn (bound in <sup>4</sup> He)	theory [22]	
1	16.8 ± 0.8	21.49 ± 2.53	17.3	
2	59.5 ± 1.4	56.54 ± 5.10	60.1	
3	23.0 ± 0.9	21.37 ± 3.18	19.6	
4	$0.7 \pm 0.2$	$0.59 \pm 0.24$	0.67	

<sup>\*)</sup> kaons are also included in 4He distributions

From inspection of Tables 1,2 one may conclude that there is no large difference in the branching ratios for annihilation of the stopped antiprotons on the free or bound nucleons.

The situation with the annihilation in flight is shown in Figs. 4,5 where annihilation cross sections on the bound proton and neutron are compared with those for the free nucleons. The results of



the PS 179 experiment, where antiproton annihilation in  $^4$ He at 192.8, 306.2 and 607 MeV/c was measured/ $^{21}$ /, are shown by crosses. In fact, the measurable quantity was the cross section of the antiproton annihilation on two protons ( or two neutrons) of  $^4$ He. In Figs. 4,5 we have shown these cross sections divided by two. A very large shadowing effects are clearly seen.

#### 3.3 Isospin dependence of the NN amplitude

The isospin dependence of the NN amplitude is an important issue of low-energy antiproton physics. Let us remind, that the antiproton-neutron (pn) system is a pure isospin state with I=1 and the wave function of the pp system is a mixture of states with I=0 and I=1

$$\Psi$$
 ( $\bar{p}p$ ) =  $-\frac{1}{2}$  (  $\Psi$ ( I=0) +  $\Psi$  (I=1) ) · (7)

From the experiments with  $\bar{p}p$  and  $\bar{n}p$  annihilation in flight we know that the ratio R

is around R=0.8-1.0 and is practically energy independent (see Fig.6). The increasing of  $\sigma_{\rm ann}({\rm pp})$  in comparison with  $\sigma_{\rm ann}({\rm pn})$  may be

explained on the language of  $N\overline{N}$  potentials as a manifestation of strongly attractive central potential in I=0 state due to coherence of  $\sigma$  and  $\omega$  exchange terms.

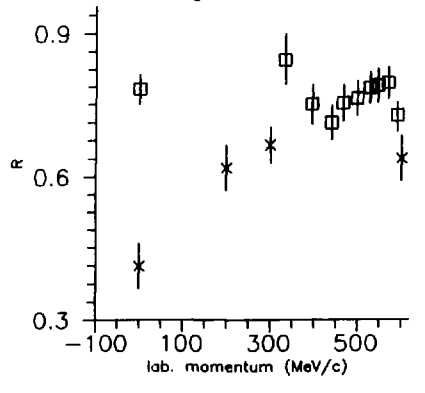


Fig. 6. Energy dependence of the ratio R from (B). Results of the PS 179 experiment/10.25/ for pHe annihilation are shown by crosses, squares correspond to the data of/19/ for p annihilation in deuterium.

For antiproton annihilation at rest in the liquid deuterium bubble chamber experiments was found that

$$R(d) = 0.75 \pm 0.02$$
 [24] (9)  
 $R(d) = 0.82 \pm 0.03$  [19].

These values are nearly twice as large as the corresponding values found from the stopped antiproton annihilation on  $^4{\rm He}$  and  $^3{\rm He}$ 

$$R(^{4}He) = 0.42 \pm 0.05$$
 [10]  
 $R(^{3}He) = 0.48 \pm 0.06$  (10)  
 $R(^{4}He) = 0.48 \pm 0.1$  [25]  
 $R(^{3}He) = 0.35 \pm 0.07$  [25]

It is instructive to compare the experimental values of R (9)-(10) with predictions of different theoretical models. In the limit of  $k \rightarrow 0$  the ratio R from (8) is connected with  $N\overline{N}$  scattering lengths in S-wave:

$$R = \frac{2 \text{ Im } a_1}{\text{Im } a_1 + \text{ Im } a_0}$$
 (11)

Table 3 the values of R from the theoretical models and the last experiments are collected.

TABLE 3. The ratio R from different NN potential models

Model	R	Ref.
Ueda 1	1.	26
Ueda 2	0.742	26
Veda BST	0.834	26
Bryan-Phillips	0.85	27
Bryan-Phillips	0.99	27
Dover-Richard	0.84	28
Paris	1.14	29
Exp.value	0.87 ± 0.14 and AGS 795 data)	30

(from pp atoma and AGS 795 data)

One can see that both theoretical and experimental results demonstrate the large value of R in obvious disagreement with helium results (10).

In our opinion, the reason is that annihilation of stopping antiprotons in helium gas proceeds mainly from the P- and D- atomic states. It is known from the electromagnetic cascade model

calculations  $^{/31/}$  that the probability to populate the S-levels in helium gas at 1 atm is only 8%, whereas the probability to annihilate from P-states is 49% and from the D-states is 43%. In principle, the annihilation from a certain antiproton-nucleus state may proceed via different NN-states and one should solve the standard hadronic atoms Coulomb-plus-strong interaction task to obtain the connection between the probabilities of snnihilation in pA and pN systems. Fortunately, in the case of helium, one may expect a simplification due to the fact that the nucleons in the helium nucleus occupy mainly the S-state, ( the admixture of S-wave states in the helium wave function is greater than 90%). Therefore, as a zero approximation one may consider that the annihilation from a certain state of the helium atom implies the dominance of the same state in  $N\overline{N}$  system, i.e. one may expect that the P- and D-contributions will be also dominant in the antiproton annihilation on nucleons bound in the 4He.

Therefore, it is impossible to compare directly the helium

results (10) with that from pd (9) or pp -annihilation (Table 3.). The reason is that in liquid hydrogen it is well known that the annihilation proceeds mainly from highly excited S-states owing to a strong Stark effect  $^{/32}$ . The difference between the helium (10) and deuterium data (9) must be regarded as an indication on a strong isospin dependence of  $N\bar{N}$  -amplitude in P- and/or D-states.

There are some arguments in favor of this statement. First of all, the fits of low-energy pp and pn data in the effective range approximation for the NN-amplitude have really demonstrated a substantial isospin dependence in the P-states 33,34/

The analog of eqs. (11) for the P-wave annihilation is

$$R_{p} = \frac{2 \text{ Im } b_{1}}{\text{Im } b_{1} + \text{ Im } b_{0}}$$
 (12)

where Im b<sub>1</sub> and Im b<sub>0</sub> stand for the imaginary parts of the scattering

volumes in the isospin states I=1 and I=0. The fit of Mahalanabis-Pirner-Shibata 33/ gives for  $R_{\rm p}$  = 0.2, the fit of Grach-Kerbikov-Simonov 34/ provides  $R_{\rm p}$  = 0.35.It is interesting to note that the same tendency is conserved for the D-state ratio  $R_{\rm D}$  = 0.42/34/.

If one assumes that there is an hierarchy between R ratios in different states R  $_{\rm B}$  >> R  $_{\rm p}$  and R  $_{\rm D}$  then the energy dependence of R in  $^4$ He (see Fig.6) may be understood as follows. Just at the threshold the R ( $^4$ He) must be small because annihilation proceeds from P- and D-states. As the energy increases—the ratio R ( $^4$ He) must grow up dus to the S-wave contribution which must appear in the NN-amplitude for the interaction in flight. However, when the antiproton energy is high enough the S-wave contribution must decrease resulting in overall decreasing of the R ratio. An indication of the existence of such energy behaviour may be obtained from the inspection of 51g.6.

The isospin dependence of the  $N\bar{N}$  amplitude may arise either from the long range part of  $N\bar{N}$  potential or from the short range one. The former is usually derived from NN potentials by G-parity conjugation, the latter, annihilation potential, is not constructed from the first priciples but chosen, in some sense, arbitrary. In most popular annihilation potentials (for example,  $^{/27,28,35/}$ ) there is no isospin dependence. It is interesting to compare the predictions of such models with our data to understand if it is possible to explain the observed isospin dependence only due to long range part of  $N\bar{N}$  potential.

On Fig.7 a comparison with results of the calculations with Dover-Richard potential  $^{28}$  is shown. The full line corresponds to the calculations of the energy dependence of the ratio R from (8). The dashed line shows the energy dependence of the ratio  $R_{\rm S}$  which is constructed only from the S-wave contributions in  $\sigma_{\rm ann}(\bar{p}p)$  and  $\sigma_{\rm ann}(\bar{p}p)$ . The dot-dashed line stands for  $R_{\rm p}$ , which is the ratio for the P-wave contributions. One can see that the behaviour of R and  $R_{\rm S}$  from these calculations is in agreement with results of  $\bar{p}d$ -annihilation experiment  $^{/19}/$  in liquid deuterium. But neither R,  $R_{\rm S}$  nor  $R_{\rm p}$  from the Dover-Richard model is comparable with the  $\bar{p}^4{\rm He}$ 

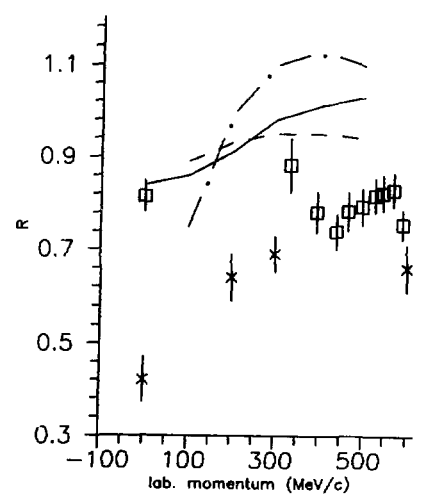


Fig. 7. A comparison with results of the calculations of R by Dover-Richard potential model  $^{\prime 28\prime}$ . The full line corresponds to the calculations of the energy dependence of the ratio R from (8). The dashed line shows the energy dependence of the ratio R  $_{\rm S}$  which is constructed only from the S-wave contributions in  $\sigma_{\rm ann}(\bar{\rm p}n)$  and  $\sigma_{\rm ann}(\bar{\rm p}p)$ . The dot-dashed line stands for R  $_{\rm P}$ , which is the ratio for the P-wave contributions. Results of the PS 179 experiment  $^{\prime 10,\,25\prime}$  for  $\bar{\rm p}$  He annihilation are shown by crosses, squares correspond to the data of  $^{\prime 19\prime}$  for  $\bar{\rm p}$  annihilation in deuterium.

results in gas. It seems to be an indication that the NN annihilation potential must depend on the isospin to provide an additional isospin dependence which demonstrated in  $p^4$ He data.

#### 4.CONCLUSIONS

The elastic and inelastic scattering of antiprotons on  $^4$ He was measured at 600 MeV/c. It was found a strong suppression of the  $^4$ He break-up reactions ( $\sigma_{\rm b.u.}$  is only 6% of the total reaction cross section  $\sigma_{\rm p}$ ).

The cross sections of antiproton annihilation on bound protons and neutrons were reconstructed at 0-600 MeV/c interval. There is no large difference in the branching ratios for annihilation of the stopped antiprotons on the free or bound nucleons.

It was found that for the stopped antiprotons ratio between annihilation probabilities on neutron and proton bounded in <sup>4</sup>He is nearly twice as small as for annihilation in deuterium. It indicates

on the strong isospin dependence of NN-amplitude in the P- and/or D-states, which seems to be not explainable in the ordinary potential models of the NN interactions which neglected isospin dependence of the annihilation potential.

#### 5. ACKNOWLEGMENTS

We are grateful to Dr.T.-A.Shibata for providing us the results Dover-Richard model calculations. We thank a lot to L.A.Kondratyuk, R.Landua, B.O.Kerbikov, D.E.Kharzeev, V.V.Pupishev for the fruitful discussions which were very useful for us.

#### REFERENCES

- Balestra F. et al., Nucl. Instr. and Meth., 1985, v.234, p.30.
   Falomkin I.V. et al., Nucl. Instr. and Meth., 1967, v.53, p.266.
- Gray L. et al., Phys. Rev. Lett., 1971, v.26, p.1491.
- Balestra F. et al., Nucl. Instr. and Meth., 1987, v.A257, p.114.
- 5. Garreta D. et al., Phys.Lett., 1984, v.B135, p.266. 6. Garreta D. et al., Phys.Lett., 1984, v 1984, v.B149, 1985, v. B151, p. 473; 1986, v. B169, p. 14.
- 1987, v.A469, p.669.
- 7. Bendiscioli G. et al., Nucl. Phys., 1987, v.A469, p. 8. Falomkin I.V. et al., Nuov.Cim., 1978, v.43A, p.219. 9. Shcherbakov Yu.A. et al., Nuov. Cim., 1976, v.31A, p.249.
- Binon F. et al., Nucl Phys., 1978, v. A298, p.499.
- Balestra F. et al., Nucl. Phys., 1987, v. A465, p.714.
   Kondratyuk L.A., Sapozhnikov M.G., prepint JINR, E4-86-487,
- Dubna, 1986; Yad. Fiz., 1987, v. 46, p.89.
  Dalkarov O.D., Karmanov V.A., Phys. Lett., 1984, v.147B, p.1.
  12. Heiselberg H. et al., Nucl. Phys., 1985, v. 4445, p.637.
- Suzuki T., Nucl. Phys., 1985, v. A444, p.659 Ingemarsson A., Nucl. Phys., 1986, v. A454, p.475.
- 13. Picklesimer A. et al., Phys.Lett., 1985, v.163B, p.311. 14. Balestra F. et al., Phys.Lett., 1987, v.194B, p.343. 15. Balestra F. et al., Nucl. Phys., 1980, v.A340, p.372.

- 16. Batusov Yu.A. et al., JINR Rapid Comm., 1985, N.12, p.6
- 17. Karmanov V.A., Trukhov A.V., Pisma ZhETP, 1988, v.47, p.70.
- Bruckner W. et al., Phys.Lett., 1985, v.B158, p.180.
   Bizzarri R. et al., Nuov.Cim., 1974, v.22A, p.225.
- 20. Parkin S.J.H. et al, Nucl. Phys., 1986, v. B277, p. 634.
- 21. Balestra F. et al., CERN preprint, EP/87-213, Geneva, 1987.
- 22. Offranidia S.J., Rittenberg V., Nucl. Phys., 1973, v. B59,p. 570.
- 23. Ghesquiere C., Symp. on Antinucleon-Nucleon Int., Liblice, Yellow Report CERN 74-18, p.436, 1974.
- 24. Kalogeropoulos T., Tzanakos G.S., Phys.Rev., 1980, v.22, p.2585.
- Batusov Yu.A. et al., Nucl. Phys., 1987, v.A474, p.651.
   Ueda T, Prog. Theor. Phys., 1979, v.62, p.1670.
- 27. Bryan R.A., Phillips R., Nucl. Phys., 1968, v.B5, p.201.
- 28. Dover C., Richard J.M., Phys.Rev., 1980, v.C21, p.1466.
- 29. Cote J. et al., Phys. Rev. Lett., 1982, v. 48, p. 1319.
- 30. Mutchler G.S. et al., Rice University preprint DOE/ER/10309-2, Houston, 1987.
- 31.Reifenrother F., Klempt E. Landua R., Phys. Lett., 1988. v.203B.p.9.
- 32. Day T.B., Snow G.A., Sucher J., Phys. Rev., 1960, v.118, p.864.
- Mahalanabis J., Pirner H.J., Shibata T.-A., CERN preprint. TH.4833/87, 1987, Geneva.
- Grach I.L., Rerbikov B.O., Simonov Yu.A., ITEP preprint, N210, Moscow, 1987.
- 35. Weise W. Proc. IV LEAR Workshop, Villars, 1987, p.287.
- 36. Bruckner W. et al., Proc. IV LEAR Workshop, Villars, 1987, p.277.
- 37. Armstrong T. et al., Phys.Rev., 1987, v.D36, p.659.

# STUDY OF LOW ENERGY ANTIPROTON INTERACTION WITH NUCLEI USING A SELF SHUNTED STREAMER CHAMBER IN A MAGNETIC FIELD

Bergen- Brescia-Dubna-Frascati-Oslo-Pavia-Torino-Collaboration
PS179 experiment at CERN

F.Balestra, S.Bossolasco, M.P.Bussa, L.Busso, L.Ferrero, A.Grasso, D.Panzieri, G.Piragino, F. Tosello Istituto di Fisica Generale A.Avogadro, University of Torino, INFN, Sezione di Torino, Italy

R.Barbieri, G.Bendiscioli, A.Rotondi, P.Salvini, A.Zenoni
Dipartimento di Fisica Nucleare e Teorica, University of Pavia and INFN, Sezione di Pavia Italy

Yu.A.Batusov,S.A.Bunyatov, I.V.Falomkin, G.B. Pontecorvo, A.M.Rozhdestvensky,M.G.Sapozhnikov,V.I. Tretyak Joint Institute for Nuclear Research. Dubna.

C.Guaraldo, A.Maggiora Laboratori Nazionali di Frascati dell'INFN,Frascati,Italy

E.Lodi Rizzini
Dipartimento di Automazione Industriale, University of Brescia and INFN, Sezione di Pavia, Italy

A. Haatuft, A. Halsteinslid, K. Myklebost, J. M. Olsen Physics Departement, University of Bergen, Norway

F.O.Breivik, T.Jacobsen, S.O.Sorensen Physics Departement, University of Oslo, Norway

(presented by F.Balestra)

#### 1. INTRODUCTION

In these last years, the experimental studies of the interaction of low energy antiprotons on nucleon and nuclei have received a vigorous impulse, due to the LEAR antiproton beams at CERN. The nuclear physics results are among the most interesting scientific outputs of the first generation of LEAR experiments. For a comprehensive review the reader is referred to the report by Guaraldo at the Villars Conference 1. The aim of the PS179 experiment was to explore:

- the dynamics of the dominant process of the low energy antiproton-nucleus interaction ,i.e. the annihilation:

- the problem of the penetration of antiproton inside a nucleus, identifying peripheral and deep unnihilation events:
- the new physics beyond the "conventional" annihilations, with its typical predicted signatures, in particular strangeness production.

In this paper we describe the results obtained by the Streamer Group studying  $\overline{p}$ -Ne annihilations at 200,300,600 MeV/c and at rest  $\overline{p}$  and also  $\overline{p}$  annihilations on nuclear emulsion (Ag/Br) at 300,400,500 MeV/c and at rest  $\overline{p}$ ).

#### 2. SPECIFIC FEATURES OF THE EXPERIMENTAL APPARATUS

The experimental apparatus consisted of a self shurted streamer chamber in a magnetic field exposed to the  $\overline{p}$  beams of the LEAR facility at CERN. The details of the apparatus and its performances are reported in ref. 4. The chamber with a sensitive volume of (70X90X18)cm<sup>3</sup>, was filled at 1 atm with gas target.

Due to the  $4\pi$  acceptance and the low density gas target the apparatus is able to detect very carefully

the charged prongs multiplicity of the events,including very slow particles and  $\Lambda^0$  and  $K_s^o$  observed through their charged decay mode. The ability to measure short nuclear fragment ranges (corresponding to energies lower than 1MeV) together with the curvature of the fast particles and the very good vertex resolution allow to obtain a very good charged prong multiplicity, to study the behaviour of momenta and angles vs. charged prong multiplicity and permit to obtain an accurate identification of the reaction channels and exclusive reactions.

#### 3. CENTRAL ANNIHILATIONS

There are two good reasons to focus a particular attention on central or deep achihilations. By definition, one may expect that any significant difference between antinucleon-nucleon and antinucleon-nucleus processes, which constitutes one of the objectives of nuclear physics research with antiprotons, is most likely to show up in such events. Moreover, the signals of the new physics which might be discovered in annihilations on more than one nucleon, the probability of which increases going deeply in the nucleus, could in principle be enhanced if these events could be distinguished from the background of surface annihilations on a single nucleon. In the PS179 experiment central from surface annihilation have been clearly identified from:

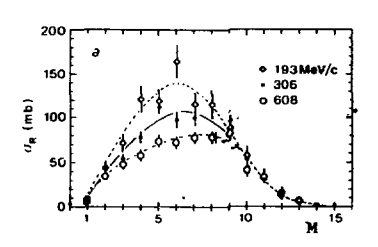
#### a) Multiplicity distributions of charged prongs

Low and high-multiplicity events present typical opposite behaviours. Examining the reactions cross section  $\sigma_R$  in Neon as a function of the multiplicity M, one can consider two regions (Fig.1). In the first one, the events with M<9, M follows the energy behaviour of the  $\overline{p}$ -N cross section, which increases as the energy decreases, typical of surface annihilations. In the second region, with M>9, M is independent on the energy, the average multiplicity is<M>=10.7,<  $n_{\pi}$ >=1.75, so that the number of heavy prongs must be about 7.5, on average. This fact means that a nucleus with atomic number 10 is almost disintegrated in free nucleons due to a transfer of energy greater than its total binding energy.

This is possible when a deep penetration has occured. Finally, it is remarkable that the percentage of the central events is increasing with energy: from some percent at rest up to about 15% at 600 MeV/c.

Similar conclusion can be drawn from the data obtained by analyzing the  $\overline{p}$  - Ag/Br annihilation events in nuclear emulsion<sup>3</sup>.

In fig. 2. the distribution of nuclear matter density  $\rho(r)/\rho(0)$  is compared with the  $\overline{\rho}$  absorption probability  $P_{ann(\%)}$  calculated by using standard INC model calculations. The annihilation probabilities in the high density nuclear matter region are in agreement with those we deduced for the annihilations in the depth of the nuclei. In fact in the central part of the nucleus were  $\rho(r)/\rho(0) > 0.75$ ,  $P_{ann(\%)}$  amounts to (15-28% for Ne and Ag/Br , respectively) over the total number of events at 600 MeV/c. In the case of  $\overline{\rho}$  at rest the probability of  $\overline{\rho}$  annihilation in the region  $\rho(r)/\rho(0) > 0.75$  is about 5% of the total number of events, in agreement with the value found for high multiplicity events.



P<sub>(1)</sub> P<sub>(2)</sub> (%) 15 15 10 10 5 8 (fm)

Fig.1. Charged prong multiplicity cross section for  $\overline{p}$  - Ne interaction.

Fig.2·The probability of  $\overline{p}$  annihilation in Ne vs. the nuclear radius. The histograms were calculated  $^{6}$  for 590 MeV/c  $\overline{p}$  - $^{12}C$ . Full line was calculated  $^{5}$  for  $\overline{p}$  at rest.

#### b) Momentum angle rapidity distributions

In a deep annihilation inside the nucleus it is expected that all pions interact, consequently they must be less energetic than those emitted in the surface (quasi-free) annihilation case; the angular distributions are more isotropic and the rapidity values compatible with the emission from many nucleons.

A comparison between momentum, angle and rapidity distribution of  $\pi^-$  and nuclear fragment for low and high-multiplicity events (in the case of Neon for M=4 and M=11, respectively) has been performed.

The results can be summarized as follows: the high-multiplicity events present, in comparison with the low-multiplicity ones, a lower number of negative pions, which have lower mean energy (Fig. 3 a,b) and are isotropically emitted (Fig. 3 c,d) from a kinematical source involving many nucleons (Fig. 3 e,f).

As far as the nuclear fragments are concerned, their number and their mean energy are higher for M=11 than for M=4, while the kinematical sources involve, in both cases, a number of nucleons. The overall degree of isotropy of the charged proofs is higher for the high-multiplicity events.

It is possible to conclude that all the experimental features are contained in the scenario pictured by the intra nuclear cascade models, according to which low multiplicity events correspond on average, to surface annihilations, while high-multiplicity events correspond on average, to central annihilations.

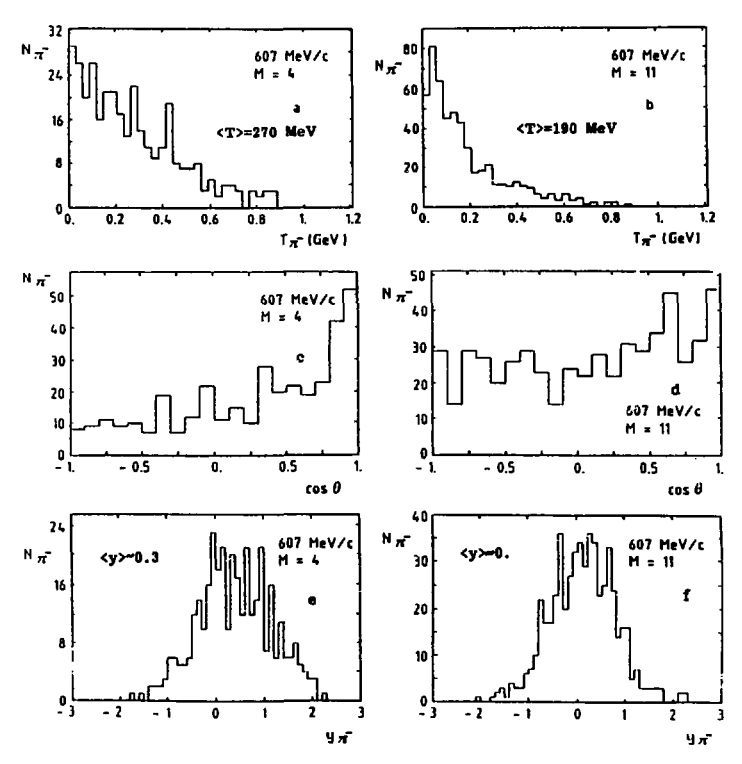


Fig. 3. p -Ne (607 MeV/c). Comparison between annihilation events with M=4 and M=11. Negative pion distributions vs.: Kinetic energy (a,b); cos θ (c,d); rapidity (e,f).

### 4 DYNAMICS OF LOW ENERGY P ANNIHILATION IN NUCLEI

#### a ) Multiplicity distributions of pions

It has been shown that high charged prongs-multiplicity events correspond, on average, to deep annihilations, which favour strong pion-nucleon interactions and consequently high-energy deposition inside the nucleus. It is reasonable to assume a correlation between high-multiplicity and high-energy deposition. From high-energy deposition it is expected a higher number and/or energy of fragments and reduced total energy of final pions.

As far as the fragments are concerned, the behaviour of the emitted fragments and their momenta vs. multiplicity are in agreement with INC previsions (confirming the assumption that the multiplicity is proportional to the deposited energy).

As far as  $\pi^-$  are concerned,it is possible to observe a striking behaviour:the mean number of  $\pi^-$  is increasing with the multiplicity. The standard INC calculations did not make any prevision taking into account the overall contribution of all the pions. However, a recent sophisticated version of an existing INC model by Golubeva et al.  $^{7}$  explains this striking behaviour. This version of the model gives a much better description of the elementary  $\bar{N}N$ -interaction, includes the effects of the local reduction of the nuclear density during the development of the cascade (trawling effect) and takes into account the de-excitation of the residual nuclei in terms of evaporation and multifragmentation. As it is shown (Fig.4b) the model predicts the correct behaviour of  $<n_{\pi^-}>vs$ . M.

The same agreement is obtained by another recent different model developed by Cugnon et al.  $^{8)}$  in which the ejection mechanism is assumed to correspond to a clan picture where the ancestors are pions. This simple model retains all the basic premises of INC and handles charge conservation exactly at each step. Good agreement is obtained for multiplicity distributions and in particular for the very strong correlations observed in Ne between <n $_{\pi}$ > and charged prongs multiplicity (Fig.4a). The agreement is a direct consequence of charge conservation and has no dynamic content.

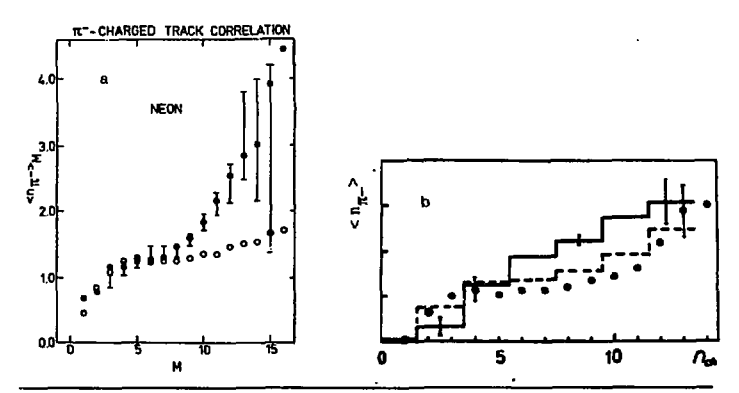


Fig. 4.  $\overline{p}$  -Ne (607 MeV/c). Correlation between the mean number of negative pions and charged prongs multiplicity. a) The bars represent the experimental data; the full circle are the prediction of the model of Cugnon et al. <sup>8)</sup>. The open circle correspond to the relaxation of the charge conservation. b) The dots are the experimental data. The solid and dashed lines represent the results of intranuclear cascade calculations by Golubeva et al. <sup>7)</sup>, with and without trawling effect.

#### b) Kinetic energy and rapidity distributions of pions.

Summing over all the multiplicities it is possible to obtain more general information on the dynamics of  $\overline{p}$  annihilations, stressing the role of pions in transferring energy to the nucleus and identifying how many nucleons participate in the annihilation and subsequent cascade in the nucleus.

The inclusive pion momentum spectrum (Fig. 5) shows a typical two bump structure with a sharp peak below 100 MeV and a broad bump around 300 MeV. Pions which have interacted with the nucleus contribute to the lower energy peak both forward and backward, pions from peripheral annihilations (primordial pions) not interacting with the nucleus contribute to the high-energy peak when emitted forward and to the low energy peak when emitted backward, due to the Lorentz factor.

Different kinematical sources for emitted pions may be recognized by inspecting rapidity distribution (Fig. 6). The pion rapidity spectra for Pt<100 MeV/c and Pt>400 MeV/c clearly show, for the latter, the quasi free  $\overline{N}$ -N origin (y=0.3), while low energy pions come from a system involving many nucleons (y=0). A phase space  $\overline{p}$  - p calculation is clearly in agreement with the primordial pion rapidity spectrum.

These last features confirm what inferred from the inclusive spectra. Assuming that nothing unusual is occurring, the method for energy deposition is pion absorption (via delta) and scattering. The large energy depositions (high-multiplicity) correspond to a production of low-energy "thermalized" pions and necessarily it will happen deeper within the nucleus involving many nucleons in the process. On the contury, high-energy "primordial" pions are associated to peripheral annihilations, which happen on a single nucleon.

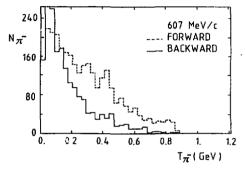


Fig. 5. p -Ne (607 MeV/c) . Negative pion distribution vs. kinetic energy.

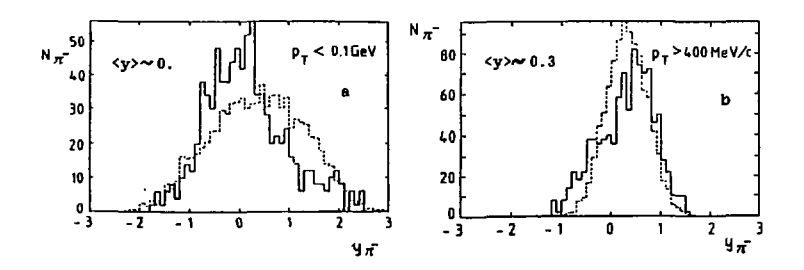


Fig. 6.  $\overline{p}$  -Ne (607 MeV/c) . Negative pion distribution vs. rapidity for :P<sub>T</sub><100 MeV/c (a) and P<sub>T</sub>> 400 MeV/c (b).Dashed line:phase space calculation for  $\overline{p}$  -p annihilations.

#### 5. STRANGE PARTICLE PRODUCTION IN NUCLEAR COLLISIONS

Hunting for new phenomena, certainly a special role must be reserved to multinucleon annihilation, which are expected to have a probability proportional to the nuclear density and thus to be preferably looked for in deep annihilations. As above stressed, central annihilations can be identified by triggering on high-multiplicity charged prongs events.

Strange particle production in nuclear collisions has become a topic of interest with the speculation that significant changes in relative and absolute abundance of strange particles(togheter with tails of high momentum protons) could serve as a probe for a quark-gluon plasma formation <sup>9)</sup>. Also in a more conventional approach enhanced strangeness production would be signature of annihilations with baryon number B>0 <sup>10</sup>.

With the streamer chamber , the inclusive production of  $V^0$  from 600 MeV/c antiproton annihilations in Neon was investigated  $^{11)}$ . The  $\Lambda^0$  and  $K^{\circ}_{\bullet}$  were observed through their charged decay modes.

The  $\Lambda^0$  and  $K_s^0$  production cross section can be compared with recent results obtained at KEK on Ta at 4 GeV/c (Miyano et al.  $^{13}$ ), on complex nuclei below 450 MeV/c (Condo et al.  $^{12}$ ) and on  $^2$ H at 450-921 MeV/c (Parkin et al.  $^{14}$ ).

### 1. $R = \sigma (\Lambda^0)/\sigma (K^2)$ behaviour vs. A and energy

The emission probability of  $\Lambda^0$  (1.95±0.43 %) confirms the results obtained on complex nuclei by Condo et al. <sup>12</sup>). Both PS179 and Miyano et al. <sup>13</sup>) experiments, on medium and medium heavy nuclei, obtain about the same value (about 2.4) for the ratio  $R = \sigma(\Lambda^0) / \sigma(K_s^0)$  independently on energy. On light nuclei, according to the recent data on deuterium <sup>14</sup>) the R value is less than unity. Preliminary data of PS179 experiment on annihilation on <sup>4</sup>He show a value for R near unity. It is possible to hypothesize a "peripherical-like" component in the production of  $K^0$ . Then, in a lighter nucleus, such a deuteron or <sup>4</sup>He, the enhanced surface production would invert the value of the ratio . If this is true, the surface character of annihilation at rest ought to give a lower value for R. The preliminary annihilation data at rest on Neon seem to confirm this mechanism.

Reaction	σ(Λ <sup>O</sup> )	σ( K <sub>s</sub> )	$R=\sigma(\Lambda^0)/\sigma(K_s^0)$
Ne (607 MeV/c) ref. 11	12.3 ± 2.8 mb	5.4 ± 1.1 mb	2.3 ± 0.7
Ta (4 GeV/c) ref. 13	193 ± 12 mb	82 ± 6 mb	$2.4 \pm 0.3$
<sup>2</sup> H (450-921 MeV/c) ref.14	0.65 %	2.55 ± 0.12 %	0.25±0.05
<sup>4</sup> He (at rest) *)			0.80±0.17
Ne (at rest) *)		i	1.14±0.17

Table 1.  $K_s^o$  and  $\Lambda^o$  production cross section .  $R=\sigma(\Lambda^o)/\sigma(K_s^o)$  behaviour vs. A and energy. \*) preliminary data from PS179 experiment.

## 2. Strangeness enhancement in PS179 and KEK 13) experiments

For the  $\overline{p}$ -Ta experiment at 4 GeV/c the  $\Lambda^O$  production is surprisingly high compared with that obtained by scaling data from  $\overline{p}$ -p strangeness production and taking into account some simplified geometrical factor.

For the Neon data the same effect is supported, scaling the data from p-d at 600 MeV/c. (see Table)

KEK				PS1	PS179 $G * A^{2/3} E = \frac{\sigma_{pNe}}{}$		
	σ <sub>pTa</sub> (mb)	σ <sub>pp</sub> * A <sup>2/3</sup>	$E = \frac{\sigma_{\overline{p}\Gamma e}}{\sigma_{\overline{p}p} * A^{2/3}}$	σ <sub>pNe</sub> (mb)	σ <sub>pd</sub> * A <sup>2/3</sup>	$E = \frac{\sigma_{pNe}}{\sigma_{pd} * A^{2/3}}$	
	(4 GeV/c)	(mb)		(.6 GeV/c)	(mb)		
۸ <sup>0</sup> +X	193 ± 12	17	11	12.3 ± 2.8	3.1	6.1	
Ks +X	82 ± 6	60	1.3	5.4±1.1	11.7	0.46	

Table 2 · Strangeness enhancement in PS179 and KEK experiments

### 3. Rapidity distributions of Λ° K° and associated π

From the analysis of rapidity distributions some conclusions on the effective target of nucleons involved in the strangeness production can be drawn.

The weighed average rapidity of  $\Lambda^\circ$  is <y>=(.07±.03) which implies an interacting system of many nucleons. This result is consistent with that deduced for  $\overline{p}$  of 4 GeV/c  $\overline{p}$ . The weighed average rapidity of K°s is y=(.33±.07) indicating a pronounced preference of forward production relative to the  $\overline{p}$  beam direction and implying an interacting system ( $\overline{p}$ ,1N) to be compared to a system ( $\overline{p}$ ,3N) deduced at higher energy  $\overline{p}$  we can conclude that in  $\overline{p}$  Ne annihilations at 607 MeV/c the data favour the hypothesis that  $\overline{k}^\circ$  and  $\Lambda^\circ$  production mechanisms are similar to those described by Miyano et al. or  $\overline{p}$  Ta

that  $K_s^*$  and  $\Lambda^o$  production mechanisms are similar to those described by Miyano et al. for p. Ta annihilations at 4 GeV/c.

The rapidity distribution of negative tracks ,mostly pions, gives a puzzling result. Both ( $\Lambda^o$  associated and  $K^o{}_S$  associated)  $\pi^-$  rapidity distributions - a parameter not measured at KEK - present different average values compared to those of the associated strange particles: as if pions were produced from totally different effective targets.

The rapidity distribution of negative tracks associated to  $\Lambda^{\circ}$  events has an average value <y> = 0.31 $\pm$  0.08 indicating the forward character of these events not correlated with the behaviour of the associated  $\Lambda^{\circ}$  distribution, whereas the rapidity distribution of negative tracks associated to  $K^{\circ}$ s events is y=-0.01 $\pm$ 0.06, which is consistent with a flat production, differently from the forward associated  $K^{\circ}$ s.

## 4. Summary of the specific features in strangeness production from P\$179 and KEK experiments

The specific features from PS179 and KEK experiments on the strangeness production in  $\overline{p}$ -nuclei annihilations can be summarized as follows:

- Strangeness enhancement on Ta at 4GeV/c (and in Neon at .6 GeV/c);
- "Two-source" hypothesis for  $\Lambda^0$ . K° production in both experiments;
- =  $R = \sigma(\Lambda^0) / \sigma(K_s^0)$  behaviour :  $K_s^0$ , "peripherical-like "production;  $\Lambda^0$ , "cluster-like "production;
- Uncorrelation between strange particles and  $\pi^-$  associated rapidity distributions ("four-source").
- 4.1 Conventional two step processes

The recent theoretical estimation by Ko and Yuan  $^{15)}$  to explain the large enhancement in strangeness production in the KEK experiment find a cross section value about 40% less than the experimental value. The various conventional two- step processes taken into account for  $\Lambda^{\circ}$  production seem to be not enough to justify the high experimental value. However, a recent calculation  $^{16)}$  which takes also into account the contribution of  $\eta$  and  $\rho$  to the two-steps processes for  $\Lambda^{\circ}$  production, fits the experimental results.

4.2. Surver cooled quark-matter in 4 GeV/c p-heavy nuclei annihilation
A model developed recently by Rafelsky 177 in the frame of the hypothesis of quark matter production  $\omega$  and  $c\in\omega$  led condition seems to explain both the strangeness enhancement and the different sources for  $\Lambda^0$  and  $K_s^0$  production together with the behaviour of R= $\sigma(\Lambda^0)/\sigma$  (  $K_s^0$  ) vs. A.

According to Rafelsky, for some magic momentum (3-4 GeV/c) the p deposits all the annihilation energy in a narrow forward cone of nuclear matter within the target nucleus. Under these favourable conditions of energy transferring it can be postulated the formation of super cooled quark-matter at rather modest temperature (T=60 MeV).

Both the strangeness enhancement and the absolute strangeness abundance of 5s pairs are explained by the model. The agreement of experimental data with rapidity distributions computed assuming a unique thermal source for the emitted strange particles at the same low temperature confirms the internal consistency of the hypothesis of a central fireball disintegrating into various particles.

#### 4.3 An observation of a leading meson in p -Ne reaction at 607 MeV/c incident momentum

In order to explain the "four sources" hypothesis for the negative pions-associated to strangeness production and to obtain further information on the dynamics of the strangeness production it is necessary to examine in more details the rapidity distributions of the negative pions associated to A 0, K. production.

The emission of the Ao's is nearly isotropic in the laboratory system, with an average rapidity <y>=0.07+-0.03. The average longitudinal rapidity of the kaons is significantly larger, namely <y>=0.33+-0.07 and can be considered, within the limits of the statistics, as the sum of two distributions: a first one, about symmetrical around zero and a second one given by the difference between the full distribution and the symmetrical one (Fig. 7). This difference is characterized by an excess of large rapidity kaons. The distribution of the excess extends from y =0.1 to y=1.3 with an average value <y>=0.7, which corresponds to a longitudinal kaon momentum of about 400 MeV/c. Thus, two groups of kaons seem to exist, one emitted from a system with an average rapidity about zero, the other emitted in the forward direction with an average rapidity about 0.7.

In the same way as for the kaons, also the rapidity of the  $\pi^-$  emitted with a  $\Lambda^0$  can be considered. within the limits of the statistics, as the sum of two distributions; one with a mean value about zero, and the other one with an excess of large rapidity pions. The distribution of the excess extends from y=0.2 to y=1.8. The average value is <y>=1., corresponding to a pion longitudinal momentum of about 200 MeV/c.

Pions or kaons as leading particles carry some fraction of the momentum of the incident antiproton in the forward direction in the final state. This fraction of the incident momentum is not absorbed by any target system. The observation of leading mesons is well known from pp reactions 18) where, in the annihilation C.M. system, in the final state the negative pions tend to follow the direction of the antiproton, and the positive ones the direction of the proton.

If a leading particle is seen in the final state, the emission of a pion or a kaon in the forward direction may be depicted as beam fragmentation through quark flow diagrams which conserve the quantum numbers (Fig.8). The leading pion or kaon are produced when an antiquark of the implinging antiproton picks-up a light or an s quark, respectively, from the sea-quark of an interacting nucleon of the target system, while the other two antiquarks are absorbed by the target.

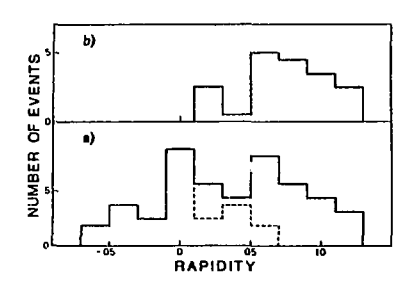


Fig.7. For events with a K's:

- a) the distribution of rapidity of kaons as sum of two distributions;
- b) the distribution of the excess.

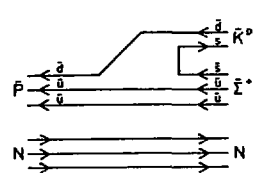


Fig. 8. Quark flow diagram describing beam fragmentation with a leading kaon.

#### REFERENCES

- C.Guaraldo, Physics at LEAR with Low Energy Antiprotons, eds. C. Amsler et al., Harwood Academic Publishers, 1988, p. 797.
- 2) F.Balestra et al., Nucl. Phys. A452 (1986) 573.
- Yu.A.Batusov et al., Europhys.Lett., 2 (1986) 115; G.Piragino, Hadronic Physics at Intermediate Energy, eds. T.Bressani, R.A.Ricci, Elsevier Science Publishers B.V., 1986, p.293.
- 4) F.Balestra et al., Nucl. Instr. and Meth. A134 (1985) 30.
- 5) A.S.Iljinov et al., Nucl. Phys. A382 (1982) 378.
- 6) M.R.Clover et al. Phys. Rev. C36 (1982) 2138.
- 7) Ye.S.Golubeva, A.S.Iljinov, A.S.Botvina and N.M.Sobolosky, Nucl. Phys. A483 (1988) 539.
- 8) J.Cugnon et al., Report of University of Liege, Institute of Physics (1988).
- 9) J.Rafelski, Phys. Lett., 91B (1980) 281; J.Rafelski and B.Muller, Phys. Rev. Lett., 48 (1982) 1066.
- 10) J.Cugnon and J.Vandermeulen, Phys.Lett. 149B (1984) 16.
- 11) F.Balestra et al., Phys.Lett.194B (1987) 192.
- 12) G.T.Condo et al., Phys.Rev. C29 (1984) 1531.
- 13) K.Miyano et al., Phys. Rev. Lett. 53 (1984) 1725.
- 14) S.J.H.Parkin et al., Nucl. Phys. B277 (1986) 634.
- 15) C.M.Ko and R.Yuan, Phys. Lett. 192B (1987) 31.
- 16) C.Dover, Private communication
- J.Rafelski, Physics at LEAR with Low Energy Antiprotons, eds. C. Amsler et al., Harwood Academic Publishers, 1988, Addendum.
- R.Armenteros and B.French, <u>High Energy Physics</u>, edit by E.H.S.Burshop, Academic Press, London 1969,pag.237.

# THE RATIONALE FOR RHIC IN THE CONTEXT OF RECENT A+A DATA

C. Chasman, O. Hansen, and H. E. Wegner Brookhaven National Laboratory, Upton, NY 11973 USA

#### 1. Introduction

RHIC stands for Relativistic Heavy Ion Collider. RHIC is designed as a collider with two beams and four intersections. The beams may be different, each can have a mass number from I to  $\simeq 200$  (in practice probably  $^{197}$ Au). The  $\sqrt{s}$  for Au+Au is designed as 200 GeV/(nucleon pair). The collider tunnel and target halls exist as does the liquid He refrigeration plant for the use of superconducting magnets in the collider configuration. Several prototype dipoles and one quadrupole have been built and tested and the project is ready for construction as soon as funding becomes available. The injection scheme for the collider consists of two tandem accelerators to provide the ion beams, and a synchrotron booster that can accelerate partially stripped ions to energies just below 1 GeV/nucleon where full stripping can be done at a reasonable efficiency. The beams will then be accelerated further in the BNL-AGS to  $\frac{Z}{A} \times 29$  GeV/c per nucleon and injected into RHIC. The tandems and the AGS are existing machines, that have delivered  $^{18}$ O and  $^{28}$ Si beams for physics experiments over the past two years at 14.5 GeV/c per nucleon. The synchrotron hooster is under construction.

The scientific foundation for RHIC is of course intimately connected with the ideas of a possible phase transition from the confined hadronic state of quark matter, to a state where quarks (and gluons) can move freely over distances many (several) times the nucleonic diameter (quark-gluon plasma). An important part of the rationale for the choice of energy of RHIC, relies on the idea of transparency developing from full "stopping" with increasing bombarding energy. It is also important that energy densities of many times that of the ground state of cold nuclear matter can be reached in ion-ion collisions. In this talk, we will examine whether the two latter premises seem to hold true in view of the data from A+A collisions at the Brookhaven AGS-Tandem Complex and at the CERN-SPS. Finally, a few comments are made on measured slopes of hadronic p<sub>1</sub> spectra.

#### 2. Comments on nuclear "stopping" results

In their analysis of p+A data, Bussa and Goldhaber<sup>1,2</sup>/ found that an incoming proton at ≈100 GeV/c (in the lab frame) would lose ≈2 units of rapidity by traversing a Pb-nucleus along a diameter. Under the assumption that this result does not depend on bombarding energy, one would conclude that nucleons with less than two units of rapidity to start with, would lose all of their rapidity in a central collision with a Pb nucleus. For a symmetric collision stopping should prevail for beam rapidities below 4 (2 in the c.m. system), i.e. for beams below  $\approx 60 \text{ GeV/nucleon}$  in the c.m. system.

There are presently two bodies of data relevant to these expectations. The first is from zero degree calorimeter measurements by CERN WA-80/3/ together with results from BNL-E802/4/.

Figure 1 shows the E-802 results. The zero degree calorimeter is limited to an acceptance of  $\pm 0.3^{\circ}$  for these data. The two upper frames show results with a minimum bias trigger for a Au target (left) and an Al target (right). The beam was <sup>28</sup>Si at 14.5 GeV/c per nucleon. Both distributions are broad, spanning from just below the beam kinetic energy at  $\approx$ 380 GeV towards zero. For the Al target the distribution falls off at low energies, while for Au a peak is observed at  $\approx$ 20 GeV. With a central trigger (high charged-particle multiplicity) the picture changes, in that the high energy part of the spectrum becomes suppressed. For Al the spectrum peaks at  $\approx$ 80 GeV, showing that there are 5 to 6 spectators, while for Au the peak at  $\approx$ 20 GeV dominates the spectrum. If the acceptance is increased to  $\pm$ 3°, the above features do not change, although the 20 GeV Au peak becomes somewhat broader.

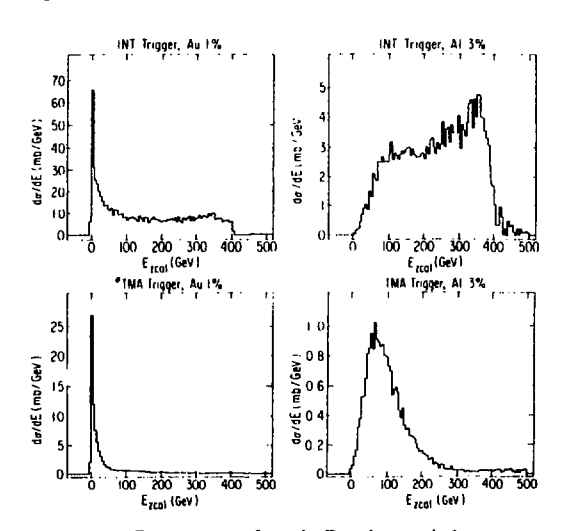


Fig. 1. Energy spectra from the E802 beam calorimeter.

The interpretation of the above observations is straightforward. For Si+Al, collisions with total overlap of the two equally sized nuclei are rare and typical central collisions have only partial overlap. For Au, the projectile is much smaller than the target, and completely overlapping collisions happen often ( $\approx$ 10% of all interactions). The fact that essentially no energy goes forward after a central Si+Au collision is indicative of "full" stopping.

In the WA-80 <sup>16</sup>O beam results<sup>/3/</sup>, at 60 GeV/c per nucleon bombarding energy, the overall trend in going from light ( $^{12}$ C) to heavy ( $^{197}$ Au) targets is similar to the trends discussed above: on the light targets few events take place with  $\simeq$ sero energy left in the beam while for Au the spectrum still peaks at  $\simeq$ 40 GeV, although the peak is less dominant than at the lower AGS energy. At 200 GeV/c per nucleon the peak in the  $^{16}$ O +  $^{197}$ Au spectrum has moved up in energy to  $\simeq$ 500 GeV, and none of the lighter targets show a low energy peak.

We may conclude that "full" stopping is still possible at 60 GeV/nucleon for central collisions of <sup>18</sup>O + Au, but at 200 GeV/nucleon there is always energy going forwards, i.e. "transparency" is setting in.

If the above interpretation of the zero-energy peak in the zero-degree calorimeter as being an indicator of "full" stopping is correct, it is implied from data of Ref. 3 that a Ag nucleus is not large enough to fully stop <sup>16</sup>O at 60 GeV/nucleon beam energy.

The second body of data comes from lead-glass calorimeters, where the electromagnetic energy from  $\pi^0 \to 2\gamma$  and  $\eta^0 \to 2\gamma$  is measured. If the lead glass calorimeter has an acceptance that covers the maxima of the pseudo-rapidity distributions for the various targets, they give a measure of the energy of created  $\pi^0$  and  $\eta^0$  that is largely free of acceptance corrections for the slightly different kinematics of targets with different masses. The lead-glass arrays used in E802/5,6/ satisfy this acceptance condition. The results of Fig. 2 are from <sup>16</sup>O+A at 14.5 GeV/c per nucleon and shows the total energy measured in an asimuthally symmetric lead-glass arrangement (for details see Ref. 5). One feature of interest is the high energy behavior of the  $E_{OT}^{0}$  spectrum for Cu and for Au. If the Cu curve is multiplied by  $\times 5$ , it coincides with the Au curve, and both corresponds to 16 geometrically weighted convolutions of the p+Au spectrum over the beam nucleons (see Ref. 6 for details). Thus the  $\pi^0$  and  $\eta^0$  energy production from <sup>16</sup>O + Au and <sup>16</sup>O + Cu are the same for the highest energies observed, no more energy is produced with Au than with Cu. We may conclude that a nucleus of the size of Cu is enough to "fully" stop <sup>16</sup>O at this bombarding energy, at least as regards energy flow from produced  $\pi^0$  and  $\eta^0$ . Preliminary E802 results for Si+A are in full accordance with the above discussion, the high energy edges for Cu, Ag, and Au are identical except for a cross section factor. The cross section factors may be interpreted geometrically, as the cross sections for complete overlap of projectile

and target. /5,6 An interpretation along these lines is not possible for the WA-80 calorimetry data, because of acceptance effects (see e.g., Ref. 3).

It may be concluded that in regard to "stopping" the present data support the picture underlying the RHIC scenario, and demonstrates the onset of transparency for energies at ~200 GeV/nucleon in fixed target mode.

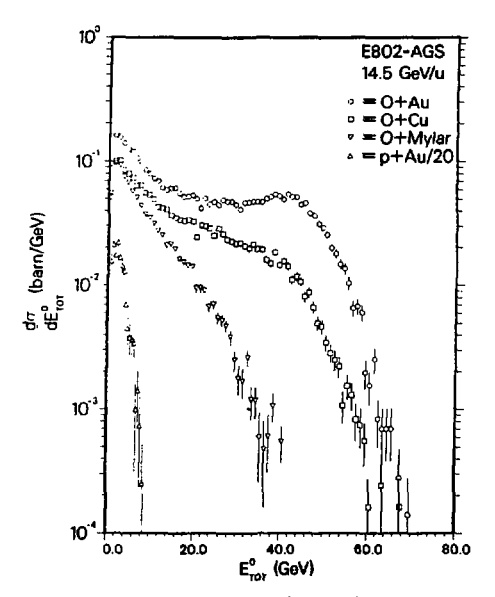


Fig. 2. Energy spectra from the E802 lead-glass array.

#### 3. Comments on energy densities

An energy density behaves under Lorentz transformation as the 44 component of the kinetic energy-momentum tensor/ $^{7}$ /, so if  $\epsilon$  is the density of a volume element in its local rest system, the density observed in the lab system is

$$\epsilon_{lab} = \epsilon \gamma^2$$
 (1)

when the local rest system travels with velocity  $\beta$  relative to the lab system, and  $\gamma = (1-\beta^2)^{-1/2}$ . Hence a discussion of energy densities involves a discussion of reference system. In the extreme limit of full transparency, Bjorken<sup>/8</sup>/ has derived a formula, that connects the measured transverse energy density  $dE_{\perp}/dy$  in rapidity to the energy density in the hot, baryon free region between

the collision partners after the nuclear encounter

$$\epsilon = \frac{dE_{\perp}}{du} (\pi R^2 \tau_0)^{-1} \tag{2}$$

R is the radius of the smaller of the colliding nuclei and  $\tau_0$  is a typical time, usually taken as 1 fm. Equation (2) evidently does not apply in the AGS/CERN energy region, but has nonetheless been used as a reference. The obvious reason for using Eq. (2) is that no experiment has so far measured the relevant volume, from which the observed radiation originated. Applied directly, Eq. (2) gives values of  $\epsilon \approx 1 \text{ GeV/fm}^3$  at the AGS energies/5,9/ and  $\approx 2 \text{ GeV/fm}^3$  at 200 GeV/nucleon (Refs. 3, 10, 11). At AGS energies use of a fireball-model to define the reference frame and the volume does not change/5,8/ the estimated  $\epsilon$ , while a Landau shock front estimate (see e.g., Ref. 12) gives a larger value.

If the values quoted above are at all realistic, the indication is that densities of interest are being reached, from 6 to maybe over 10 times those of nuclear ground states. Thus, accepting the rather uncertain state of affairs, we may conclude that nothing argues strongly against the premise, that considerable densities may be reached in nucleus-nucleus collisions.

#### Comments on slopes of p<sub>⊥</sub>-spectra

It is customary to present particle momentum spectra as  $E(d^3\sigma/dp^3)$  plotted versus  $p_\perp$ . Equivalent forms are often used,

$$E(d^3\sigma/dp^3) = d^3\sigma/(dp_x dp_y dy) = d^3\sigma/(p_\perp dp_\perp d\theta dy)$$
 (3)

and sometimes the invariant cross section is integrated over the azimuthal angle ( $\theta$ ) and/or over rapidity (y),

$$\int_{0}^{2\pi} E \frac{d^{3}\sigma}{dp^{3}} d\theta = 2\pi \frac{d^{2}\sigma}{p_{\perp}dp_{\perp}dy}$$
 (4)

assuming that there is no explicit dependence on  $\theta$ .

Data of  $E(d^3\sigma/dp^5)$  plotted against  $p_{\perp}$  often look as an exponential and are parameterized as

$$E(d^3\sigma/dp^3) = \alpha(y)e^{-p_{\perp}/t(y)}. \tag{5}$$

Sometimes the data are integrated over rapidity y before parametrisation, and the resulting slope then represents an averaging over the rapidity interval

$$\int_{a_1}^{y_2} dy E(d^3\sigma dp^3) = \alpha' e^{-p_{\perp}/t}.$$
 (6)

A tabulation of selected slope parameters from the CERN experiments are given below.

Table

		Siope Parameter t					
Reaction	Particle	E/A (GeV)	t (MeV/c)	<i>y</i> 1	y <sub>2</sub>	y(mid)	Ref.
<sup>16</sup> O+W	$(\pi^-)$	200	190	0.9	1.9	3.0	13
<sup>16</sup> O+Au	$(\pi^{-})$	200	153	2.0	3.0	3.0	14
<sup>16</sup> O+Au	$\pi^0$	200	210	1.5	2.1	3.0	15
<sup>16</sup> O+Au	$\pi^0$	60	200	1.5	2.1	2.0	15

 $(\pi^-)$  stands for negatively charged particles, dominated by  $\pi^-$ . Errors on the slopes are typically less than  $\pm 10$  MeV/c and the  $p_\perp$  range (which differs from experiment to experiment) is from 0.5 GeV/c to  $\simeq 2$  GeV/c. Preliminary data/<sup>16</sup>/ from E802 at 14.5 GeV/c <sup>28</sup>Si+Au show  $\pi^+$  slope parameters near 170 MeV/c for rapidities just below mid-rapidity and  $\simeq 150$  MeV/c just forward of mid-rapidity. The data show a rapidity dependence towards smaller slope parameters with increasing rapidity. Within the spread of the numbers, it is fair to say that there is little variation in the  $\pi$  slope parameter at mid-rapidity in going from 14.5 GeV/nucleon <sup>28</sup>Si to 200 GeV/nucleon <sup>18</sup>O. p+A data from CERN exhibit very similar slopes; there are no p+A data from BNL.

Recalling that  $\pi$  slope parameters at the Bevalac (see e.g., Ref. 17) were much smaller ( $\leq$ 100 MeV/c), it is clear that a "saturation" sets in with increasing bombarding energy.

One may ask: Is it possible to give a thermal interpretation of  $E(d^3\sigma/dp^3)$  versus  $p_\perp$  slopes? The experimental data at present are not sufficient to answer this question. We shall nonetheless offer a few remarks on the subject. Assume that the particles are emitted from a single thermal source with a Boltzman distribution in total energy E,

$$P(p) = (4\pi m^2 T K_2(\frac{m}{T}))^{-1} e^{-E/T}$$
(7)

where P(p) is the probability of finding a particle of rest mass m with momentum between p and p + dp. T is the temperature of the source, and  $E^2 = p^2 + m^2$ .  $K_2$  is a function related to a Hankel function of second order of purely imaginary argument/18/.

Equation (7) can be recast into the variables  $p_{||}$ ,  $p_{\perp}$ , and  $\theta$  and integrated over  $\theta$  and  $p_{||}$ , (see also Eq. (3))

$$P(p_{\perp})p_{\perp}dp_{\perp} = \int_{-\infty}^{\infty} dp_{\parallel} \int_{0}^{2\pi} d\theta P(p)p_{\perp}dp_{\perp} = (m^{2}TK_{2}(\frac{m}{T}))^{-1}m_{\perp}K_{1}(\frac{m_{\perp}}{T})p_{\perp}dp_{\perp}$$
(8)

where  $m_{\perp} = (m^2 + p_{\perp}^2)^{1/2}$  and  $K_1$  is a function related to a Hankel function of the first order (Ref. 18). Noting that  $p_{\perp}dp_{\perp} = m_{\perp}dm_{\perp}$ , Eq. (8) can be written

$$P(m_{\perp}) = (m^2 K_2(\frac{m}{T}))^{-1} \frac{m_{\perp}}{T} K_1(\frac{m_{\perp}}{T})$$
(9)

i.e., for given mass and temperature the entire dependence on kinematical variables is in  $m_{\perp}$ . For large values of  $\frac{m_{\perp}}{L}$ , i.e. for

$$m_{\perp} \gg T$$
 (10a)

K<sub>1</sub> becomes near exponential/18/, and

$$P(m_{\perp}) = (m^2 K_2(\frac{m}{T}))^{-1} (\frac{\pi}{2})^{1/2} (\frac{m_{\perp}}{T})^{1/2} e^{\frac{-m_{\perp}}{T}}.$$
 (10)

Thus a plot of  $\frac{d\sigma}{dm_{\perp}}$  versus  $m_{\perp}$  gives a near exponential fall off with increasing  $m_{\perp}$  with a slope parameter that equals the temperature, when  $m_{\perp} \gg T$ .

Turning back to an interpretation of slope parameters from plots of Eqs. (5) or (6), we note that Eq. (8) gives a complicated behavior as function of  $p_{\perp}$ ,

$$N(p_{\perp})dp_{\perp} \propto (m^2 + p_{\perp}^2)^{1/2} K_1 \left(\frac{(m^2 + p_{\perp}^2)^{1/2}}{T}\right) dp_{\perp}$$
 (8a)

where  $N(p_{\perp})$  is the number of emitted particles with transverse momentrum between  $p_{\perp}$  and  $p_{\perp}+dp_{\perp}$ . While Eq. (8a) is near exponential in  $m_{\perp}$  for  $m_{\perp}\gg T$ , it is not exponential in  $p_{\perp}$  until  $p_{\perp}$  satisfies

$$p_{\perp} \gg m$$
. (8b)

We thus have two conditions to satisfy for an exponential behavior of  $d^2\sigma/dp_\perp^2$ , namely Eqs. (8b) and (10a); the latter may be written (taking  $\gg$  to mean  $> 2\times$ ),

$$p_{\perp} > (4T^2 - m^2)^{1/2}$$
. (10b)

For pions the requirement is  $p_{\perp} > 400 \text{ MeV/c}$  for  $T \simeq 200 \text{ MeV}$ , which is fulfilled by the numbers quoted above. For knons, Eq. (8b) is the sharper and requires  $p_{\perp} > 1 \text{ GeV/c}$  (using  $\gg$  to mean  $> 2 \times$ ). Proton spectra plotted as invariant cross section versus  $p_{\perp}$  are not expected to be near exponential in  $p_{\perp}$  until  $p_{\perp} > 2 \text{ GeV/c}$ . The curvature of the  $K_1$  function for  $p_{\perp}$  values near m, may easily yield a totally erroneous temperature. The natural variable is not  $p_{\perp}$  but  $m_{\perp}$ .

Let us finally note, that the systematics of pion spectral slope parameters may possibly reflect a statement about a temperature saturation. The fact that p+A spectra exhibit a very similar tend certainly means that the phenomena is not exclusive for A+A collisions. It will be very exciting to see spectra from very heavy beams and at much higher energies. Is there really a universal maximum slope value of  $\approx 200 \text{ MeV/c}$  for pion spectra? We need RHIC badly!

# Acknowledgements

This research was supported by the U. S. Department of Energy, Division of Basic Energy Sciences under Contract No. DE-AC02-76CH00016.

# References

- 1. W. Busza, Nucl. Phys. A418 (1984) 635c.
- 2. W. Busza and A. Goldhaber, Phys. Lett. 139B (1984) 235.
- 3. S. P. Sorensen et al., The WA-80 Collaboration, Z. Phys. C 38 (1988) 3.
- E. Duek et al., The E-802 Collaboration, Contribution to the Third Int. Conf. on Nucleus-Nucleus Collisions, Saint Malo, France, 1988.
- 5. T. Abbott et al., The E-802 Collaboration, Phys. Lett. B197 (1987) 285.
- 6. L. P. Remsberg et al., The E-802 Collaboration, Z. Phys. C 38 (1988) 35.
- 7. The Theory of Relativity, C. Moller, University Press, Oxford, 1955.
- 8. D. Bjorken, Phys. Rev. D27 (1983) 140.
- 9. P. Braun-Munzinger et al. Z. Phys. C 38 (1988) 45.
- 10. F. Corriveau et al., The Helios Collaboration, Z. Phys. C 38 (1988) 15.
- 11. W. Heck et al., The NA-35 Collaboration, Z. Phys. C 38 (1988) 19.
- 12. M. Gyulassy, Z. Phys. C 38 (1988) 361.
- 13. H. W. Bortels, The NA-34 Collaboration, Z. Phys. C 38 (1988) 85.
- 14. H. Stroebele, The NA-35 Collaboration, Z. Phys. C 38 (1988) 89.
- 15. H. Loehner, The WA-80 Collaboration, Z. Phys. C 38 (1988) 97.
- G. Stephans, The E-802 Collaboration, Contribution to the Third Int. Conf. on Nucleus-Nucleus Collisions, Saint-Malo, France, 1988.
- S. Nagamiya, Nucl. Phys. <u>A418</u> (1984) 239c.
- M. Abramowitz and I. A. Stegun, Handbook of Mathematical Functions, Dover Publications, Inc., New York, 1972.

# PRESENT STATUS OF THE GSI-SIS/ESR PROJECT

# Paul Kiente Gesellschaft für Schwerionenforschung mbH. D~6100 Darmstadt, BRD

# 1 SIS/ESR Project

Fig. 1 gives an overview of the heavy ion acceleration complex under construction at GSI\*. It consists of an upgraded UNILAC used as an injector into a medium energy (1-2 GeV/u) heavy ion synchrotron SIS 18\*\* which is connected with a storage cooler ring ESR\* of half the circumference of SIS 18. The combination of these two rings should allow to produce completely stripped heavy ion beams up to U\*\* with the highest possible phase space densities achievable by various beam cooling techniques. In addition SIS/ESR will provide beams of radioactive nuclei in the energy range from several MeV/u up to 1-2 GeV/u again cooled to the highest possible phase space densities. The beams in the ESR may be used either circulating with high currents or extracted with a great variety of time structures and intensities. They may be also reinjected into SIS for further acceleration or deceleration. There will be a large experimental area with several experiments set up on beams from both SIS and ESR. Further experimental areas are located directly behind SIS, between SIS and ESR and around the ESR. In future one can think of injecting the high phase space density completely stripped beams in superconducting collider rings with small apertures, modest size and prize to achieve very high c.m. energies (> 20 GeV/u) at as high as possible luminosities.

Very recently we changed our injector, concept into the UNILAC, such that we can run a truly independent low energy program with a free choice of ion species and energy parallel to a low duty factor high current injection cycle into SIS 18. The SIS injection is based on recently developed high intensity ion sources? for low charge states (U\*\*) which will be accelerated by 27 MHz RFQ structures up to 130 keV/u and after stripping injected straight into the second Wideroe tank. This high current injector will be operated with a duty factor of 1.%, which is sufficient for synchrotron injection. It can provide 100-1000 times more injection current than the present UNILAC.

For the low energy UNILAC program we plan to construct an independent injector<sup>6</sup> consisting of a 10 or 16 GHz ECR-source, a RFQ linac up to energies of 300 keV/u, followed by an interdigital line structure up to the injection energies of the Alvarez section (1.4 MeV/u). These structures will be operated at 108 MHz with 50 % duly factor.

The heavy ion beam accelerated in the UNILAC up to 11.4 MeV/u and stripped to an adequate high charge state for the desired energy and intensity, is injected into SIS 18 during 10 to 30 turns and accelerated with a repetition rate between 3 Hz (up to 1.2 T) and 1 Hz (up to 1.8 T) to maximum energies, depending on the charge states of the ions as shown in Fig. 2.

For uranium ions with a charge state of q=78, after stripping at 11.4 MeV/u with a foil largel, 1 GeV/u is achieved as maximum energy. The maximum beam intensities from SIS 18 are shown in Fig. 3 for Ne- and U-

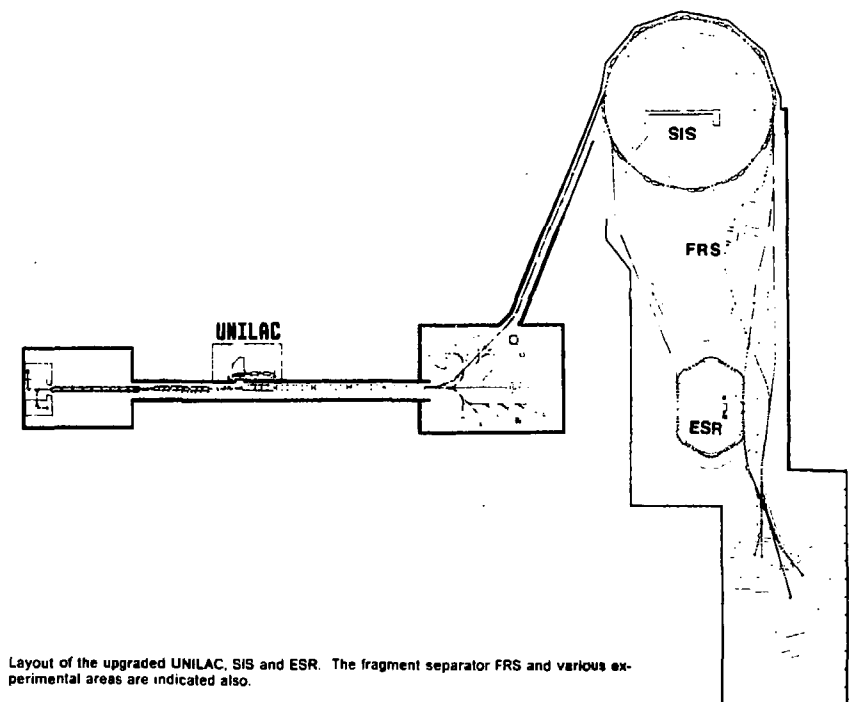


Fig. 1.

Fig. 2. Maximum achieveable energies at SIS 18 as a function of nuclear charge, the elergies are given for a gas- or a foll-stripper at an energy of 1.4 MeV/u. resulting in relatively low degrees of ionization. If a second stripper at 11.4 MeV/u is added or if completely ionized particles from the experimental storage ring ESR are reinjected into the synchrotron higher energies can be achieved.

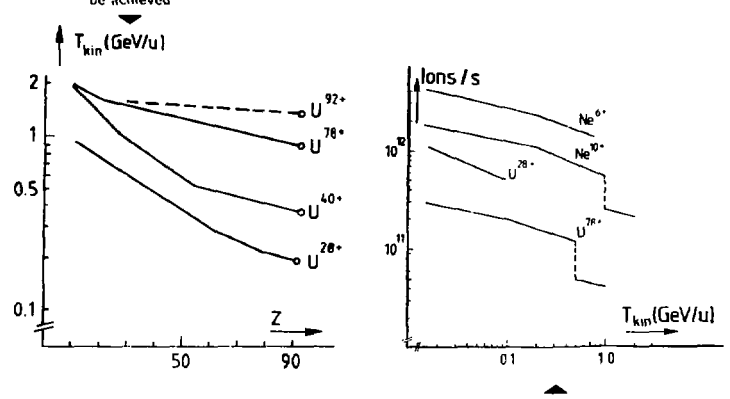


Fig. 3 - Beam currents for various charge states of Ne- and U-ions, gained with the stripping procedures described in Fig. 2 as function of the energy. The intensity drops by a factor of 3 for Ne<sup>-104</sup> and U<sup>-104</sup> are due to a decrease of the repotition rate from 3 Hz to 1 Hz.

ions of various ionic charges, depending on the stripping procedure, as function of their specific energies. The decrease of the intensities towards higher energies is caused by a small decrease of the synchrofron repetition rate, the drop for 1 GeV/u Ne and 500 MeV/u U is due to a change of the repetition rate from 3 to 1 Hz.

Between SIS 18 and ESR the beam may be stripped once more to the highest desired charge state. The ESR with a bending power of  $Bp = 10^{\circ}$  Tm allows to store ions up to  $U^{97^{\circ}}$  with the following maximum energies. Ne<sup>104</sup> (8/34 MeV/u). Ar<sup>147</sup> (709 MeV/u). Kr<sup>147</sup> (669 MeV/u), Xe<sup>244</sup> (609 MeV. /u) and  $U^{924}$  (556 MeV/u). The uranium ions can be fully stripped at this energy with an efficiency of 60.% in a Cu-target of 100 mg/cm<sup>2</sup> thickness. The stripping yield in creases strongly with decreasing nuclear charge, thus one expects a yield of 70.% for Pb<sup>924</sup>-ions (574 MeV/u) and already 100.% for Xe<sup>344</sup>-ions (609 MeV/u). Alternatively one can install a reaction target for projectife fragmentation. The favourable kinematic focussing of the products around the heam direction and velocity allows effective mass-separation in a special mass-separator between SIS and ESR, followed by accumulation of rudioactive beams with the ESR, which accepts beams with  $\phi p/p = \pm 0.5.\%$  and transverse emittances of 20.8 min mrad.

The ESR (Fig. 4) has two 9.5 m long straight experimental sections, in one of which an electron cooling device will be installated. The other 4 straight sections will be used for the installation of rf cavities, slow and fast extraction elements. The rf cavities are used for acceleration, deceleration and especially also for bunching of the beam together with the Liei fron cooling for reduction of the occupied longitudinal phase space volume. With the fast extraction system of the ESR one can transfer a highly ionized and cooled beam back to SIS 18 for further acceleration, or specially also deceleration. The optics of the ring allows three modes of operation, one with moderate dispersion along the ring specially suited for accumulation of beams with large momentum spread ( $\delta p/p = -1.05$ %) and emittance ( $\epsilon_{hy} = 0.00$  m mm mrad), one with zero dispersion in the straight

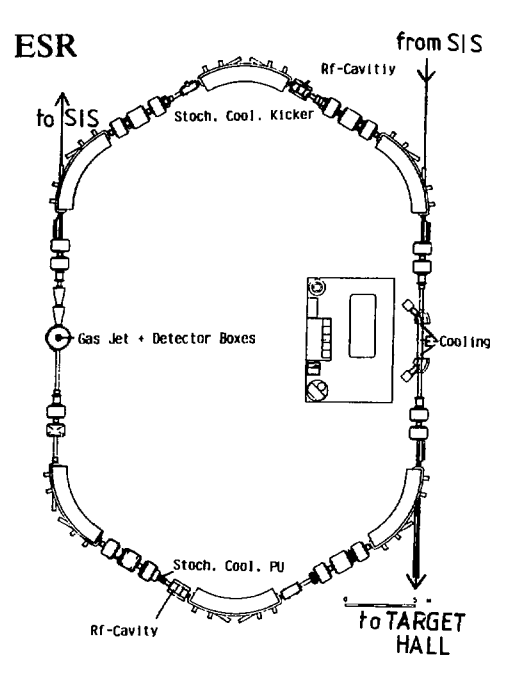


Fig. 4. The magnetic lattice lay out of the ESR ring, with stochastic and electron cooling devices, recavities and a straight section with an optional gas jet target.

sections, which allows multi-charge operation (U\*\*\* - U\*\*\*) and one with large dispersion to accommodate two beams of slightly different momenta, which then may be brought to merge with a well defined angle of about 100 mrad.\* This can be used to study collisions of two highly ionized beams at fixed target equivalent energies of up to 7.2 MeV/u and an energy definition of better than 10 %.

The most important facilities of the ESR are various cooling devices which can be applied complementary. For low phase space density secondary beams stochastic pre-cooling may be used. For cooling to very high phase space density, electron cooling of completely stripped heavy ions is foreseen in an interaction zone of 2 m length. A "cool" electron beam of 5-10 A is focused within an area of 5 cm diameter collinearly along the ion beam at the corresponding average velocity. For cooling of beams between 30 MeV/u and 560 MeV/u, electron energies in the range of 16.5 keV and 310 keV are required. With an electron beam current density of up to 1 A/cm² and ion beams of initially  $\delta p/p = 0.1$ % and  $\epsilon = 4 \pi$  mm mrad cooling times of 30 ms for U°2\* at 500 MeV/u are expected. Heavy ion beams with emittances as small as 0.1  $\pi$  mm mrad and momentum spreads of less than 10 -5 may be produced. Space charge effects limit the number of ions to be cooled in a circulating heam."

While the cooled beam circulates in the ring it may be used in the second straight section for the study of collision processes with internal targets, which may be atomic or electron beams (unpolarized or even polarized) gas jets or fibres. For all experiments which need thin targets a high gain in luminosity may be achieved compared with a single pass experiment due to the increase of the circulating beam current (~ 2x10°). Also the interaction of collinear laser and electron beams with the circulating ions of high intensity and small momentum spread may be favourably studied.

The building construction started in November 1986 and is completed now. All dipole magnets and several locussing groups are installed in the SIS-funnel and connected to power supplies and cooling circuits. In beginning of July we expect to make the first power test runs together with the electric power companies, which will probe the line loads and the reaction of the generator sets. We expect to have SIS 18 completely assembled by the end of 1988 to start first injection test. After a comissioning period of half a year, we hope to start first experiments with beams from SIS in fall of 89.

The ESR is constructed parallel to SIS. The magnets, power supplies, UHV systems and the electron cooling device are under construction. In summer 1988 we plan to begin the installation of the ESR magnets with the goal to start commissioning and first cooling experiments only shortly after SIS has taken up production.

# 2 EXPERIMENTAL FACILITIES FOR FIRST NUCLEAR PHYSICS EXPERIMENTS AT SIS/ESR

a) Projectile Fragment Separator (FRS)

In the experimental area between SIS and ESR (Fig. 1) a high resolution projectile fragment isotope separator (FRS) will be installed. Radioactive beams can be transported into a small cave close to the FRS, into all experimental facilities of the large target hall and most important into the ESR. The FRS is constructed following a scheme which has been successfully used by the separator LISE at GANIL'. A high energy, high intensity beam from SIS hits a target in which projectile fragments are produced with similar velocities as the beam and well focused in the direction of the beam ( $\Theta_{1/2} < 0.5 \cdot 1^{\circ}$ ). The first two dipole magnets separate fragments with a certain A/Z values, from the projectiles and fragments with different A/Z. For an isotope separation from a selected A/Z-fraction, the nuclei are passed through an absorber, in which they loose energy proportional to Z<sup>2</sup>. T<sup>2</sup> is nuclei with a certain Z can be separated completely by the following two dipole magnets. By shaping the absorber chromaticity corrections may be introduced.

The physics programs at the FRS is expected to become very diversified. First we will focus on the study of the fragmentation process especially with heavy masses. Beside the measurement of A and Z distributions the study of the momentum and energy transfer on the fragment should shed light on the reaction dynamics. With separated isotopes detailed nuclear structure studies of heavy neutron rich nuclei should be possible. Then of course high energy radioactive beams may be produced and used for reaction studies, especially also in context with the ESR, in which they may be cooled and decelerated.

A very different class of reactions which may be favourably investigated in the FRS are fusion reactions high energies using inverse kinematics, like  $^{12}\mathrm{C}$  (p.  $\gamma$ ,  $^{0}$ ,  $^{13}\mathrm{N}$ . The heavy fusion products emitted in a small forward cone may be identified and completely momentum analyzed with 100 % detection efficiency. Thus very rare processes may be studied. Another interesting field is connected with the proposed study of  $\Delta$ -production in quasielastic collisions, for which the FRS may be used as a high resolution spectrometer. Very rare processes like the subthreshold production of K<sup>-</sup> and antiprotons can advantageously be studied at the FRS as well as the search for exotics like neutrons bound by negative pions.

The radioactive beams of the FRS may be injected into the ESR, accumulated and cooled by stochastic precooling and electron line cooling to the highest phase space densities possible. Their energies may be adjusted in a large range by acceleration or deceleration in the ESR. These radioactive beams may be used as high current circulating beams in the ESR or they may be slowly extracted and transported in the experimental hall. The ESR may be also favorably used as a high resolution mass spectrometer or mass separator. With a scan of the revolution frequencies of cooled coasting radioactive beams in the ESR, high resolution mass measurements may be performed. The relative (A/Z) resolution given by the expression  $\delta(A/Z)/(A/Z) = (< \delta B/B >^2 + (1/\gamma^2 - 1/\gamma_1^2) \gamma_1^4 < \delta p/p >^2 1/2$  is determined by the variation of the magnetic field  $\delta B/B$  and the momentum spread becomes very small if one could store the ions with a relativistic factor  $\gamma$  close to the transition point  $\{\gamma_1\}$ . With well controlled magnetic fields and well cooled beams, mass resolutions of  $10^{-5}$  to  $10^{-6}$  may be achieved. The ESR is also equipped with a resonance extraction system, which may be used as a mass separator. In such an operation the electron energy of the cooling system would be used for fine adjustment of the revolution frequency to the extraction resonance for one particular isotope which would be kicked out of the ring.

It was suggested to use cooled circulating radioactive beams of 200 - 400 MeV/u energy for high resolution nuclear reaction spectroscopy on nuclei far off stability. All standard quasi elastic reactions, like inelastic scattering and transfer reactions may be investigated by bombarding atomic beam targets of H. D. T.  $^3$ He,  $^4$ He,  $^6$ Li  $^7$ Li etc. with circulating cooled, radioactive beams and detecting the light recoils at angles, which correspond to forward angles in the c m -system. The resolution is critically dependent on the accuracy to measure the recoil angle and thus on the emittance of the cooled beam. With an emittance of 0.1  $\pi$  mm mrad one expects for inelastic scattering at 160 MeV/u a Q-value resolution of about 50 keV.

One class of ESR experiments is concerned with the β-decay of a completely stripped nucleus to its isobar with the decay electron becoming bound in the 1s state. This process which is interesting for the nuclear synthesis<sup>13</sup> and neutrino physics<sup>14</sup> has not been observed before. Because the final state is energetically favoured relative to the initial one by about the binding energy of the 1s electron, nuclei which are stable as atoms may decay if the following condition is fulfilled.

$$Q = [m(Z) - m(Z+1)] c^2 + [B(Z) - B(Z+1)] + [B(1s)]_{Z+1} > 0.$$

In this expression  $[m(Z) - m(Z + 1)]c^2$  is equal to the mass difference of the neutral atoms, [B(Z) - B(Z + 1)] denotes the total binding energy difference of the electrons in the atom Z and Z + 1,and  $[B(1s)]_{Z+1}$  the binding energy of the electron captured in the atomic 1s-state of the nucleus with atomic number Z + 1

There is an interesting proposal to study the groundstate hyperfine splitting of hydrogen-like ions either by detection of the M1-transitions between the hyperfine levels after production of the hydrogen-like ions in a stripper foil or more ambitiously by collinear laser spectroscopy. The transition energies are in the optical region and one can also use the large Doppler shifts for funing purposes. The radiative lifetimes of typical groundstate hyperfine structure transitions are between 100 ms and 100 us.

Studies of nuclei far off stability were proposed using Coulomb-excitation, complete fusion and possibly transfer reactions with radioactive beams of fragmented projectiles, cooled in the ESR and decelerated to energies close to the Coulomb-barrier. Such reactions will allow to study nuclei close to the proton dripline.

# c) Hot Dense Nuclear Matter

Following the exploring work on the properties of healed, compressed, and baryon excited nuclear matter studied by medium energy nucleus-nucleus collisions at the Bevalac, second generation experiments are designed to study the dynamics of dense and hot matter including the rare processes like the production of y-rays, strange hadrons and antiprotons in the SIS target half.

Fig. 1 shows the tentative lay out of the beam transport system leading to three targe caves in which the first experimental facilities will be installed during the next two years. Two caves are anticipated for nucleus-nucleus collision studies at the beginning. The third cave is reserved for biology, atomic physics and smaller nuclear physics experiments.

For the study of central collisions we decided to construct an advanced 4π-detector for charged particles including a forward-spectrometer and large BaF<sub>2</sub>-detector arrays for high energy photon spectroscopy. This device is designed to measure the complete momentum flow (d<sup>3</sup>σ/dp<sup>3</sup>) of all charged particles originating from a hard collision, which will allow to analyze in substantial detail the collective nuclear matter flow first observed in exclusive experiments by Gustafson et al.<sup>15</sup>

A schematic lay out of the  $4\pi$ -detector is shown in Fig. 5. The target B is surrounded by a drift chamber E placed within the magnetic field (0.5.1) of a superconducting solenoid J. Particles emitted in a forward cone between  $30^{9}$  and  $7^{9}$  are identified with three planes of tracking detectors F, a detector to measure energy loss H and the TOF plastic wall G, placed about 4 m downstream the target. For handling high multiplicity events the plastic wall is segmented into about 1500 thin plastic scribillators recording  $\Delta E$  and the time of flight of particles. A complete particle identification is aimed at by measuring the magnetic rigidity (Bp), the velocity v, and the energy loss  $\Delta E$  through several detectors. The momentum vector  $\vec{p}^*$  can also be determined for each

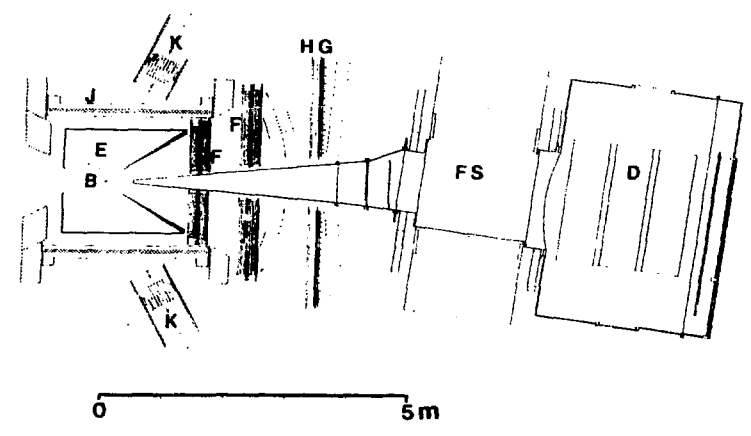


Fig. 5. Schematic lay out of the 4r-detector. The target B is surrounded by a central drift chamber E in a magnetic field produced by a superconducting solenoid. J. The forward cone between 7 and 30° is covered with tracking chambers F, a cluster detector. H and a lime of flight wall G. The products emitted in heam direction are analyzed with a forward spectrometer FS and a Detector D. High energy 7-rays are detected with BaF<sub>2</sub> arrays K.

charged particle. In order to cover also the forward cone  $\Theta < 7^{O}$  a forward spectrometer (FS) using a large magnetic dipole field is under discussion. Such a device would complete the momentum flow analysis in the important forward direction. The complete  $4\pi$ -detector can of course also be used to study in detail certain selected particle-particle correlations including multifragmentation.

The production of  $\gamma$ -rays,  $\pi^0$  and  $\eta^0$ mesons will be studied with a Two Arm Photon Spectrometer "TAPS" consisting of at least two arrays of 64 BaF $_2$ crystats each being 12 radiation lengths deep. High energy  $\gamma$ -spectroscopy may be a useful probe to investigate the temperature and possibly the energy density of the hot matter in an unambiguous way. It may also be possible to study directly the production and decay of baryonic resonances. At higher bombarding energies the combinatorial background of many  $\gamma$ -rays from  $\pi^0$  decay may prevent single photon spectroscopy or will make it very difficult. In this energy regime complete  $\pi$ -meson creation studies seem to be most important. At still higher bombarding energies, the complete  $\pi$ -detector should allow to observe also K  $^+$ -production. The forward spectrometer of the  $4\pi$ -detector will be extremely useful tor nuclear reactions, in which lighter target nuclei are bombarded with heavy projectiles. The projectile fragments should be all contained within a forward cone and can be analyzed simultaneously by a spectrometer with large angular acceptance. For first experiments moderate momentum resolution might be adequate

There are also plans to construct a detector for high energy neutrons, having very high efficiency and the best possible time of flight resolution to study Coulomb break up of relativistic projectiles. Such a detector consisting of a sandwich structure of iron converter plates and plastic scintillators could be put 15 m downstream from the target.

With the highest SIS energies and high bram intensities it will be possible to study the subthreshold production of strange particles like K\* and K^ and hopefulty also anliprotons as function of bombarding energy and mass of the colliding nuclei. These rare processes should give further information on collective effects. Like compression and correlations of quarks and antiquarks in the high density fireballs produced in medium energy nucleus-nucleus collisions. Several magnetic spectrometers and transport devices are suggested for these investigations, including the use of the projectile fragmentation isotope separator for the measurement of K^ and p-production in forward direction. Fig. 6 shows the design values of a Kaon Spectrometer, which is discussed to study specially K \* -production at energies as far as possible below the threshold.

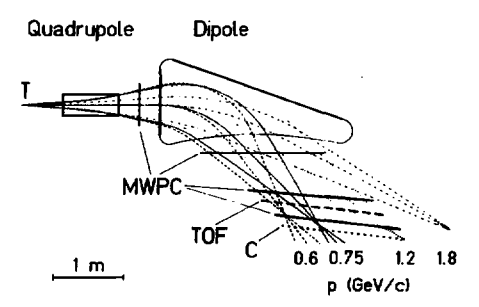


Fig. 6. Design schematic of a Kaon Spectrometer.

# 3 CRYSTALLINE BEAMS

At the end of my review I like to draw attention on a phenomenon which seems to open up very exciting physics with cold heavy ion beams available.

It was pointed out " that by cooling beams of highly stripped high Z ions ( $U^{9/4}$ ) in the ESR to low enough temperatures a phase transition to an ordered state should occur. If the order parameter  $\Gamma = (Z^4e^3/a)/k\Gamma$  exceeds 170 Molecular dynamics simulations (Fig. 7) show that in such a beam a novel form of ordering occurs with the particles being placed on cylindrical shells encircling the beam axis. New crystallographic symmetries occur that differ from those in an infinite Coulomb lattice. The lattice constants are in the order of several tens of micrometer, thus a piece of condensed ordered matter is formed with a density  $10^{14}$  times smaller than ordinary matter. The practical absence of Doppler broadening will be extremely beneficial for some nuclear physics experiments discussed above. A momentum spread  $\Delta p/p$  of  $10^{-8}$ , characteristic for crystalline beams, would allow high precision mass measurements (Schottky scan) and resonance laser spectroscopy with lower power recurrements

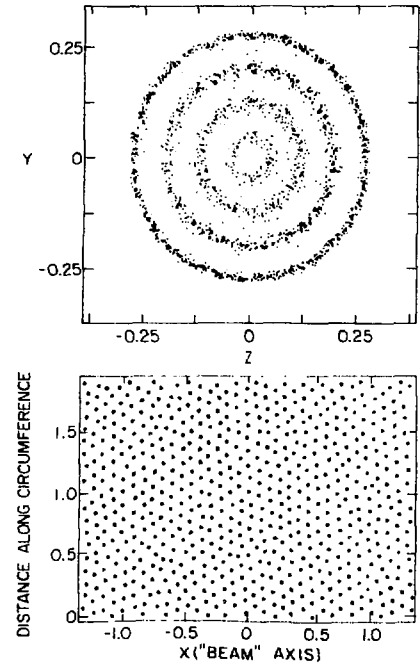


Fig. 7. Crystalline beams. Upper part: Projection of 2000 particles in a molecular-dynamics calculation<sup>19</sup> onto the plane perpendicular to the beam (x-axis) for Γ = 170. Lower part: distribution of particles in the outer shell with the shell unfolded into a plane. All shells but the innermost show a similar pattern.

# REFERENCES

- Die Ausbauplane der GSI, March 1984
- SIS Ein Beschleuniger für schwere Ionen hoher Energie, GSI-Bericht 82-2
- 3 K. Blasche, D. Bohne, B. Franzke, H. Prange, 1985 Particle Acc. Conf. 1985, Vancouver, IEEE Trans. NS32.
- B Franzke et al., Zwischenbericht zur Planung des Experimentier-Speicherrings (ESR) der GSI, GSI-SIS-INT/84-5 August 1984 and Information about ESR, GSI-ESR-TN/87-02.
- R. Keller et al., Proc. Int. Ion Engineering Congress, Kyoto (1983)
- N Angert, internal report
- H Gould et al., Phys. Rev. Lett. <u>52</u>, 180 (1984) B Franzke, Ch. Schmetzer, GSI-Scientific Report 1984, p.341
- I Hofmann, GSI Scientific Report, 1985, p. 387
- 10 G Münzenberg, GSI-Nachrichten 11-87, p. 3
- 11 M Langevin et al. Phys. Lett. 150B, 71 (1985)
- 12 J Homolka et al., Nucl Instr Meth A260, (1987) 418
- K. Takahashi and K. Yokoi, Nucl. Phys. A404 578 (1983)
- 14 P Kienle in Proc. of "10 Years of Uranium Beams" GSI Conference 86-19 and Prec. of "Int. Conf. on Solar
- Neutrino Detection" GSI preprint 86-57
- 15 H A Gustafson et al., Phys.Rev.Lett 52, 1590(1984)
- 16 J.P. Schiller and P. Kienle, Z. f. Physik, A321, 181 (1985)
- J P Hansen, Phys. Rev. A11, 1025 (1975)
   A Rahman, J P. Schiffer, Phys. Rev. Letters 57, 1133, (1986)

Рукопись поступила в издательский отдел 1 ноября 1988 года.

Ответственные за выпуск сборника В.В.Буров, А.Д.Коваленко, Ю.А.Панебратцев

Редакторы: Е.Б.Колесова, **Макет** Р.Д.Фоминой, Э.В.Ивашкевич. Т.Е.Полеко.

Подписано в пачать 27.01.89.

Формат 60х90/16. Офсетная печать. Уч.-надлистов 24,21. Тирых 400. Заказ 41563.

Издательский отдел Объединенного института ядерных исследований. Дубна Московской области.